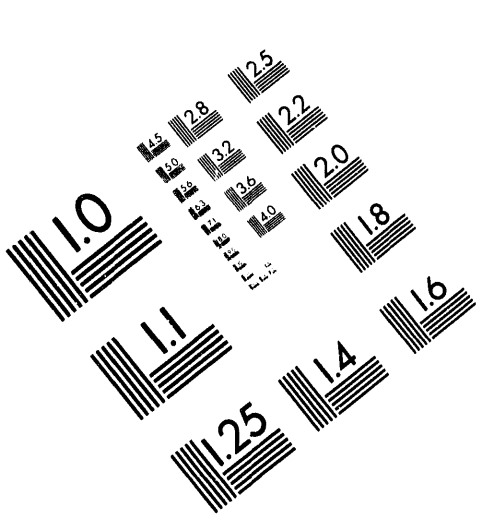

Association for Information and Image Management

1100 Wayne Avenue, Suite 1100
Silver Spring, Maryland 20910

301/587-8202

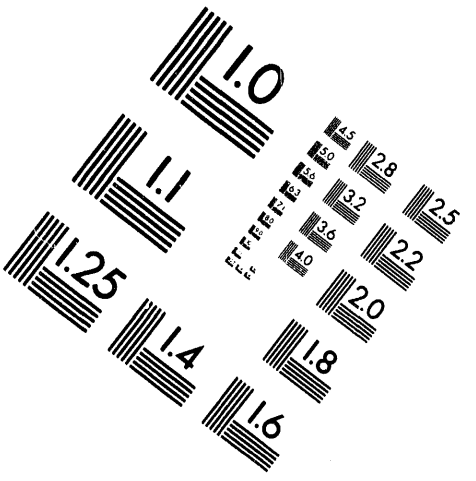

Centimeter

Inches

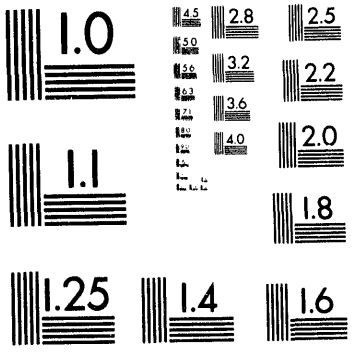

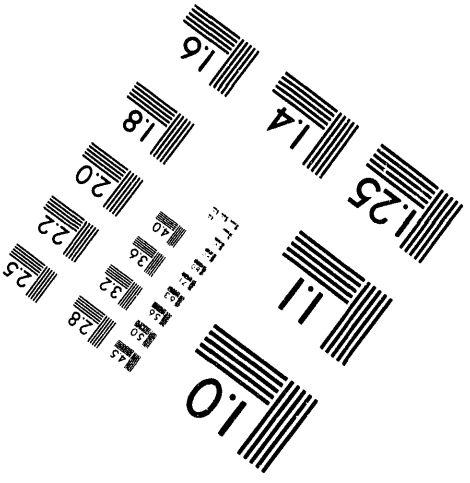

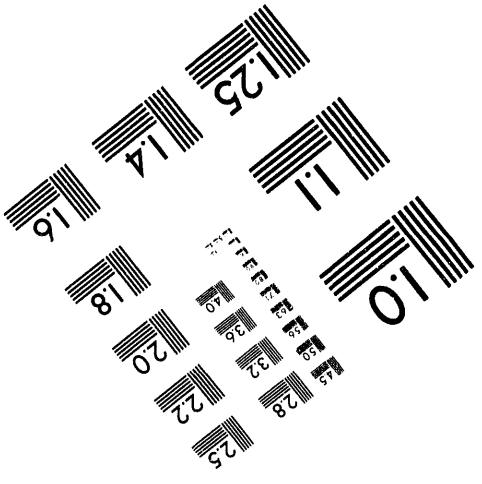

1 of 8

CONF-940190--

SAND94-0753
Unlimited Release
Printed April 1994

PROCEEDINGS OF U.S.-JAPAN WORKSHOP Q-181

on

High Heat Flux Components and Plasma-Surface Interactions for Next Devices

University of California at San Diego
San Diego, California
January 24-27, 1994

Edited by R. T. McGrath, Sandia National Laboratories
and T. Yamashina, Hokkaido University

Sandia National Laboratories
Albuquerque, New Mexico

Table of Contents

Workshop Summary

Session II: PFC Issues for Future Machines
Chairmen: O. Motojima and K. Wilson

II.1	O. Motojima	Present Status of the Large Helical Device (LHD)
II.2	S. Tanaka	Design of ITER Plasma Facing Components
II.3	R. Matera	R&D for ITER Plasma Facing Components
II.4	D. Hill	Power Handling in the TPX Tokamak—Tokamak Physics Experiment

This session focused on three new fusion reactors: LHD, ITER, and TPX. The missions of these devices are quite varied, but they all provide tremendous challenges in the development of plasma-facing materials and components. Each device relies on a magnetic divertor system employing steady state, active heat removal on the order of 10 MW/m^2. All divertor systems are also actively pumped for plasma particle control. A number of common issues for divertor technology R&D exist, including low atomic number materials development, joining of plasma-facing materials to a copper alloy heat sink substrate, conditioning in a high magnetic field, and finally the lifetime and performance testing to provide a reliable and long-lived divertor system. This session provided the opportunity to confirm the steady progress of each project in achieving its goals.

The mission of the LHD is to produce currentless, steady state helical plasmas that are complementary to the tokamak approach. A second goal is the achievement of physics conditions that are extrapolatable to fusion reactor conditions, with contribution to fusion technology. LHD is an eight-year project that is in its fifth year and is presently under construction in Japan. It has a continuous helical divertor, with carbon fiber composite as the plasma-facing material chosen for the 10 MW/m^2 . The design and R&D for the vacuum chamber and divertor plate are now underway. A new idea of the Local Island Divertor (LID) was presented as an effective boundary control method utilizing the artificial m/n = 1/1 island and a cylindrical pumping structure with a graphite head. While LHD is based on a different magnetic configuration from the tokamak concept, an important point is that both are complementary. Therefore, the results of the R&D for high heat flux components and the development of edge control will provide the necessary data bases for future reactors.

ITER's mission is the demonstration of the scientific and technological feasibility of fusion through controlled ignition and extended burn of D-T plasmas, with steady state as the ultimate goal. ITER is using a radiative, gas target divertor concept in combination with beryllium as the plasma-facing material. Power balance and momentum balance are intensively investigated to determine a stable plasma solution, and a practical design for the divertor is progressing. A critical issue is the necessity to withstand transient heat loads such as ELMs and disruptions. The divertor must dissipate on the order of 200 MW leading to a divertor heat flux of approximately 5 MW/m^2 with as much as 200 MJ/m^2 energy deposition during a disruption. Beryllium bonded to a water-cooled copper alloy heat sink is the reference design. Fiber reinforced materials are also under development, and helium or liquid metal cooling is also being considered as back-up options. Details were also presented on ways to achieve improved beryllium microstructures by mechanical alloying with reduced oxygen content, and on the concept of a compliant layer attachment between a sacrificial component and the permanent heat sink that uses low melting solders.

The goal of TPX, which is under design in the U.S., is the testing of the compatibility of steady-state power and particle control techniques with advanced tokamak operation including noninduction current drive with high beta and high confinement. TPX relies on a radiative divertor with edge radiation from impurities, with a resultant wall loading of 15 MW/m^2. The divertor structure consists of a carbon fiber composite brazed to copper and cooled by water.

The lifetime of the carbon based component was estimated to be twice that of beryllium for the conditions of TPX.

Collaborations among these three devices look fruitful due to the common nature of their plasma-facing components. Further work is necessary in materials development and in the evaluation of the boundary control techniques. Existing fusion devices, as well as off-line test facilities, will be needed to control the plasma-facing component issues for future machines.

Session III: Recent PMI Results from Several Tokamaks
Chairmen: N. Yoshida and D. K. Owens

III.1	D. K. Owens	Results from the Initial D-T Experiments on TFTR
III.2	N. Yoshida	PFC and PSI Studies on TRIAM-1M
III.3	B. LaBombard	Initial Results from Alcator C-Mod
III.4	N. Noda	High Z Limiter Experiments in TEXTOR
III.5	T. Ando	PFCs and PSI in JT-60U
III.6	M. Caorlin	DT-Relevant PMI Studies on TFTR
III.7	P. West	Divertor Plasma and Plasma Facing Wall Research on DIII-D

This session contained many interesting reports of progress on device performance, plasma materials interaction and plans for future work. The groups reporting were TRIAM-1M, C-Mod, TEXTOR, JT-60U, DIII-D, and TFTR.

Contributions to PMI from this session fall into three categories:

1. Wall Conditioning and Low Z Materials
   (DIII-D, TFTR, JT-60U)

2. High Z Limiters and Divertor Tiles
   (TRIAM-1M, C-Mod, TEXTOR, JT-60)

3. Radiative Divertors, Divertor Pumping
   (C-Mod, DIII-D)

1. Wall Conditioning and Low Z Materials

DIII-D reports dramatic improvement in N-τ-T, doubling the value every two years. Wall and conditioning techniques are credited with this improvement. Wall coverage has gone from 9% to 100% graphite and carbonization, boronization, and He glow discharge cleaning are employed.

Similar performance improvements in the high-βp mode were reported by JT-60U. CFC divertor tiles were B_4C converted on the surface and installed at the outer divertor strike point. These tiles survived 30 MW of NBI for 2 seconds without significant damage. By optimizing tile shape and B_4C thickness to reduce erosion, they have obtained record values of N-τ-T.

The attainment of fusion powers in excess of 6 MW on TFTR was possible only with a low Z carbon limiter, the reduction in hydrogen isotope recycling by discharge cleaning and the reduction in carbon influx by coating the limiter with lithium, also low Z.

The effect of Li coatings on deuterium retention was investigated on the Tokamak de Varennes, with the result that D retention is increased slightly, from 40% (without Li) to 50% (with Li).

The initial retention measurements for T on the graphite TFTR limiter are at least 9% (values of 50-80% are expected).

2. High Z Limiters and Divertor Tiles

Analysis of the PM-Mo movable limiter on TRIAM-1M and TiC/Mo limiter and divertor tiles on JT-6C shows melting and cracking. The estimated heat flux to the edge of the JT-60 divertor tiles was in the range of 140-200 MW/m^2. The melting appears to initiate cracking at the grain boundaries. The high heat load also initiates grain growth and recrystallization above 1200°C, resulting in reduced intergranular strength. Alloying of the TiC and Mo was observed on JT-60. Intergranular fracture was the failure mechanism.

On TRIAM-1M, the Mo cracking has been understood on the basis of 3d finite element stress analyses. The cure to the problem is to raise the recrystallization temperature. Possible improvements are summarized in the following table:

Alloy	Recrystallization Temperature
Pure Mo	1200°C
Mo + Ti, Ce, Th - TZM	1300-1400°C
Mo + rare earth metals - TEM	1200-1800°C
Mo + TiC	1800-2000°C

C-Mod has a Mo first wall. During normal operation (no auxiliary heating), the dominant impurities are C, O, and H. The carbon flux is typically two to three times the oxygen flux and comes mostly from the walls. Mo is not observed. However, with Ar puffing, Mo is observed. This is attributed to the increased sputtering of Mo by Ar.

Extensive work was done on TEXTOR with high Z limiters since tungsten is the primary candidate for the divertor plates in the ITER/CDA (technical phase). It was suggested that the question should not be whether high Z materials are acceptable, but under what conditions high Z materials can be allowed for use as plasma facing materials.

With the Mo movable limiter on TEXTOR, no strong dependence of Z_{eff}, density or radiated power on limiter position was seen. (Note that the limiter was sharing power with the ALT-II limiter. The power fraction going to the limiter was less than 7%.)

Effects on plasma stability were observed in high density ohmic discharges which had unstable, hollow T_e profiles. Peaked tungsten radiation profiles were sometimes seen in auxiliary heated plasmas, though conditions were found which did not have such behavior.

An interesting observation is that central Mo radiation did not increase in spite of melting of the Mo limiter.

3. Radiative Divertors, Divertor Pumping

Normal operation of the C-Mod divertor is "radiative," with the radiated power fraction in the divertor region on the order of 40%. With gas puffing, detached divertor operation is achieved with greatly reduced conducted power flow to the target plates. The radiating region moves from a volume near the target plates to the x-point.

Radiative divertor operation was also accomplished in DIII-D with a factor of 2 reduction in conducted power flow to the target plates with heavy gas puffing.

The divertor cryopump is in operation in DIII-D with 30 kl/s pumping speed for D_2 and 10 kl/s pumping speed for He using the argon frost technique. For He pumping, $\tau^*_{He}/\tau_E \approx 11\text{-}14$, comparable to the values required for ITER (7-15).

The pump divertor has also permitted density control independent of plasma current in H-modes. Confinement is found to be weakly dependent on density.

Summary of Discussions on Sessions I, II, and III
Monday Afternoon, January 24, 1994
Provided by: P. West

The primary focus of the afternoon session was recent results from existing tokamaks, with presentations from TRIAM-1M and JT-60U from the Japanese side, C-Mod, TFTR, and DIII-D from the U.S. side. There was also a presentation on work done on TEXTOR.

In general, it seems that the tokamak community has been very responsive to the primary needs of the PFC community. One of the major suggestions over the last few years has been that the existing tokamaks should find plasma based solutions to disperse the peak heat flux incident on the divertor strike plates near the separatrix over a wider area than predicted by scaling from experimental previous results. At this conference we heard reports from DIII-D and C-Mod on heat flux reduction due to high gas pressures in the divertor region and due to injection of radiating impurities. DIII-D has observed, transiently, heat flux reduction by a factor of about 5 with either D2 or Ne injection. C-Mod reports the formation of a high pressure zone and detachment of the plasma in its relatively narrow slot divertor with no gas puffing. These results are very promising and suggest that the present ITER plans to limit peak divertor heat flux to 5 MW/m^2 may be very reasonable. Although not presented here, tokamaks in the European Community have also been conducting radiative divertor (JET) and radiative boundary (TEXTOR and Tore Supra) experiments, also with success.

Tokamak experiments on the effects of various wall materials on the plasma and vice versa were also reported. High Z limiter experiments on TEXTOR produced mixed results. Positive results on the use of a thick boron carbide coating on graphite in the divertor of JT-60U were reported. It was also reported from C-Mod that for their low power ohmic discharges studied to date, typically little Mo is seen in the plasma. DIII-D has initiated DiMES experiments, and results of erosion/redeposition measurements were reported. There seems to be some variety of first wall/divertor plate materials being used in diverted tokamaks worldwide, for example, Be in JET, carbon in JT-60U and DIII-D, and Moly in C-Mod and TRIAM-1M.

TFTR reports very good results from its initial DT operation. At 6.2 MW of fusion power, no alpha instabilities were observed, and the fast ion loss to the wall was not anomalous.

During the discussion, it was suggested that existing tokamaks should continue the active investigation of PFC-related problems. The opportunity to study tritium uptake during the TFTR DT operation phase should not be missed. An understanding in some detail of the advantages/disadvantages of the high Z walls on C-Mod is obviously important. DiMES is also a valuable resource.

One area of importance to the future that has not been pursued by today's tokamaks is wall conditioning for long-pulse machines with superconducting toroidal field coils. Later in the workshop, some ideas were presented that perhaps could be pursued on TRIAM-1M or Tore Supra.

Session IV: High Heat Flux Technology
Chairmen: M. Ulrickson and M. Akiba

IV.1	M. Akiba	Development of High Heat Flux Components at JAERI
IV.2	N. Noda	HHFC Development at NIFS
IV.3	C. Baxi	Design, Fabrication and Testing of Helium Cooled Divertor Module
IV.4	S. Suzuki	Heating Tests on JT-60 Actively Cooled Divertor Mock-ups
IV.5	K. Sato	Thermal Cycling Experiment on 1D CFC/W-Cu Divertor Mock-up
IV.6	D. Youchison	Recent EBTS Results and Planned HHF Tests on Beryllium Armored Mock-ups
IV.7	R. Castro	Plasma-Spraying of Beryllium for Fusion Applications
IV.8	F. Kudough	High Heat Flux Load Experiments on Functionally Graded Materials
IV.9	T. Hua	Liquid Metal Coolants for Blanket and Divertor
IV.10	K. Kitamura	Residual Stress Measurements in Tungsten-Copper Duplex Structures after Cyclic Thermal Testing

Development of high heat flux components has been performed extensively in both the U.S. and Japan. These efforts have been oriented to develop high heat flux components for not only operating fusion devices but also next fusion devices, in particular for ITER. The U.S.-Japan collaboration in this field has successfully been carried out as before. This session can be summarized as follows:

Contributions from Japan:

1. The divertor plates for LHD have been developed successfully at NIFS, which could endure a heat load of 10 MW/m^2, 30 seconds for 5000 thermal cycles.

2. The divertor plates for JT-60U have been developed at JAERI, which successfully satisfied the design values.

3. The 1m-long divertor plates with a sliding support structure have been developed at JAERI, which successfully demonstrated the sliding performance and suppress deformation less than 0.5 mm.

4. The divertor plates with 1-D CFC armors brazed onto W-Cu alloy heat sinks endured a heat load of 15 MW/m^2, 30 seconds for over 1000 thermal cycles in a flat plate type. The W30Cu alloy can be a promising candidate for the ITER divertor plate.

5. Development of functionally gradient materials has been performed intensively at Mitsubishi Heavy Industries, which will be a promising technique to reduce stresses at a bonding interface of the ITER divertor plate.

6. Residual stresses of bonded structures have been measured intensively and compared with numerical analyses at Toshiba Corp., whose efforts are necessary to design the ITER divertor plate in a bonded structure.

Contributions from the United States:

1. The results of testing of carbon brazed to copper are very encouraging for TPX and ITER. The samples have survived large numbers of cycles at heat fluxes above 10 MW/m^2.

2. Activation of silver used in most of the carbon-copper braze joints is a potential problem for ITER. Development of non-silver containing brazes should be pursued.

3. Helium cooled divertor heat removal modules have been tested at ITER relevant heat fluxes. The results indicate helium should be further developed as a back-up to the baseline water cooling planned for ITER.

4. The plasma sprayed Be materials being produced are very promising for use in ITER. Further optimization to improve the thermal conductivity is required. This technique has potential for being used for in-situ repair of ITER PFCs.

5. Functionally graded layers are being developed to reduce braze stresses.

6. Liquid metal coolants for the divertor were discussed. Insulating layer development is the major R&D issue. Healing of cracked insulating layers is the most critical topic.

Session V: Plasma Facing Component Design and Applications
Chairmen: A. Komori and J. Davis

V.1	A. Komori	Local Island Divertor Concept for LHD
V.2	R. Nygren	Tore Supra Phase III Outboard Pump Limiter (OPL) (Phase III denotes water-cooled PFCs)
V.3	J. Davis/ D. Driemeyer	U.S. Design Studies for ITER PFCs

This session addressed the engineering issues associated with the design and fabrication of high heat flux components for current and near-term experimental fusion experiments. Papers presented described the design of a divertor for the Large Helical Device (LHD), the manufacture of actively cooled limiters for the Tore Supra tokamak, and the optimization studies for a cold gas divertor for the ITER tokamak. The following sections briefly summarize the key points made at this session.

1. Local Island Divertor Concept for LHD, A. Komori (NIFS)

A closed, full helical divertor provides the primary edge control of the LHD; however, the high cost and uncertainty in physics make the use of this approach risky on the LHD at this time. Instead, considerable insight can be gained into the relationship between the plasma edge and the core through the use of a small and cheaper local island divertor. The local island divertor takes advantage of the currentless helical device, which allows for the creation of a unique (m/n = 1/1) magnetic island. With a divertor head and a pumping duct, this island can be used as a divertor. Some of the advantages of a local island divertor are

- ease of fabrication because of toroidally localized recycling,
- high pumping efficiency (up to 50%) for low recycling mode and high plugging efficiency for high recycling mode, and
- no leading edge.

The preliminary design consists of an actively cooled carbon-carbon divertor, approximately 60 cm wide and 60 cm long. Testing is estimated to begin in 1998.

2. Tore Supra Phase III Outboard Pump Limiter (OPL), R. Nygren (SNL/NM)

The Phase III limiter is roughly 70 x 70 cm in size and contains approximately 1200 pyrolytic graphite tiles, which were brazed onto copper tubes with less than 2% of the tiles requiring rebrazing. The component was successfully operated for 82 plasma shots in Tore Supra withstanding power loads of up to 0.8 MW for 8 seconds. Because of a flaw in the primary Tore Supra control system, on the 83rd shot the controlling computer turned off the cooling water to the limiter. Even though the limiter was not cooled, it was still able to withstand the plasma power for roughly 4 seconds, which attests to the robustness of the design. Eventually, the braze melted at two tile locations on the leading edge tube, which was receiving heat flux in excess of 10 MW/m^2.

In manufacturing this component, one of the greatest difficulties was in finding a reliable, nondestructive analysis technique to show the unbonded areas. To inspect these parts, a unique inspection technique was developed using infrared thermography. In this technique, hot water flowed through the tubes, while the tile surface temperatures were measured with an infrared

camera. The tiles which did not have good thermal contact due to braze flaws or graphite cracking were readily identified and tagged for repair. The successful operation of an actively cooled limiter for multiple plasma shots increases the confidence that actively cooled components can be used in advanced fusion devices. The damaged Tore Supra limiter has been repaired and will again be installed on the tokamak in the spring of 1994.

3. U.S. Design Studies for ITER PFCs, J. Davis/D. Driemeyer (MDA)

The U.S. presented the results of a series of design trade studies initiated to define the operational constraints for materials used in a cold gas type of divertor. In addition to identifying material constraints, alternative design options were also presented. These design options help to increase the design margin for this type of divertor. The results of this study have been documented in a report which will be distributed to the ITER community. In general, it was found that for graphite with a surface temperature of 1200°C, either copper, niobium, or vanadium alloys could be used as a structural material. In the case of beryllium with a surface temperature limit of 700°C, only copper and niobium alloys could be used, assuming a beryllium thickness of 5 mm. If the beryllium surface temperature is limited to 500°C, then only copper could be used, assuming the coolant temperature was less than 100°C. A key point is that the designers need to be very careful in establishing material use limits, because these limits can significantly restrict the design options. Future design studies are going to look at alternative divertor side wall concepts such as a ribbed channel and helium cooling.

Summary of Session

In general three key points can be derived from these presentations:

1. The LID for LHD should be very useful for developing actively cooled divertor components as well as benefiting the LHD.

2. The results of the Tore Supra pump limiter development have shown that perfect brazing of plasma facing materials to cooling tubes is not required. This increases the likelihood that actively cooled components can be developed for future devices.

3. The U.S. ITER divertor design study has shown that there are several clear optimizations that can be made in divertor design once the materials are chosen.

Session VI: Plasma Facing Component Materials and Irradiation Damage
Chairmen: T. Muroga and L. Snead

VI.1	T. Muroga	Radiation Damage of Plasma-Facing Materials
VI.2	L. Snead	ORNL Irradiation Effects Program
VI.3	S. Miki	Development of PFC Materials at Toyo Tanso
VI.4	W. Wampler	Enhancement of Hydrogen Isotope Trapping in Damaged B and Ti Doped Russian Graphites
VI.5	Y. Gotoh	Development of C/C with Controlled Fiber Orientation
VI.6	Y. Kikuchi	Development of B4C Coated Carbon Materials by Conversion Method
VI.7	P. Trester	Preparation of Plasma Facing Materials Coatings at General Atomics

Japanese activity of irradiation damage of PFC materials was introduced by T. Muroga. Irradiation experiments of heat sink materials such as Cu and Mo-Re alloys have been performed by using FFTF/MOTA. It was emphasized that soiid transmutation effects were new and very important issues in neutron irradiation effects. Transmuted Ni and Zn in Cu reduce its thermal conductivity and enhance void swelling. In the case of Mo-Re alloys, quick transmutation of Os from Re results in copious precipitation and relating hardening.

Radiation effects of Cu-C/C joint were reported. It was pointed out that Ag in the filler might act as an enhancer of swelling in the materials.

Neutron irradiation effects of PFC are the next important issues on which our community should concentrate.

Low energy H ion irradiation of W was reported. Purity effects on defect accumulation are very strong. It is expected that high purity, single crystal W (99.99%) is very resistant to hydrogen ion irradiation.

R&D of PFC is being carried on very actively in Japanese companies. S. Miki introduced R&D activity of PFC in his company, Toyo Tanso USA, Inc. Manufacturing process and physical properties of advanced materials such as TiC mixed, boronized and siliconized graphite were introduced.

Y. Gotoh proposed active cooling C/C composite armor with controlled fiber orientation. It is expected that this structure will show better thermal performance than the conventional type structures.

Development of B4C coated carbon materials by conversion method was reported by Y. Kikuchi. Its structure and chemical composition were well characterized by X-ray diffraction, SEM, AES, SAM. The B4C converted carbon tiles with 300 μm-thick B4C layer have been installed in JT-60U since December 1993.

The effect of neutron damage on thermal conductivity (TC) was presented for very high TC graphites and composites. Serious degradation in TC was evidenced for low temperature irradiations. For the case of the highest TC material, a saturation value of 10% of original TC was seen following 100°C irradiation. However, annealing studies indicate that for ITER relevant temperatures (> 600°C), irradiated material will retain ~60% of original conductivity. An algorithm for the irradiation induced degradation in high TC composites has been developed as a function of temperature and displacement damage. Such an algorithm can be applied to calculate the temperature gradient which can be expected for a C/C PFC under irradiation. Also

of note is that RGTi has not evidenced the superior irradiation performance to other high TC graphites previously reported.

Deuterium retention in several Russian graphites has been measured for unirradiated and carbon irradiated materials. Following room temperature (RT) carbon beam implantation, a significant increase in D retention occurs in all materials studied with the highest perfection (larger grain size) materials showing the largest retention. Above 1 dpa (peak), a saturation in retention was seen for the RT implantation. Irradiation at 400°C yielded approximately a factor of two decrease in retention. The saturation seems not to occur at the higher temperature irradiation. Also seen was that small boron additions to RGTi significantly reduce the D retention.

An oxide getter coating for graphite has been developed which shows excellent surface adherence. The coating system takes advantage of the SiC/B_4C eutectic to produce a gradient from graphite to B_4C. Thermal shock testing has been conducted in the Judith facility up to the melting temperature of B_4C (at 12 MW/m^2). Spallation did not occur. Such a coating may lend itself to surface repair of damaged PFCs or for general (in-situ) PFC coverage. The thickness of the oxide getter coating appears to be easily controlled.

Session VII: Boundary Layer Plasmas
Chairmen: N. Noda and L. Schmitz

VII.1	L. Schmitz	ITER Gas Target Divertor Modeling and Experimental Simulation
VII.2	R. Campbell/ D. Knoll	Modeling of Radiative and Gaseous Divertor Operation
VII.3	A. Grossman	Modeling of Gas Target Scenarios Using Degas

Control of plasma boundary is one of the critical issues in next devices.

- Heat flux and particle flux to target plates and side walls of a divertor are determined by the boundary control.
- Design of divertor pumping scheme is also strongly dependent on the boundary control.
- The boundary control is not well established in the existing plasma experimental devices.
- A lot of efforts are ongoing to have a reasonable and reliable modeling of the boundary plasmas.

Bob Campbell (SNL/NM) described recent progress in the modeling of radiative divertor regimes in collaboration with D. Knoll (INEL). Capabilities of the 2-D code, NEWEDGE, include an "average impurity ion" or multispecies impurity models, and non-orthogonal grid geometry. Modeling of Alcator C-Mod ohmic shots indicates that carbon radiation is located very close to the divertor target. After deuterium puffing, however, the radiation zone was observed to move to the x-point. Both deuterium and argon puffing were found to reduce the divertor heat load substantially (by 60-85%). Two-D modeling showed that the radiation layer was extended poloidally in the case of argon puffing and localized closer to the target for D_2 puffing.

One-D calculations have been performed for DIII-D radiative divertor scenarios. A steady-state solution with 28 torr-l/s argon puffing demonstrated 11 MW radiated power, for 16 MW power crossing the separatrix. The Z_{eff} at the outboard midplane was increased to 3.3. In the case of neon puffing, an increase from $Z_{eff} \approx 1$ to $Z_{eff} \approx 1.8$ was observed at the symmetry point. Two-D simulations indicate that the peak heat flux can be reduced by a factor ≥ 2 for a tilted target (75 degrees).

One-D ITER simulations indicated also that the radiation zone can be extended with combined puffing of argon and deuterium. Entrainment of the injected impurities in the vicinity of the targets was found to be satisfactory, if the separatrix density and recycled hydrogen flux in the divertor were high. Ninety-five percent of the input power (325 MW) was radiatively dissipated. The residual target heat flux was 1.4 - 2.6 MW/m^2. However, at lower separatrix density, the entrainment deteriorated and Z_{eff} was found to increase substantially.

Lothar Schmitz (UCLA) described ongoing modeling work on gas target divertors relying entirely on deuterium radiation. Modeling capabilities at UCLA include a 1 1/2-D fluid code (coupled with a diffusion neutral model for atomic and molecular deuterium) and a 2-D code (fully implicit Newton solver, capable of non-othogonal geometry, can be coupled with multi-species, multi-group neutral models). Both codes are benchmarked with data from the PISCES-A linear plasma device.

ITER modeling results were reported. A localized ionization front, very low target electron temperatures and plasma detachment were obtained at input power levels up to 200 MW from the 1 1/2-D code. Two regimes have been modeled: (1) A regime relying on volume recombination of the plasma in the vicinity of the target, and (2) a regime relying on strong target gas injection and recirculation. The volume recombination scenario is attractive since no external gas injection is required and the pumping requirements remain moderate. The radiation layer is extended poloidally and is effective in redistributing the divertor heat flux onto the side walls. A fairly closed divertor structure is needed to retain the required deuterium neutral pressure of several torr. The solutions were found to be sensitive to radial plasma momentum transport. Very robust solutions were found for the second scenario—relying on massive deuterium injection through the target. This regime requires enhanced radial plasma transport ($D \geq 10\ m^2/s$) and strong pumping along the divertor side walls in order to avoid a plasma flow reversal. The required gas puffing rate is very large ($\geq 10^{24}/s$) and necessitates internal gas recirculation. Both regimes require a closed divertor "channel" and neutral densities on the order of 10^{21}-10^{22} in the vicinity of the target.

Experiments in the PISCES-A linear device have demonstrated a stable, detached ionization front in a closed "tube" divertor channel mock-up for electron heat fluxes $\leq 7\ MW/m^2$. In a hydrogen plasma, the target heat flux could be reduced by 97%. The neutral pressure at the target was found to balance the plasma pressure. The plasma pressure was found to peak at the ionization front, and a subsonic flow reversal was observed in the region of reversed pressure gradient. One and one half-D modeling results agree very well with the experimental data. In an argon plasma, the target neutral pressure was much lower than the plasma pressure. This was attributed to the increased radial dissipation of plasma momentum by the lack of radial ion confinement in argon. The electron heat flux was found to be classical.

Two-D Degas modeling results for ITER gas target scenarios were presented (A. Grossman, UCLA). A 30 x 60 grid was used to resolve the structure of the ionization layer in a closed divertor channel (0.2 m wide and 1.5 m long). The plasma input data for Degas were constructed by assembling "slices" of 1-D plasma solutions with the proper upstream boundary conditions in the radial direction. For the gas injection scenario, it was found that the atomic deuterium density at the upper end of the divertor structure was sufficiently high to produce excessive backflow to the main plasma. This problem may be avoided in the volume recombination scenario (radial transport may be very small here). The volume recombination scenario shows a distributed radiation layer, which is beneficial in spreading out the heat load onto the side walls. Direct wall loading by neutrals was found to be small in both regimes. The fraction of radiated power (plus neutral power loss to the side walls) is limited in the gas injection scenario ($\leq 45\%$ of the input power), but can reach 85% in the volume recombination scenario. Ten to twenty percent of the input power is carried to the channel side walls by fast neutrals.

During the discussion, the feasibility of supporting neutral pressures of 1 torr or higher in the divertor area was questioned. Extensive baffling would be required, possibly severely limiting diagnostic access to the divertor region. Existing tokamaks have demonstrated pressure differentials of 10^{-3}, at best. Lower neutral pressure would be required if a substantial fraction of the input power can be radiated by impurities inside or outside the separatrix. The feasibility of impurity radiation in the outer layers of the core plasma was discussed. It was pointed out that the radiating volume in TFTR shrinks with increasing input power, making it difficult to obtain high fractions of radiated power in high power discharges. Radiative divertor experiments in C-Mod, DIII-D, etc., may provide additional insight into these limitations in the future. Also, radial impurity transport in the core is not understood and needs to be investigated in conjunction with scrape-off layer transport. The use of intrinsic or injected impurities may impact the choice

of PFCs in ITER and needs to be considered when evaluating candidate materials. It was also pointed out that the effect of drift flows in the scrape-off layer needs to be addressed in the modeling of highly radiative divertor regimes.

Session VIII: Disruptions
Chairmen: N. Yoshida and A. Hassanein

VIII.1	M. Akiba	Overview of Disruption Simulations at JAERI
VIII.2	P. Rockett	Recent Results from the US/RF Disruption Collaboration
VIII.3	A. Hassanein	Status of Disruption Modeling and Simulations
VIII.4	J. Gilligan	Upgrade to MAGFIRE Code Modeling of Disruptions and Comparison with Experimental Results

This session described current activities in both disruption modeling and simulation experiments in the United States and Japan.

Disruption simulations at JAERI were overviewed by M. Akiba (JAERI). Erosion of many kinds of materials such as graphites, CFCs, B_4C-overlaid CFCs for JT-60U, W and Mo caused by simulated disruption heat load has been studied. It was shown that weight loss by the heat load (1800 MW/m^2, 1.5 ~ 2.0 ms) increased with increased base temperature and is very material dependent. The necessity of international collaboration in this field for next fusion devices such as ITER was emphasized.

The US/RF exchange is working well to complement the strength of each side. Dr. Hassanein of ANL reported on their joint work with TRINITI, RF on a comprehensive radiation transport model which is implemented in the new version of A*THERMAL-S computer code. Recently, Dr. Hassanein has perfected and upgraded the model into a two-dimensional transport model. This addition greatly improved the ability to accurately simulate the radiation generated in impulsive plasma-material interaction. This yielded more confidence in erosion predictions as well as providing a spectroscopic diagnostic against experimental data from various simulation experiments.

Dr. Rockett of SNL/NM complemented this work with a detailed spectral analysis in the VUV (20-400 Å) of two RF plasma guns VIKA, at Efremov Laboratory and 2MK-200 at TRINITI. These experiments attempted to elicit the plasma temperature and density profiles and the impurity distributions in plasma guns. A*THERMAL-S correctly predicted the observed high plasma temperatures (10-20 eV), sufficient to strip carbon (POCO graphite) to its helium-like and hydrogen-like states. Previously, it was believed that ablated plasma temperatures were much lower (~ 1-4 eV).

Additionally, Dr. Rockett's work revealed the presence of fluorine impurities in the VIKA plasma gun and of material sample impurities at 2MK-200. The abundance of spatially and temporally resolved data will now be compared against code calculations. New data will be taken in the summer of 1994 with high spectral resolution in a more limited spectral region.

The drastic differences observed in VIKA and 2MK-200 emphasized the need for plasma characterization during in-situ tokamak disruptions. Dr. Hassanein reported a collaboration with TEXTOR to improve predictive capabilities of erosion prediction with impulsive loads of ~ 10^9 W/m^2. He also showed the first estimates of damage to substrate materials below armor tiles, under disruption loads. Dr. Hassanein's new 2-D calculational ability should aid in this work.

Dr. J. Gilligan of NCSU made a case that plasma characterization was extremely important in low temperature, high density plasma gun sources. These are different from the high temperature, lower density plasmas expected from an ITER disruption. Dr. Gilligan displayed his extensive data base of erosion for many graphites, CFCs, and metals as obtained from

SIRENS, his electrothermal plasma gun. He described a difference between his erosion data and that recorded on PLADIS, VIKA, and 2MK-200. He argued that his 1-D code, MAGFIRE, (plus other data) suggests that the vapor shield is transmitting at least 5% of incident disruption energy.

Finally, it was rewarding to see the results shown by Dr. Akiba of JAERI and Dr. Gahl of the University of New Mexico on disruption-related erosion measurements at their facilities. Dr. Akiba reported increased erosion rates of 2-3 times with increased bulk material temperatures (up to 1000°C) in graphite. Dr. Gahl reported initial results of increasing pulse length on PLADIS at 5 MJ/m^2, from 100 μs to 230 μs, erosion rates surprisingly in this lower power region. These results are under investigation.

Session IX: Conditioning and Tritium
Chairmen: A. Sagara and R. Causey

IX.1	A. Sagara	Boronization in Japan
IX.2	K. Okuno	Studies on Tritium Retention, Permeation and Recovery of Plasma Facing Materials at JAERI
IX.3	R. Causey/ D. Cowgill	Report on the Tritium Plasma Experiment (TPE) Tritium Inventory and Permeation in ITER Outgassing and Conditioning
IX.4	H. Kugel	Real-Time Boronization in PBX-M Using Erosion of Solid Boronized Targets
IX.5	B. Doyle	Measurements of Fusion Synthesized T and T Fuel in JET, TFTR, DIII-D and TEXTOR

Boronization in Japan, A. Sagara (NIFS)

Boronization has been applied in plasma devices, JT-60U, Heliotron-E, CHS and JIPP T-IIU. Results are summarized as follows: (1) Decaborane has been commonly used with He. (2) Fast conditioning is commonly achieved every morning and after exposure to air. (3) Boronization once every few weeks gives stable wall condition. (4) Oxygen impurity is effectively reduced. (5) Reduction of carbon and metal impurities depends on wall material and plasma operation. (6) H recycling seems to depend on boronization condition and/or method. (7) STB has been confirmed to be clearly effective as quick conditioning to reduce both impurity and H recycling, while its lifetime is limited within a few shots.

Present state of R&D on boronization for LHD is summarized as follows: (1) Oxygen penetrates into deeper layers over 50 nm, and B film of about 100 nm thick is sufficient for oxygen getter. This result coincides with the thickness needed in plasma devices, but the penetration mechanism is not clear yet. (2) B film after O_2 glow keeps a quite passive state in the air. This result explains the fast conditioning observed in plasma devices. (3) Decaborane is comparable with diborane as far as oxygen getting capacity is concerned. (4) H in B film desorbs at lower temperature than that in carbon. This result explains the good discharges due to low H recycling in JT-60U, but R&D at room temperature is still required for the V/V in LHD, because its temperature is limited below 100°C.

Studies on Tritium Retention, Permeation and Recovery of Plasma Facing Materials at JAERI, M. Akiba (JAERI) on behalf of K. Okuno

The Tritium Processing Laboratory (TPL) was discussed. It is capable of handling 40 grams of tritium. The tritium permeation and inventory in plasma facing materials was discussed. The experimental facilities used in these experiments were shown. Permeation studies performed so far have used only deuterium. The R&D schedule for studies on tritium retention and recovery of plasma facing materials was shown. Tritium permeation experiments are scheduled to begin this year.

Report on the Tritium Plasma Experiment (TPE) Tritium Inventory and Permeation in ITER Outgassing and Conditioning, R. Causey and D. Cowgill (SNL/CA)

This talk covered three different areas: (1) Tritium Plasma Experiment (TPE), (2) tritium inventory prediction for ITER, and (3) conditioning. The TPE has been moved to the Tritium System Test Assembly (TSTA) at Los Alamos National Laboratory. It should be ready for operation in June of this year. Dr. Causey suggested TPE is available for collaborative research by ITER researchers from Japan, the European Community, and Russia.

Tritium inventory predictions for ITER were given to be as high as several kilograms. The upper limit is determined by the amount of trapping. Permeation into the coolant could be as high as 300 grams per day.

ICR was given as the recommended way to condition plasma machines with permanent high magnetic fields.

Real-Time Boronization in PBX-M Using Erosion of Solid Boronized Targets, H. Kugel (PPPL)

Evaporative, real-time boronization is being performed routinely on PBX-M using boronized probes. The most recent STB probes consist of 86% boronized graphite-felt composite containing loose 40 μm diameter boron particles. Three graphite-felt probes have been tested to date, resulting in more than 17 g deposited in PBX-M to date (1-2 hours per application, up to several applications per week, 29 applications total).

Effectiveness is summarized as follows: (1) During continuous real-time boronization and post boronized discharges, low Z and high Z impurities are significantly lower. (2) During disruptive conditions on new regimes, 3-4 applications per week seem adequate. (3) Rapid recovery from an air leak followed by N_2 vent. (4) Reduced impurities during IBW core confinement mode. (5) Disruptions redistribute and reactivate boron. (6) Significantly accelerate conditioning to new regimes.

STB may provide a possible method for achieving target plasmas with steep, highly peaked density profiles.

Measurements of Fusion Synthesized T and T Fuel in JET, TFTR, DIII-D and TEXTOR, B. Doyle (SNL/NM)

Motivation for measuring T was discussed: to provide data on the behavior of high energy ions in tokamak plasmas and T safety issues.

T measurement techniques were characterized with respect to sensitivity and analysis range. A new T-monitor by counting β's using a PIN diode in air or vacuum was introduced, which provides quick, real-time, nondestructive measurement of tritium near surface. Another new technique, neutron elastic recoil detection (NERD) method, was introduced for H isotope depth profiling.

Tritium measurement data on materials in tokamaks, JET, TFTR, DIII-D and TEXTOR, were shown and discussed from points of view of T cleanup, behavior of high energy T, and deposition patterns of T and D.

Future research and development were discussed concerning portable or in-situ T-monitor and their applications for advanced tokamaks, TPX and ITER.

Session X: Erosion/Redeposition
Chairmen: T. Hino and Y. Hirooka

X.1	Y. Hirooka	Recent Progress in the ITER-R&D Related Erosion and Redeposition Studies at UCLA
X.2	C. P. C. Wong	DiMES Program 1993 Activities and 1994 Plan
X.3	N. Brooks	Characterization of Divertor Plasma During DiMES8 Sample Exposure
X.4	W. Wampler	Measurements of Erosion and Deposition of Carbon and Tungsten by the DIII-D Divertor Plasma
X.5	J. Brooks/ T. Hua	Erosion/Redeposition Analysis for ITER, DIII-D, and PISCES and Tokamak Sheath Modeling

In this session, Y. Hirooka discussed recent results from PISCES and described the system established on PISCES so that erosion measurements can be made on Be samples.

Several presentations were devoted to results and plans for the DiMES experiment on DIII-D. C. Wong outlined the experimental system and program plan for DiMES. At the conclusion of the workshop, a tour of DiMES was available. N. Brooks described diagnostics available on DIII-D which provide valuable data on heat and particle fluxes necessary for accurate modeling of erosion/redeposition measurements on DIII-D. W. Wampler then described measurements of carbon and tungsten erosion/redeposition on DIII-D divertor tiles. Finally, J. Brooks described computational modeling results. Agreement between experimental measurements and model predictions is very good, providing some confidence that erosion/redeposition for future machines, such as LHD, TPX and ITER, can be confidently predicted.

Session I

Welcome/Organization and Overviews

Opening Remarks

by

Professor T. Yamashina
Hokkaido University

U.S. - JAPAN WORKSHOP Q181

HIGH HEAT FLUX COMPONENTS AND PLASMA SURFACE INTERACTIONS FOR NEXT DEVICES

SAN DIEGO, CALIFORNIA
JANUARY 24-27, 1994

CURRENT STATUS OF NUCLEAR FUSION DEVELOPMENT IN JAPAN

- **RESEARCH ORGANIZATION AND COLLABORATION**
- **NATIONAL BUDGET FOR FUSION DEVELOPMENT**

RESEARCH ACTIVITIES IN NUCLEAR FUSION ENGINEERING IN JAPAN

- **RESEARCH GROUPS IN UNIVERSITIES AND JAERI**
- **RESEARCH SUBJECTS WITH HIGH PRIORITY**
- **FORMATION OF RESEARCH NETWORK IN FUSION ENGINEERING**

NUMBERS OF RESEARCH GROUPS AND RESEARCHERS IN JAPANESE UNIVERSITIES MOE

NUCLEAR FUSION ENGINEERING FIELD

	RESEARCH GROUPS	RESEARCHERS STAFFS	RESEARCHERS STUDENTS
• PLASMA FACING MATERIALS	13	60	40
• STRUCTURAL MATERIALS	51	133	105
• TRITIUM SCIENCE (1) HANDLING AND TECHNOLOGY	17	51	39
• TRITIUM SCIENCE (2) ENVIRONMENTS	23	54	22
• THERMAL-ELECTROMAGNETIC TECHNOLOGY	19	51	61
• FUSION NEUTRONICS	20	41	61
• MAGNET TECHNOLOGY	27	89	75
• REACTOR DESIGN AND SAFETY	15	30	15
TOTAL	185	509	387

900

NUMBERS OF RESEARCHERS IN NAKA NUCLEAR FUSION INSTITUTE (JAERI) STA

• **NUCLEAR FUSION ENGINEERING SECTION**

RESEARCH STAFFS 56
(PLUS TECHNICAL STAFFS 20)

76

• **OTHER SECTION**

RESEARCH STAFFS 140
(PLUS TECHNICAL STAFFS)

TOTAL RESEARCH STAFFS 200

(PLUS 150 TECHNICAL STAFFS)

350

JAPANESE NATIONAL BUDGET FOR NUCLEAR FUSION DEVELOPMENT

1993 FISCAL YEAR

SCIENCE AND TECHNOLOGY AGENCY (STA)

JAPAN ATOMIC ENERGY RESEARCH INSTITUTE (JAERI)

• ITER PROJECT (EDA)	7000 M-¥ (64 M-$)
• JT-60U PROJECT	10000 M-¥ (91 M-$)
• FUNDAMENTAL RESEARCH (FUSION ENGINEERING AND PLASMA PHYSICS)	5000 M-¥ (45 M-$)
STA TOTAL	22000 M-¥ (200 M-$)

MINISTRY OF EDUCATION (MOE)

• NATIONAL RESEARCH • INSTITUTE OF FUSION • SCIENCE (NIFS) (LARGE HELICAL DEVICE, LHD)	9100 M-¥ (83 M-$)
• OSAKA UNIVERSITY (LASER FUSION, GEKKO-XII)	1240 M-¥ (11 M-$)
• KYOTO UNIVERSITY (HELICAL, HELIOTRON-E)	750 M-¥ (7 M-$)
• TSUKUBA UNIVERSITY (MIRROR, GAMMA-10)	460 M-¥ (4 M-$)
• OTHERS	1140 M-¥ (10 M-$)
MOE TOTAL	13000 M-¥ (120 M-$)

TOTAL SUM IN JAPAN 35000 M-¥ (320 M-$)

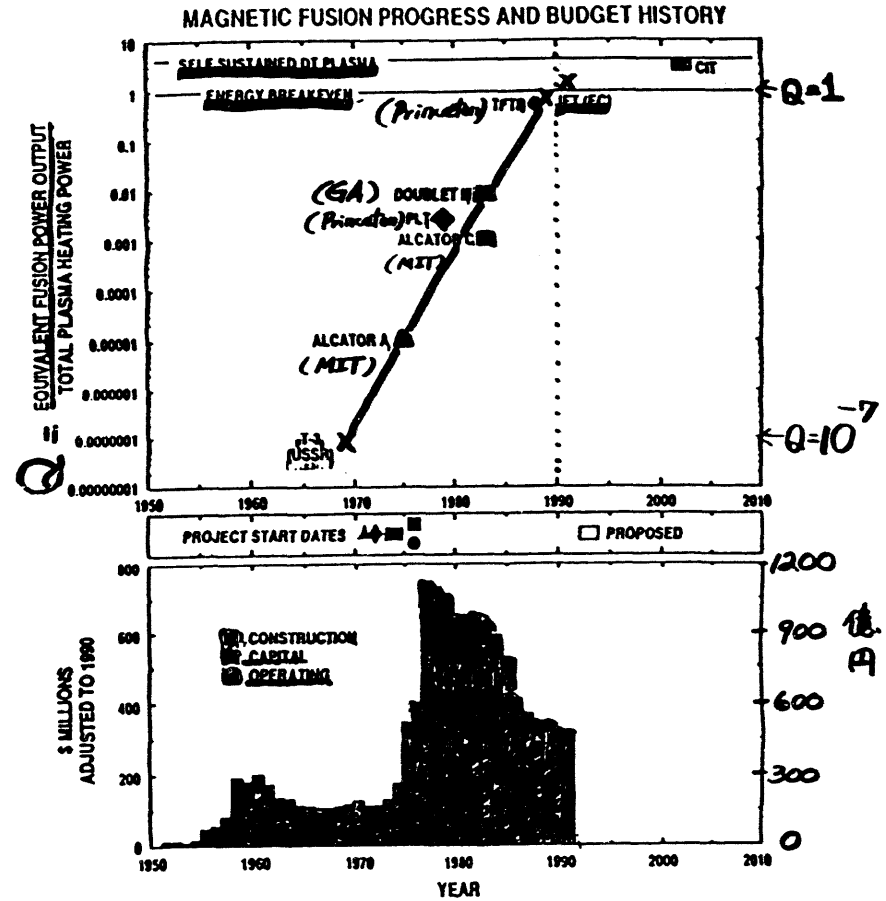

Fig. 1. Comparison of progress in equivalent-fusion-power gain[4] with the US magnetic fusion budget profile estimated in 1990 dollars. The progress in the 1980s was made possible by the investment in new facilities made during the peak funding years.

Tokamak (PLT → PDX → TFTR Princeton
DIII → DIID GA
AlcatorA → AlcatorC MIT

RESEARCH SUBJECTS OF FUSION ENGINEERING FIELDS WITH HIGH PRIORITY IN JAPANESE UNIVERSITIES

FUEL PARTICLE AND FIRST WALL TECHNOLOGY

- PLASMA-FIRST WALL INTERACTION IN FUSION
- CONDITIONS ELECTROMAGNETIC CONTROL OF PLASMA NEAR FIRST WALL
- EROSION OF MATERIALS AND FUEL RECYCLING

HEAVY IRRADIATION TECHNOLOGY

- STRONG HIGH ENERGETIC NEUTRON SOURCE
- NEUTRON ENGINEERING AND RADIATION DAMAGE OF MATERIALS
- LOW ACTIVATION MATERIALS

BLANKET AND SAFETY TECHNOLOGY

- RECOVERY AND BREEDING OF FUEL IN BLANKET
- BEHAVIORS OF BLANKET MATERIALS AT TROUBLE OF OPERATION
- SAFETY DESIGN METHODS

TRITIUM TECHNOLOGY

- BEHAVIORS OF TRITIUM IN MATERIALS (5000 Ci)
- PRECISE INSTRUMENTATION OF TRITIUM
- ENVIRONMENTAL PROTECTION

NETWORK PLAN - FUSION REACTOR ENGINEERIN(

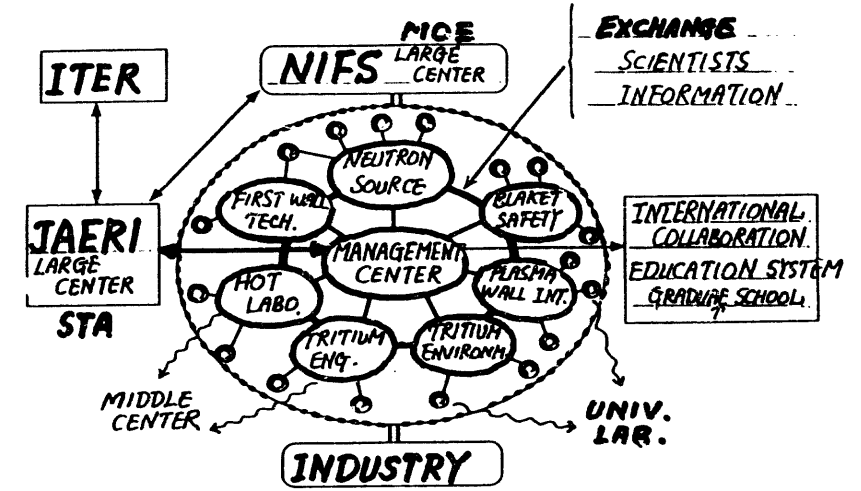

RESEARCH PROJECT OF JAPANESE MINISTRY OF EDUCATION (MOE)

PLANNING AND PROMOTION OF NUCLEAR FUSION STUDY IN JAPANESE UNIVERSITIES

1990~1993

CURRENT STATUS, FUTURE PLAN AND PROMOTION OF RESEARCH WORKS ON NUCLEAR FUSION DEVELOPMENT IN JAPANESE UNIVERSITIES

THREE FIELDS RELATING TO NUCLEAR FUSION

- PLASMA SCIENCE
- FUSION SCIENCE
- FUSION ENGINEERING

→

- CURRENT STATUS: NUMBER OF RESEARCH GROUPS IN DIFFERENT FIELDS IN JAPANESE UNIVERSITIES
- PROMOTION OF STUDY: SELECTION OF RESEARCH ITEMS WITH HIGH PRIORITY AND TIME SCHEDULE
- ORGANIZATION AND COLLABORATION: CONSTRUCTION OF NETWORK FOR UNIVERSITY GRUOPS AND INTERNATIONAL COLLABORATION (ITER)

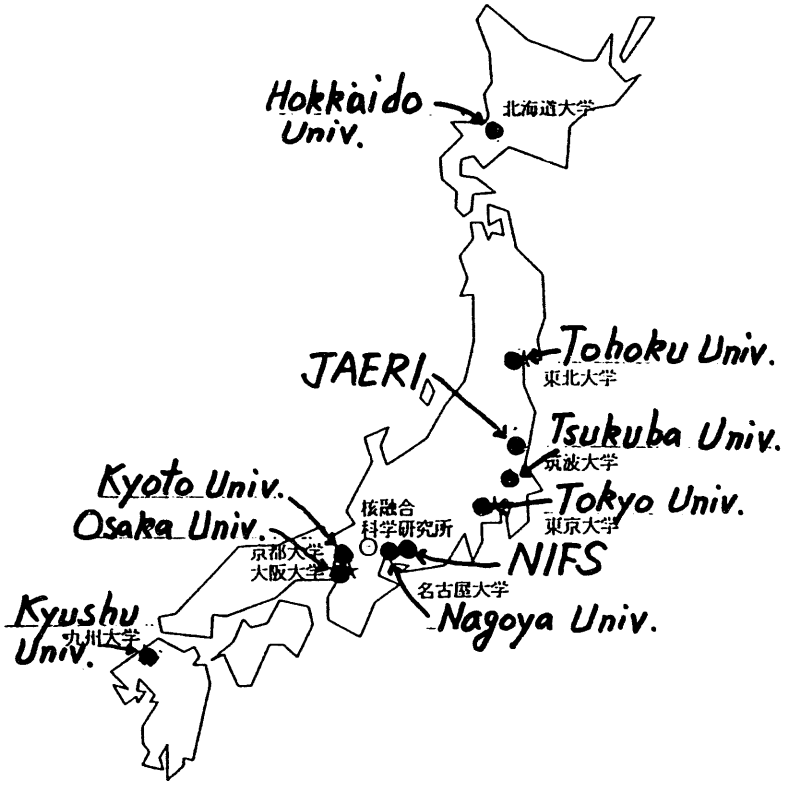

U.S.-JAPAN FUSION RESEARCH COLLABORATION

日米核融合研究協力の概要

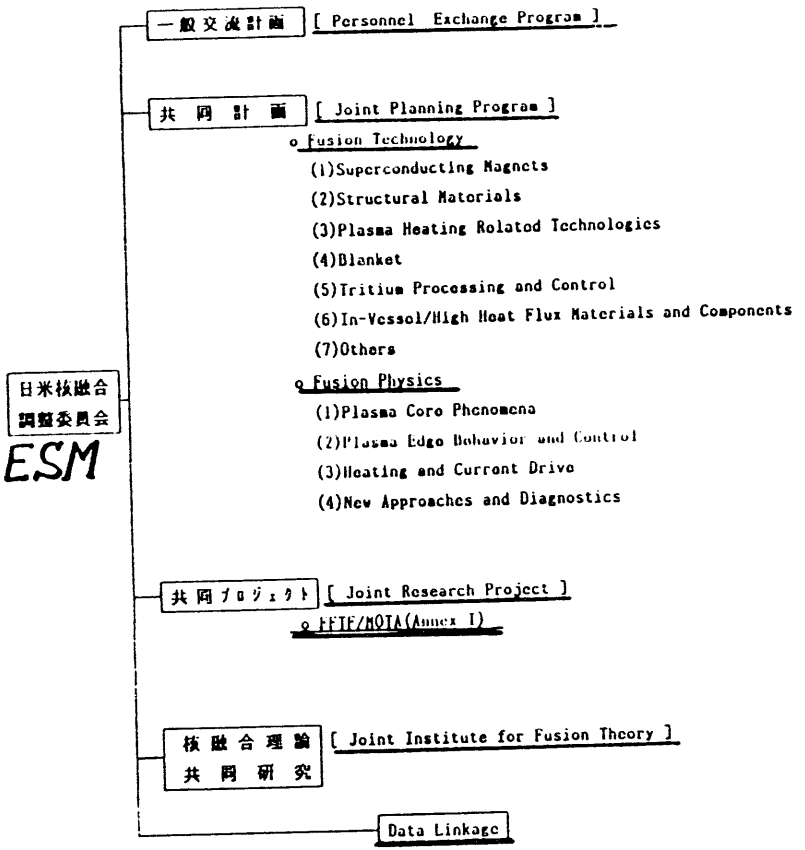

Jan.24-27,1994
US-Japan Workshop Q181 on High Heat
Flux Components and Plasma Surface
Interactions for Next Devices

Overview of HHFC and PMI Studies in Japan

T.Hino
Deaprtment of Nuclear Engineering,
Hokkaido University,Sapporo,060 Japan

Content

(1)PFC and PSI Studies in Japan

Organization

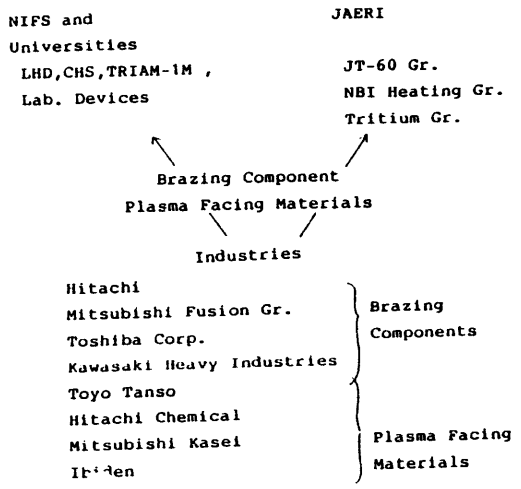

Information Exchange(Meetings)

(1)NIFS Collaborative Study (60-70 Members)
Study on Plasma Facing Wall and Plasma Surface Interactions for LHD (T.Yamashina)

(2)Research Committee,Plasma and Fusion Research Society in Japan (40 Members)
Overall Evaluation Study on Plasma Facing Material (M.Akiba)

(3)Research Meeting, Institute of Future Energy Development (60-70 Members)
Evaluation and Development of Plasma Facing Material (N.Yoshida)

(4)PFC Meeting in JAERI (M.Akiba)

(2)PFC and PSI Studies in Tokamaks

* Fusion Devices in Japan
* JT-60U

Experimental Plan
Recent Results - Fusion Performance
(Max. Fus. Triple Products)
Boronization
Decaborane $B_{10}H_{14}$ - 12 Gas Feedings
Uniform Film Thickness:100-400nm
Recycling Rate:50-80% Reduced
Oxygen Impurity: 50% Reduced
Installation of B_4C Coated CFC
No Major Damage
More B_4C Tiles be Installed
Brazing Component (CFC plus Cu)
1000 Cycles - 10MW/m^2 Heat Pulse

Fusion Devices in Japan

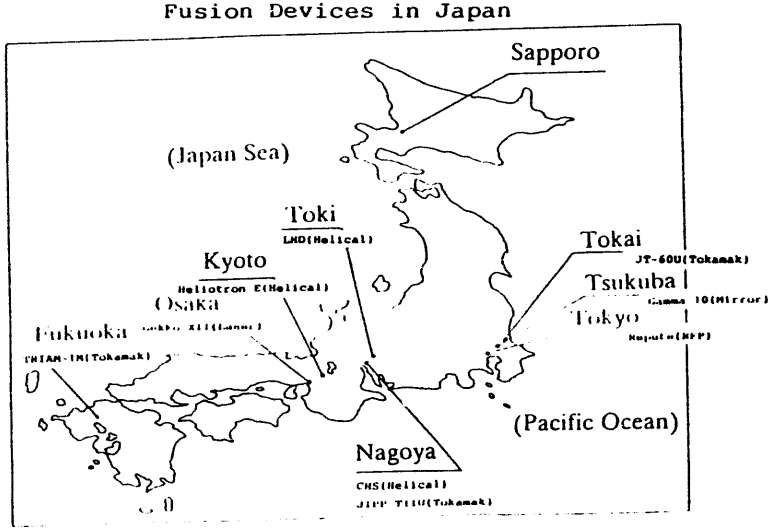

EXPERIMENTAL PLAN FOR JT-60U

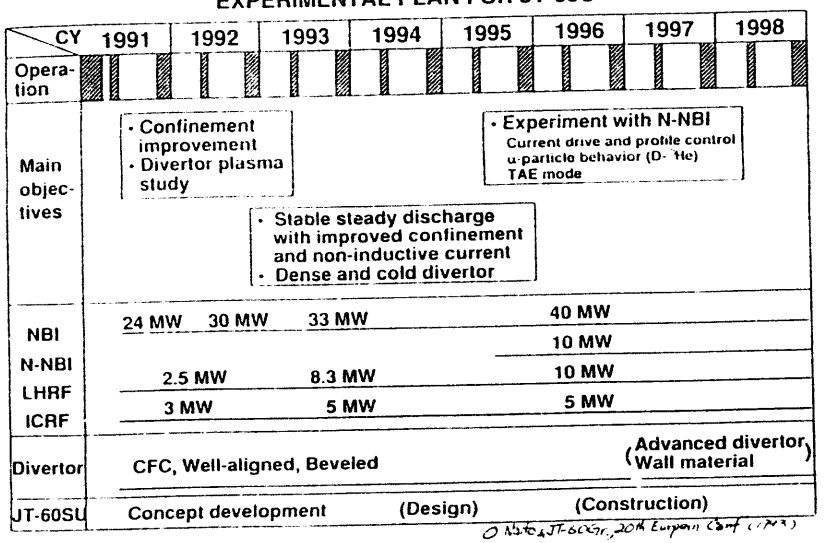

O. Naito et al., JT-60 Team, 20th European Conf. (1993)

Fusion Performance Summary

1. High performance is achieved in high-β_p H-mode

year		1992	1993
regime	H-mode	high-β_p mode	high-β_p H-mode
$n_D(0)\tau_E T_i(0)$ (keV s m^{-3})	2.5×10^{20}	4.4×10^{20}	1.1×10^{21}
Q_{DT}	0.2	0.3	0.6
W (MJ)	7.7	6.1	8.7
		peaked $n_e(r)$, core heating	

2. β_p limit is raised in high-β_p H-mode due to pressure profile broadening

3. Steady improved state is achieved with ELMs

O. Naito et al., JT-60 Team, 20th European Conf. (1993)

Achieved Fusion Performance

- $n_D(0)\tau_E T_i(0) = 1.1\times10^{21}$ keV s m^{-3}
- $Q_{DT} = 0.6$, $n_D(0) = 4.3\times10^{19}$ m^{-3}
- $T_i(0) = 37$ keV, $\tau_E = 0.68$ s
- High-β_p H-mode

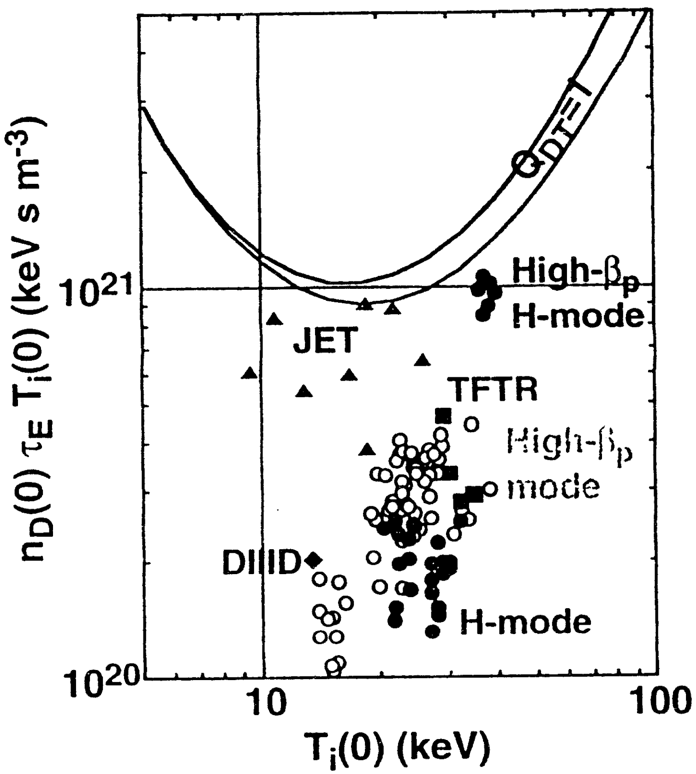

TRIAM-1M

Mo Limiter Discharge: To July 1993

Single X Point Discharge: From Oct.1994

(Mo Divertor with Active Cooling)

Long Pulse Operation

Damage due to Heat Load

Impurity Emission

Recycling

High Heat Load Tests(Electron & Laser Beam Sources)

Hydrogen Retention Properties such as Depth Profile

Mo,W,SS - SIMS,RBS

(3)Divertor Development for LHD

* Construction of Vacuum Vessel: From 1995
* Before the use of helical divertor, Local Island Divertor, LID, be used from Apr.1998. (S. Motojima)
* Heat Load Condition

	Helical Divertor	
Steady State	3MW Input	$0.75MW/m^2$
10s Pulse	20MW Input	$5MW/m^2$
5s Pulse	>30MW Input	$10MW/m^2$

Heat Load Test for Brazing Components in Electron Beam Facility, ACT

C/C-Cu Brazing Comp.: 5000 Cycles (Flat Plate Type) ($10MW/m^2$ & 1min) (Y. Ueda)

Local Island Divertor (N. Chiyaba)

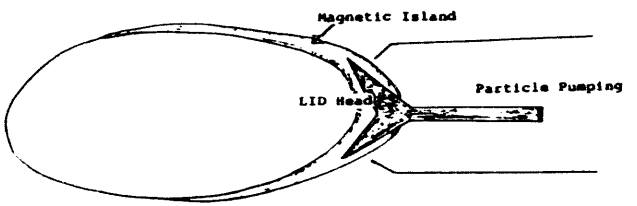

Heat Load Area < 1 m^2

Steady State: $5.5MW/m^2$

10s Pulse : $10MW/m^2$

Heat Load Test for LID Module: From FY 1994

Candidate LID Head

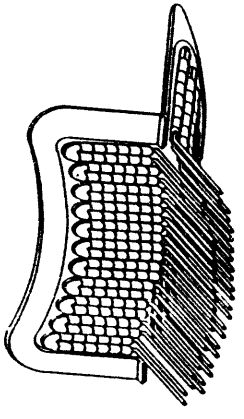

(4)Development of High Heat Flux Component for ITER

* CFC-Cu Brazing Component
  (Swirl Tube,Saddle Type)

  1000 Cycles(20MW/m^2 ,30S)

* Heat Load Testing for
  Brazing Comp. with
  Supporting Structure

  Deformation
  Thermal Stress

M. Akiba
S. Suzuki

High Heat Flux Component

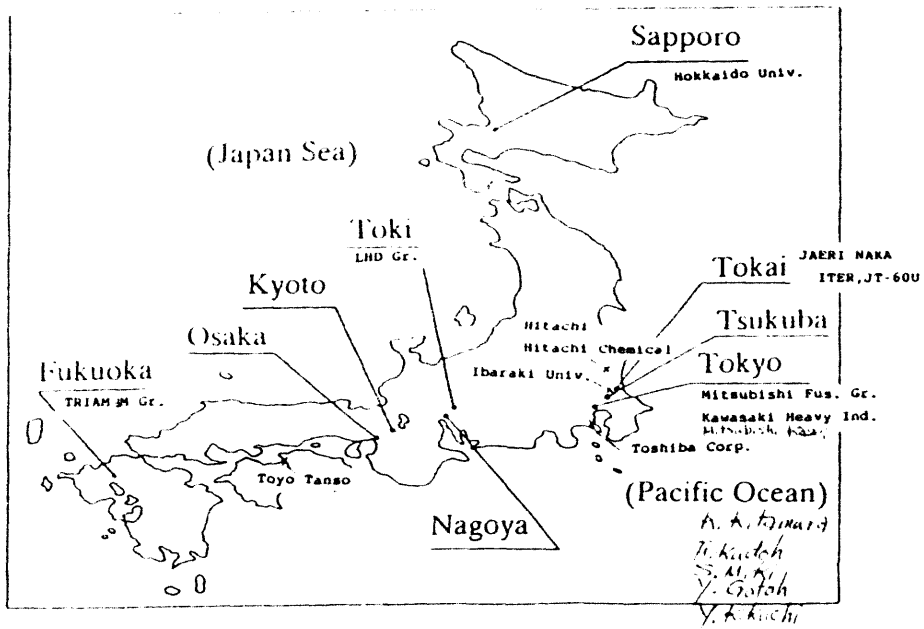

Development of HHFC

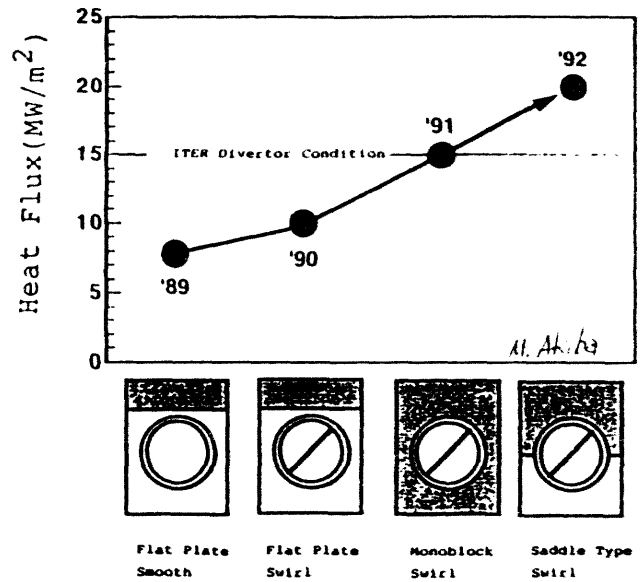

(5)Boronization and Low Z Plasma Facing Material

* Institute

- Nagoya Univ.(H.Sugai)–Boronization (Decaborane, Diborane)
  Li Coatongs
- JT-60 Gr.(M.Saidoh) — Boronization
  Decaborane
  300 C
- NIFS
- Hokkaido Univ. — Boronization(SUT)
  Diborane
  Decaborane
- Toyo Tanso
  Hitachi Gr.
- JAERI
- Hokkaido Univ. —— B_4C Coated Graphite
  Hitachi (Erosion, Retention)
- Hitachi Chemical —— B_4C Coated Graphite
- Toyo Tanso —— B_4C, SiC Coated Graphites
  Bulk Boronized Graphite

Boronization and Low Z PFM (Except Graphite)

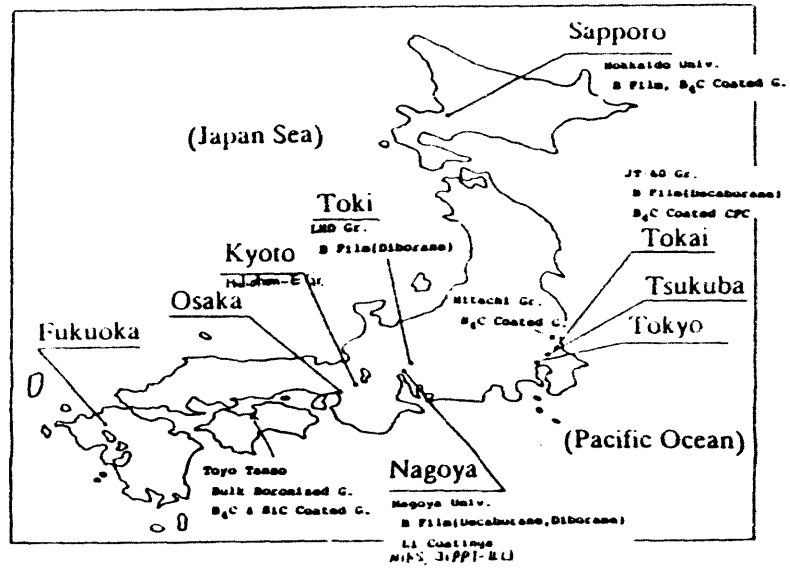

* Major Results

Hydrogen Retention

H Desorption Temperature of B Film : 300-350 C

(Less Than That of Graphite, 600-700 C)

- Hokkaido U.,NIFS

Hydrogen Concentration

Film Made by Decaborane at 300C: 10% - M.Saidouh

B/C Film in TEXTOR: 29% - J.Winter

B Film by Diborane at RT(SUT): 26-37% - Hokkaido U., NIFS

Oxygen Gettering Capability

Approximately 10^{17} O atoms/cm^2

(Both for Films Made by Decaborane and Diborane)

- NIFS, Hokkaido U.,Nagoya U.

Decrease of O_2 Partial Pressure During O_2 Discharge After Boronization(SUT in NIFS)

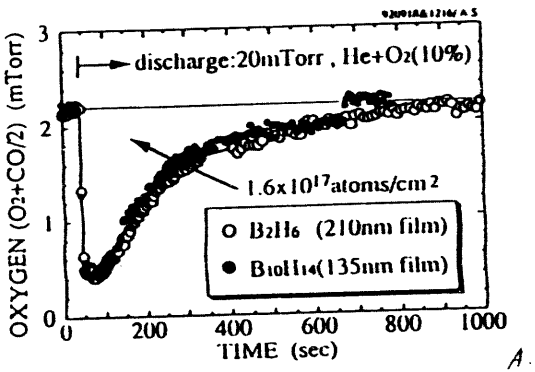

A. Sagara

(6)Tritium Study

JAERI Gr.(K.Okuno)

T Retention and Recovery

T Permeation Through PFM

↓

Permeation of D^+ Ion

for Several Materials

Toyama Univ.(K.Watanabe)

Basic Study on T - Material Interaction

Diagnostics for T (Detector)

Recovery and Separation

Storage in Metal Hydride

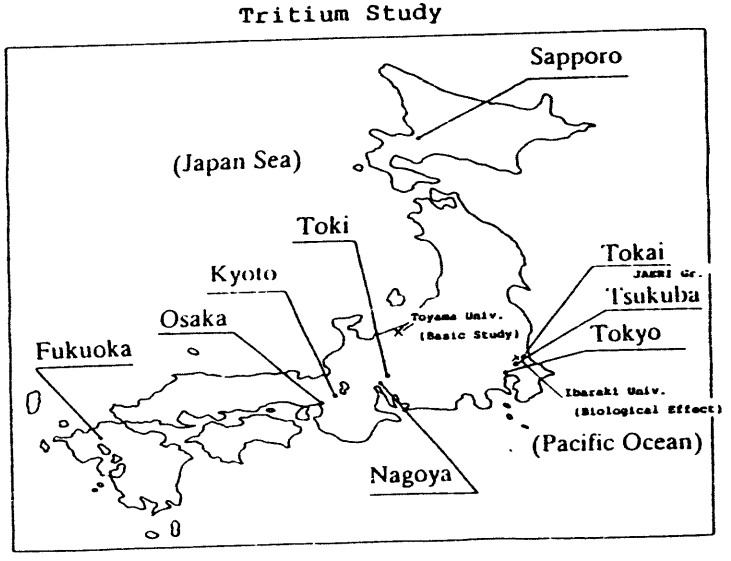

R&D SCHEDULE FOR TRITIUM PERMEATION STUDY

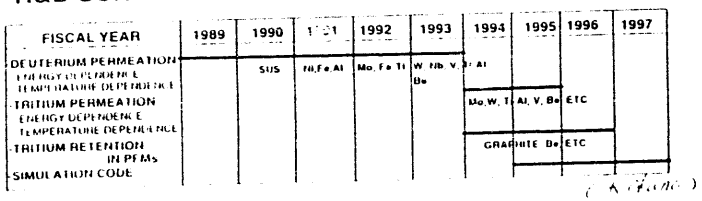

D Permeation for SS,Ni,Al,Al-Li Alloy,Mo,Fe-Ti Alloy

R&D SCHEDULE FOR STUDIES ON TRITIUM RETENTION, AND RECOVERY OF PLASMA FACING MATERIALS

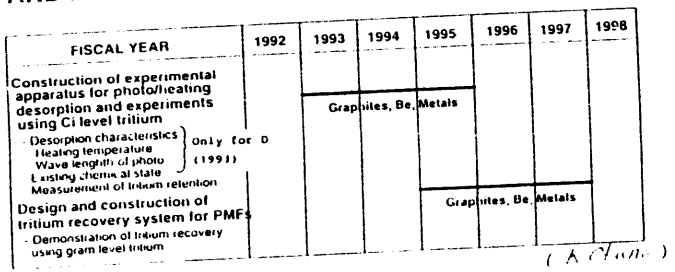

Tritium-Material Interactions

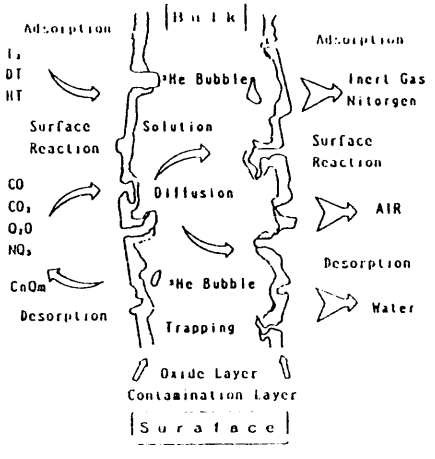

(7)Damage of Plasma Facing Material

* Decrease of Thermal Conductivity
  Isotropic Graphites,CX2002U and
  Bulk Boronized Graphite
* Recovery by Annealing

* Carbon Material Irradiated in
  FFTF/EBR-II
  failure
  Deformation

* Metals of Brazing Component
  Cu,Re - Nuclear Transformation

Special Thanks

T.Ando, M.Akiba, K.Okuno - JAERI
O.Motojima, N.Noda, A.Sagara, A.Komori - NIFS
N.Yoshida, T.Muroga - Kyushu Univ.

M.Okada/S.Miki - Toyo Tanso
Y.Gotoh - Hitachi
Y.Kikuchi - Hitachi Chemical
K.Kitamura - Toshiba Corp.
F.Kudoh - Mitsubishi Fusion Gr.
T.Ikeda/T.Maeda - Mistubishi Kasei

Overview of HHFC and PMI Studies in the U.S.

Michael Ulrickson
Sandia National Laboratories

Presented at the US-Japan Workshop Q181
High Heat Flus Components
and
Plasma Surface Interactions for Next Devices
San Diego, CA
January 24-27, 1994

- Divertor Design Support Study
- Beryllium Development
- Disruption Studies
- Electron Beam Testing
- Cooling Studies
- Tritium Retention and Permeation
- Plasma Facing Material Erosion

Plasma Facing Components Highlights

Design

The Divertor Design Support Study was initiated in February 1993 to provide support to the JCT in the design of the ITER divertor.

The group merges U.S. industries, national labs and universities.

- McDonnell Douglas, Ebasco, General Atomics, Rocketdyne, Westinghouse
- ANL, INEL, LANL, LLNL, ORNL, PPPL, SNL
- GIT, UCLA, UIUC

Activities have focused on:

- developing divertor target options
- evaluating thermal, mechanical and lifetime performance limitations
- collecting and evaluating materials databases
- performing preliminary safety assessments of design options
- identifying R&D needs

The design analysis was based on the gaseous/radiative divertor concept

- reference peak and average heat loads 5 MW/m2 and 2 MW/m2 respectively were assumed
- divertor plasma modeling from the ITER Divertor & Disruption Physics Task Area (Sam Cohen) were used in divertor performance evaluation

Divertor Design Window Summary

MDA-HES

(For Beryllium Armor Thickness of 5 mm and 5 MW/m² heat load)

- **Liquid Metals**
  - **Lithium/Nb combination has a narrow operating window (350-450°C)**
  - **Lithium/Cu conbination is chemically incompatible**
  - **NaK/DS Cu combination can be used at temperatures up to ~400°C**
  - **NaK/CuCrZr combination limited to ~300°C**
  - **Insulator must be provided between coolant and structure**
- **Water**
  - **Limited to maximum temperature of ~160°C based on critical heat flux margin**
- **Helium**
  - **Viable if peak beryllium temperatures > 700°C are acceptable**
  - **Maximum coolant temperature of 170°C if beryllium limited to 800°C**

Materials Development for ITER PFCs

- Beryllium: Development of high quality, high thermal conductivity plasma sprayed coatings for PFC fabrication and *in-situ* repair at LANL.

  Plasma spray-Be adhesion to copper, vanadium and stainless steel substrates.

  Reliable Be armor bonding to heat sink structures.

  Thermal fatigue Gleeble measurements for S-65-B, porous Be, Cu/Be bonded joints, and other Be samples. The Gleeble is approved for thermal cyclic measurements of neutron-irradiated Be samples.

  Thermal shock of neutron-irradiated beryllium could be performed in SNL's Hot Cell-Electron Beam Test System (HC-EBTS description and status provided below).

- CFC's: Investigations of high thermal conductivity graphites
  - high conductivity fibers and CFCs
  - doped graphites

  Design correlation for the loss of thermal conductivity with neutron fluence and temperature.

  Improved brazing techniques for CFCs to Copper and Niobium.

Plasma Facing Components Highlights

R&D

Plasma-Facing Materials Development

- Beryllium has been successfully plasma sprayed, with densities of 95%, low oxygen content (0.35 weight percent), and efficiencies of over 60%.
- A number of carbon fiber composites have been irradiated to ITER-relevant fluences (0.001 to 1 dpa) and temperatures (100° to 1100° C), and an algorithm for loss of thermal conductivity has been developed.

High Heat Flux Testing

- Helium coolant tests have been successfully conducted on several prototype heat exchangers.
- The EB-1200 High Heat Flux Facility has been completed and acceptance tests are underway.
- Disruption simulations in PLADIS show high beryllium ablation, in good agreement with A*THERMAL calculations.

Plasma Compatibility Testing

- The DIMES probe in the DIII-D divertor is operational, and initial measurements have been made on erosion during normal operation. The results are in good agreement with REDEP calculations.
- The PISCES-B Facility is being made beryllium-compatible.

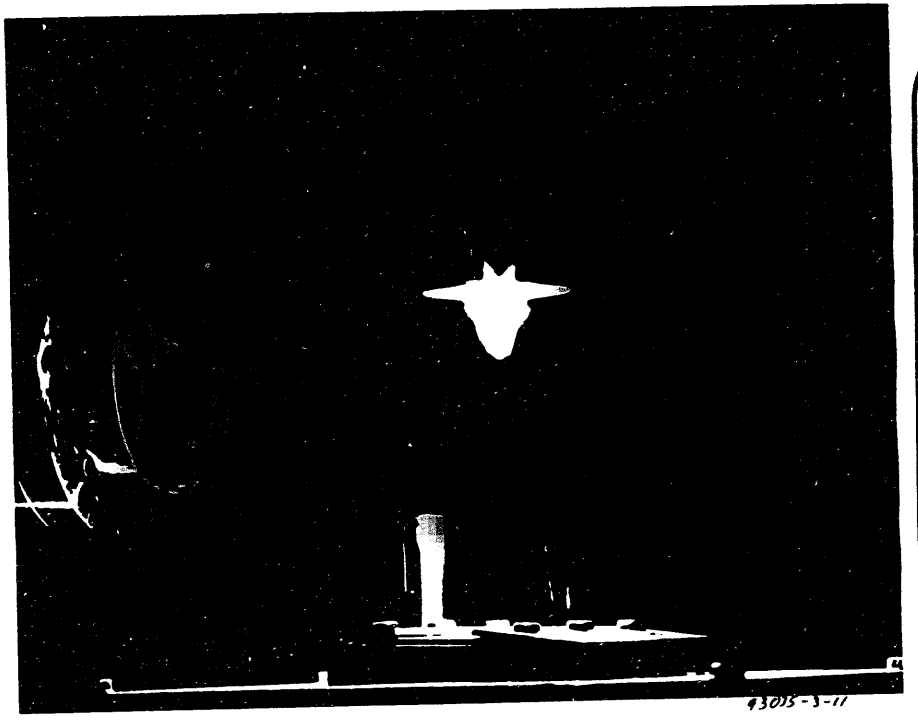

Unmelted particles increase porosity in plasma sprayed beryllium coatings.

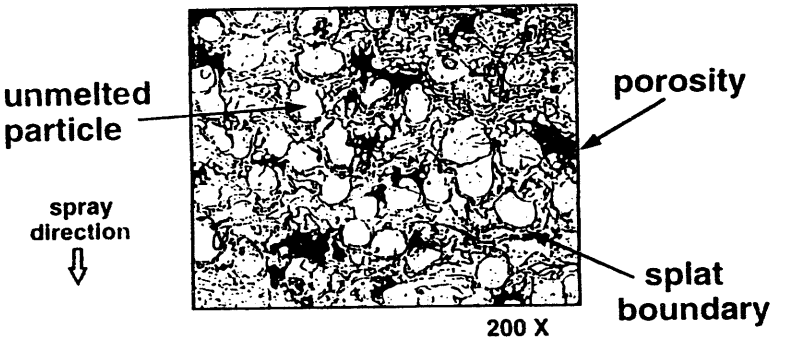

⇨ *This reduces the thermal conductivity.*

Plasma-Sprayed Beryllium Outgasses Similar to Graphite

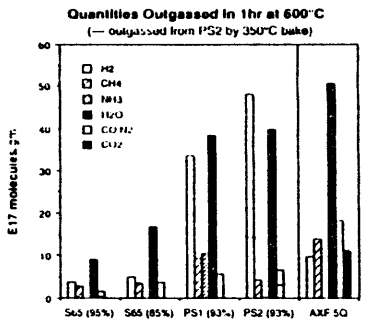

- Primary impurities are water and hydrogen:
  - quantities & desorption temps (~350°C) similar to AXF-5Q *plus 0.4e17 Ar/gm (PS gas)*
  - 4 times more water than for S65 of comparable porosity
- Data for two plasma-spray samples differ by effects of 350°C bake:
  - hydrogen released by bake is not available for conversion to methane and ammonia at 600°C
  - nitrogen is released by bake, but carbon monoxide is not

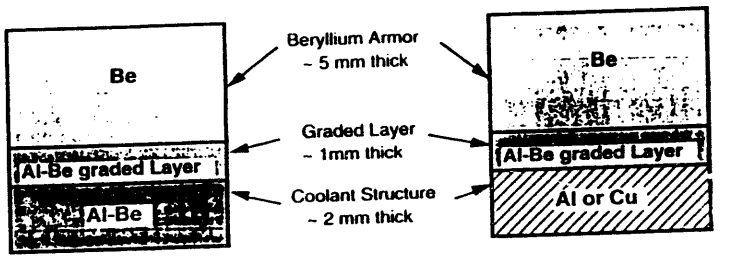

Concept 1

Figure 1(a)

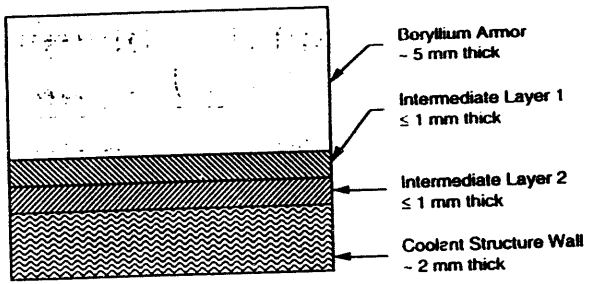

Concept 2

Figure 1 (b)

Figure 1 Alternate divertor target design concepts.

"Ductile" Beryllium History

- 1975 - Kawecki Berylco Industries produced an ingot of electrolytically-refined beryllium exhibiting a grain size of 2.5 μm with an impurity level of 0.12 BeO and 200 wppm impurites. The strength parameters were: 455 MPa YS(.2% offset), 600 MPa UTS with 5% isotropic ductility.
- 1977 - *Ivanov, et al* report using a superplastic thermomechanical treatment on high purity (500 wppm impurities) ingot beryllium, to produce fine grains (3-5 μm). This material was reportedly isotropic at room temperature, with a total ductility from 17 to 22% and a yield strength of 430 MPa. No other room temperature data were presented. This work has not been reproduced.

In Search of "Ductile" Beryllium

- Review DOE and industrial efforts at producing ductile Be over the past two decades.
- Develop zone-refining capability at National Laboratories with industrial participation. Apply thermomechanical treatments to zone-refined Be to validate *Ivanov et al* results.
- Develop cost/timetable estimate for redeveloping electrolytic Be capability

Beryllium Joining Effort

Two Approaches:

1. Friction (Inertia) Welding - evaluate and optimize the process and joint designs for the inertia welding process. Evaluate both the mechanical and metallurgical qualities of the bond between:
   - Be/Cu
   - Be/Be

2. Brazing - review, evaluate, and optimize the brazing parameters to produce a bond between:
   - Be/Cu

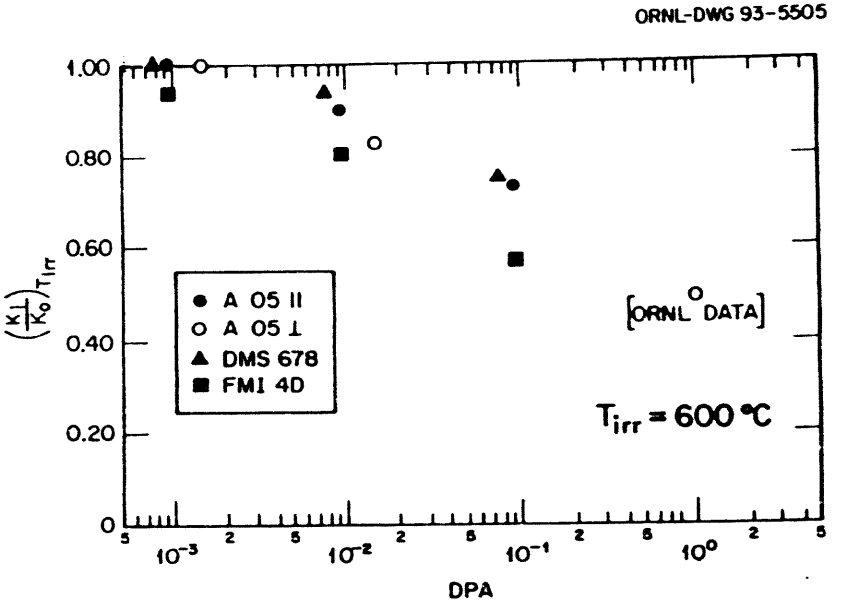

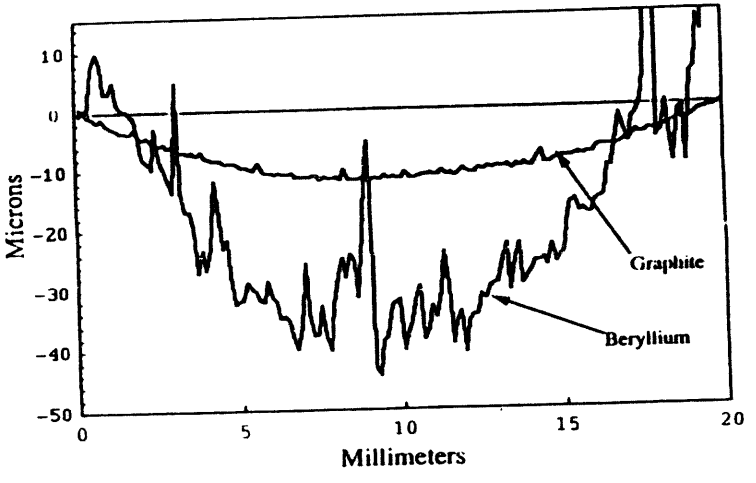

Theoritical Modeling versus Plasma Gun Simulation Experiments of Be and Graphite Disruptions

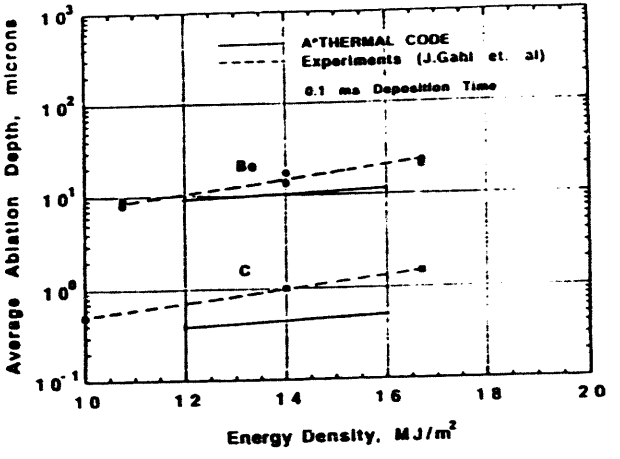

Estimated maximum number of disruptions tolerated for both Be and graphite PFC surfaces in ITER based on experimental data.

- Disruption load 12 MJ/m²
- Disruption time 0.1 ms

PFC Material	Initial Coating/ Tile Thickness (mm)	Sacrificial Layer (mm)	Erosion Thickness per Disruption (μm)	Maximum Tolerable Number of Disruptions
Be	3	1.5	50	30
Graphite	10	5	10	500

Critical Issues for Lifetime and Reliability

- Statistically robust database for thermal fatigue lifetime of both unirradiated and n-irradiated PFC mockups.
- Synergistic effects of normal high heat flux cycling plus multiple thermal shocks from disruption heat loads.
- Neutron damage effects: differential swelling-induced stresses, embrittlement, irradiation creep.

EB-1200, a 1200 kW Electron Beam Test System (modifications in progress--on line February 1994)

Power	1200 kW (cw)
Heat flux	1000 MW/m^2 (12 cm^2) or 4 MW/m^2 (3000 cm^2)
Target size	Up to 0.5 m x 1.5 m
Maximum heated area	0.4 m x 0.8 m
Sweep frequency	10 kHz
Beryllium compatible	Yes
Non-uniform beam profile	Yes
Total power handling capacity for water cooled samples	2.0 MW (cw)
Extensive diagnostics	IR imaging, video imaging, calibrated spot pyrometers, coolant pressure and ΔT measurements, . . .
Computer control system	Feedback control, safety interlocks and data acquisition

PMTF - Upgrade
Phase-I
1200 kW Electron Beam Test System

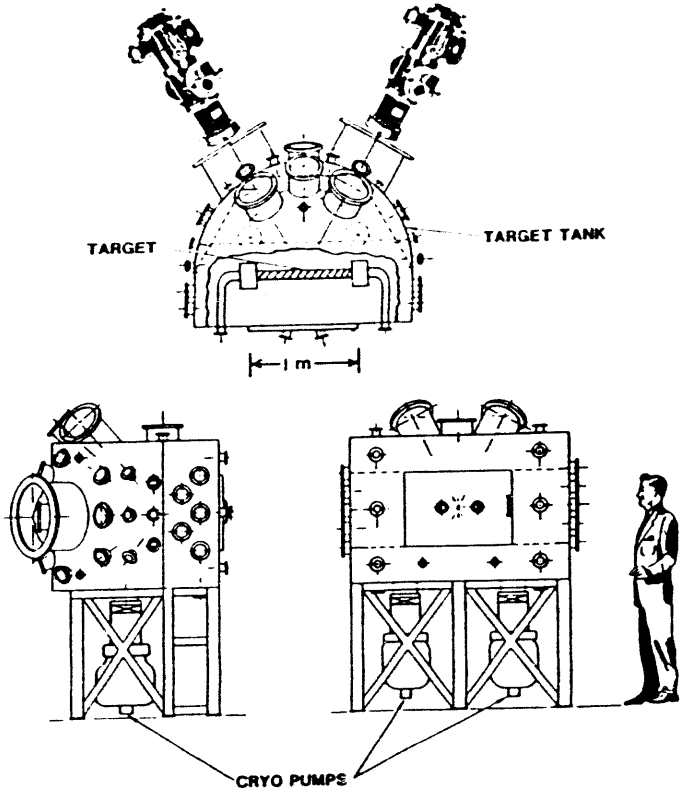

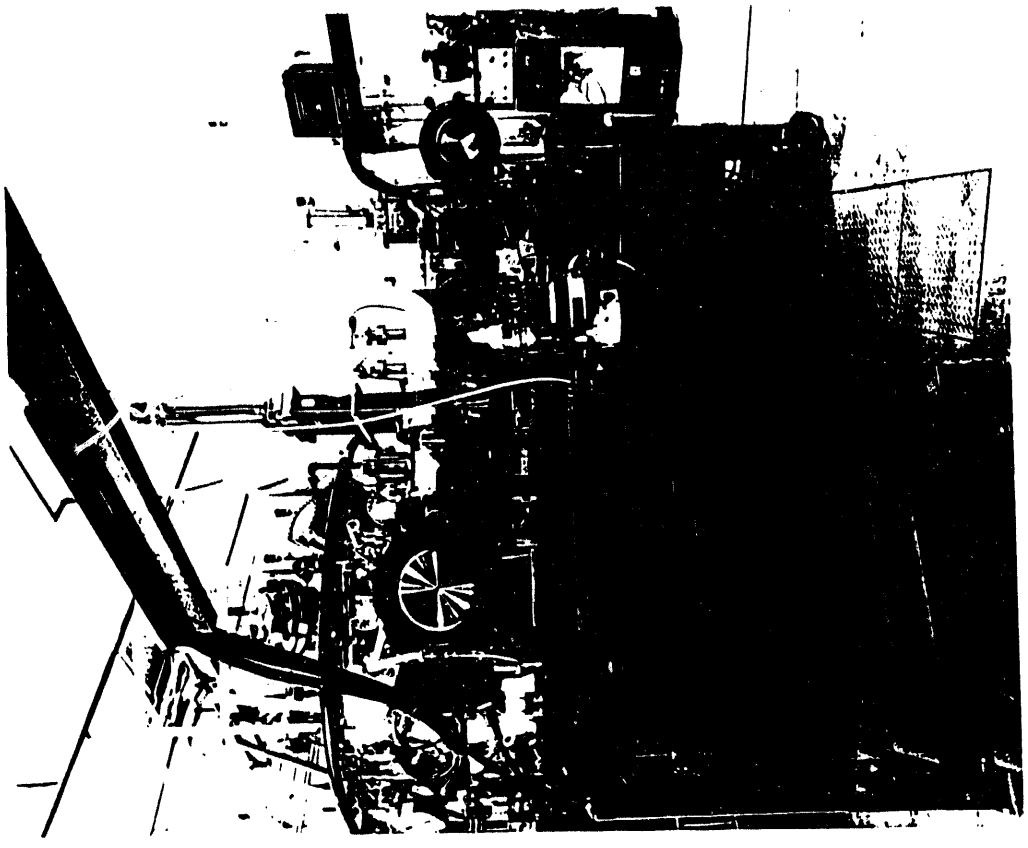

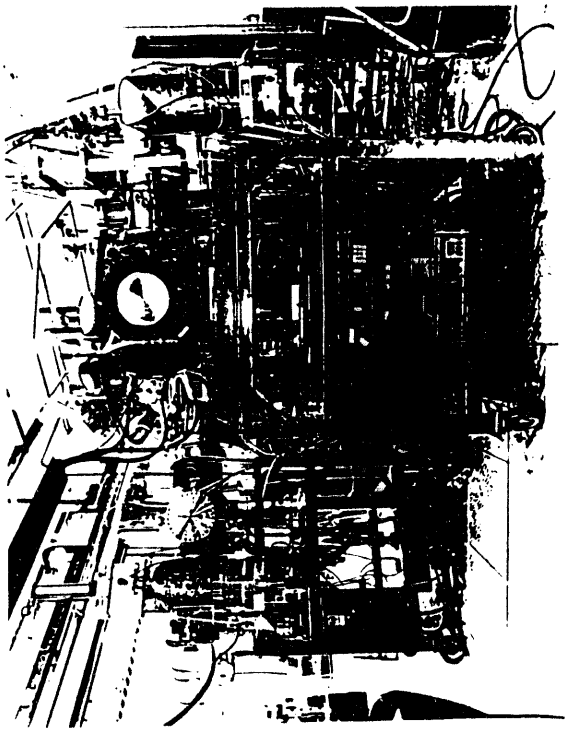

Electron Beam Test Facilities

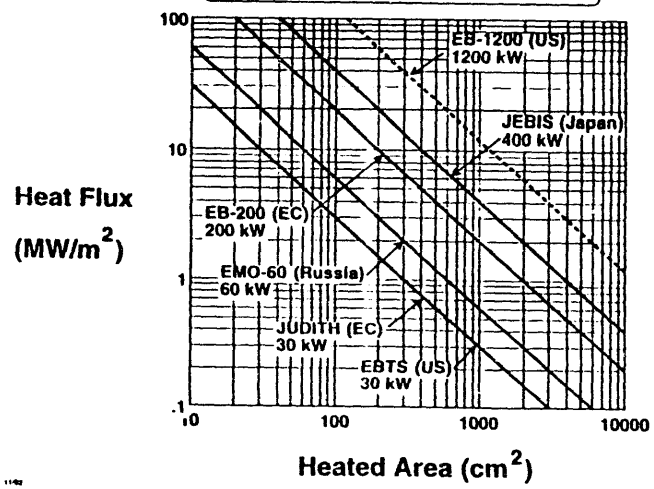

SNL's Electron Beam Test System (EBTS) has operated for over 15 years and meets the needs of ITER by quickly evaluating the performance and durability of new divertor and first wall design options.

- Total Power = 30 kW
- Variable spot size and rastered area
- Water flow loop
  - 20 - 280 °C
  - 0.3 - 7 MPa
  - 0 - 30 l/s
  - Water purity control
  - Computer controlled
  - 2.0 MW total capacity
- Helium Flow Loop
  - 24 - 450 °C
  - 0.25 - 4 MPa
- Extensive diagnostic systems
  - IR imaging, thermocouples, spot pyrometers, video imaging, coolant pressure and ΔT measurements....
  - Active feedback control and safety interlocks
  - Automated data acquisition
- Extensive beryllium testing for JET has been conducted on this system.

The Hot Cell - Electron Beam Test System (HC-EBTS) is a 30 kW cw test stand designed for a shielded or full hot cell environment.

Present Status

- The electron beam gun, vacuum chamber, remote sample manipulation system, vacuum pumps, power supply and large frame for remote relocation have been fabricated.
- A hot cell within the SNL Nuclear Reactor Facility has been identified for HC-EBTS use. Space adjacent to the hot cell requires minor modifications.
- A detailed cost estimate and schedule for HC-EBTS completion is being prepared.

1. The 1 MJ Disruption Simulator will deliver ≥20 MJ/m^2 of energetic protons over 100 cm^2 with simultaneous E-beam exposure of 15-30 MW/m^2.
2. Plasma guns of this sort have already been built and demonstrated at well beyond those energy and power levels. Thus there is a sound historical path to refer to.
3. Techical concerns of physical safety, EMP, and scaling to long pulses will be addressed in EBTS-IID.
4. A high degree of confidence of success is expected because of the prior demonstrated technology and because of the evolutionary nature of this program -- from PLADIS to EBTS-IID to MegaSim.
5. Cost and schedule estimates have recently been reviewed based upon known salaries, rates, and in-place contracts.

The US is studying both water and helium cooling for the ITER divertor

- High velocity, highly subcooled water with turbulence promoters.

  ⇨ *CHF up to 100 MW/m^2 have been achieved.*
  (T_{inlet}=20 C, velocity = 13 m/s)

- High pressure helium gas, with extended surface areas.

Helium Coolant Tests

·Creare, Inc. Microchannel, Normal Flow Heat Exchanger
Tested to an absorbed heat flux of 4 MW/m²
(6 MW/m² incident heat flux) using 7.3 g/s of helium
@ 1.4 MPa [M. Izenson]

·General Atomics Divertor Module
Tested to an absorbed heat flux of 9 MW/m²
(12 MW/m² incident heat flux) using 22 g/s of helium
@ 4.0 MPa [C. Baxi]

·Thermacore Porous Metal Heat Exchanger
Tested to an absorbed heat flux of 16 MW/m²
(25 MW/m² incident heat flux) using 1 g/s of helium
@ 4.0 MPa [J. Rosenfeld]


channel width = 150 micron

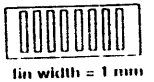
fin width = 1 mm
gap width = 1 mm


50% dense sintered copper wick

The Tritium Plasma Experiment (TPE) is a Unique Facility Devoted to Tritium-Material Interaction Studies

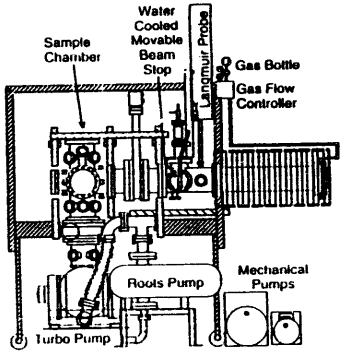

- TPE is presently being moved to the Tritium System Test Assembly (TSTA) at Los Alamos National Lab
- It should be ready for operation in June 1994
- It is capable of delivering a 100 eV tritium ion flux of 10^{19} T/cm^2 -s to a 5 cm diameter sample

Sandia National Laboratories

Divertor Tritium Retention and Permeation

MDA-HES

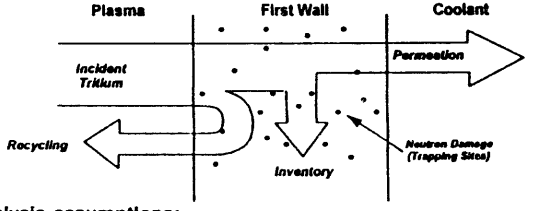

Analysis assumptions:

4 mm Be; 10^{19} cm^{-2}s^{-1} D-T flux; 930°C Be temp; 0.001 trap density; 200 m^2 surface

Results:

- **Divertor inventory of 600-700 grams within one operating week**
- **Coolant permeation of 4.5 grams per 1000 second shot**
- **With no trapping, 100°C lower temperature reduces inventory and permeation by factor of 2**
- **No change in permeation or inventory with temperature when trapping included**

Divertor Surface Erosion/Redeposition Summary

MDA-HES

- Analysis based on idealized gas-target plasma configuration
  - UCLA and Ruzic solutions qualitatively similar
- Includes effects of:
  - Charge-exchange D-T neutrals (5-75 eV)
  - D, T, He (5%), Be or Mo ions with 3 kT_e sheath potential
  - Be ionization, transport and redeposition

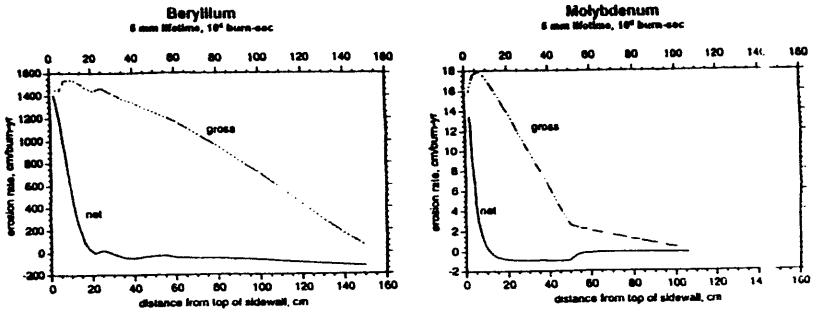

McDonnell Douglas Aerospace

DiMES
Divertor Materials
Exposure System

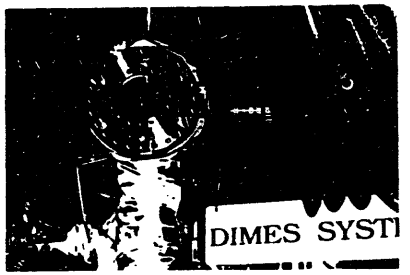

K 880(2)
5 11 93/mac

GENERAL ATOMICS

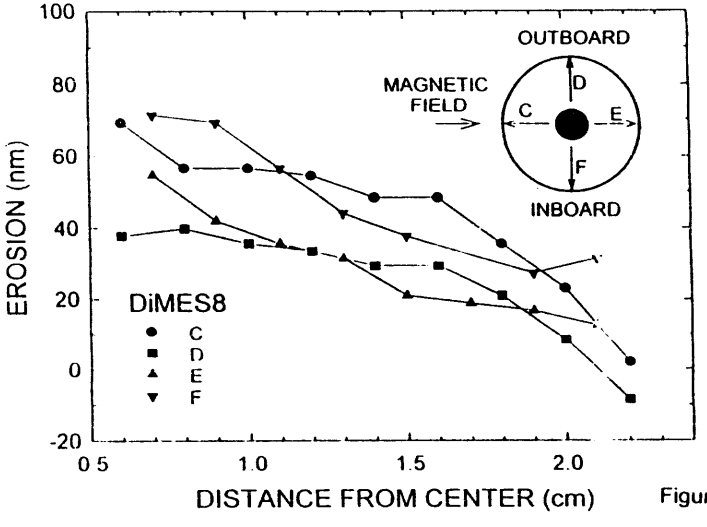

Figure 7

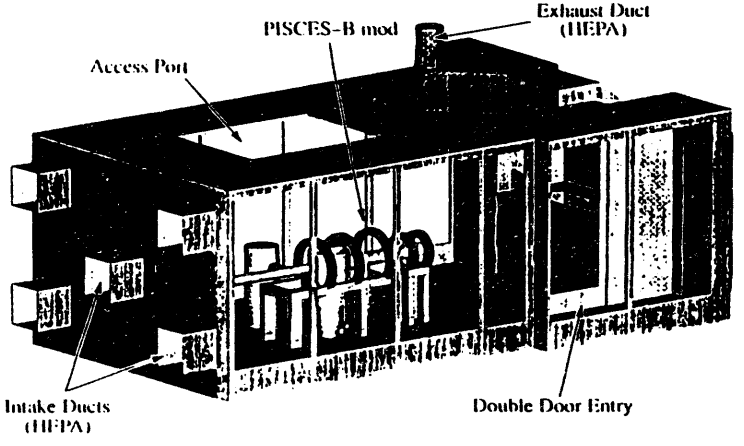

Fig. 10 The beryllium handling facility for PISCES-B mod.

Comparison between PISCES-B, PISCES-Upgrade and ITER Divertor Plasma Conditions

	PISCES-B	PISCES-Upgrade	CDA ITER Divertor
n_e	3.5×10^{19} m^{-3}	1×10^{20} m^{-3}	$1\text{-}6 \times 10^{20}$ m^{-3}
T_e	5-20 eV	5-20 eV	5-50 eV
T_i	1-2 eV	1-20 eV	5-20 eV
Ion species	D,He,C,O	D,He,C,O	D,He,C,O,T
E_{ion}	10-300 eV	10-300 eV	20-200 eV
Γ_{target}	2×10^{23} m^{-2}s^{-1}	4.9×10^{23} m^{-2}s^{-1}	1.5×10^{23} m^{-2}s^{-1}
Target angle	90°	25°	1-2°
P_{target}	1-9 MW/m^2	3-35 MW/m^2	10-30 MW/m^2
B_{target}	0.1 T	0.3 T	5 T
A_{target}	30 cm^2	65-150 cm^2	---
Pulse duration	1 sec - S.S.	1 sec - S.S.	400 sec - S.S.
Target materials	C,W,Be	C,W,Be	C,W,Be

Session II

PFC Issues for Future Machines

Present Status of the Large Helical Device (LHD)

by

Professor O. Motojima
National Institute for Fusion Science

US-JAPAN WORKSHOP ON IIHFC
24 TO 27 JANUARY, 1994 SAN DIEGO, U.S.A.

STATUS OF LHD PROJECT AND CONSTRUCTION

1. BRIEF SUMMARY OF LHD PROJECT
2. PRESENT STATUS
3. INTRODUCTION TO COMPONENTS OF LHD UNDER CONSTRUCTION
   HELICAL COIL, POLOIDAL COIL, CRYOSTAT, etc.
   BUILDINGS
4. VACUUM CHAMBER AND DIVERTOR
   DESIGN CHARACTERISTICS
   R&D
5. RESULTS OF OTHER R&D
   CONDUCTOR DEVELOPMENT, POWER SUPPLY,
   HEATING SYSTEM, DIAGNOSTIC SYSTEM, etc.
6. RECENT DEVELOPMENT OF PHYSICS PROGRAM
   EDGE CONTROL BY LOCAL ISLAND DIVERTOR
7. INTRODUCTION TO LHD TYPE REACTOR DESIGN PROGRAM
   AND FUTURE PROSPECT

OM0115

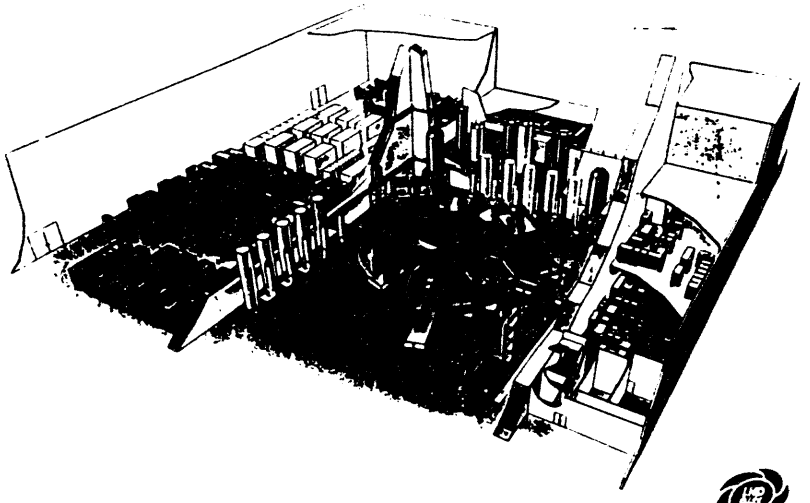

GOAL OF LHD PROJECT

1. PHYSICS EXPERIMENT EXTRAPOLATABLE TO FUSION CONDITION
   - HIGH $n\tau T$ > 10^{20} $keVm^{-3}s$ (Q~0.35)
   - HIGH T > 10 keV
   - HIGH β > 5 %
2. CURRENTLESS STEADY PLASMA PRODUCTION
   DIVERTOR EXPERIMENT
3. COMPLEMENTARY TOROIDAL DEVICE TO TOKAMAK APPROACH
4. CONTRIBUTION TO FUSION TECHNOLOGY

OM0115

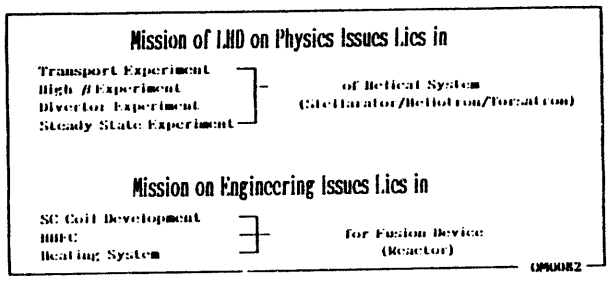

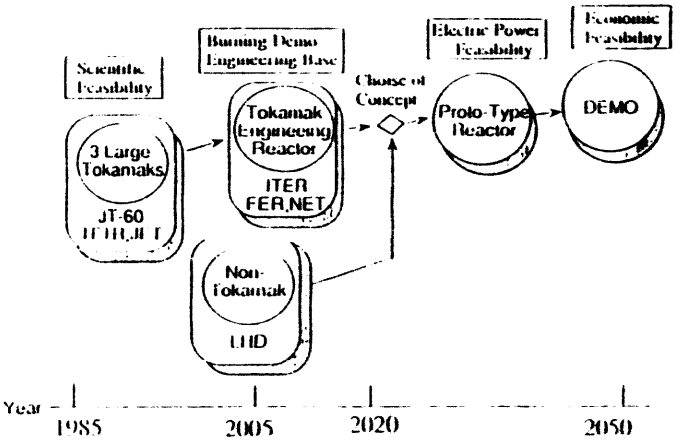

Strategy of Magnetic Fusion Reactor Development in Japan

Annual Budget for Fusion Reseach

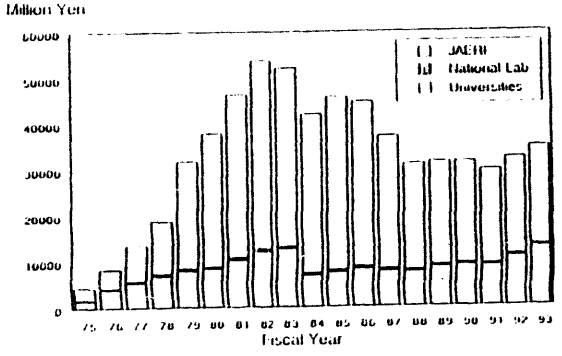

Budget for Fusion Research (M.O.E)

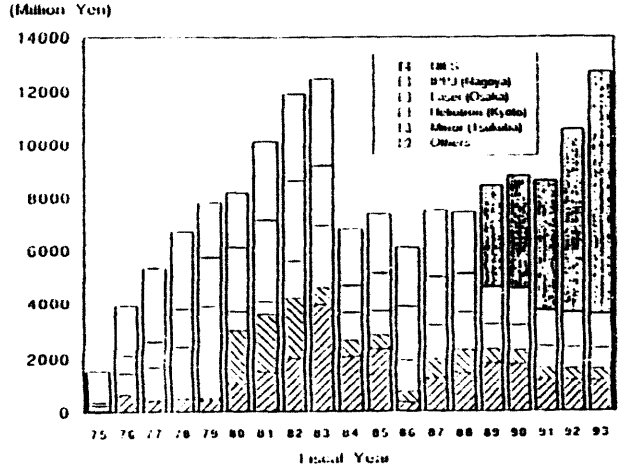

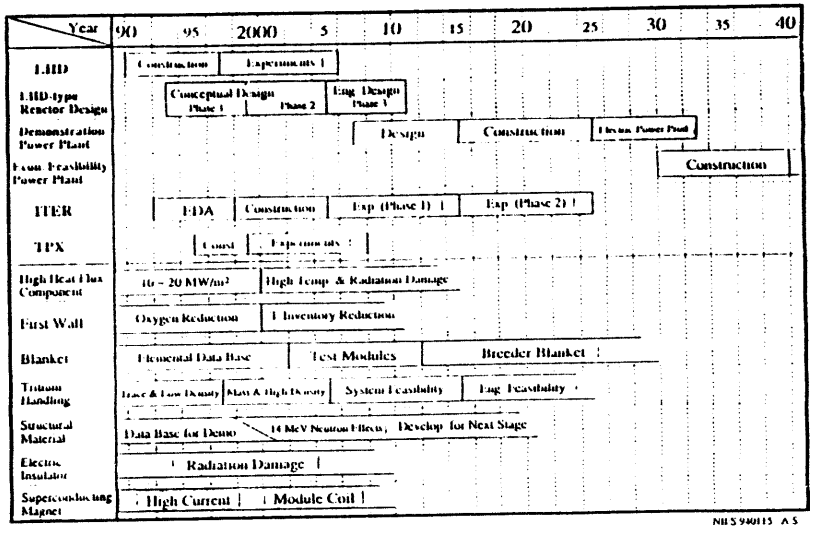

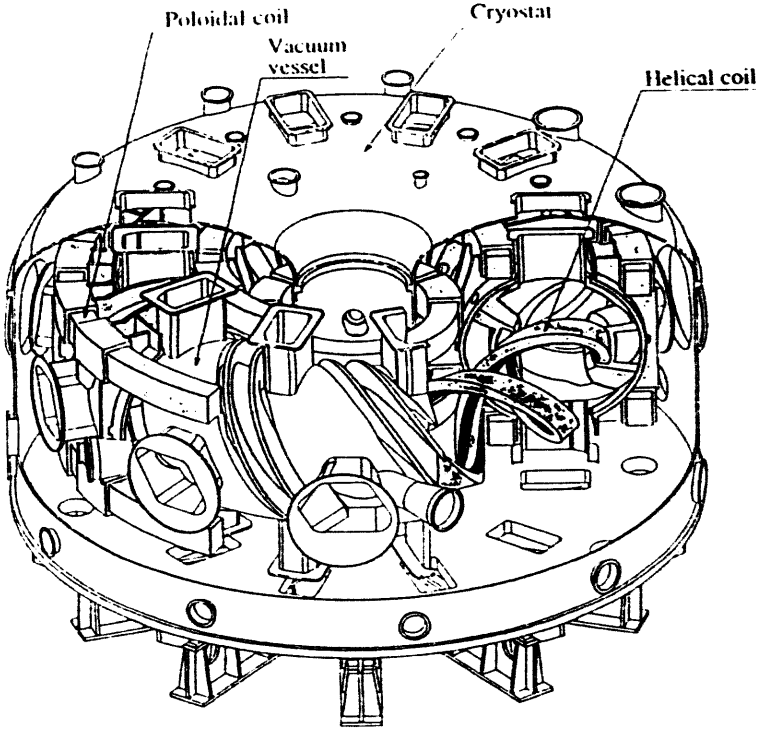

Table 1. Construction schedule for LHD

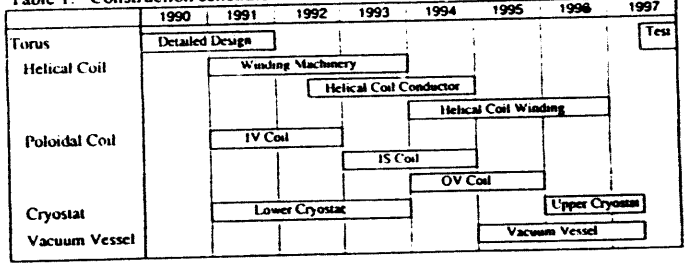

SPECIFICATIONS OF LHD

	PHASE I	PHASE II
MAJOR RADIUS	3.9 m	←
COIL MINOR RADIUS	0.975 m	←
AVERAGED PLASMA RADIUS	0.5～0.65 m	←
PLASMA ASPECT RATIO	6～7	←
ℓ	2	←
m	10	←
γ c=m/2·a_c/R (PITCH PARAM.)	1.25	←
α (PITCH MODULATION FACTOR)	0.1	←
MAGNETIC FIELD		
CENTER	3 T	4 T
COIL SURFACE	6.9 T	9.2 T
HELICAL COIL CURRENT	5.85 MA	7.8 MA
COIL CURRENT DENSITY	40 A/mm^2	53 A/mm^2
NUMBER OF LAYERS	3	←
LHe TEMPERATURE	4.4 K	1.8 K
POLOIDAL COIL CURRENT	STEADY	REAL TIME
INNER VERTICAL COIL	5.0 MA	←
INNER SHAPING COIL	-4.5 MA	←
OUTER VERTICAL COIL	-4.5 MA	←
LHe TEMPERATURE	4.5 K	4.5 K
PLASMA VOLUME	20～30 m^3	←
ROTATIONAL TRANSFORM		
CENTER	< 0.5	←
BOUNDARY	≃ 1	←
HELICAL RIPPLE AT SURFACE	0.2	←
PLASMA DURATION	10 s	←
REPETITION TIME	5 min	←
HEATING POWER		
ECRH	10 MW	←
NBI	15 MW	20 MW
ICRF	3 MW	9 MW
STEADY	-----	3 MW
$D^0 \rightarrow D^+$	-----	PRACTICE
NEUTRON YIELD	-----	2.4×10^{17} n/shot
COIL ENERGY	0.9 GJ	1.6 GJ
REFRIGERATION POWER	9 kW	～15 kW

OM0100

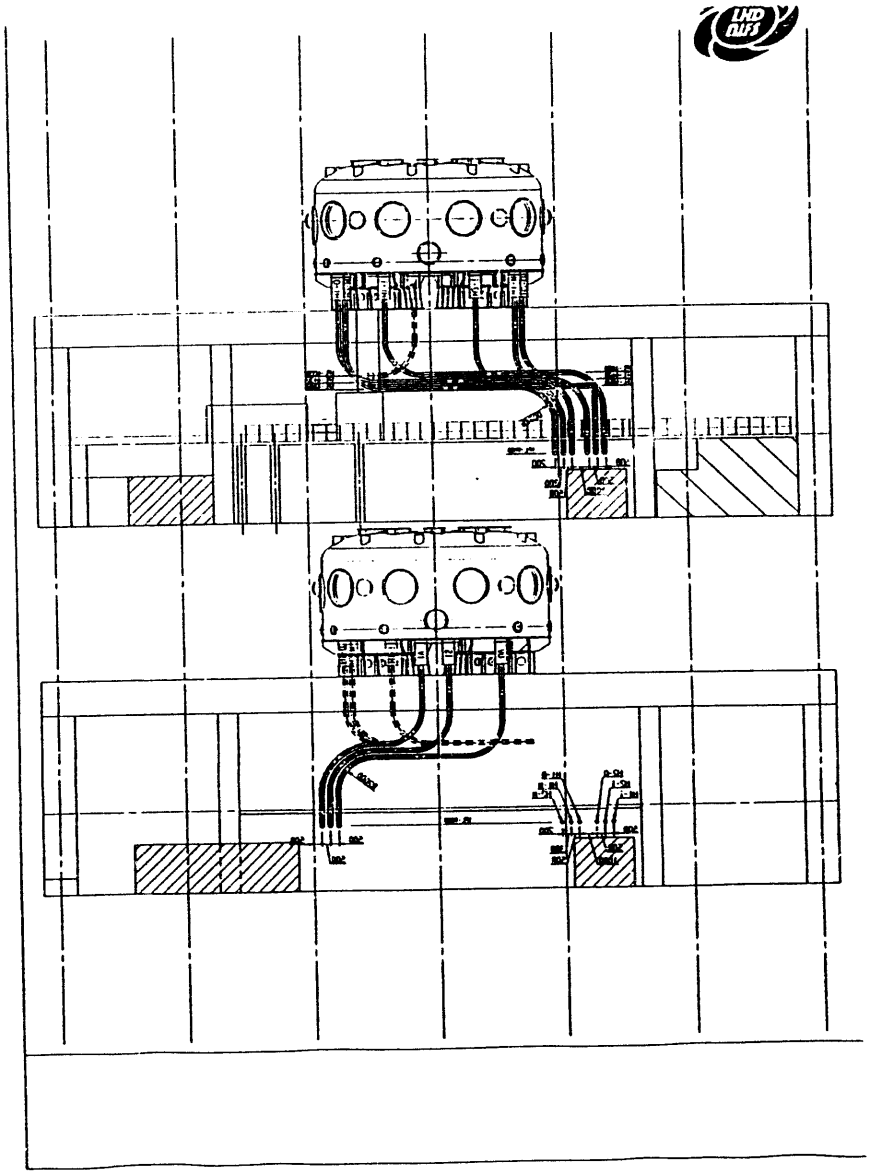

CURRENT DIRECTION OF LHD PROJECT

CONTINUATION OF LHD CONSTRUCTION
(1) 1994, 5TH YEAR OF 8 YEAR PROJECT
(2) COMPLETION OF FINAL ENGINEERING DESIGN
(3) FABRICATION OF MAJOR COMPONENTS IN THE FACTORY (FROM 1991)
- POLOIDAL COILS (UNTIL 1994)
- LOWER HALF OF CRYOSTAT (UNTIL 1993)
- HELICAL COIL FABRICATION MACHINE (UNTIL 1993)
- HELICAL COIL CONDUCTOR (UNTIL 1996)
- LHe REFRIGERATOR (UNTIL 1993)
- POLOIDAL COIL POWER SUPPLY (1993)
- COOLING SYSTEM (1993)

(4) STARTING CONSTRUCTION IN TOKI SITE
- HELICALI COIL FABRICATION
- POLOIDAL COILS
- CRYOSTAT
- SUPPORTING STRUCTURE etc.

(5) BEGINNING COMPONENT TEST
- INNER VERTICAL COIL TEST

(5) ACCELERATION OF R&D
- SC (BUS LINE, etc.)
- FIRST WALL MATERIAL AND COOLING SYSTEM
- POWER SUPPLY AND CONTROL SYSTEM
- PLASMA HEATING EQUIPMENT (NEGATIVE ION SOURCE, GYROTRON, etc.)
- DIAGNOSTICS

(5) DETAILED PLANNING OF LHD EXPERIMENTS FROM 1998
- TRANSPORT, MHD, DIVERTOR, STEADY STATE EXPERIMENT, etc.

(6) KEEP CONTINUING CONSTRUCTION OF BUILDINGS AND FACILITIES
- MAJOR EXPERIMENTAL BUILDING (1994, MARCH)
- MG BUILDING (COMPLETED)
- COMPUTER CENTER BUILDING (COMPLETED)
- HEATING SYSTEM R & D BUILDING (COMPLETED)
- SC RESEARCH BUILDING (COMPLETED)

OM0115

Progress in construction of the main body of LHD

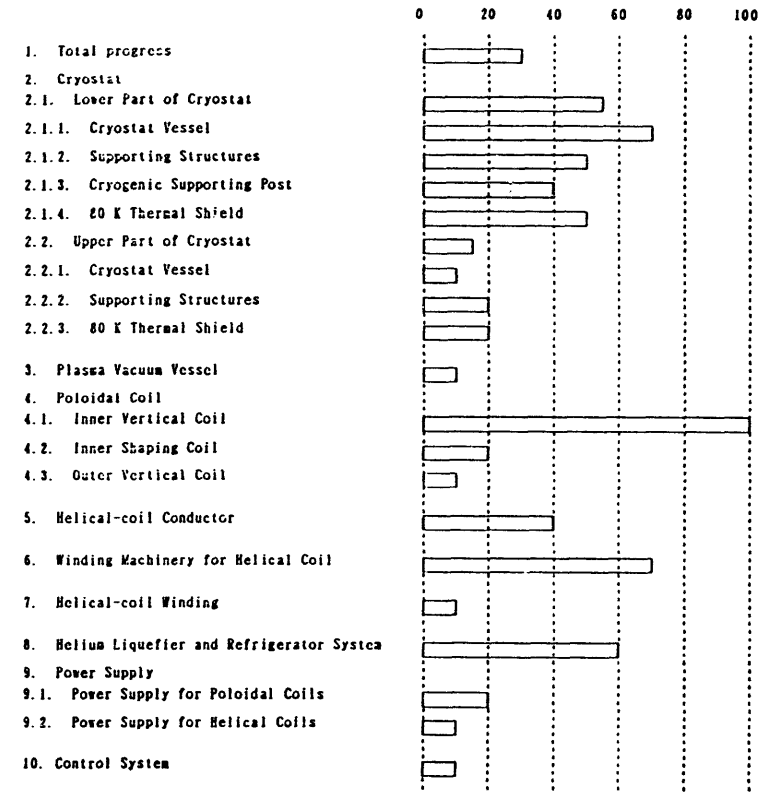

Items of research and development for the main body of LHD

1. Whole system of the main body of LHD
(1) Layout of components
(2) Layout of piping and cabling
(3) Planning construction schedule and coordinating work area in the main building
2. Cryostat
2.1. Lower Part of Cryostat
(1) Conceptual design, Determination of major specifications, Drawing specifications for purchase
2.1.1. Cryostat Vessel
(1) Layout of ports for diagnostics, pumping, heating equipment, and maintenance
(2) Structural analyses for atmosphere pressure (deformation and stress)
(3) Design of bellows (Evaluation of fatigue caused by thermal expansion and deformation by electromagnetic force)
(4) Design of sealing mechanism of flange
2.1.2. Supporting Structure
(1) Determination of design loadings and allowable stress
(2) Evaluation of electromagnetic force on coils
(3) Selection of the method to support poloidal coils
(4) Optimization of thickness and shape of supporting structure
(5) Structural analyses for electromagnetic force (deformation of coils and stress on structures)
(6) Thermal analyses for cooling down and heating (temperature difference during cooling down, temperature raise by eddy current, heat load)
(7) Analyses of thermal stress during cooling down and at quench of superconducting coils
(8) Evaluation of eddy current at field varying mode and plasma disruption
(9) Development of high precise measuring system for large scale device
2.1.3. Cryogenic Supporting Post
(1) Structural analyses for gravity (bucking and stress)
(2) Structural analyses for earthquake (static analysis, analysis of natural frequency, dynamic analysis)
(3) Thermal analyses for cooling down and heating
2.1.4. 80 K Thermal Shield
(1) Evaluation of electromagnetic force caused by eddy current
(2) Thermal analyses for cooling down and heating (heat input by eddy current, thermal conduction, and radiation)
2.2. Upper Part of Cryostat
(1) Layout of in-vessel piping
others are same as 2.1.
2.2.1. Cryostat Vessel
same as 2.1.1.
2.2.2. Supporting Structures
same as 2.1.2.
2.2.3. 80 K Thermal Shield
same as 2.1.3.
3. Plasma Vacuum Vessel
(1) Conceptual design, Determination of major specifications, Drawing specifications for purchase
(2) Determination of design loadings and allowable stress
(3) Determination of heat loading from plasma
(4) Structural analyses for atmosphere pressure (deformation and stress)
(5) Structural analyses for earthquake (static analysis, analysis of natural frequency, dynamic analysis)
(6) Discussion on manufacturing method and assembling error
(7) Discussion on cooling method
(8) Discussion on baking method
4. Poloidal Coil
4.1. Inner Vertical Coil
(1) Conceptual design, Determination of major specifications, Drawing specifications for purchase
(2) Determination of detailed specifications for conductors
(3) Structural analyses for electromagnetic force and thermal stress
(4) Thermal analyses for cooling down and heat generating
(5) Evaluation and reduction of error field caused by feeder and across region of the conductor
4.2. Inner Shaping Coil
same as 4.1.
4.3. Outer Vertical Coil
same as 4.1.
5. Helical-coil Conductor
(1) Conceptual design, Determination of major specifications, Drawing specifications for purchase
(2) Evaluation of magnetic field in the helical coil
(3) Determination of detailed specifications for conductors
(4) Structural analyses for electromagnetic force
(5) Estimation of Hall effect of pure aluminium composite conductors
(6) Thermal analyses for cooling down and heat generating
(7) Development of method of non-destructive inspection
6. Winding Machinery for Helical Coil
(1) Conceptual design, Determination of major specifications, Drawing specifications for purchase
(2) Optimization of condition for shaping helical coil conductors
7. Helical-coil Winding
(1) Conceptual design, Determination of major specifications,
Drawing specifications for purchase
(2) Brushing up of winding method
(3) Optimization of exposure factor of conductors
(4) Determination of detailed specifications of the electrical insulator
(5) Structural analyses of helical coil conductor and can for electromagnetic force
(6) Development of the method to measure location of each conductor high precisely
8. Helium Liquefier and Refrigerator System
(1) Conceptual design, Determination of major specifications, Drawing specifications for purchase

(2) Evaluation of heat generation of each component
(3) Detailed design of control system
9. Power Supply
9.1. Power Supply for Poloidal Coils
(1) Conceptual design, Determination of major specifications, Drawing specifications for purchase
9.2. Power Supply for Helical Coils
(1) Conceptual design, Determination of major specifications, Drawing specifications for purchase
10. Control System
(1) Conceptual design, Determination of major specifications, Drawing specifications for purchase

INTRODUCTION TO PRESENT STATUS OF CONSTRUCTION

1. HELICAL COIL FABRICATION MACHINE

2. STRUCTURAL SHELL

3. POLOIDAL COIL (INNER VERTICAL COIL)

4. LHe REFRIGERATOR

5. BUILDING

OM0100

637
100
Helical-coil can
Shell arm
116
6
92.5
57.5
6
92.5
124.5
33
12.5
18
Ground insulation
Layer to layer insulator
Turn to turn insulator
R975
Minor radius
Superconductor

CRITICAL ISSUES OF ENGINEERING DESIGN FOR LHD

1. STRUCTURAL SUPPORT FOR LARGE MAGNETIC FORCE
2. HELICAL COIL WITH HIGH RELIABILITY AND ACCURACY
3. POLOIDAL COILS FOR REAL TIME OPERATION
4. VACUUM CHAMBER AND HIFC FOR STEADY STATE OPERATION
5. LARGE CRYOSTAT

OM0100

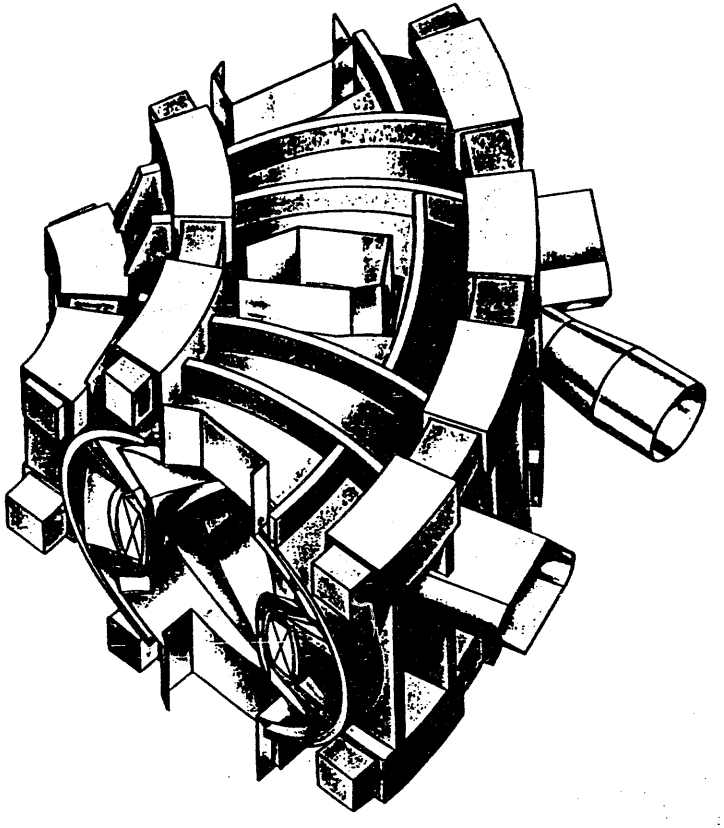

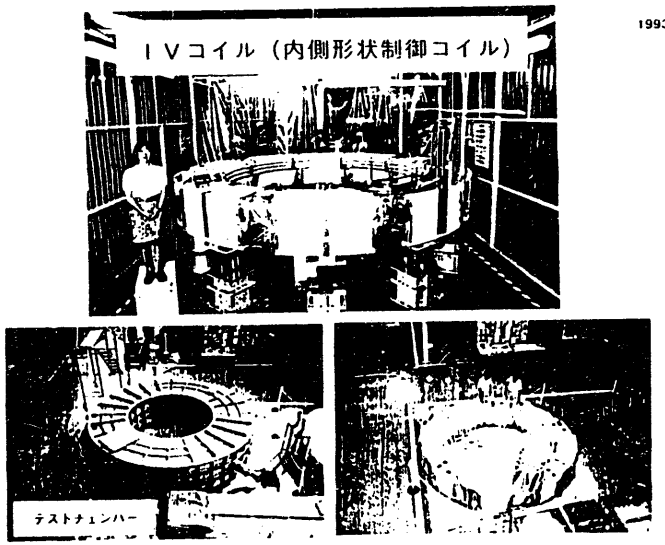

1993.10.

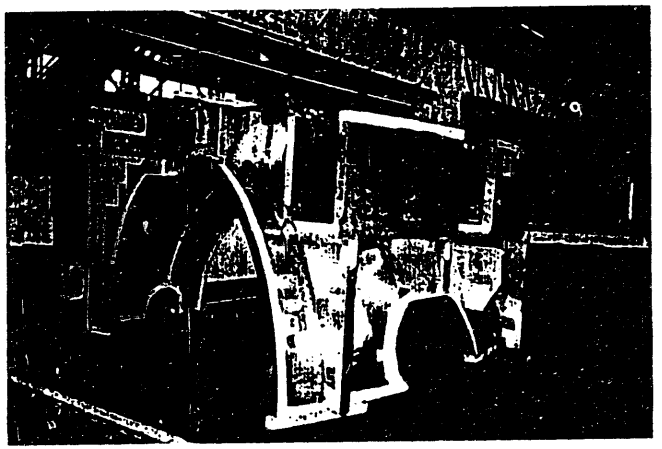

(3/8)

R&D PROGRAM

(1) R&D activities on superconductors, vacuum and high heat flux components, power supplies, control systems, heating systems, and diagnostic system are being pursued.

(2) SC Research Building was completed by the end of 1990.

(3) Construction of superconducting material and test coil have been completed. Final Liquid Helium cooling tests are being performed on various test components.

(4) Heating System R & D Building and MC Building have been completed. Test facilities for negative ion source, ICRF antenna system, and gyrotron are began in operation.

(5) A test facility for developing vacuum and high heat flux components has been completed in the SC Research Building, and is under operation.

(6) Main missions of R & D are developments of advanced technology based on new ideas and positive confirmation of performance.

(7) A great deal of technical knowledge has been obtained as expected.

- Development of stable large current conductor
- Development of large magnet
- Development of refrigeration technology
- High heat flux components
- Negative Ion Source
- Gyrotron
- ICRF antenna system

OM0100

LHD Plasma Vacuum Vessel

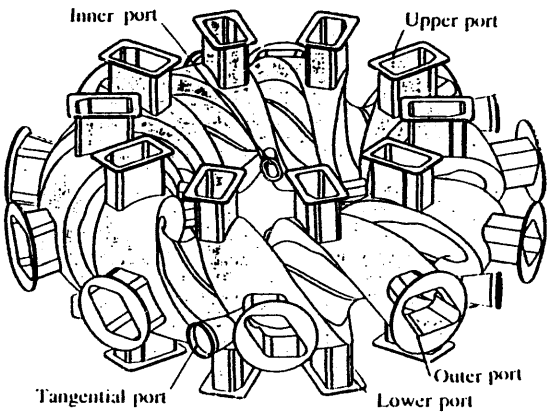

Design Properties of LHD plasma vacuum vessel

The vacuum vessel maintains high vacuum pressure, removes heat from the plasma and protects superconducting coils from the plasma heat.

Size ; major radius 3.9 m, minor radius 1.6 m, thickness 15 mm
Material ; stainless steel
Construction ; segments are patched together by welding
Heat Flux ; 3MW(CW), 20MW(10s)
Cooling System ; water cooling pipes (vessel surface), divertor plates
Thermal Insulation ; 80K sheeld (between helical coils and vessel)
Rigidness ; 1atm (against inner and outer pressure)

5 types of ports ;
(a) Upper and Lower ports; for cooling water pass and director across
(b) Inner and Outer Horizontal ports; for Diagnostics and ICRF heating
(c) Tangential ports; for NBI

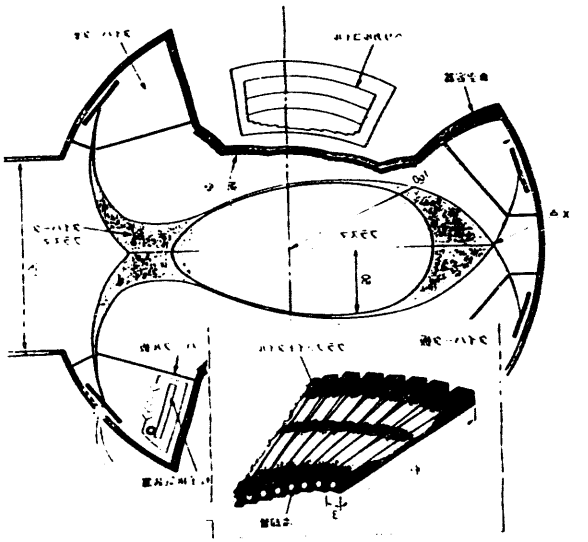

Research Items on IIIIFC

(1)Evaluation for Candidate Plasma Facing Materials
Materials: CFC, C/C Composite, Iso. Graphite, B Doped or Coated Graphite, Boronization, ...
Major Analysis: PSI Issues
Retention, Erosion, Gas Desorption, Effective Surface Area, Sublimation and Cracking due to Heat Load
(2)Evaluation for Candidate Brazing Components(US and Japan)
Materials: (CFC, C/C Components, B-Doped or Coated Graphite)
plus
(Water or Helium Cooling)
Major Items:High Heat Load Tests in ACT and EBT
Correlation between Heat Load and Temperature Profile
Damage in Heat Removal Structure
Damage of PFM
(3)Evaluation for Limiter or Divertor Components Irradiated in LHD, and TRIAM-1M

Materials: Small Pieces of Limiter/Divertor Module Used in LHD, and TRIAM-1M
Major Items: New Erosion, Retention, Damage in Structure, Damage of PFM
(4)Suggestions/Proposal to Limiter/Divertor Component of a Helical Reactor
Based on the results of (1) and (2), suitable divertor component for LHD is considered. In addition, these analysis be helpful to understand the behavior of discharge plasma and damage of the components.
Analysis for post irradiated limiter/divertor components, suggested is the suitable limiter/divertor component of a helical reactor.

C93103

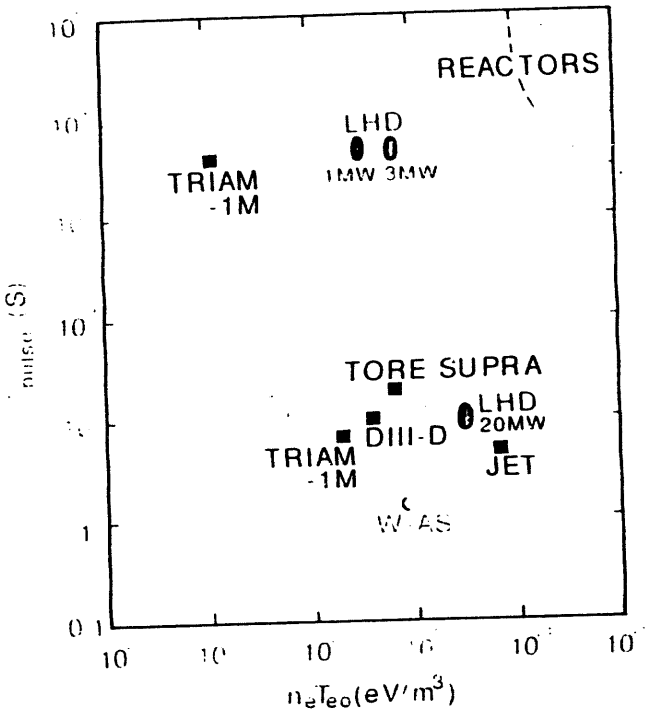

Fig. Energy density and confinement time of torus plasma.

Divertor Magnetic Geometries for LHD

Helical Divertor (HD)	Local Island Divertor (LID)
* Natural Configuration	* Addition of m/n=1/1 field
* Open Divertor With Baffle, Closed Div	* Closed Divertor
* Vague Boundary (~50mm) (ergodic layer + edge surface layer)	* Sharp Boundary (1mm) between closed and open regions.

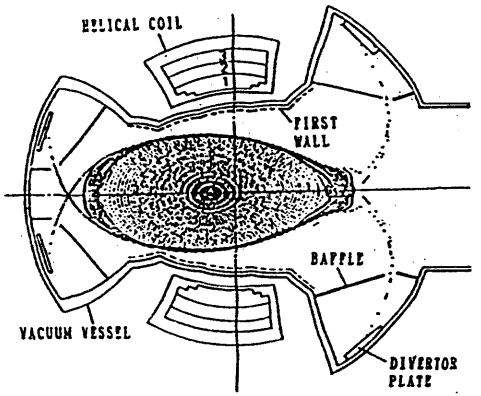

Helical Divertor

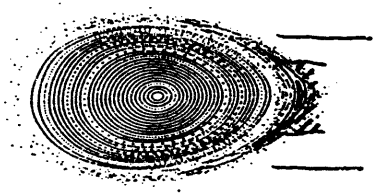

Local Island Divertor

LHD DIVERTOR PROGRAM

Objectives

(1) to improve LHD core plasma performance through divertor edge control.

(2) to provide a testing ground for high heat flux plasma facing components.

(3) to develop reactor relevant divertor systems or concepts through the experiment.

Concepts and experimental results obtained in the tokamak research programs and in the LHD design program will be incorporated into the LHD divertor experiment to improve helical plasma performance.

(1) Concepts from tokamak programs

* High density divertor plasma
* Radiative cooling
* Impurity trapping by plasma flow
* H-mode
* Boron coating

(2) Concepts from the LHD program

* High Temperature Divertor Operation
* Local Island Divertor(LID)
* Carbon Sheet Pumping
* Metal Membrane Pumping
* LID Discharge Cleaning

SUMMARY

(1) Construction of LHD is progressing.
(2) Presently at the final stage of engineering design. Design activities are carried out by the LHD Construction Team (LOH Team) at NIFS.
(3) R&D is progressing on superconductors, vacuum and high heat flux components, power supplies, control system, heating systems, and diagnostic systems. A large amount of technical knowledge has been obtained, especially a large contribution has been made to the area of superconducting research.
(4) Fabrication has been started on major components and is growing.
(6) Construction of buildings is under progress.
(7) On site fabrication and assembly in Toki site are scheduled to start in April, next year, 1994.

OPD100

DIVERTOR OPERATIONAL MODES

High Recycling ⇒ Low Recycling

Low Divertor Temperature High Divertor Density	High Divertor Temperature Low Divertor Density
Impurity Trapping in the Edge by Plasma Flow ⇓ Radiative Cooling (a Safe Heat Removal)	High Efficient Pumping ⇓ High Edge Temperature ⇓ Enhancement of τ_E

Either operation mode will require successful both plasma flow control and impurity control.

Plasma flow (recycling) control will be done by combination of efficient hydrogen pumping and deep fuelling (pellet, NBI).

Two pumping schemes are being developed for this purpose.

Carbon Sheet Pumping
Membrane Pumping

Design of ITER Plasma Facing Components

S.Tanaka
Divertor & Plasma Interface Division
ITER Garching Joint Work Site

US-Japan Workshop on High Heat Flux Components and Plasma Surface Interactions for Next Devices

University of California,San Diego
January 24-27,1994

Structure of Divertor & Plasma Interface Division

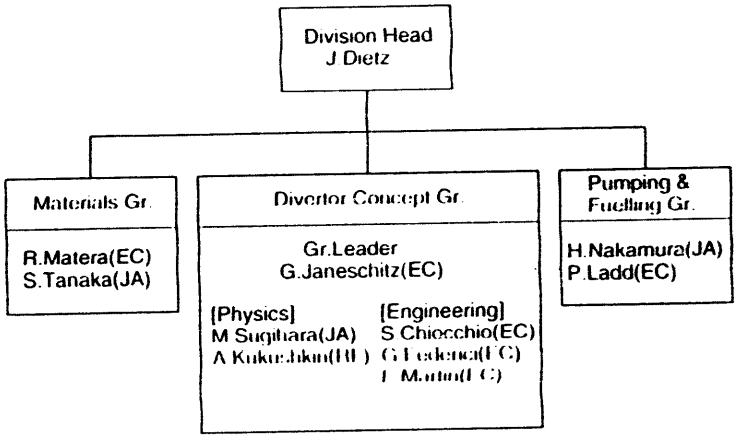

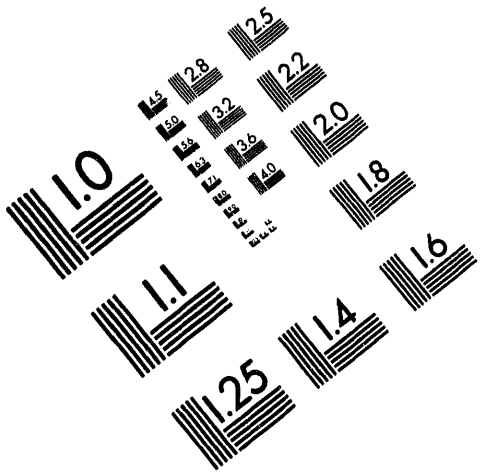

Association for Information and Image Management
1100 Wayne Avenue, Suite 1100
Silver Spring, Maryland 20910
301/587-8202

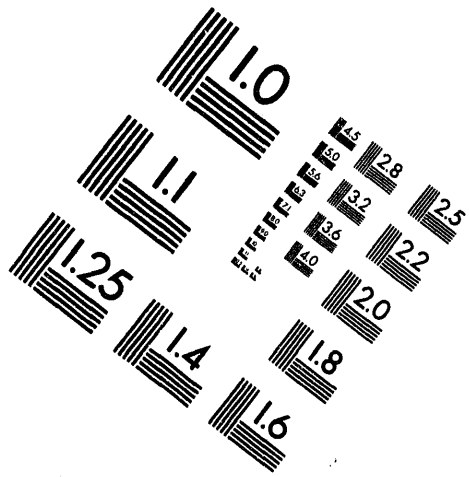

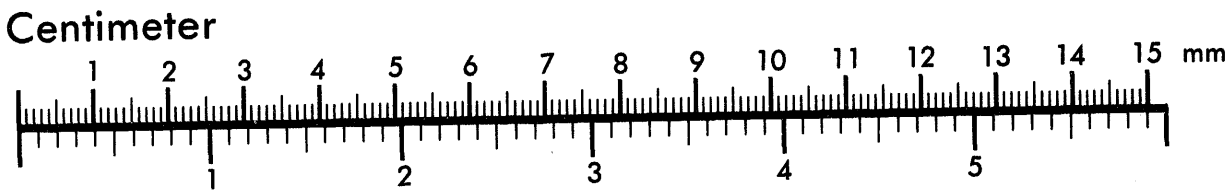

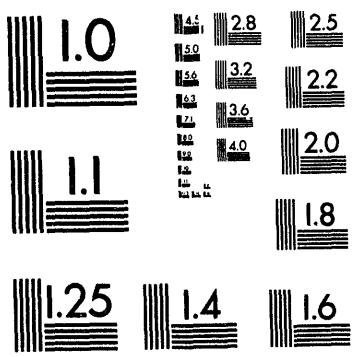

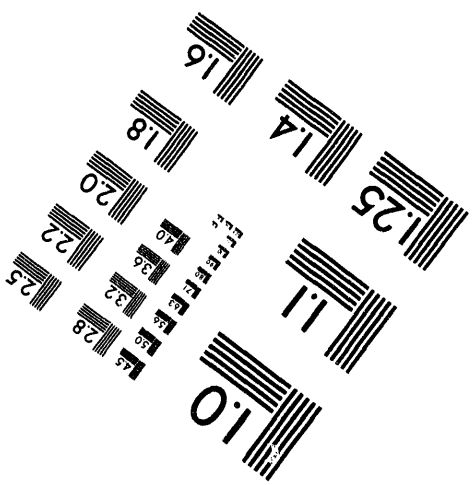

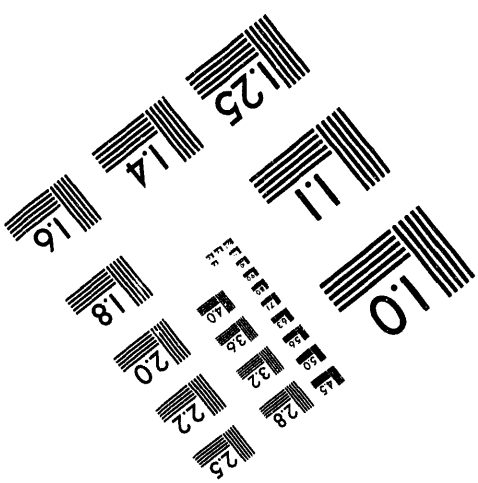

2 of 8

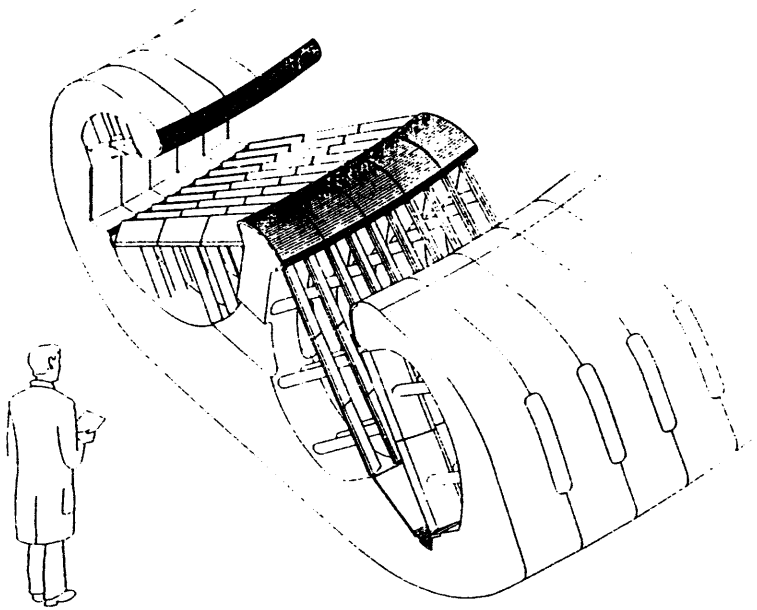

Fig. 4 Three dimensional view of a divertor cassette

Design Requirements

1.Divertor Baffles

Function

- Maintain a relatively high neutral gas pressure (1~10 Pa) inside the divertor chambers.
- Lower neutral density around the main plasma.
- Improve the retention of recycling impurities in the divertor.

Shape

- Follow the 6 cm(~ 6x power decay length) flux line for about 1 m of poloidal length from the X-point upwards.

Heat Load

- Direct deposition of the SOL plasma.
- CX neutrals.
- Strong radiation from the SOL near the X-point.

To be designed to:

- withstand, with acceptable life time, normal (up to 5MW/m^2) and abnormal conditions;
- define, together with the divertor dome, the size and configuration of the slot at the divertor chamber entrance to prevent excessive neutral back flow in the main chamber;
- provide electrical continuity in the toroidal direction to minimize the effects of eddy current circulation;
- resist the impulsive forces due to halo current;
- prevent gas flow through the gaps between two adjacent modules.

2.Divertor Dome

Function

- Prevent the SOL plasma (parallel power flux ~1GW/m^2) to directly hit the lower components in case of large vertical displacement events or during plasma start up and ramp down, together with the baffles.
- Host and protect mirrors to enable a diagnostic coverage of the critical parts of the divertor.

Shape

- Dome-like structure at the center.

Heat Load

- Energy load during disruptions and ELMs.
- CX neutrals and radiation (steady state)

To be designed to:

- withstand, with acceptable life time, normal operation and disruptive loads;
- define, together with the divertor baffles, the size and configuraton of the slot at the divertor chamber entrance;
- provide electrical continuity in the toroidal direction to minimize the effect of eddy current circulation;
- resist the impulsive forces due to halo current;
- provide shielding to protect the lower parts of the divertor chamber including diagnostic penetrations and instruments;
- minimize the misalignment between different modules of the surface exposed to the plasma.

3.Transparent Wall ("Air Fins")

Function

- Efficiently thermalize the hot neutrals which exit the plasma, and receive the momentum transported by these neutrals.
- Keep the highest possible transparency for neutrals (i.e.,maximize recirculation of neutrals).
- Receive most of power radiated along the divertor throat.

Shape

- A set of wing-like structure tilted by 45° in the toroidal direction towards the incomimg magnetic field lines.
- Louver like structure ~ 10 cm away from the last flux line entering divertor through the baffle.

Heat Load

- Power (~200MW) radiated in the divertor region.

To be designed to:

- withstand, with acceptable life time, a heat flux of 5MW/m^2 radiated under normal operation from the divertor plasma;
- be close to the plasma to dump the momentum transported by neutrals;
- provide a barrier to radiative heat while allowing neutral gas circulation.

4.Energy Dump Target

Function

- Accomodate the remaining steady state power load of < 10% of the energy conducted in the SOL.
- Absorb heat pulses originating from ELMs as well as from disruptions.

Shape

- Plates tilted poloidally to reduce heat flux on the surface by a factor of 3.

Heat Load

- Power load of < 10% of the energy conducted in the SOL.
- Energy load during ELMs and disruptions.

To be designed to:

- withstand, with acceptable life time, 2.5~5MW/m^2 under normal operation and 100 ~ 200 MJ/m^2 during ELM's and disruptions;
- be actively cooled to limit the temperatures below 800 C during normal and transient operations;
- be replaceable as a whole without requiring cutting and rewelding of pipes.

Materials and Coolants

Plasma facing material

Reference :Beryllium

Back-up :Fiber based materials with a Be or graphite matrix

Structure Material

Reference : Copper alloy (Cu-Cr-Zr)

- compatible with neutron irradiation up to 10 dpa at temparatures below 300 C.
- joining techniques well established.

Options : Cu-Be-Ni,DS copper

Coolant

Reference : water

The inlet temperature 100~150 C is chosen to maintain surface temperatures below 600 C to avoid swelling and, on the other hand,to keep Be in the ductile range.

Options :He gas, Liquid metal

Engineering Design

Transparent Wall

- estimation of surface heat flux distribution on the fins.
- thermo-mechanical analysis of the fins.
- electromagnetic analysis of the fins.

Energy Dump Target

Conduction cooled design proposed:

- metal fiber/metal foam compliant layer concept.
- solder/rheocast alloy compliant layer concept.

At present, the engineering design and analyses are immature. New proposals and further studies are required.

R & D for ITER
Plasma Facing Components

R. Matera
Divertor & Plasma Interface Division
ITER Garching Joint Work Site

Us-Japan Workshop on High Heat Flux
Components and Plasma Surface Interactions for
Next Devices

University of California, San Diego
January 24-27, 1994

TASK T1 Development of Ductile Beryllium and Study of Manufacture and Joining Techniques

TASK T2 Development, Manufacture and Test of Divertor Elements

TASK T4 Development of In-Situ Beryllium Plasma Spray Techniques

TASK T6 Test of Divertor Bumper Cooling

TASK T62 Tritium Permeation and Invertory for ITER Divertor and First Wall

R. Matera US-Japan Ws Q 181 San Diego - Jan '94

TASK T3 Assessment, Characterization and Development of Composite Plasma-Facing Materials

TASK T5 Study of Compliant Layer between Wall Protection and Blanket Segments

MECHANICAL ALLOYING

High Energy Milling Elemental Powders for Extended Time (1-100 hrs)

GOAL

Isotropic, Nanocrystalline Beryllium Reinforced by a Finer Dispersion of an Insoluble Hard Phase e.g. Be Carbide

- Grain Size 100-500 nm
- Size od Dispersed Phase = 10 nm
- Reduced Oxigen Content or
- Reduced Size of Oxide Particles
- Improved Mechanical Properties
- Pinning He Bubbles
- Improved Radiation Resistance

R. Matera US-Japan Ws Q 181 San Diego - Jan. '94

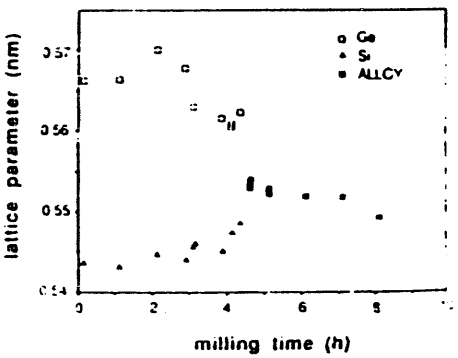

Figure 5-4. Lattice parameter vs milling time for Si and Ge powder for the composition Ge-72 at.% Si

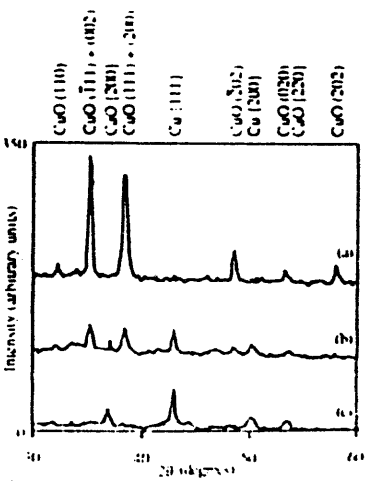

FIG. 1. X-ray powder diffraction patterns of mechanically alloyed CuO and Cu (a) 7.5 min, (b) 60 min, (c) 1440 min

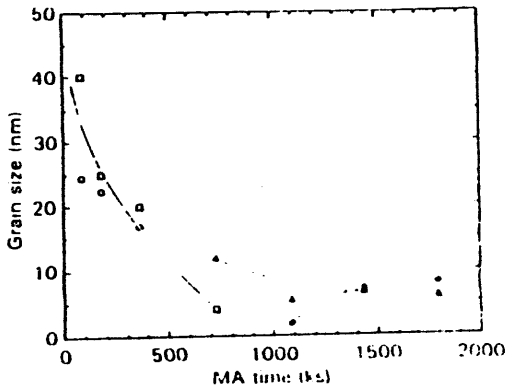

Figure 2 Elemental particulate and grain sizes measured from the line-broadening versus MA time for Nb-54.5 wt.% Al mixture (○) Al, (□) Nb, (△) Nb_2Al, (▲) $NbAl_3$

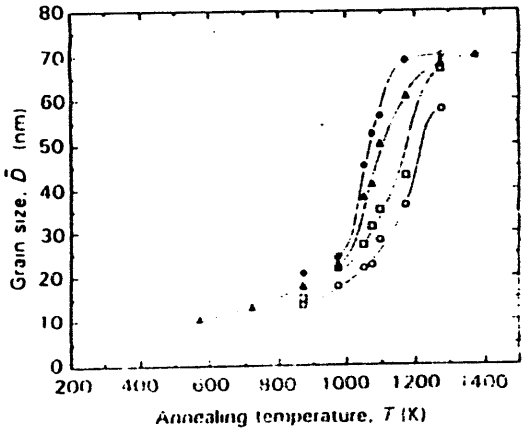

Figure 4 Measured grain sizes plotted against anneal temperature as a function of anneal time for $NbAl_3$ produced by MA 1800 ks (●) as alloyed (□) 1.8 ks, (△) 3.6 ks, (▽) 10.8 ks, (○) 18.0 ks

Table 2 Mechanical properties of 2.50vol%TiC- and 2.50vol%ZrC-dispersion-strengthened coppers prepared by mechanical alloying and hot extrusion.

Dispersoid	Hardness (Hv)	Ultimate tensile strength (MPa)	Elongation (%)	Reduction of area(%)
TiC	190	667	11	41
ZrC	201	7.5	12	44

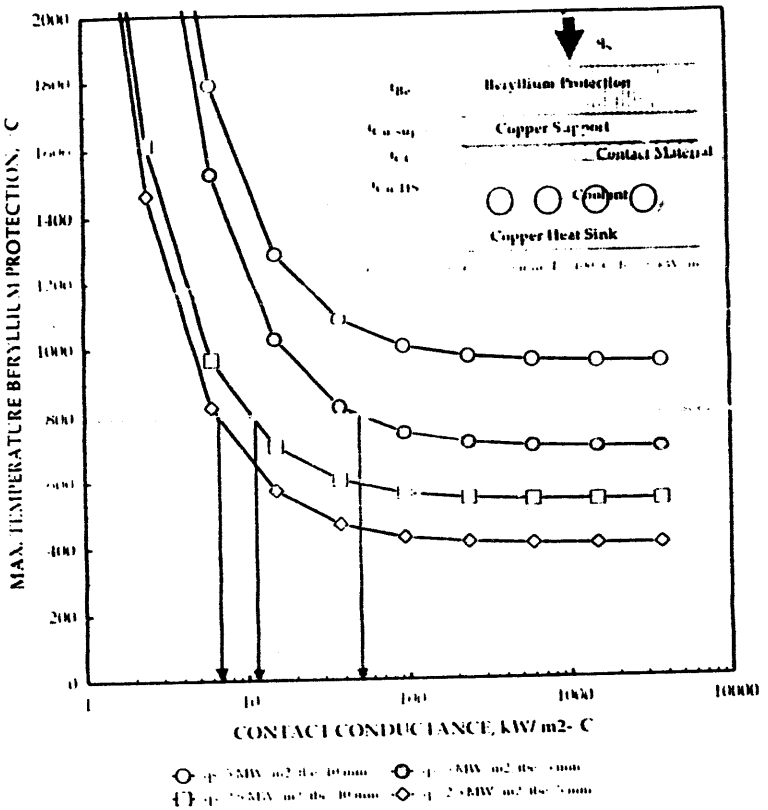

Conductance Evidence
January 18, 1994

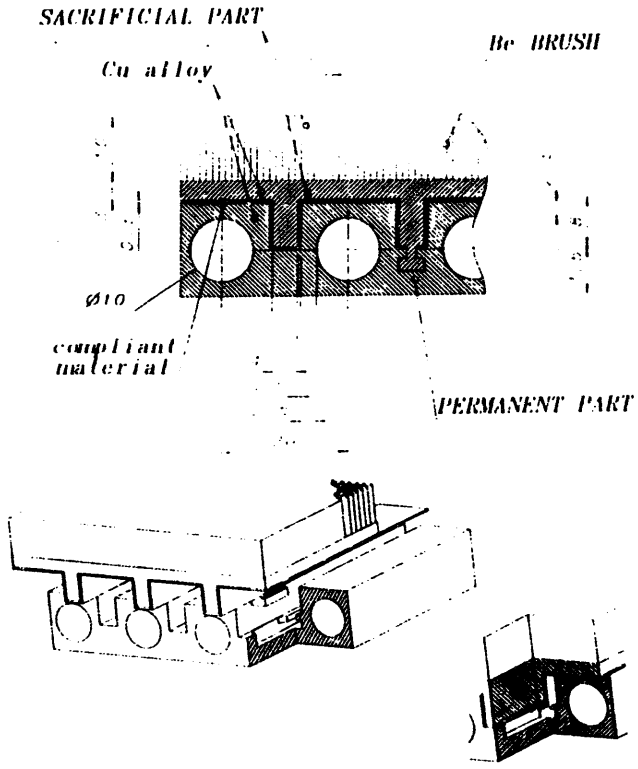

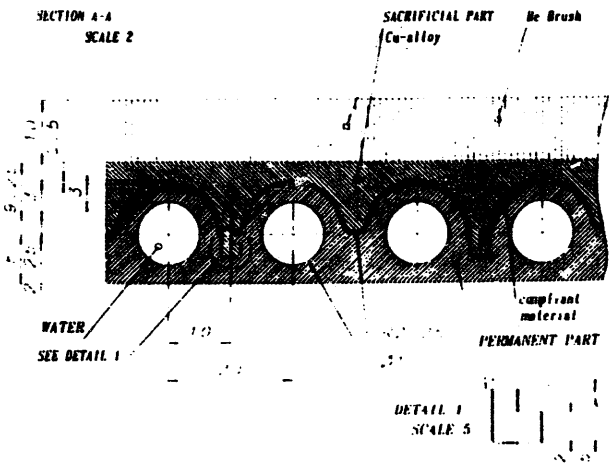

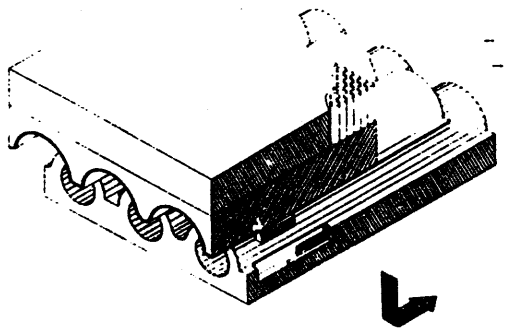

ENERGY DUMP TARGET.

Brush-like Structure

DRASTIC REDUCTION OF THERMAL AND DIFFERENTIAL SWELLING STRESSES

DAMAGE BY HIGH ENERGY DUMP REMAIN LOCALISED

NO FREE PATH FOR CRACK PROPAGATION

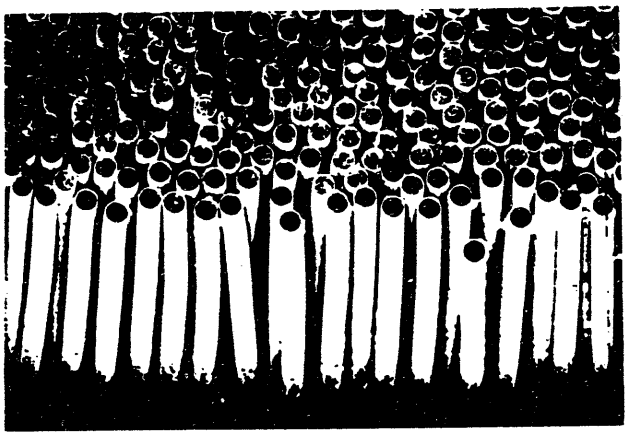

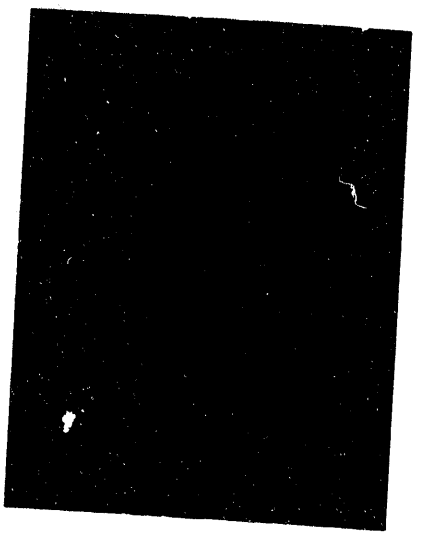

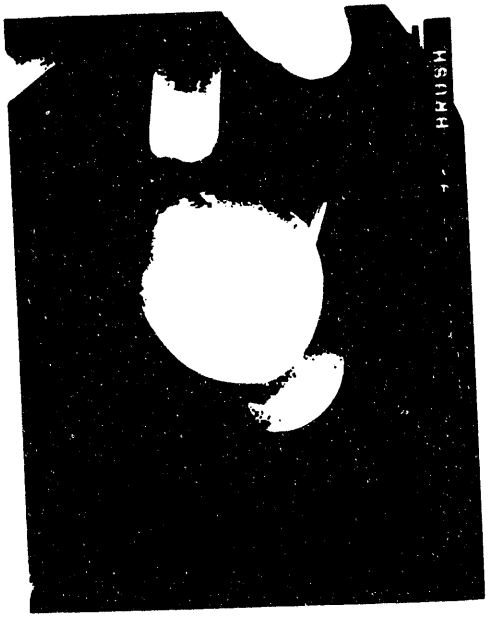
HMIISH

RHEO-CAST ALLOYS

Thixotropy

Time, shear rate-dependent viscosity

When the material is sheared it thins; when undisturbed it thickens again

Reversible from solid to semi-solid provided the temperature does not exceed rheo-cast temperature

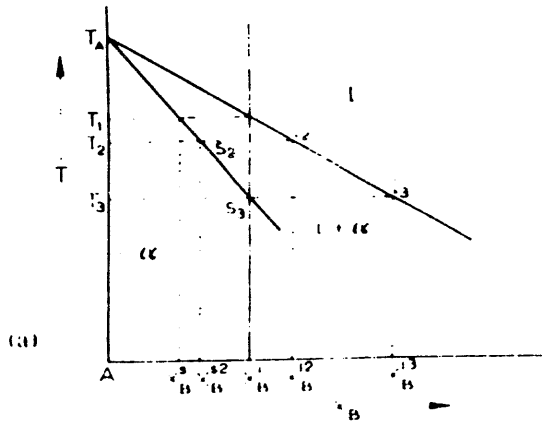

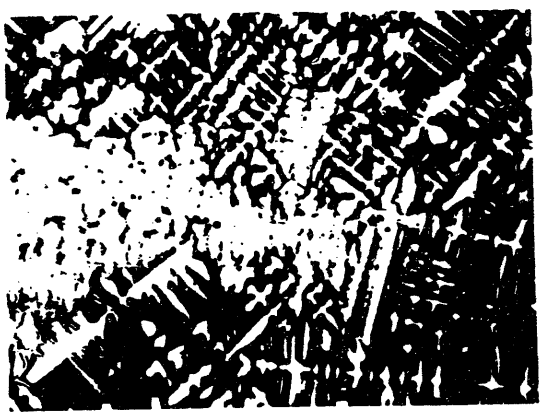

APPARENT VISCOSITY Pa
SHEAR STRESS MPa

Table I. Some Typical Viscosities

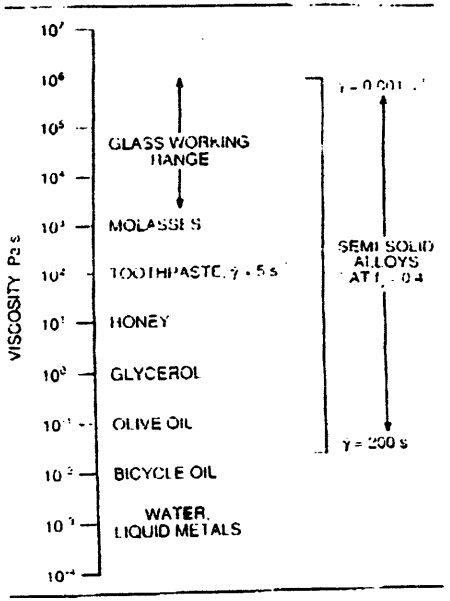

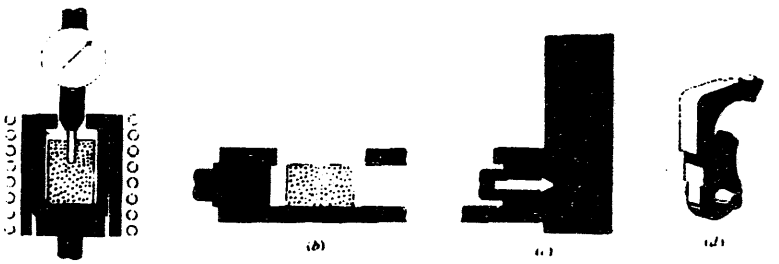

Solidus C	Thixotropic Range C	Systems	Commercial solder
118	132-144	In-Sn	71
138	154-169	Bi-Sn	281
144	172-222	Ag-In	3
155	180-228	Al-In/Ca-In/Ba-In/As-In	-
221	246-285	Ag-Sn	132
227	242-263	Cu-Sn/Al-Sn	160
270	300-400	As-Bi	
311	350-450	Al-Tl	
271-630	300-550	Bi-Sb	

Solidus C	Thixotropic Range C	Systems	Commercial solder
118	132-144	In-Sn	71
138	154-169	Bi-Sn	281
144	172-222	Ag-In	3
155	180-228	Al-In/Ca-In/Ba-In/As-In	-
221	246-285	Ag-Sn	132
227	242-263	Cu-Sn/Al-Sn	160
270	300-400	As-Bi	
311	350-450	Al-Tl	
271-630	300-550	Bi-Sb	

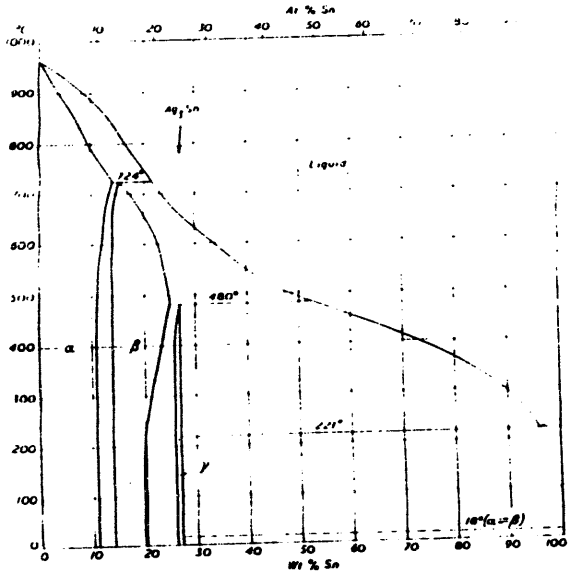
At. % Sn
Wt. % Sn
Liquid
480°
221°
α
β
γ

Ag - Sn

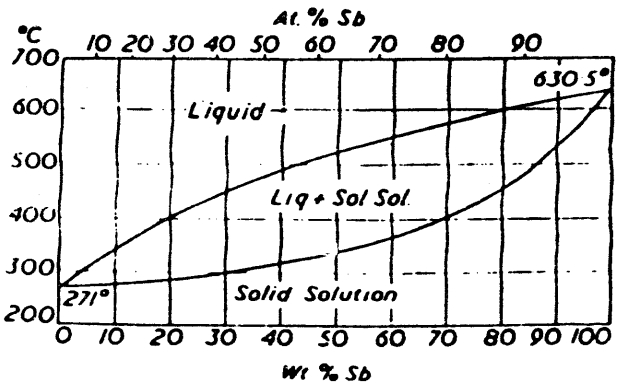
At. % Sb
°C
Liquid
630.5°
Liq + Sol Sol.
Solid Solution
271°
Wt. % Sb

Bi–Sb

POWER HANDLING IN THE TPX TOKAMAK

TOKAMAK PHYSICS EXPERIMENT

Work performed by the TPX Coceptual Design Team

Presented by
David N. Hill
Lawrence Livermore National Laboratory

OUTLINE

Brief overview of the TPX

Expected power loads for the divertor and first wall

PFC conceptual design

Radiative divertor operation in TPX

Presented at the US/Japan HHF/PMI Workshop
UCSD, San Diego, CA
January 24–27, 1994

TPX OBJECTIVES

The mission of the TPX is to develop the scientific basis for an economical, more compact, and continuously operating tokamak fusion reactor.

Toward these ends, our goals are to obtain:

- Efficient current drive via high bootstrap fraction (NBCD, LHCD, and FWCD)
- Advanced tokamak operation:
  $\beta_N = 4-5$ and $H = 3-4$ at $q_{95} \sim 4$
- Steady–state power and particle exhaust, extrapolation to ~ 3 MW/m^2 neutron flux & ~10% He ash.
- High plasma and component reliability: 80% availability of all components, ~ 1 disruption per 10 hours operation.

Tokamak Parameters

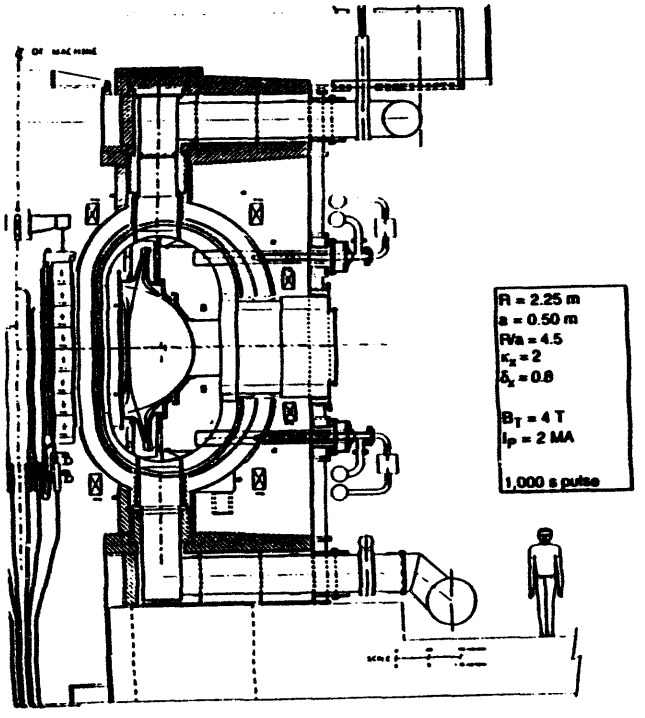

Tokamak Physics Experiment Proposed Schedule

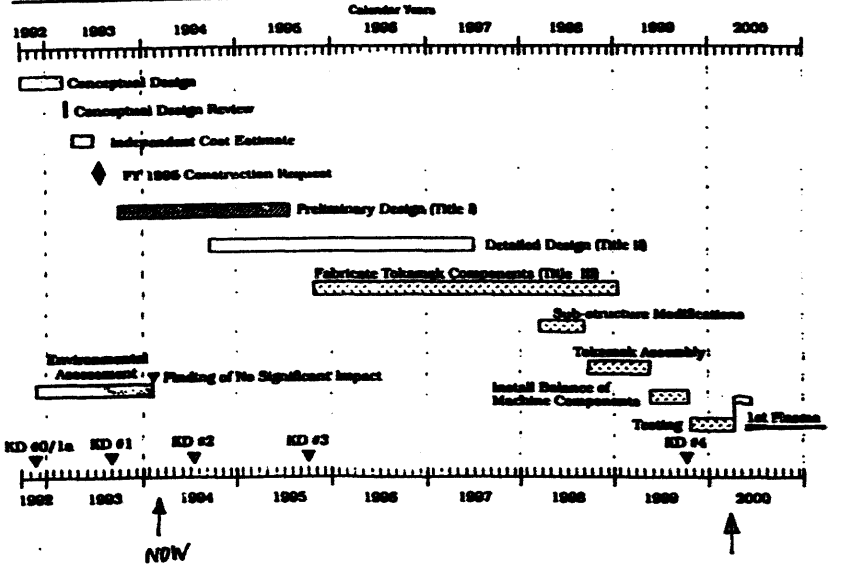

EXPECTED DIVERTOR HEAT FLUX (simplest possible calculation)

• P_{in} (MW) =	18	45
• f_{rad} =	0.4	0.4
• DND: P_{out}^{div} (MW) = 0.8×0.55×(1-0.4)×18	4.75	12
SND: P_{out}^{div} (MW) = 0.67×(1-0.4)×18 (1.5× higher than DND)	7.2	18
• λ_q at midplane (cm)	0.5	0.5
λ_q at divertor ($\lambda_{q,div}$) (cm) [= $\lambda_q \times 2.5 \times 1/\sin(16^o) = 9.1\lambda_q$]	4.5	4.5
R_{div} (m)	2	2
$q_{max} = \frac{P_{div}}{2\pi R_{div} \lambda_{q,div}}$ (MW/m^2)	8.4	21
• with a correction for diffusion into private flux region (0.5 -- 0.7)	4-6	11-14

ACCEPTABLE DIVERTOR CONDITIONS SHOULD BE OBTAINED WITH THE BASELINE HEATING COMPLEMENT

- With 18 MW, TPX should be in the marginally collisional flux-limited regime. Ions and electrons are not fully equilibrated in the SOL.

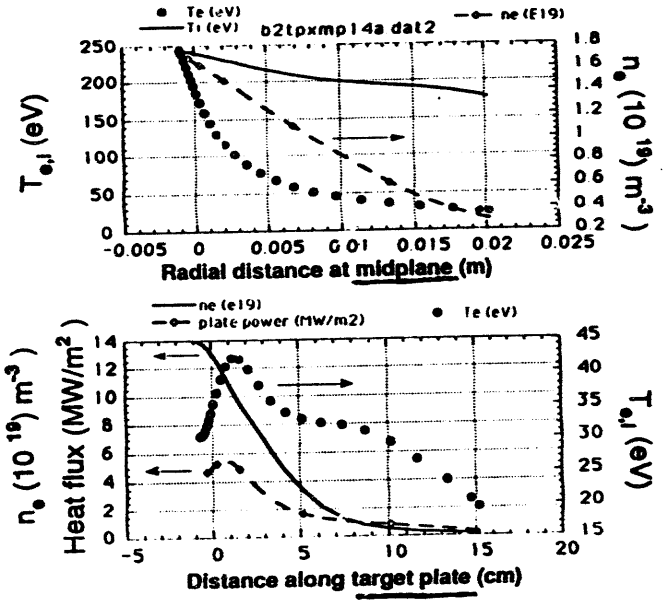

45 MW OPERATION WILL PRODUCE REACTOR-LIKE EDGE PLASMAS AND REQUIRE A RADIATIVE DIVERTOR

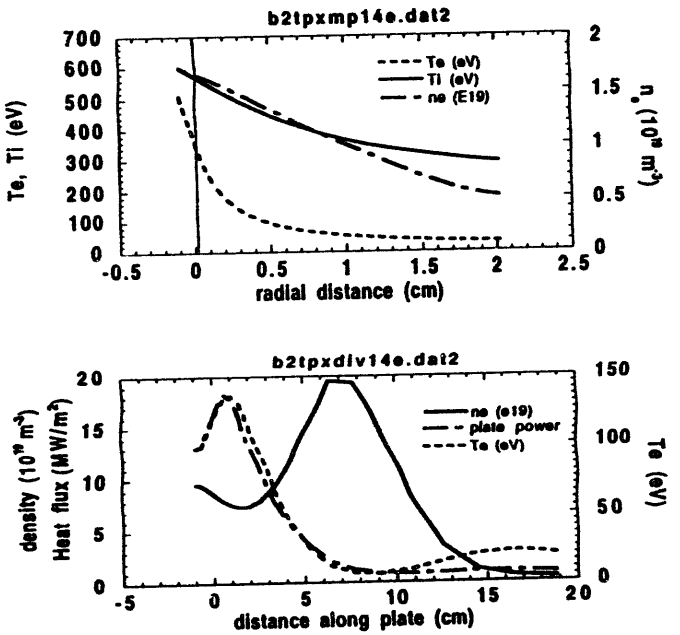

- Upstream values are comparable to those predicted for ITER.

TPX PLASMA FACING COMPONENTS

low activation

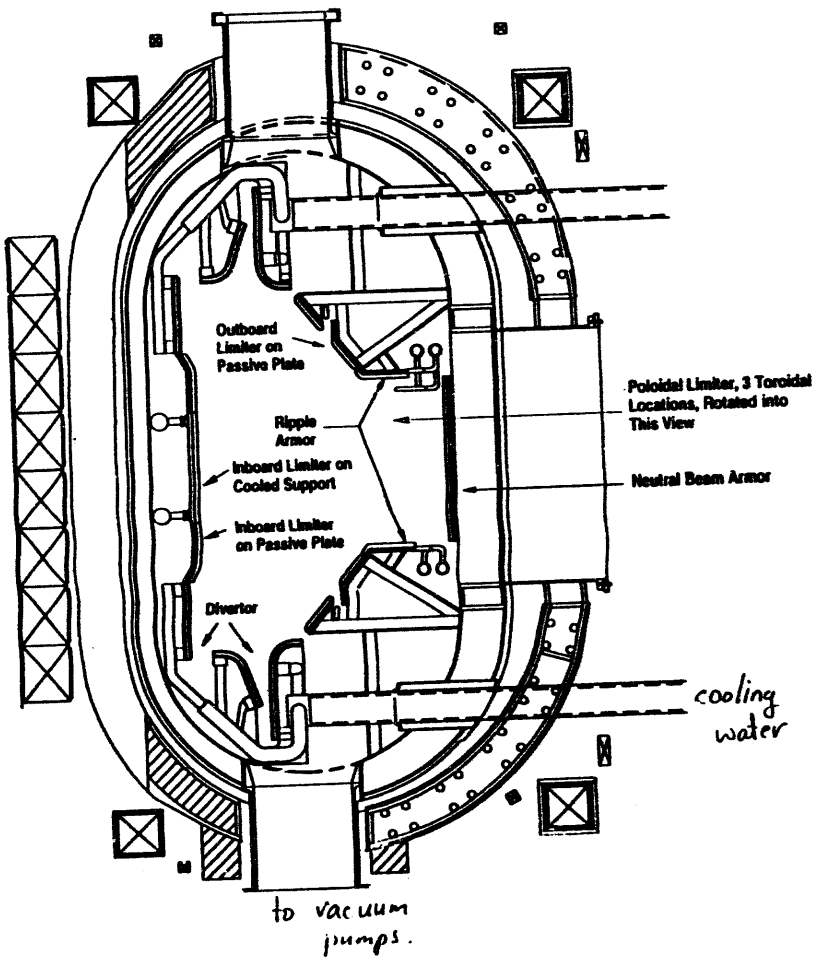

PFC PEAK DESIGN HEAT LOADS and MATERIAL CHOICES

Component	Peak Power for 18 MW (MW/m^2)	Peak Power for 45 MW (MW/m^2)
Divertor targets	15 (7.5)	15 (7.5)
Divertor baffle	4	4
Inboard limiter	0.15	0.4
@NBI strike point	1.45	1.7
Outboard limiters	0.15	0.4
Neutral beam armor	2.7	3.8
Ripple armor	0.72	2..1

- Active water cooling is required.
- Carbon–fiber composite materials are preferred for all high heat flux and disruption–damage locations:
  - — high thermal conductivity
  - — excellent disruption resistance
  - — low Z
  - — lots of operating experience
  - — longer erosion lifetime than Be

CFC MONOBLOCK CONSTRUCTION FOR HIGH HEAT FLUX DIVERTOR SURFACES

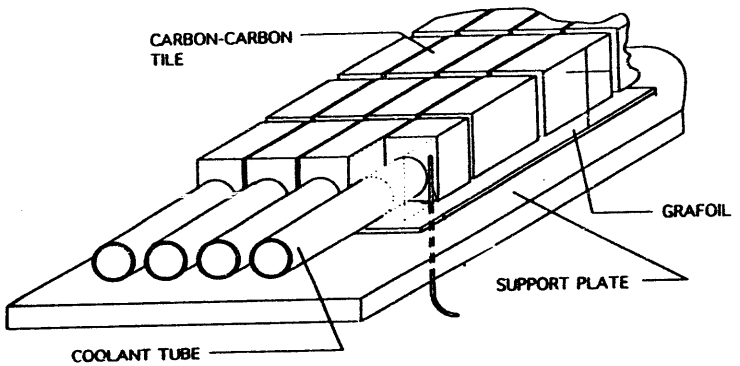

- Water-cooled copper tube for heat removal. Design for 15MW/m2 is difficult and will require extensive R&D program for material development, braze fabrication, and high heat flux testing. CDR result. Preliminary design will reexamine.

INBOARD LIMITER PANEL

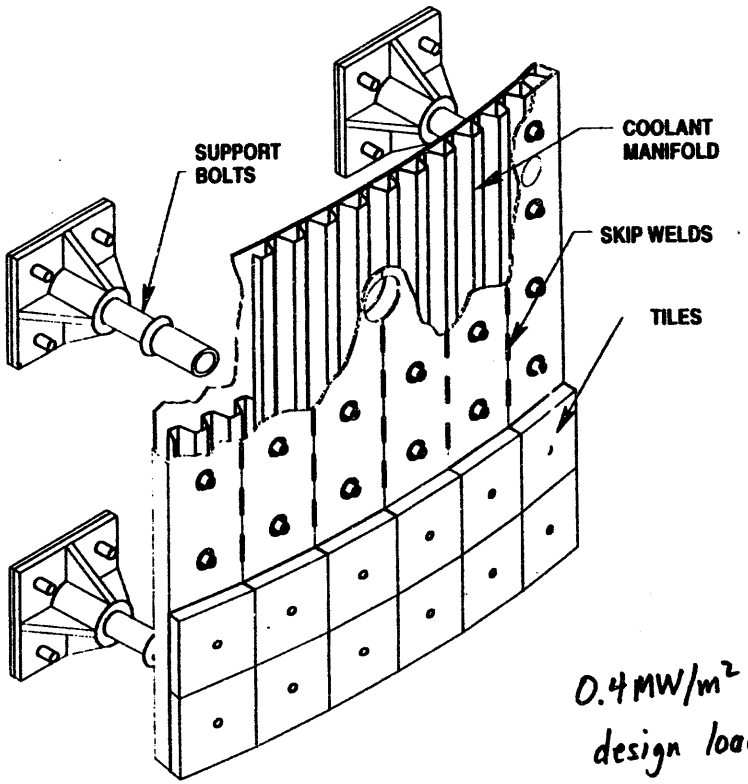

0.4 MW/m² design load.

GENERAL ATOMICS MCDONNELL DOUGLAS

IN-VESSEL MANIPULATOR
[SHOWN WITH TELEMATE (SM-229): DEXTROUS ARM]

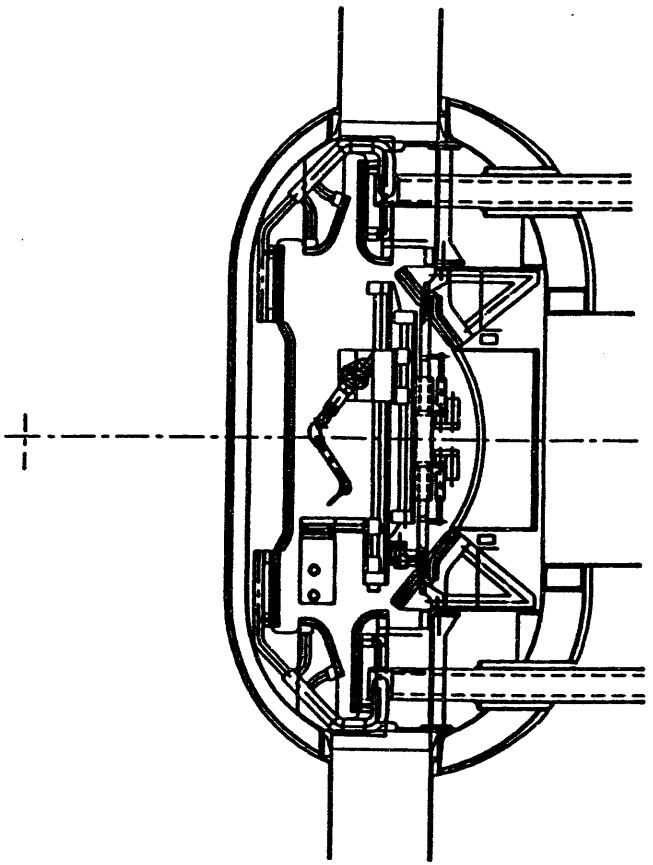

DIVERTOR-PLATE EROSION LIFETIME

- Erosion calculated using the REDEP code (Brooks, ANL), with plasma conditions in front of the surfaces obtained from the Braams b2 code.

- For the standard 18 MW operating scenario we have:
  - $T_e = 42$ eV, $T_i = 100$ eV, $T_{plate} = 1200$ C, and $n_e = 1.4 \times 10^{19}$ m^{-3}
  - 9.0×10^4 sec/mm for carbon
  - 1.3×10^5 sec/mm for beryllium
  - $>3.3 \times 10^7$ sec/mm for tungsten
  - expected operating time is $\leq 5 \times 10^5$ sec/year

- Note that the lifetime of a carbon divertor could be as much as twice as long as a beryllium divertor because the higher thermal conductivity of CFC allows for much thicker armor (10 mm vs. 3.5 mm).

WALL CONDITIONING

- We require that the TPX vacuum vessel be baked to 350° C.
- Based on experience from DIII-D, JT-60U, and JET, the operating temperature of the vessel will be below 150° C.
- Pulse discharge cleaning between shots is also being studied.
- Experiments with cryo-pumping inTore Supra and DIII-D show that it is possible to reduce the gas inventory in the carbon walls of the tokamak by pumping on the plasma during the pulse. This suggests that future long-pulse, actively pumped devices may not need preliminary GDC before the start of each discharge.

BASIC STRATEGY FOR DIVERTOR HEAT FLUX REDUCTION

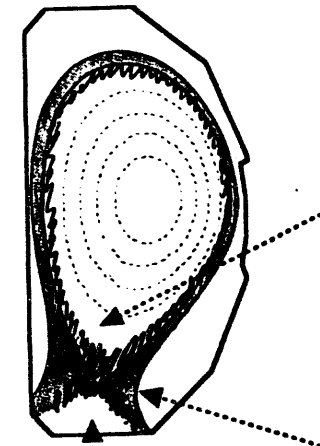

EDA ITER
200MW
20 cm
5MW/cm²

When the plasma temperature in front of the divertor targets falls below 10 eV, charge exchange can become an important loss mechanism.

Ion-neutral collisions reduce the plasma pressure and allow the SOL plasma to partially detach from the divertor targets.

The ability to have adequate particle exhaust for density control and helium ash removal under these conditions remains an issue.

GENERAL ATOMICS

Divertor Heat Flux Reduction is Sustained with Neon Injection

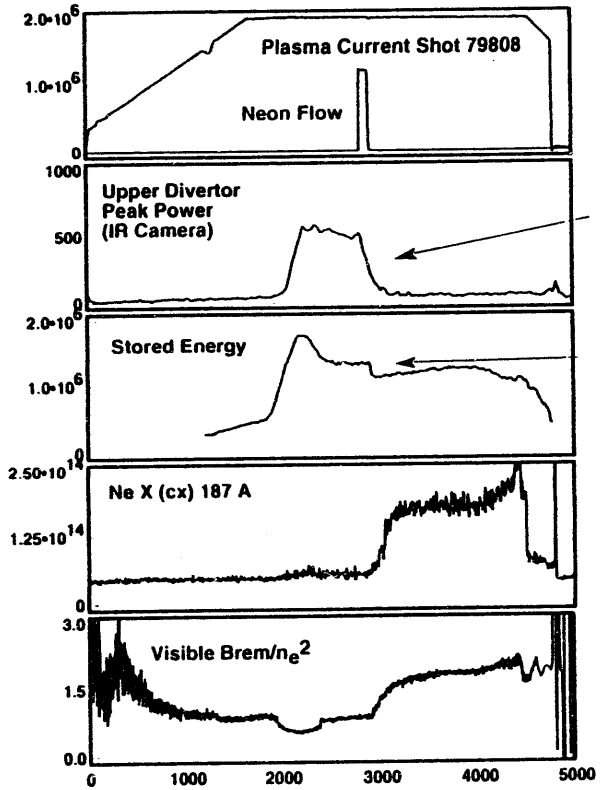

- Beam Power 14 MW
- Heat Flux Reduction
- Small Effect on Energy
- Core Neon Constant
- Vis. Brem. Increases

Radiation Profile for Radiative Divertor Neon Puffing

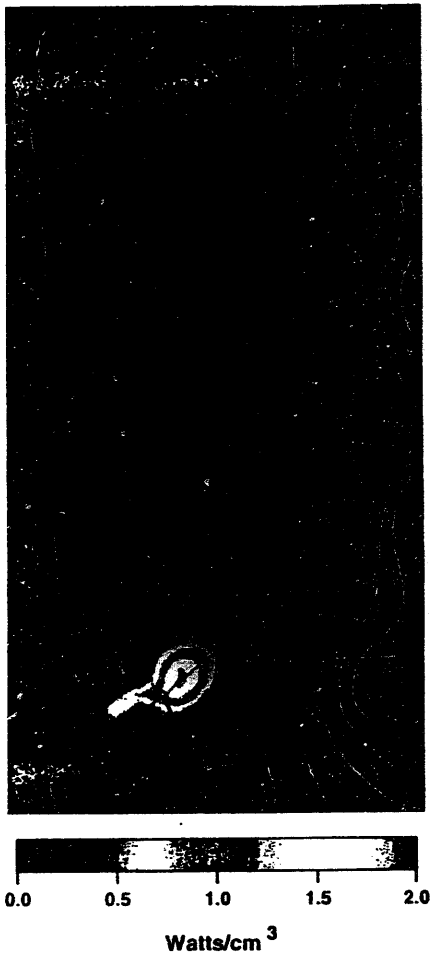

SUMMARY

- The TPX tokamak will test the compatibility of steady-state power and particle control techniques with advanced tokamak operation (non-inductive current drive with high beta and high confinement).

- A deep double-null divertor configuration is planned to enhance recycling at the target plate, spread out the heat flux, and facilitate pumping for density control.

- The carbon-carbon composite materials used for PFC construction should provide reliable operation with the initial heating complement, but considerable component testing will be required.

- High power operation will require active reduction of the peak divertor heat flux: i.e., a dissipative divertor concept. Such a concept is now being tested in operating tokamaks.

Session III

Recent PMI Results from Several Tokamaks

Results from the Initial D-T Experiments on TFTR

presented by

D. K. Owens
for the TFTR Group

TFTR Collaborations & Industrial Participants

PPPL

UNIVERSITIES
- Colorado School of Mines, Golden, CO
- Columbia University, New York, NY
- Cornell University, Ithaca, NY
- Courant Institute, New York University, New York, NY
- Georgia Institute of Technology, Atlanta, GA
- Massachusetts Institute of Technology, Cambridge, MA
- University of California, Los Angeles, CA
- University of California, Dan Diego, CA
- University of California, Irvine, CA
- University of Illinois, Urbana, IL
- University of Tokyo, Japan
- University of Wisconsin, Madison, WI

INDUSTRIES
- Burns and Roe Company, Oradell, NJ
- Canadian Fusion Fuels Technology Project, Canada
- Ebasco Services, Inc., New York, NY
- Fusion Physics and Technology, Inc., Torrance, CA
- General Physics Corporation, Columbia, MD
- Grumman Aerospace/Energy Systems Program, Bethpage, NY
- General Atomic, San Diego, CA
- Lodestar, Boulder, CO
- Radiation Science, Inc., Belmont, MA

LABORATORIES
- Environmental Measurement Laboratory, New York, NY
- Idaho National Engineering Laboratory, Idaho Falls, ID
- I.V. Kurchatov Institute of Atomic Energy, Russia
- Ioffe Physical-Technical Institute, Russia
- Japan Atomic Energy Research Institute, Japan
- JET Joint Undertaking, United Kingdom
- Lawrence Berkeley Laboratory, Berkeley, CA
- Lawrence Livermore National Laboratory, Livermore, CA
- Los Alamos National Laboratory, Los Alamos, NM
- Oak Ridge National Laboratory, Oak Ridge, TN
- Sandia National Laboratory, Albuquerque, NM and Livermore, CA
- Savannah River Plant, Aiken, SC

Overview of TFTR D-T Results

- Hardware modifications on TFTR for Tritium Operation are completed.
- The operation of the neutral beams in tritium was very successful.
- We have completed Phase I of our high power D-T experiments.
- It was observed during D-T injection that
  - the stored energy in the ion and electron channels increased
    - ⇒ improved plasma confinement
    - ⇒ indications of alpha heating
  - the fusion power was increased to 6.2 MW
  - there was no enhanced loss of alpha particles observed by the lost - alpha detectors.

TFTR Goals and Objectives for the D-T Experiments

Phase I Initial Tritium Experiments

Technical Objectives	Research Objectives
• Integrated Test of tritium systems Completed	• 5 MW of Fusion Power with NBI Completed
• Shipping of waste with Type A and B containers Completed	• Measure Escaping α's and test confined-α diagnostics Completed
• Evaluate diagnostic performance in high flux of 14 MeV neutrons Completed	• Measure tritium transport Completed
• Evaluate tritium retention Completed	

Phase II TFTR Tritium Experiments

Technical Objectives	Research Objectives
• Commission Tritium Purification System in tritium	• Confinement and heating in D-T plasmas
• ~ 20 high concentration tritium plasma shots every operational week	• Maximize fusion power and α driven effects
	• Document/evaluate α collective instabilities
	• Document/evaluate energetic α transport
	• Evaluate RF heated and pellet fueled plasmas for different modes of operation in DT plasmas

Fusion Power of 6.2MW has been achieved on TFTR

TFTR

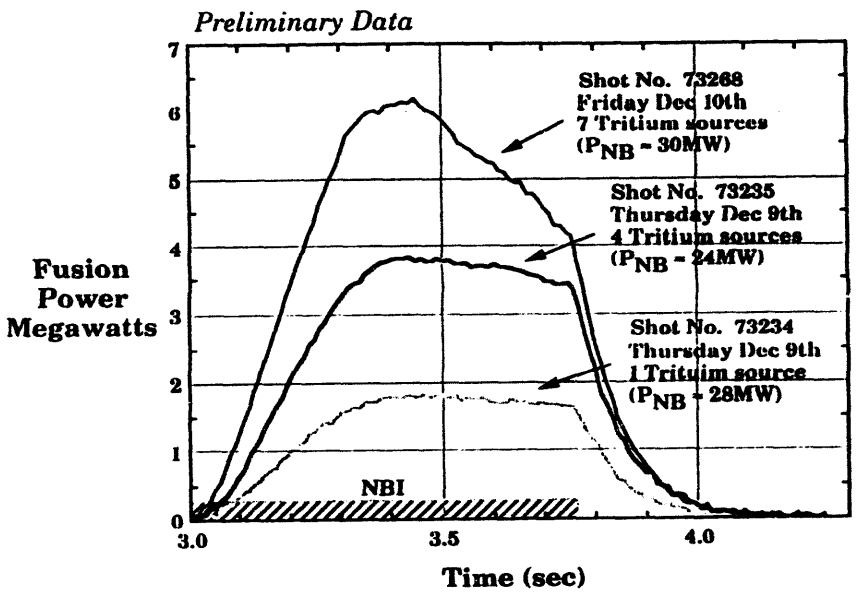

L. Johnson
J. Strachan

Calculated Neutron Emission Components

Experimental Proposal DT-7
Fusion yield ~ 6.2 MW

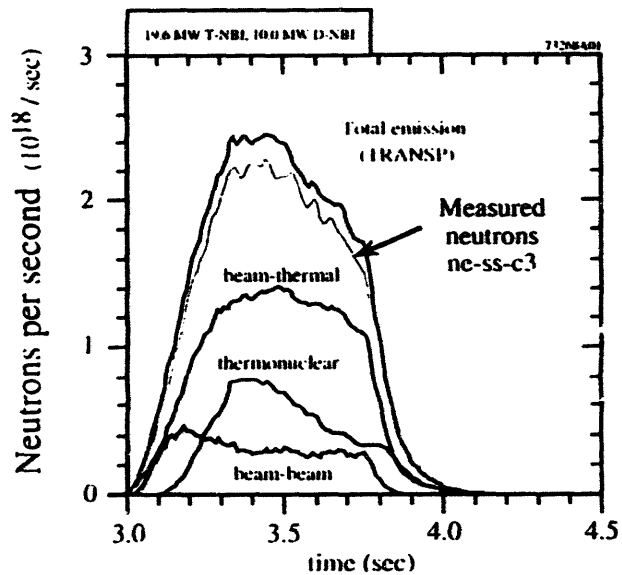

- Neutron emission is ≈ 30% thermonuclear reactions

B. Budny

The Fusion Power Density in the Core of TFTR is Comparable to ITER

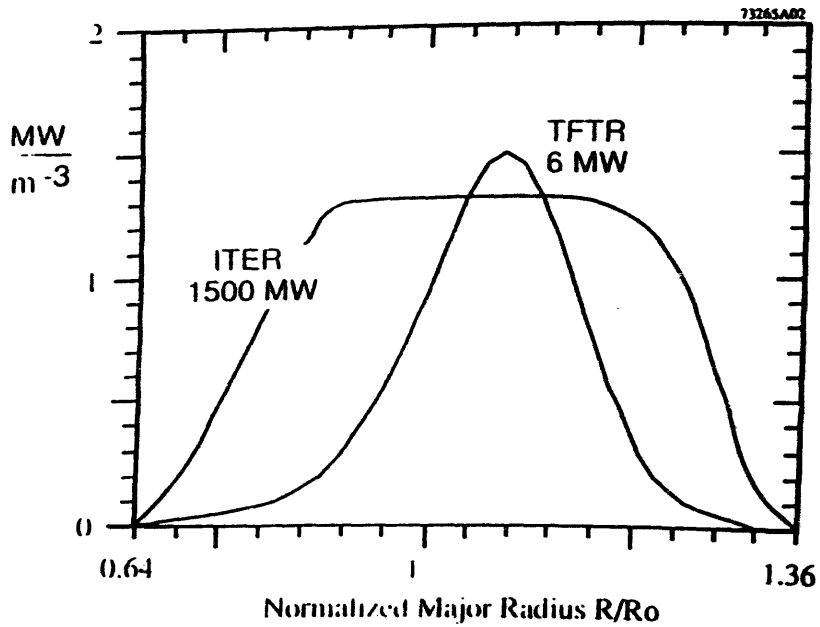

The Stored Energy Increased in the D - T Plasma

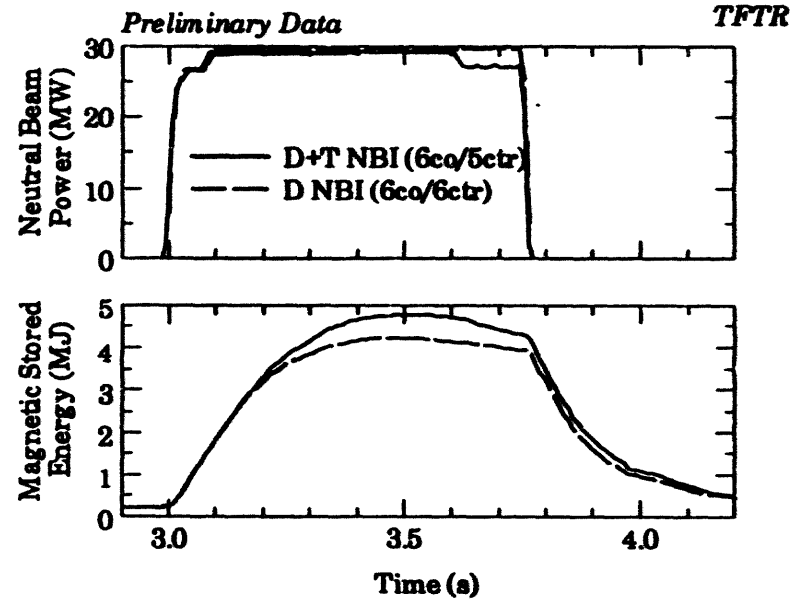

- Increased confinement time in D - T.
- Possible isotope scaling in D - T plasma.

M. Bell

Ion Temperature appears to increase during D-T operation

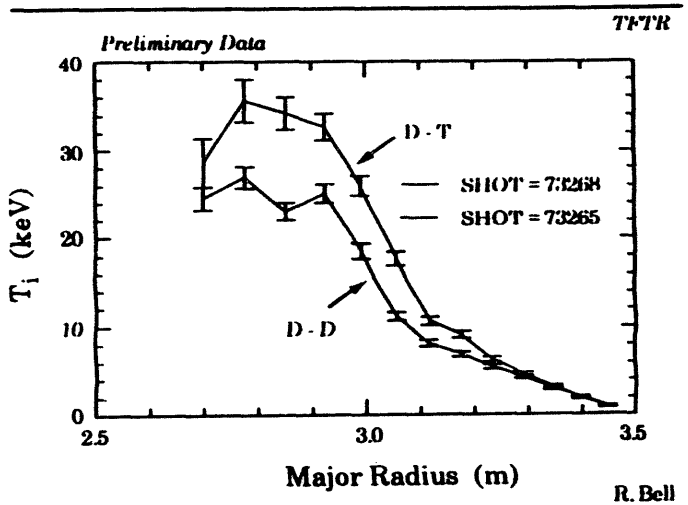

- χ_i decreases by a factor of 2

R. Bell
C. Bush ORNL
E. Synakowski

Electron Temperature increased during D-T operation

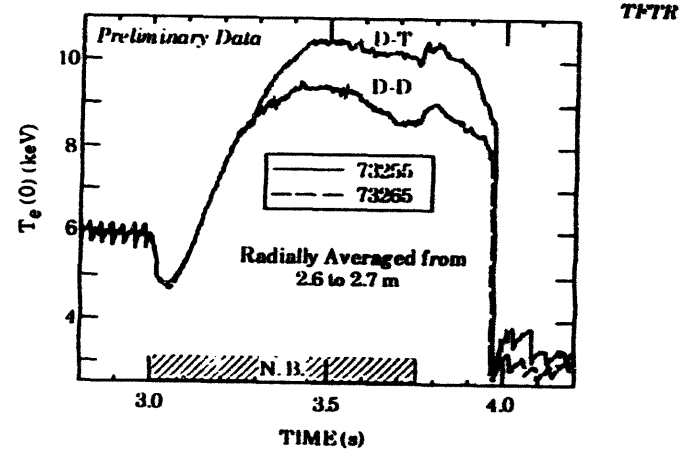

- Is this Alpha heating or isotope scaling?

G. Taylor

Abel Inverted D - T Neutron Profile

Preliminary Data TFTR

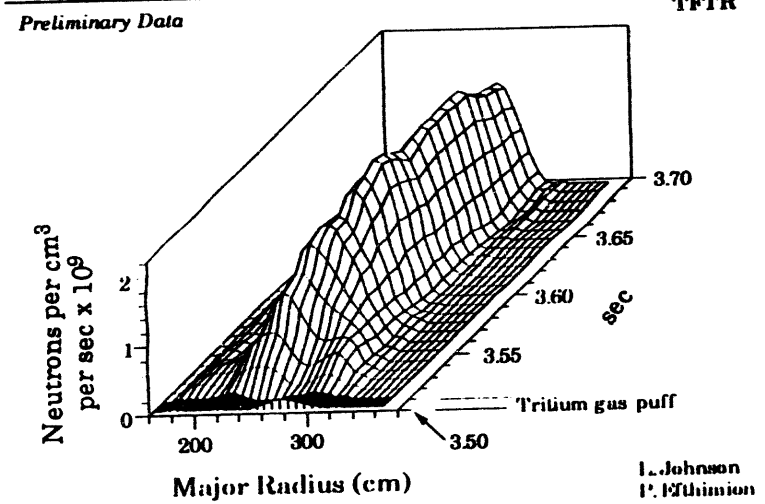

L. Johnson
P. Efthimion

Measured Alpha loss for TFTR D-T experiments

Preliminary Data TFTR

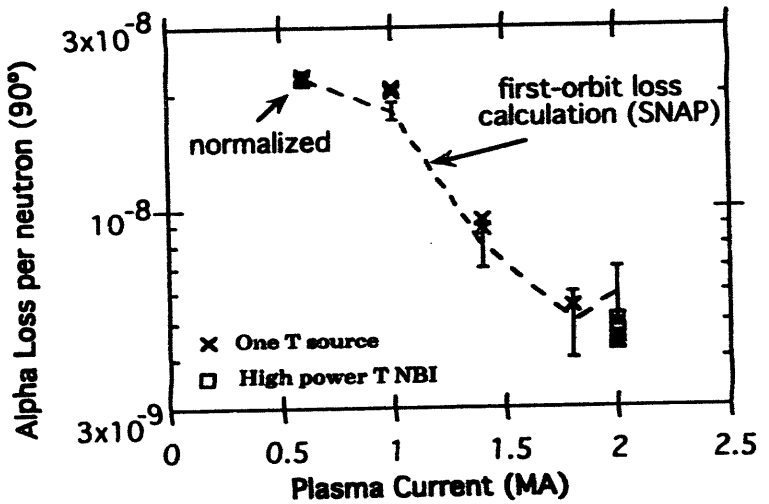

- Good agreement between measured and calculated alpha loss

S. Zweben
D. Darrow

Alpha loss does not increase strongly with Fusion Power

TFTR

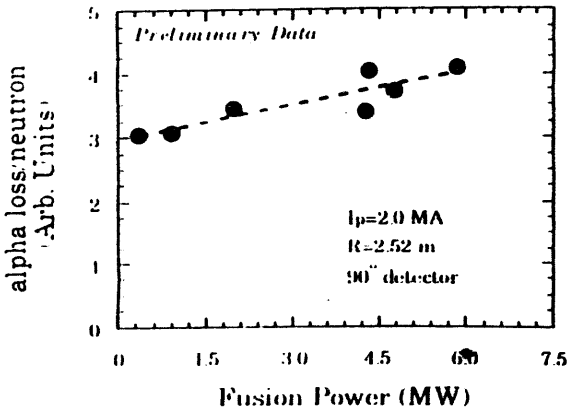

S. Zweben
D. Darrow

Alpha driven TAE instability signature not observed in the D-T plasmas

Preliminary Data

TFTR

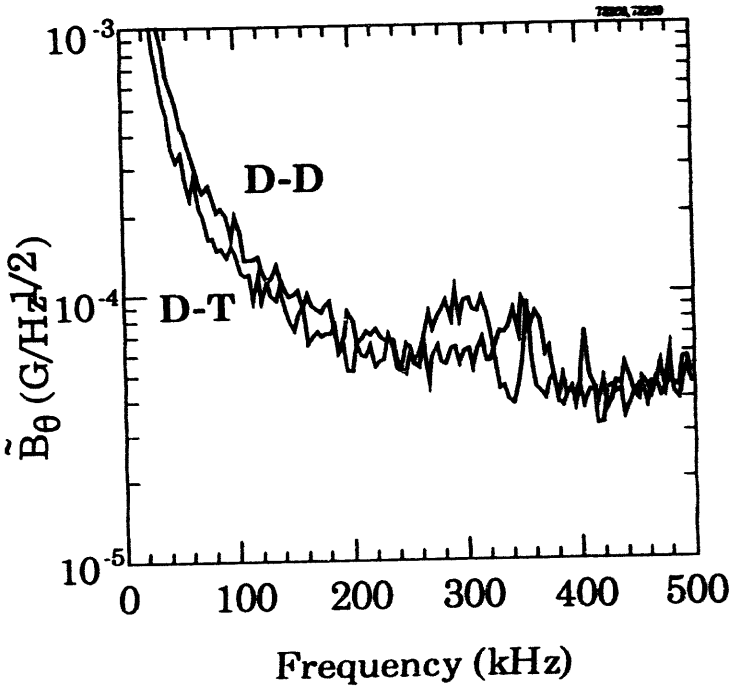

- TAE mode is excited by neutral beams with $V_f / V_A \geq 0.2$

E. Fredrickson

Future Plans

- Start Phase II of the D-T Plan
  - Clarify physics issues such as:
    - confinement in D-T plasmas
    - alpha driven instabilities
    - alpha heating while producing fusion reactor power densities
    - alpha ash buildup
    - ICRF heating of a D-T plasma

Summary

1. Significant differences were observed in confinement time in going from D-D to D-T plasma.
2. We obtained $P_{fusion} \approx 6.2$ MW with $P_{\alpha} \approx 1.2$ MW.
3. Confined alpha diagnostics are operational.
4. No enhanced loss of alpha particles was observed
   - Profile maybe stable to TAE modes.
5. From trace tritium experiments we will be able to obtain D and V for the tritium transport.

US–Japan PMI–HHF Workshop
January 24–27, 1994, San Diego, CA, USA

PFC AND PSI STUDIES ON TRIAM–1M

N. YOSHIDA

Research Institute for Applied Mechanics
Kyushu University
Japan

OUTLINE

1. **Present Status of TRIAM–1M and Plans of PSI Experiments in 1994–1995**

2. **Performance and Issues of High–Z (Mo) PFC used in TRIAM–1M and JT–60**

3. **Preliminary Results of High Heat Flux Experiments of C/C Composite**

PRESENT STATUS OF TRIAM-1M

1. Repair and Improvement

- shutdown in June 1992
- Repair of some poloidal field coils, etc.
- Addition of divertor (single X point configuration)
- Improvement of mobile limiter (Mo cover)

2. Schedule

- Installation on January 19, 1994
- Start of Operation in August 1994

3. Expected Plasma Parameters
(LHCD 8.2GHz, 200kW)

- Density $\geqq 4 \times 10^{13}$ /cm^3
- Discharge duration time $\geqq$ 60s

DIVERTOR PLATE OF TRIAM-1M

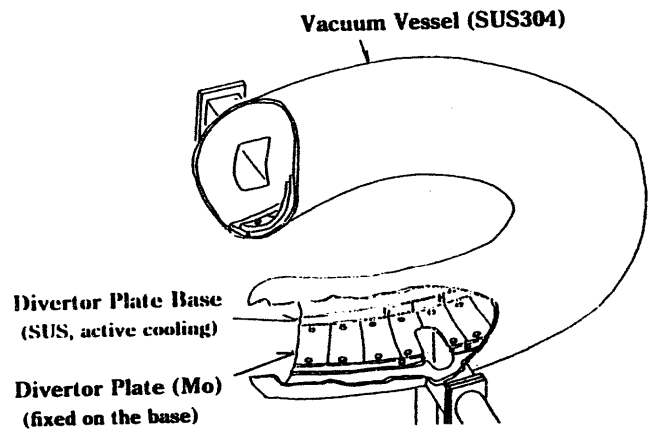

DIVERTOR PLATE OF TRIAM–1M

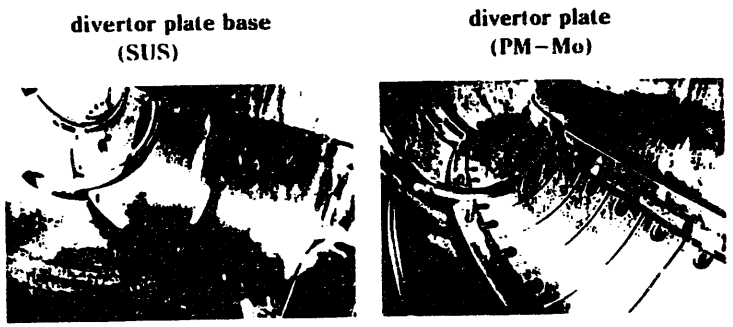

PSI EXPERIMENTS IN 1994–1995

- **Macroscopic Damage Analysis of Divertor Plate**
  - –identification of impurity sources and its mechanism
  - –material performance under high density long pulse operation
- **Time Resolvable Collector Probe Experiments**
  - –behavior of impurities under long pulse discharge
    surface analysis (SIMS, AES)
  - –radiation effects of energetic particles
    damage structure observation (TEM)
    measurement of retained hydrogen (SIMS, TDS)
- **High Heat Loading Test Using Mobile Limiter**
  - – evaluation and development of HHFM
    Mo → Mo Alloys → C/C composite
    long pulse operation

TRIAM–1M MOBILE LIMITER

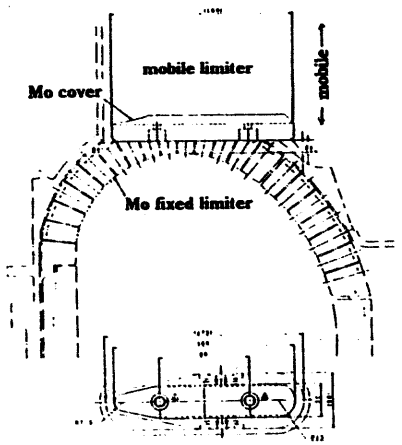

- Mo plate fixed on SS base
- Forced cooling
- TC fixed on SS base
- TV monitoring

SUBJECTS

- Behavior of impurities in plasma
- Material test
  Mo → Mo alloys → C/C
- Steady state heat removal
  (preliminary experiment of LID project)

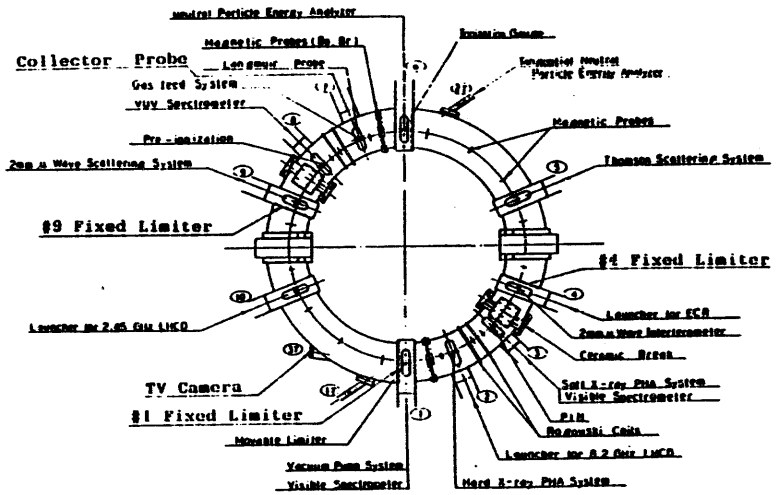

PERFORMANCE OF HIGH–Z MATERIALS

Examined PFC

- **TRIAM–1M Poroidal Fixed Limiter (long pulse discharges)**
  PM–Mo (Tokyo Tungsten Co.)

- **JT–60 Divertor and Limiter (1985.5–1987.3)**
  TiC coated PM–Mo (Plansee Co.)

DAMAGE OF MO–LIMITER (Inner Limiter, E–side)

Initiation of cracking at the grain boundaries (emblittlement at the G.B.)
high heat load → grain growth & recrystalization (above 1200 °C)
→ reduction of intergranular strength

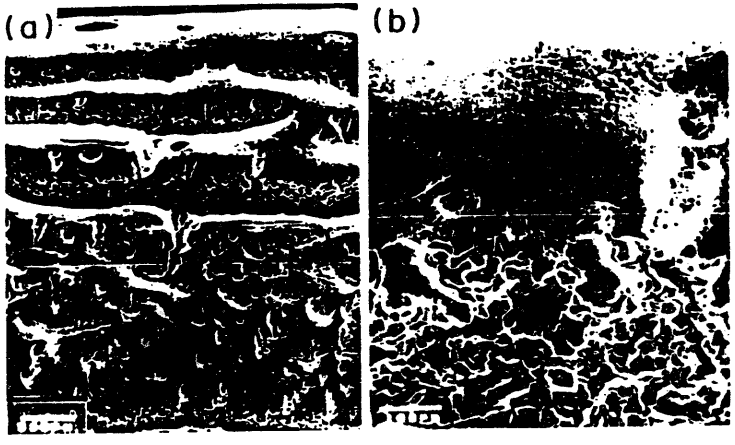

JT−60 TiC/Mo LIMITER

- Melting and Alloying (Mo−Ti (−C))
- Intergranular fracture

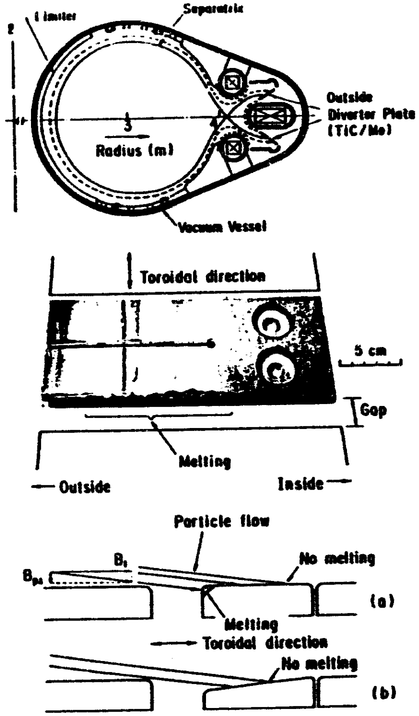

図6 TiC/Moダイバータ板の端部熱集中と溶融[13]

JT-60 TiC/Mo DIVERTOR (5U-18)

Top Surface

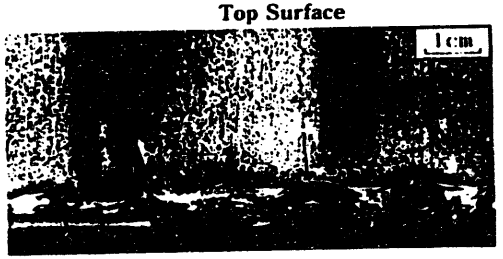

Front Surface

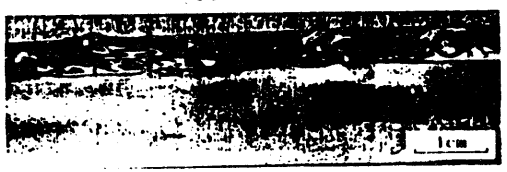

- high HF concent. at the edge
  - −top surface: 13−20MW/m^2
  - −front surface: 140−200MW/m^2
- melting at the edge
- large crack parallel to the top surface
  - −initiation of crack intergranular fracture

3D FEM THERMAL STRESS ANALYSIS

(W.X. Wang et al.)

Block Subjected to Local Thermal Shock

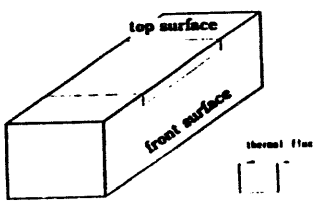

Finite Element Meshes

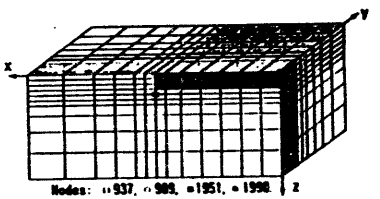

Fig 2 Finite element meshes of size: 50 × 25 × 20 mm, elements: 1560, nodes: 2002, deep shadow area: 25 × 3 mm and impinging energy flux = 200MW/m^2, light shadow area: 25 × 25 mm and impinging energy flux =20MW/m^2.

MO PROPERTIES AND TEMP. VARIATION

Table 1 Properties of Molybdenum

Density kg/m³	Coeff. of thermal expansion 1/℃	Heat conductivity cal/(m sec ℃)
1.022×10^{-4}	5.1×10^{-6}	3.29×10^{-2}
Specific heat	**Young's modulus**	**Poisson's ratio**
59cal/(kg℃)	3.3×10^{4}kgf/mm²	0.30

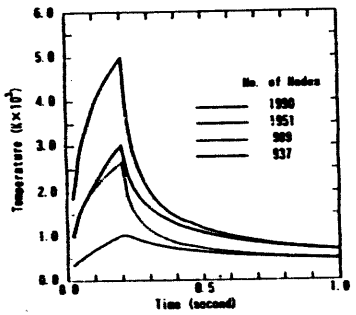

TEMPERATURE DISTRIBUTION

z=0.5mm section (T.S.)

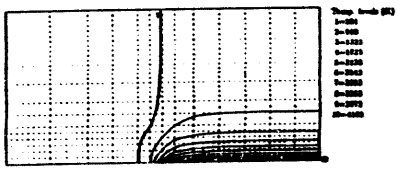

x=0.5mm section

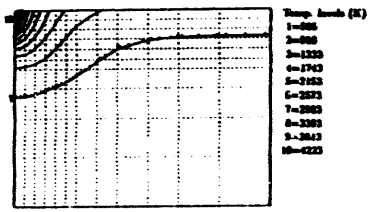

y=0.5mm section (F.S.)

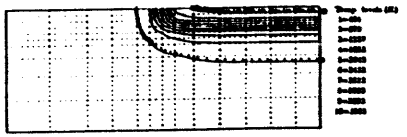

CRACK PERPENDICULAR TO X–AXIS

JT–60 TiC/Mo Divertor

View from Top Surface

Surface of Crack

ELASTIC THERMAL STRESS ANALYSIS

Thermal Stress Distribution

(Ef =200MW/m², Et =20MW/m², t=0.2sec)

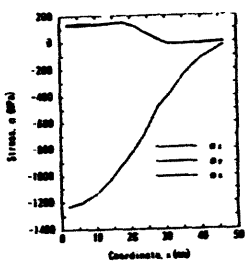

along x direction
y=z=2.5mm

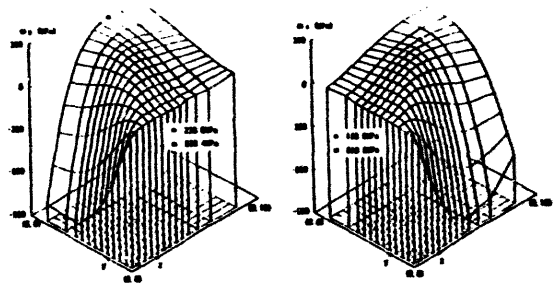

distribution on the symmetry section of x=0

ISSUES OF PM-MO AS HIGH HEAT FLUX COMPOMENT

(1) EMBRITTLEMENT

* anisotropy of strength of hot-rolled PM-Mo
  (low elongation perpendicular to the direction of the hot rolling)
* recrystallization of surface layer by heating above 1100-1200 ℃ (pure Mo)
  → reduction of intergranular strength
  → easy initiation of cracks along grain boundaries by low thermal stress

(2) CRACKING

→ increasing of surface temperature due to reduction of thermal transfer
→ enhancement of melting , evaporation and cracking

DAMAGE SCENARIO OF BRITTLE MATERIALS BY HEAT LOADING

Heat Loading → Recrystalization
→ Embrittlement at grain boundaries
→ Cracking
→ Melting / Evaporation

COUNTERPLANE AGAINST EMBLITTLEMENT

(1) Increasing of recrystalization temperature:

critical heat load for recrystalization in pure Mo (Tr ~ 1200 ℃) :
15MW/ m^2 , 30sec ← EB bombardment experiment

* addition of carbite, oxide and nitride former (Ti, Ce, Th, etc)
  ····· TZM (Tr=1300-1400 ℃)
* addition of rare earth metals
  ····· TEM (Tr=1200-1800 ℃)
* addition of TiC ····· (Tr=1800-2000 ℃)

(2) Mo-Re Alloy (Rhenium Alloying Effect)

SURFACE MODIFICATION DUE TO HEAT LOADING

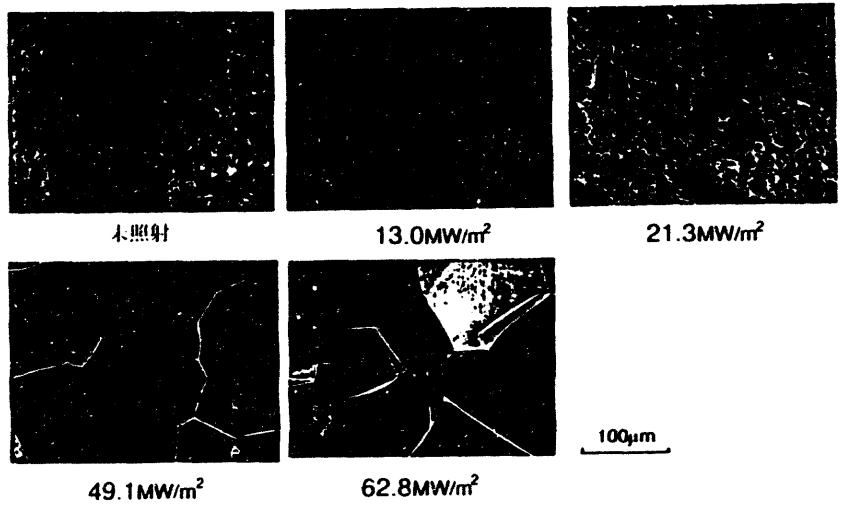

MAXIMUM TEMPERATURE REACHED BY HEAT LOADING

--Electron Beam Bombardment Experiment (20keV, 30sec)--

Material: PM-Mo

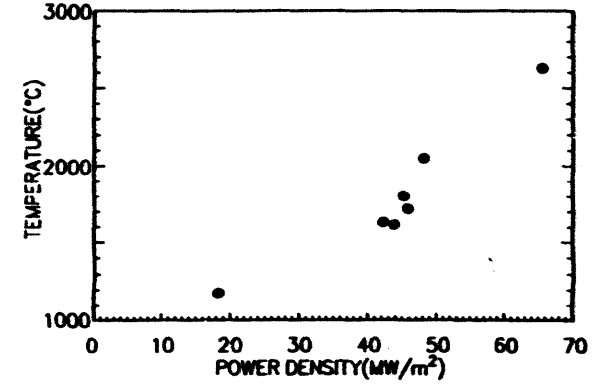

HEAT FLUX DEP. OF EMITTED PARTICLES FROM CX2002U BY E.B. IIEATING

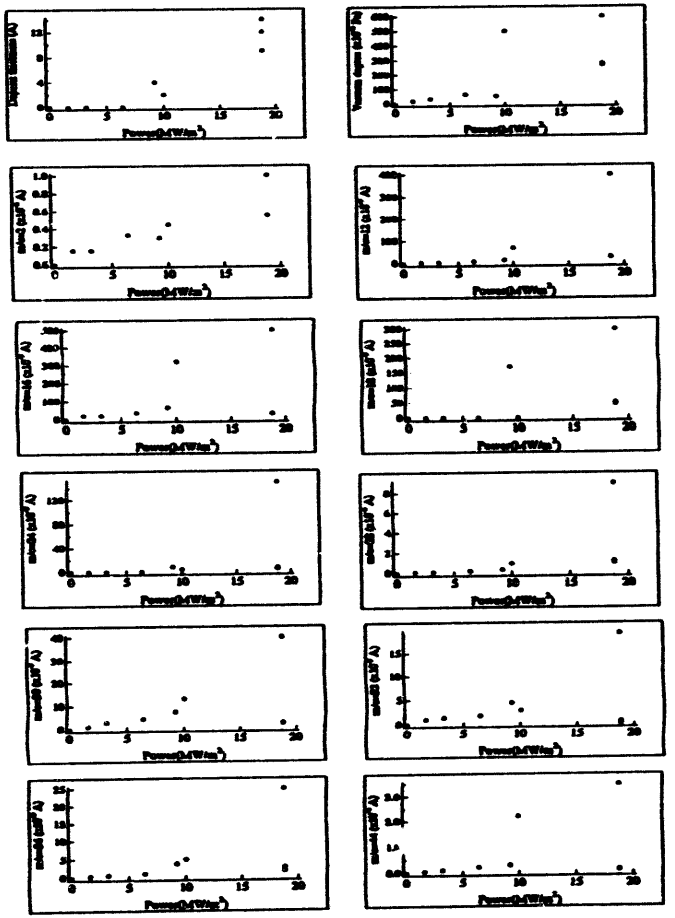

MASS ANALYSIS OF EMITTED PARTICLES FROM C/C BY ELECTRON BEAM HEATING

- Sample: CX2002U
- Heat Flux: 1.6–18.8MW/m^2
- Beam Diameter: 8mm ϕ
- Beam Energy: 20keV

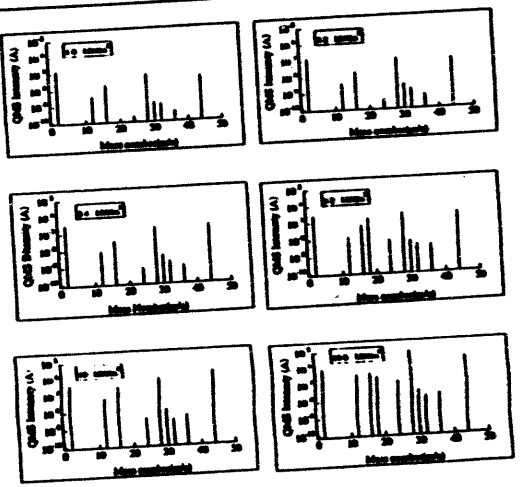

HEAT FLUX DEP. OF EMITTED PARTICLES FROM CX2002U BY E.B. HEATING

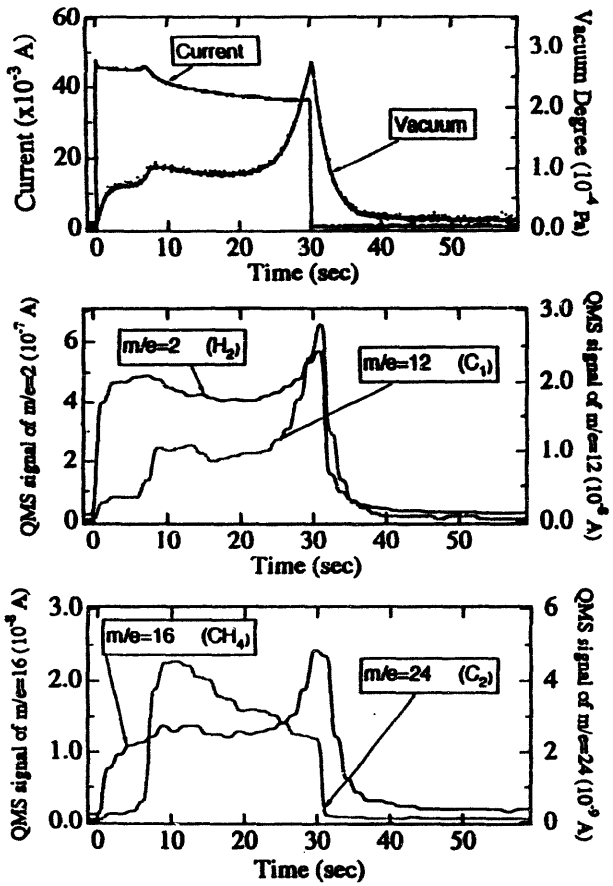

QMA OF EMITTED PARTICLES FROM CX2002U BY E.B. HEATING (9.2MW/m^2)

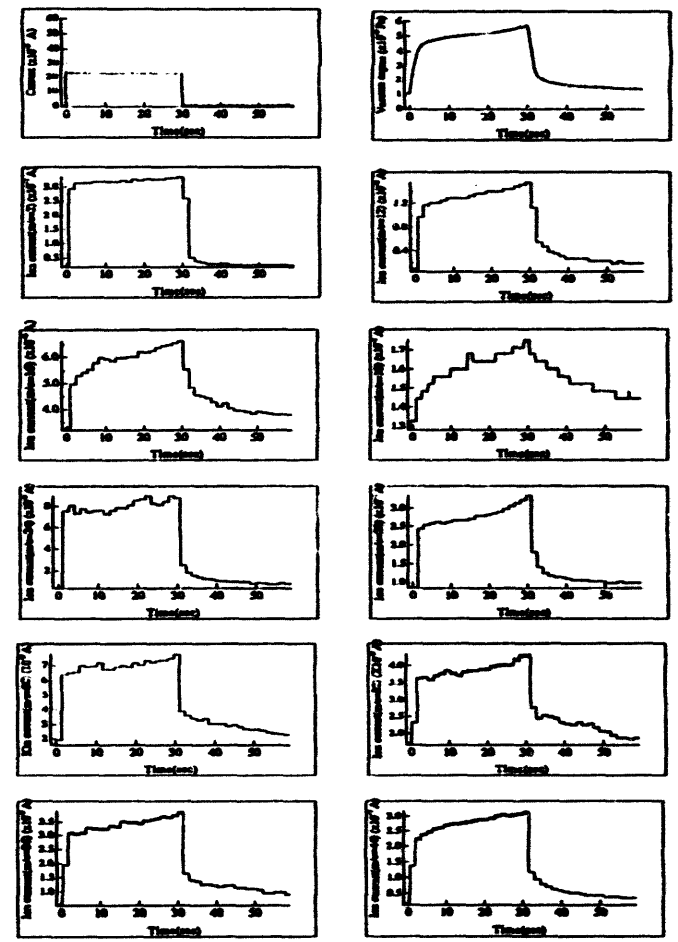

Initial Results from Alcator C-Mod

Outline:

Alcator C-Mod Overview & Current Status

First Results from Divertor Experiments

Plans for Next Run Period

presented by B. LaBombard
for the M.I.T. Alcator Group
at the U.S./Japan HHF/PMI Workshop, San Diego California,
January 24-27, 1994

Alcator C-Mod Crossection

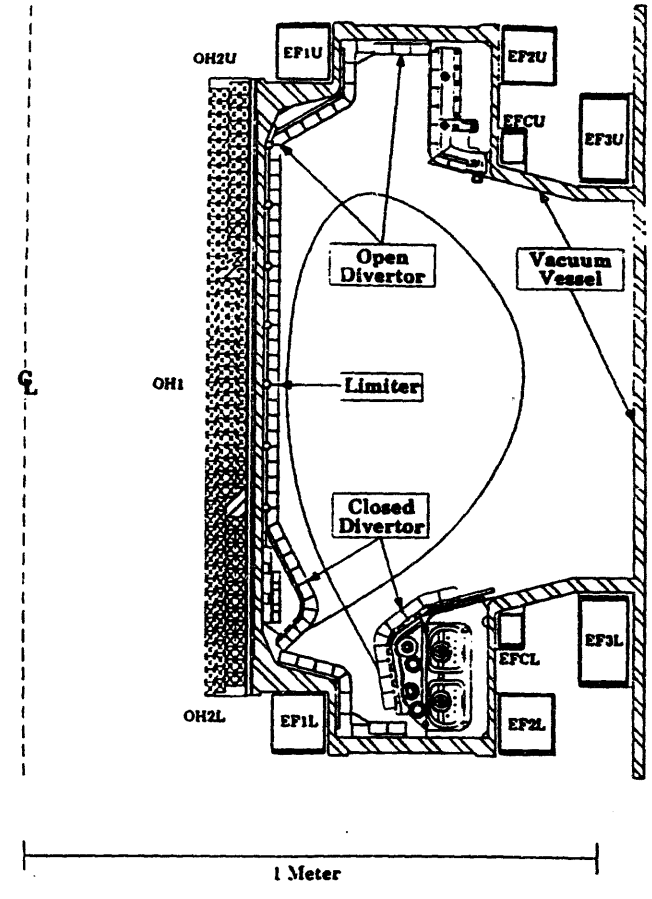

Alcator C-Mod Schedule

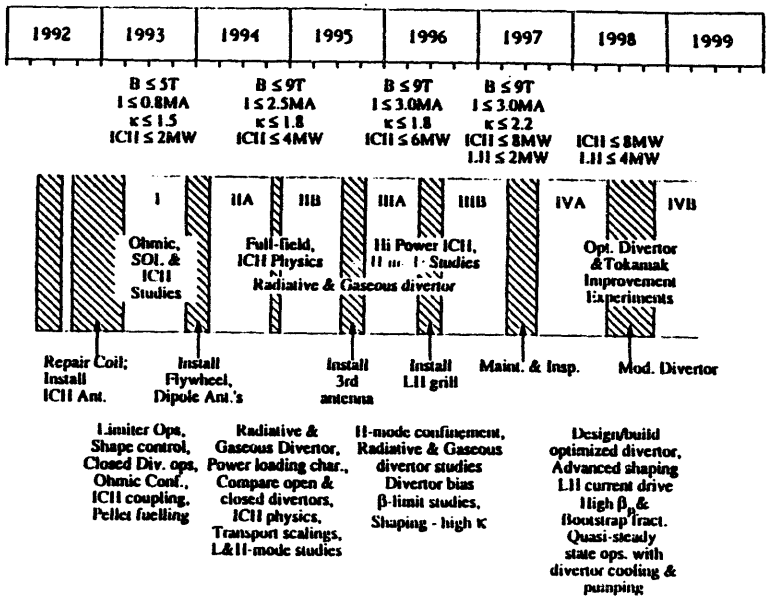

Unique Characteristics of Alcator C-Mod → **Related areas of research**

- Closed divertor geometry
- High density

→ Radiative divertor; $P_{rad} \propto n_e n_z$

→ Gaseous divertor; $P_{cx} \propto n_e n_n$

→ Compare 'closed' vs. 'open' geometry

→ Impurity Retention

→ Edge physics database

- Highly inclined divertor plate → Reduce heat loads

- High-Z first wall → Density Control

→ Reactor relevant material

- Unlike lower-field tokamaks, P_{sep} is not limited by central plasma beta.

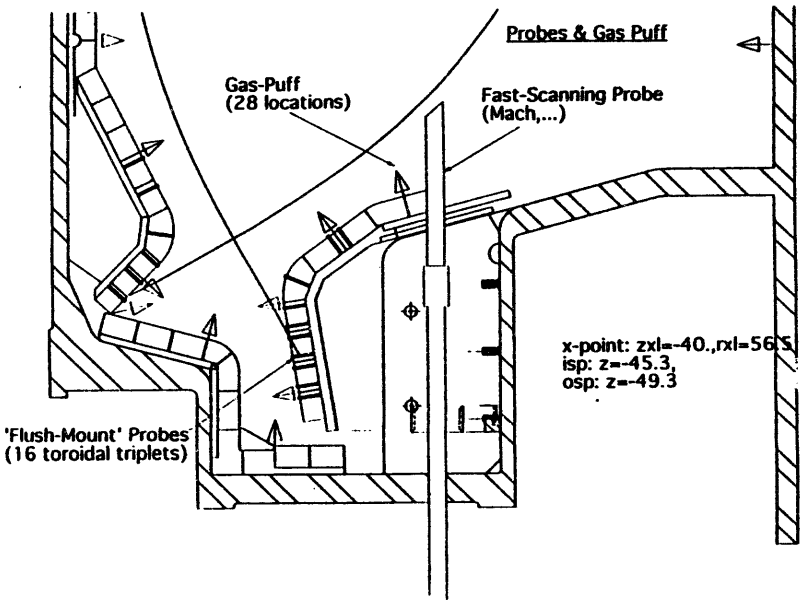
Probes & Gas Puff
Gas-Puff
(28 locations)
Fast-Scanning Probe
(Mach,...)
x-point: zxl=-40.,rxl=56.5
isp: z=-45.3,
osp: z=-49.3
'Flush-Mount' Probes
(16 toroidal triplets)

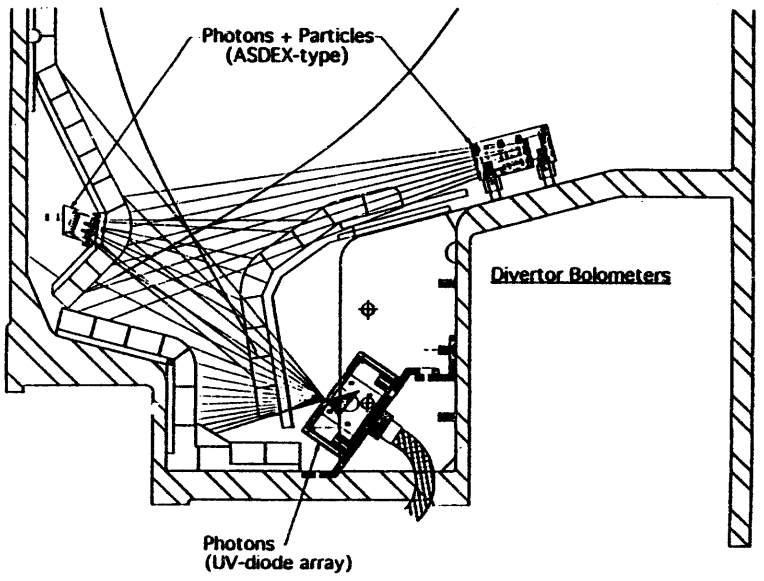
Photons + Particles
(ASDEX-type)
Divertor Bolometers
Photons
(UV-diode array)

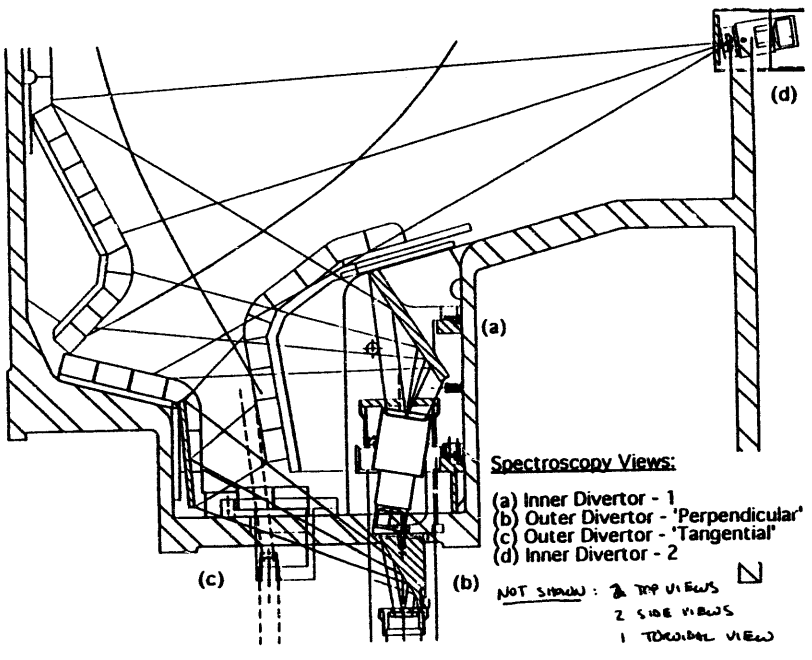

FIRST RESULTS:

OUTLINE

- NORMAL DIVERTOR
  → "RADIATIVE DIVERTOR"
- DETACHED DIVERTOR
- IMPURITY MEASUREMENTS

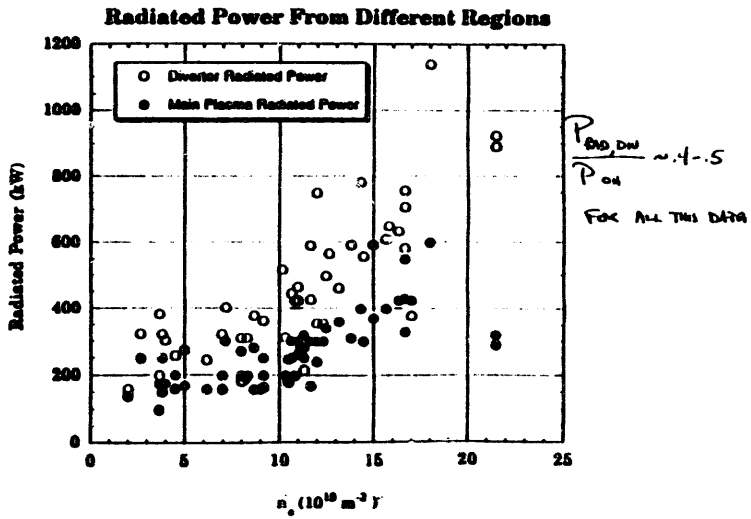

$\frac{P_{RAD,DIV}}{P_{OH}} \sim .4-.5$

FOR ALL THIS DATA

J. GOETZ
B. LIPSCHULTZ

RADIATIVE DIVERTOR CHARACTERISTICS

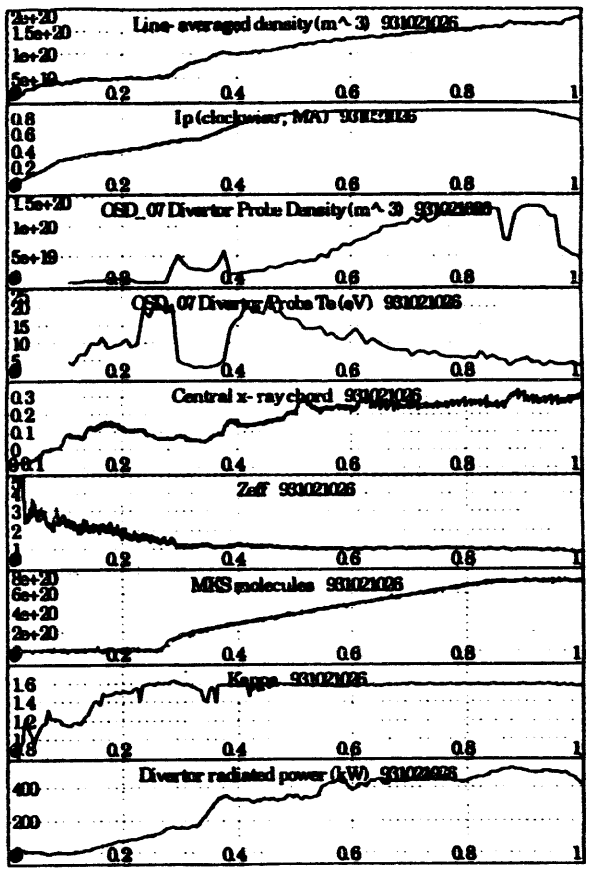

→ $n_{e,DIV}$ HIGH, $T_{e,DIV}$ LOW

→ Z_{eff} LOW

→ $P_{RAD,DIV} \sim .4 \times P_{IN}$

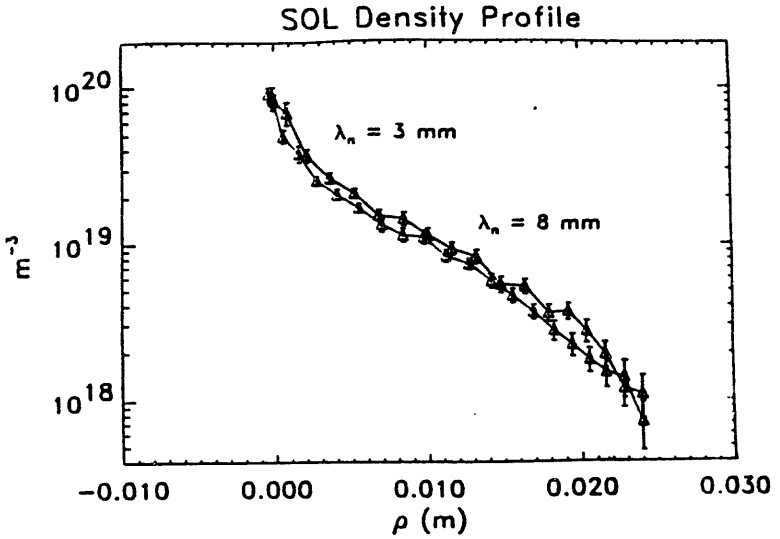

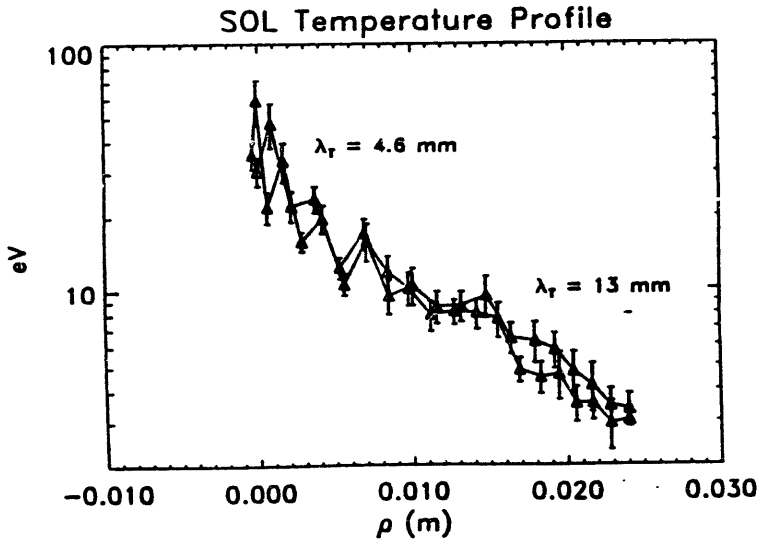

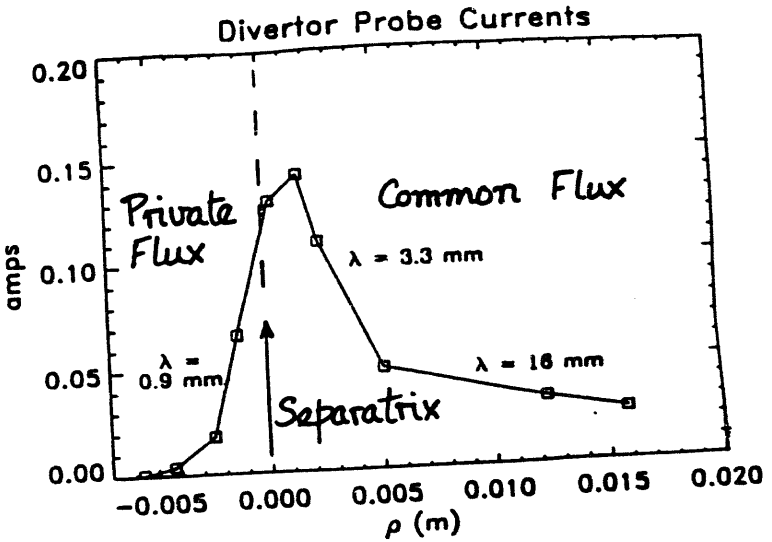

Flushmount probes in the outer divertor provide profile of the strikepoint current, mapped to the distance from separatrix.

Private flux region thickness << common flux.

B. LaBombard

Radiative Divertor Characteristics

- Radiation near the inner & outer divertor surfaces accounts for ~ .4 - .5 x P_{OH}.
- High recycling -> $n_{e,sep}$ can be high; 3 - 6 x10^{20} m^{-3}
- Radiation dominated by C, O & H
- Mo source rate normally insignificant in the divertor
- SOL profile fairly steep with two e-folding lengths 'near' and 'far' from the separatrix
  - $\lambda_{n,\,near}$ typically ≤ 5 mm
  - $\lambda_{n,\,far}$ typically ≥ 8 mm
  - λ_T ~ 1.5 - 2 x λ_n
- Pressure ~ const. along flux surface from SOL to divertor.

'Detached' Divertor

- ➥ Induced by D_2 or He puffing in the divertor or main chamber.
- ➥ Abrupt drop in divertor ion current near separatrix
- ➥ Rearrangement of the strong divertor radiation
- ➥ Profiles of n_e, T_e in SOL flatten

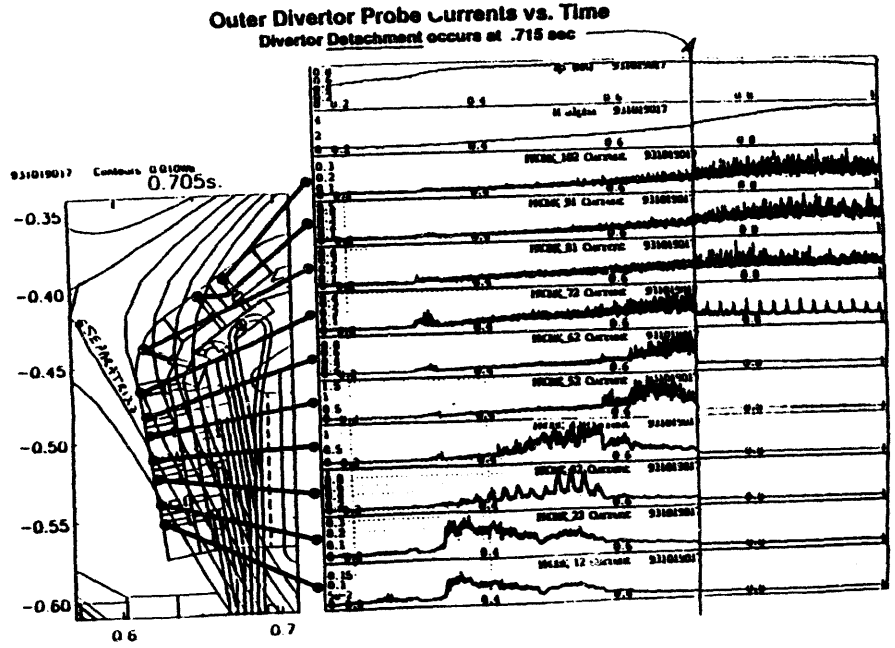

DIVERTOR PARAMETERS BEFORE & AFTER DETACHMENT

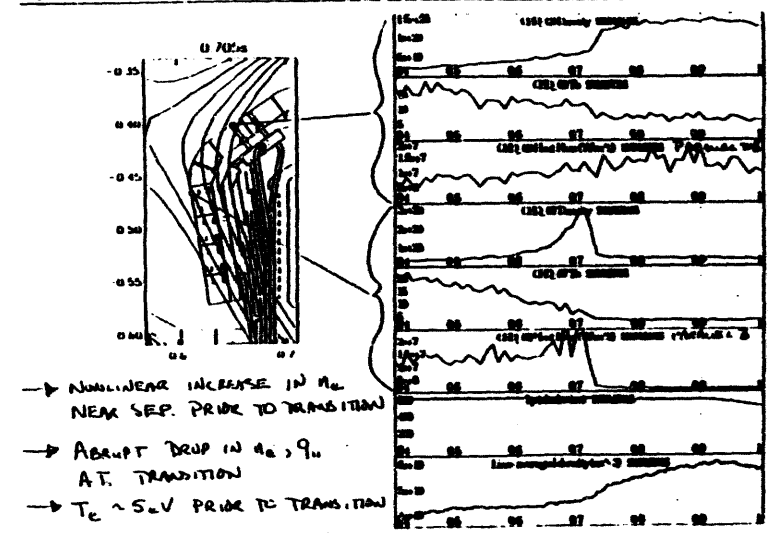

→ NONLINEAR INCREASE IN n_e NEAR SEP. PRIOR TO TRANSITION

→ ABRUPT DROP IN $q_e > q_H$ AT TRANSITION

→ $T_e \sim 5$eV PRIOR TO TRANSITION

B. LaBombard

REARRANGEMENT OF CIII RADIATION DURING DETACHMENT

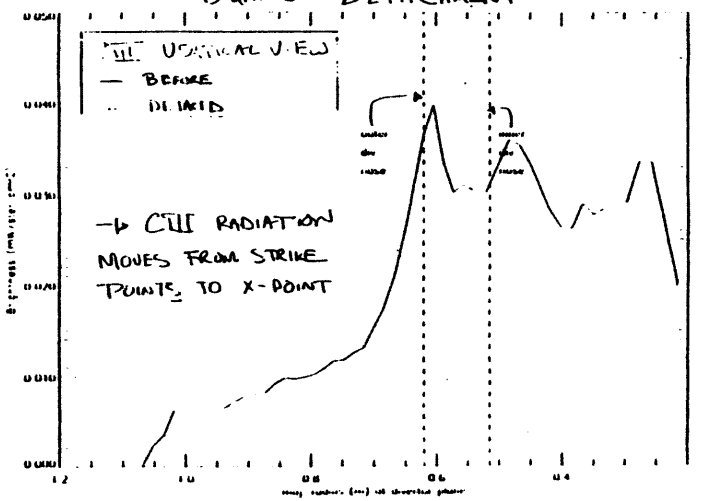

J. GOETZ
B. LIPSCHULTZ

RADIATION PEAK MOVES UP

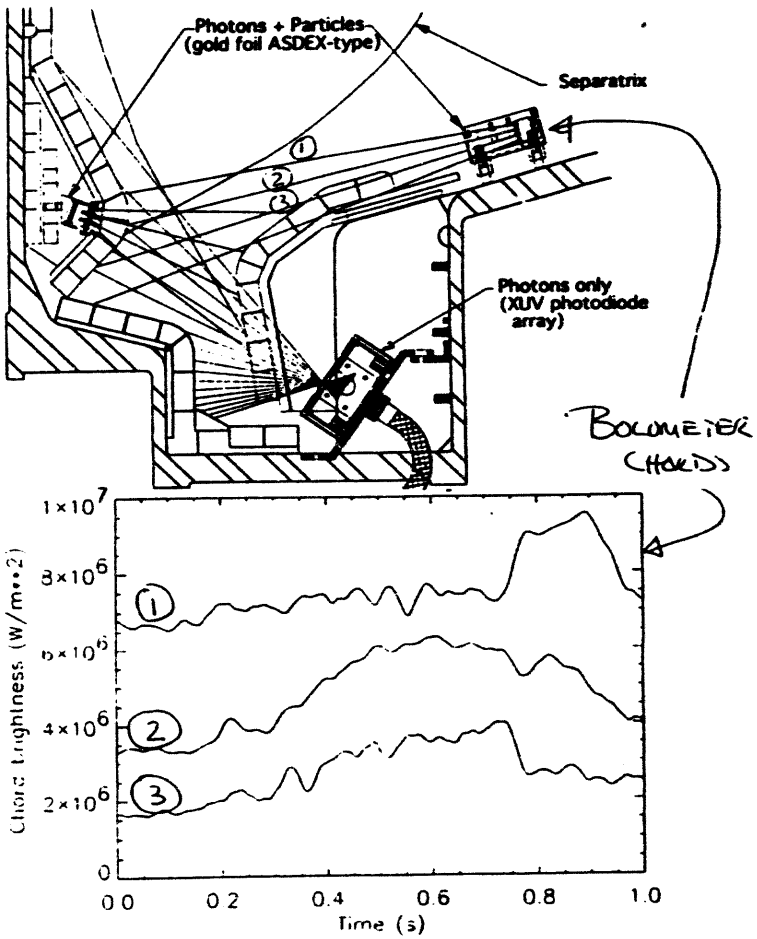

J. GOETZ
B. LIPSCHULTZ

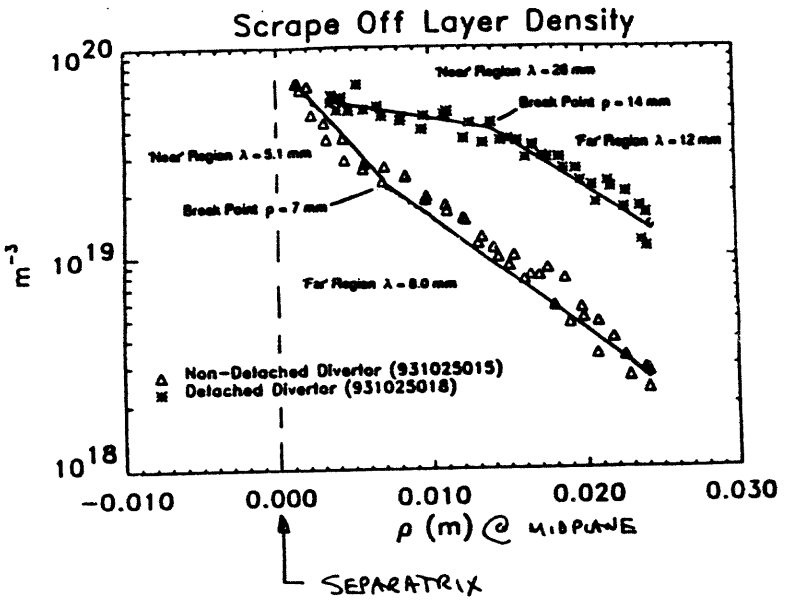

→ DENSITY PROFILE 'FLATTENS' AFTER DETACHMENT

B. LaBombard
D. Jablonski

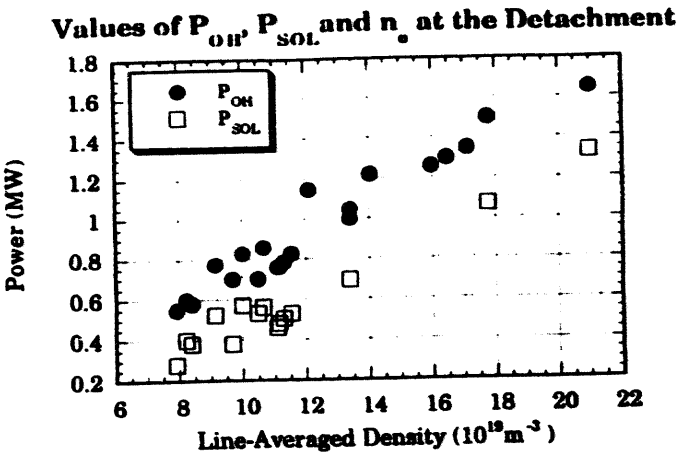

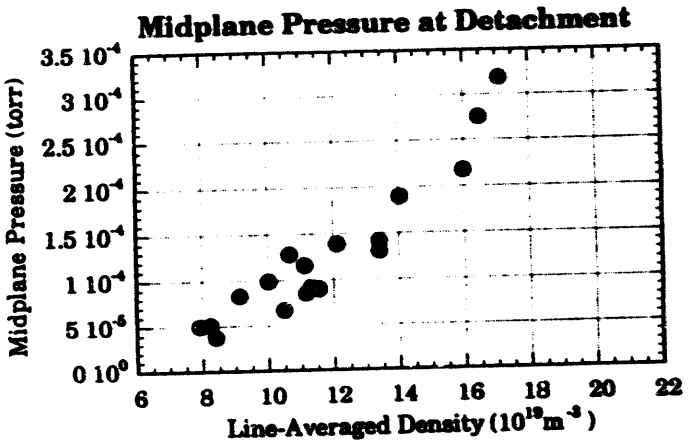

J. Goetz
A. Niemczewski
B. Lipschultz

'Detached' Divertor Characteristics

- Detachment of plasma occurs at both divertor plates
  - drop in n_e is primarily in region of the separatrix.
  - constant or increasing n_e @ pts 1 - 1.5 x λ_n from sep.
  - up to a factor of 20 decrease in local heat flux.
- Rearrangement of the strong divertor radiation; movement towards the x-point.
  - C radiation appears to be concentrated above x-point.
  - H radiation on both sides of the x-point.
- Strong effects in the general SOL as well:
  - Profiles of n_e, T_e flatten, particularly near separatrix.
  - T_e at separatrix drops.
- Pressure no longer constant along flux surface.
- 'Critical' central plasma density for detachment $\propto P_{OH}$.
- Outer divertor T_e always ~ 5 eV prior to detachment.

Impurity Transport

- Carbon
  - Γ_C ~ 2 - 3 x O source rate
  - Γ_C is higher at the walls than from the divertor.
  - Γ_C increases slowly with $\bar{n}_e$.
  - contribution to Z_{eff} -1 decreases with $\bar{n}_e$ (SOL screening efficiency is better at higher $\bar{n}_e$).
  - C/H influx ratio indicates C coverage of Mo surfaces of order 5%.
- Molybdenum
  - $\Gamma_{Mo} < \Gamma_O, \Gamma_C$ at limiter.
  - Γ_{Mo} negligible in divertor; below sputtering threshold.
  - Contribution to central radiation 'normally' < than from carbon.
- Ar puffing experiments:
  - Divertor retention of Ar increases with $\bar{n}_e$.
  - Location of Ar puff does not affect the Ar density in main plasma.
  - Puff @ inner wall delays entry of Ar into the main plasma compared to divertor puff

CARBON SOURCE RATE FROM THE WALLS & DIVERTOR

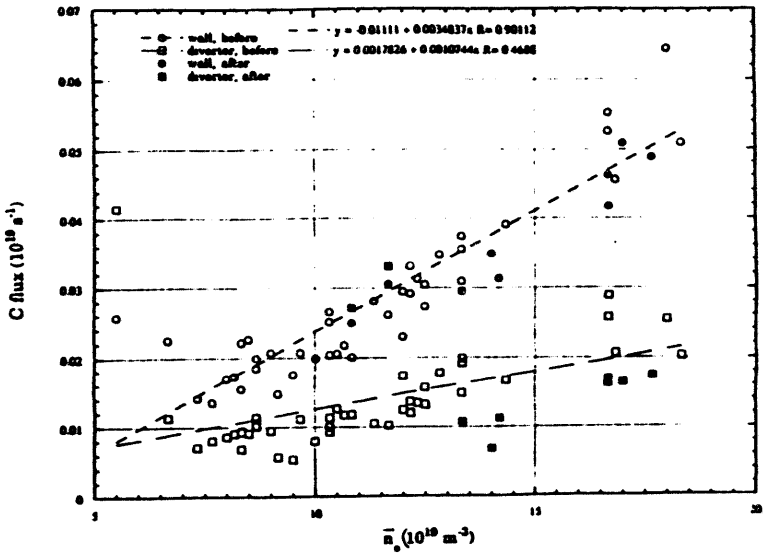

→ C INFLUX FROM THE WALLS GREATER THAN FROM THE DIVERTOR

C. KURZ
B. LIPSCHULTZ

DEPENDENCE OF DIVERTOR MO INFLUX RATE ON $T_{e,DIV}$

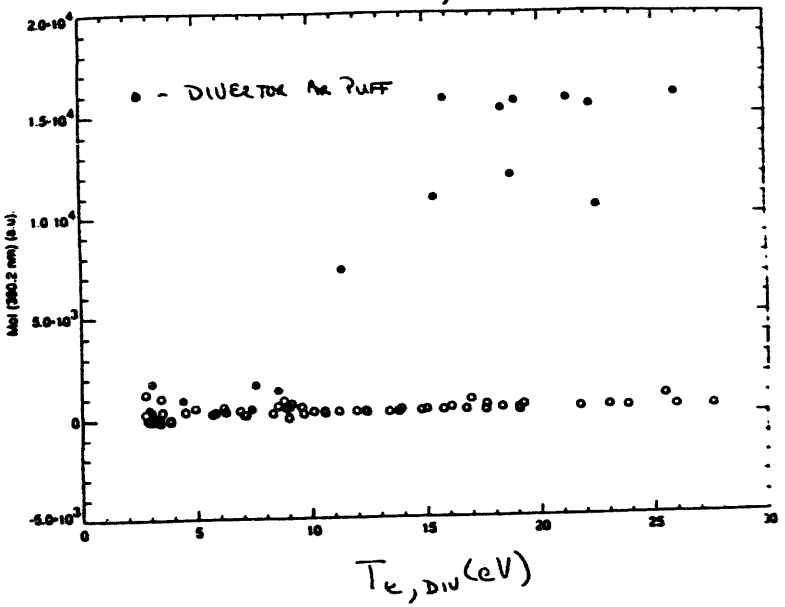

→ MO SOURCE RATE IN THE DIVERTOR IS 'NORMALLY' LOW.

→ AR PUFF IN THE DIVERTOR LOWERS THRESHOLD FOR MO SPUTTERING

C. KURZ
B. LIPSC

Plans For Upcoming Run Period (3/94)

➥ Improve the SOL and divertor plasma characterization:

(A) Better measurements of n_e, T_e and T_i.
- install 1 'domed' probe at each of 16 poloidal triplets.
- upgrade scanning probe head.
- new spectrograph for doppler shift T_i.

(B) Plasma flow measurements
- 'Mach' operation of scanning probe
- U. Md. 2-D detector + 2m spectrograph for flow and T_i measurements.

➥ Divertor power balance:

(A) Divertor Heat Load Profile
- Install 12-channel InGaAs infrared surface temperature measurement
- Install prototype single HgCdTe infrared detector

(B) Magnitude and location of divertor radiation.
- Reorient views of existing div. bolometer arrays.
- Add 3rd array with perpendicular view.

(C) Relative contributions from different impurities.
- Add more diode array views of the divertor

Summary

- Radiative divertor operation obtained
  - with significant divertor P_{rad}.
  - with a range in $\bar{n}_e$.
  - with a low Z_{eff}.
  - without a need to inject impurities.
  - $n_{e,div} > n_{e,sep}$ & $\bar{n}_e$.

- Operation with the plasma 'detached' from the divertor can be obtained
  - The SOL becomes broader
  - The power to the divertor plates is reduced
  - Pressure is not constant from the SOL to the divertor.
  - The divertor radiation shifts to the x-point region.

- Future experiments are aimed at
  - higher I_p, n_e, P_{in}, providing ITER-like conditions
  - better diagnosis of divertor radiation & power balance.
  - determining perpendicular and parallel transport.
  - impurity source rates and transport.

Plans For Upcoming Run Period (3/94)

- Impurities:
  - (A) Source rate magnitude and location
    - 2-D detector (λ+28 spatial channels) with 0.25 m spectrograph .
    - remote-controlled filter wheels for diode arrays.
  - (B) Transport
    - measurement of spatial distribution of different impurity charge states.
    - upgrade the number of available capillary gas-puff locations.

- Modeling:
  - (A) External Collaborations - modeling of C-Mod data
    - NEWEDGE (D. Knoll) : non-orthogonal geometry.
    - DDC83 (A. Kukushkin) 2-D fluid code
    - DEGAS (D. Stodtler) model neutrals and H_α recycling
    - NEWT-1D (R. Campbell) -> impurity transport
  - (B) Internal Work - modeling of C-Mod data
    - MIST modeling of impurity transport.
    - Kinetic code (Krasheninnikov et al)
    - analytic modeling of flows and edge transport (Krasheninnikov)

Japan-U.S. Workshop Q181 High Heat Flux Components and Plasma Surface Interactions for Next Devices
San Diego, January 24-27,1994

High Z Limiter Experiments in TEXTOR

Y. Ueda[1], V. Philipps[2],T. Tanabe[1], M. Wada[3], B. Unterberg[2], A. Pospieszczyk[2], B. Schweer[2], P. Wienhold[2], M. Rubel[4], B. Emmoth[4], M. Toker[2], L. Könen[2], N. Hawkes[5], R. Kosh[2] and the TEXTOR Team[2]

presented by N. Noda
(National Institute for Fusion Science)

1) *Faculty of Engineering, Osaka University, Japan*
2) *Institute fur Plsmaphuysik, KFA Jülich, Germany*
3) *Faculty of Engineering, Doshisha University, Japan*
4) *Royal Institute of Technology, Sweden*
5) *Culham Laboratory, United Kingdom*

Contents

TEXTOR Parameters

Major Radius : 1.75 m
Minor Radius : 0.46 m (ALT-II Pump Limiter)

Plasma Current : 340 kA
Toroidal Field : 2.25 T
NBI : 1.25 MW Co-injection (for this experiment)

Wall Condition : Siliconization for Mo experiment
Bolonization for W experiment

Main Plasma Diagnostics

A. Interferometer : Ne Profile
B. ECE : Te Profile
C. Bolometry : Radiation Profile
D. VUV Spectrometry : Impurity Line
E. SX Spectrum : Impurity Line

Edge Plasma Diagnostics

A. He Beam : Ne and Te in plasma edge

Test Limiter Diagnostics

A. CCD Camera1 (Normal) : Thermography
B. CCD Camera2 (Tangential) : Impurity Flux
C. Thermocouple : Deposition Energy

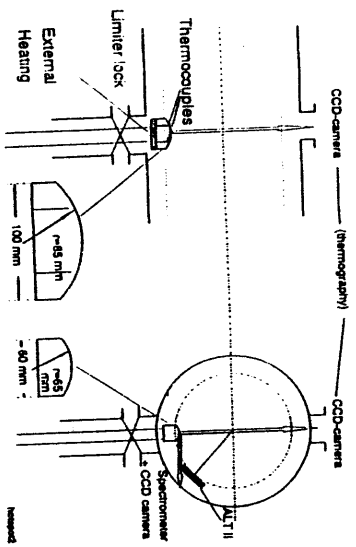

Background

- Possible problems in C/Be in future
- Tungsten was the primary candidate for divertor plates in ITER/CDA (tech. phase)
- It has been said that T_{edge} must be < 50 eV
- No data available for high Z materials especially their impact on core plasmas
- Most of tokamks have been operated with lowZ walls for these 10 years
- TEXTOR is assigned an experimental device dedicated to PSI and PFM
- Well furnished edge diagnostics and a lot of experiences in TEXTOR on PSI studies
- Some Japanese colleagues proposed a systematic study for high Z PFM

Aims

-To evaluate impacts of high Z limiters on core plasmas

-To get a database of influx and impurity concentration on plasma axis as a function of edge temperature

-To find conditions for which high Z metals can be applied as PFM

The question must not be

"whether high Z materials are OK or not OK ?"

but should be

"in which condition, high Z materials are allowed to be used as PFM ?"

How is the maximum tolerable edge temperature ?

Can they be used for limiter and/or divertor config. ?

Can they be used for a good confinement scheme or for only L-mode scheme ?

.....

Comparison surface temperatures Mo and C : deposited energy 85kWs

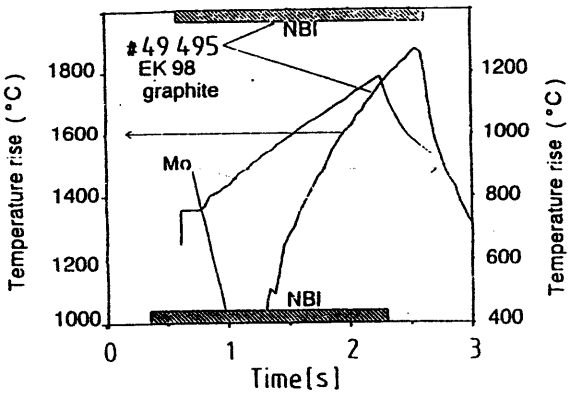

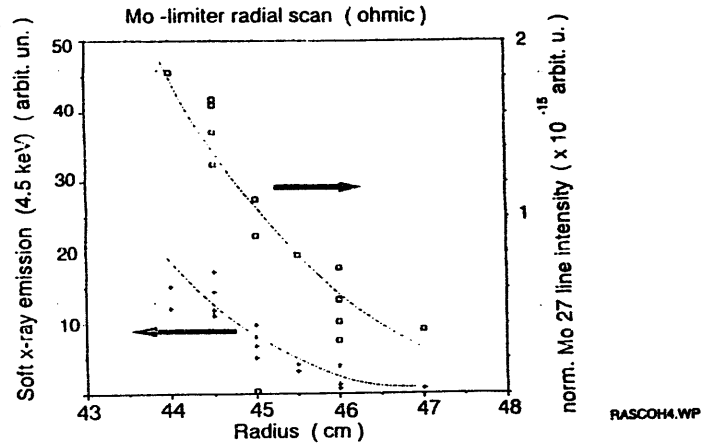

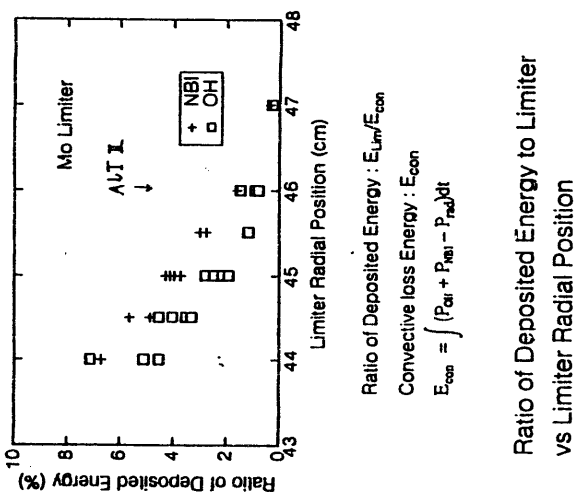

Ratio of Deposited Energy : E_{Lim}/E_{con}

Convective loss Energy : E_{con}

$E_{con} = \int (P_{OH} + P_{NBI} - P_{rad})dt$

Ratio of Deposited Energy to Limiter vs Limiter Radial Position

Dependences of Z_{eff}, Radiation and line average density on limiter position

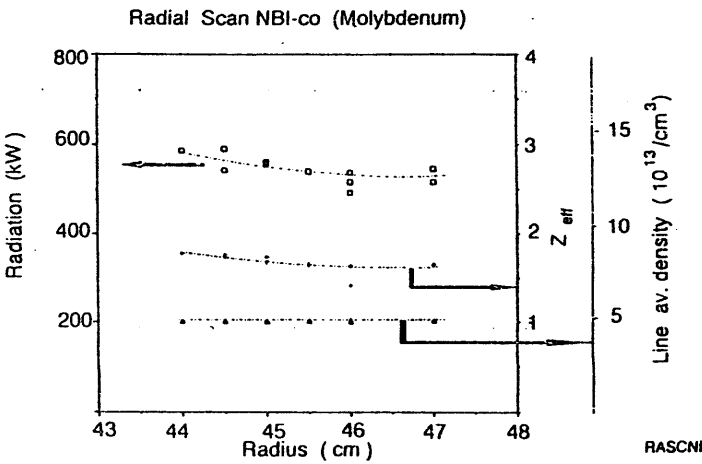

Mo density(Moxxvii & Soft X-ray) vs. Line averagde density.

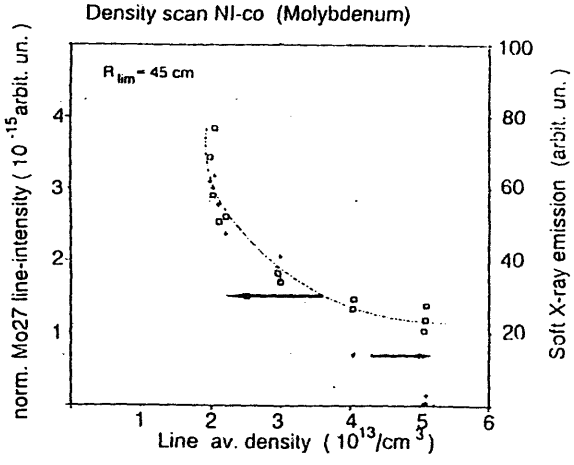

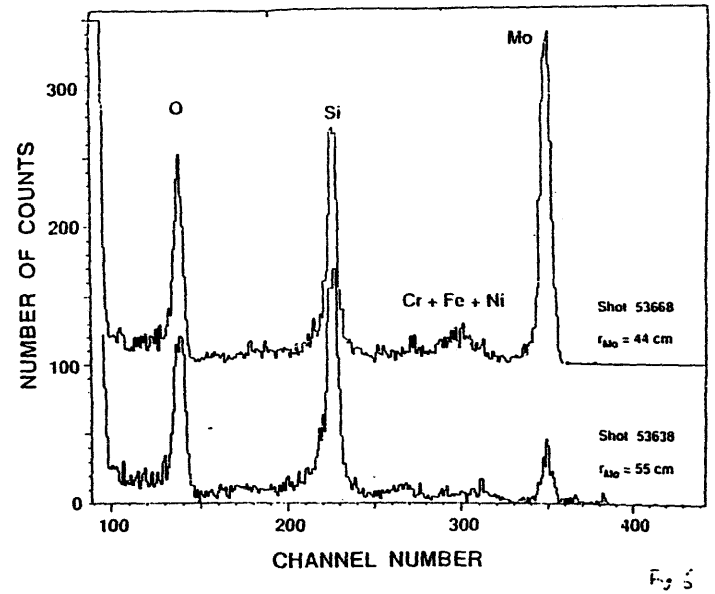

Fig 5

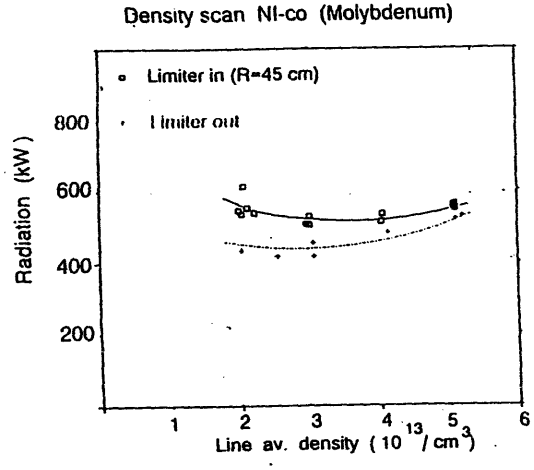

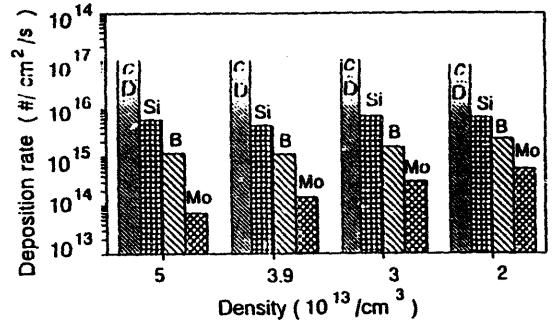

Fig. 7

High Density OH Shot with Instability

$\bar{n}_e > 3.0 \times 10^{13} cm^{-3}$

Impurities accumulate in the plasma center and hollow temperature profile appears.

Radiation Profile in OH Case

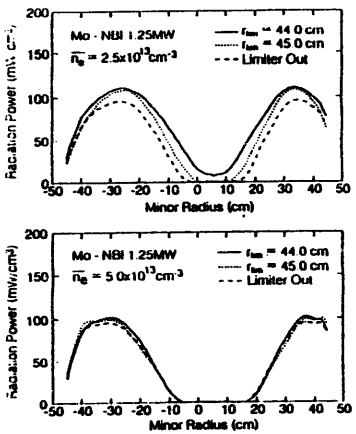

Radiation Profile in NBI Case

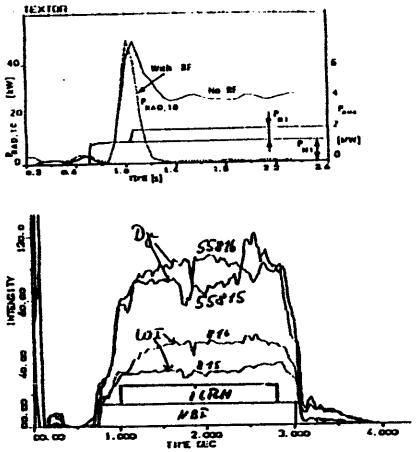

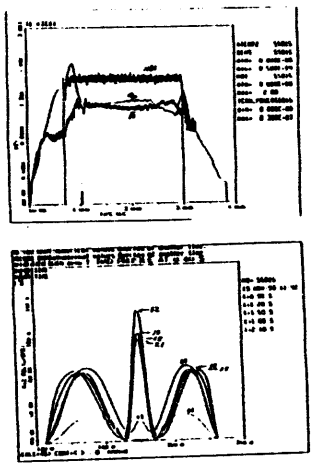

Fig. 2 Plasma operation with NBI on and ICRH off. (a) Electron density, temperature and NBI power plotted as functions of time. Note that electron temperature signal is quiet and does not show any saw-tooth oscillation. (b) Spatial distribution of radiation power of the plasma.

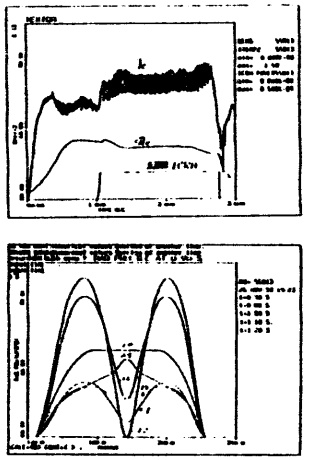

Fig. 3 Plasma operation with ICRH on and NBI off. (a) Electron density, temperature and ICRF power plotted as functions of time. (b) Spatial distribution of radiation power of the plasma.

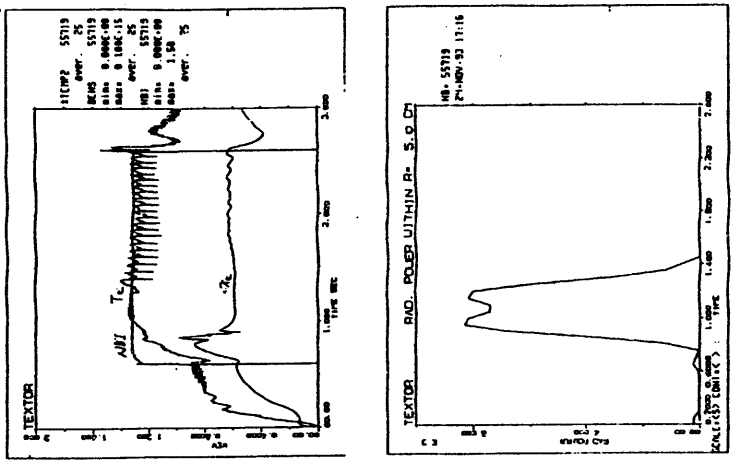

Fig. 4. Plasma operated with NBI only. (a): Electron density, temperature and ICNF power plotted as functions of time. (b): Radiation power from the central region of plasma. The spatial distributions of the radiation power are similar to those shown in Fig. 2(b)

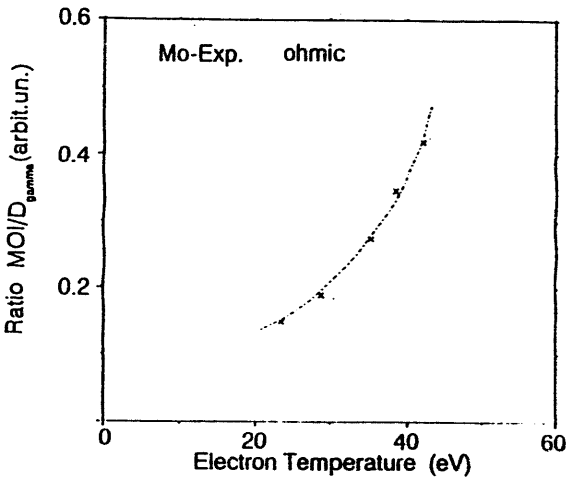

OH

DSCMOTE.WPG

Tanabe, Noda (Last PSI conf. in Monterey)

n_z/n_e n_z T_{LCFS} T_{DV}

Table 1
Central density of metal impurities in ohmic and neutral beam heated discharges in tokamaks

n_z/n_e (10^{-4})	n_z (10^{18} m^{-3})	n_e (10^{19} m^{-3})	I_p (MA)	P_{in} (MW) (NBI)	Gas	Conf. figur.	Material Lim/Div	Wall	T_{LCFS} (eV)	T_{DV} (eV)	Other conditions and remarks	Machine	Ref
Ti: 0.6	2.4	4.0	1.5	20(1)	H_2	div	TiC/Mo	TiC/Inconel	–	–	P_{rad}(total) ~ 10%	JT-60	a
											n(oxygen) ~ 4 $\times 10^{-17}$ m^{-3}		
Ti: 40	40	1.0	1.5	11–14(1)	H_2	div	TiC/Mo	TiC/Inconel	–	–		JT-60	a
Fe: 2.6	12	4.7	0.3	OH	He	lim	Ti	SS	–	–		ASDEX	a
Fe: 4.0	12	3	0.3	OH	He	lim	Ti	SS	–	–		ASDEX	a
Fe: 0.9	4.1	4.7	0.3	OH	He	div	Ti	SS	–	–		ASDEX	a
Fe: 1.8	5.3	3	0.3	OH	He	div	Ti	SS	–	–		ASDEX	a
Fe: 0.4	1.9	4.7	0.3	OH	D_2	lim	Ti	SS	–	–		ASDEX	a
Fe: 0.5	1.5	3	0.3	OH	D_2	lim	Ti	SS	–	–		ASDEX	a
Mo: 93	650	7.0	0.2	OH	D_2	lim	Mo	SS	–	–	hollow $T_e(r)$	ALCATOR C	a
Mo: 1.0	20	20	0.2	OH	D_2	lim	Mo	SS	–	–		ALCATOR C	a
W: 15–257	30–307	2	0.4	OH	H_2	lim	W	SS	–	–	hollow $T_e(r)$?	PLT	a
Ni: 0.11	0.2	1.9	3	OH	He	lim	Inconel	Inconel	–	–		JET	a
Ni: 0.03	0.06	1.9	3	OH	D_2	lim	Inconel	Inconel	–	–		JET	a

[a] T. Sugie et al., Kakuyugo-Kenkyu 65 (Suppl.) (1991) 287, in Japanese.
[b] G. Fussmann et al., J. Nucl. Mater. 145–147 (1987) 96.
[c] B. Lipschultz et al., J. Nucl. Mater. 179 & 129 (1984) 555.
[d] E. Hinnov et al., Nucl. Fusion 18 (1978) 1305.
[e] K. Behringer et al., J. Nucl. Mater. 162–164 (1989) 398.

no data before TEXTOR!

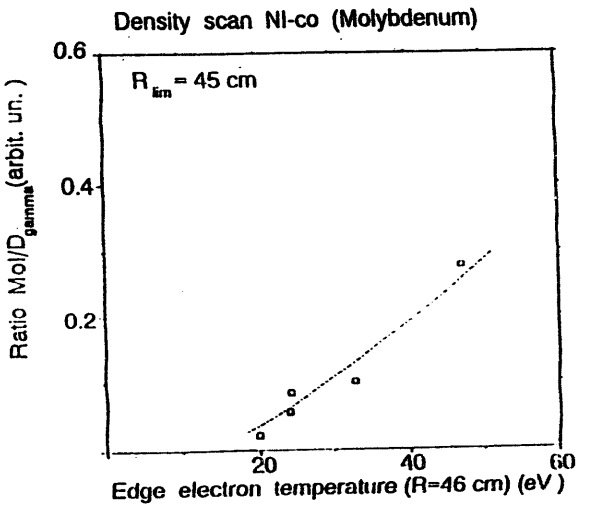

NB

DSCNBS2

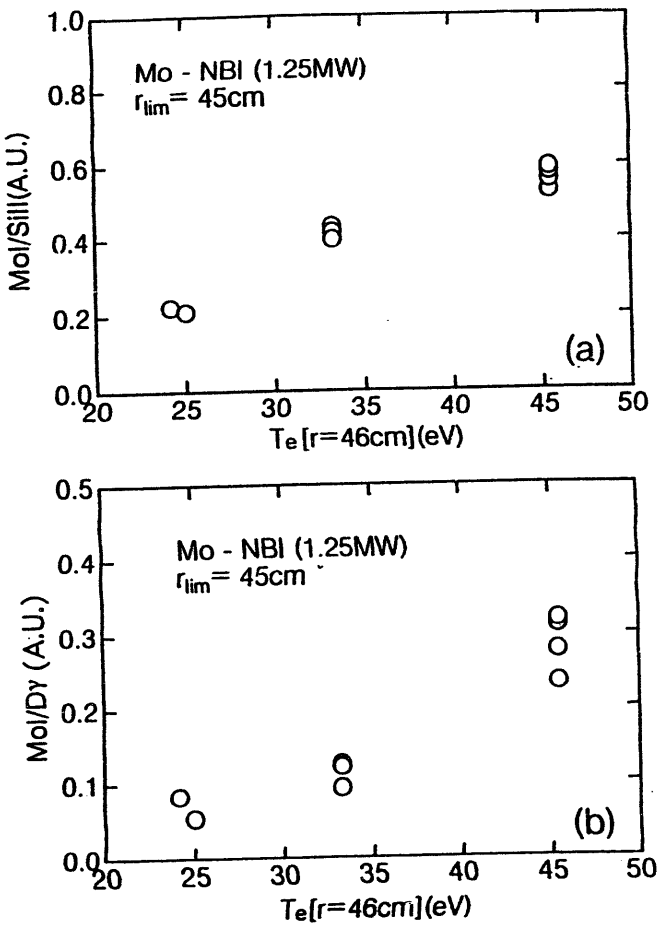

Ratios of Mo Flux to Si Flux (a) and
D Flux (b) vs Edge Electron Temperature

MoI line inensity vs edge Te

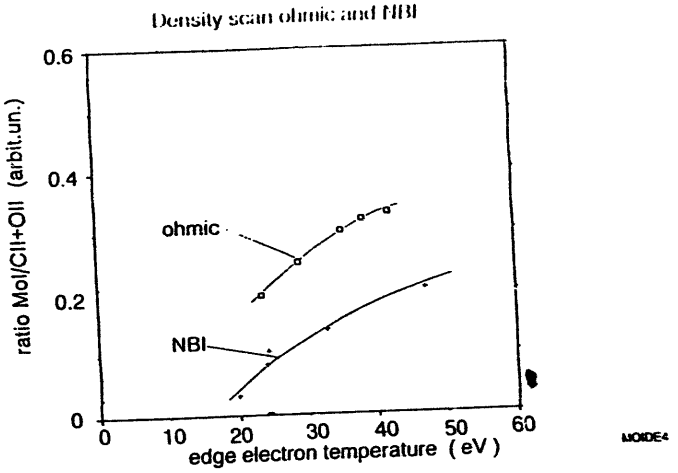

Ratio of sputter flux produced by deuterium impact to that
produced by carbon impurity impact as function of edge temperature

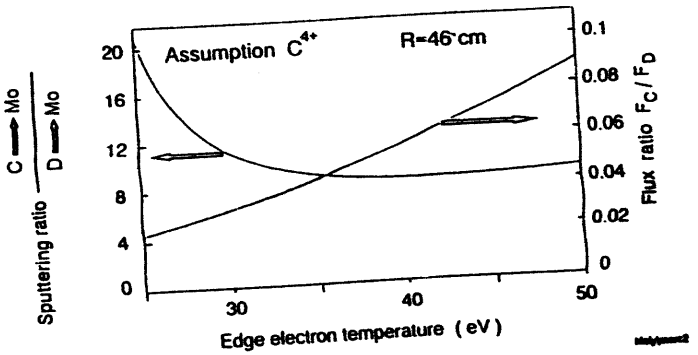

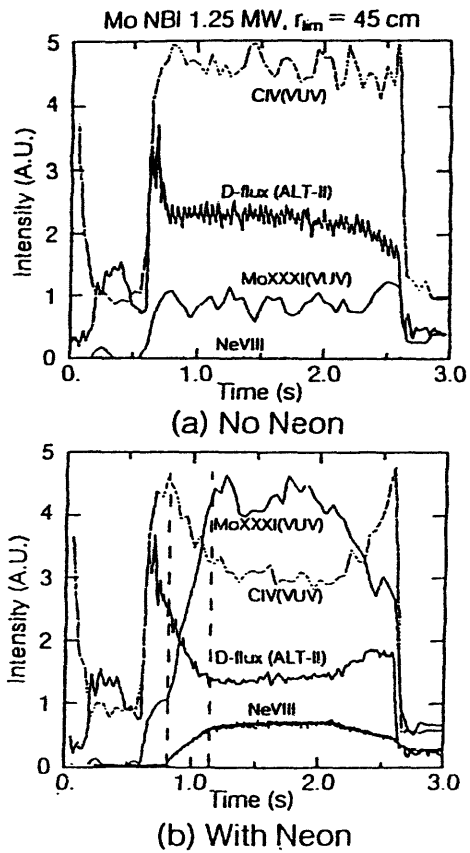

Time Evolution of VUV Lines (Mo, C)
and D Flux from ALT-II without (a) and with (b)
Neon Injection

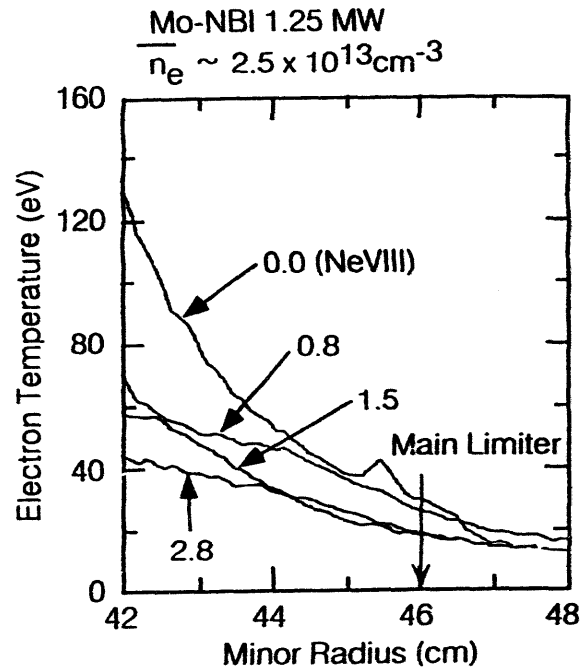

Edge Electron Temperature
Profile in Neon Injection

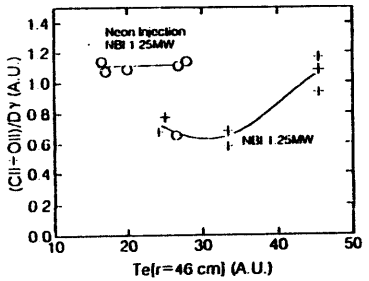
Neon Injection
NBI 1.25MW
NBI 1.25MW
(CII+OIII)/DY (A.U.)
Te[r=46 cm] (A.U.)

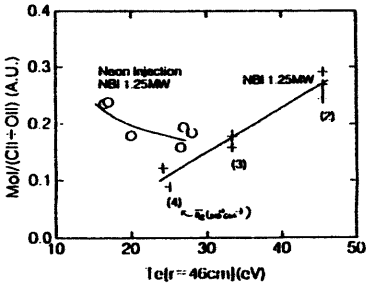
Neon Injection
NBI 1.25MW
NBI 1.25MW
(2)
(3)
(4)
MoI/(CII+OII) (A.U.)
Te[r=46cm](eV)

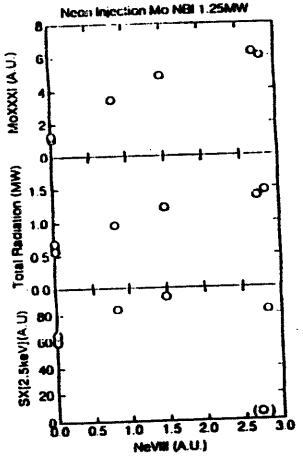
Neon Injection Mo NBI 1.25MW
MoXXXII (A.U.)
Total Radiation (MW)
SXI[2.5keV](A.U.)
NeVIII (A.U.)
(c)

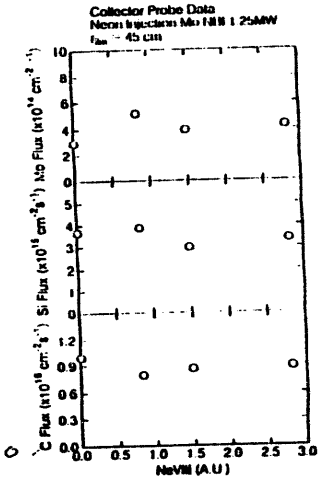
Collector Probe Data
Neon Injection Mo NBI 1.25MW
NeVIII (A.U.)

Photograph of Mo limiter after the experiments

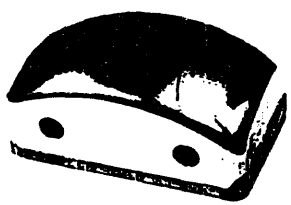

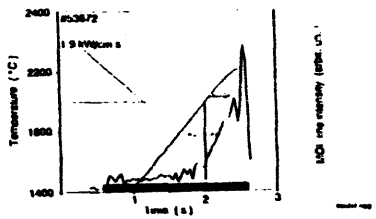

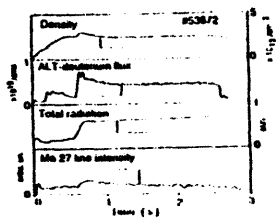

Summary

1. The hollow Te profiles could be seen in relatively high density OH operations, but could not seen for NB and ICRF heated plasmas.
2. The hollow Te condition is unstable.
3. Concentration of n_{Mo}/n_e on axis in the order of 10^{-4}
4. Tungsten radiation is occasionally central peaked in NB heated plasmas, but both for NB and RF heating plasmas, a condition was found in which the radiation peaking does not occur.
5. Dependence of Mo influx on T_{edge} has been investigated systematically.
6. Neon injection enhanced Mo radiation in spite of lower edge temperature
7. Central Mo radiation does not increase in spite of enhanced influx of Mo at the limiter surface with melting.

US-Japan Workshop on HHFC and PSI for Next Devices
San Diego, California, January 24-27, 1994.

PFCs and PSI in JT-60U

T. Ando
Japan Atomic Energy Research Institute

Contents

US-Japan Workshop Q181 on HHFC and PSI for Next Devices, San Diego, California, January 24-27, 1994.

PFCs and PSI in JT-60U

T. Ando, JT-60 Facility Div. II, JAERI

SUMMARY

The application of the B_4C-converted carbon fiber composite (B_4C/CFC) divertor tiles and the performance in high power neutral beam (NB) heated discharges are reported. Wall damages in the recent operation are also shown.

The B_4C/CFC is a surface-boronized material with a B_4C-layer thickness of a few hundreds μm, which is produced by a chemical vapor reaction of gaseous boron oxide and the carbon substrate at ~2000°C. The B_4C/CFC tiles were installed on the outboard striking point of the divertor plate in late 1992.

The operation of JT-60U in 1993 has been carried out successfully with a NB injection power up to 36 MW for 2 s. The number of total discharges and NB heated ones are 2335 and 1089, respectively. The plasma parameters have been improved significantly. In March, the highest fusion triple product (1.1×10^{21} keVsm^{-3}) has been achieved in high β_p H-mode plasma in which the evaluated Z_{eff} is 2.3 with relatively low carbon concentration. The impurity influx from the B_4C/CFC tiles is not large during ELM-free phase, but the rapid increase of boron as well as carbon is observed in strong ELMy phase with decreasing stored energy. However, moderate ELMs with almost constant stored energy do not cause the significant increase of boron and carbon. The behavior of oxygen is different from that of boron and carbon.

The in-vessel inspection in late 1993 showed that the tapered-edges of the B_4C/CFC tiles were eroded slightly and melting of the surface was observed. The slight erosion was also observed on two CFC tiles which were installed to compare to the B_4C/CFC ones. The tile shape and the thickness of the B_4C layer should be optimized further. The additional B_4C/CFC divertor tiles have been installed in December 1993.

The mechanical fracture of three CFC armor tiles was observed. A possible cause of this failure is an electromagnetic force due to halo current. The required force and current are estimated to be about 1 ton / tile and 20 kA / tile, respectively, based on the material strength. It was also found from the plasma TV monitor that the broken tile of 131 x 147 mm in size and 0.8 kg in weight was rotated poloidally around the plasma with a speed of ~10 m/s during the following discharge. This fact indicates that electromagnetic interactions between plasma and plasma facing components are also an important issue.

In late August 1993, one CFC divertor tile was disconnected due to loosening of the bolt. It was also found that about 80 units of divertor tiles were loosened and erosions of 2~3 mm in depth were observed on seven divertor tiles due to protrusion during discharges.

Based on the US-Japan collaboration, beta back scatter measurements of JT-60U tiles have been carried out successfully and B_4C-converted graphite samples have been fabricated for DIII-D DiMES test.

The electron beam heating test (JEBIS) of the water-cooled divertor mock-ups for JT-60U advanced divertor has been made and the promising result was obtained.

Installation of B_4C-converted CFC Divertor Tiles (Dec. 1992)

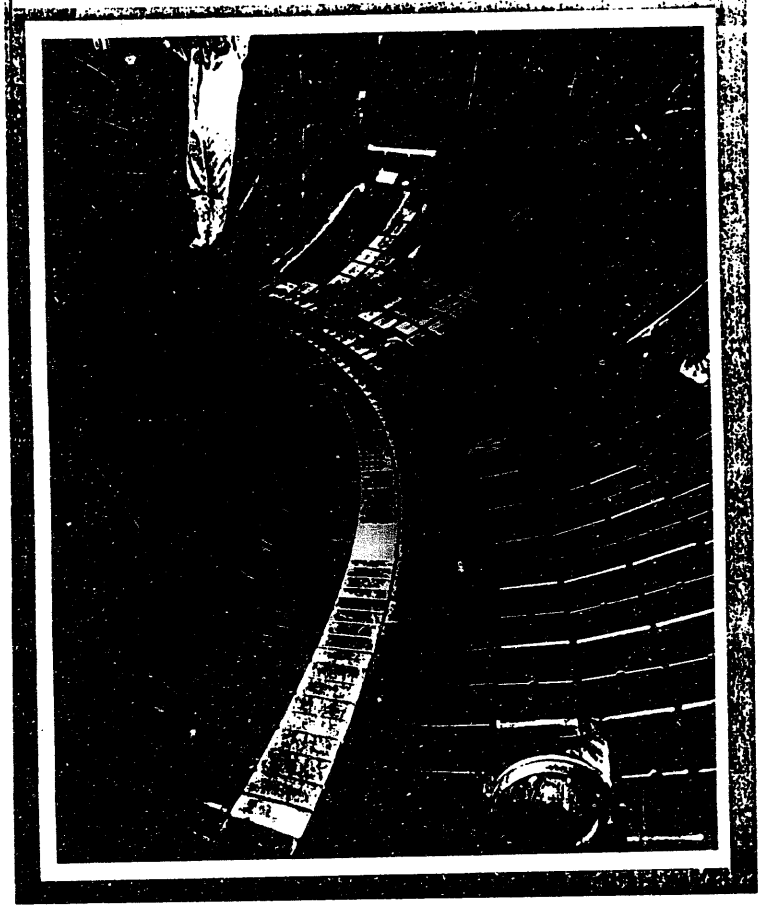

B_4C-converted Layer

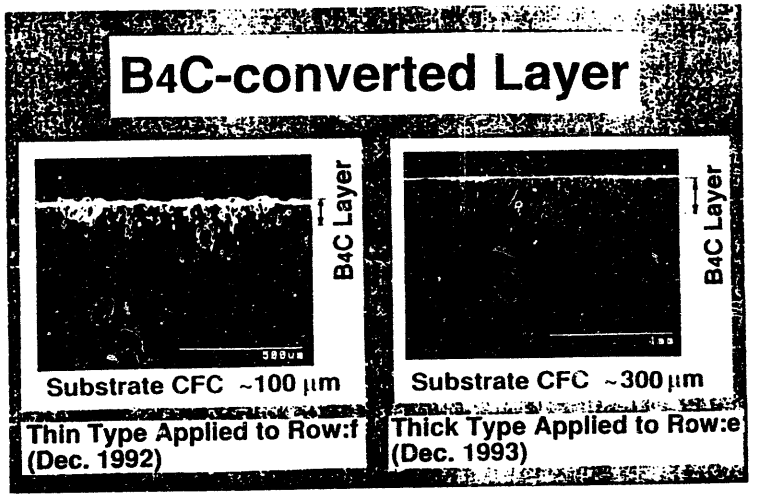

Equilibrium Configuration of High ßp H-mode

E17110, t=6.0 s

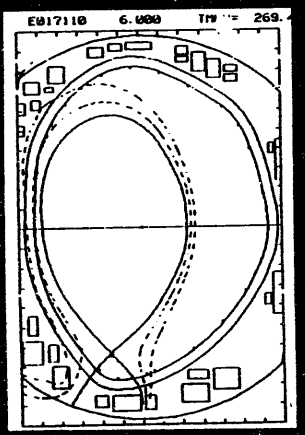

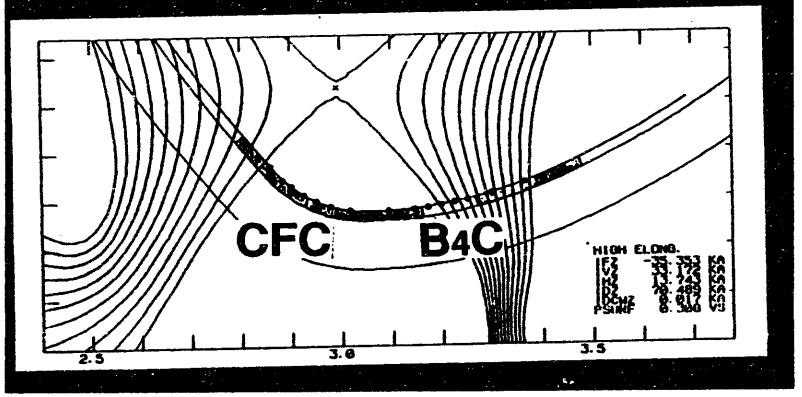

Typical Divertor Discharge Using B4C-converted CFC Tiles (E17110)

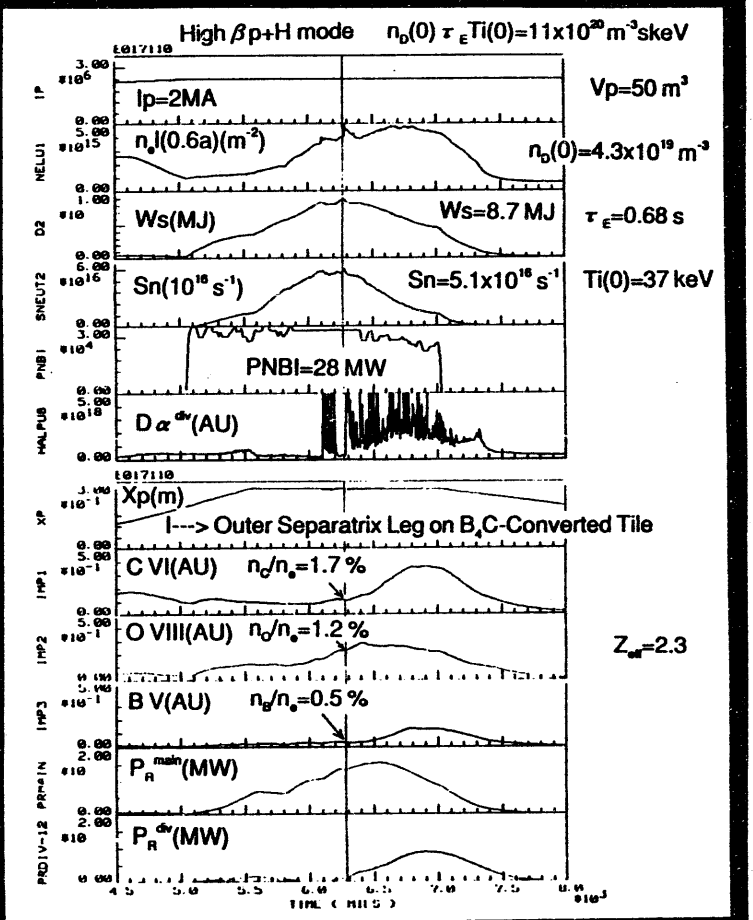

Typical Divertor Discharge Using B_4C-converted CFC Tiles (E17268)

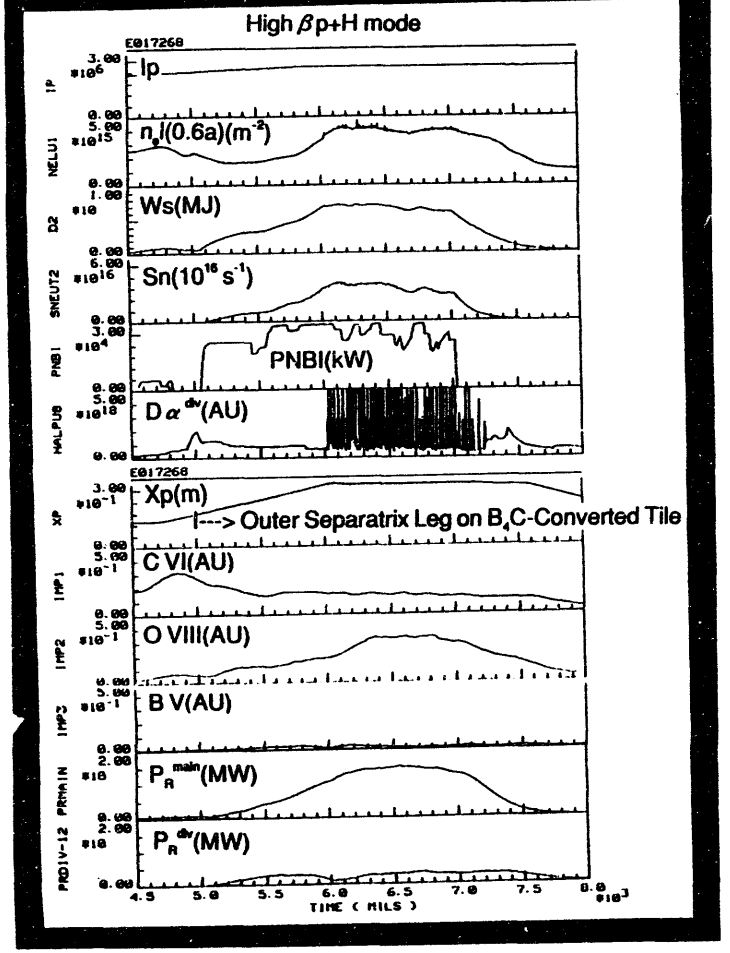

Typical Divertor Discharge Using CFC Tiles (E16045) (Aug. 1992)

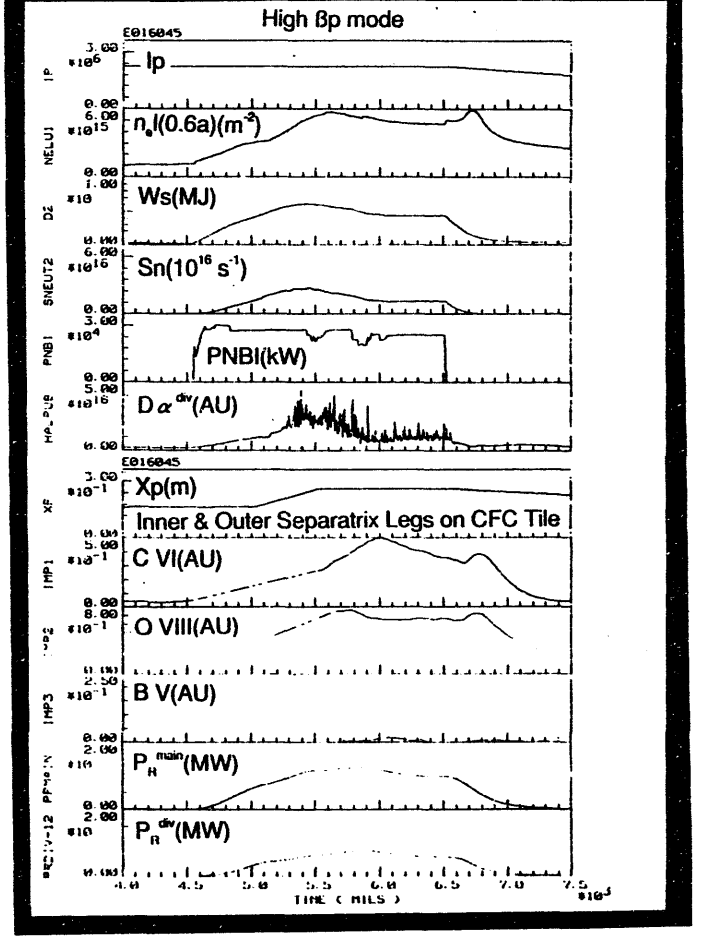

Typical Divertor Discharge Using CFC Tiles After Third Boronization (E16989)

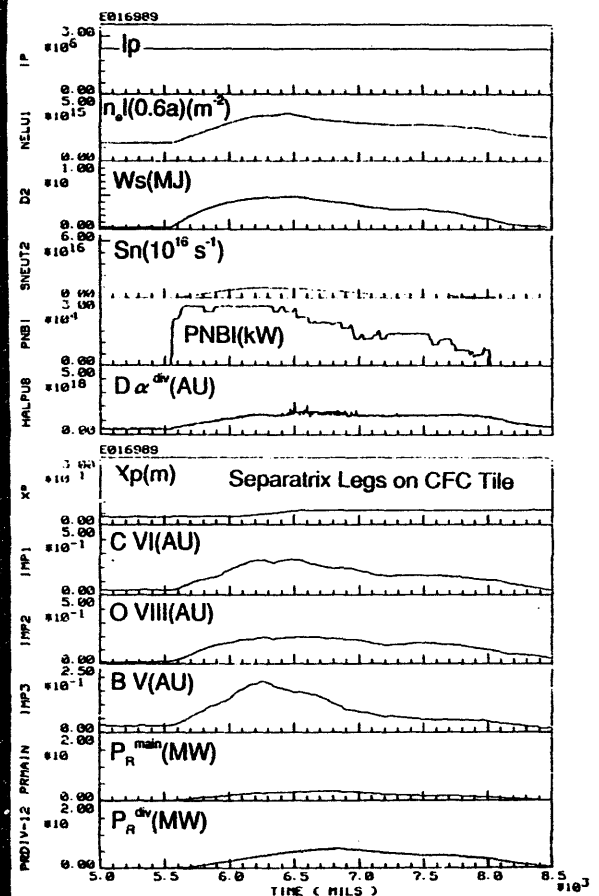

Damage of Outboard Divertor Tiles Slight Edge Erosion on B_4C-converted Tiles (Sep. 1993)

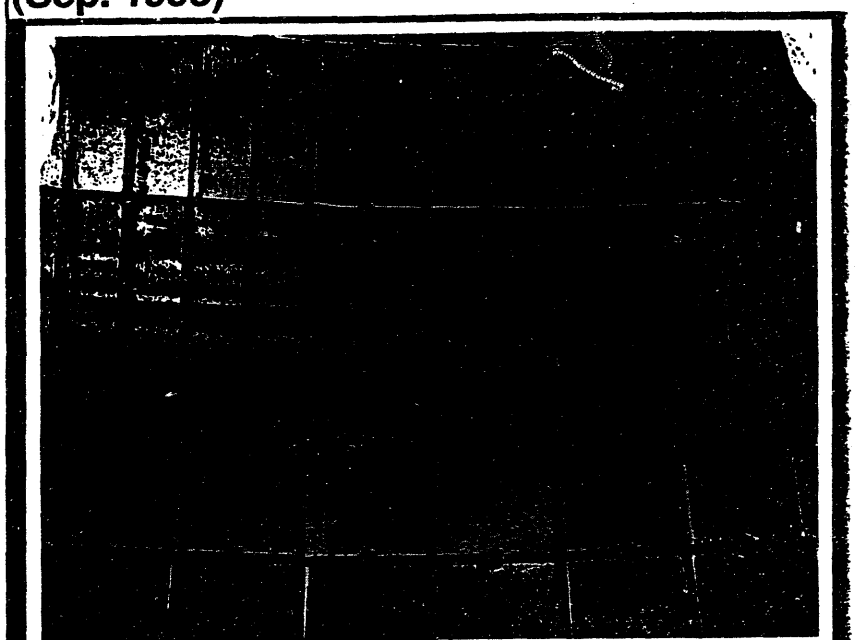

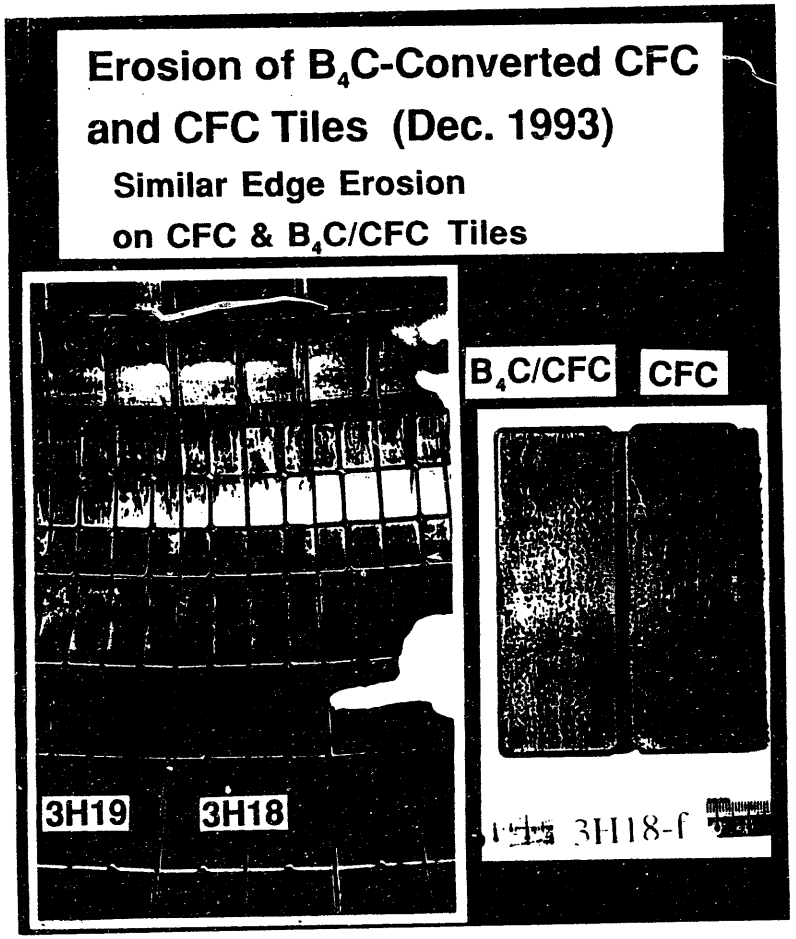
Erosion of B_4C-Converted CFC and CFC Tiles (Dec. 1993)
Similar Edge Erosion on CFC & B_4C/CFC Tiles
B_4C/CFC
CFC
3H19
3H18
3H18-f

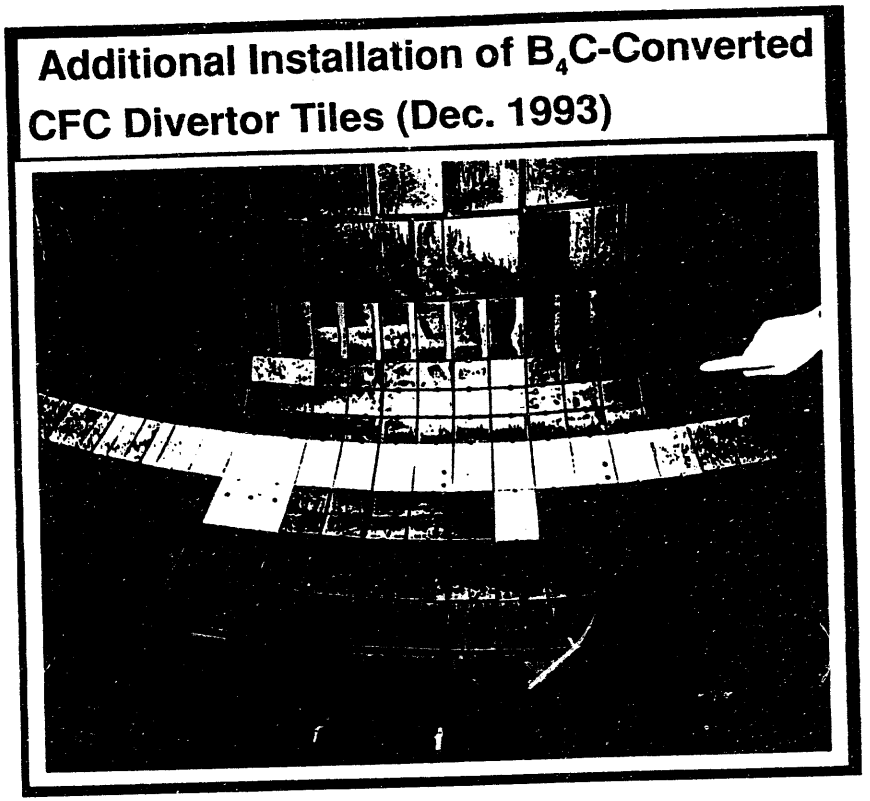
Additional Installation of B_4C-Converted CFC Divertor Tiles (Dec. 1993)

Mechanical Fracture of CFC Tiles Possibly due to Halo Current (Sep. 1993)

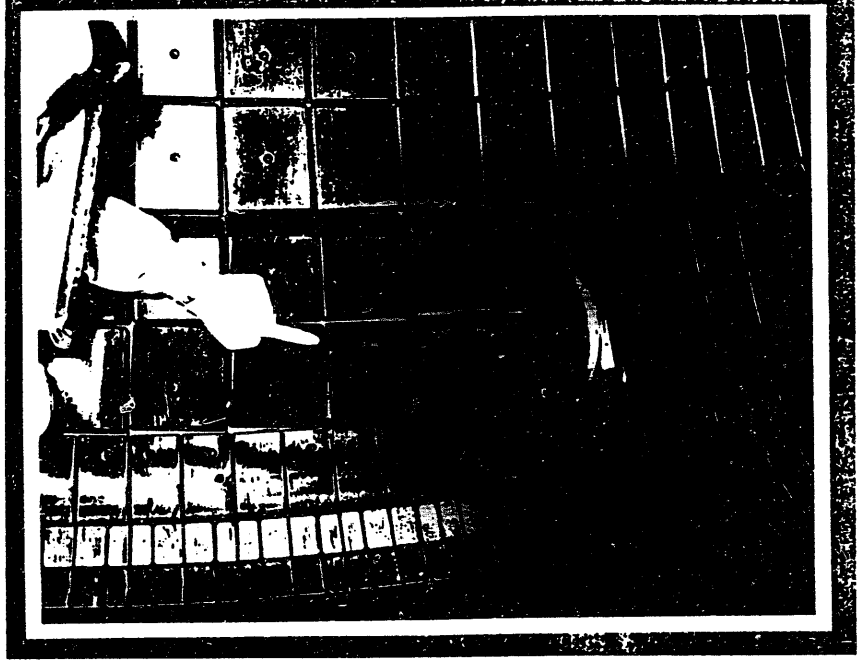

Electromagnetic Force due to Halo Current

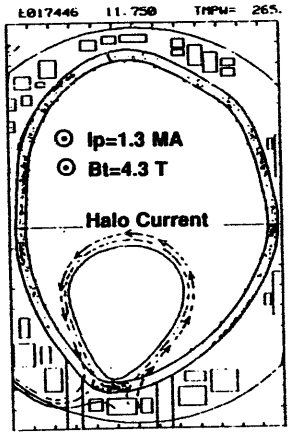

Estimation from CFC Strength
~20 kA/tile(~1 ton/tile)
Measurement of I_{halo} at Divertor Tile
~5 kA or more
x factor 2 (port opening)

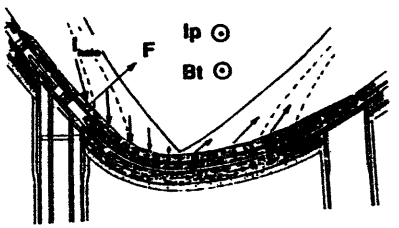

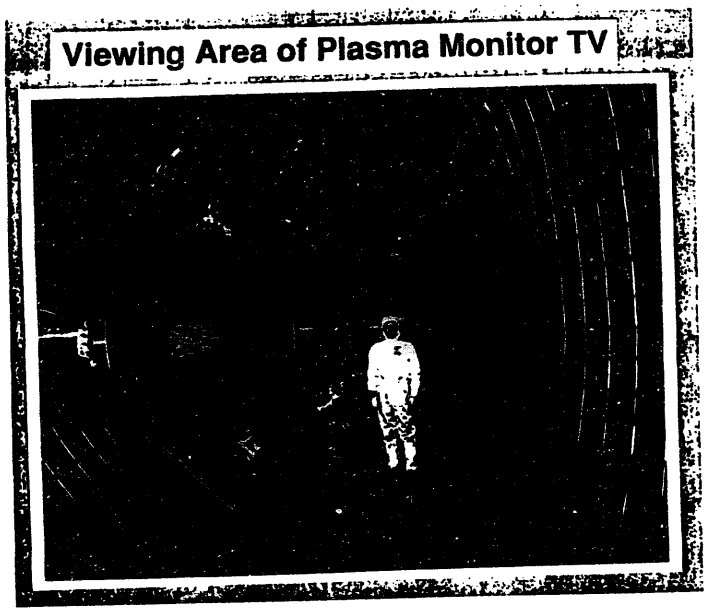
Viewing Area of Plasma Monitor TV

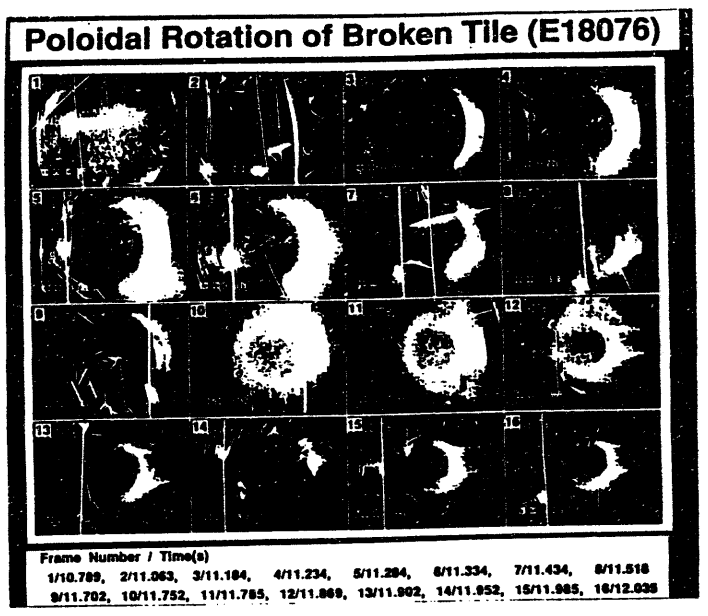
Poloidal Rotation of Broken Tile (E18076)
Frame Number / Time(s)
1/10.789, 2/11.063, 3/11.184, 4/11.234, 5/11.284, 6/11.334, 7/11.434, 8/11.516
9/11.702, 10/11.752, 11/11.785, 12/11.869, 13/11.902, 14/11.952, 15/11.985, 16/12.035

Poloidal Rotation of Broken Tile (E17448)

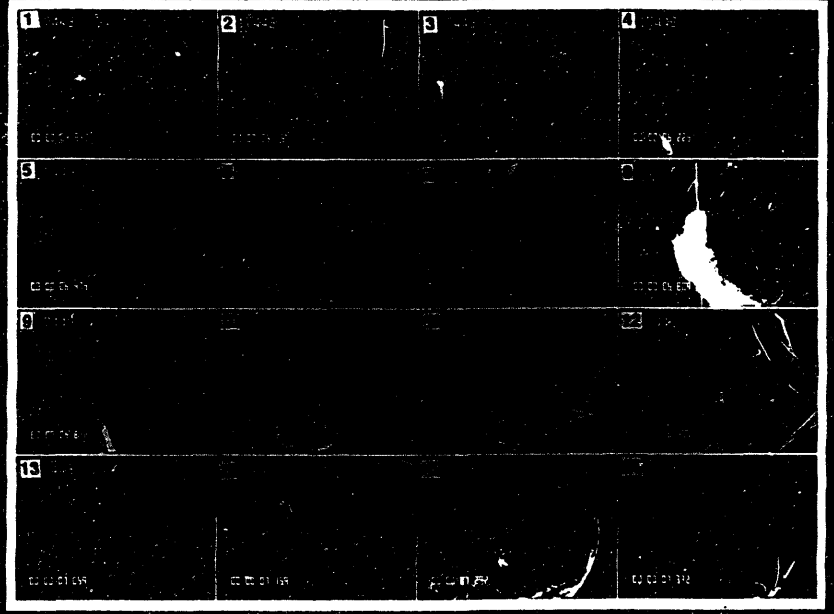

Frame Number / Time(s)
1/4.890, 2/5.154, 3/6.174, 4/6.224, 5/6.474, 6/6.541, 7/6.759, 8/6.809
9/6.842, 10/6.875, 11/6.925, 12/6.959, 13/7.059, 14/7.159, 15/7.292, 16/7.392

Poloidal Rotation of Tile During Plasma Discharge

Tile Size : 131 x 147 x 22 mm, Weight : ~0.8 kg

Speed : ~10 m/s

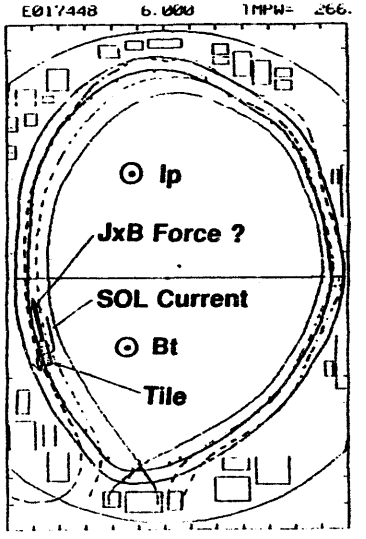

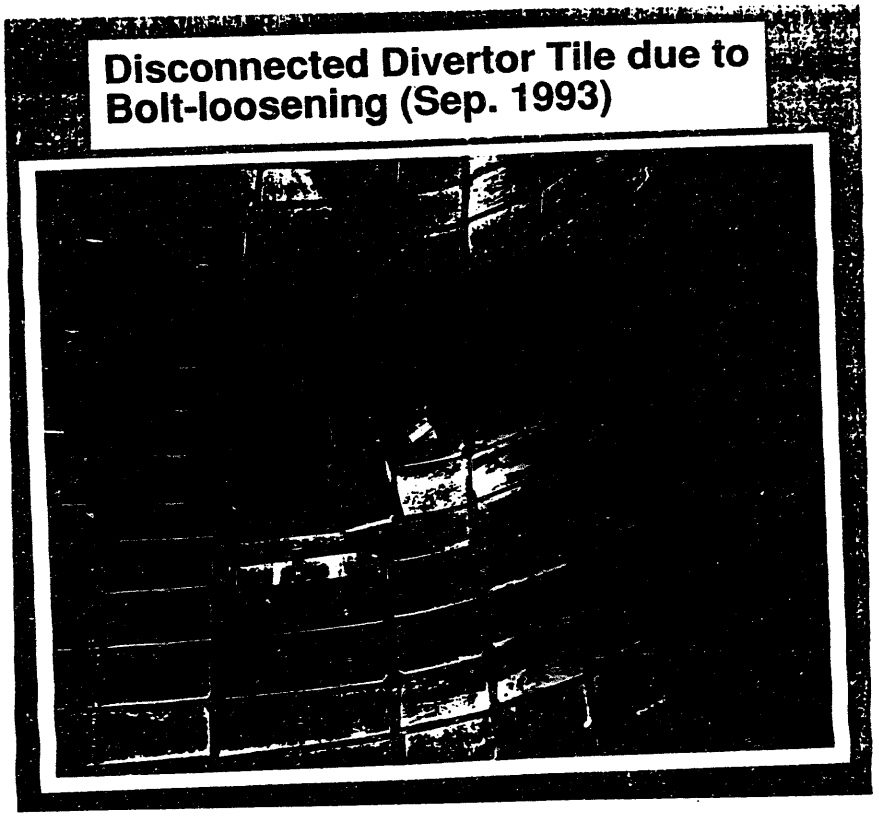

US-Japan Collaboration on JT-60 PFC (P214)

-Beta Backscatter Measurement of JT-60U Divertor Tiles

Row f (Dark Zone) - B_4C-Converted CFC Tiles

2H3 (Bright Zone) - Metal Deposits (March 1992)

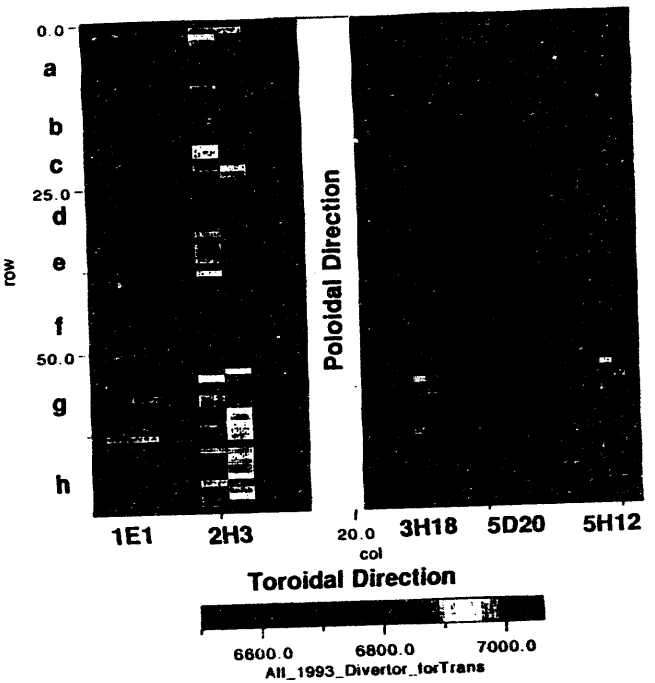

US-Japan Collaboration on JT-60 PFC (Q183)

- Evaluation of a B_4C-converted Coating on Graphite Tiles on DIII-D

Fabrication of DIMES Samples

Materials: ATJ, PD-330S, etc.

Heat Load Test Using JEBIS

10 MW/m^2 x 5 s

No Exfoliation, Melting of B_4C

B_4C Conversion

B_4C/ATJ Graphite

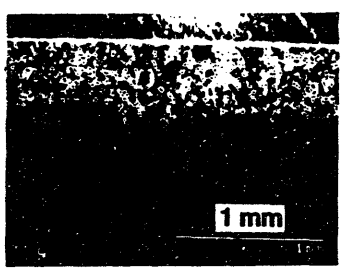

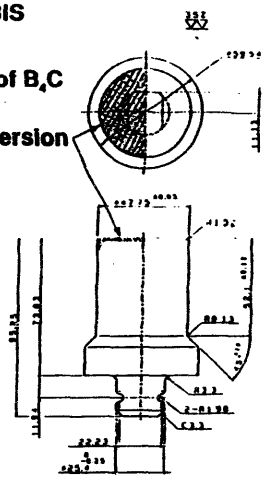

DIMES Sample

SUMMARY

- High plasma performance (1.1×10^{21} keVsm^{-3}) has been achieved in high βp-H mode using boron/carbon-based plasma facing materials.
- B_4C-converted CFC divertor tiles show good PMI performance in high power NB heating operation (~30 MW x 2 s).
- Optimization on tile edge shape and B_4C layer thickness is neccessary to reduce erosion.
- Plasma wall interactions are becoming severe in the recent NB heating and LHCD operations.
- Mechanical fracture of CFC armor tiles was observed.
- Electromagnetic interactions during disruption are also an important issue on PFCs.

DT-RELEVANT PMI STUDIES ON TFTR

Presented

by

Marco Caorlin

Princeton University
Plasma Physics Laboratory

US-Japan Workshop Q181 on High Heat Flux Components and Plasma Materials Interactions for Next Devices

University of California - San Diego
January 24-27, 1994

ACKNOWLEDGEMENTS

The material discussed in this talk is the result of the dedicated work of the following researchers (in alphabetical order)

At PPPL - Princeton

C Barnes (LANL)
M Caorlin
L Johnson
J Kamperschroer
P La Marche
M Loughlin (JET - UK)
D Mueller
D K Owens
J Strachan

At CCFM and INRS - Varennes, Canada

G Abel
M Ennaceur
J-L Gauvreau
H Y Guo
E Haddad
H H Mai
D Keroack
R Paynter
N Richard
G G Ross
B L Stansfield
B Terreault
W Zuzak
and the TdeV Team

CONTENTS

1. INTRODUCTION

TWO PMI AREAS OF STUDY FOR TFTR'S DT

A. <u>INFLUENCE OF LITHIUM ON TRITIUM IN-VESSEL RETENTION</u>

- ABUNDANT USE OF Li-PELLET CONDITIONING IN TFTR'S D-T CAMPAIGN
- WILL LITHIUM DRAMATICALLY INCREASE THE IN-VESSEL TRITIUM INVENTORY ?

B. <u>TRITIUM-CLEANUP OF THE VESSEL DURING DT CAMPAIGN</u>

- TRITIUM BUILDS UP ON THE WALLS AND LIMITERS DURING DT PULSES (INVENTORY CONCERN)
- THEN TRITIUM FROM WALLS AND LIMITERS ENTERS PLASMA (ADDITIONAL FUELING)
- CAN WE TAKE ACTION ON THESE TWO ISSUES ? AND HOW ?

2. LITHIUM EXPERIMENTS AT TdeV
July-August, 1993

2.1 GOAL

- STUDY EFFECT OF Li DEPOSITED LAYERS ON DEUTERIUM SHORT-TERM VESSEL RETENTION

2.2 THE EXPERIMENT

- BORONIZE, He GDC, H_2 SHOTS
- LITHIUM SOLID DEPOSITION:

  Li ON CRUCIBLE INTO SOL DURING D SHOTS

- GRAPHITE AND Si SAMPLES ALSO EXPOSED TO PLASMA AND BORONIZATION
- MEASURE DEUTERIUM INPUT AND PUMPOUT BY RGAs. DIFFERENCE IS CALLED *RETENTION*
- ANALYZE SAMPLES (SIMS, PLD)
- REPEAT SEQUENCE: NEW SAMPLES, NO LITHIUM DEPOSITION

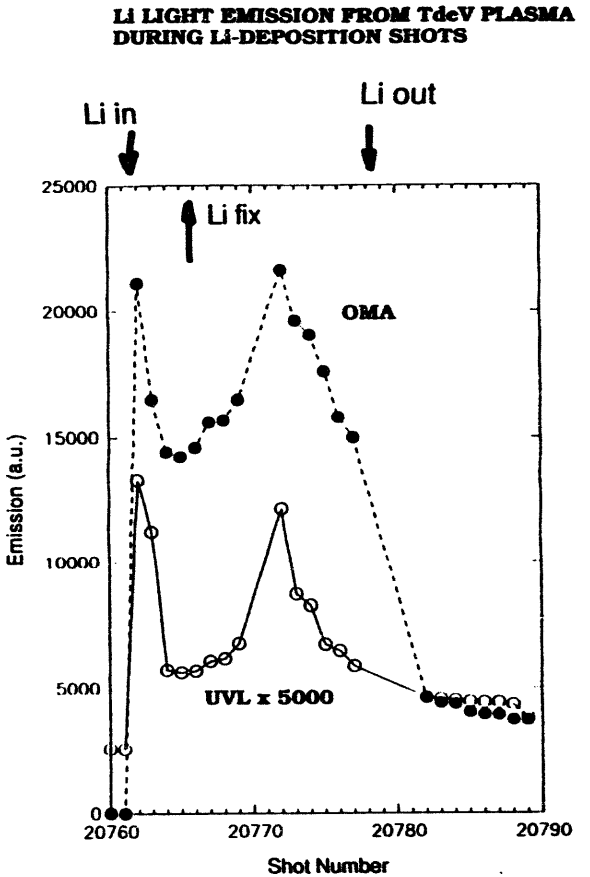

OMA looks above Li crucible
UVL looks at plasma edge

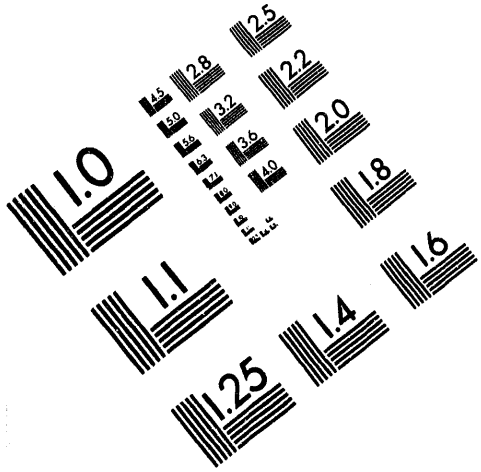

Association for Information and Image Management
1100 Wayne Avenue, Suite 1100
Silver Spring, Maryland 20910
301/587-8202

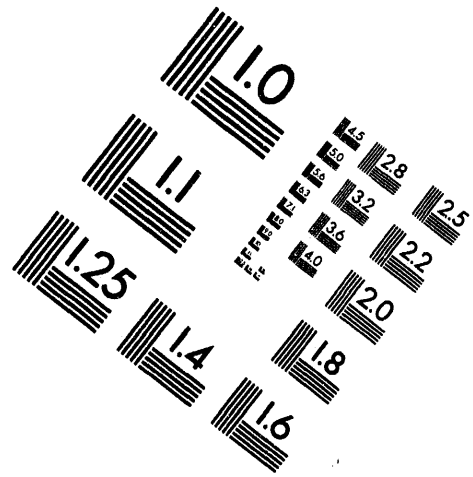

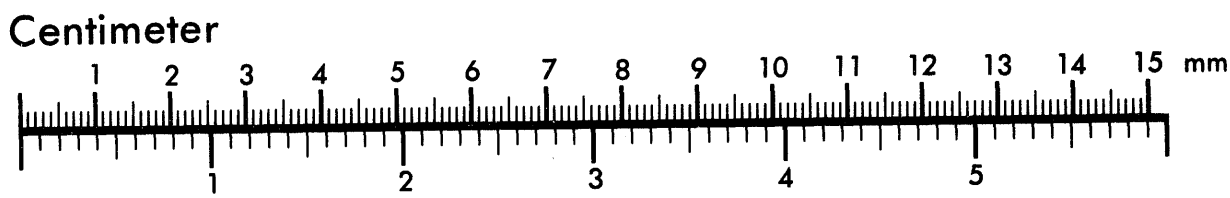

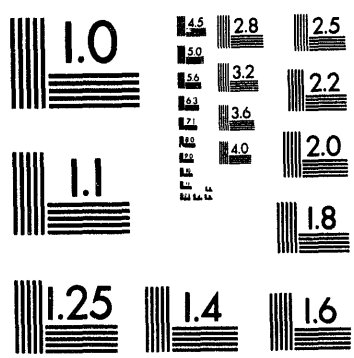

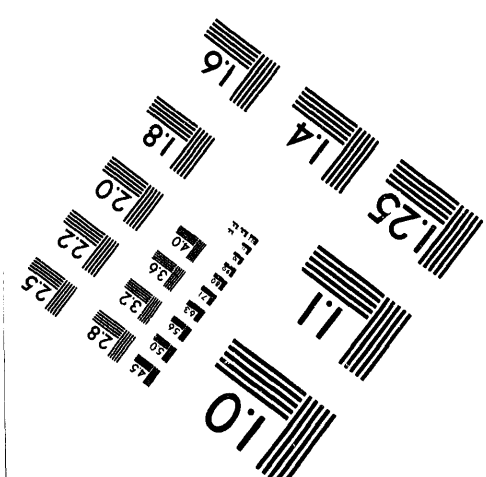

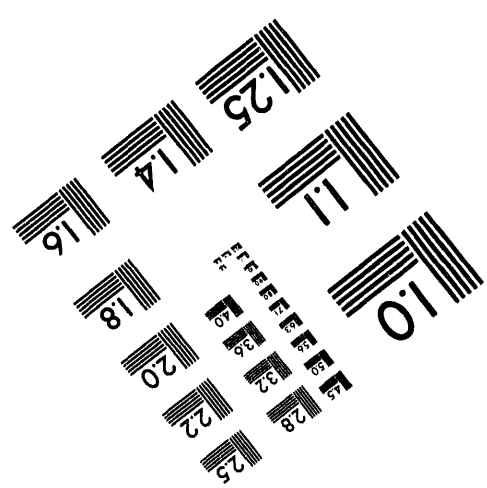

3 of 8

2. LITHIUM EXPERIMENTS AT TdeV (cont'd)

2.3 PRELIMINARY RESULTS

1. *0.2 g OF LITHIUM CONSUMED, 10^{21} Li atoms/m^2*
2. *VERY LITTLE DIFFERENCE BETWEEN Li AND NO-Li CASE*

- Li DETECTED ON GRAPHITE AND Si SAMPLES (SIMS) AND IN PLASMA EDGE
- PLD: D DESORBED WAS 35 % HIGHER WITH LITHIUM, ONLY ON ION-DRIFT SIDE
- RGAs: D RETENTION INCREASED WITH LITHIUM TO 50% FROM 40% OF D INPUT
- MORE WORK UNDER WAY

3. TFTR EXPERIMENTS ON T-CLEANUP

3.1 GOAL

- ATTEMPT A T-CLEANUP DURING DT-CAMPAIGN
- COMPLY WITH MACHINE AND OPS CONSTRAINTS (NO DECONDITIONING, SCHEDULE, TIMING ...)
- ATTEMPT COLLECTING AND MEASURING AMOUNT OF REMOVED TRITIUM

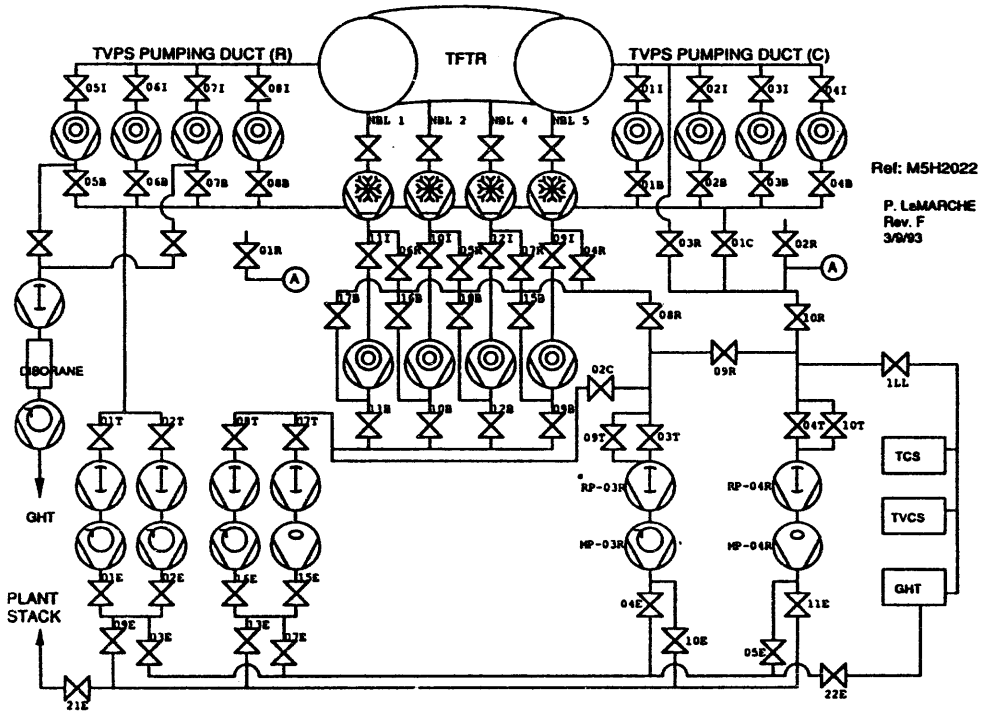

3. TFTR EXPERIMENTS ON T-CLEANUP
(cont'd)

3.2 THE EXPERIMENTS

- USE ONE NB LINE (# 1) TO PUMP TORUS AND TO INJECT D BEAMS
- 4 OHMIC CLEANUP SHOTS AT R_p = 2.62 m.
- 2 D NB SHOT, W_{NB} = 5 - 7.5 MW, R_p = 2.62 m, TO MEASURE NEUTRONS
- REPEAT 4 OH + 2 NB SEQUENCE 5 TIMES
- STOP OPS AND REGEN NBL INTO GHT
- MEASURE AMOUNT OF TRITIUM RECOVERED IN GHT

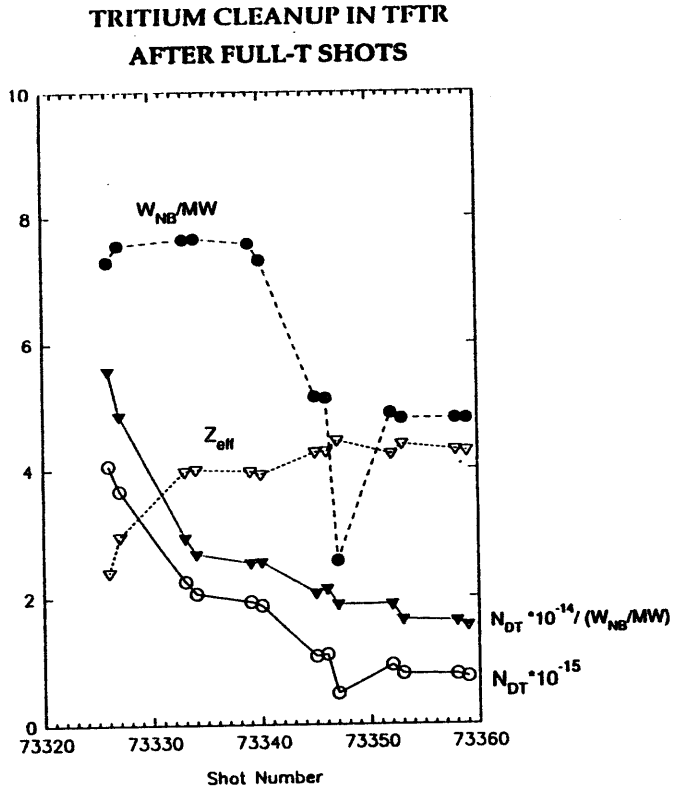

N_{DT} = DT-NEUTRONS
W_{NB} = D-NB POWER
Z_{eff} = Z EFFECTIVE

3. TFTR EXPERIMENTS ON T-CLEANUP (cont'd)

3.3 PRELIMINARY RESULTS

- DT-NEUTRONS DECREASE,
- Zeff INCREASES

  ALONG THE RUN.
- AMOUNT OF T RECOVERED:

  G_T = 37 Ci
- AMOUNT OF T PREVIOUSLY INJECTED INTO TORUS:

  F_T = 395 Ci
- LOWER BOUND ON RETENTION FACTOR:

  G_T/F_T = 37/395 = 9.4 %
- UPPER BOUND ON INVENTORY:

  $F_T - G_T$ = (395 - 37) Ci = 358 Ci

4. CONCLUSION

A. TdeV/Li

- SOLID LI DEPOSITION DEVELOPED
- LI DETECTED IN PLASMA EDGE AND ON SAMPLES
- D RETENTION SLIGHTLY INCREASED BY LI

B. T-CLEANUP AT TFTR

- T RETENTION FACTOR WAS HIGHER THAN 9%
- INVENTORY WAS LESS THAN 358 Ci
- T RECYCLING FROM LIMITER CAN BE REDUCED BY OH SHOTS - but *SLOWLY*
- PLASMA SHOTS NOT VERY EFFECTIVE IN REMOVING TRITIUM FROM VESSEL.
- ANALYSIS UNDER WAY

GENERAL ATOMICS

Divertor Plasma and Plasma Facing Wall Research on DIII-D

By The DIII-D Team

Presented by Phil West

at the US/Japan Workshop on HIIF/PMI

UCSD

24 January 1994

GENERAL ATOMICS

DIII-D PROGRAM MISSION AIMS AT DEMO

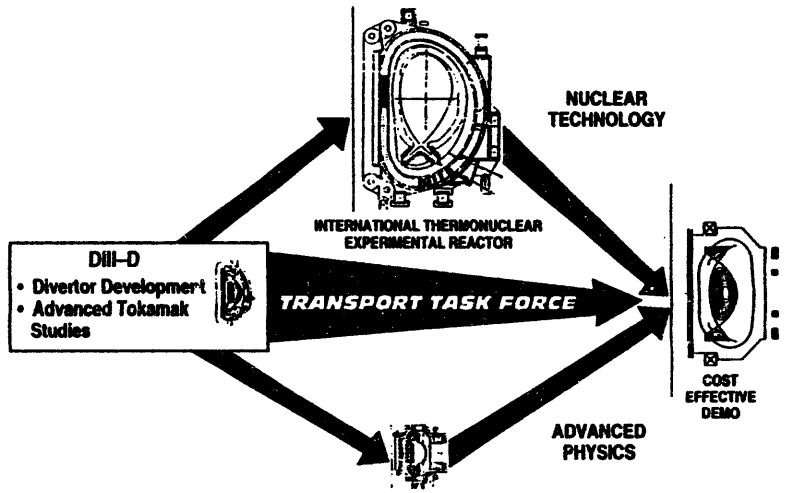

GENERAL ATOMICS

INCREASED PERFORMANCE IS OBSERVED WITH LOWER Z_{wall} MATERIALS

DIII-D FUSION PERFORMANCE HAS DOUBLED EVERY TWO YEARS

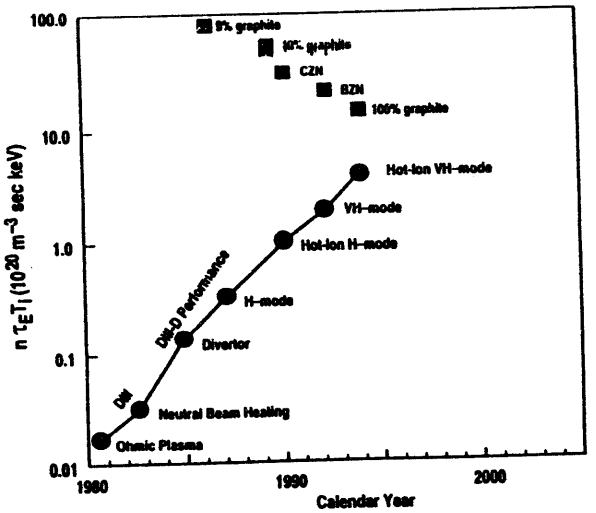

GENERAL ATOMICS

DIII-D's Contribution to Progress in Divertor and PFC Development

- **Divertor Plasma Characterization:**
  - -Better Understanding of the Divertor Plasma
  - -Empirical Scaling to Next Generation Devices
  - -Modeling Code Validation
- **Radiative Divertor:**
  - -Reduce peak heat and energetic particle loads on the strike plate
    → reduced materials and engineering requirements.
- **Advanced Divertor Program: Pumping and Biasing**
  - -Particle Control
  - -He Ash Removal
- **DIMES: Divertor Materials Erosion Studies**
- **International Collaborations on First Wall Materials and Coatings**

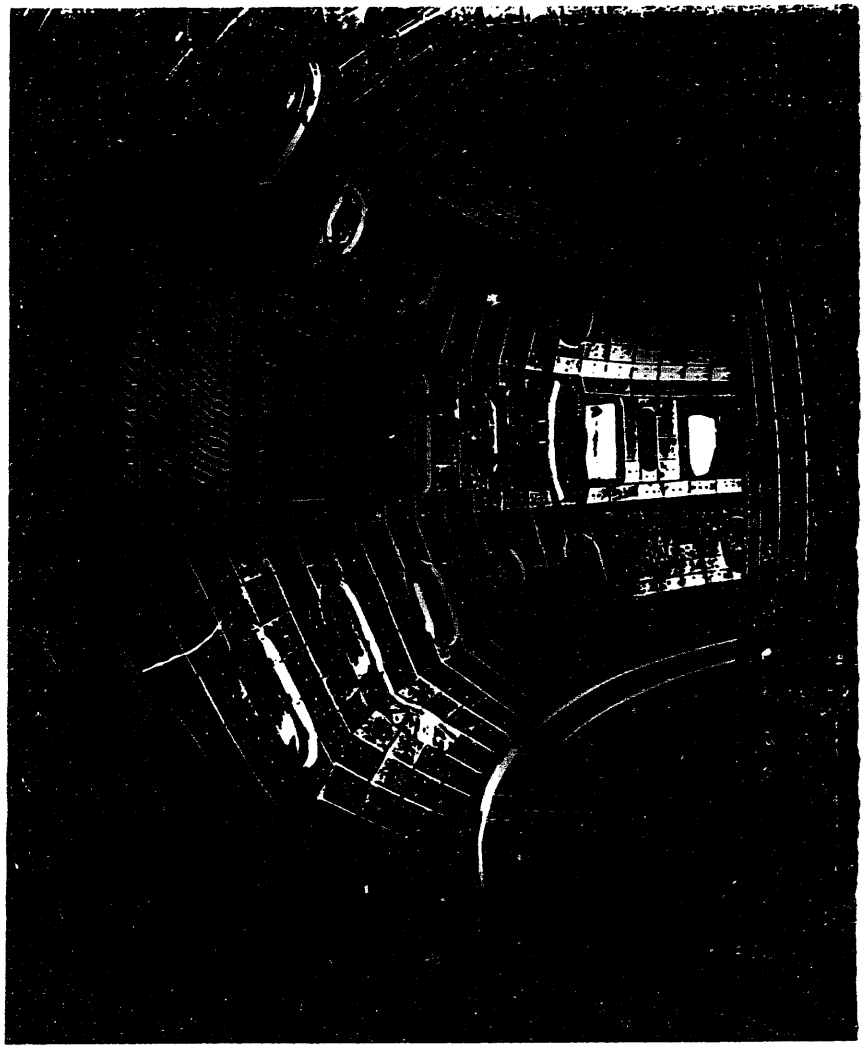

DIVERTOR AND SCRAPE-OFF LAYER DIAGNOSTICS

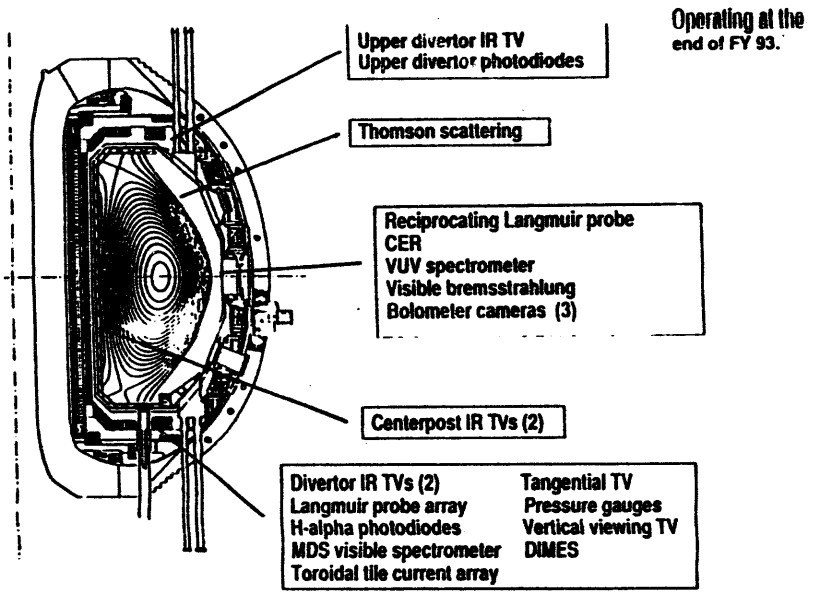

Sandia National Laboratories

Scrape-off layer measurements help determine divertor slot width:

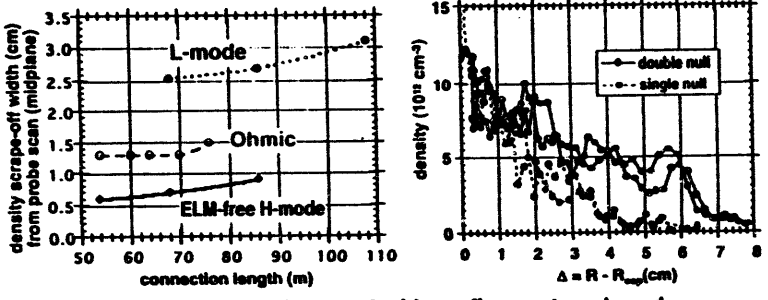

- The SOL width varies by a factor 5-6 with confinement mode and configuration ⇒ "openness" of divertor varies with operating conditions.
- SOL profiles are used to benchmark the models used for design of the DIII-D Radiative Divertor, TPX, and ITER.
- Reciprocating probe measurements also give us turbulence driven particle and heat transport and help determine the SOL transport processes.

SIMULATION OF SHOT 78037, 2800 ms

GENERAL ATOMICS

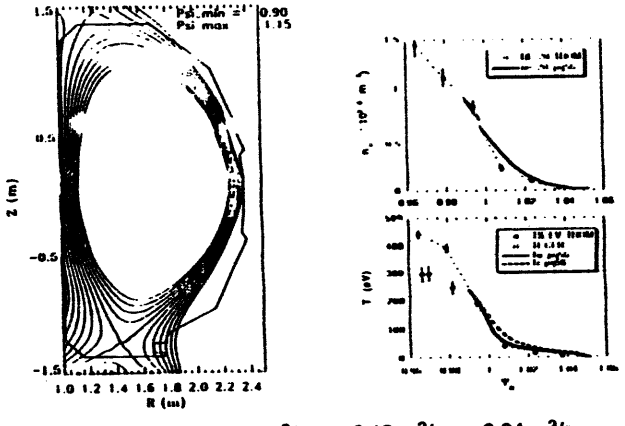

- Simulation with Ω_i=0.035 m^2/s, χ_e=0.12 m^2/s, χ_i=0.04 m^2/s

DIVERTOR POWER SIMULATION FOR 78037

GENERAL ATOMICS

- Calculated peak power at outer strike point is within 30% of experiment
- Outer profile shape is consistent with experiment

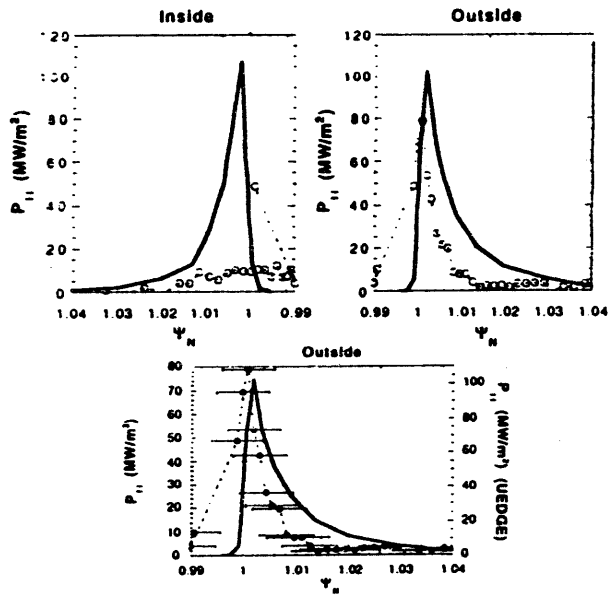

GENERAL ATOMICS

Divertor Heat Flux is Reduced with Deuterium Gas Puffing

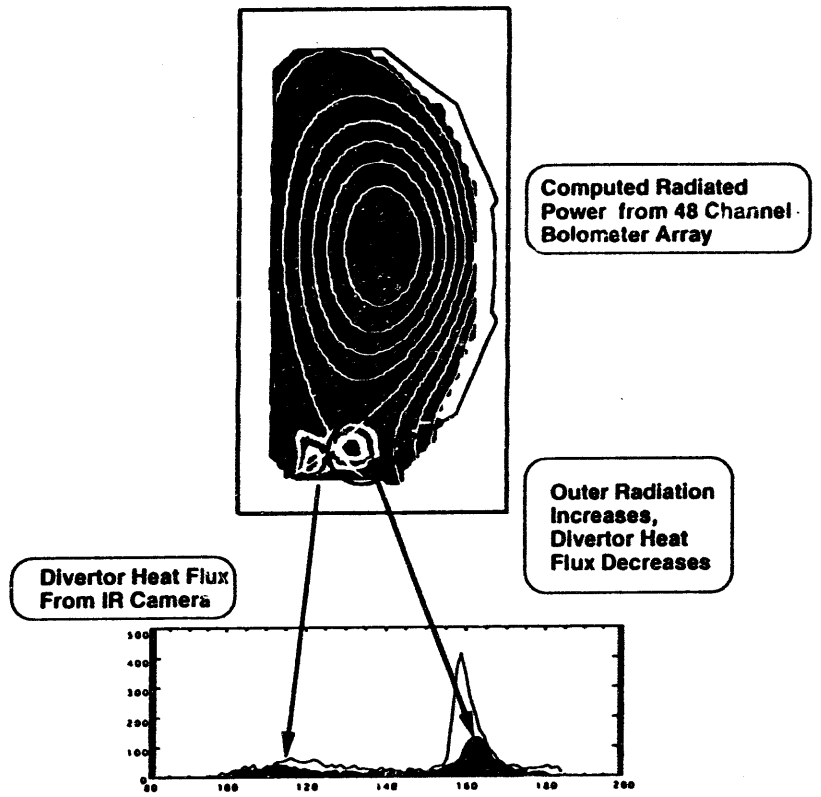

Shot 79341 @ 3200ms

GENERAL ATOMICS

Divertor Heat Flux Reduction in D2 Puffing Experiments

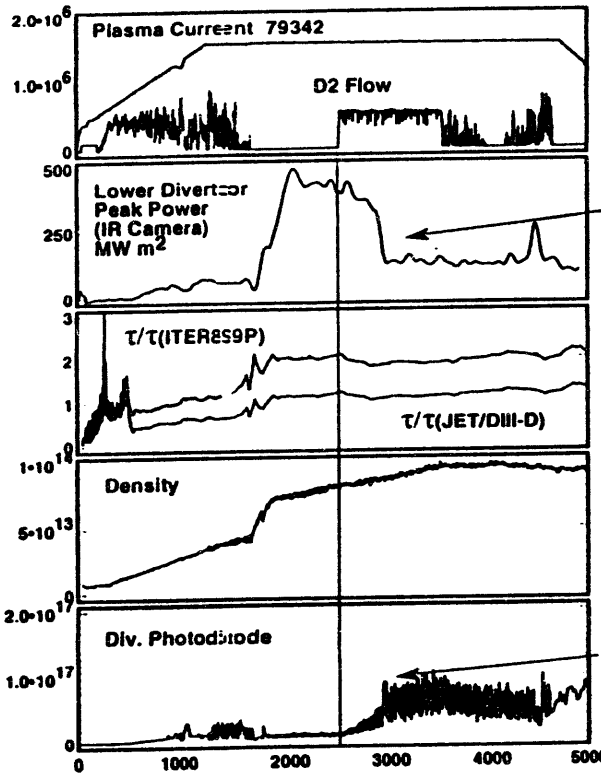

- Beam Power 9 MW
- Heat Flux Reduction
- Small Effect on τ
- Core Density Increases
- ELMs Change

GENERAL ATOMICS

Neon Radiates Inside of the Separatrix

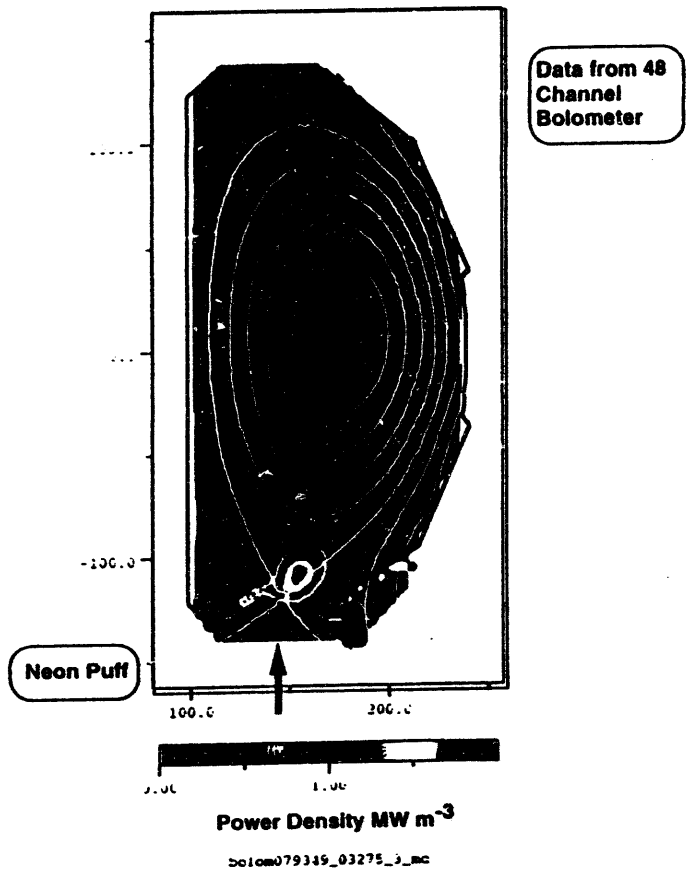

GENERAL ATOMICS

Divertor Heat Flux Reduction in Neon Puffing Experiments

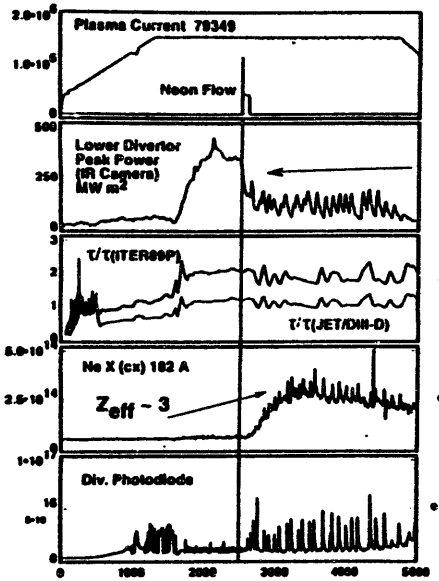

- Beam Power 9 MW
- Heat Flux Reduction
- Small Effect on τ
- Core Neon Decreasing
- ELMs Change

GENERAL ATOMICS

ADVANCED DIVERTOR HARDWARE FOR PARTICLE CONTROL

COMPLETE CARBON-TILE COVERAGE

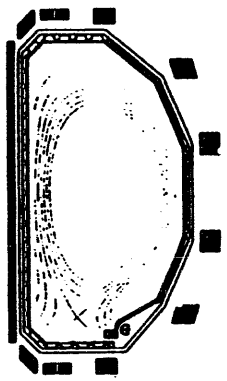

CRYOPUMP UNDER DIVERTOR BAFFLE

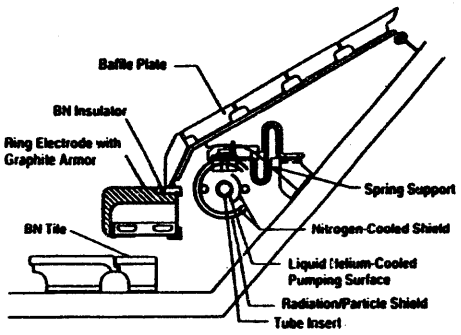

Helium Exhaust in ELMing H-mode Plasmas in DIII-D

- Exhaust of helium has been demonstrated in ELMing H-mode plasmas using Argon frost on the ADP cryopump.
- Preliminary analysis indicates that $\tau^{*}_{He} / \tau_{E} = 11 - 14$ has been achieved, within the acceptable range for successful operation of a reactor of 7-15.

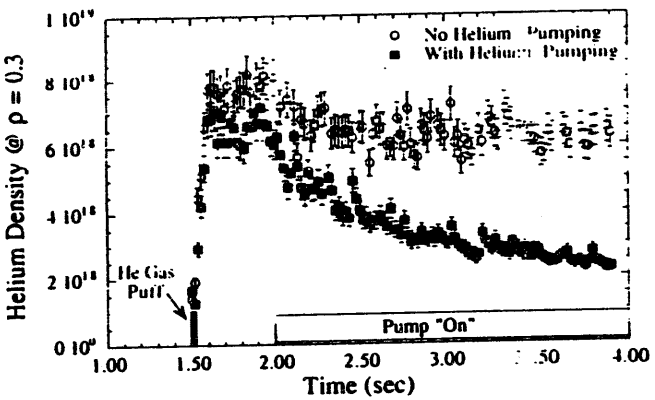

orn1

GENERAL ATOMICS

GENERAL ATOMICS

WITH DIVERTOR CRYO-PUMPING H-MODE DENSITY IS DECOUPLED FROM CURRENT

Different Densities – Same Current

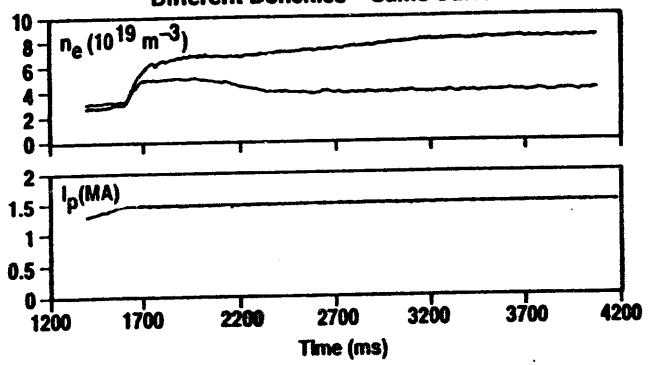

Different Currents – Same Density

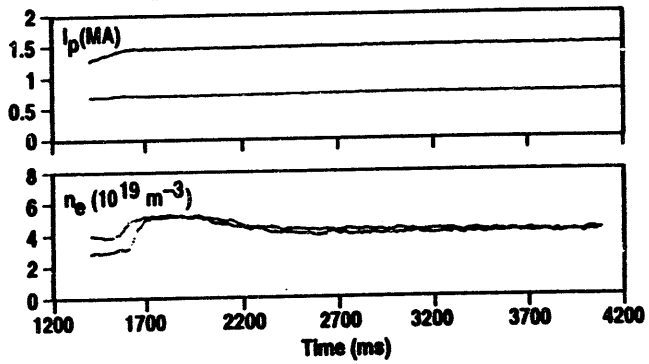

Profile Evolution with Helium P... ping

- During pumping, the helium density profile remains essentially the same.

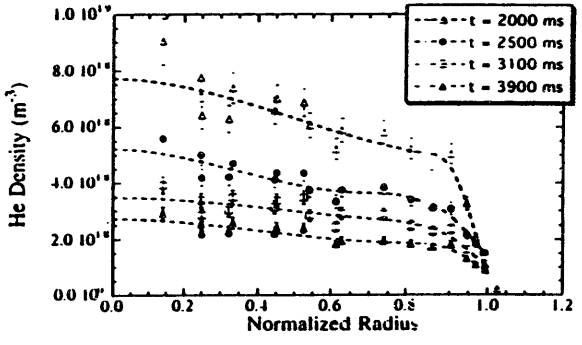

- This observation suggests that the removal of helium in these experiments is limited by the effective cryopump pumping speed and not by helium transport to the plasma edge (i.e., that the helium confinement time τ_{He} is much shorter than τ^{*}_{He}).

ornl

GENERAL ATOMICS

SPRED Spectra Before and After Installation of Tiles

Vessel Boronized

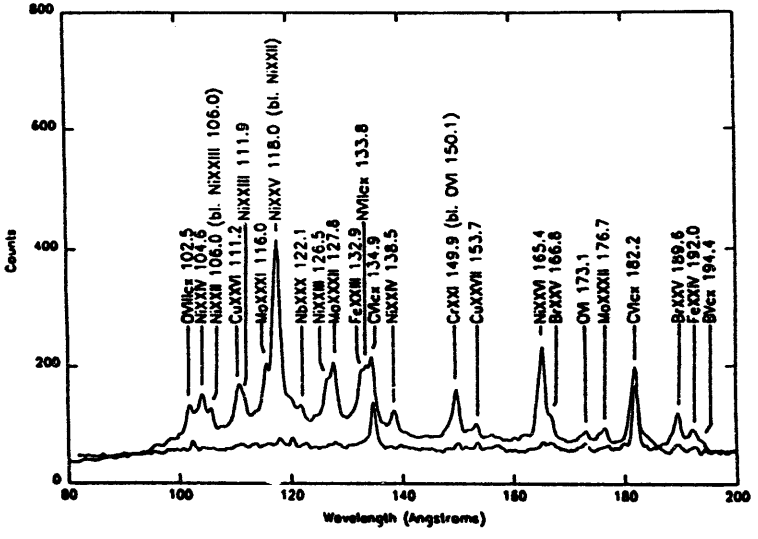

Primary Contributors to Z_{eff} for Three Wall Conditions*

	n_i/n_e	
	Carbon	Oxygen
40% Carbon 60% Inconel Boronized	.034	.0098
100% Carbon Unboronized	.023	.0050
100% Carbon Boronized	.031	.0023

*measured using the SPRED spectrometer during VH-mode operation

Metallic Impurities and Radiated Power Significantly Lower after Installation of the All Carbon Wall

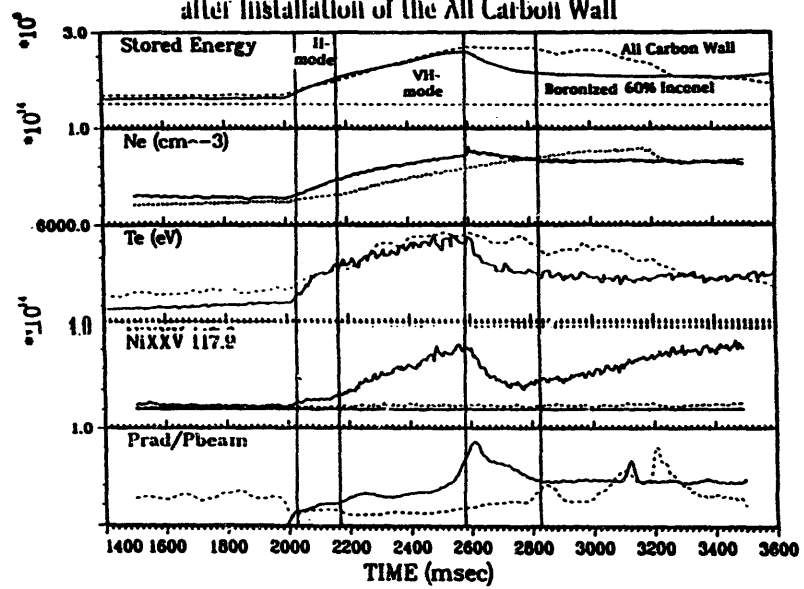

GENERAL ATOMICS

MATERIAL EVALUATION EXPERIMENTS IN DIII-D DIVERTOR

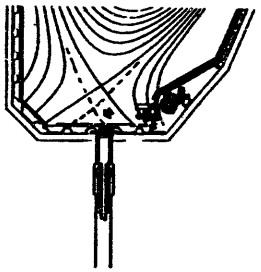

DIMES Sample Insertion

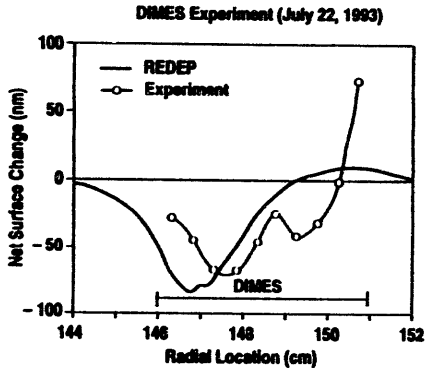

Comparison of Net Erosion with REDEP Model

HIGH HEAT FLUX TESTING
B_4C COATED RGT
(TITANIUM DOPED RECRYSTALLIZED GRAPHITE)

RGT has high thermal conductivity (- 400W/mK), of interest for long pulse applications in DIII-D

Sample provided by TRINITI LABS, Troitsk, Russia

E-Beam testing at SANDIA NATIONAL LABS, New Mexico

110 Cycles, from 2.5 to 10 seconds each

Heat flux raised from 2.3 To 13 MW/cm^2

No damage observed even at the highest level tested

Peak surface temperature at 13 MW/cm^2 for 5 seconds was 940 C

GENERAL ATOMICS

DIII-D Radiative Divertor Program: Objectives

- Demonstrate Reduction of Divertor Heat Flux (10X)
  - -Consistent with ITER and TPX needs
  - -Consistent with the DIII-D Advanced Tokamak (AT) Program
- Demonstrate Simultaneous Particle Control and He Ash Removal
  - -ITER Relevant
  - -Support the DIII-D Advanced Tokamak (AT) Program
- Develop Physics Understanding
  - -Provide Diagnostics
  - -Benchmark Models
  - -Participate in Data Base development with other tokamaks
  - -Continue PMI studies
- Schedule
  - -Conceptual Design nearing Completion
  - -Final Design FY94
  - -Fabrication FY95
  - -Installation Mid FY96

FUTURE DIVERTOR AND SCRAPE-OFF LAYER DIAGNOSTICS

We are now working to install the following diagnostics according to the schedule given.

Diagnostic	Institution	First Operation	Measurement
Divertor-throat Langmuir probes	SNLA, LLNL	April — May 1994	particle flux into baffle during pumping experiments
Bias-ring IR TV	GA, LLNL	May 1994	heat flux on bias ring and in divertor throat during biasing/pumping exps.
Laser blow-off system	GA	May 1994	impurity-ion confinement time
Divertor interferometer	LLNL	April — May 1994	time-resolved line density across inner/outer divertor legs
Divertor reflectometer	UCLA	June 1994	peak density, private-region-side profile of divertor density at each leg
X-point plunging Langmuir probe	SNLA, UCLA	July 1994	2-d profiles of divertor density, temp, and plasma flow (@ low power)
Divertor Thomson scattering	LLNL, GA	June 1995	2-d profiles of divertor density, temperature (@ high power)
Divertor Thomson LIDAR	LLNL, UCD	1997	2-d profiles of divertor density, temperature (after RDP hardware)

GENERAL ATOMICS

Features of the DIII-D Radiative Divertor Design

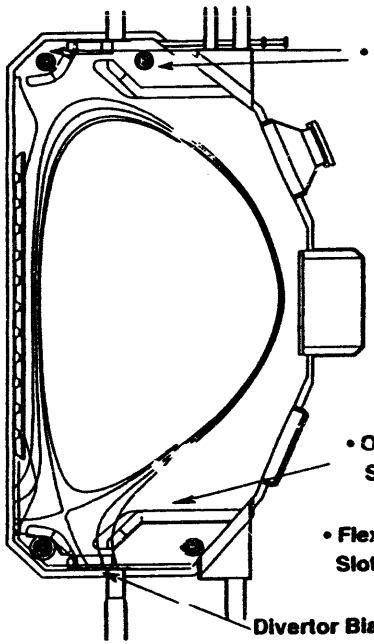

- Pumping of Either Inner or Outer Strike Points
- Either Single or Double Null Operation
- Diagnostic Access Similar to Present DIII-D Machine
- Operation on Top of Shelf Possible
- Flexible Design-Vary Slot by Changing Tiles

Divertor Biasing

GENERAL ATOMICS

Summary

- The plasma facing wall and wall conditioning have played a significant role in the steady increase of DIII-D performance over the past several years.
- DIII-D has provided valuable divertor data for the ITER and TPX design.
- DIII-D radiative divertor experiments have demonstrated significant heat flux reduction in an open divertor configuration.
- Particle control and He ash exhaust have been demonstrated in an enhanced confinement regime.
- DIMES has provided divertor materials erosion data for the benchmarking of erosion/redeposition codes and has the capability to provide more benchmarking data on ITER and TPX relevant materials, to study disruption induced erosion, and to provide divertor plasma diagnostic support.
- Future work in diagnostic development, benchmarking models, and radiative divertor development will provide direct support to ITER and TPX, as well as support the DIII-D Advanced Tokamak Program.

Session IV

High Heat Flux Technology

US/J Workshop on HHF & PSI for
Next Fusion Devices,
San Diego, CA,
Jan. 24-27, 1994

JAERI

Development of High Heat Flux Components at JAERI

M. Akiba (JAERI)

- Overview of 1993
- Recent Topics

Overview of 1993

JAERI

- Tests of Divertor Mock-ups
  - 1m-long mock-ups with a support structure
  - Mock-ups for JT-60U (IV.4 - Suzuki)
  - Mock-ups with W-Cu heat sinks (IV.5 - Sato)
- Heat Transfer Experiments
  - Smooth & swirl tubes
  - CHF dependence on subcooling (SNL+JAERI)
- Tests of Advanced Cooling Technique
  - Gas-solid suspension flow (JAERI/Tokai)

Overview of 1993 (continued)

- Simulated Disruption Experiments
  - CFCs, W at ~1000 °C
  - B_4C-overlaid CFCs for JT-60U
  - Experiments in a plasma gun (UNM/SNL + JAERI)
- High Ion Flux Experiments
  - Development of an ion source for high ion flux experiments
- Gas Absorption and Desorption of CFCs (Prof. Yamashina)

- US/J Workshop: M. AKIBA -

Overview of 1993 (continued)

- Code Development
  - Vapor shield effect (JAERI/Tokai)
  - Heat deposition of runaway electrons (JAERI/Tokai)
  - Neutron irradiation stress (JAERI/Tokai)

Overview of 1993 (continued)

- Neutron Irradiation
  - CFCs ; JRR-3, JMTR
  - Irradiation on CFC+Cu bonded structures and Be will start in 1994.
- E-beam Test Facility in Hot Cells
  - The 60 kW e-beam test facility in the JMTR Hot Cells is under designing.
  - Licensing has already been obtained.
  - Installation to the hot cells will start in September 1994.

1m-long Divertor Mock-ups with a support structure were tested.

- Test conditions
  - 15 MW/m², 30s, heating length of ~ 5 cm
  - 10 m/s, 25 °C, 2.5 MPa, pure water
- Mock-ups
  - monoblock type + rail sliding support
  - monoblock type + pin sliding support
- Results
  - Both types of sliding supports show sufficient sliding performance of 0.5 mm, and can suppress the deformation within 0.5 mm.

Sliding Structures

JAERI

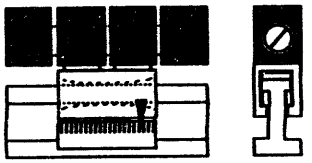

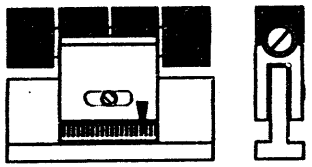

- Rail sliding structure
  - High sliding resistance
  - Temperature of rails will be low.
- Pin sliding structure
  - Low sliding resistance
  - Temperature of pins will be high.

1m-long Divertor Mock-ups

JAERI

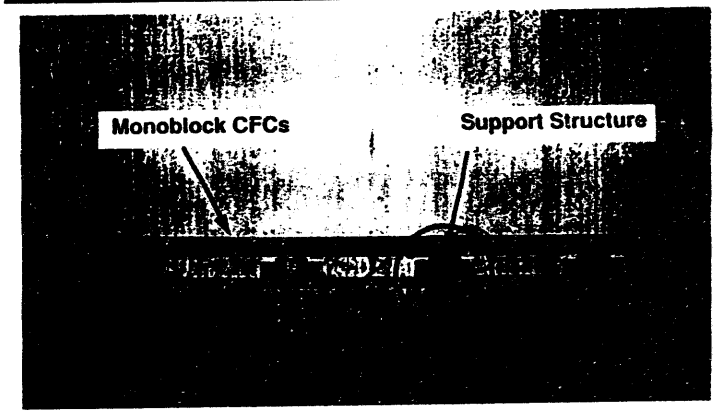

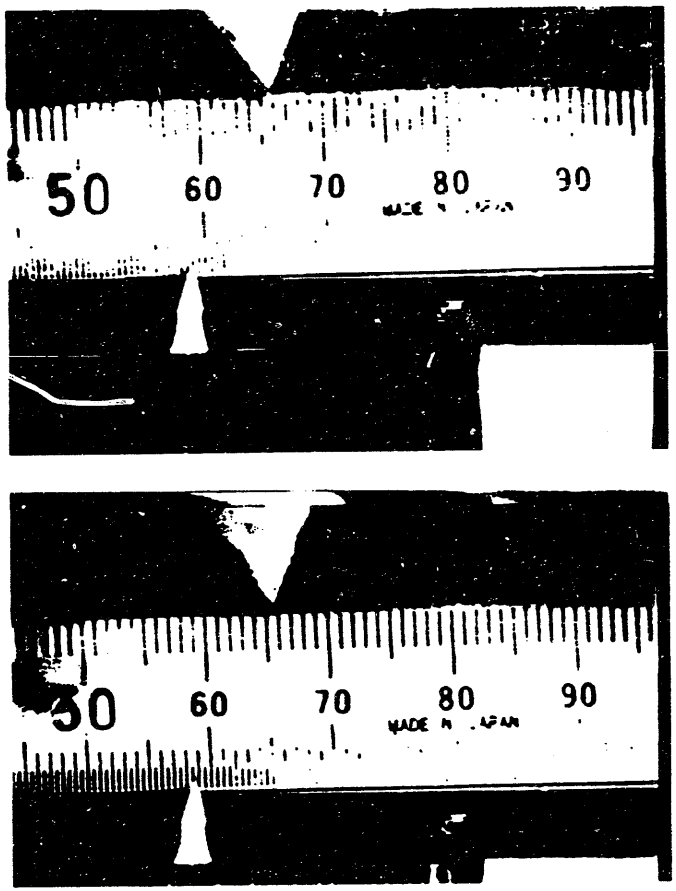

There is no correlations under the one-sided heating conditions for;

JAERI

- boiling/subcooled boiling heat transfer correlations,
- forced convection heat transfer correlations of a swirl tube.

- Heat transfer experiments have been performed under the one-sided heating conditions with
  - smooth and swirl tubes

Development of High Flux - Low Energy Ion Source

JAERI

- To measure material erosion by ions, a high flux - low energy ion source has been developed.
  Target is;
  - Beam energy 50 ~ 1000 V
  - Ion flux ~ 10^{17} ions/cm^2•s
- New acceleration grids, 0.5 mm ϕ W-wires, have been developed.
- Ion flux of 6 x 10^{16} ions/cm^2•s was achieved. The ion flux is limited by the arc power supply.

- US/J Workshop: M. AKIBA -

High Flux - Low Energy Ion Source

JAERI

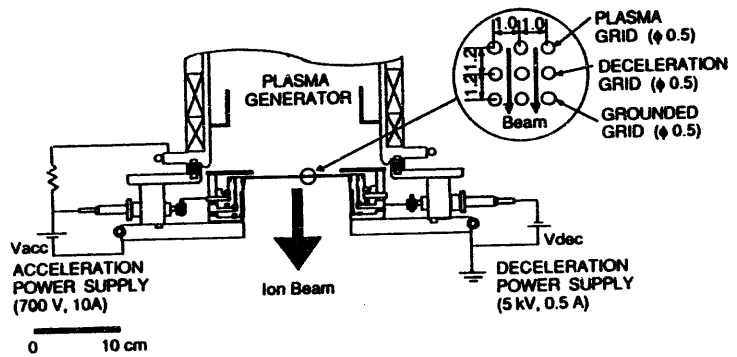

Beam Profile at Sample Surface

JAERI

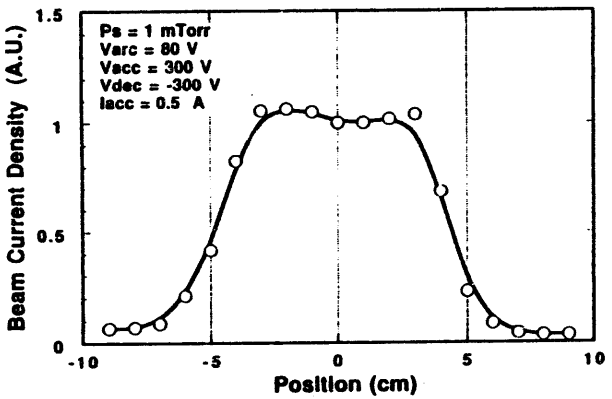

JAERI's Activities under US/J Collaboration in FY1993 (April 1993 ~ March 1994)

JAERI

- US to Japan (JAERI)
  - P214 Beta Backscatter in JT-60U
  - P215 Erosion-Redeposition Modeling (deferred in 1994)
  - PL123 High Heat Flux Test on Tungsten Armor
- JAERI to US
  - Q183 Evaluation of a B_4C-converted Coating on Graphite Tiles on DIII-D
  - QL142 Critical Heat Flux Studies
  - QL143 Disruption Simulation
- Workshop
  - Q181 High Heat Flux Components & Plasma Surface Interacts for Next Devices (this workshop)
  - Q182 Helium-cooled High Heat Flux Components Design (deferred in 1994)

Japan-U.S. Workshop Q181 High Heat Flux Components and Plasma Surface Interactions for Next Devices
San Diego, January 24-27,1994

HHFC Development in NIFS

N. Noda, Y. Kubota, A. Sagara, N. Inoue, O. Motojima

National Institute for Fusion Science

With the contributions from

Professor Yamashina's laboratory
in Hokkaido University

Toyo Tanso Co. Ltd.

Kawasaki Heavy Industry Co. Ltd.

Hitachi Chemical Co. Ltd.

Hitach Works, Hitachi Ltd.

Pechinei Japon Co. Ltd.

Contents

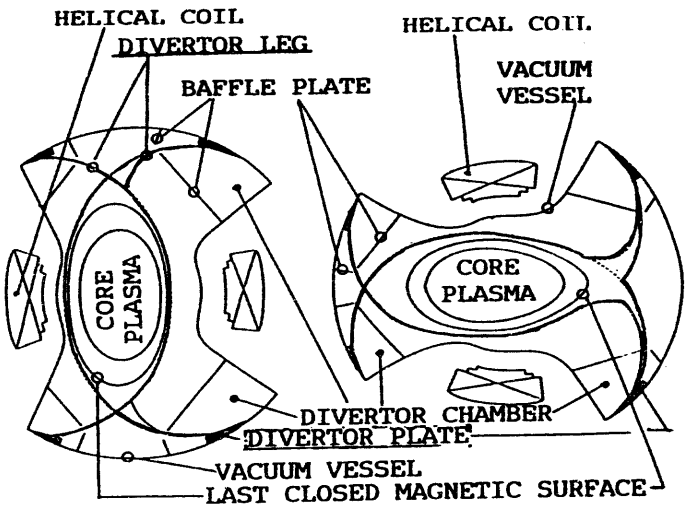

Fig. 1 Cross sectional view of the LHD device
Torus axis is on the left hand side.

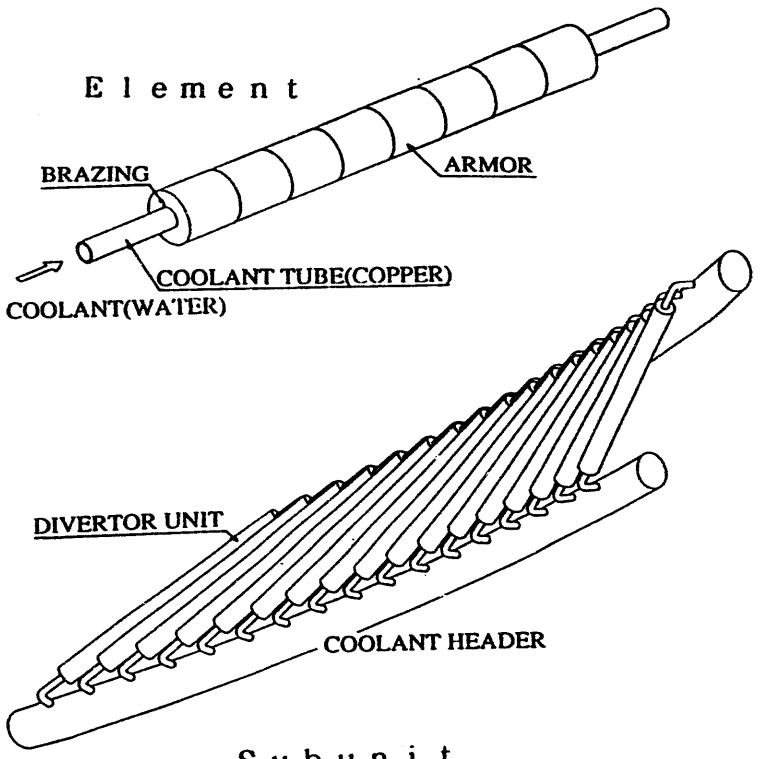

Present Status of Vacuum Vessel and Divertor Plates Design

- finalizing the detail design of the vacuum vessel and the divertor plates
- fabrication of mock-ups of the vacuum vessel and the helical divertor divertor plates

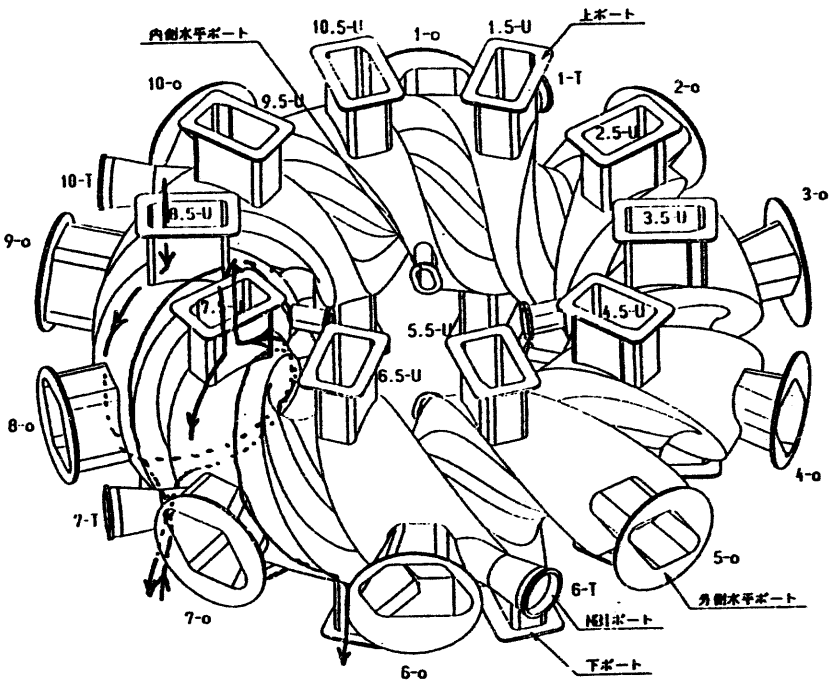

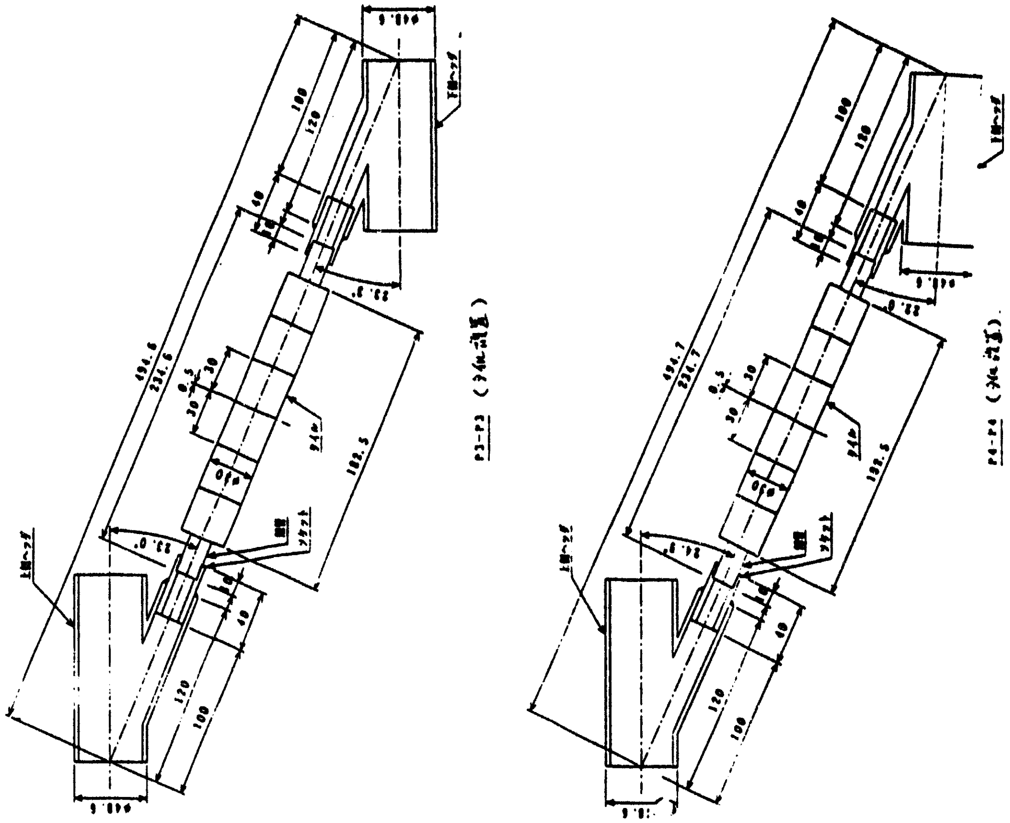

図3 ヘッダと要素の接続構造（2/3）

図1 ヘッダ付きモックアップ試験体形状（参考図）

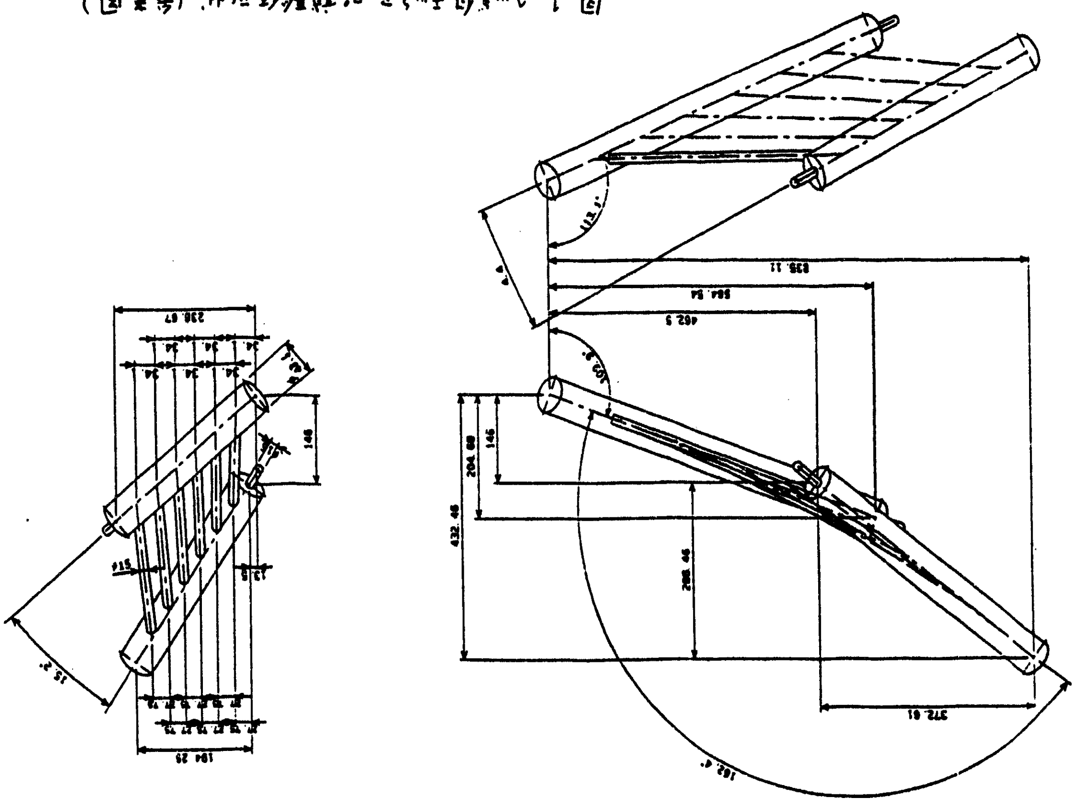

Schedule for Vacuum Vessel and Divertor Plates

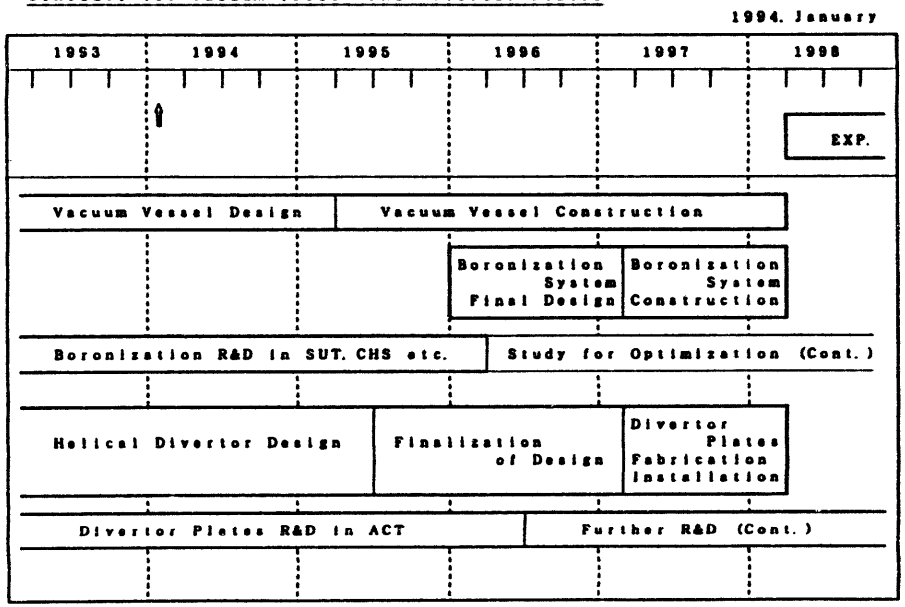

Goal of the HHFC Study in NIFS

- to find several possible candidates for LHD divertor plates

  carbon armor tiles brazed to copper cooling tube

  max. heat load of 10 MW/m^2

  criteria : surface temperature $Ts < 1200$ °C

  no large deterioration after 1000 shots

- to assess availability of graphite as armor tiles (heat load limit for graphites)

- to find other possible materials and geometry for future use

  advanced C-based materials

  PFC for higher heat load

Table 1. Heat load condition in LHD

total heating power (MW)	heat load (MW/m^2)	duration (sec.)
3	0.75	steady
20	5	10
>30	10	5

Outline of Test Pieces

- two types of brazing geometry were tested

  flat-plate type (F-type)

  mono-block type (M-type)

- felt type CC composite (CC) and isotropic graphite (IG) as armor tiles

  CX-2002U (Toyo Tanso)
  PCC-2S (Hitach Chemical)
  A05 (Le Carbone)

  IG-430U (Toyo Tanso)
  PD-330S (Hitach Chemical)

  PD-330S (Hitach Chemical)
  (with B_4C)

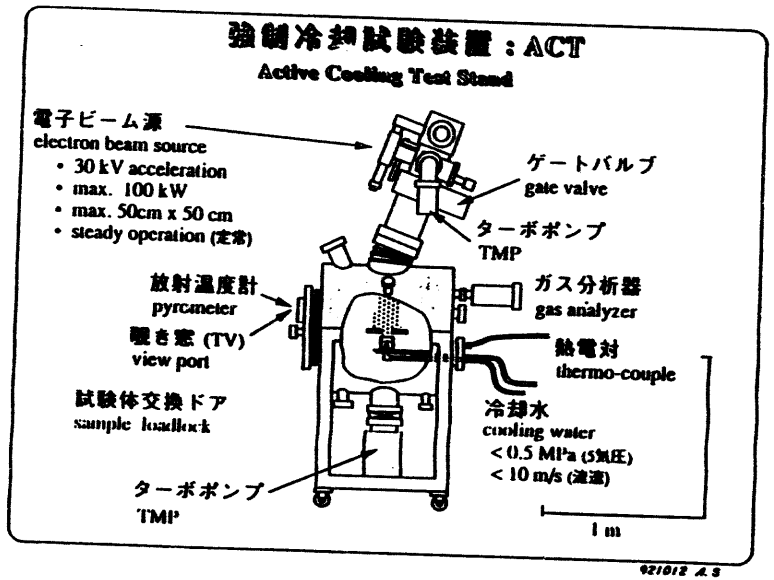
強制冷却試験装置：ACT
Active Cooling Test Stand
電子ビーム源
electron beam source
• 30 kV acceleration
• max. 100 kW
• max. 50cm x 50 cm
• steady operation (定常)
ゲートバルブ
gate valve
ターボポンプ
TMP
放射温度計
pyrometer
覗き窓 (TV)
view port
ガス分析器
gas analyzer
熱電対
thermo-couple
試験体交換ドア
sample loadlock
冷却水
cooling water
< 0.5 MPa (5気圧)
< 10 m/s (流速)
ターボポンプ
TMP
1 m
921012 A S

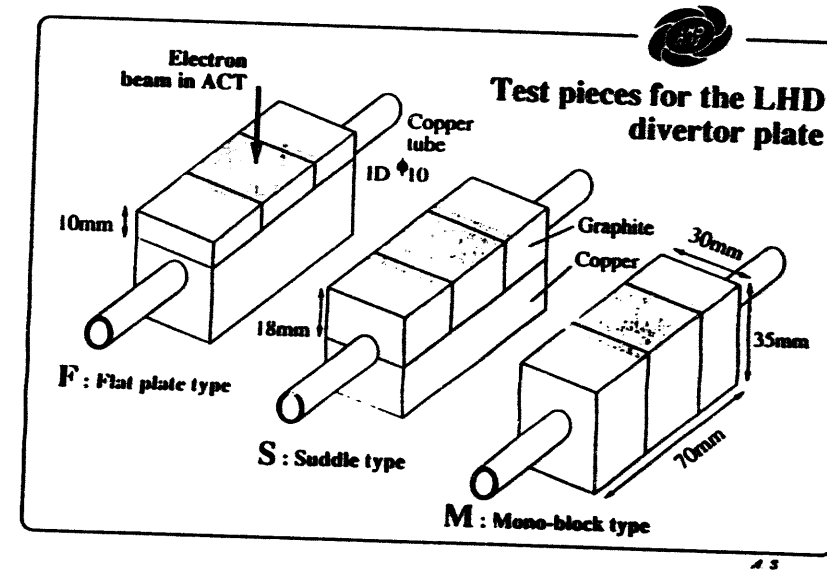
Test pieces for the LHD divertor plate
Electron beam in ACT
Copper tube
ID φ10
10mm
Graphite
Copper
30mm
18mm
35mm
F : Flat plate type
S : Suddle type
70mm
M : Mono-block type
A S

Automatic Control of Beam Power
DPCを使用した繰り返し電子ビーム照射の自動制御法2 (ターゲット温度制御)

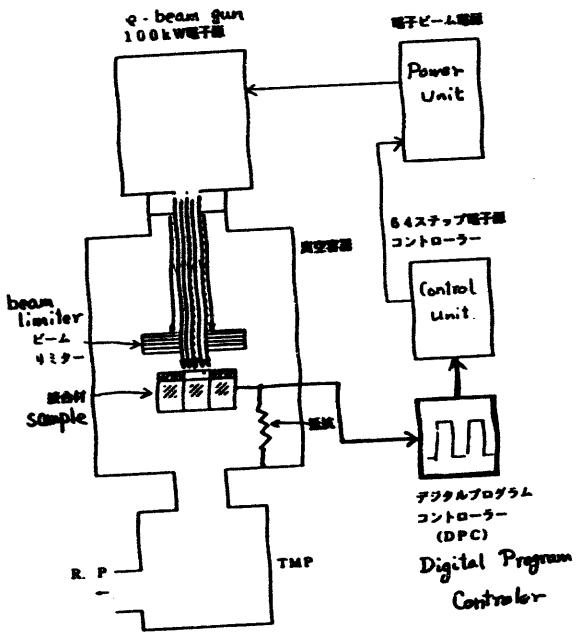

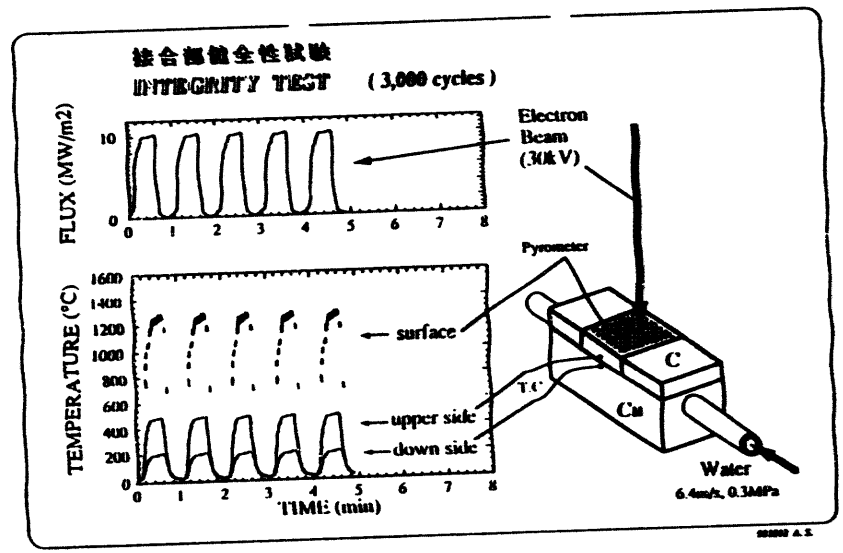

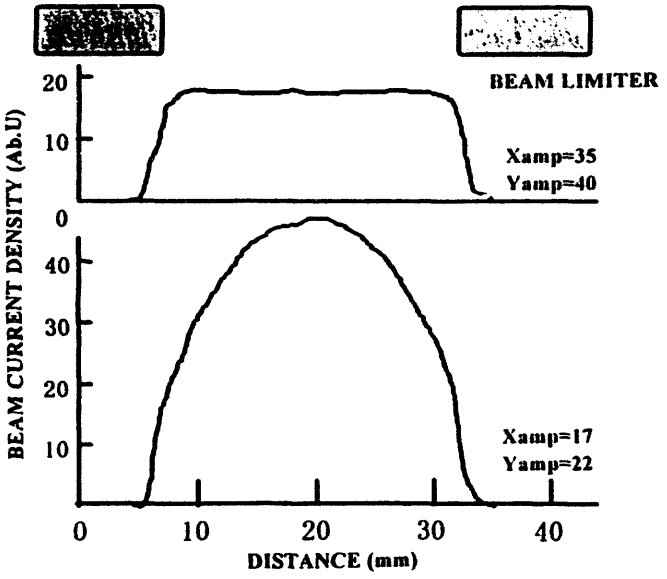
BEAM LIMITER
BEAM CURRENT DENSITY (Ab.U)
20
10
0
40
30
20
10
Xamp=35
Yamp=40
Xamp=17
Yamp=22
0
10
20
30
40
DISTANCE (mm)

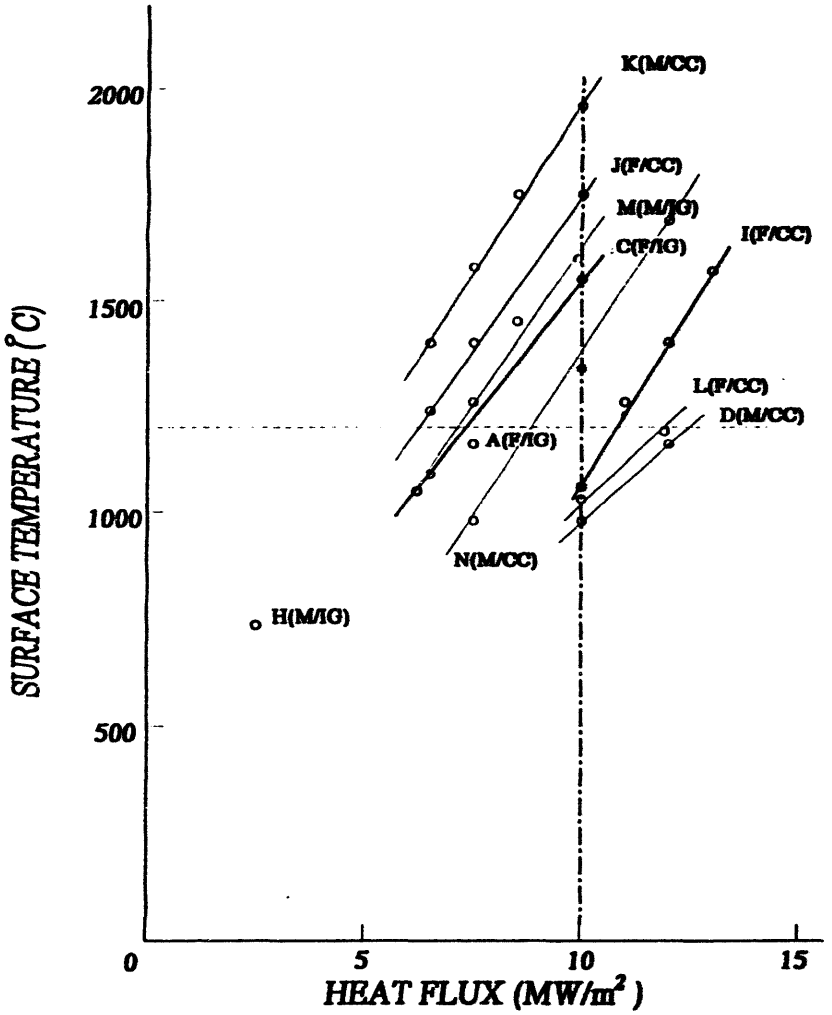
SURFACE TEMPERATURE (°C)
2000
1500
1000
500
0
5
10
15
HEAT FLUX (MW/m²)
K(M/CC)
J(F/CC)
M(M/G)
C(F/G)
I(F/CC)
L(F/CC)
D(M/CC)
A(F/G)
N(M/CC)
H(M/G)

HEAT LOAD (MW/m²)
SHOT NUMBER
0
1000
2000
3000
4000
5000
6000
5
10
15

Ts(°C)
Tiu(°C)
q(MW/m2)
FCT1013A
Ts(°C)
q(MW/m2)
shot#
0
500
1000
1500
2000
0
5
10
15
20
1000
2000
3000
4000
5000
6000

F/CC type
after 5100 cycles test
with 10MW/m2 for 30sec
water : 7.2m/s, 0.6MPa
Ts
before tests
Tiu
Tid
h
Heat Transfer Coefficient (kW m-2K)
Heat Flux (MW/m2)
Temperature (°C)
0
20
40
60
80
100
0
500
1000
1500
2
4
6
8
10
12

Case 2: PFC - Mo - Cu Brazing

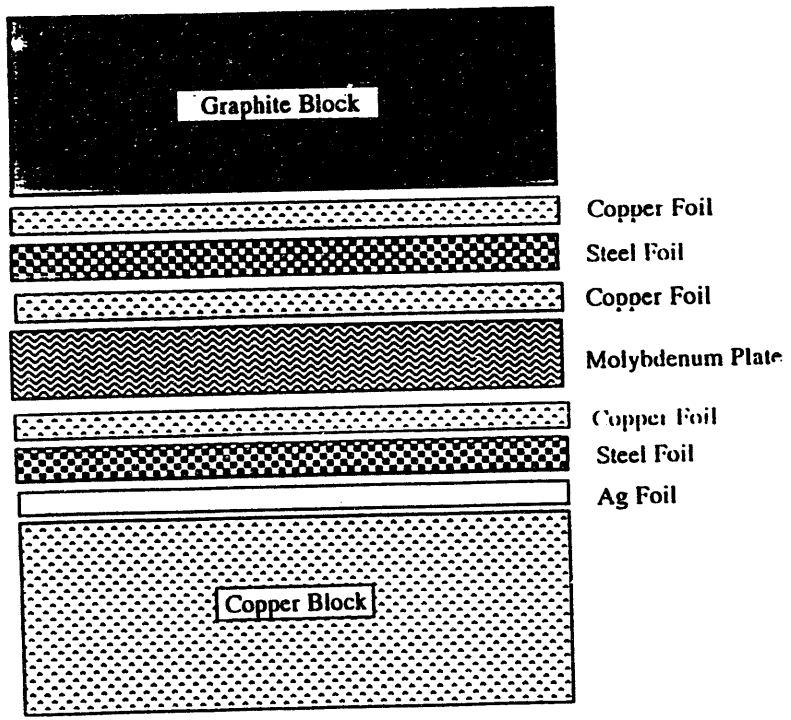

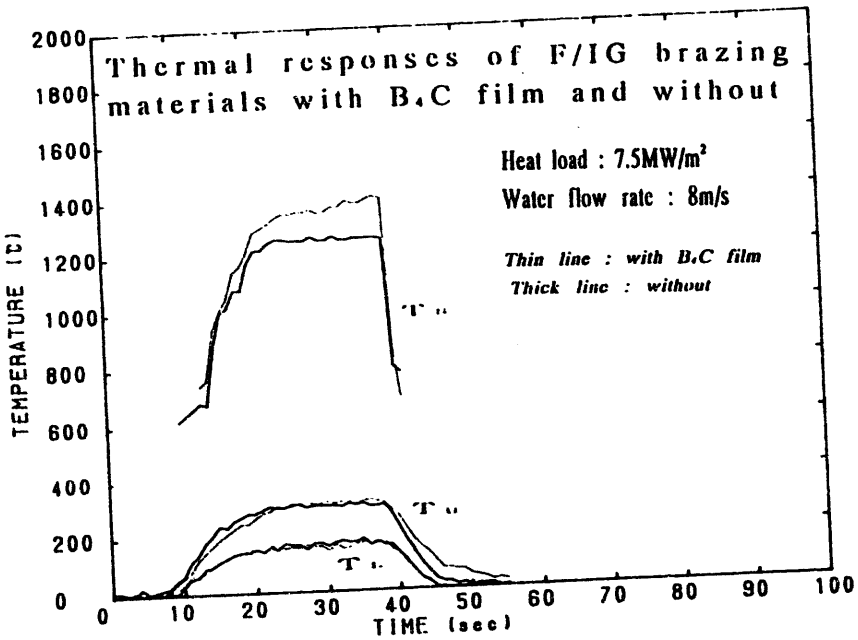

Summary of Results

1. 4 types clear the LHD criteria

max. heat load 10 MW/m^2

criteria : surface temperature Ts < 1200 °C

no large deterioration after 1000 shots

F/CC CX2002U brazed by Toyo Tanso
CX2002U brazed by KHI
PCC-2S brazed by Hitach Works

M/CC CX2002U brazed by KHI

2. Graphite armor is available up to 7 MW/m^2

3. Less than 10 % loss in Overall Thermal Transmission in B_4C Coated Graphite Armor of PD-330S Compared to Pure Graphite

DESIGN, FABRICATION AND TESTING OF HELIUM COOLED DIVERTOR MODULE

C. Baxi

GENERAL ATOMICS
&
SANDIA NATIONAL LABORATORY,
ALBUQUERQUE

Presented at
U.S./Japan HHF/PMI Workshop
San Diego, California
January 24-27, 1994

GENERAL ATOMICS

SUMMARY

- The peak heat flux on the ITER divertor surface is estimated to be 5 MW/m^2 and an average heat flux of 2 MW/m^2.
- A requirement of minimum temperature (100°C) and maximum temperature.
- Coolants considered for fusion reactors are water, liquid metals, and helium.
- Helium cooling is attractive from safety and other considerations
- The challenges are:
  - Manifold sizes
  - Pumping power
  - Leak prevention
- A variety of heat transfer enhancement techniques are considered and experimental studies presented.

GENERAL ATOMICS

TEST MODULE DESIGN AND TESTING

- Design basis
- Thermal/hydraulic design
- Fabrication
- Testing

GENERAL ATOMICS

DESIGN BASIS

- To design, fabricate, and test a helium-cooled divertor module for ITER-relevant heat flux conditions.
- To be tested at Sandia National Laboratory, Albuquerque (SNL)
- The module was designed for:
  - Heat flux = 10 MW/m^2
  - Pressure = 4 MPa (580 psia)
  - Size: 25 mm wide and 80 mm long
  - Made from DS-copper (T_{max} = 500°C)

SNLA HELIUM LOOP

- Pressure = 4 MPa
- Flow = 23 g/sec
- Pressure drop = 0.5 bar
- Helium inlet temperature 20° to 45°C
- Heat flux source electron beam
  - Beam power 30 kW
  - 57 cm diam. and 96 cm long vacuum chamber
  - Maximum sample size = 25 cm long

He FLOW LOOP

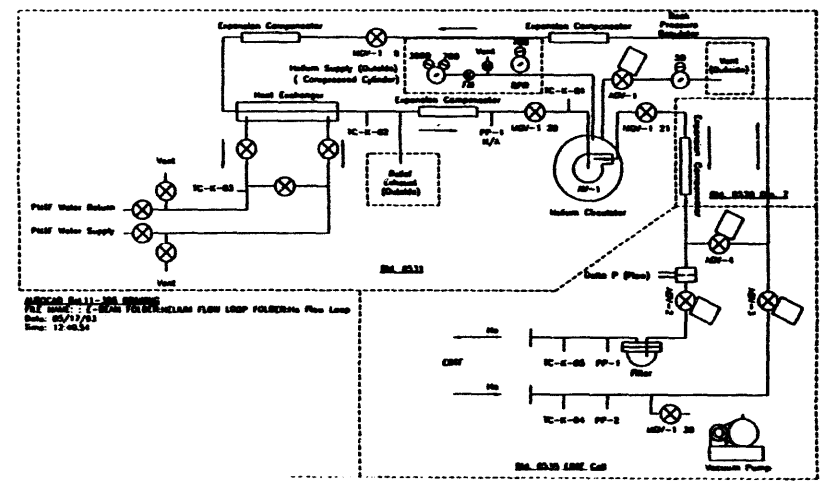

GENERAL ATOMICS

PUMPING POWER AND FLOW

$$\frac{Q}{N}=\frac{Q}{\left(M\Delta p/\rho_1\eta\right)}$$

$$\frac{Q}{N}=\frac{8\eta P^2 L^2\left(Tw-\bar{T}\right)^3}{Q^2}\rho_1\bar{\rho}Cp^3\frac{St^3}{f}$$

$$V=\frac{Q}{\rho_2 Cp\left[Tw_{max}-T_1-\left(\frac{q''_{max}}{\alpha}\right)\right]}$$

The pumping power and volumetric flow rate could be reduced by:

- Increasing the coolant pressure,
- Increase the heat transfer coefficient,
- Reducing the length,
- Reducing the peak heat flux and the power to be removed,
- Reducing the inlet coolant temperature,
- Increasing the allowable peak temperature.

HEAT TRANSFER ENHANCEMENT TECHNIQUES

O ROUGHNESS

- o HTC INCREASED BY FACTOR OF 2 TO 3
- o FRICTION INCREASED BY FACTOR OF 4 TO 7

O JET IMPINGEMENT

- o HTC INCREASED BY FACTOR OF 3
- o FF INCREASED BY FACTOR OF 7

O EXTENDED SURFACE

- o HTC INCREASED BY A FACTOR OF 10
- o FF INCREASED BY A FACTOR OF 20

EXTENDED SURFACES

LARGER HEAT TRANSFER COEFFICIENT IS OBTAINED BECAUSE:

- o REDUCED FLOW AREA: HIGHER VELOCITY
- o LARGER HEAT TRANSFER AREA
- o SMALLER HYDRAULIC DIAMETER

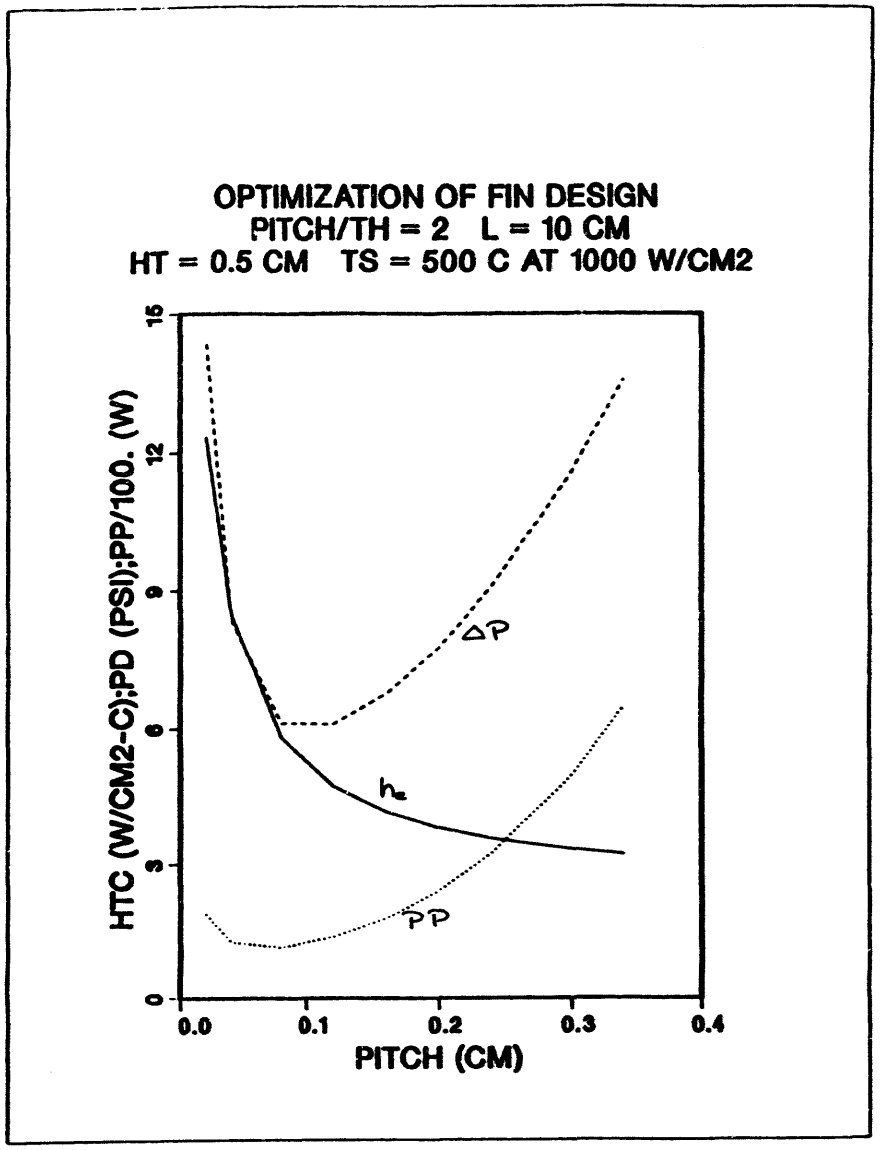

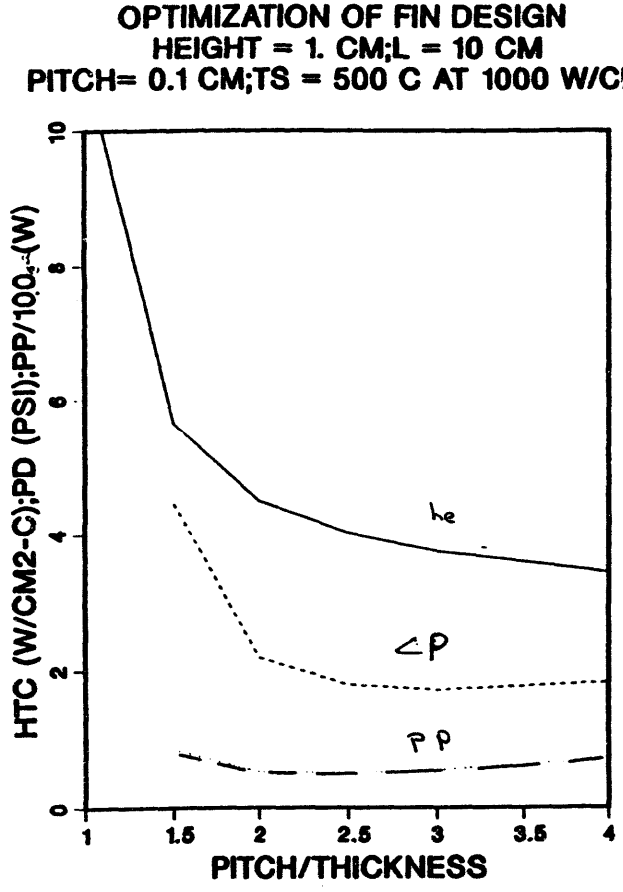
OPTIMIZATION OF FIN DESIGN
HEIGHT = 1. CM;L = 10 CM
PITCH= 0.1 CM;TS = 500 C AT 1000 W/CM2
HTC (W/CM2-C);PD (PSI);PP/100.;(W)
PITCH/THICKNESS
he
ΔP
PP
0
2
4
6
8
10
1
1.5
2
2.5
3
3.5
4

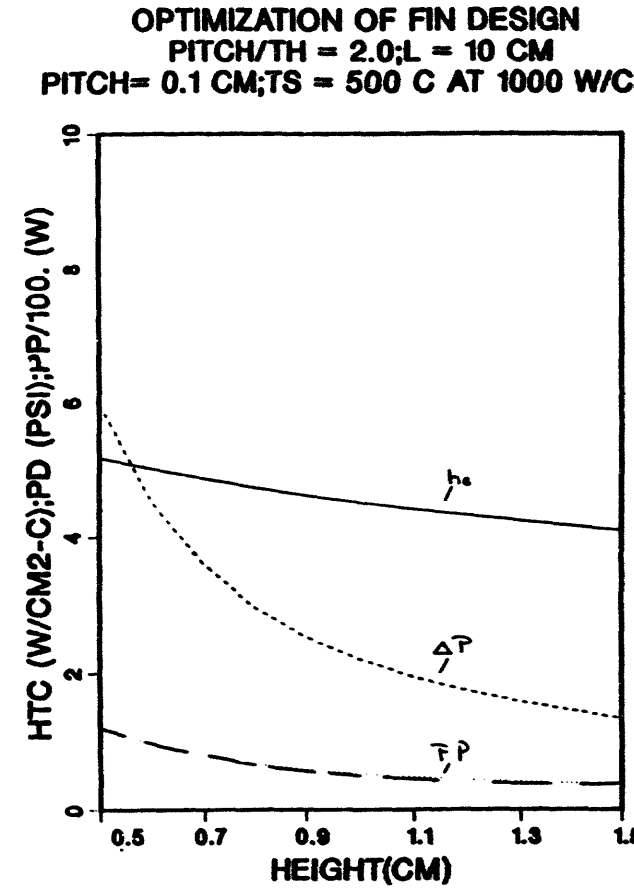
OPTIMIZATION OF FIN DESIGN
PITCH/TH = 2.0;L = 10 CM
PITCH= 0.1 CM;TS = 500 C AT 1000 W/CM2
HTC (W/CM2-C);PD (PSI);PP/100. (W)
HEIGHT(CM)
he
ΔP
PP
0
2
4
6
8
10
0.5
0.7
0.9
1.1
1.3
1.5

GENERAL ATOMICS

THERMAL HYDRAULIC OPTIMIZATION

Thermal analysis of different concepts to achieve a surface temperature of 500°C. Heat flux = 10 MW/m^2; wall thickness = 3 mm, helium pressure = 4 MPa (580 psia). The module is 80 mm long and 25 mm wide.

Material	Concept	Flow Required (kg/s)	Heat Transfer Coefficient (MW/m^2-°C)	Pressure Drop (MPa)	Pumping Power [W (%)]
Cu	Smooth tubes	0.230	0.026	0.064	2300 (11.5%)
Cu	2-D rough tube	0.120	0.028	0.066	1180 (5.9%)
Cu	3-D rough tubes	0.072	0.029	0.044	480 (2.4%)
Cu	Jets	0.026	0.040	0.1	490 (2.45)
Cu	Optimized fins	0.026	0.040	0.012	50 (0.25%)
Cu	Offset fins	0.025	0.042	0.01	40 (0.20%)
Be	Optimized fins	0.040	0.040	0.035	200 (1%)

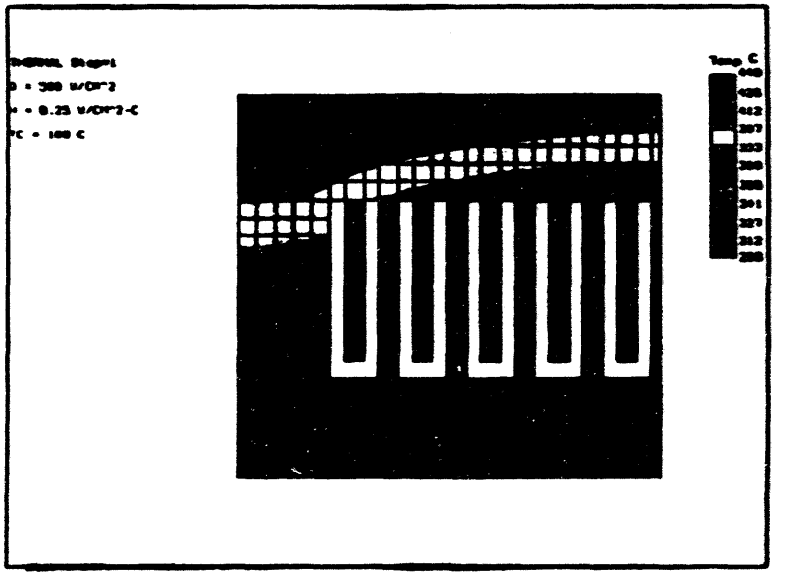

GENERAL ATOMICS

MODULE FABRICATION

- Heated length of 80 mm, fin height of 5 mm, fin pitch of 1 mm and a fin thickness of 0.4 mm
- Fabricated out of DS-Cu material
- Electro discharge machining (EDM) process
- Fin height of the fabricated module is half the value found in optimizing study, for ease of fabrication

GENERAL ATOMICS

GENERAL ATOMIC MODULE

- DS-copper
- Heat flux area = 20 cm²
- 10 MW/m²; with Ts < 450°C; at pumping power < 1%

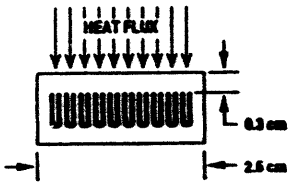

MATERIAL: Dispersion strengthened copper (GLIDCOP by SCM)

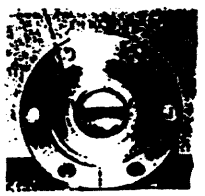

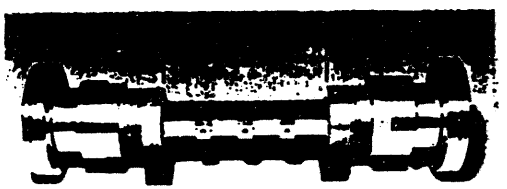

GENERAL ATOMICS

TEST RESULTS

The tests were conducted at the plasma materials testing laboratory of the Sandia National Laboratory. The heat source was an electron beam. Following are some preliminary results at the highest helium pressure (4 MPa). The pulse length was 60 seconds, which is adequate to achieve steady state. No damage was detected at the end of these tests.

Flow Rate (kg/s)	Heat Flux (MW/m^2)	Peak Surface Temperature (°C)	Pumping Power (W) [% of power removed]
0.022	10	380	157 (0.8)
0.011	6	422	21 (0.2)
0.0064	3	424	3.4 (0.06)

Tests at smaller loop pressure increased the pressure drop and pumping power.

The above results confirmed the design predictions.

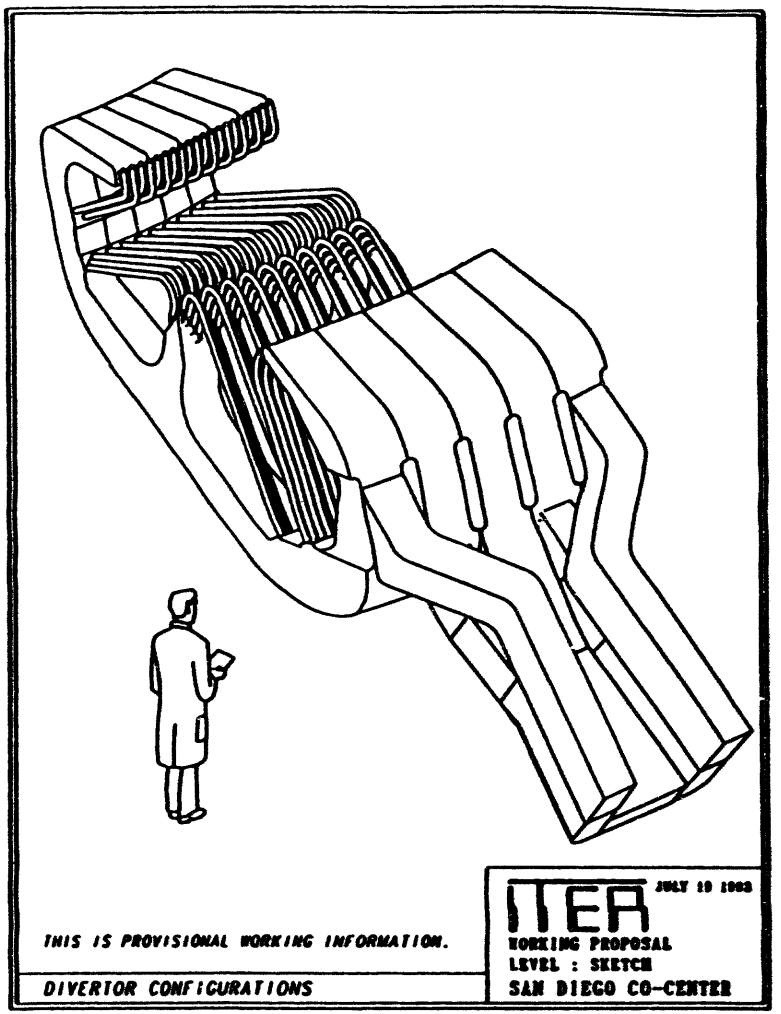

Cross section of Channel

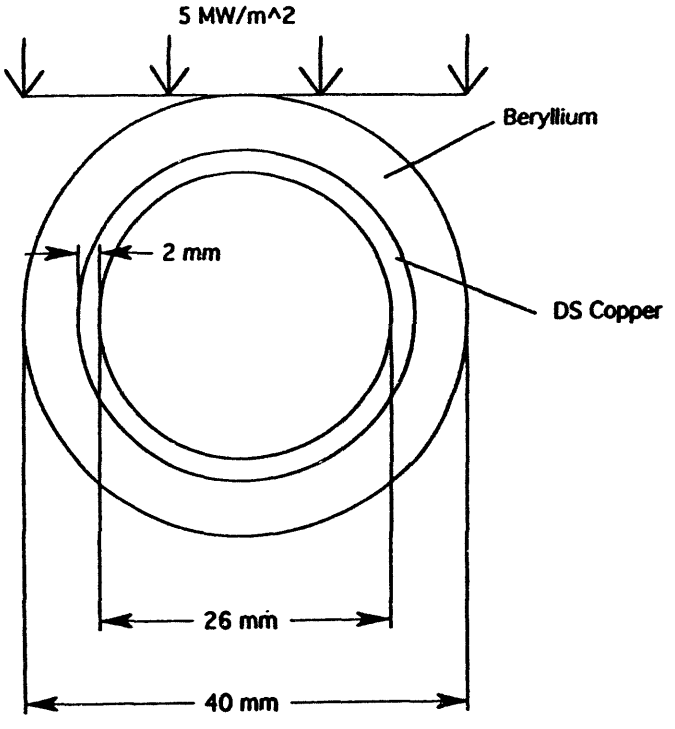

Smooth Channel

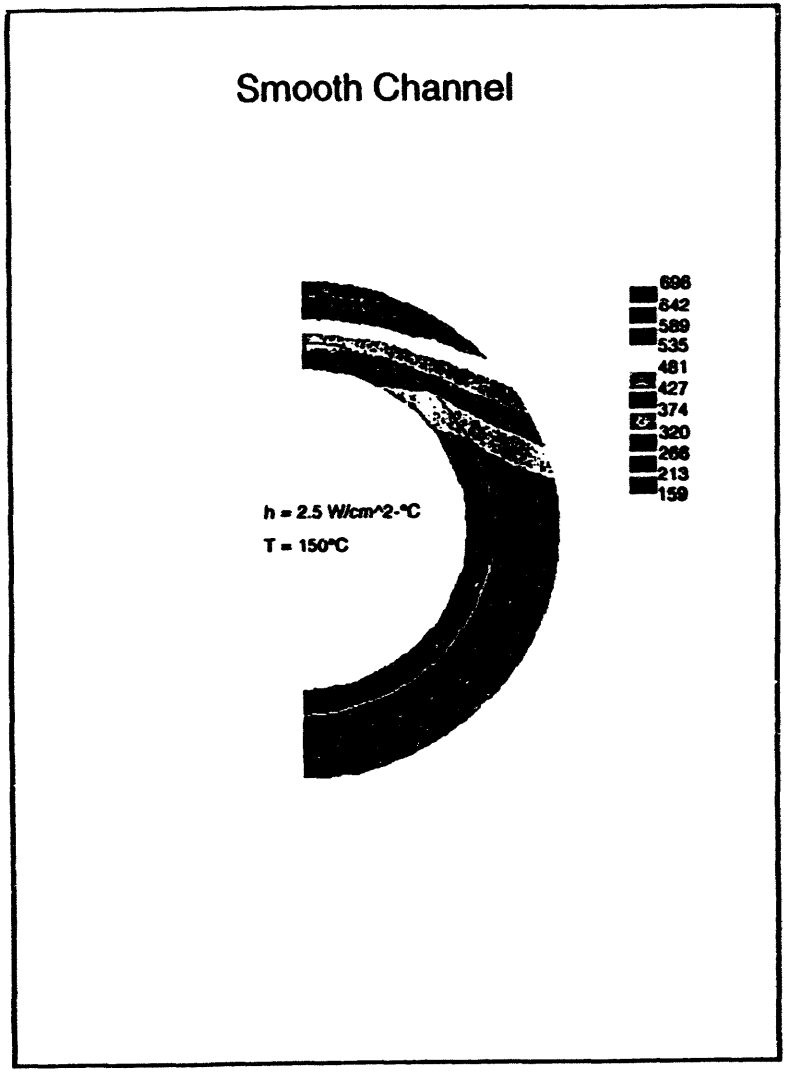

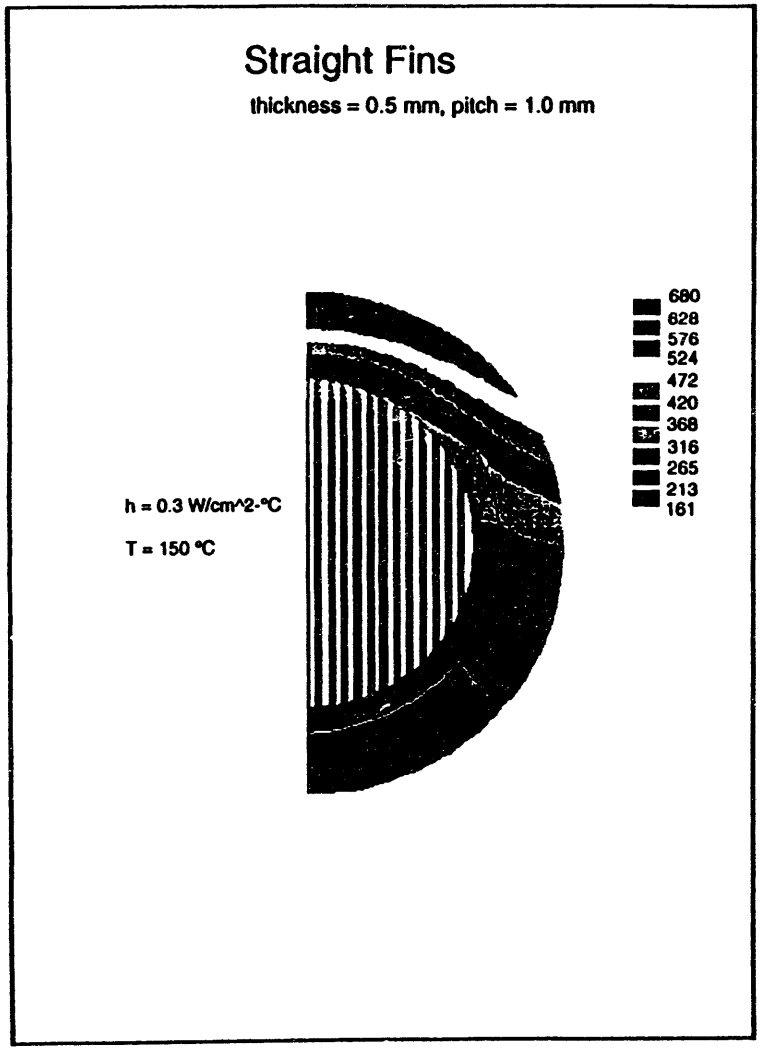
Straight Fins
thickness = 0.5 mm, pitch = 1.0 mm
h = 0.3 W/cm^2-°C
T = 150 °C
680
628
576
524
472
420
368
316
265
213
161

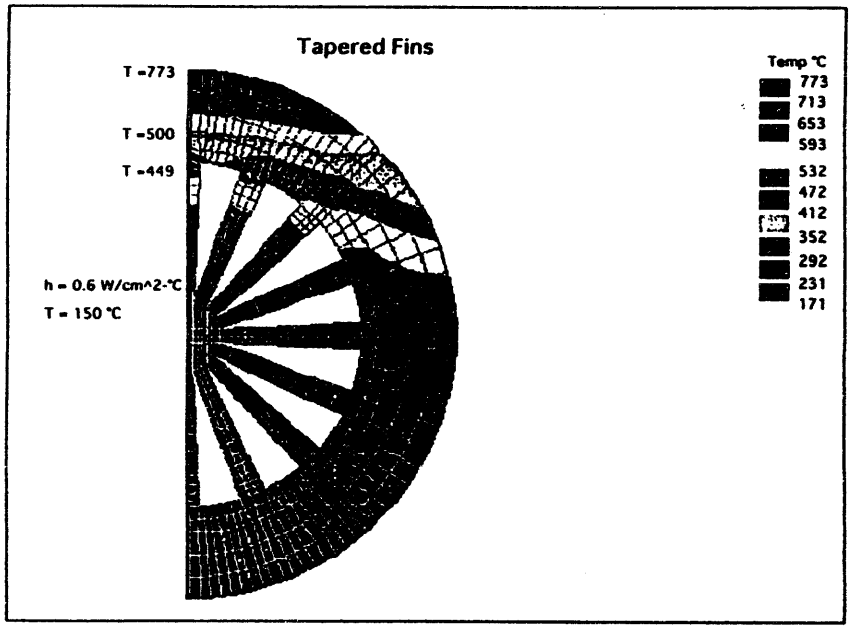
Tapered Fins
T =773
T =500
T =449
h = 0.6 W/cm^2-°C
T = 150 °C
Temp °C
773
713
653
593
532
472
412
352
292
231
171

GENERAL ATOMICS

SUMMARY OF ANALYSIS FOR 5 MPa DESIGN

DATA

Pressure = 5 MPa, q''_{max} = 5 MW/m^2, q''_{av} = 2 MW/m^2, total Q = 480 MW, T_{in} = 150°C, T_{max} for Be = 700°C, Be thickness = 5 mm, Cu thickness = 2 mm, length = 3 m

RESULTS

Geometry	Flow (kg/s)	Reynolds Number	Velocity (m/s)	Pressure Drop (MPa)	Pumping Power [MW (%)]
Smooth	2800	2.8×10^6	510	1.1	615 (128)
2-D rough	1500	1.6×10^6	270	0.47	130 (27)
Twisted tape	1250	1.3×10^6	230	0.3	71 (15)
3-D rough	920	9.7×10^5	170	0.24	42 (9)
Extended surface	430	4.6×10^5	84	0.21	20 (4.1)

GENERAL ATOMICS

MANIFOLD SIZES

- The flow required is 430 kg/s
- The manifold sizes inside the machine will be:
  - Number: 12 inlet and 12 outlet
  - Inlet diameter 15 cm
  - Outlet diameter 17 cm

GENERAL ATOMICS

EFFECT OF AREA WITH HHF

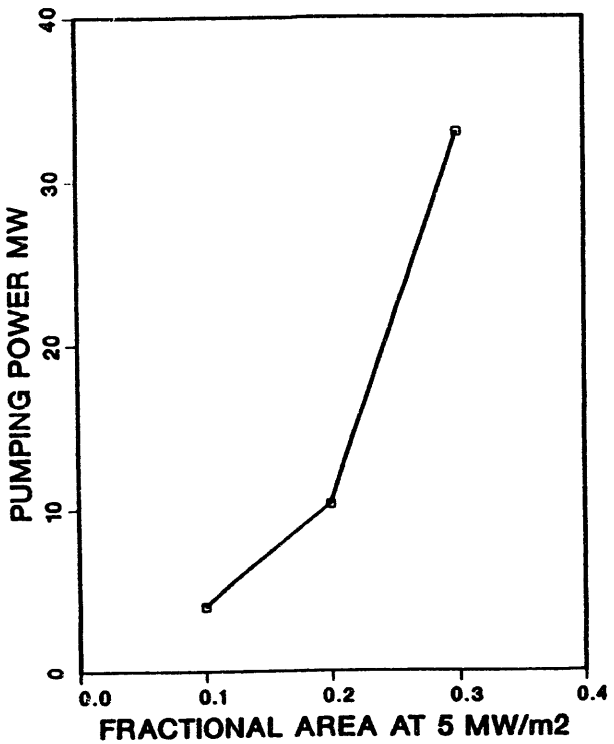

GENERAL ATOMICS

EFFECT OF He PRESSURE

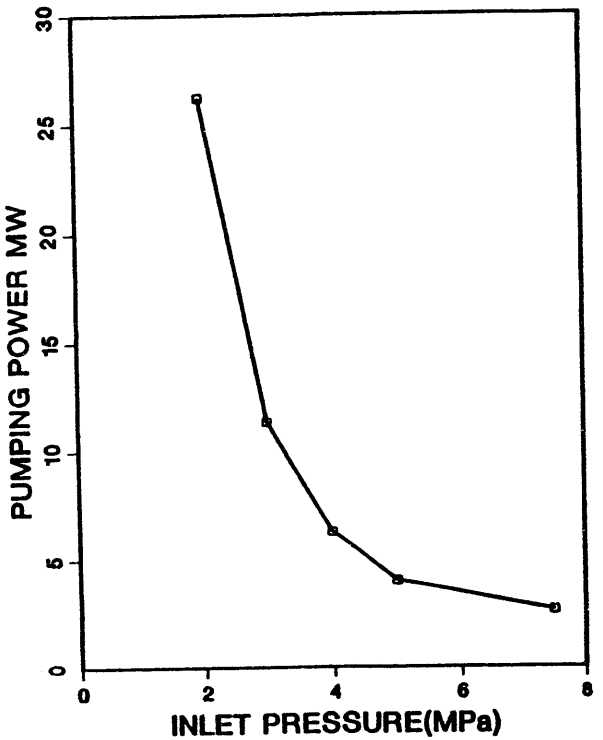

GENERAL ATOMICS

EFFECT OF Be SURFACE TEMPERATURE

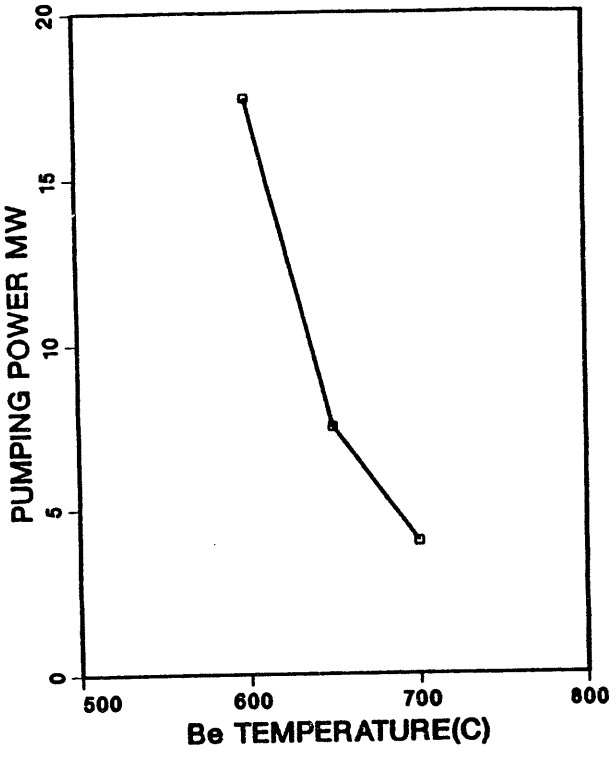

GENERAL ATOMICS

CONCLUSIONS

- Objectives of the Task Were Fulfilled
- At an inlet Pressure of 4 MPa, GA Divertor Module Tested to a Heat Flux of About 9 MW/m^2, Over an Area of 20 cm^2, at a Surface Temperature Less Than 400 ^{o}C.
- The Pumping Power was about 1 % of Power Removed for the Highest Heat Flux.
- The Experimental Results Confirmed the Analysis.
- The Concept Can be Applied to ITER Divertor to Produce a Robust Design.

Heating Tests on JT-60 Actively Cooled Divertor Mock-ups

S. Suzuki, M. Akiba, M. Araki, T. Ando*, K. Sato, K. Yokoyama, M. Fairaku

NBI Heating Laboratory
*JT-60 Facility Division II
Fusion Research Establishment, JAERI Naka

Divertor mock-up (Flat plate design)

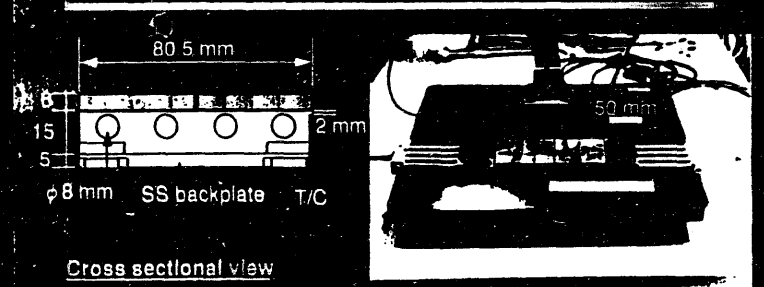

Cross sectional view

Design values of JT-60 divertor plate and test conditions

	JT-60	Thermal cycling test
Incident heat flux	up to	x 10 MW m^{-2}
Heating time		
Coolant flow velocity		
Coolant pressure		
Coolant temperature		

Thermal cycling test

Results of thermal cycling test

Surface temperatures through 1,000 cycles

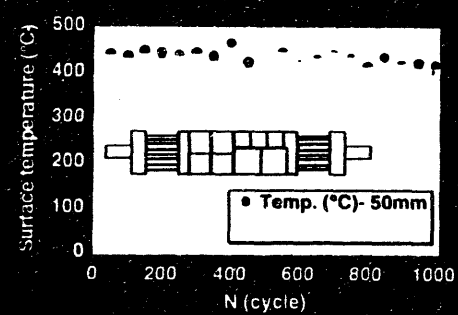

Screening test (Flat plate divertor mock-up)

Test conditions

- Coolant inlet pressure = 1.5 MPa (Temp. R.T.)
- Flow velocity = 5 m/s
- Heat flux = 10 MW/m²

Dimensions of the armor tile

Temperature chabges of
the mock-up at 13 MW/m
Temp. at heat sink
Surface temp.
Over ranged
Temperature (C)
1400
1200
1000
800
600
400
200
0
0 1 2 3 4 5 6 7 8
Time (s)

16:38:24 93.08.26
16:38:44
16:38:57 93.08.26

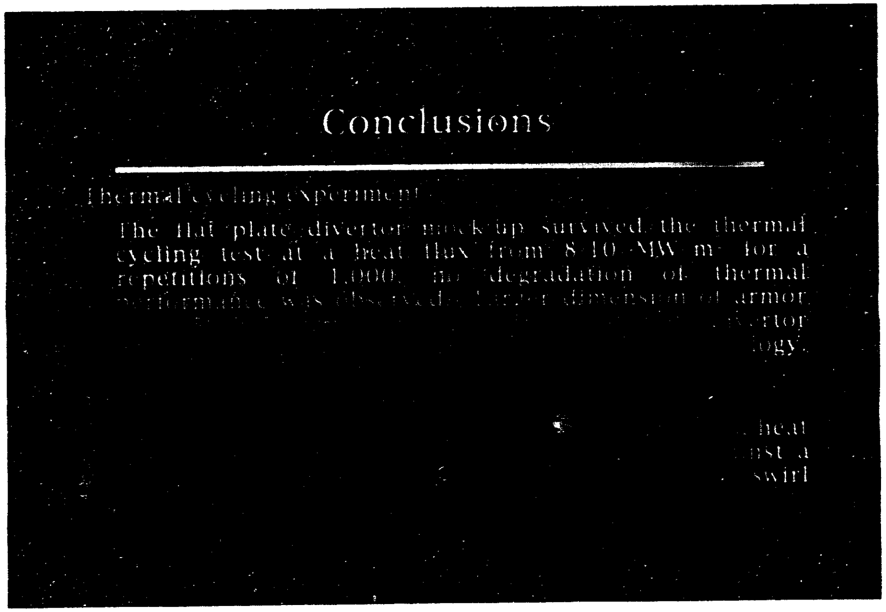
Conclusions
Thermal cycling experiment
The flat plate diverter mock-up survived the thermal
cycling test at a heat flux from 8-10 MW m for a
repetitions of 1,000, no degradation of thermal

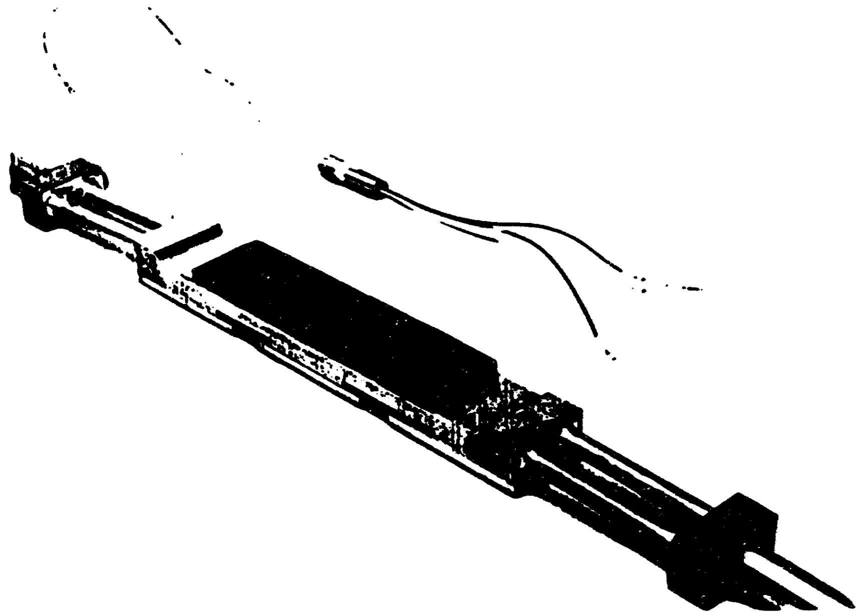

Mitsubishi MFC-1 on OFHC Copper, 29MW/m², 10s

H. D. Falter, M. Araki, et al, JET-Report (1994).

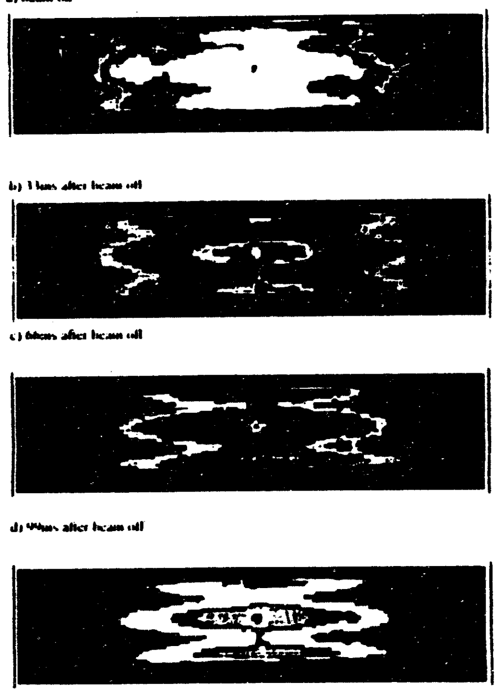

Thermal cycling Experiment on 1D CFC/W-Cu Divertor Mock up

K. Sato, M. Akiba, M. Araki, S. Suzuki,
K. Yokoyama, M. Dairaku

NBI Heating Laboratory

Japan Atomic Energy Research Institute

Objective

To investigate the durability of 1D CFC/W-Cu divertor mock-up

Advantages of use of W-30Cu

W-30Cu proposed is made by an infiltration of copper into a skeleton of tungsten.

The thermal expansion coefficient of W-30Cu matches well with that of 1D CFCs. The residual stresses at the braze interface can be reduced.

Ultimate strength of W-30Cu is two times higher than that of OF-Cu at R.T.

At high temperature high yield strength would be expected.

Thermal conductivity of W-30Cu is as high as 290 W/mK at R.T.

Thermal expansion coefficient

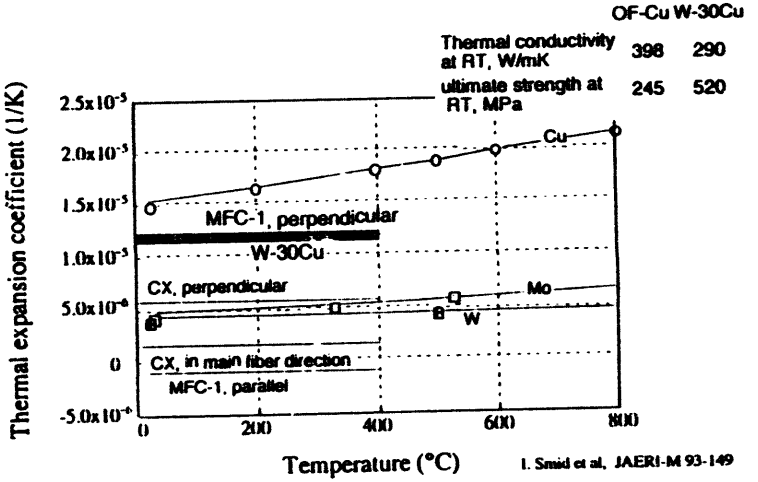

I. Smid et al, JAERI-M 93-149

Result of stress analyses

Braze solidification at 750°C

Incident heat flux is selected at 15 MW/m^2 and coolant velocity at 10 m/s

predicted maximum stresses (MPa) in the MFC-1			Residual stress (MPa)	Thermal stress (MPa)	ultimate strength (MPa)
MFC-1/W-30Cu Bond	x-x	tensile	0.33	0.38	3.
		compressive	0.01	7.4	16.
	y-y	tensile	8.2	14.	400.
		compressive	0.90	8.0	216
	z-z	tensile	0.34	0.05	3.
		compressive	—	4.7	16.

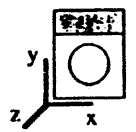

I. Smid et al, JAERI-M 93-149

1D CFC/W-Cu divertor mock-up

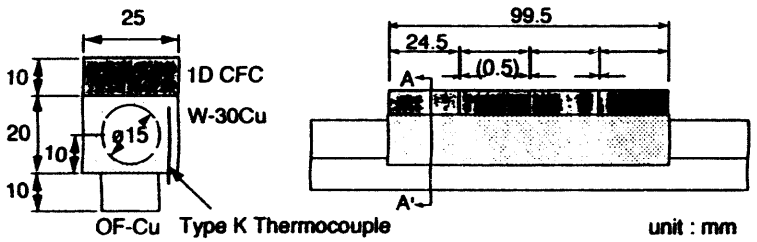

NBI Heating Laboratory

Experimental conditions

Surface heat flux	15 MW/m^2
Duration/Interval time	20 s/ 10 s
Cooling condition	
flow velocity	10 m/s
Local pressure	2.0 MPa
Inlet temperature	27 °C
Heat transfer coefficient	Thom's correlation
Number of cycle	1000

NBI Heating Laboratory

Comparison of temperature between experiment and the calculations

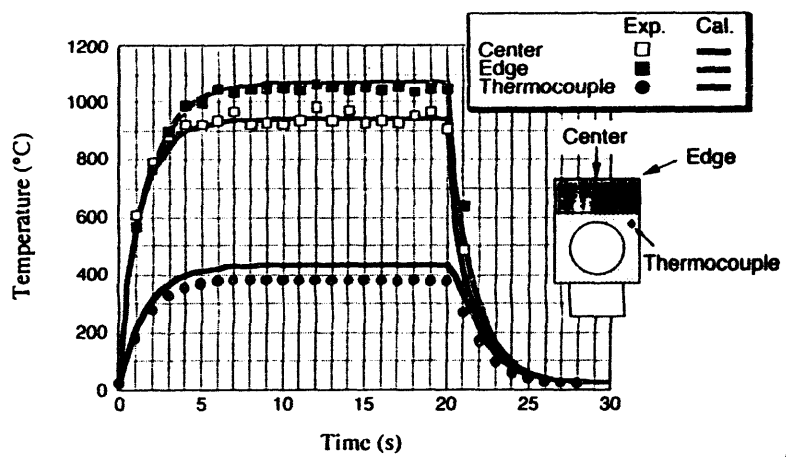

NBI Heating Laboratory

No cracks have been found at the interface with SEM

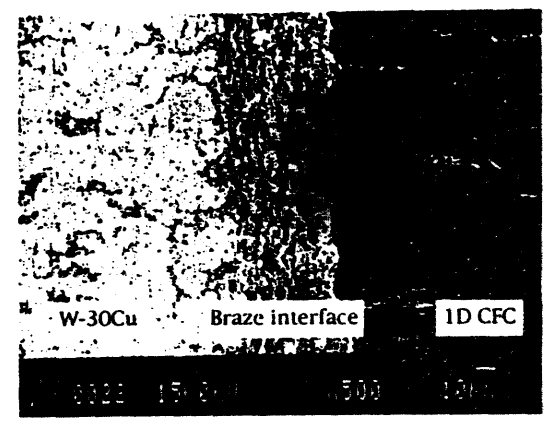

NBI Heating Laboratory

Conclusion

The 1D CFC/W-30Cu divertor mock-up could succcessfully endure a cyclic heat load of 15 MW/m^2, 20 s for 1000 cycles.

No crack or detachment at the interface were found after the thermal cycling experiment.

The material combination of 1D CFCs and W-30Cu is promissing for the ITER divertor plate.

U.S.-Japan Workshop on HHF-PSI

Reactor Engineering Technology Center

DLY 01/25/94

Recent EBTS Results and Planned HHF Tests on Beryllium Armored Mock-ups

Dennis L. Youchison
Sandia National Laboratories

January 25, 1994
San Diego, CA

Sandia National Laboratories

HHF Testing on the EBTS

- Synopsis of Helium Coolant HHF Test Results
- CHF Tests of Russian Porous Coating Mock-ups
- Tore Supra Braze Flaw Mock-ups
- ITER Divertor Dump Plate Compliant Layer Mock-ups
- Plans for Beryllium Armored Mock-ups

Sandia National Laboratories

PMTF Helium Flow Loop

•Operating Pressure:	0-4.0 MPa (600 psi)
•Maximum Allowable Pressure:	4.8 MPa (700 psi)
•Helium Temperature:	0-230 °C
•Helium mass flow rate:	0-20 g/s @ 4.0 MPa*
•pressure drop:	0-7.5 psi @ 4.0 MPa*

*Present blower: 55 scfm air, ΔP=1.7 psi @ atm.
Blower upgrade: 600 scfm air, ΔP=6.2 psi @ atm.
He mass flow rate ≈ 200 g/s @ 4.0 MPa
ΔP≈27 psi He @ 4.0 MPa

Blower upgrade tentatively scheduled for 04/94

Sandia National Laboratories

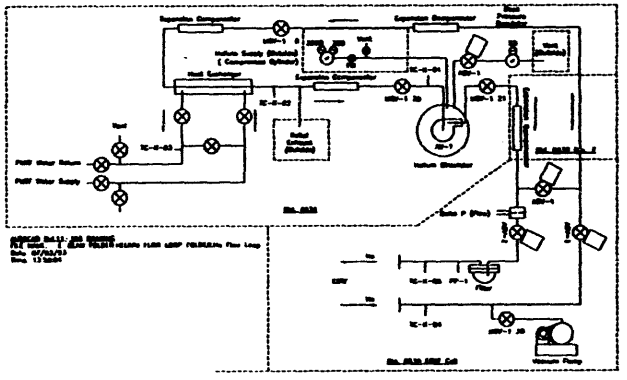

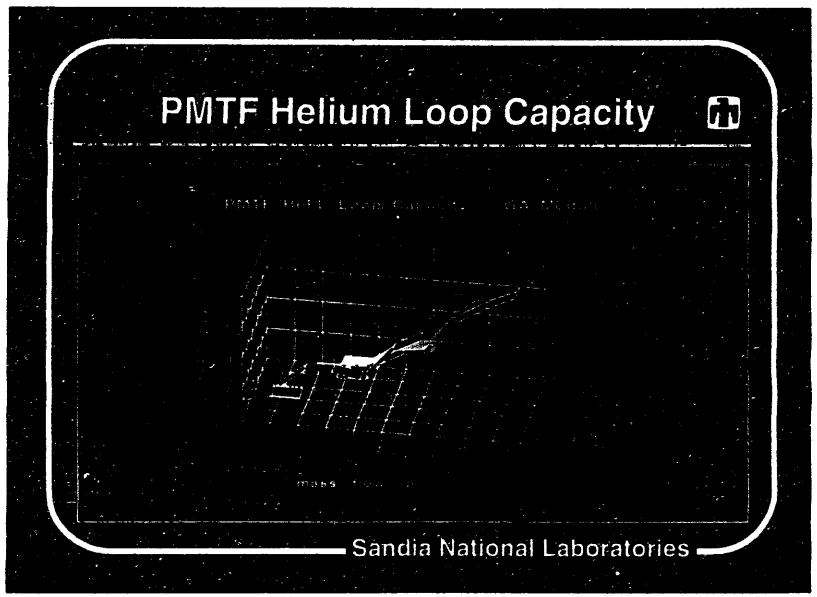

Helium Test Objectives

- Survivability, integrity
- Maximum heat flux, heat removal capacity
- Investigate parameter space for efficient heat removal
  Dependence on pressure, mass flow rate and pressure drop

Sandia National Laboratories

1993 Helium HHF Experiments

Creare, Inc. Normal Flow, Microchannel Heat Exchanger

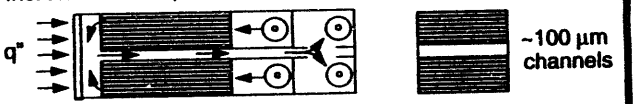

General Atomics Helium-Cooled Divertor Mock-up

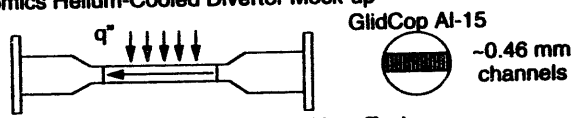

Thermacore Porous Metal, Helium-Cooled Heat Exchanger

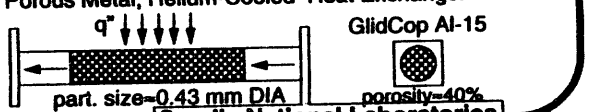

Sandia National Laboratories

Helium Coolant Tests

- **Creare, Inc. Microchannel, Normal Flow Heat Exchanger**
  Tested to an absorbed heat flux of 4 MW/m²
  (6 MW/m² incident heat flux) using 7.3 g/s of helium
  @ 1.4 MPa [M. Izenson]

- **General Atomics Divertor Module**
  Tested to an absorbed heat flux of 9 MW/m²
  (12 MW/m² incident heat flux) using 22 g/s of helium
  @ 4.0 MPa [C. Baxi]

- **Thermacore Porous Metal Heat Exchanger**
  Tested to an absorbed heat flux of 16 MW/m²
  (25 MW/m² incident heat flux) using 1 g/s of helium
  @ 4.0 MPa [J. Rosenfeld]

Sandia National Laboratories

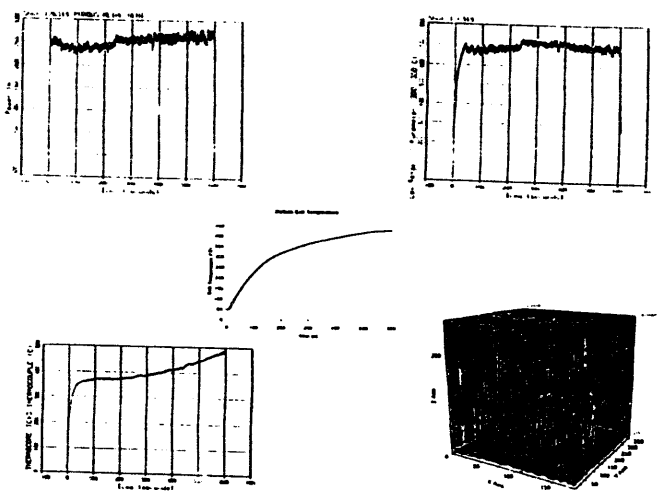

HHF Testing with Helium

Important Issues

- Increase flexibility to accommodate diverse samples
  - upgrade blower capacity
  - new pressure vessel for blower
  - parallel channel, 2 stage flow meter (outlet)
  - turbine flow meter (inlet)
  - enhanced data acquisition system

- Investigate helium calorimetry techniques
  - repositioned and shielded thermocouples
  - alternative temperature measurement techniques
  - benchmark tests against water calorimetry

Sandia National Laboratories

CHF/PC Test Objectives

- Study the bimodal evolution of the boiling crisis for one-sided heating: -local crisis -global crisis
- Study of porous coating intensifier to increase heat removal and ultimate absorbed critical heat flux (UHF)
- Study of post-crisis heat removal regime

impact:

•Define operating parameter space that does not lead to crisis

•Reduction in accident consequences - development of burnout detection techniques for active safety systems.

Sandia National Laboratories

Boiling Crisis

- Burnout is due to global crisis. Local crisis may be tolerable
- Heat loading significantly greater for global crisis than for local crisis
- Simultaneous coexistence of all heat exchange regimes are possible at the pre-burnout conditions

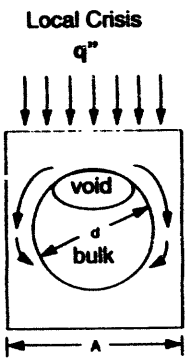

Sandia National Laboratories

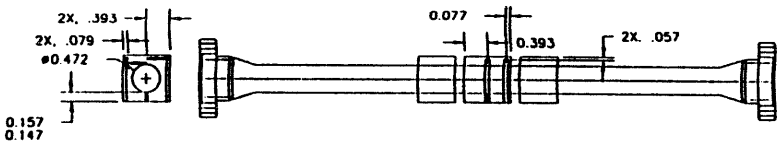
2X, .393
2X, .079
ø0.472
0.157
0.147
0.077
0.393
2X, .057

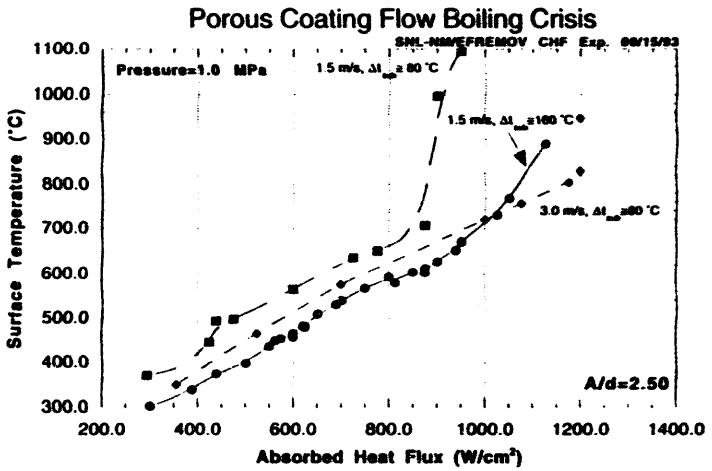
Porous Coating Flow Boiling Crisis
SNL-NM/EFREMOV CHF Exp. 09/15/93
Pressure=1.0 MPa
1.5 m/s, Δt_sub ≥ 80 °C
1.5 m/s, Δt_sub ≥160 °C
3.0 m/s, Δt_sub ≥80 °C
A/d=2.50
Surface Temperature (°C)
Absorbed Heat Flux (W/cm²)
1100.0
1000.0
900.0
800.0
700.0
600.0
500.0
400.0
300.0
200.0
400.0
600.0
800.0
1000.0
1200.0
1400.0

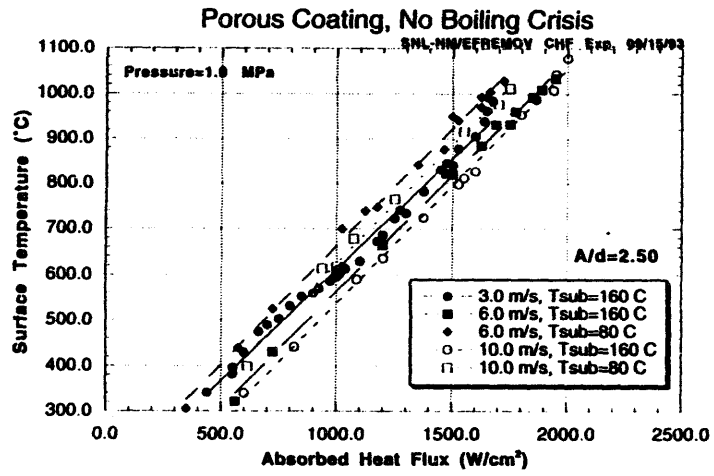
Porous Coating, No Boiling Crisis
Pressure=1.0 MPa
A/d=2.50
3.0 m/s, Tsub=160 C
6.0 m/s, Tsub=160 C
6.0 m/s, Tsub=80 C
10.0 m/s, Tsub=160 C
10.0 m/s, Tsub=80 C
Surface Temperature (°C)
Absorbed Heat Flux (W/cm²)
1100.0
1000.0
900.0
800.0
700.0
600.0
500.0
400.0
300.0
0.0
500.0
1000.0
1500.0
2000.0
2500.0

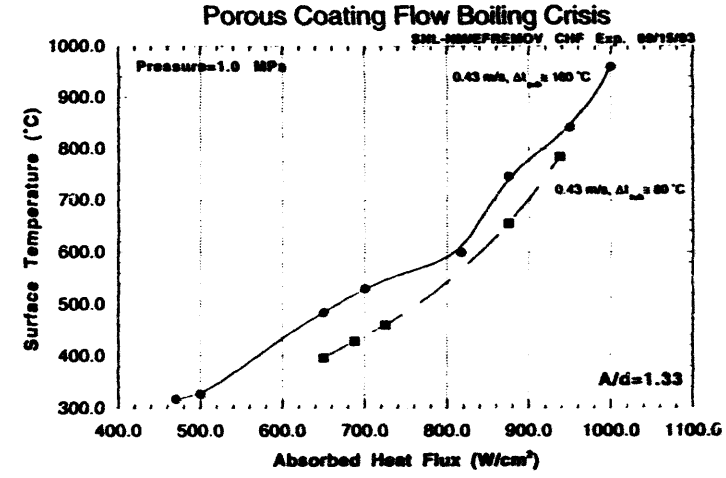
Porous Coating Flow Boiling Crisis
Pressure=1.0 MPa
A/d=1.33
Surface Temperature (°C)
Absorbed Heat Flux (W/cm²)
1000.0
900.0
800.0
700.0
600.0
500.0
400.0
300.0
400.0
500.0
600.0
700.0
800.0
900.0
1000.0
1100.0

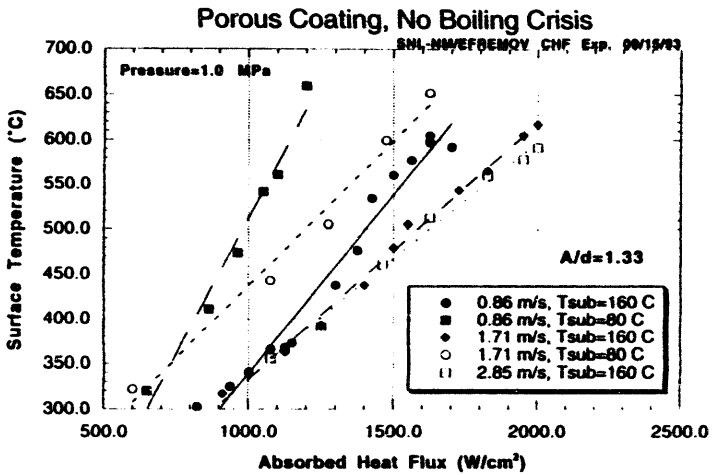
Porous Coating, No Boiling Crisis
SNL-NM/EFREMOV CHF Exp. 09/15/93
Pressure=1.0 MPa
A/d=1.33
0.86 m/s, Tsub=160 C
0.86 m/s, Tsub=80 C
1.71 m/s, Tsub=160 C
1.71 m/s, Tsub=80 C
2.85 m/s, Tsub=160 C
Surface Temperature (°C)
Absorbed Heat Flux (W/cm²)
700.0
650.0
600.0
550.0
500.0
450.0
400.0
350.0
300.0
500.0
1000.0
1500.0
2000.0
2500.0

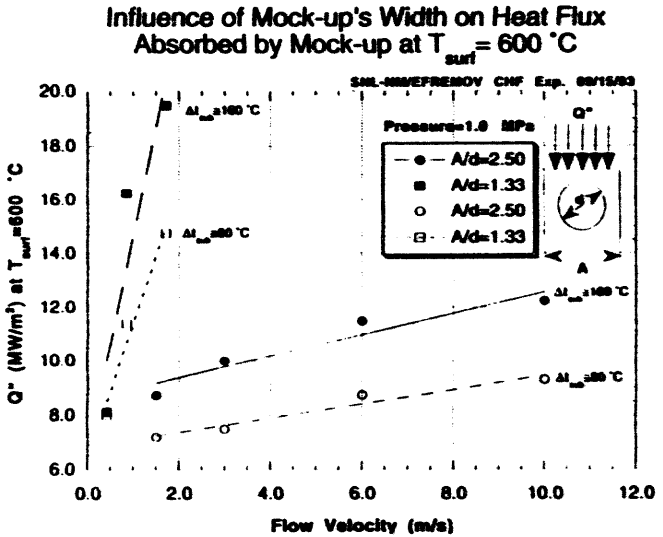
Influence of Mock-up's Width on Heat Flux
Absorbed by Mock-up at T surf = 600 °C
SNL-NM/EFREMOV CHF Exp. 09/15/93
Pressure=1.0 MPa
A/d=2.50
A/d=1.33
A/d=2.50
A/d=1.33
Q"
A
Q" (MW/m²) at T surf=600 °C
Flow Velocity (m/s)
20.0
18.0
16.0
14.0
12.0
10.0
8.0
6.0
0.0
2.0
4.0
6.0
8.0
10.0
12.0

Influence of Wall Thickness on Absorbed Heat Flux at T_{surf} = 600 °C

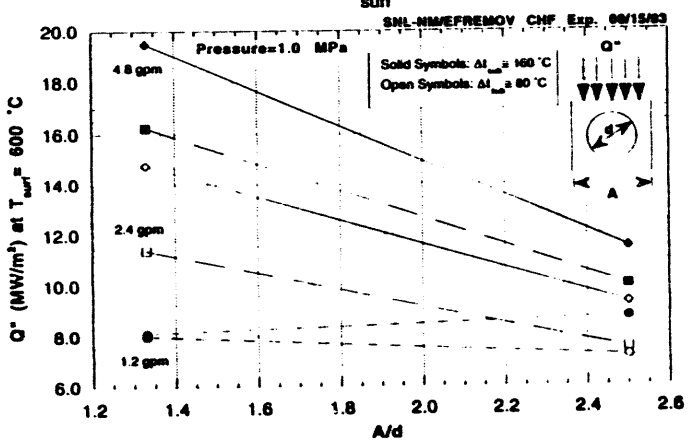

Tore-Supra Test Objectives

- Study effects of braze flaws on thermal conductivity/heat removal
- Characterize boiling in braze-flawed mock-ups. Correlate ultimate heat fluxes to braze void content
- Establish a definition of acceptable "quality" for void content in the braze

Sandia National Laboratories

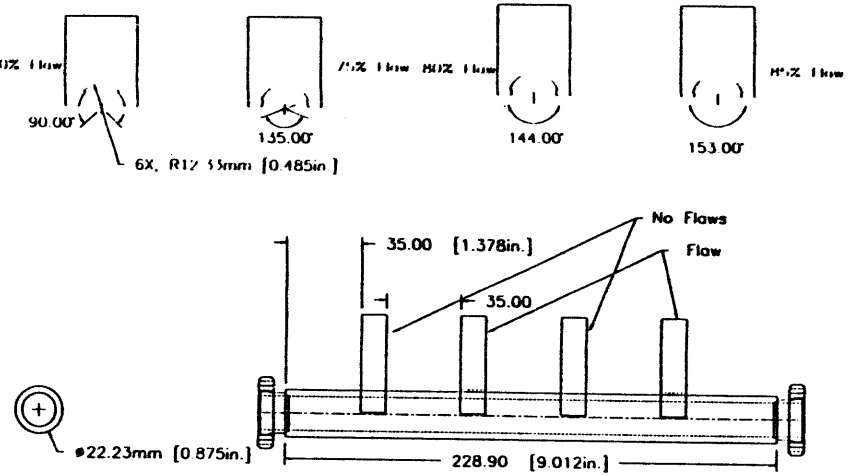
90.00°
135.00°
144.00°
153.00°
6X, R12.55mm [0.485in.]
35.00 [1.378in.]
35.00
No Flaws
Flaw
ø22.23mm [0.875in.]
228.90 [9.012in.]

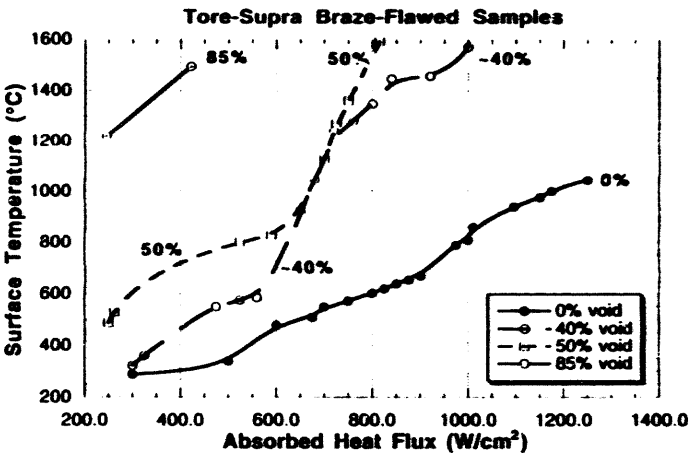
Tore-Supra Braze-Flawed Samples
Surface Temperature (°C)
Absorbed Heat Flux (W/cm²)
1600
1400
1200
1000
800
600
400
200
200.0
400.0
600.0
800.0
1000.0
1200.0
1400.0
85%
50%
40%
50%
40%
0%
0% void
40% void
50% void
85% void

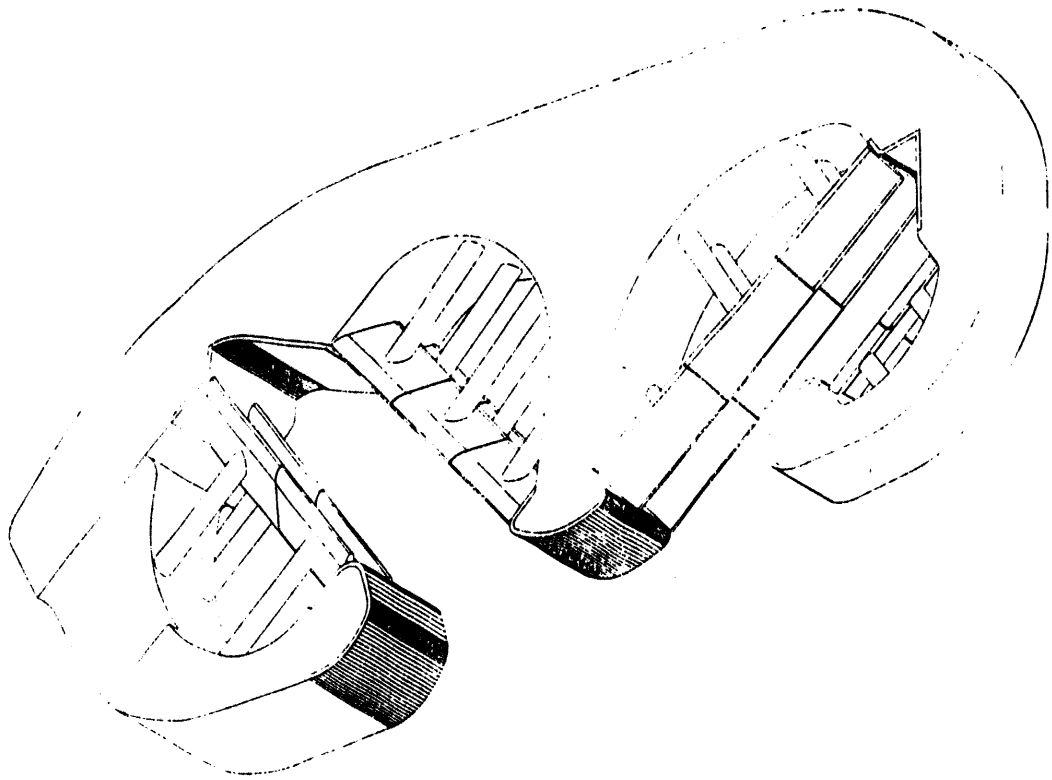

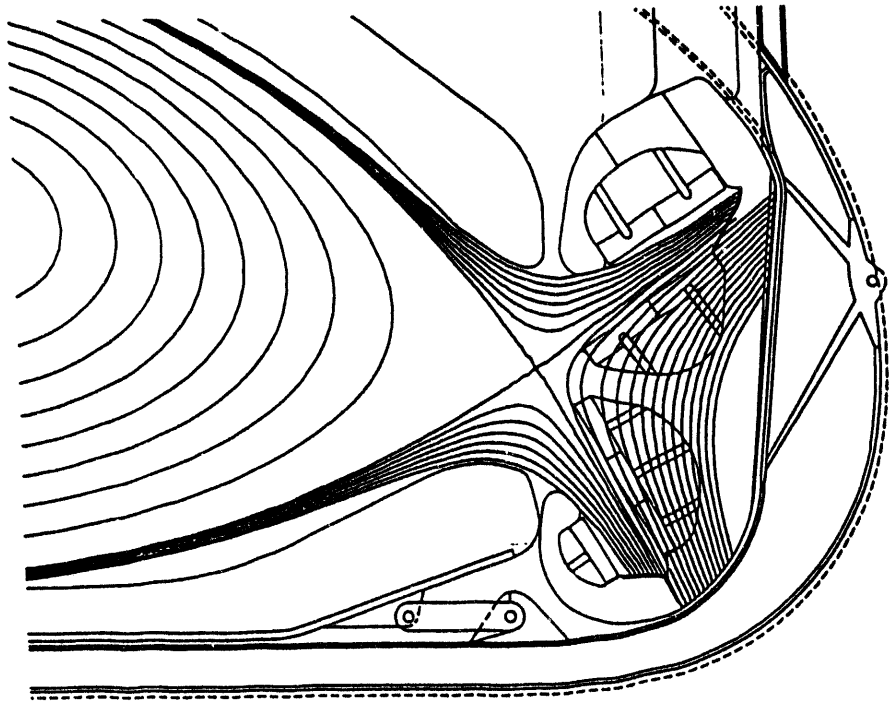

ITER cross-section with superimposed magnetic field lines

Compliant Layer Test Objectives

- Thermal conductivity studies across compliant layer
- Lifetime, survivability tests — Compliant Layer
- Vacuum performance

1. 90% In / 10% Sn
2. 90% Sn / 10% Ag
3. 99% Sn / 1% Ge
4. 97% Sn / 3% Cu

Sandia National Laboratories

Compliant Layer Assembly – Side View

Sandia National Labs

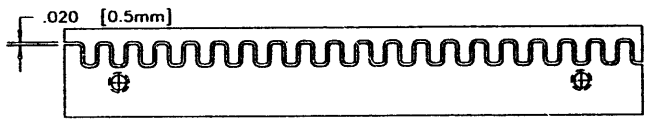

Fusion Technology
JAH 01/18/94

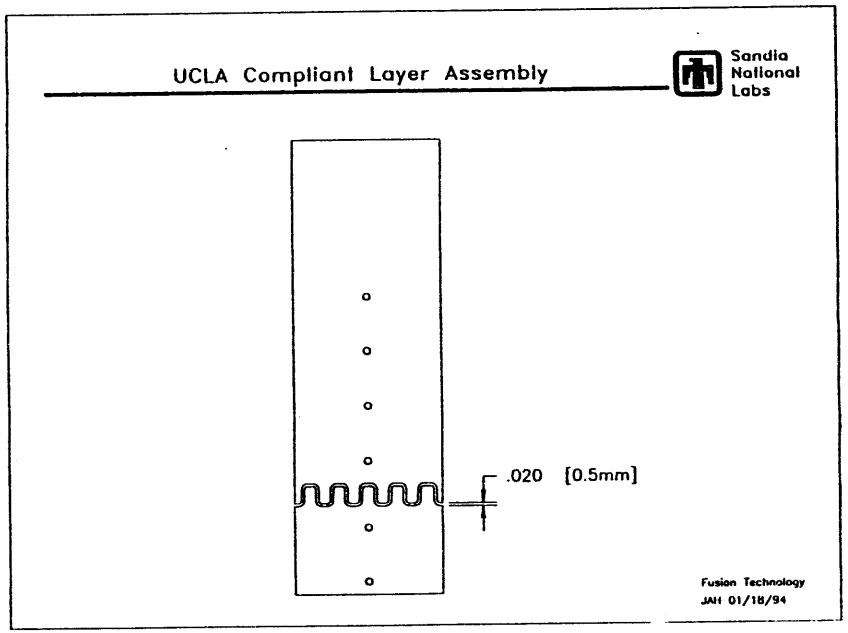

Beryllium Test Objectives

- Study the quality of diffusion bonding
- Lifetime-fatigue tests
- Thermal conductivity screening tests
- Compare performance of two mock-up designs
- Ascertain effectiveness of porous coatings

Sandia National Laboratories

Floor Plan of Building 6530 Beryllium Facility and Regulated Areas

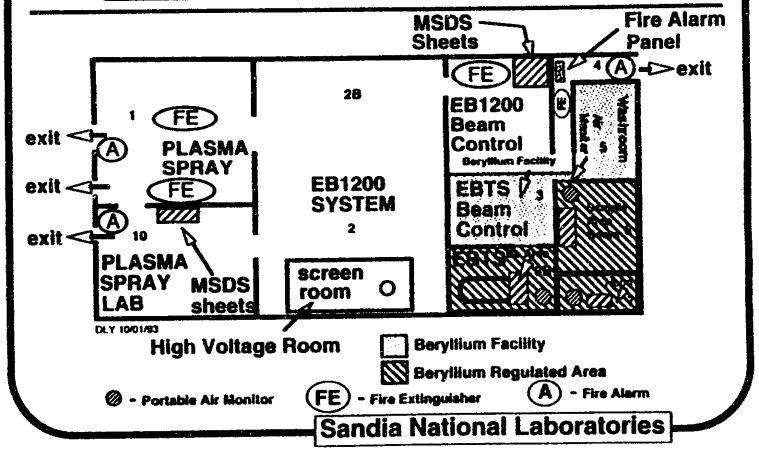

Sandia National Laboratories

'94 Beryllium Campaign

HHF testing of beryllium in the EBTS is scheduled for March and April 1994.

Two mock-ups will be tested:

1. Russian Mock-up - 5 mm and 10 mm thick beryllium tiles diffusion bonded onto an OFHC copper saddleblock which is also diffusion bonded onto a MAGT tube (2)

2. U.S. Mock-up - Brush Wellman beryllium monoblock diffusion bonded onto an OFHC copper tube with twisted tape insert (1)

* Russian Mock-up - 5 mm and 10 mm thick beryllium tiles diffusion bonded directly onto a MAGT tube (2)

Sandia National Laboratories

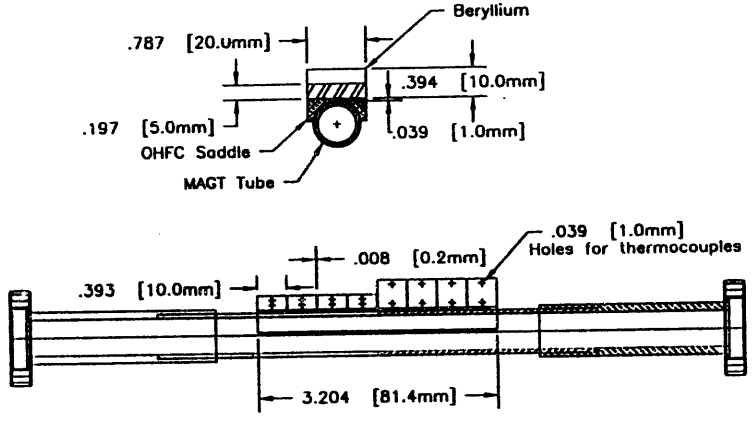

Beryllium Sample Mockup #1

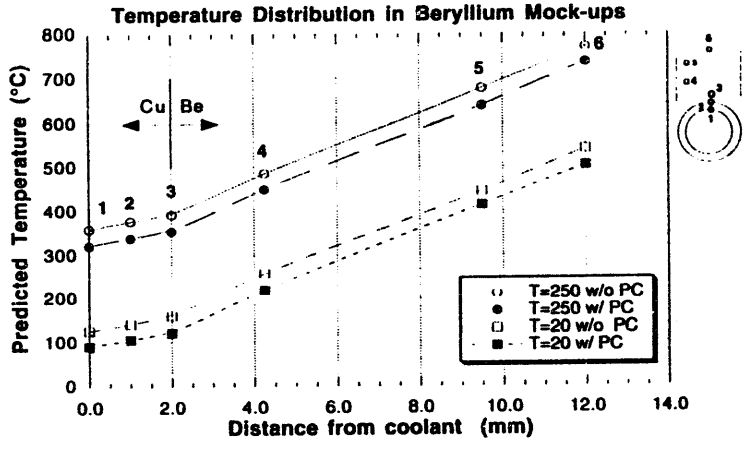

Beryllium Monoblock Divertor Mockups

Three Samples are being fabricated by Brush Wellman:

1. **Slotted surface, 6 mm grid**
2. **Unslotted surface**
3. **90% dense beryllium***

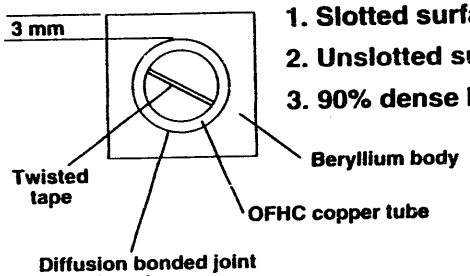

*This may reduce fatigue cracking.

Sandia National Laboratories

RDW Sandia 10/92

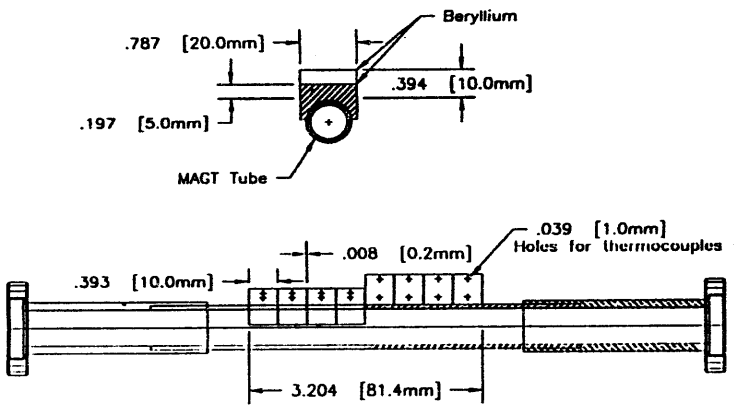

Beryllium Sample Mockup #2

Future Beryllium HHF Tests

1. Russian Mock-up - 5 mm and 10 mm thick beryllium saddleblocks diffusion bonded directly onto a MAGT tube (2)

2.. U.S. Mock-up - Brush Wellman slotted beryllium monoblock

3. U.S. Mock-up - Brush Wellman porous beryllium monoblock

Sandia National Laboratories

Plasma-Spraying of Beryllium for Fusion Applications

Richard G. Castro

Materials Division
Los Alamos National Laboratory
Los Alamos, NM 87545

US-Japan Workshop on
PMI-HHF Components
San Diego, California
January 24-27, 1994

Outline

- Facilities
- Results (FY1993)
- Critical Research Issues

Beryllium Atomization and Thermal Spray Facility

- 2000 ft² of laboratory space filtered through high efficiency HEPA filters using a 20,000 cfm ventilation fan.

  - Controlled access room (respirator only)

    powder production
    powder handling
    plasma spraying

  - Characterization/support facilities

    metallography
    heat treating/melting

  - Consolidation facilities

    hot isostatic pressing

Centrifugal Atomization of Beryllium

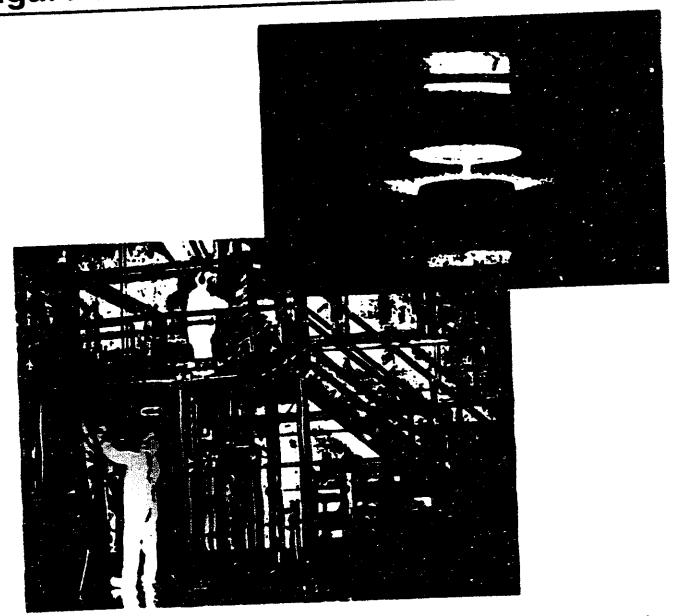

Los Alamos

Centrifugal Atomizer Schematic

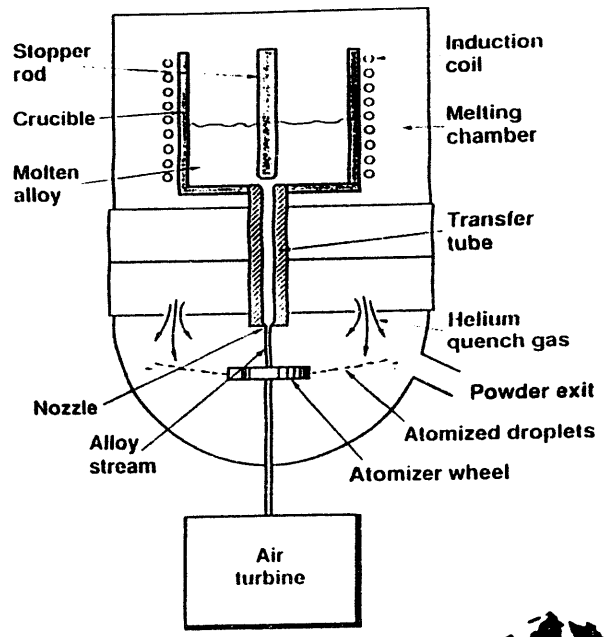

Beryllium Powder Morphology

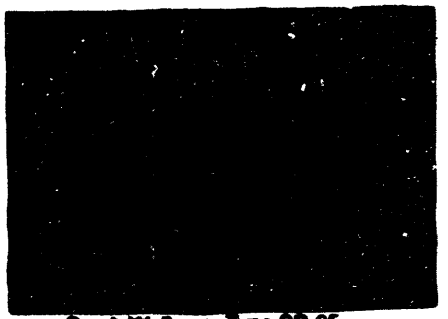

Brush Wellman: Type SP-65
impact attritioned

LANL: Type XSR
centrifugal atomized

Atomized Beryllium Powder
- 400 mesh

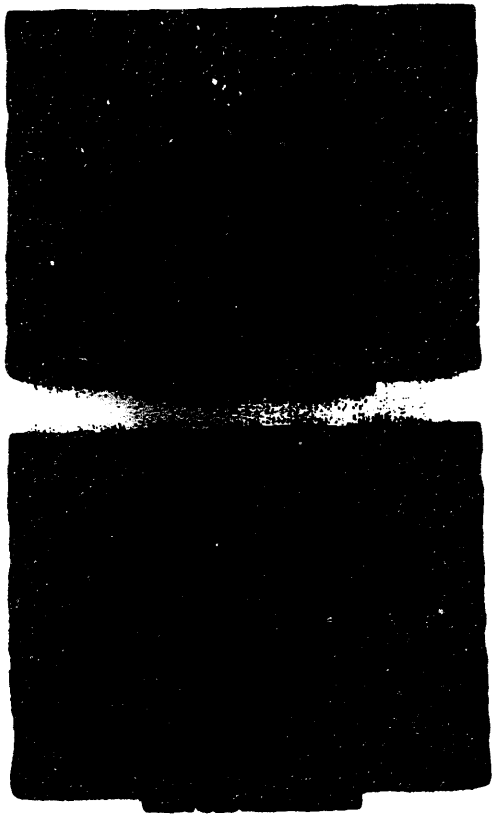

Vacuum Plasma Spraying of Beryllium

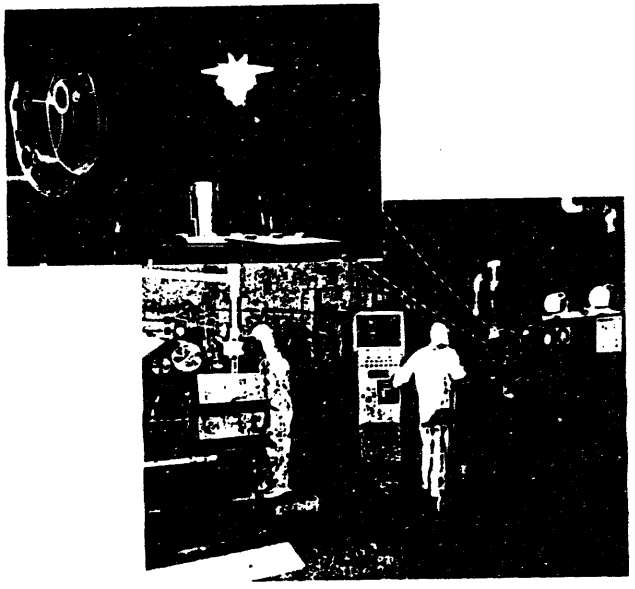

Los Alamos

Optimizing Spray Deposits of Beryllium

- Increase particle melting:
  - *particle morphology*
  - *particle size distribution*
  - *substrate temperature*
  - *particle dwell time:*
    - *low velocity laminar flow*
    - *high flame temperature*

Plasma Spraying of Beryllium for ITER

- Applications:
  - *In-situ repair of sputter eroded and disruption damaged beryllium armour tiles in high heat flux regions.*
  - *Fabrication of large area (1000 m^2) beryllium coatings (1-2mm) over stainless steel or vanadium first wall surfaces.*
- Requirements:
  - *high density*
  - *high deposit efficiency*
  - *good thermal conductivity*
  - *good bond strength between coatings and substrate materials (Be, S.S etc.)*
  - *enhanced mechanical behavior under pulse fusion conditions*
  - *others.....*

Materials Science and Technology Div...

Microstructure of Plasma-Sprayed Beryllium

As-sprayed microstructure (optical)

Optical metallography (

Oxides in Beryllium

Plasma-sprayed beryllium

Hot-pressed beryllium

A Comparison of Oxygen Levels in Beryllium Spray Deposits and Beryllium Powders

Materials Science and Technology Division

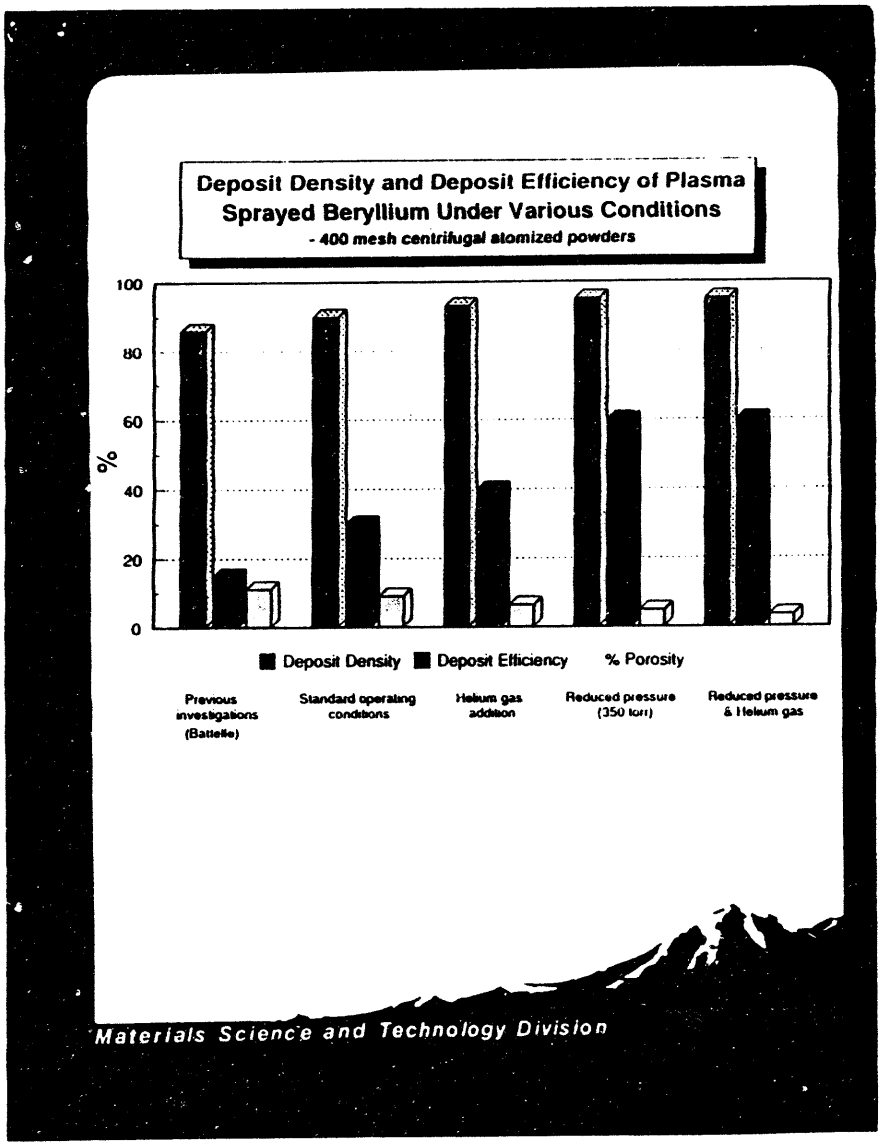

Thermal Conductivity

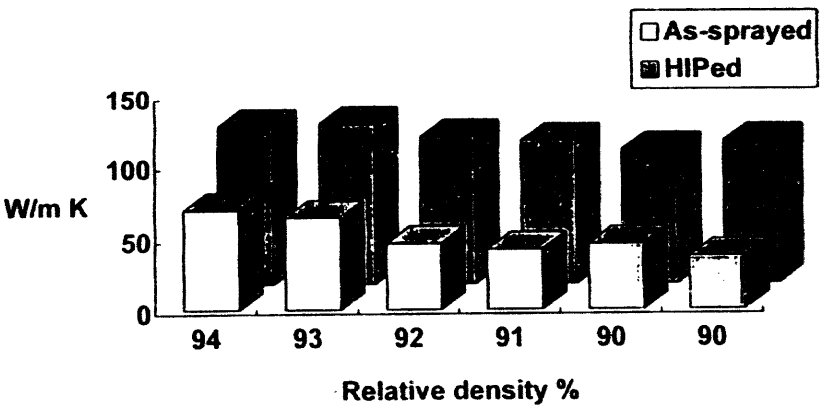

AIIM

Association for Information and Image Management

1100 Wayne Avenue, Suite 1100
Silver Spring, Maryland 20910
301/587-8202

Centimeter

Inches

MANUFACTURED TO AIIM STANDARDS
BY APPLIED IMAGE, INC.

4 of 8

Deposit Density and Deposit Efficiency of Plasma-sprayed Be vs. Be-Al-4%Ag

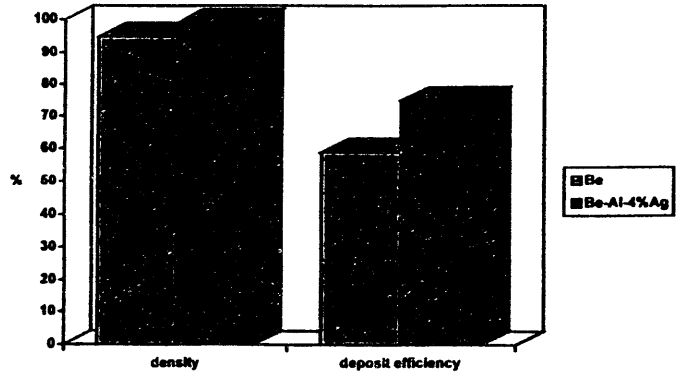

Materials Science and Technology

Effect of Processing Parameters on the As-deposited Microstructure of Be-Al-4%Ag

Arc Gas - 35 slm (Ar)
Arc gas - 35 slm (He)
Fwd gas - 2.5 slm (Ar)
Fwd feed - .5 lb/hr
Distance - 3in
Pressure - 600 torr
Current - 500 amps

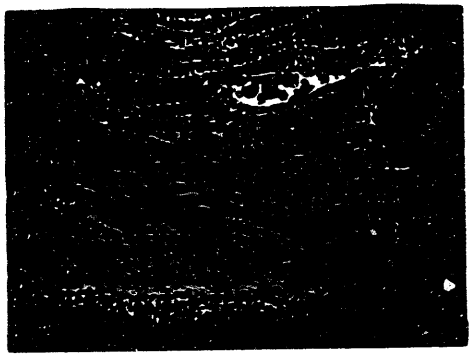

Arc Gas - 35 slm (Ar)
Arc Gas - 35 slm (He)
Fwd gas - 2.5 slm (Ar)
Fwd feed - .5 lb/hr
Distance - 3 in
Pressure - 600 torr
Current - 500 amps

Plasma Spraying of Beryllium for ITER

- **Critical Research Areas:**

  - ***Optimize powder processes (centrifugal, inert atomization) to produce high yields of low oxide, -400 mesh spherical beryllium powder.***

  - ***Optimize plasma spray parameters to produce high density/high thermal conductivity, and high deposit efficiency deposits of beryllium.***

  - ***Characterization/performance of plasma-sprayed beryllium coatings under pulse fusion conditions.***

  - ***Investigate surface preparation techniques on the bond strength of plasma-sprayed beryllium to beryllium, stainless steel and vanadium.***

  - ***Demonstrate remote manipulation and in situ repair***

High Heat Flux Load Experiments on Functionally Graded Materials

F.Kudough, M.Morimoto, K.Namiki, K.Ioki
Mitsubishi Atomic Power Industries, Inc.
4-1 Shibakoen, 2-Chome, Minato-Ku
Tokyo 105 Japan

and

H.Tsunoda, M.Toyoda, M.Onozuka
Mitsubishi Heavy Industries, Ltd.
4-1 Shibakoen, 2-Chome, Minato-Ku
Tokyo 105 Japan

Abstract

The use of Functionally Graded Layers (FGLs) for Plasma Facing Components (PFCs), owing to piecewise transition in material properties from low-Z surface materials to metal substrates, can provide reduction in thermal stresses, and also provide high thermal resistance to PFCs. Mitsubishi started the study on PFCs using FGLs in 1990. This article addresses the Mitsubishi's activity on the development of PFCs using FGLs.

OBJECTIVE

To Develop Plasma-Facing Components (PFCs)

1) Which Are Capable of Reducing Thermal Stresses, and
2) Which Are Capable of Possessing High Thermal Load Resistance.

APPROACHES

Study Started on Developmental Manufacturing Basis.

Procedures Taken in This Study Are:

1) Determine Material Combination of
   Surface Material
   FGLs
   Metal Substrate
2) Bond Them together to Provide Test Sample,
3) Subject Test Sample to Heat Loads, and
4) Examine Integrity of Test Sample.

Study Is in Progress in the Following Steps.
Procedure 2) in Step 3 Has Finished Now.

Step 1:

Use of Experienced Materials Attempted as First Step.
Material Combination Was:

Surface Material : Graphite
FGLs : ZrO_2/SUS 304L
Metal Substrate : SUS 304L
(SUS 304L : Japanese Notation
Equivalent to Type 304L Stainless Steel)

Interfaces Successfully Diffusion-Bonded by Hot Press.
Test Sample Subjected to Constant Heat Flux of 1KW/cm2.
Incremental Durations : 3s, 5s, 7s. and 10s

Crack Found in Graphite for Case with Exposure Time of 7s.
Rupture Occurred for Case with Exposure Time of 10s.

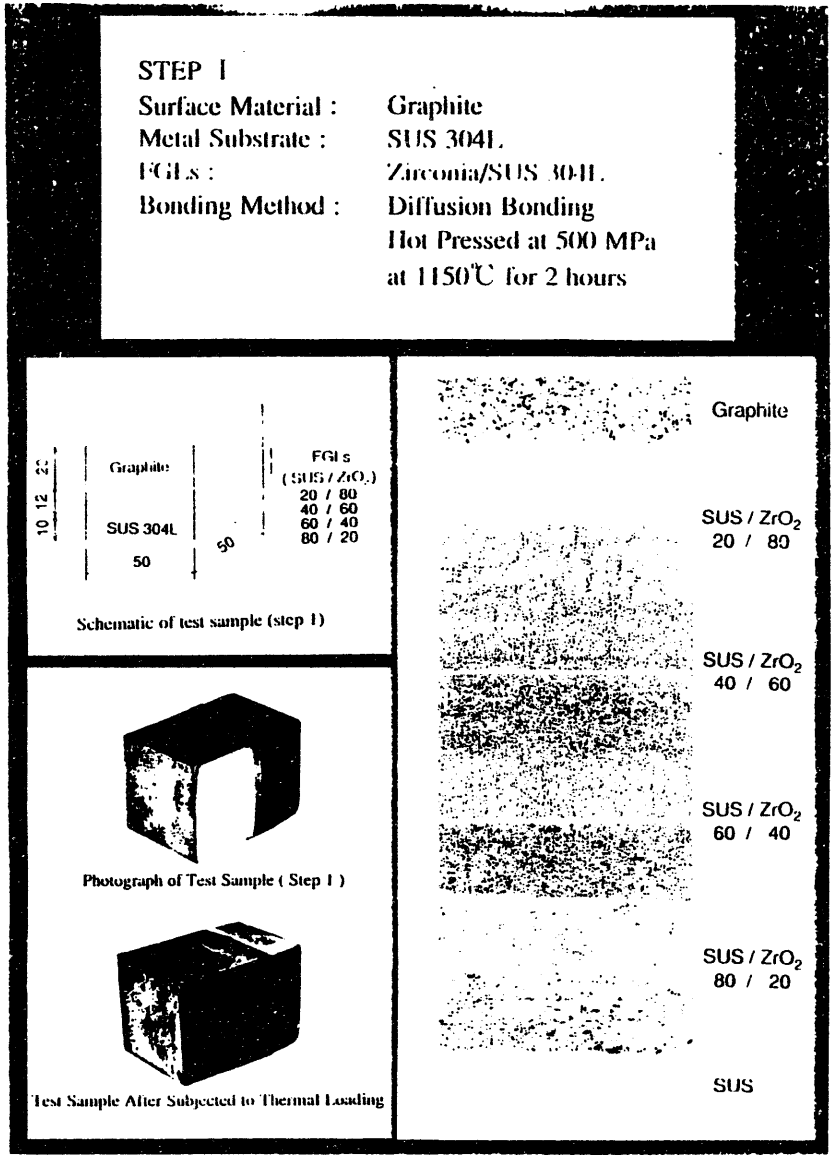

Step 2:

In What Follows, More Thermally Resistant and Thermally Conductive PFCs Attempted.

Material Combination Selected with Ultimate Goal in Perspective.
Diffusion Bonding of CFC Composite and TiN/Cu Attempted in Vain.
Graphite Adopted for Surface Material as Preliminary Step.

	Ultimate goal	Step 2
Surface Material	CFC composite	Graphite
FGLs	TiN/Cu	TiN/Cu
Metal Substrate	Cu	Cu

Successfully Diffusion-Bonded by Hot Press.
Subjected to 50 Times of Thermal Loading.
Each Having Constant Heat Flux of 1 KW/cm2 for 2s.

No Harmful Damage Found in Sample.
Structural Integrity Demonstrated.

STEP II

Surface Material :	Graphite
Metal Substrate :	Copper
FGLs :	TiN/Copper
Bonding Method :	Diffusion Bonding Hot Pressed at 5000 MPa at 1029℃ for 2 hours

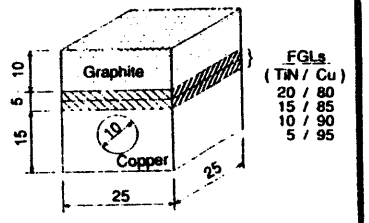

Schematic of test sample (step 2)

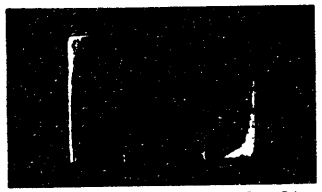

Photograph of Test Sample (Step 2)

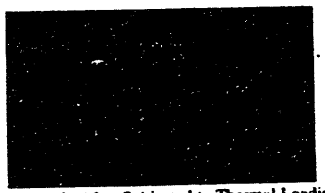

Test Sample After Subjected to Thermal Loading

Step 3:

As Diffusion Bonding of CFC Composite and TiN/Cu Ended in Vain, Brazing Between Interfaces Applied.
Sample Successfully Brazed in High Vacuum Environment.

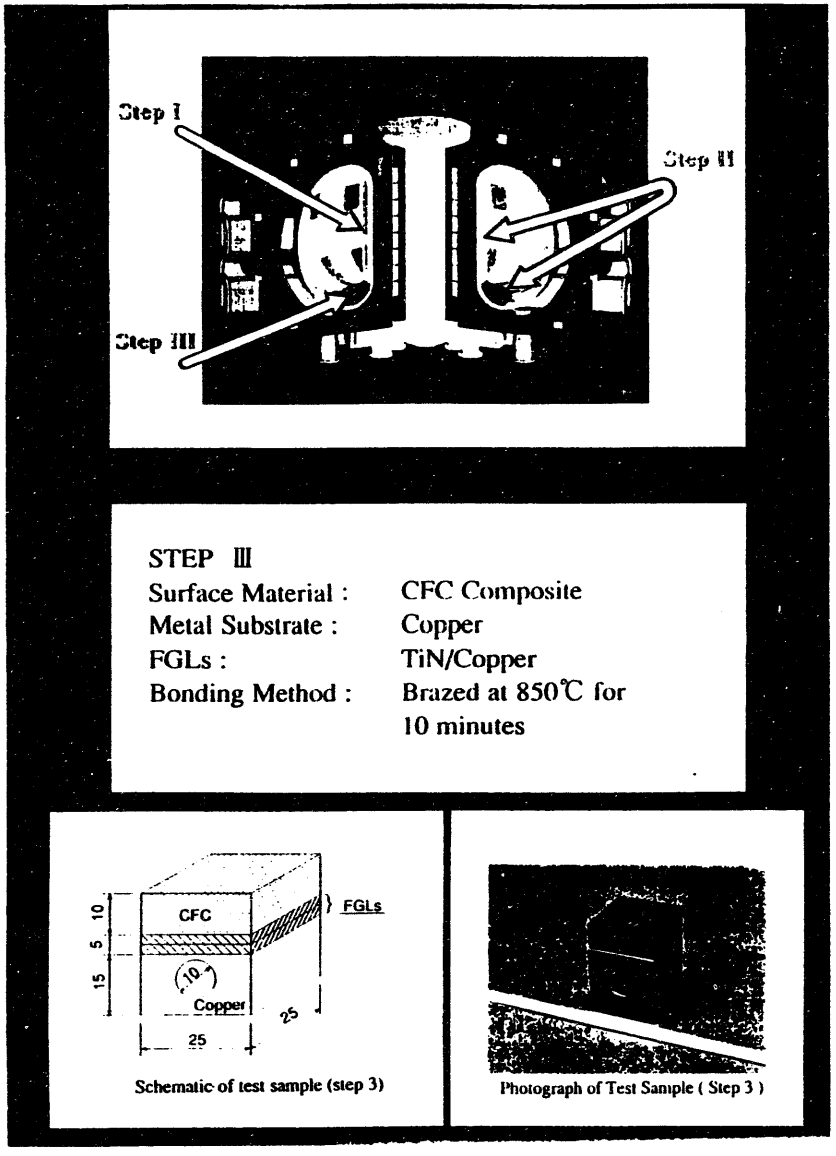

FUTURE WORK

Procedure 2) in Step 3 Has Finished.

Thermal Loading Tests on Step 3 Test Sample Slated for Next Month.

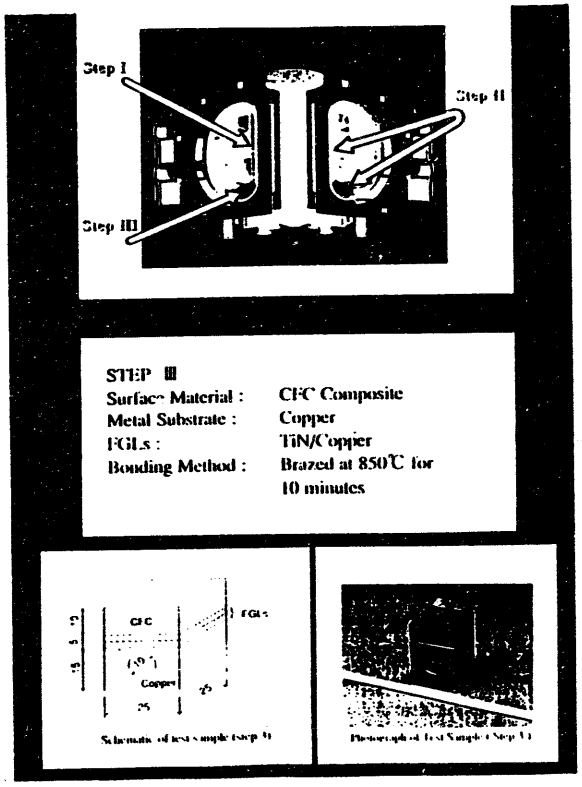
Step I
Step II
Step III
STEP III
Surface Material : CFC Composite
Metal Substrate : Copper
FGLs : TiN/Copper
Bonding Method : Brazed at 850℃ for 10 minutes
CFC
FGLs
Copper
25

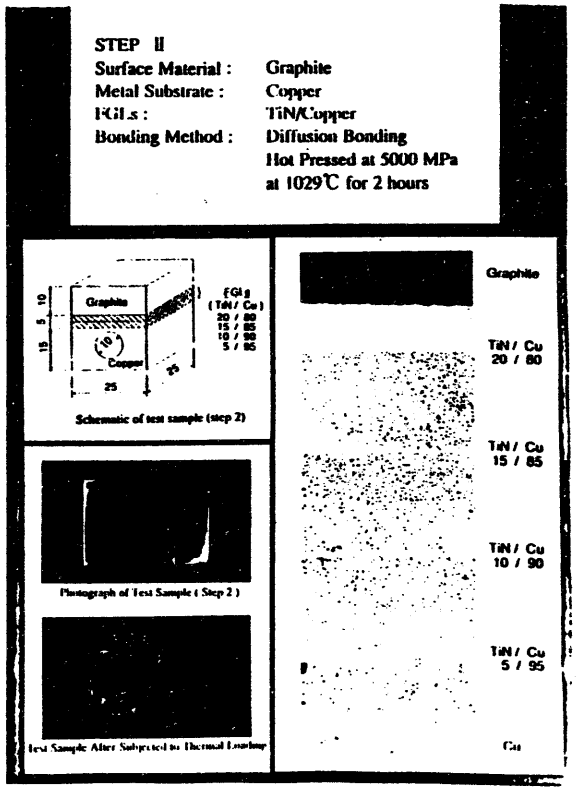
STEP II
Surface Material : Graphite
Metal Substrate : Copper
FGLs : TiN/Copper
Bonding Method : Diffusion Bonding
Hot Pressed at 5000 MPa
at 1029℃ for 2 hours
Graphite
Copper
25
Schematic of test sample (step 2)
Photograph of Test Sample (Step 2)
Test Sample After Subjected to Thermal Loading
Graphite
TiN / Cu 20 / 80
TiN / Cu 15 / 85
TiN / Cu 10 / 90
TiN / Cu 5 / 95
Cu

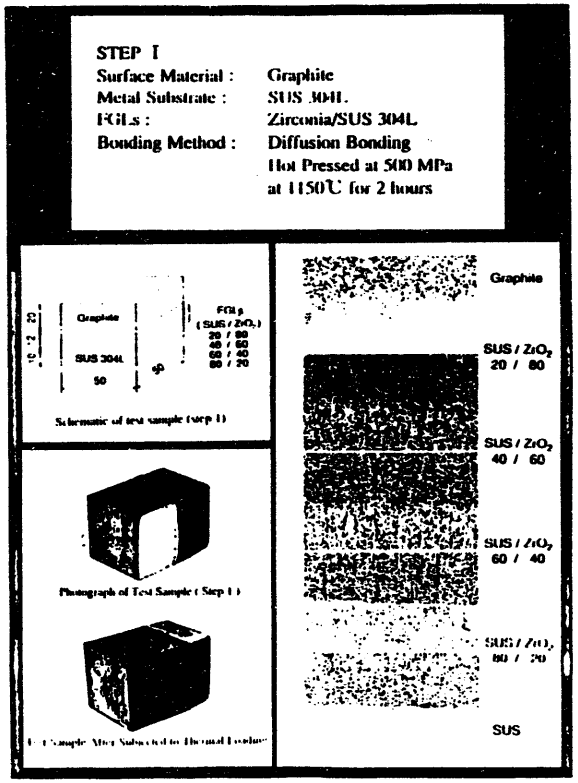
STEP I
Surface Material : Graphite
Metal Substrate : SUS 304L
FGLs : Zirconia/SUS 304L
Bonding Method : Diffusion Bonding
Hot Pressed at 500 MPa
at 1150℃ for 2 hours
Graphite
SUS 304L
50
FGLs
(SUS / ZrO2)
20 / 80
40 / 60
60 / 40
80 / 20
Graphite
SUS / ZrO2
20 / 80
SUS / ZrO2
40 / 60
SUS / ZrO2
60 / 40
SUS / ZrO2
80 / 20
SUS

LIQUID METAL COOLANTS FOR BLANKET AND DIVERTOR

T. Q. Hua
R. F. Mattas

Fusion Power Program
Argonne National Laboratory
Argonne, IL 60439

Presented at the US-Japan HHF/PMI Workshop
January 24-27, 1994, San Diego, California

LIQUID METAL COOLANT ASSESSMENT FOR ITER BLANKET

- Coolant assessed:

  Li, $Li_{17}Pb_{83}$, Na, NaK, K, Ga, Pb, BiPb

- Advantages:

  - low pressure system
  - High temperature capability
  - Li provides both the cooling and tritium breeding functions
  - Li is low activation material
  - low tritium inventory
  - good capability to accommodate power excursion
  - simple first wall, blanket, and shield design

- Disadvantages:

  - requires electrical insulator to reduce MHD pressure drop
  - coolant activation except for Li
  - melting point above room temperature except for NaK (-12°C)
  - safety concern related to reactivity with air and water

Performance of the Different Liquid Metal Coolant for the Twisted Tubes Concept with 2 m Helical Pitch and the Same Δt at 300°C

Property or Relative Factor	Material				
	32Na68K	Na	Ga	Li	17Li83Pb
ρ, Kg/m^3	796	879	5900	505	9500
cp, J/Kg.K	890	1300	400	4260	190
K, W/m.K	26	75.7	55.6	46	13.2
μ, Pa.s, x10^{-4}	2.5	4.4	11	4.5	21.5
σ, S/m, x10^{-6}	2.0	6.0	3.3	3.3	0.79
α, m^2/S x10^{-5}	3.7	6.6	2.4	2.1	0.73
Avg velocity factor	1	0.62	0.30	0.33	0.39
ΔP factor	1	1.42	0.78	0.57	0.73
h factor	1	1.72	2.25	1.35	0.71

LIQUID METAL COOLANT FOR DIVERTOR

- Water is not allowed for cooling the divertor during the Extended Performance Phase (Li/V blanket).
- Other coolant options for divertor include liquid metal or He.
- NaK coolant may be used with vanadium or Cu structure (Be surface) at low or high temperature. Requires Al_2O_3 insulator coating.
- Li coolant may be used with vanadium structure (Be surface) at high temperature (T > 220°C). Requires AlN insulator coating.

KEY ISSUES INVOLVING LIQUID METAL COOLED SYSTEMS

- Insulator coating:
  - chemical compatibility with liquid metal
  - self-healing (in situ regeneration) to repair cracks or faults through the coating
  - electrical resistivity under the combined effects of neutron irradiation and electric field
- Structured material, V-5Cr-5Ti (Li coolant)
  - data base and fabrication experience
  - cost
- Tritium recovery and purification from liquid Li
  - removal of impurities if salt method is used

CRACKS THROUGH INSULATOR COATING

- Thermal cycling may induce cracks through the coating. The self-healing process will repair cracks or faults.
- The increase in pressure drop is negligible if self-healing regenerates new layers of as little as 1% of the original coating thickness.

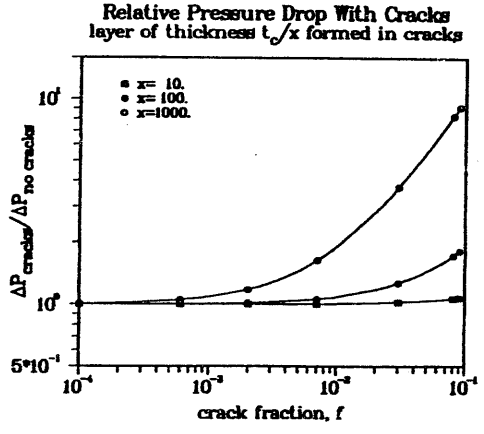

Pressure drop as a function of crack fraction

$$\text{crack fraction} = \frac{\text{total crack area}}{\text{total surface area}}$$

Liquid Metal Heat T nsfer

- The heat transfer coefficient is design dependent
  - Flow conditions
  - Geometry
  - Fluid properties
  - Heat flux distribution
- Use Nusselt number to characterize heat transfer

$$Nu = \frac{hD}{k}$$

h = heat transfer coefficient
D = pipe diameter
k = thermal conductivity

- For uniform heat flux, laminar flow

Nu ≡ 4-5

h ≡ 20,000-25,000 W/m^2 K for Li

- For uniform heat flux, laminar flow in high ⊥ magnetic field (slug flow)

Nu ≡ 7-8

h ≡ 35,000-40,000 W/m^2 K for Li

rfm/01-06-93/01

Liquid Metal Heat Transfer
(continued)

- For step heat flux on one side, laminar flow in a high magnetic field

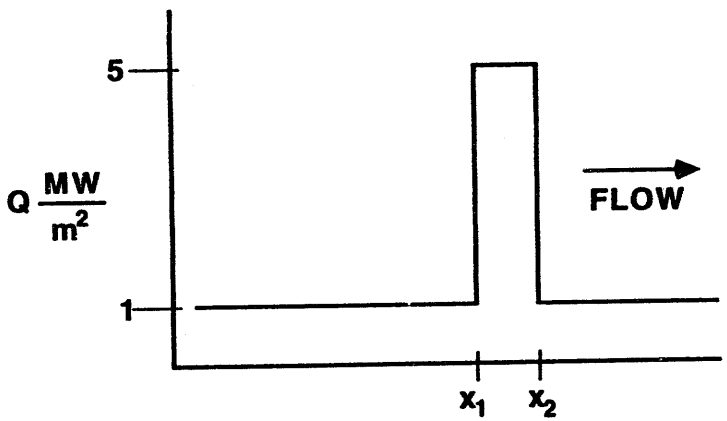

$$x_1 = 2.0\,m, x_2 = 2.20\,m, \bar{v} = 1\,m/s, D = .01\,m$$

$$h_{x_2} \cong 90{,}000\,w/m^2\,K\ for\ Li$$

- The effective heat transfer coefficient for liquid metal flow will be high

rfm/01-06-93/02

Enhanced Heat Transfer with Flow Mixing

- Laminar to turbulent transition region
- Previous experimental results show

$$Nu \tilde{>} 12$$

- Recently completed heat transfer experiment at ANL on Russian test section indicates this transition occurs at N $\tilde{<}$ 1000.
- For ITER divertor conditions

$$\bar{v} \cong 1\,m/s, N = 1000$$

- Enhanced heat transfer is probable for liquid metals in the divertor
- Detailed analysis is needed to reduce the uncertainties in heat transfer

CONCLUSIONS

- A liquid metal cooled divertor should be considered for the ITER Extended Performance Phase
- Issues concerning the performance and reliability of the insulator coatings are critical to the success of liquid metal cooled blanket and divertor. An extensive R&D program for insulator coating development is planned during the Engineering Design Activities.

IV-93

Residual Stress Measurements in Tungsten-Copper
Duplex Structures after Cyclic Thermal Testing

Kazunori Kitamura
Heavy Apparatus Engineering Laboratory, Toshiba Corporation
2-4, Suehiro-cho, Tsurumi-ku, Yokohama, 230 Japan

To safely manage the high heat loads expected in next fusion devices, great efforts have been focused on the development of the actively cooled divertor plate which consists of carbon-fiber-composite(CFC) and tungsten armor tiles bonded to copper heat sink [1] . Since the bonding with these materials often causes fabrication problems, many bonded concepts for the divertor plate have been proposed and tested under the simulated heat loads [2] . However, several important problems still remain unsolved including the interface damages due to formation and redistribution of the residual stress.

Author previously conducted to evaluate the residual stress that developed during cool down of W/Cu test specimens and to compare the residual stress around the interface edge for the several types of bonded structures, through the measurement by the strain gauge method and thermoelasto-plastic FEM analysis [3] , [4] .

Then, cyclic thermal tests have been performed on W/Cu duplex structures using an electron beam test facility with a maximum power of 30 kW, forcusing on the redistribution of the residual stress. The residual stresses on the radiated test specimens have been measured by the strain gauge method to investigate the mechanical behavior on the residual stress after the cyclic heat loads.

Test specimens were made of a 30 mm diameter tungsten plate with a 5 mm thickness brazed to the copper block with a 33 mm diameter and 20 mm thickness. Brazing was carried out at 850 ℃ for 15 min under vacuum (10^{-5} Torr) using a titanium content silver-based braze alloy with a thickness of 50 μm.

Thermal tests were carried out under three heat load conditions of varying the number of shots (1, 10 and 100 cycles) with the same heat flux distribution on the test specimens (maximum heat flux of 14 MW/m^2).

The 3-element 45° stacked strain gauges with 1 mm gauge length were used on the tungsten top surface and 5-element strip gauges with 0.15 mm length on the side surface. The copper heat sink was removed by cutting carefully along the interface with a cutting machine. The residual stresses in four specimens radiated with the different heat load cycles, including unradiated specimen, were compared.

As the results, both the radial and hoop stress components σ_R, σ_θ of the residual stresses on the tungsten top surface decreased with increase of the number of heat load cycles, and relaxation of the residual stress occurred with the elastic-plastic deformation of the copper heat sink. Axial stress component σ_z on the tungsten side surface was also reduced with the increase of the number of the heat load cycles, but hoop stress component increased.

[1] T .Kuroda et al., ITER plasma facing components, ITER documentation series no. 30, IAEA, Vienna, 1990.
[2] C.D. Groessman et al., Fusion Tech.(1988)pp796.
[3] K. Kitamura et al., Fusion Enng. Des. 18(1991)pp173-178.
[4] K. Kitamura et al., 15th SOFE, Tara Hyannis(1993) inpress.

Residual Stress Measurements in Tungsten-Copper Duplex Structures after Cyclic Thermal Testing

Kazunori Kitamura

Heavy Apparatus Engineering Laboratory,
Toshiba Corporation,
2-4, Suehiro-cho, Tsurumi-ku, Yokohama,
230 Japan

US-Japan Workshop Q-181
on PMI-HHFC
San Diego, California
January 24-27, 1994

TOPICS

- Introduction
- Experimental Procedure
  - Test Apparatus
  - Test Specimen
- Cyclic Heat Load Testing
- Residual Stress Measurement
- Summary

Mechanical Assessment of Bonded Interface

Critical Issues

Microcrackings around Interface Edge

Debonding of Armor from Copper Heat Sink

⇩

Residual Stress Formation Developed during Cool Down from Brazing Temperature

Redistribution of the Residual Stress due to Heat Loads

⇩

Investigation of the Residual Stress Behaviors of Bonded Test Specimens after Cyclic Thermal Testing

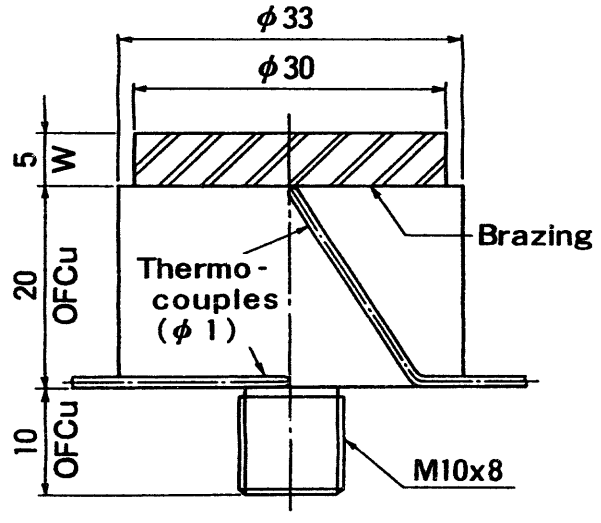

Fig. Test Specimen of Tungsten-Copper Duplex Structure for Cyclic Thermal Testing

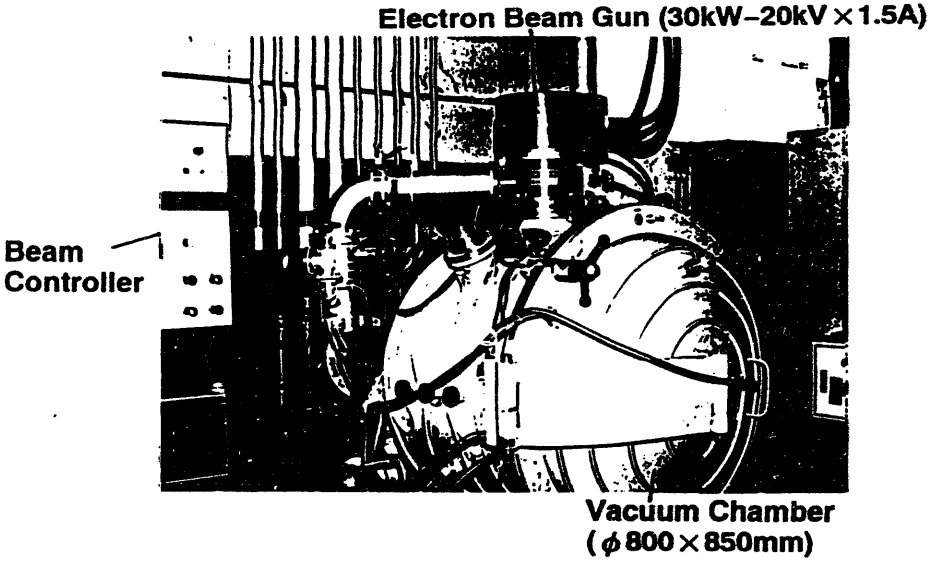

Fig. Overview of High Heat Flux Test Device Utilizing the Electron Beam Gun.

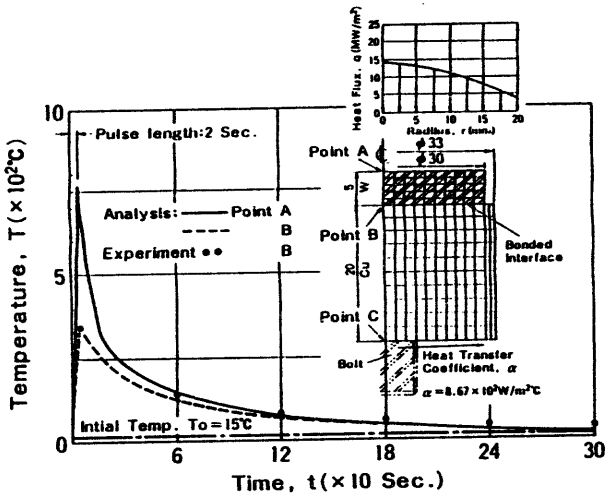

Fig. Temperature Changes in W/Cu Test Specimen to a Heat Load of 14MW/m²-2sec.

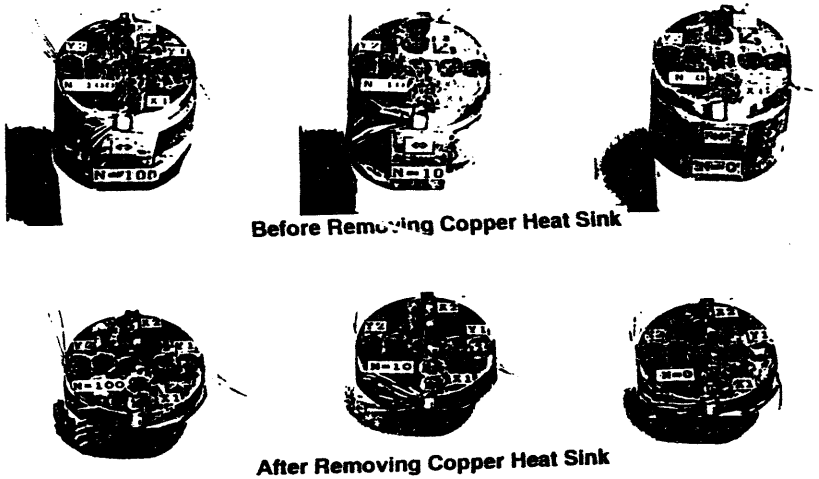

Fig. W/Cu Test Specimens with Strain Gauges on the Top and Side Surfaces of the Tungsten Plate.

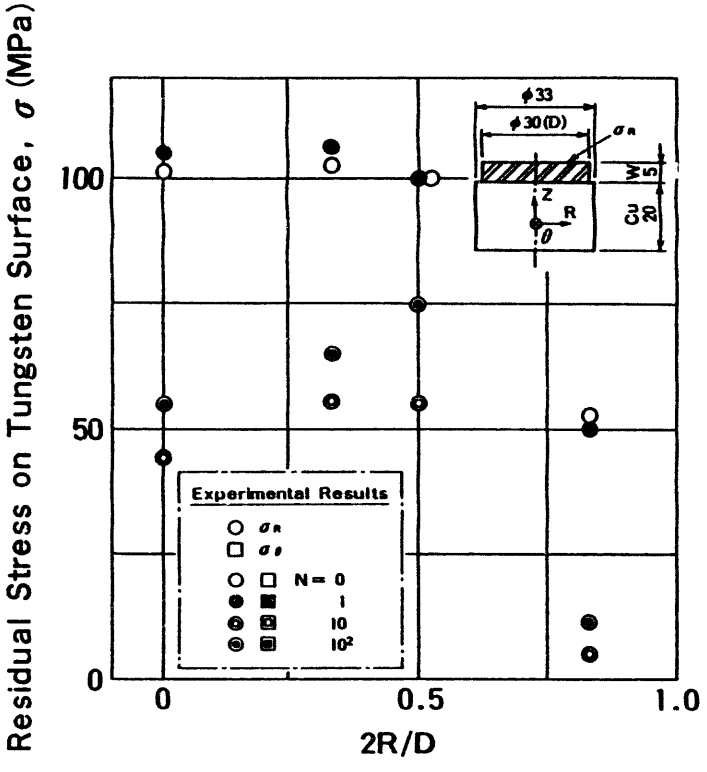

Fig. Distribution of ~~Hoop~~ Radial Stress Components on Tungsten Top Surface

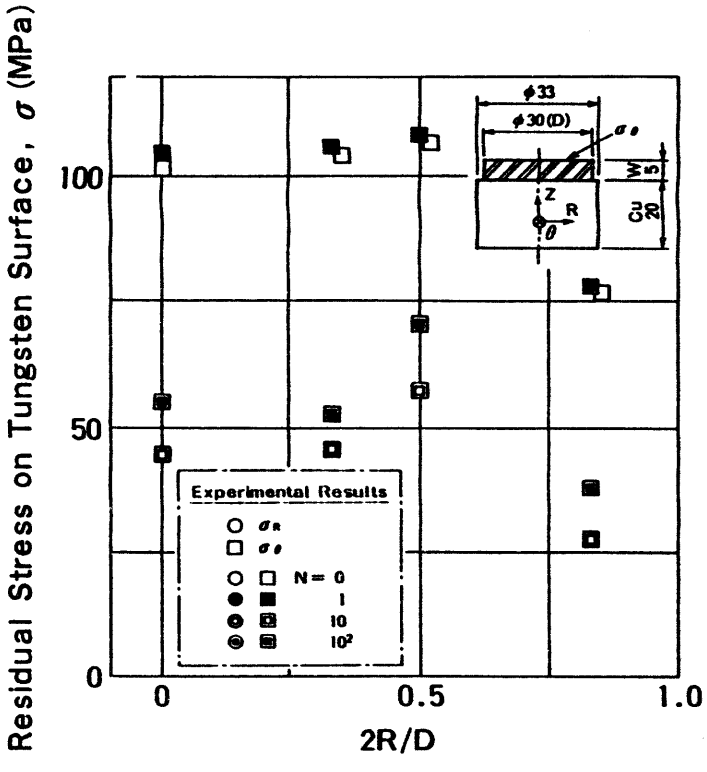

Fig. Distribution of ~~Radial~~ Hoop Stress Components on Tungsten Top Surface.

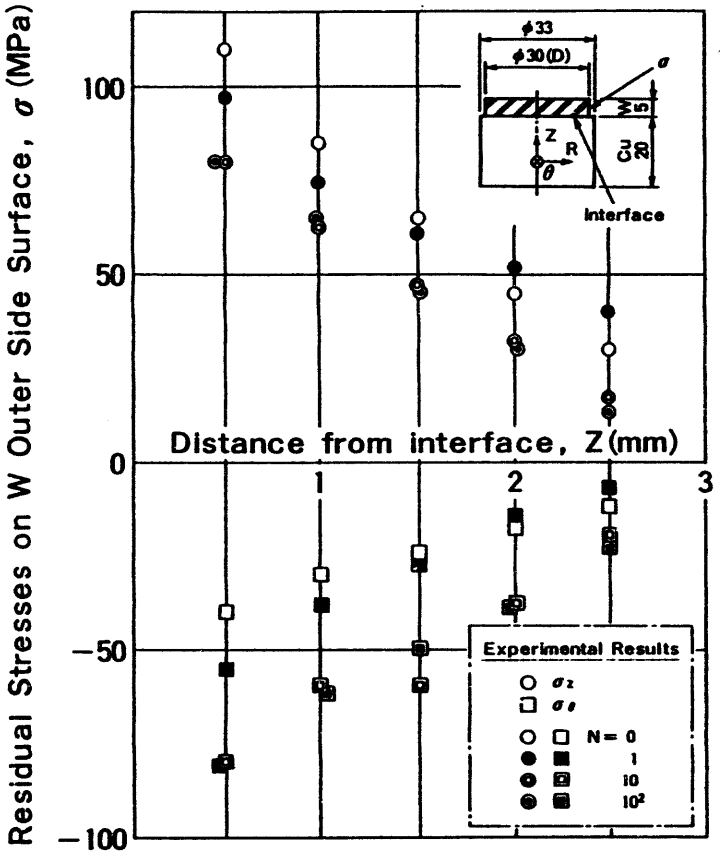

Fig. Residual Stress Distribution on Tungsten Side Surface.

Summary

Residual stresses in test specimens of W/Cu bonded structures after cyclic thermal testing were measured by the strain gauge method.

- Both radial and hoop stress components σ_R, σ_θ of the residual stresses on the tungsten top surface decreased with increase of the number of heat load cycles, and relaxazation of the residual stress occured with elasto-plastic deformation of the copper heat sink.

- Axial stress component σ_Z on the tungsten side surface was also reduced with increase of the number of heat load cycles, but hoop stress component increased.

Future Works

- Further more experimental data base of residual stress measurements of W/Cu test specimens, especially the experimental data for a large number of heat load cycles(~1000 cycles).

- Comparision of experimental results with those by thermoelasto-plastic FEM analysis.

- Experimental and analytical studies for other bonded structures consisting of several matenials (C/Cu, CFC/Cu, CFC/DsCu etc.)

Session V

Plasma Facing Component Design and Applications

US-JAPAN WORKSHOP ON IIIFC
24 TO 27 JANUARY, 1994, SAN DIEGO, USA

LOCAL ISLAND DIVERTOR CONCEPT FOR LHD

A. Komori, N. Ohyabu, H. Suzuki, T. Watanabe,
A. Sagara, N. Noda, and O. Motojima

National Institute for Fusion Sience
Nagoya 464-01, Japan

Contents

1. Introduction

A. *Motivation & Rationale of LID Project*

* Closed full helical divertor is the major LHD edge control scheme. However, it will not be completed in the early experimental phase, because of large production costs.

↓

The proposed local island divertor is ideal to control the LHD edge plasma with modest cost, and hence, will be available in the early experimental phase.

* Information about edge plasma behavior, obtained with LID, will be utilized for optimizing the design of the closed full helical divertor.

* It is a good test bed for high heat flux component system.

* The LID experiment will provide insights into the relation between edge and core plasma confinement, and will motivate exploration of advanced divertor concepts.

B. *Local Island Divertor for LHD*

* Utilize a magnetic island (m/n=1/1) as a divertor magnetic configuration, which can be generated by an additional set of small island control coils.

* A closed local divertor
  - High pumping efficiency (up to 50%) for low recycling operation
  - "Vague" boundary is eliminated.
  - Good impurity control

↓

High edge temperature

↓

A significant enhancement in the core energy confinement
(deep fueling such as NBI or pellet fueling is needed.)

  - High plasma plugging efficiency for high recycling operation

* Localized recycling
  - Easier pumping → Modest cost
    Membrane pumping?
  - No leading edge problem
  - Plasma heating power up to 3 MW (steady state)
  - Efficient discharge cleaning

Divertor Operational modes

Closed full helical divertor
Local island divertor

1. Low recycling

High temperature and low density

High efficient pumping

↓

High edge temperarue

↓

Enhancement of τ_E

2. High recycling

Low temperature and High density

Impurity trapping in the edge
by plasma flow

↓

Radiative cooling (a safer heat removal)

Principle of LID

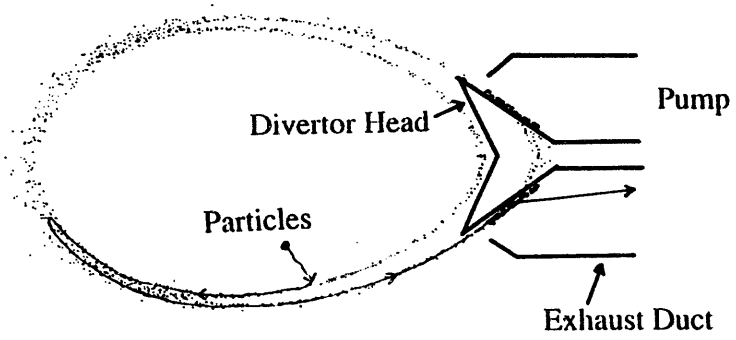

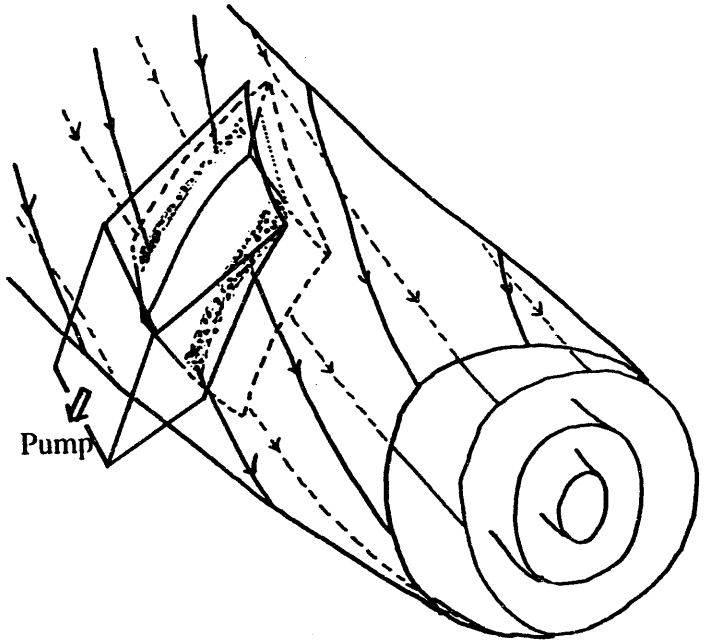

STUDY OF EDGE GEOMETRY EFFECT ON τE

Comparison Among Four Geometries

Limiter

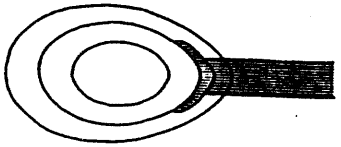

Limiter with island

Lack of low and medium
m rational surfaces
near the last closed surface.

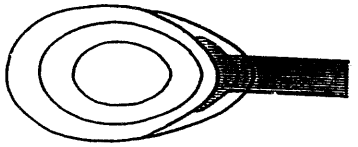

Open island divertor

Existence of separatrix

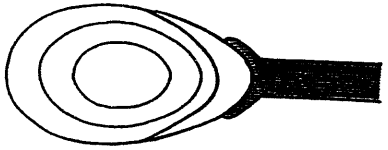

Closed island divertor

Pumping capability

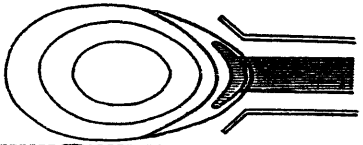

Ergodic boundary

Edge radiative cooling

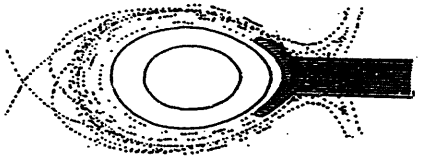

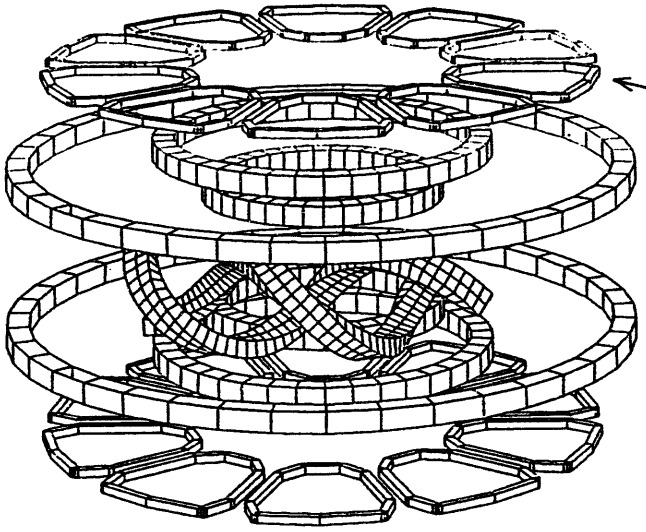

(a)

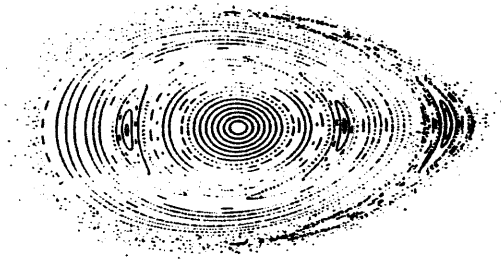

· Application of m/n=1/1 component to the LHD configuration
· Toroidal coupling → m/n=2/1 island

(b)

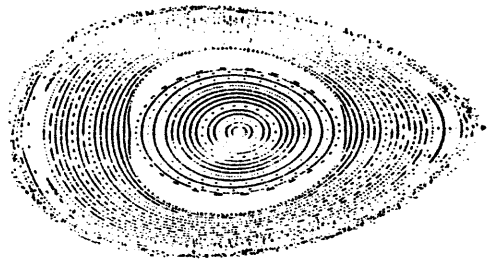

· Application of m/n=2/1 component to the LHD configuration

(c)

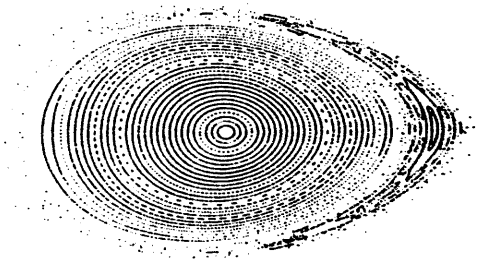

· Complete elimination of m/n=2/1 island by substracting (b) from (a)

Closed surfaces

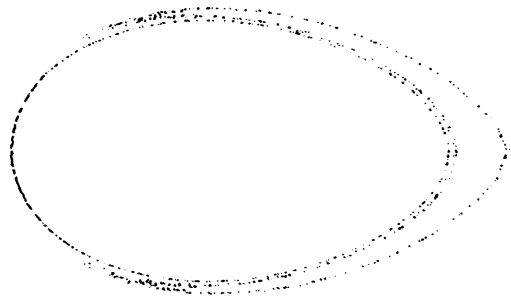

Ergodic layer between the closed surfaces

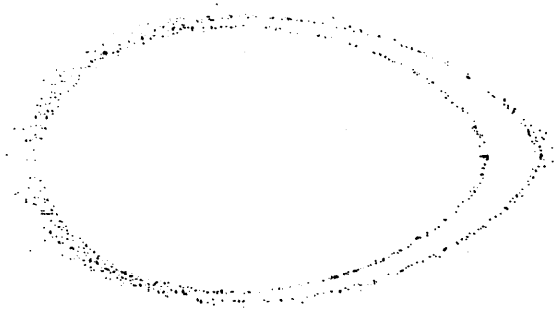

Number of toroidal circulation

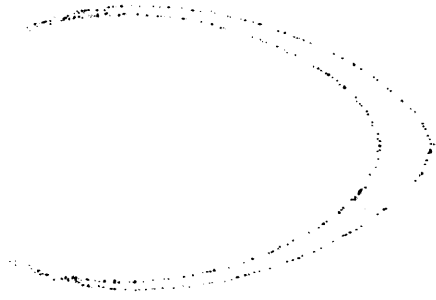

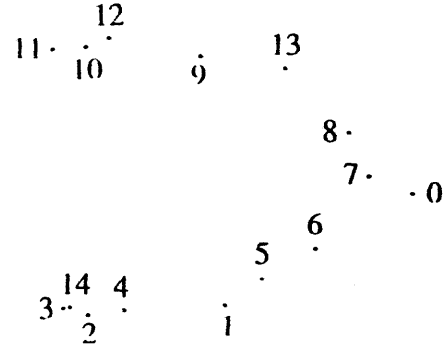

Obtained Local Island Divertor Geometry

* Magnetic field = 3 T
  Currents of island control coils = 80 ~ 100 kAT

  · Island full size ~ 15 cm

  · Number of toroidal circulation ~ 10

  · Width of the divertor head ~ 60 cm

  · Length of the divertor head ~ 60 cm

* λ_n and q

  · $\lambda_n \sim 3$ cm, $\lambda_n = (LD/C_s)^{1/2}$
  $L \sim (10/2)2\pi R$, $D \sim 1\ m^2/s$, $C_s \sim 10^5\ m^2/s$
  E x B motion may make λ_n smaller.

  · q (steady state)=2 MW/0.2 $m^2 \sim 10\ MW/m^2$

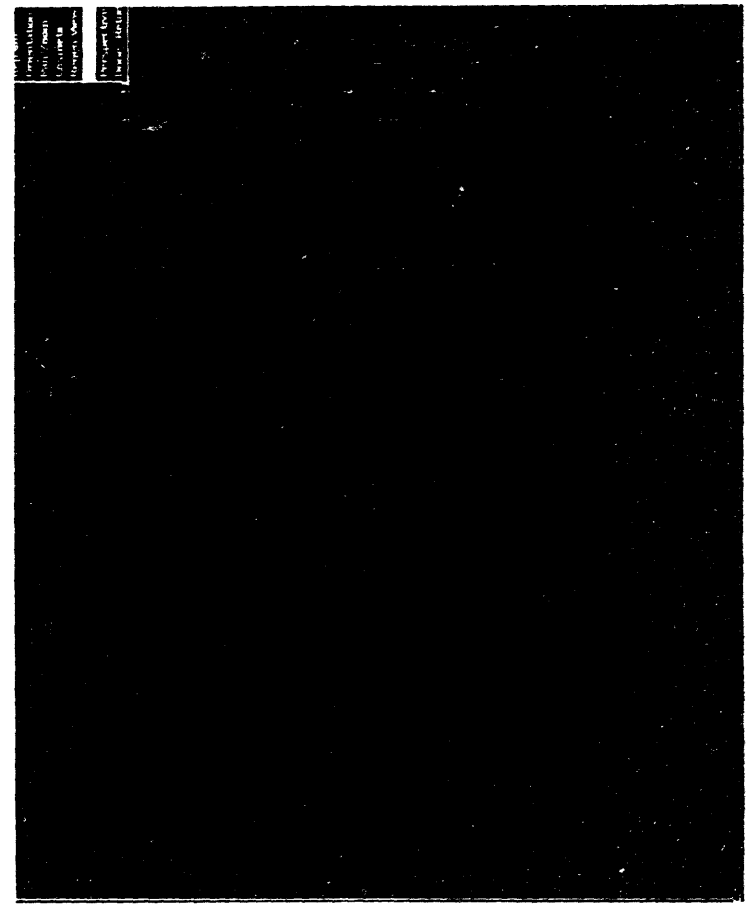

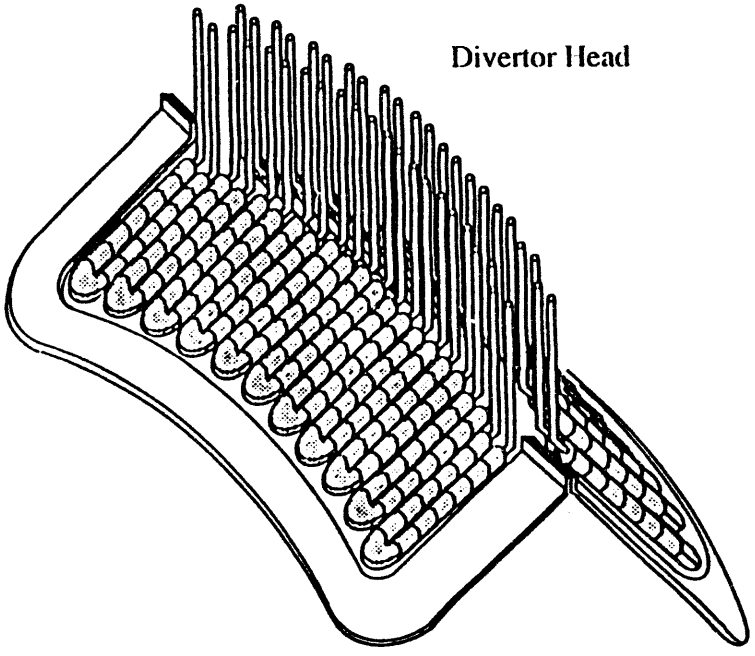
Divertor Head

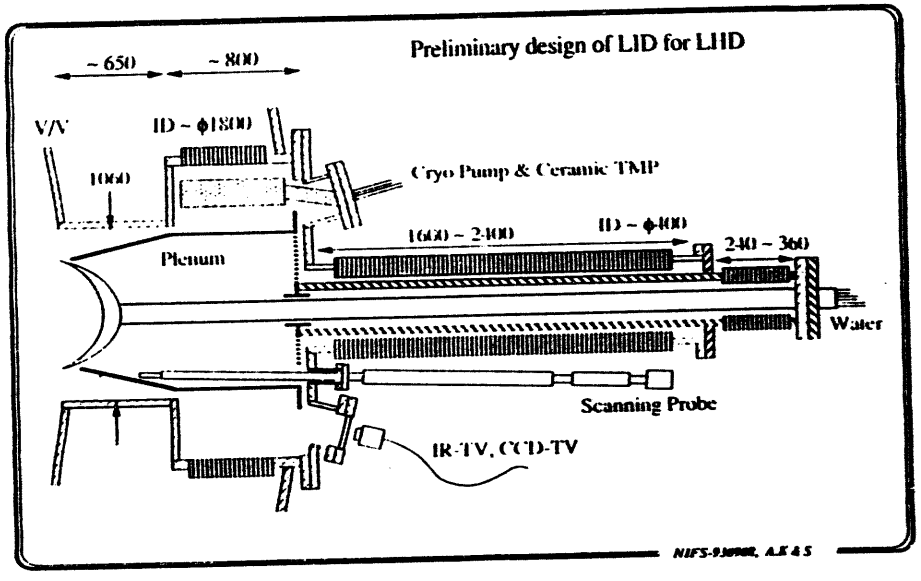
Preliminary design of LID for LHD
~ 650
~ 800
V/V
ID ~ ϕ1800
1000
Cryo Pump & Ceramic TMP
1600 ~ 2400
ID ~ ϕ400
240 ~ 360
Plenum
Water
Scanning Probe
IR-TV, CCD-TV

Schedule of LHD Divertor Experimental Study

	Local Island	*Helical Divertor*
1998	Start of divertor experiments Low power pulse operation	
		No Baffle (Open) No Pumping
1999	High power pulse operation Start of detailed physics study	
	Pumping Capability	
2000	3 MW steady state operation Evaluation of LID	
2001		Upgrade Baffle (Closed) Pumping 3 MW steady state operation High power steady state operation

4. Summary

* The concept of LID was introduced.

* It was demonstrated that the magnetic configuration necessary for LID can be generated by an additional set of small island control coils.

  Magnetic field = 3 T
  Currents of island control coils = 80 ~ 100 kAT
  ↓
  Island full size ~ 15 cm
  Number of toroidal circulation ~ 10
  Divertor head ~ 60 cm x 60 cm
  λ_n ~ 3 cm
  q (steady state)=2 MW/0.2 m^2 ~ 10 MW/m^2

* The preliminary design of divertor head, *etc.* was presented.

Tore Supra Phase III Outboard Pump Limiter (OPL)
(Phase III denotes water-cooled PFCs)

Richard Nygren, Tom Lutz @ CE, Bob McGrath, Chuck Walker,
Ben Tafoya, Paul Freshour, Jon Watkins, Joe Koski - Sandia
Dominique Guilhem, Philippe Chappuis, Thierry Loarer,
Jean Jacques Cordier - CE Cadarache
Chris Klepper, Tanner Uckan - ORNL
Steve Tobin - MFE Fellow, University of Michigan @ CE

- operational experience with Phase III OPL
- fabrication of water-cooled PFCs
- thermal-hydraulic modeling
- *all of the above*

presentation at the US-Japan Workshop on High Heat Flux Components
January 24-27, 1994 -- La Jolla, California

1454 140/RE:IV/102094

Sandia Fusion Program

We design, build, test and operate PFCs for the rest of the world.

- TEXTOR: ALT-I
- TEXTOR: ALT-II
- TEXTOR: ALT-II upgrade
- Tore Supra: Phase I Limiter
- Tore Supra: Phase II Limiter
- ☛ Tore Supra: Phase III Limiter (actively cooled PFC)
- JET redesign: tessellated Be tiles
- ITER CDA: monoblock divertor tiles
- TFTR poloidal rf antenna limiter: anisotropic 3-D analysis of CFC tiles
- ISX-B: Be limiter

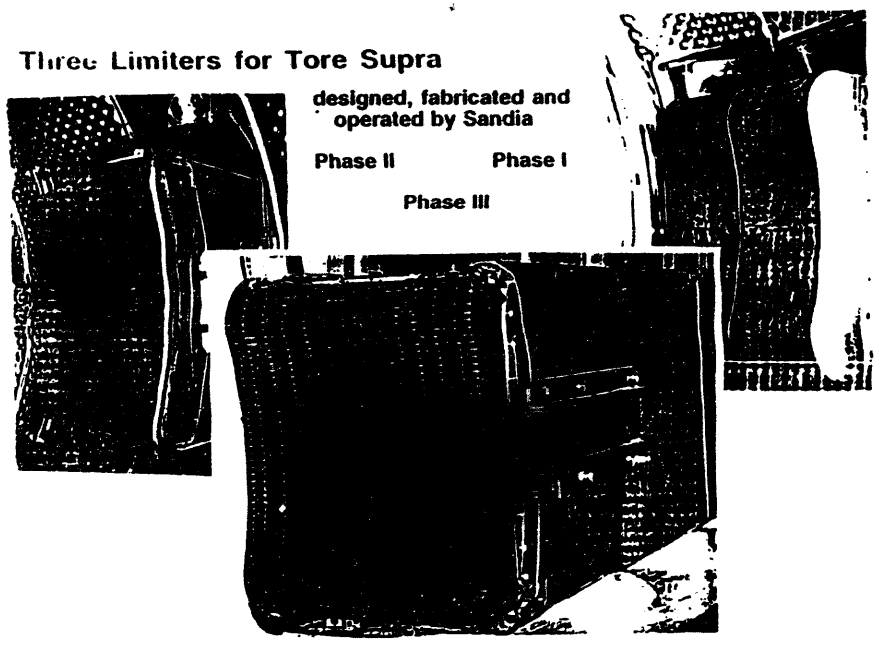

Why should ITER care about Tore Supra?

Tore Supra has no divertor.

Tore Supra's technology includes:

- long pulse operation
- actively cooled PFCs

- design of duplex heat sink (carbon on copper -- ITER startup limiter)
- thermal-hydraulic design, testing and QA
- fabrication of brazed duplex structure
- instrumentation
- reliable operation (monitoring program)

Sandia National Laboratories

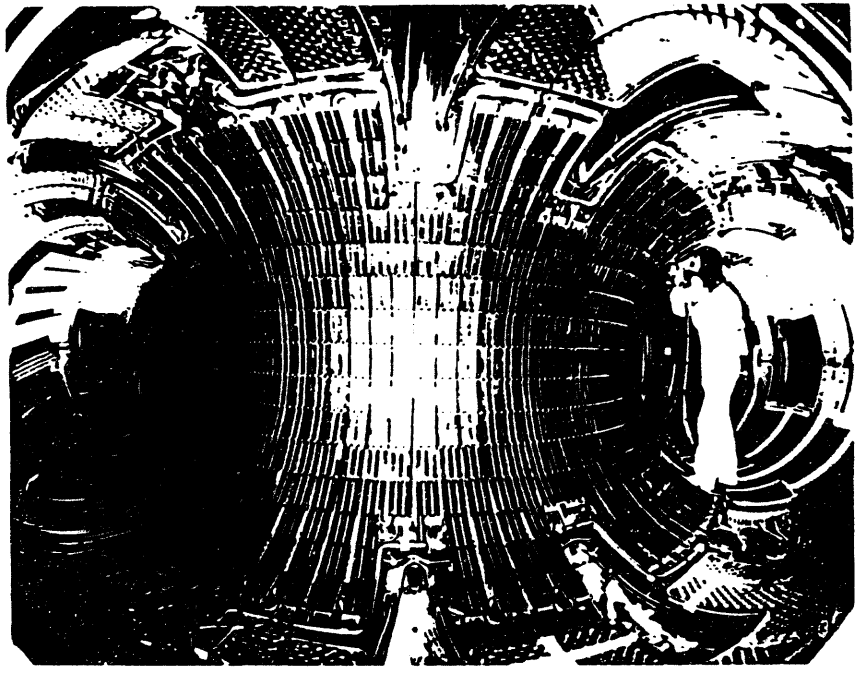

Tore Supra Phase III Outboard Limiter During the 1993 Campaign

Richard Nygren, Tom Lutz @ CE, Bob McGrath,
Chuck Walker, Jon Watkins, Joe Koski - Sandia
Dominique Guilhem, Philippe Chappuis,
Thierry Loarer, Jean Jacques Cordier - CE Cadarache
Chris Klepper, Tanner Uckan - ORNL
Steve Tobin - MFE Fellow, University of Michigan @ CE

Sandia National Laboratories

Initial Operation May 13th - 14th (Thurs.- Fri.)

Shots 11002-11084

•Phase III Outboard Pump Limiter (OPL) operated successfully.

Tests at progressively higher powers, longer shots
example: shot 11044
~0.8 MW absorbed for 8 seconds
$n_e = 3 \times 10^{19}\ m^{-3}$, $T_e = 42$ eV, $I_p = 1.5$ MA

- TCs (32) and flowmeters (10) provided excellent data.
- Limiter surface was surveyed with endoscope (large lens) - minor hot spots where expected. (Grafoil inserted between tiles was a problem.)
- "Cold wall" operation (T<100°C) did not appear to be a problem.
- Limited data on pumping (ducts open versus closed) were obtained.

Sandia National Laboratories

1454 140/RENI110583

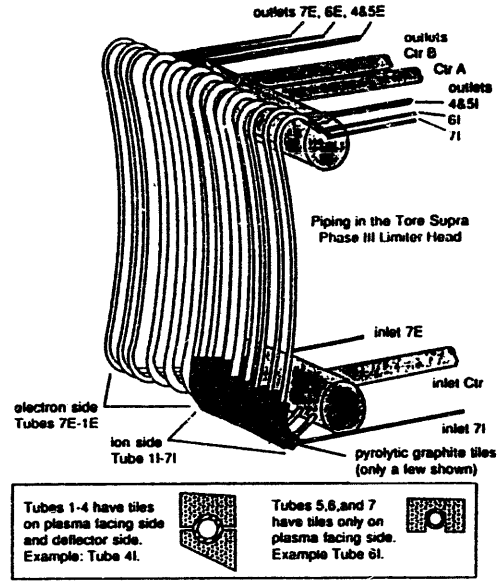

Figure 1. Piping in the Phase III Outboard Pump Limiter -- From left to right the tubes are numbered from 7I (leading edge tube) to 1I on the ion side and 1E to 7E (leading edge tube) on the electron side. The leading edge tubes, 7I and 7E, and Tubes 6I and 6E each have (separate) flowmeters. Tubes 4I and 5I are joined to a single manifold which has a flowmeter; the same is true for 4E and 5E. The center tubes flow into a single header which has two outlet pipes (Center A and Center B). Tubes 1-6 one each side plus the shelves (the heat sink and armor just outboard of the throat) are fed from a single header supplied by one large inlet pipe. The leading edge tubes (7I and 7E) are fed by a separate inlet line that splits into two lines before the diagnostic flange. (See also Figure A1 in Appendix A.)

Cross Section: Tore Supra Phase III Outboard Limiter Head

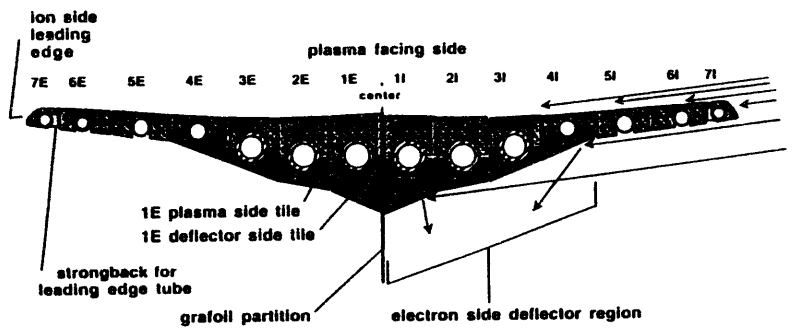

Thermocouples and Flow Meters on Phase III Limiter Module

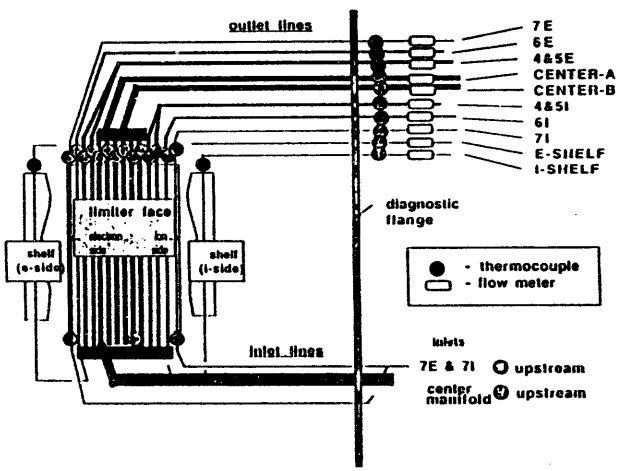

Sandia National Laboratories

Choc 11044 14/05/1993 18:08:10

CHOC TORE SUPRA (1.2)

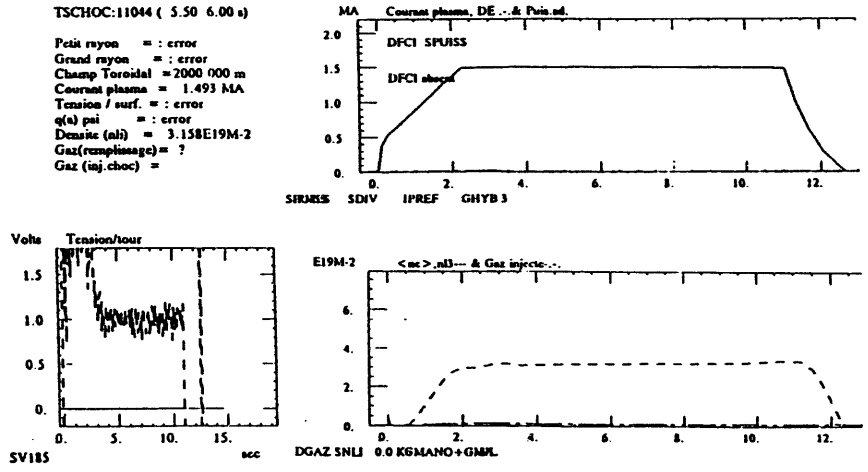

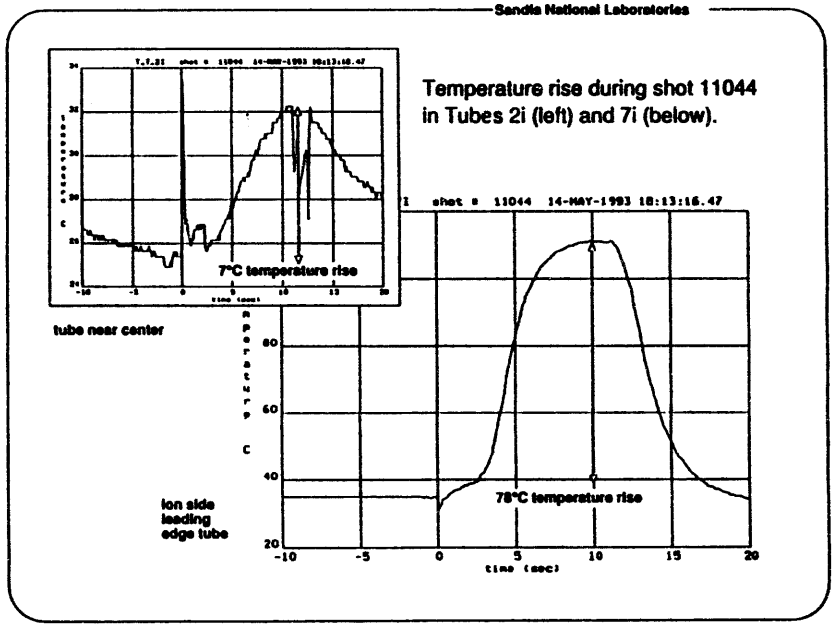

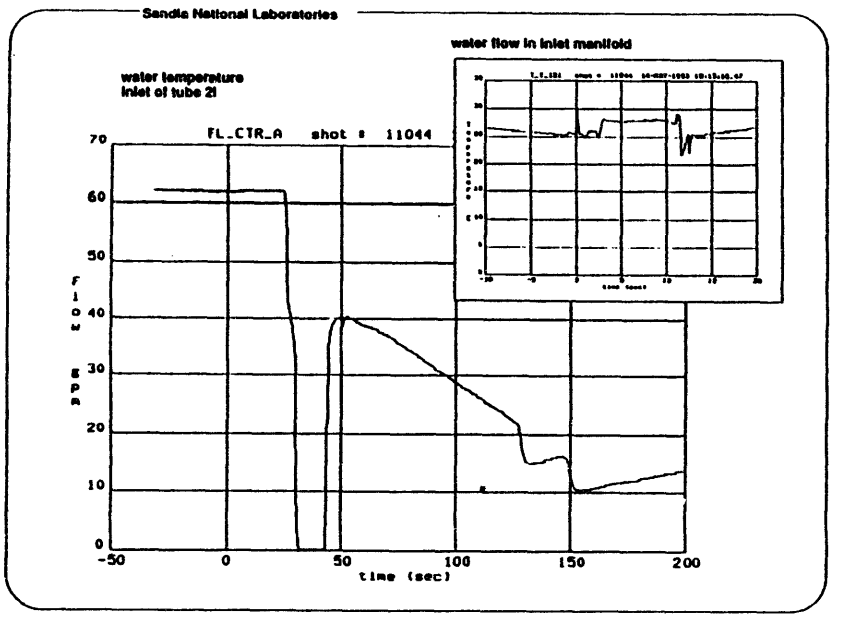
Sandia National Laboratories
water temperature
inlet of tube 2i
FL_CTR_A shot # 11044
water flow in inlet manifold
70
60
50
40
30
20
10
0
-50
0
50
100
150
200
time (sec)

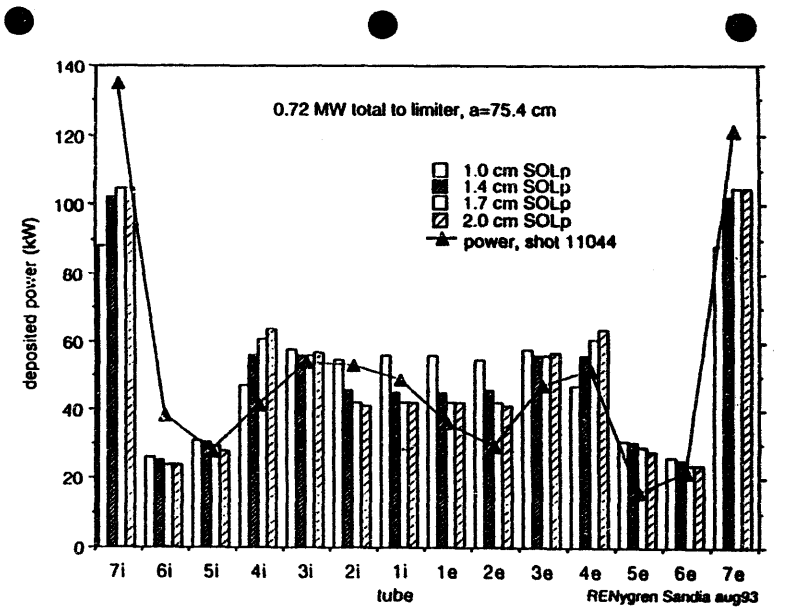
0.72 MW total to limiter, a=75.4 cm
1.0 cm SOLp
1.4 cm SOLp
1.7 cm SOLp
2.0 cm SOLp
power, shot 11044
deposited power (kW)
140
120
100
80
60
40
20
0
7i
6i
5i
4i
3i
2i
1i
1e
2e
3e
4e
5e
6e
7e
tube
RENygren Sandia aug93

Table 2. Comparison of Calorimetric Results from Shot 11044 with Results from a 3-D Model of Heat Load on the Limiter

tube	comparison meas:calc heat load	calc heat load kW	calc. front face kW	calc. back face kW	ratio back:total
7i	132%	102.2	99.5	2.7	3%
6i	151%	25.1	22.9	2.3	9%
5i	92%	30.5	26.1	4.4	14%
4i	73%	56.1	27.7	28.4	51%
3i	97%	56.0	43.5	12.5	22%
2i	115%	45.8	41.9	3.9	9%
1i	109%	44.8	40.7	4.1	9%
1e	81%	44.8	40.7	4.1	9%
2e	63%	45.8	41.9	3.9	9%
3e	84%	56.0	43.5	12.5	22%
4e	93%	56.1	27.7	28.4	51%
5e	51%	30.5	26.1	4.4	14%
6e	89%	25.1	22.9	2.3	9%
7e	118%	102.2	99.5	2.7	3%
total		**720.8**	**604.5**	**116.3**	**16%**

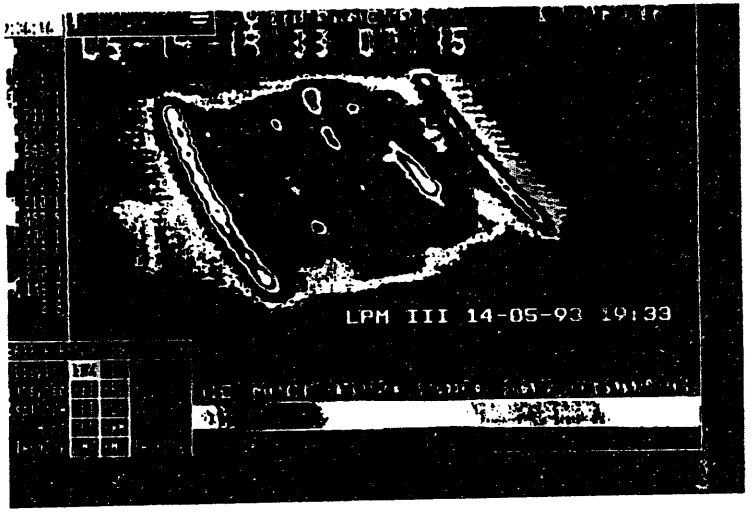

Surface temperature and peak heat flux on the inner wall of the tube are calculated with 2-D heat transfer model for tiles with flawed brazes.

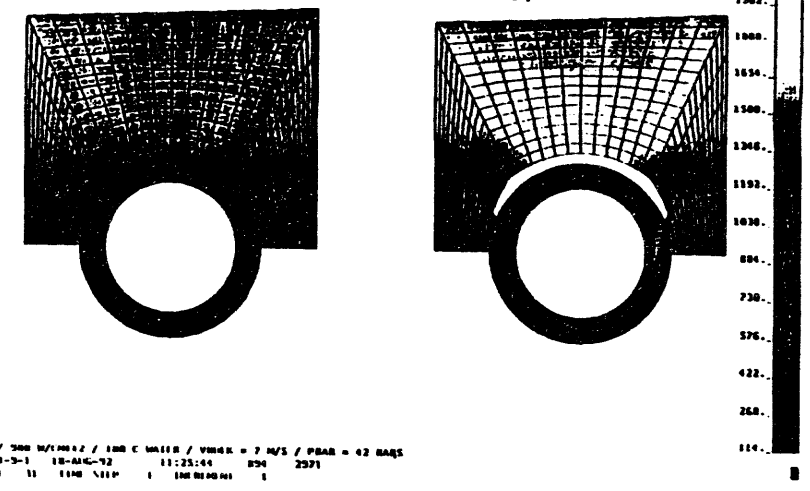

What can we deduce?

$Q_{incident} = \boxed{Q_{absorbed}} + Q_{radiated}$ — *measure: calorimetry*

$Q_{absorbed} \leftarrow \boxed{T_{surface}} = f\{ Q_{abs}, k_{PyG}, k_{Cu}, flaw \}$ — *measure: IR camera*

$Q_{absorbed} \leftarrow$ heat flux $= f\{ Q_{abs}, \theta, k_{PyG}, k_{Cu}, flaw \}$ (into water)

peak heat flux $= f\{ Q_{abs}, flaw; k_{PyG}, k_{Cu} \}$

correlations:
- $T_0 : Q_{abs}$
- flaw : T_1, T_0, Q_{abs}
- peak heat flux : Q_{abs}, flaw
- peak heat flux : $T_{surface}$, flaw

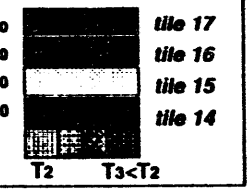

Limiter Monitoring Program

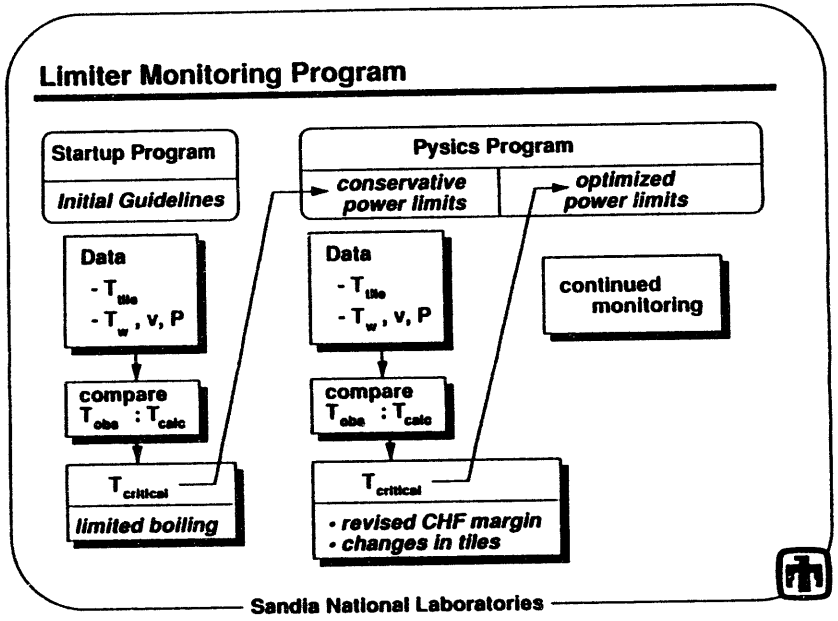

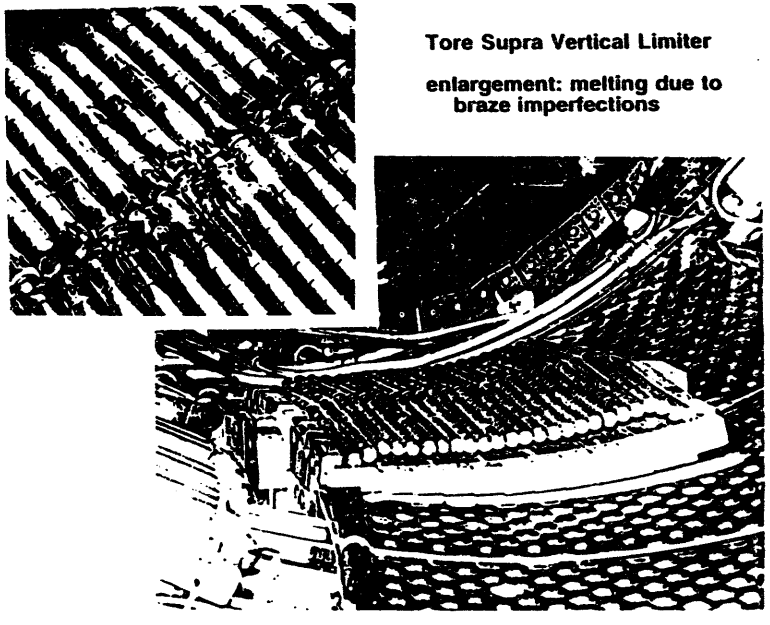

Tore Supra Vertical Limiter

enlargement: melting due to braze imperfections

Brazing: Very Tight Tolerances

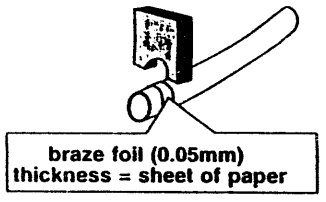

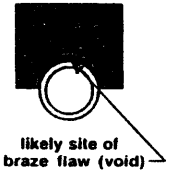

- tolerances: ± 0.02 mm (0.001 in) in key locations
- mating of curved surfaces is difficult
- CTE_{Cu} /CTE_{PG} = 20:1
  brazing difficult; residual stresses high

Sandia National Laboratories

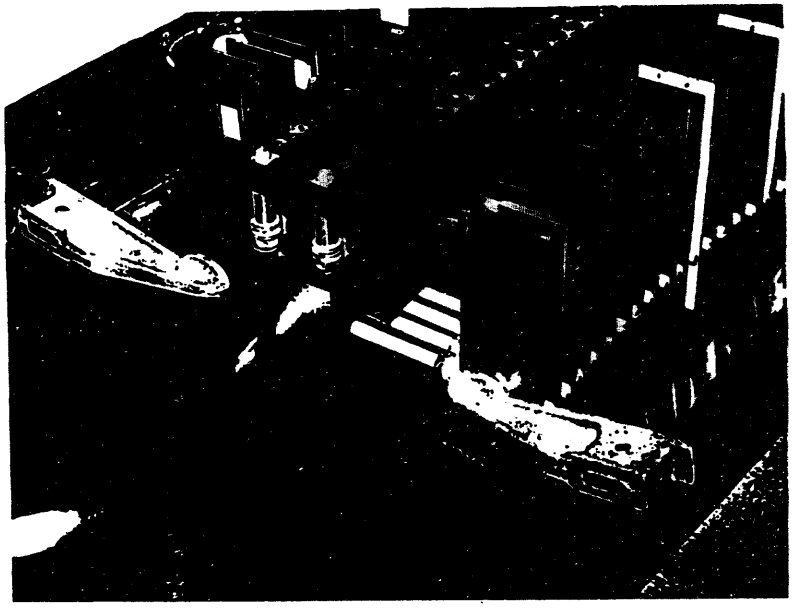

Transient heating of tiles in hot water test used to evaluate braze flaws

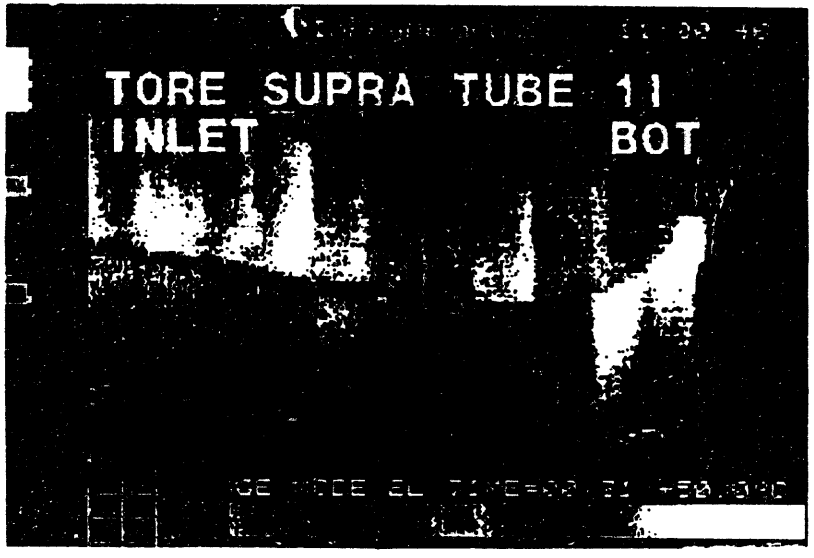

Thermal-hydraulic Analyses Supporting the

Tore Supra Phase III Limiter Monitoring Program

Richard Nygren 6531

Joel Miller 6522

(CEN, May 1993)
Specialists' Workshop on
High Heat Flux Component Cooling
September 22-24, 1993 CEN, Cadarache

Sandia National Laboratories

Modeling of Power Deposition in Tore Supra

specify surface heat load on each tile on the limiter

3-D model using ABAQUS/PATRAN

- **3-D field configuration including ripple**
- **power deposited per SOL model, i.e. exp(-x/λ), onto specified surfaces**
- **total power or parallel heat flux at last closed flux surface can be specified**

determine peak heat flux at tube/water interface (& temperatures)

2-D model using ABAQUS/PATRAN

- **tile/tube configurations**
- **flaws: 0, 27, 53, 76, 92% center; 12, 32, 50, 68% side**
- **tubes 1-6, 60 or 69°C, 7 m/s, 4.2 MPa, 600-1400 W/cm2**
- **tube 7, 93°C, 10 m/s, 4.2 MPA**

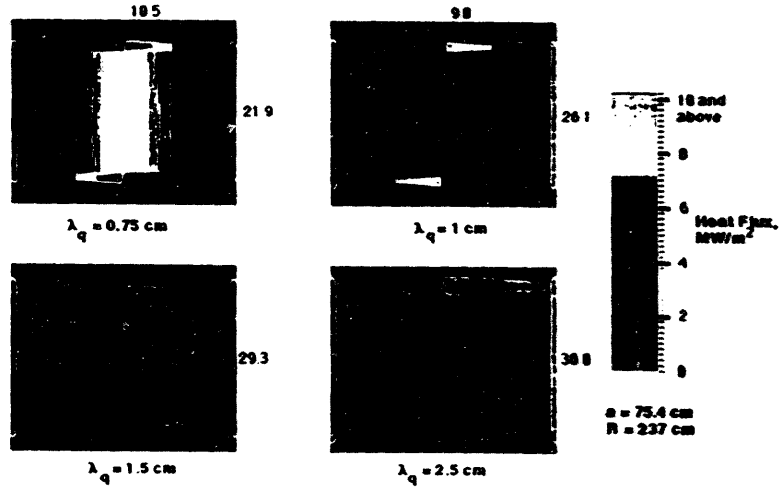

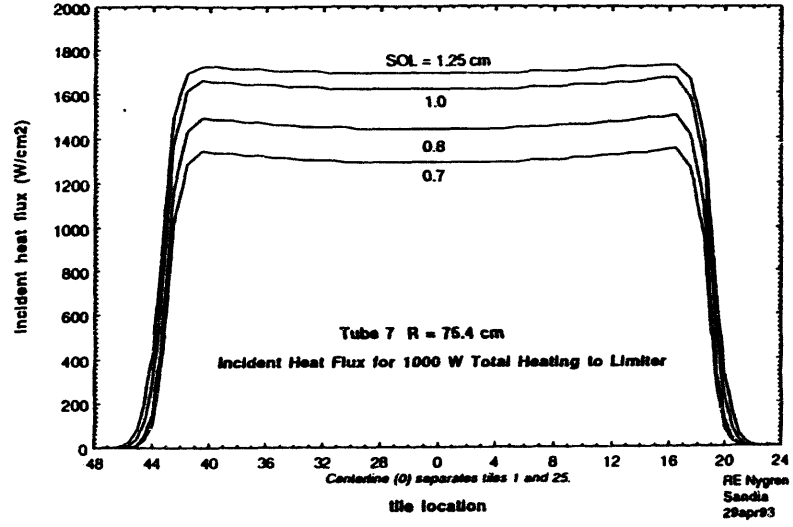
SOL = 1.25 cm
1.0
0.8
0.7
Tube 7 R = 75.4 cm
Incident Heat Flux for 1000 W Total Heating to Limiter
Incident heat flux (W/cm2)
Centerline (0) separates tiles 1 and 25.
tile location
RE Nygren
Sandia
29apr93

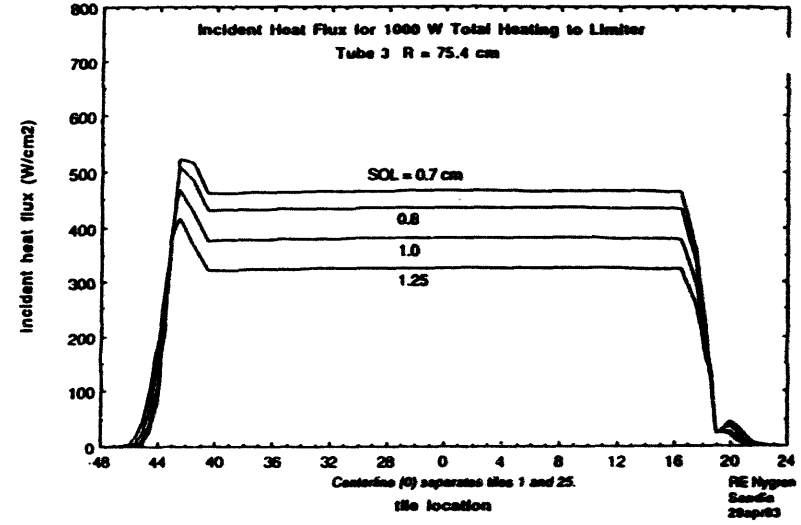
Incident Heat Flux for 1000 W Total Heating to Limiter
Tube 3 R = 75.4 cm
SOL = 0.7 cm
0.8
1.0
1.25
Incident heat flux (W/cm2)
Centerline (0) separates tiles 1 and 25.
tile location
RE Nygren
Sandia
29apr93

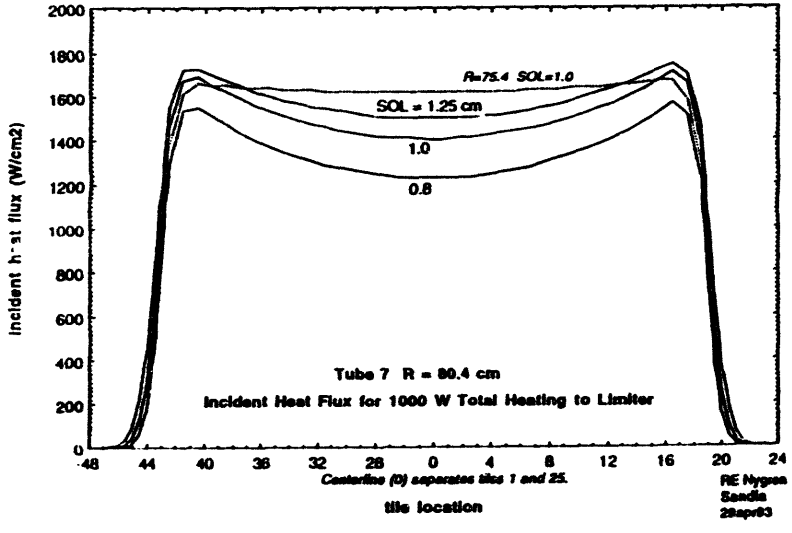
R=75.4 SOL=1.0
SOL = 1.25 cm
1.0
0.8
Tube 7 R = 80.4 cm
Incident Heat Flux for 1000 W Total Heating to Limiter
Incident heat flux (W/cm2)
Centerline (0) separates tiles 1 and 25.
tile location
RE Nygren
Sandia
29apr93

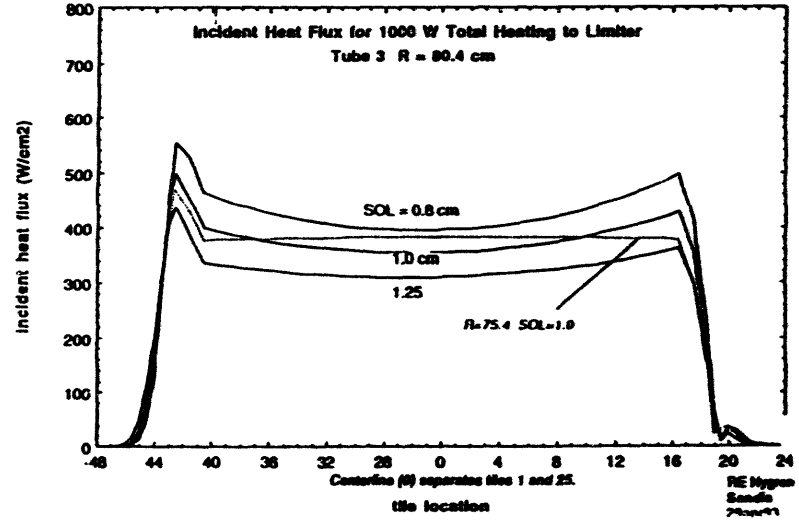
Incident Heat Flux for 1000 W Total Heating to Limiter
Tube 3 R = 80.4 cm
SOL = 0.8 cm
1.0 cm
1.25
R=75.4 SOL=1.0
Incident heat flux (W/cm2)
Centerline (0) separates tiles 1 and 25.
tile location
RE Nygren
Sandia

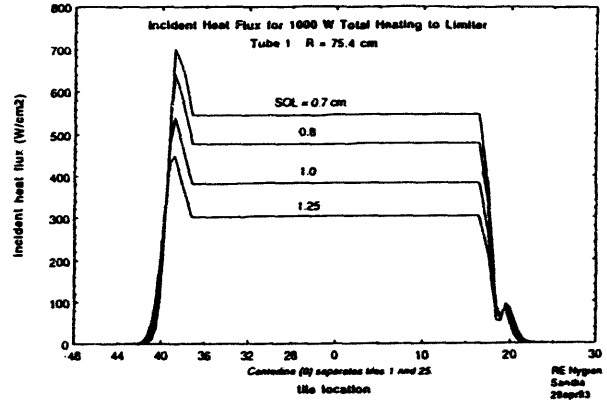
Incident Heat Flux for 1000 W Total Heating to Limiter
Tube 1 R = 75.4 cm
SOL = 0.7 cm
0.8
1.0
1.25
Incident heat flux (W/cm2)
tile location
RE Nygren
Sandia
29apr83

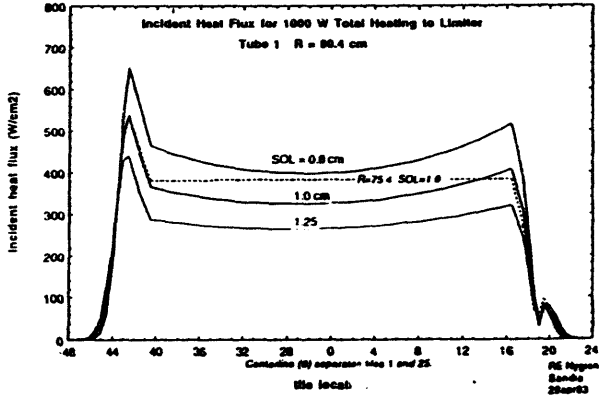
Incident Heat Flux for 1000 W Total Heating to Limiter
Tube 1 R = 88.4 cm
SOL = 0.8 cm
1.0 cm
1.25
Incident heat flux (W/cm2)
RE Nygren
Sandia
29apr83

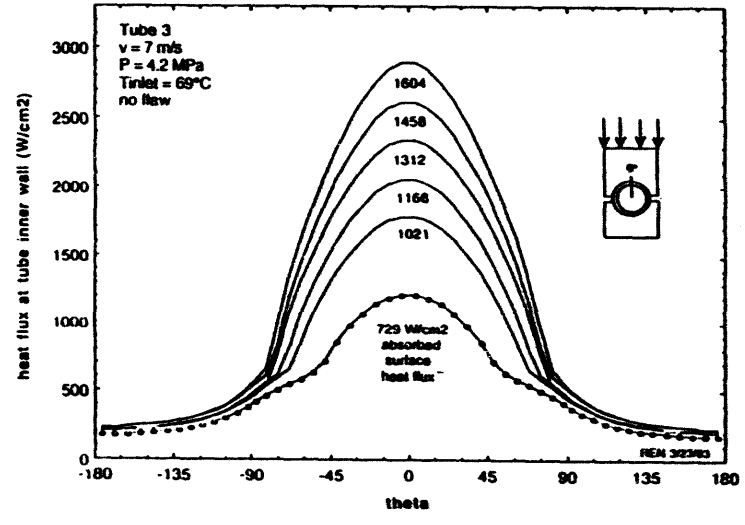
Tube 3
v = 7 m/s
P = 4.2 MPa
Tinlet = 69°C
no flaw
1604
1458
1312
1166
1021
729 W/cm2
absorbed
surface
heat flux
heat flux at tube inner wall (W/cm2)
theta
REN 3/23/83

heat flux (W/cm2)
Tube 3
v = 7 m/s
P = 4.2 MPa
T bulk = 60°C
Qi absorbed = 1013 W/cm2
no flaw
27%
92% center flaw
theta
REN rev4/2003

heat flux (W/cm2)
Tube 7
P = 4.2 MPa
v = 10 m/s
no flaw
incoming plasma
angle (° from toroidal arc a leading edge)

Tube 7
P = 4.2 MPa
v = 10 m/s
no flaw
size of centered flaw
120° (67%)
90° (50%)
60° (33%)
30° (16%)
no flaw
incoming plasma
REN
Sandia
3may93
heat flux (W/cm2)
angle (degrees)
6000
5000
4000
3000
2000
1000
0
-180
-150
-120
-90
-60
-30
0
30
60
90
120
150
180

Tube 7
P = 4.2
v = 10 m/n
Tbulk = 93°C
RE Nygren
Sandia
4may93
peak heat flux
maximum surface temperature (°C)
flaw size (%)
6000
5500
5000
4500
4000
3500
3000
2500
1500
1400
1300
1200
1100
1000
900
800
700
0
20
40
60
80
100

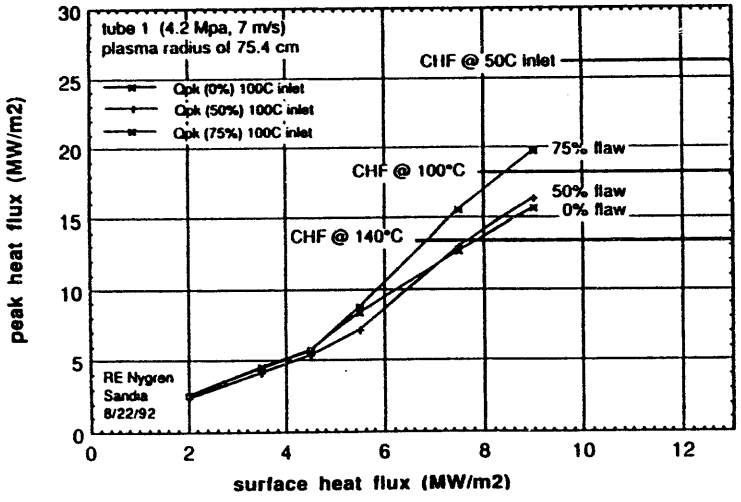
tube 1 (4.2 Mpa, 7 m/s)
plasma radius of 75.4 cm
Qpk (0%) 100C inlet
Qpk (50%) 100C inlet
Qpk (75%) 100C inlet
CHF @ 50C inlet
CHF @ 100°C
CHF @ 140°C
75% flaw
50% flaw
0% flaw
RE Nygren
Sandia
8/22/92
peak heat flux (MW/m2)
surface heat flux (MW/m2)
0
5
10
15
20
25
30
0
2
4
6
8
10
12

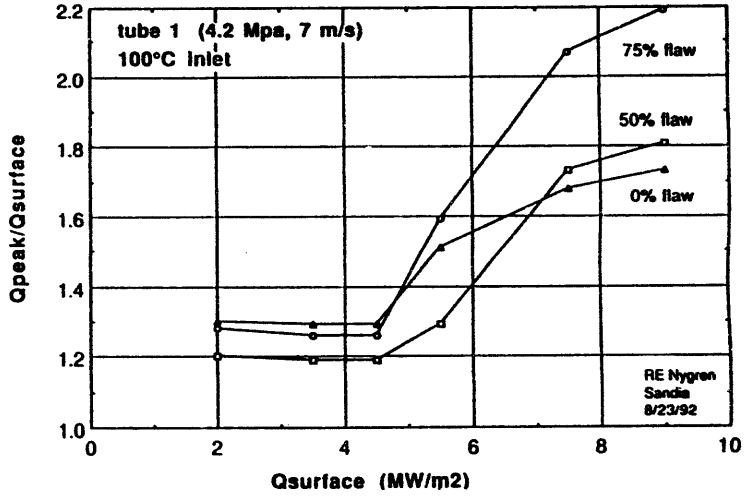
tube 1 (4.2 Mpa, 7 m/s)
100°C Inlet
75% flaw
50% flaw
0% flaw
RE Nygren
Sandia
8/23/92
Qpeak/Qsurface
Qsurface (MW/m2)
1.0
1.2
1.4
1.6
1.8
2.0
2.2
0
2
4
6
8
10

Personal Comments Regarding Actively Cooled PFCs

On Tore Supra's Phase III Limiters:

a) the most advanced working HHF technology in fusion and wonderful engineering accomplishments

b) technology with difficult quality control and supported by an an inadequate engineering data base

c) already out of date but, together with JET hypervapotron technology, our only base of practical experience

On future development of PFCs:

1) CFC's can provide structure as well as armor; this can radically affect the design of large area carbon PFCs.

2) Joining and quality control will probably limit the reliability and performance of many duplex structures (e.g., C/Cu and Be/Cu). Designers should address these issues at the outset.

3) Some basic engineering tools (e.g., heat transfer correlations) need further development to be adequate for the demands of ITER and the fusion program in general.

Sandia National Laboratories

U.S. DESIGN STUDIES FOR ITER PFCs

J. W. DAVIS
D. E. DRIEMEYER
MCDONNELL DOUGLAS AEROSPACE

24 JANUARY 1994

The U.S. ITER PFC Design Studies Are a Team Effort

Industry	Laboratories	Universities
McDonnell Douglas Aerospace	Sandia National Laboratories	Univ. of Illinois – Champaign-Urbana
Rocketdyne	Argonne National Laboratory	Univ. of California – Los Angeles
Westinghouse	Oak Ridge National Laboratory	
General Atomics	Los Alamos National Laboratory	
	Princeton Plasma Physics Laboratory	
	Idaho National Engineering Laboratory	

24 Jan 94

Objectives

- Identify Alternate HHF Target Designs for Cold-Neutral-Gas Divertor
- Identify Material Constraints and Limitations for a Cold-Neutral-Gas Divertor
- Identify Critical R&D Needs for Cold-Neutral-Gas Divertor Approach
- Assemble Material Properties Database for Candidate Target Materials
- Perform Initial Materials Compatibility and Safety Assessments

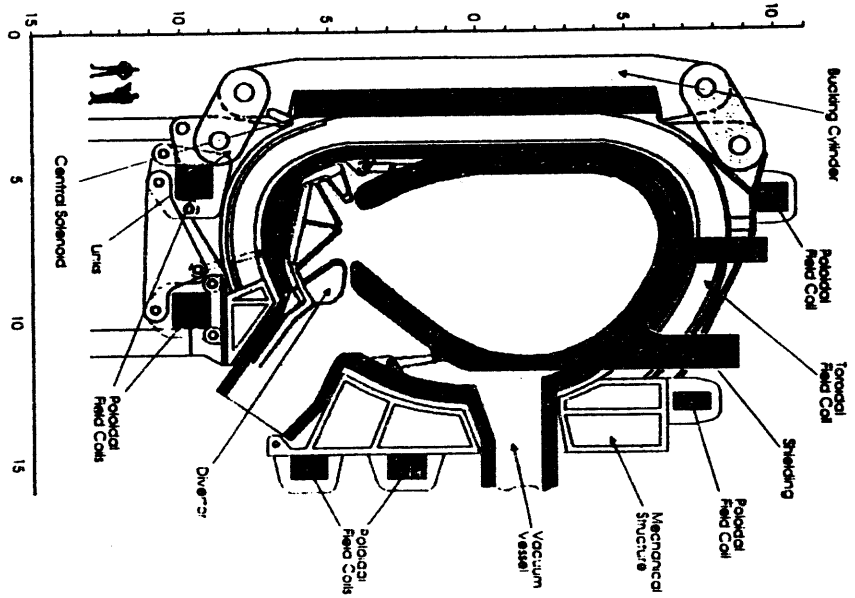

24 Jan 94

Cold Gas Target Divertor Overview

Typical Electron Temperature Contours (eV)

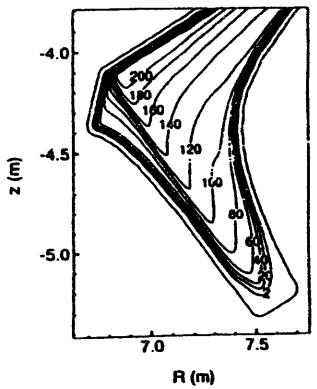

Physics Concept

- Exhaust Edge-Plasma Power into a High Density Cold-Neutral Target
- Distribute Power to Divertor Structure by Radiation (Impurities and Hydrogen) and Charge-Exchange Processes (Peak Heat Flux 5 MW/m^2)
- Use Transparent Sidewall Structure to Enable Recirculation of Neutrals Along Divertor Channel and Control Neutral Pressure (~1 mTorr)

24 Jan 94

System/Component Requirements

- Materials Facing Plasma Must Have Low Atomic Number to Minimize Plasma Contamination (Beryllium and Carbon Are Candidates)
- Plasma Facing Materials Must Have High Thermal Conductivity (≥ That of Copper) to Withstand 5-15 MW/m^2 (Heat Fluxes Approaching Those of Reentry Vehicles)
- Structural Materials (V or Cu) Must be Compatible with Coolants (Helium, Liquid Metals, or Water)
- Components Must Operate Several Hours with Surface Temperatures of ~1000°C Carbon or ~500°C Beryllium
- Components Must Have High Reliability (Maintenance is Time Consuming and Expensive)

24 Jan 94

Assumptions for Divertor Materials Trade Studies

Heat Flux	5.0 MW/m^2
Armor Material	Beryllium
Heat Sink Material	Dispersion Strengthened Copper, Niobium Alloy Cb-753, or Vanadium Alloy V-5Cr-5Ti
Armor Material Thickness	2–10 mm
Heat Sink Material Thickness	2 mm
Convective Heat Transfer Coefficient	50 kW/m^2-K
Coolant Operation Temperature	50°-350°C
Thermal Contact Resistance Between Armor and Heat Sink	0 (Bonded/Brazed)
Upper Limit on Beryllium Temperature	500–700°C

Thermal-Mechanical Evaluation Parameters

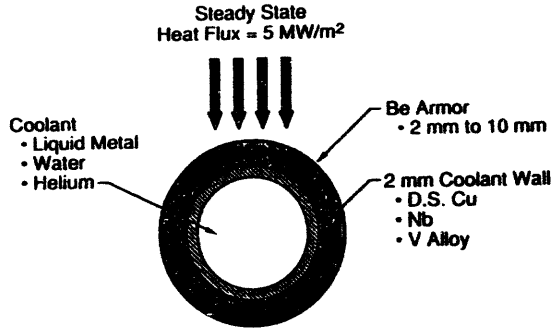

Be Is a Viable Armor Material at Lower Heat Fluxes

- Coolant Temperature = 150°C
- Convective Heat Transfer Coefficient = 50 kW/m²-K
- 10 mm Thick Armor
- 2 mm Thick Copper Structure

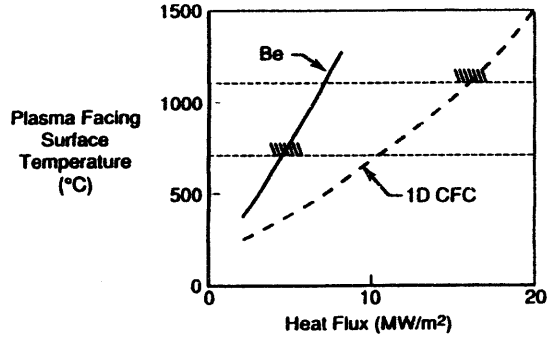

Thermal Performance Limits for Be With Water or Liquid Metal Coolants

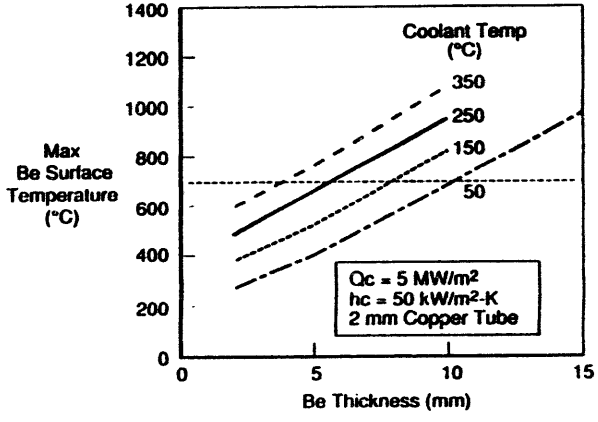

Thermal Performance Limits for Divertor Depend on Tube Material Selection

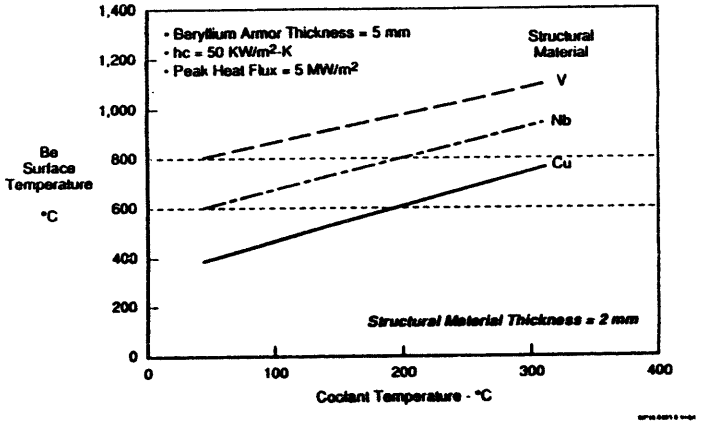

Duplex Structure Design Concepts

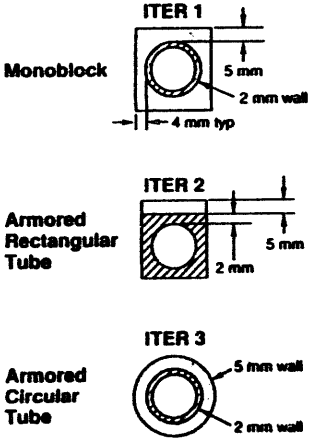

Beryllium Surface Temperatures
(Steady State, 5 MW/m² Operating Condition)

Model	Temperature
ITER 1	463°C
ITER 2	358°C
ITER 3	391°C

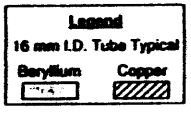

Thermal Stress Summary for Duplex Structure Concepts

Configuration	Ref. Temp. (°C)	Conditions	Max Von Mises Stress (MPa)	
			Beryllium Armor	D.S. Copper Structure
Armored Rectangular Tube	800 800	Braze Cooldown RT-ST State	333 93	124 154
Monoblock	800 800	Braze Cooldown RT-ST State	329 397	462 436

2 X Yield Strength

~350 for Beryllium
~600 for D.S. Copper
~800 for Niobium (753)

Conclusions

- Cold Gas Divertor Mode Allows Use of Beryllium Armor and Helium or Liquid Metal Coolants
- Self-Supported Beryllium Tubes Have Large Thermal Stresses/Deflections
- Duplex/Segmented Beryllium Armor Design Presents Most Attractive Divertor Design Option
  - Beryllium Armor Thickness ≤ 5 mm
  - Copper and Niobium Alloy Heat Sink Materials Offer Most Design Flexibility

FY'94 Activities

ITER Water-Cooled Divertor Configuration

Divertor Cassette Configuration
(15° Sector, 5 Segments)

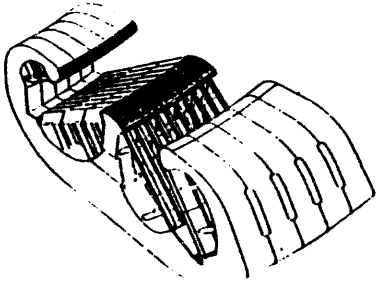

Cross Section Through Divertor
Showing Key Design Elements

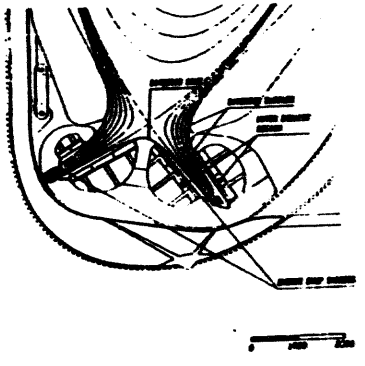

24 Jun 94

Divertor Channel Sidewall Design Concepts

Baseline Configuration

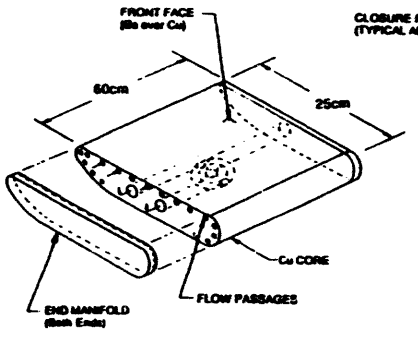

Ribbed Channel Alternative

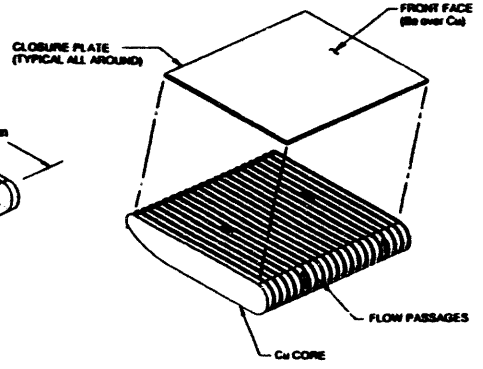

24 Jun 94

Sacrificial Dump Plate Concept

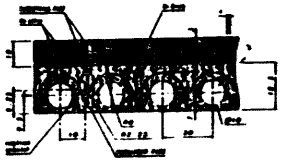

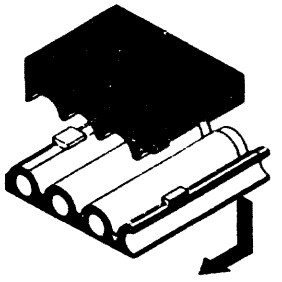

- Attached Using Compliant Material That:
  - Maintains Good Thermal and Electrical Contact with Cooled Sub-Structure
  - Has Low Melting Temperature (250-300°C) to Promote Remote Maintenance
  - Has Sufficient Thickness to Compensate for Fabrication and Assembly Tolerances
  - Provides Compliancy to Accommodate Differential Thermal Expansion

- Compliant Layer Development Issues:
  - Capability to Fill Required Gap Thickness
  - Stability Over Repeated Thermal/Mechanical Cycling Including Off-Normal Events
  - Degradation of Joint Quality Following Successive Detach/Reattach Cycles (10-15)
  - Effect of ITER Radiation Environments

Session VI

Plasma Facing Component Materials and Irradiation Damage

US-Japan Workshop on PMI-HHF
January 24-27, 1994
San Diego, CA

RADIATION DAMAGE OF PLASMA-FACING MATERIALS

T. MUROGA

Research Institute for Applied Mechanics
Kyushu University
Japan

OUTLINE

1. Neutron radiation effects on Cu and Mo-Re alloys. Solid transmutant effects - a new issue

2. Radiation effects of Cu-C/C joint

3. Low energy hydrogen ion irradiation on W

Major contribution
1. K. Abe, M. Satou (Tohoku Univ) F.A. Garner (PNL)
2. H. Watanabe, T. Sato, N.Yoshida (Kyushu Univ.) Akiba (JAERI)
3. R. Sakamoto, N. Yoshida (Kyushu Univ.)

1. Neutron radiation effects on Cu and Mo-Re alloys. Solid transmutant effects - a new issue

(1) Generation of nickel and zinc in copper

Recent transmutation calculation
Thermal conductivity degradation
Measurement of Ni in irradiated Cu
Impact on void swelling resistance

NEUTRON RADIATION EFFECTS ON METALLIC PFM

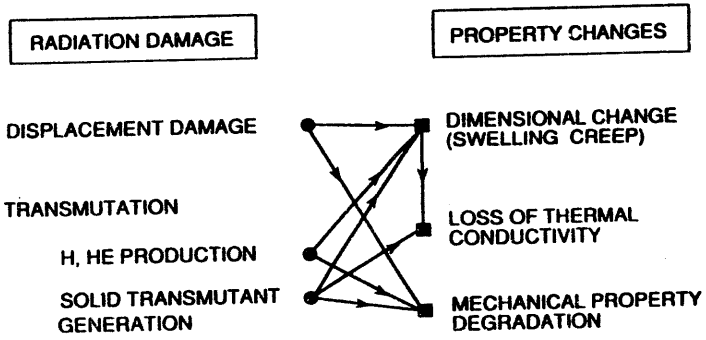

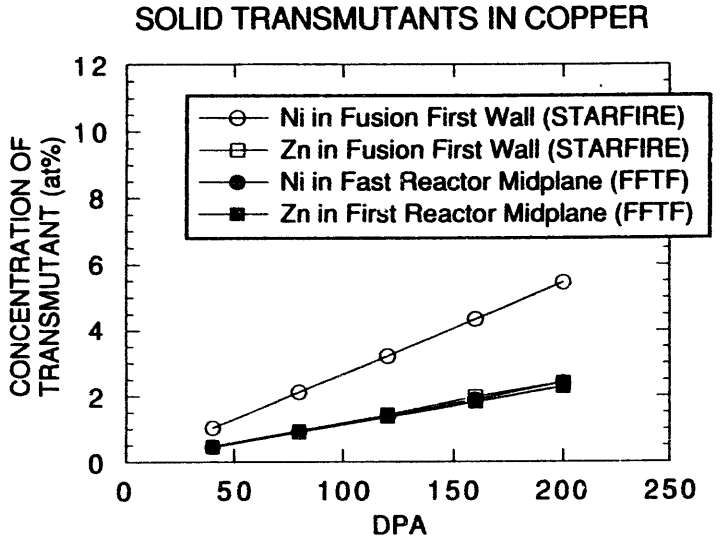

(Greenwood, 1993)

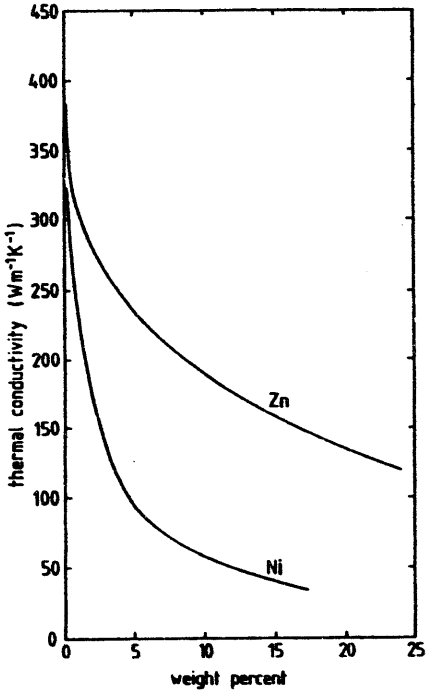

Thermal conductivity of Cu-Ni and Cu-Zn
(Butterworth 1985)

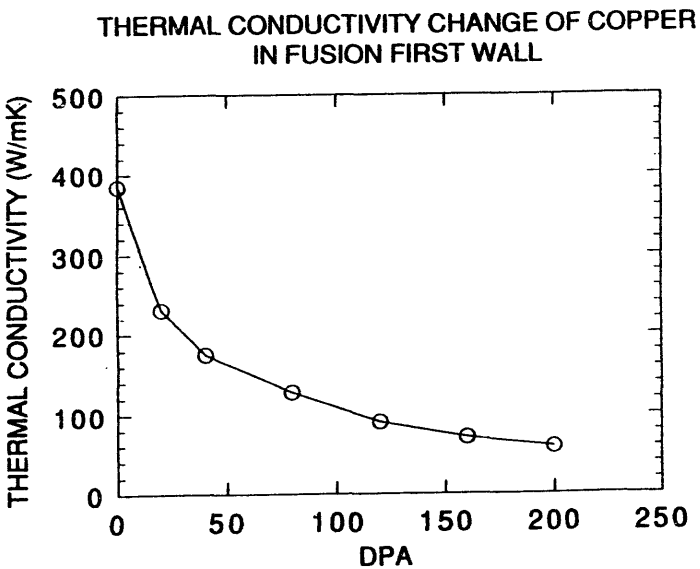
THERMAL CONDUCTIVITY CHANGE OF COPPER
IN FUSION FIRST WALL
THERMAL CONDUCTIVITY (W/mK)
500
400
300
200
100
0
0
50
100
150
200
250
DPA

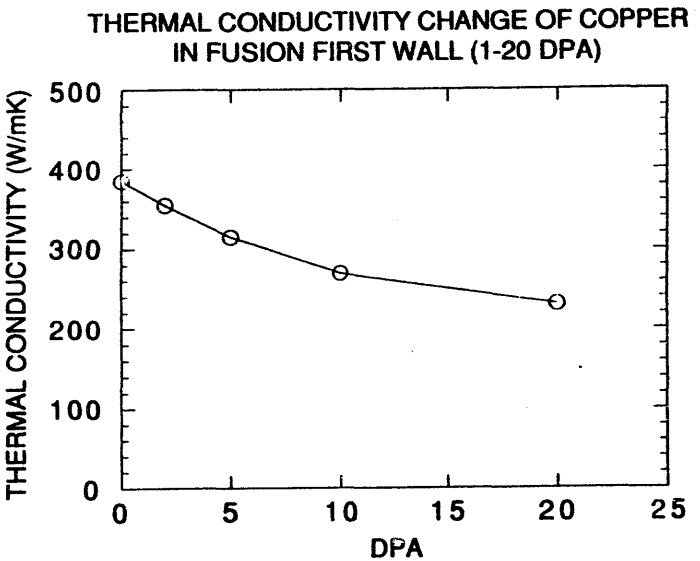
THERMAL CONDUCTIVITY CHANGE OF COPPER
IN FUSION FIRST WALL (1-20 DPA)
THERMAL CONDUCTIVITY (W/mK)
500
400
300
200
100
0
0
5
10
15
20
25
DPA

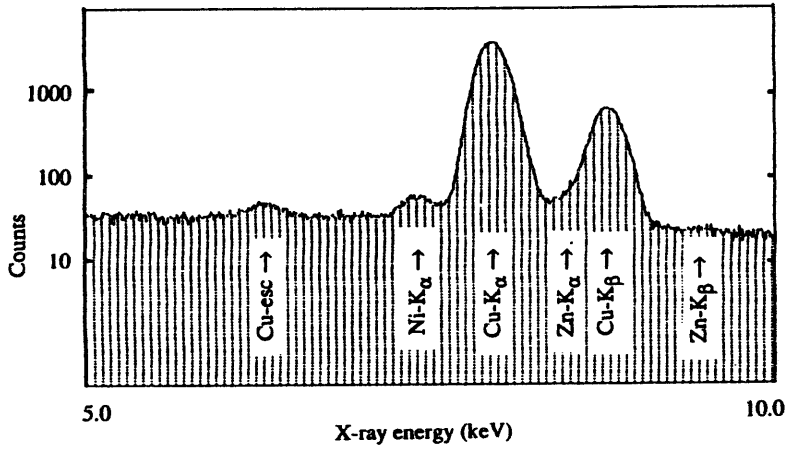

X-ray spectrum extracted from Cu irradiated with fast neutrons (FFTF) at 696 K to 95.4 dpa

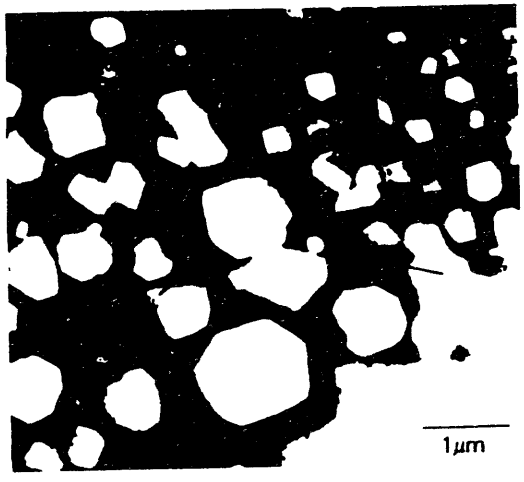

FFTF/MOTA 696K 95.4dpa

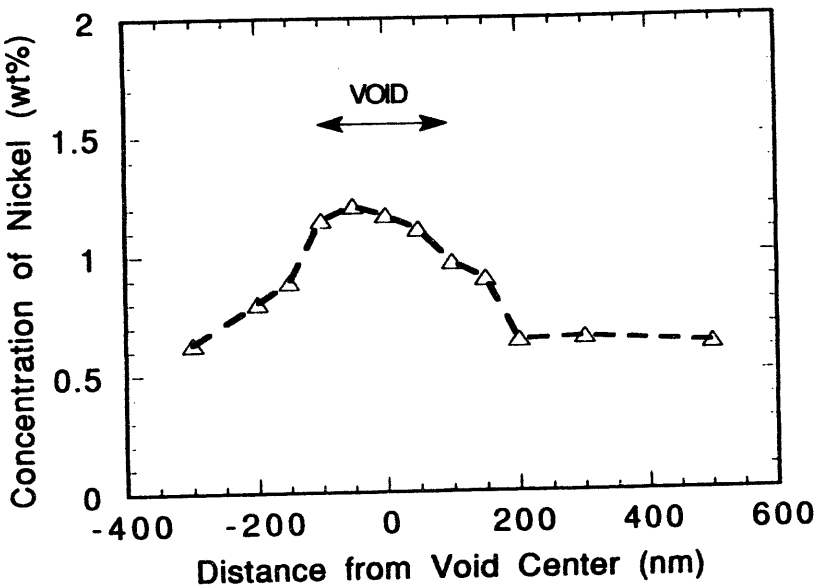

Nickel concentration profile near a void in Cu irradiated with fast neutrons at 696K to 95.4 dpa

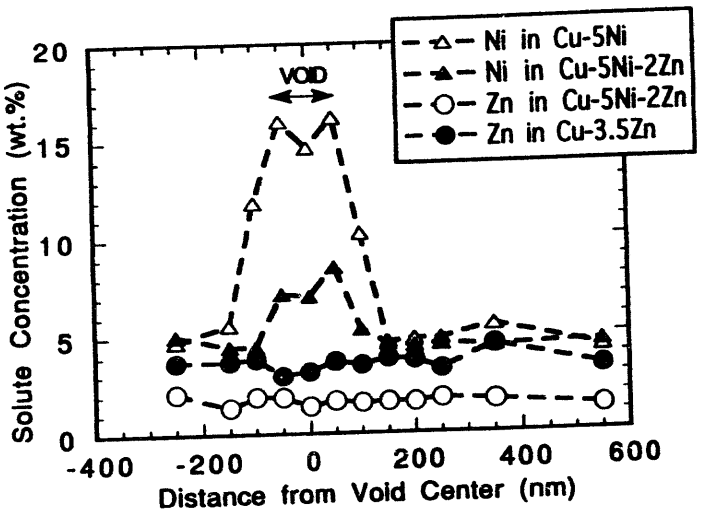

Nickel concentration profile near a void in Cu-Ni, Cu-Ni-Zn and Cu-Zn alloys irradiated with fast neutrons at 647 K to 6.3 dpa

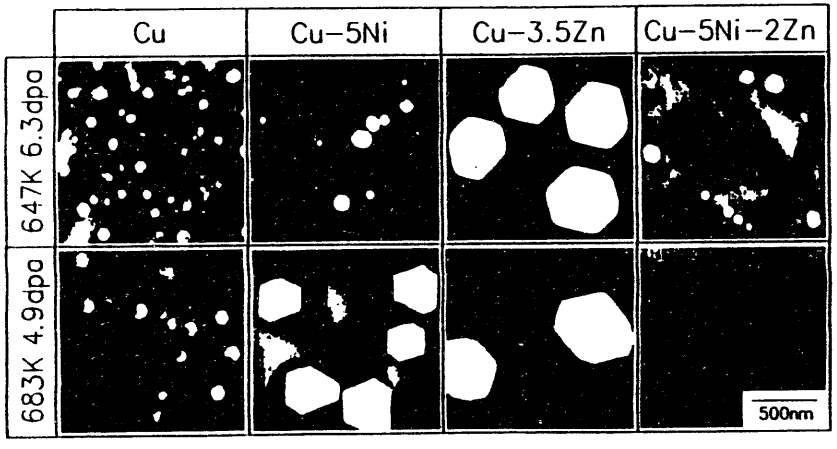

FFTF/MOTA Below Core Void Images

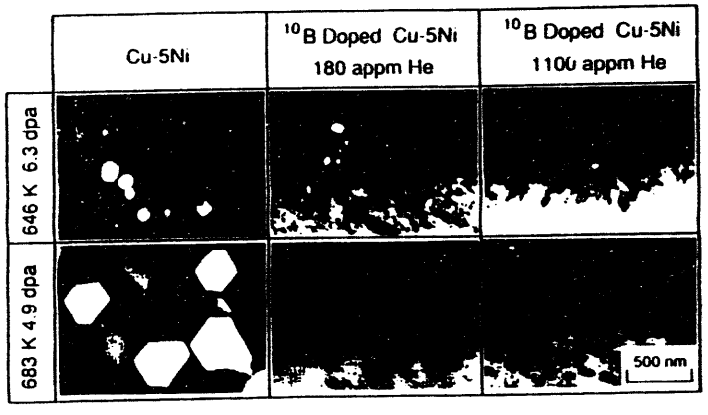

FFTF/MOTA Cycle 12 Below Core

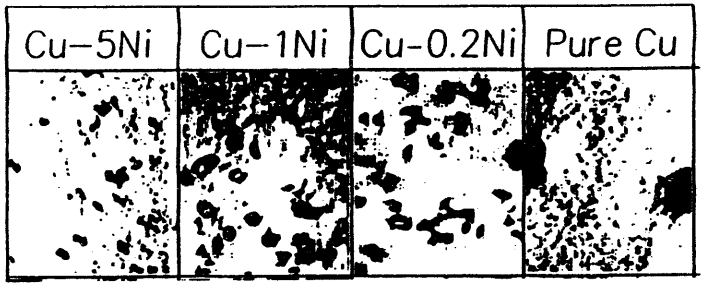

Evolution of loops in Pure Cu and three Cu–Ni alloys
573K, 1.0 MeV e^-
Foil Thickness ~ 530 nm

Summary - 1.1 Solid transmutant effects in Cu

Generation of Ni and Zn in Copper during neutron irradiation reduces its thermal conductivity.

Transmutant nickel interacts with radiation-induced defects affecting radiation response of copper. Void swelling can be strongly enhanced by nickel generation.

Synergistic effect of nickel and helium generation should be explored

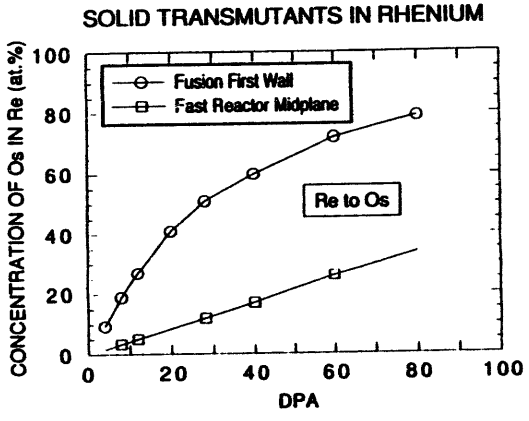

(Greenwood, 1993)

(2) Re transmutation into Os in Mo-Re alloys

Recent transmutation calculation
Os-related precipitation during irradiation
Hardness change by precipitation
Impact on alloy design/selection

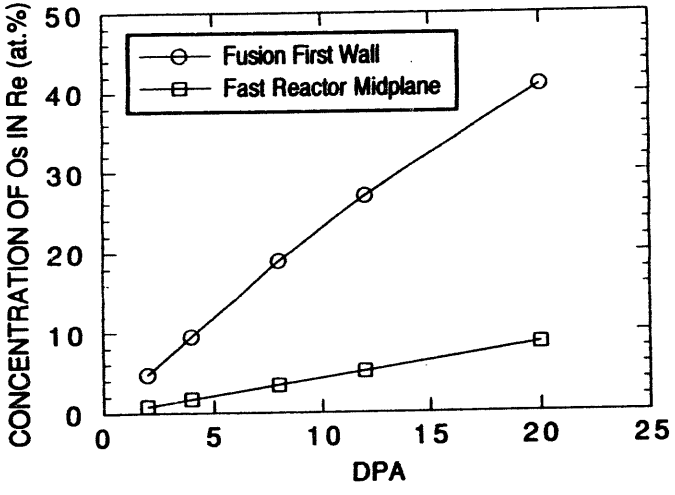

(Greenwood, 1993)

Mo-41Re, 1073 K, 14 dpa, FFTF/MOTA
(Abe and Satou, 1993)

Mo-5Re, 1073 K, 14 dpa, FFTF/MOTA
(Abe and Satou, 1993)

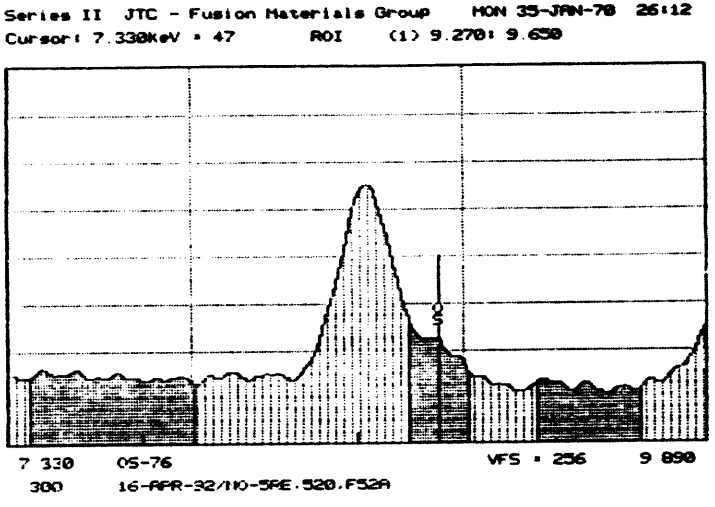

X-ray spectrum extracted from Mo-5Re alloy irradiated with fast neutrons at 792 K and 23 dpa (Abe and Satou,1993)

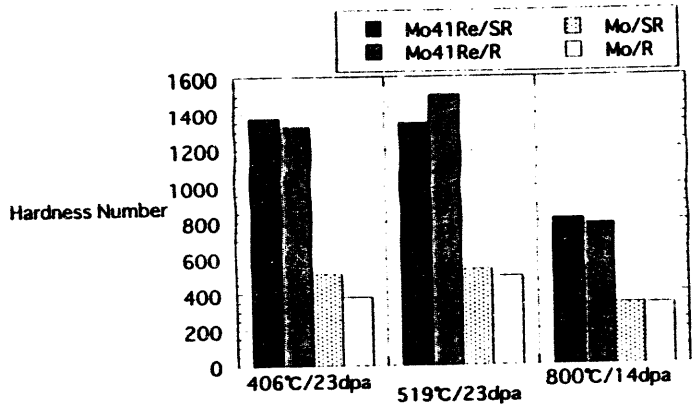

Vickers hardness of neutron irradiated Mo and Mo-41Re alloy

(Abe and Satou,1993)

Summary - 1.2 Solid transmutant effects in Mo-Re

Re transmutation into Os is very quick during fusion neutron irradiation.

The Os generation results in copious precipitation and relating hardening in Mo-Re.

In Mo-Re system, Re content should be low if it is to be used in neutron irradiation environment.

2. Radiation effects of Cu-C/C joint

Material:	Cu	OFHC
	C/C	CX2002U
	Filler	Ag-38Cu-1.8Ti
		supplied by JAERI

Experiment:

Microstructure of interfaces

Microstructural change by ion irradiation

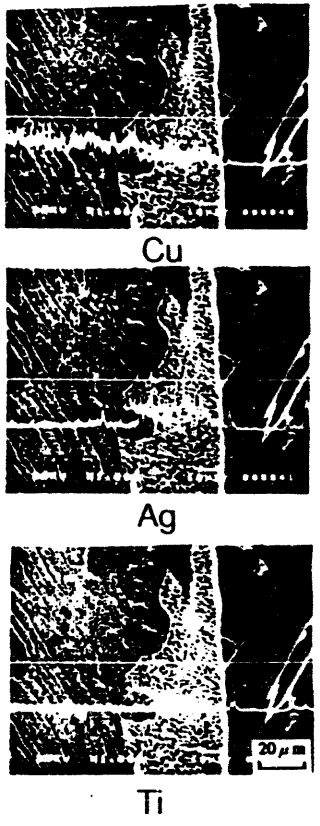

TEM MICROSTRUCTURE OF A C/C-Cu JOINT

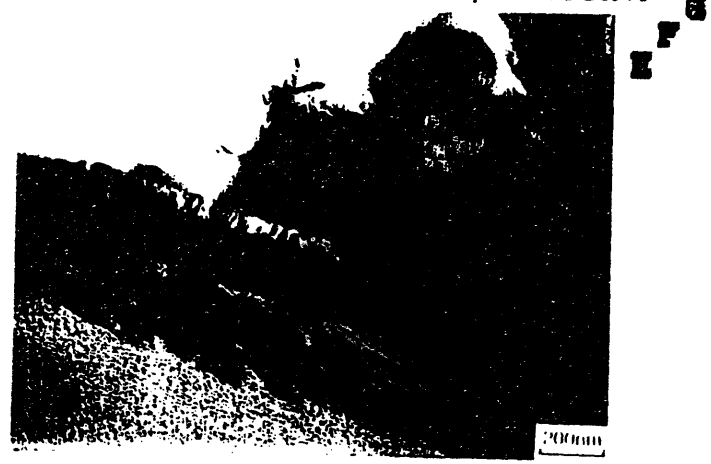

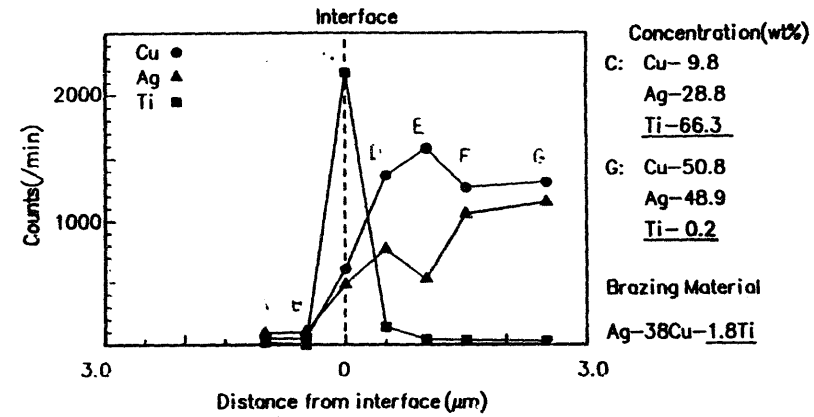

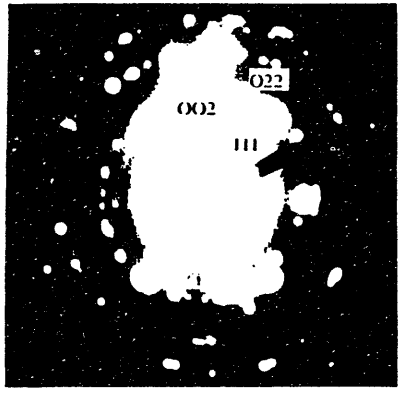

ELECTRON DIFFRACTION PATERN OF
Ti-LAYER IN C/C-Cu JOINT

TEM MICROSTRUCTURE OF A C/C-Cu JOINT

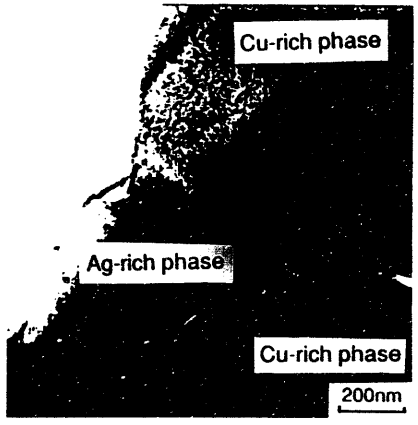

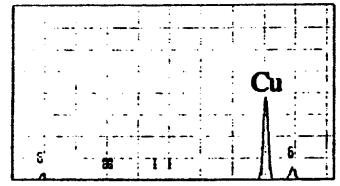

Cu-rich phase

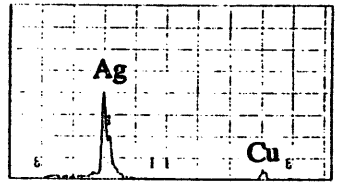

Ag-rich phase

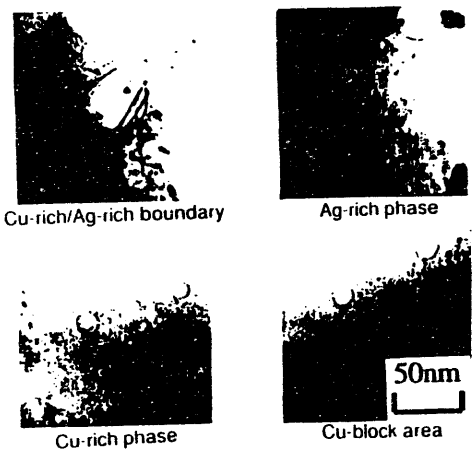

VOID CONTRAST IN DIFFERENT PARTS OF A C/C-Cu JOINT IRRADIATED WITH 4MeV HEAVY ION TO 10dpa AT 573K

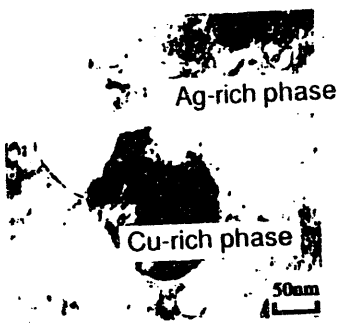

TEM MICROSTRUCTURE OF A C/C-Cu JOINT UNDER 4MeV HEAVY ION IRRADIATION TO 10dpa AT 473K

Vois swelling of Cu-block, Cu-rich phase in the filler and Ag-rich phase in the filler after irradiation to 10 dpa

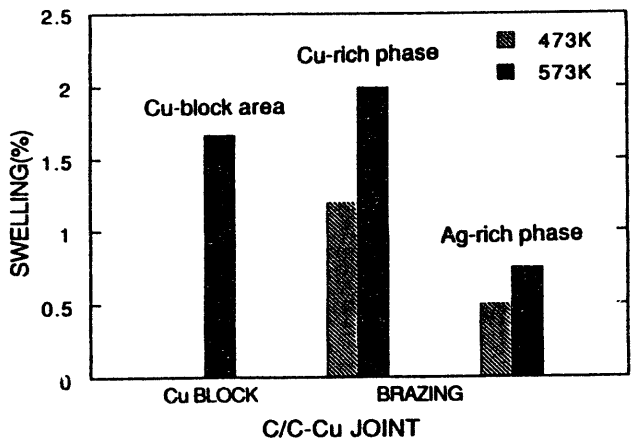

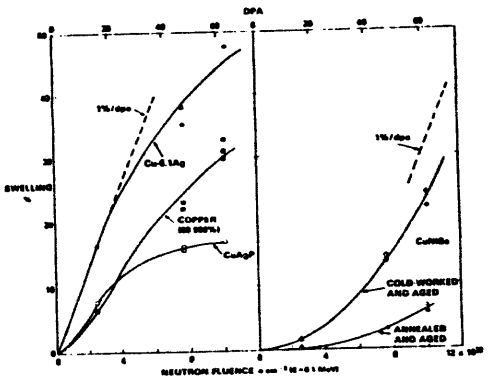

Swelling behavior of zone-refined copper and copper alloys which exhibit a moderate to high amount of swelling.

(Brager, 1986)

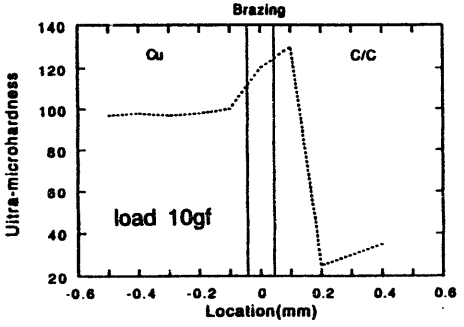

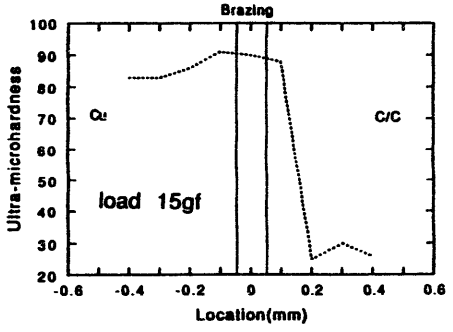

Ultra-microhardness of Cu-C/C interface

Summary - 2 Radiation effects of Cu-C/C joint

TiC layer was observed between C/C and filler. This layer seems to enhance the adhesion of interface.

In the filler area, coarsened voids were observed at the boundary of Cu-rich and Ag-rich phase.

Ag in the filler may act as a enhancer of swelling

Neutron-induced microstructures and correlation with hardening are in progress

3. Low energy hydrogen ion irradiation on W

Summary of previous reports on Mo
- Temperature dependence of microstructure
- Ion energy dependence of microstructure
- Themal stability of defect clusters

Present study on W
- High threshold energy for displacement
- Purity effects (99.99%SC and 99.9%PC)

0.5~8keV H^+, RT~1073K

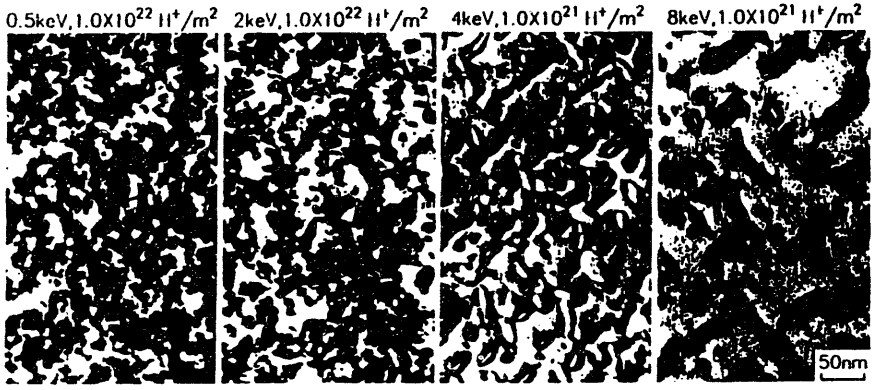

Mo, irradiated with H^+ at R.T.

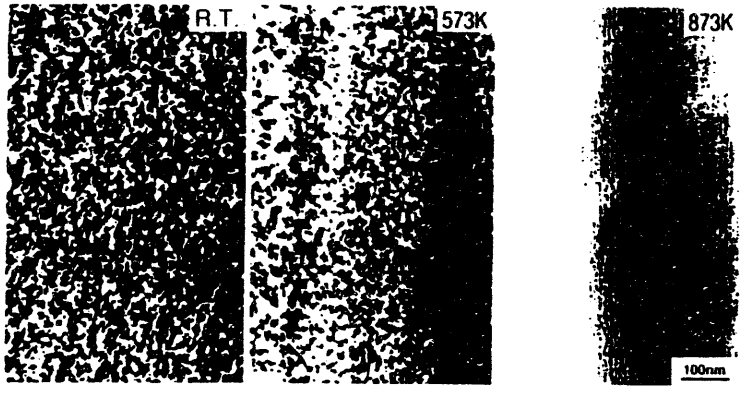

Mo, irradiated with 0.5[keV] H^+

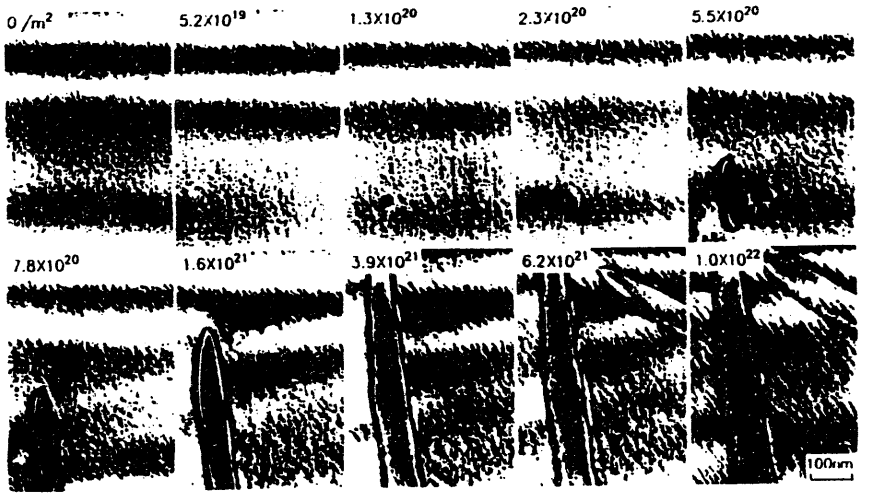

Mo, irradiated with 8keV $H^+(2.6X10^{18}/m^2/s)$ at 873K

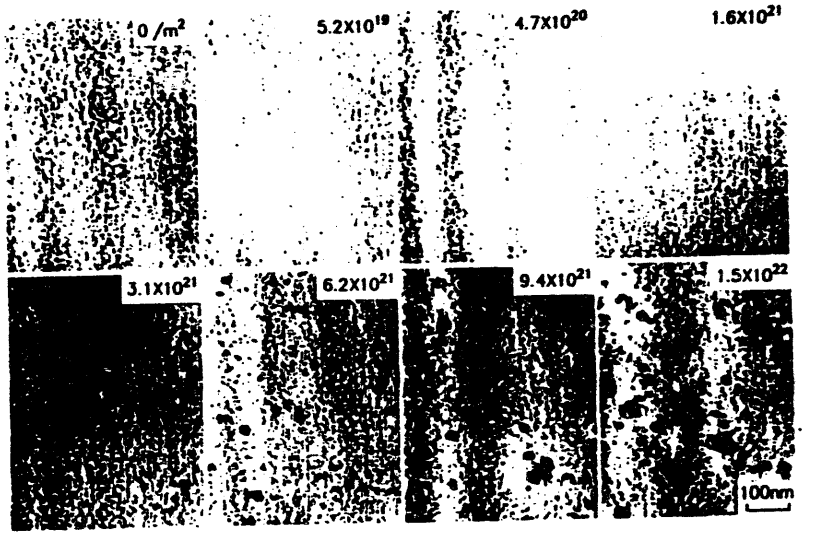

W, irradiated with 8keV $H^+(5.2X10^{18}/m^2/s)$ at 473K

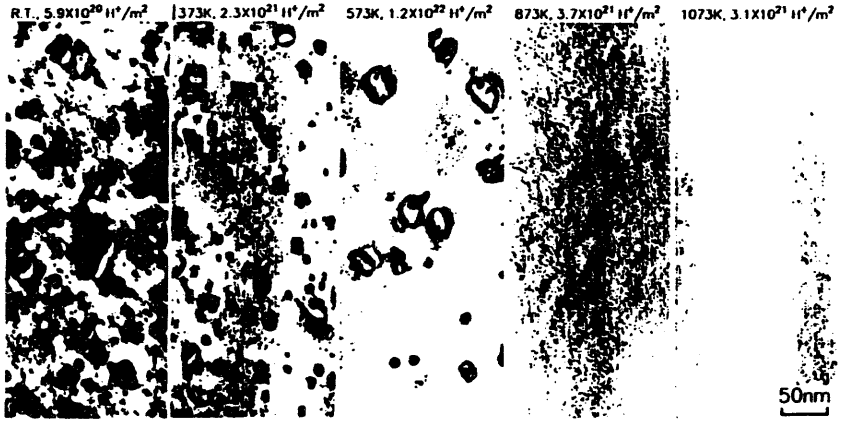

W, irradiated with 8keV H^+

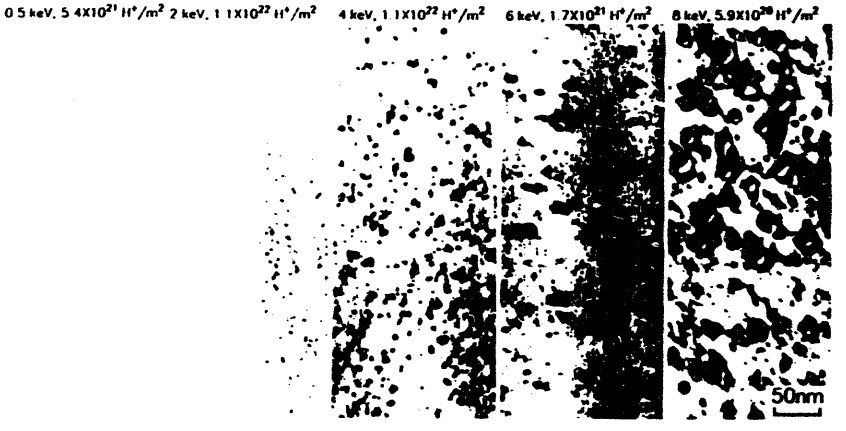

W, irradiated with H^+ at R.T.

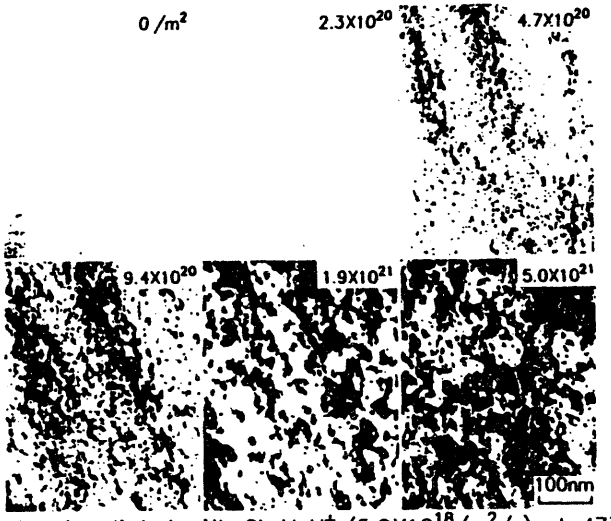

poly W, irradiated with 8keV H^+ ($5.2X10^{18}/m^2/s$) at 473K

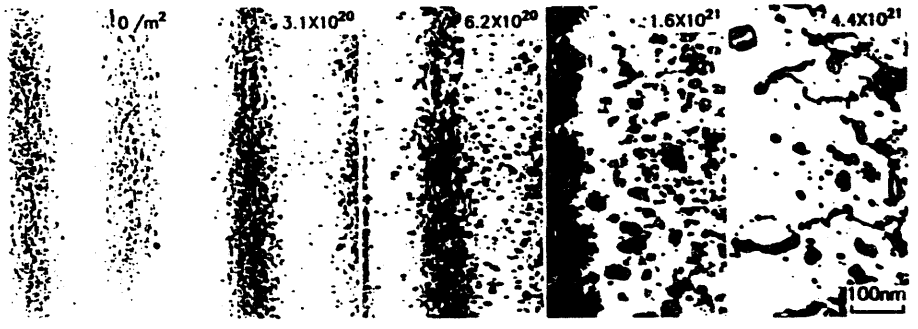

poly W, irradiated with 8keV H^+ ($5.2X10^{18}/m^2/s$) at 873K

	Mo	W
M	95.94	183.85
E_d	35 eV	44 eV
$E_H = \frac{E_d}{\frac{4M}{(M+1)^2}}$	860 eV	2050 eV

Threshold energy for atomic displacement

M : Taget mass
Ed : Displacement threshold energy
EH : Displacement threshold energy for hydrogen ions

Summary - 3 Low energy H ion irradiation on W

High purity W is very resistant to hydrogen ion irradiation
- High displacement threshold energy of H^+ ion
- Hydrogen clusters not observed
- Loop slipping out at surfaces

Low hydrogen retention and small property degradation by hydrogen are expected

Defect accumulation is more prominent in lower purity W

ORNL Irradiation Effects Program

L. L. Snead and T. D. Burchell

Metals and Ceramics Division
Oak Ridge National Laboratory

Thermal Conductivity Degradation of High TC Graphites

- Steady improvements have been made in industry in both fiber technology and C/C processing.
  - fibers approaching 2000 W/m-K thermal conductivity
  - 1D composites approaching 800 W/m-K
  - 3D composites approaching 500 W/m-K
- At elevated temperatures (> 600 °C), the thermal conductivity degradation of very high TC composites does not appear as bad as that of lower TC graphites.

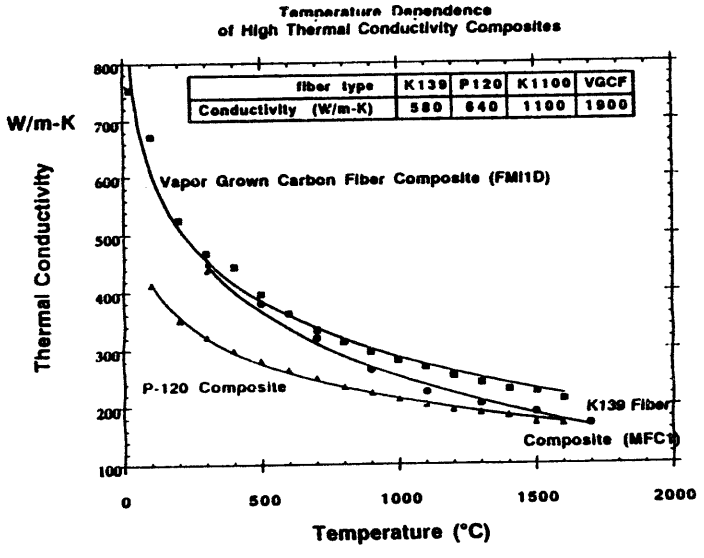

Irradiation of High Thermal Conductivity Graphite Materials

- Selected materials were irradiated in core of the HFIR reactor at Oak Ridge National Laboratory at 100 and 800 °C from 0.01 to 1.6 dpa.
- Thermal flash diffusivity measurements were made followed by annealing

ORNL

Irradiation of High Thermal Conductivity Graphite Materials

- Six candidate materials were chosen with a range of conductivities :

Material	Manufacturer	Structure	Room Temperature Conductivity (W/m-K)
H451	Segri-Great Lakes	Graphite	115
FMI-222	Fiber Materials	3-D Composite	200
Hercules 3D	Hercules	3-D Composite	345
RGTI	Efremov Institute	TI Doped Graphite	450
MFC-1	Mitsubishi Kasei	1D Composite	555
FMI 1D	Fiber Materials	1D Composite	650
Glidcop Copper	SEM Metals	dispersion strengthened	350

ORNL

THERMAL CONDUCTIVITY DEGRADATION

- Presently, the major drawback to the use of C/C in high heat flux regions is the serious thermal conductivity degradation expected in DT systems.
- The thermal conductivity of graphite is dominated by three factors.
  1) Grain Boundary Scattering (Kgb)
  2) Umklapp Scattering (Ku)
  3) Defect Scattering (Kd)

$$K_{th} = \beta \left[1/K_{gb} + 1/K_u + 1/K_d \right]^{-1}$$

- Defect scattering is highly dependent on temperature.

ORNL

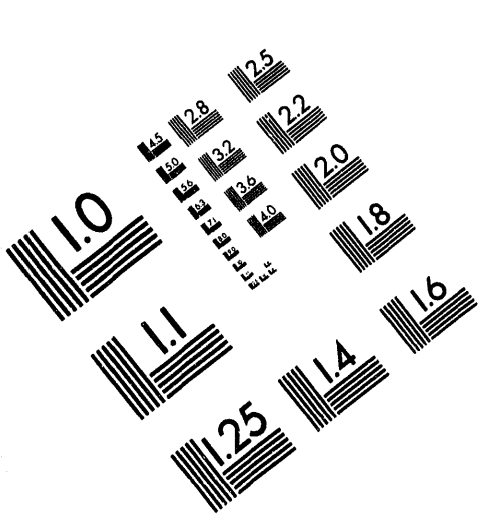

AIIM

Association for Information and Image Management
1100 Wayne Avenue, Suite 1100
Silver Spring, Maryland 20910
301/587-8202

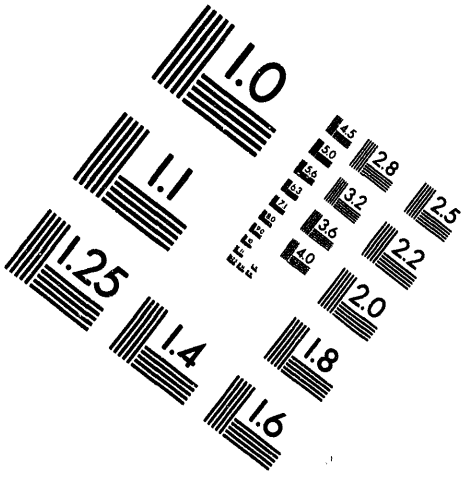

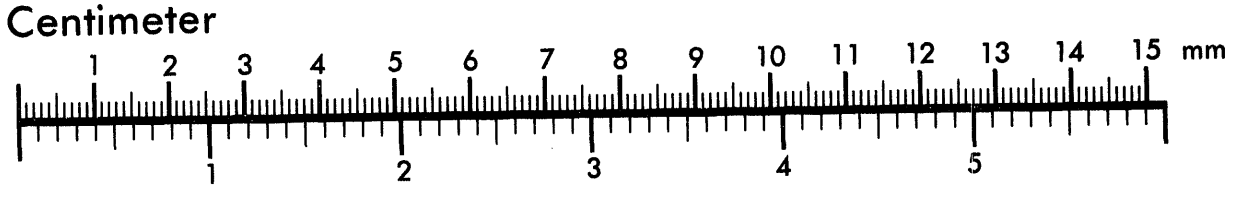

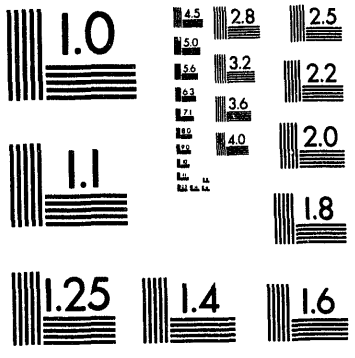

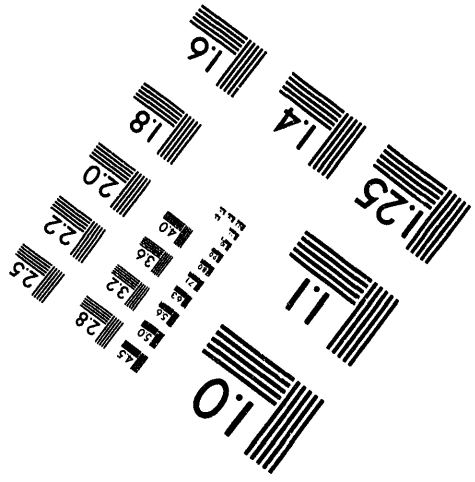

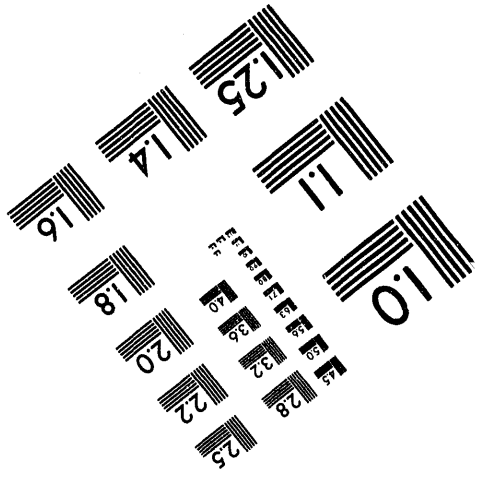

MANUFACTURED TO AIIM STANDARDS
BY APPLIED IMAGE, INC.

8 of 15

Temperature Dependence of Thermal Conductivity Degradation

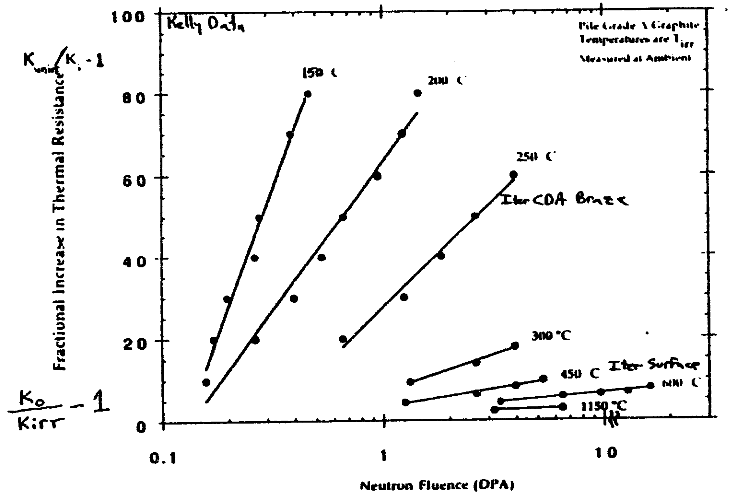

Thermal Conductivity Degradation of Selected Graphite Materials

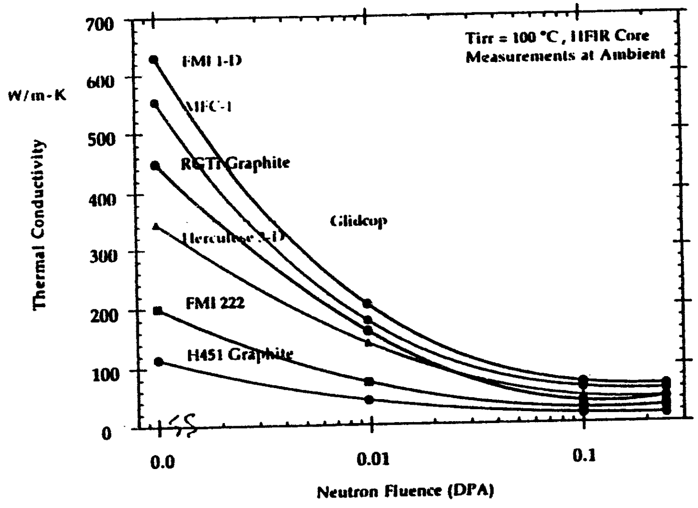

Effect of Annealing on Room Temperature Thermal Conductivity

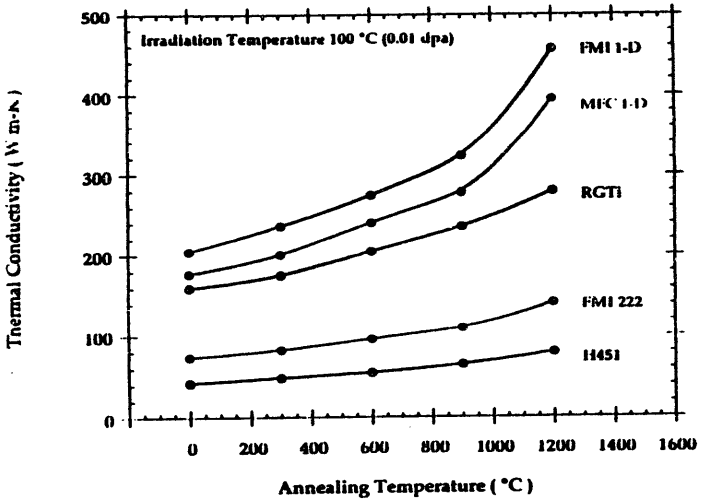

Discussion/Conclusions

- Low temperature irradiation yielded severe reduction in high thermal conductivity materials:

Material	Structure	Room Temperature Conductivity (W/m-K)	Percent of Initial Conductivity
H451	Graphite	115	12.7 %
FMI-222	3-D Composite	200	14 .0
Hercules 3D	3-D Composite	345	12.8
RGTI	Ti Doped Graphite	450	9.7
MFC-1	1D Composite	555	10.1
FMI 1D	1D Composite	650	10.3

ORNL

Beryllium Studies

- Three beryllium samples are being studied

Material	Manufacturer	Structure	Density g/cc	Thermal Conductivity W/m-K
S-65C	Brush Wellman	Poly X	1.83	~ 200
Zone Refined	Max Plank Inst.	Single X	1.85	~ 220
Plasma Sprayed	Sandia	Layered Poly X	~ 1.7	~ 100

- HFIR irradiations beginning in 94 in displacement range of 0.001 to 1 dpa at 100 to 400 °C.

Russian Recrystallized Graphite (RGTI)

- High TC graphites which use Ti as a recrystallizing agent have shown promise for fusion FW applications.
- A series of heat treatments have been carried out to reduce the titanium levels of as-processed material.
- Only a limited amount of Ti is easily removed by heat treatment.
- Radiation induced TC degradation of RGTI is no different than other graphite materials (contrary to published work.).

ORNL

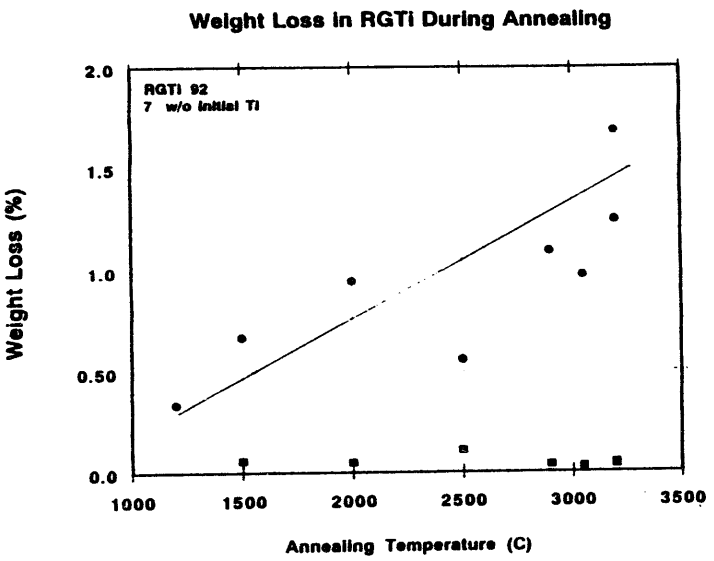

Discussion

- With the possible exception of cost, RGTi shows no clear advantage over conventional graphites.

SIC Matrix/Graphite Fiber Composite

- Two composites are being developed for high TC and low tritium retention.

Matrix	Fiber	Weave	Thermal Conductivity
CVD SIC	K1100 graphite	3-D	~ 400 W/m-K
CVD SIC	VGCF graphite	1-D	400 - 600 W/m-k

- Highly graphitized fibers have significantly reduced tritium retention.
- Further enhancement in thermal conductivity mat be achieved by beryllium doping of matrix.

ORNL

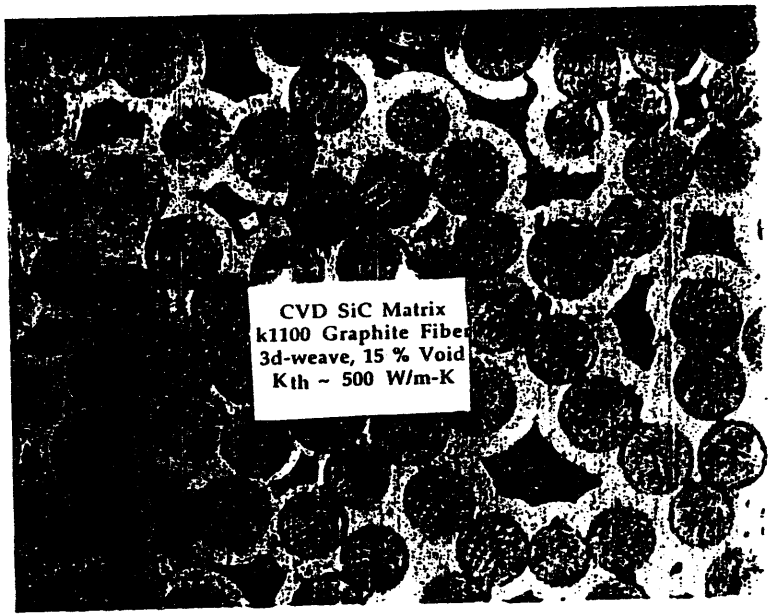

Hydrogen Solubility (H/C)
ppm
1000
100
10
0
20
40
60
80
100
Asumi et al.

DEVELOPMENT OF PFC MATERIALS AT TOYO TANSO

Presented by
Sokan Miki, Toyo Tanso USA, Inc.

With Contribution From
M. Okada, T. Sogabe, T. Matsuda, S. Nogami M. Mitsuishi, S. Goda, H. Inoue
Toyo Tanso Co., Ltd. Ohnohara Plant

US - Japan Workshop on PMI - IIIF
San Diego, CA January 24 - 27, 1994

PRESENTATION TOPICS

BACKGROUND

1. Carbon and graphite materials have been widely developed and used as plasma facing components (PFC) in fusion devices because of their low Z and excellent thermal properties.

2. At present, large fusion devices have achieved energy break-even. However, further gains in performance require advanced graphite materials with superior thermal properties.

BACKGROUND *(cont.)*

3. Problems with graphite components in fusion devices relate to degradation of plasma quality. Hydrogen and oxygen are retained by the graphite and recycled to the plasma. This causes sputtering and erosion of the graphite, and impaired plasma performance due to high levels of hydrogen, oxygen and carbon. Modified graphite materials will target these problems. Boronization is seen as an excellent choice.

4. The next generation of large fusion devices, such as LHD and ITER, promise excellent thermal stability under high heat loads. Even with these conditions and improved graphite materials, diverter components are limited to a surface temperature of about 1000° C to avoid radiation enhanced sublimation. Therefore, active cooling of the PFC is required, and must be developed.

OBJECTIVES

1. To develop graphite materials that have superior thermal properties, including high thermal conductivity and high resistance to thermal shock and sublimation.
   - (1-1) Isotropic Graphite: IG-430U
   - (1-2) Felt-type CFC: CX-2002U
   - (1-3) TiC mixed CFC

2. To develop boronized materials in order to have good control of H_2 and O_2 and to reduce chemical sputtering.
   - (2-1) B_4C mixed graphite
   - (2-2) B_4C mixed CFC
   - (2-3) B_4C coated materials
     - --B_4C coated materials by paste method
     - --B_4C coated materials by CVD method

OBJECTIVES *(cont.)*

3. To develop siliconized materials in order to reduce erosion and chemical sputtering by H_2 and O_2.
   - (3-1) Conversion method by CVR
   - (3-2) Si impregnation method .
   - (3-3) Combine: Conversion-SiC / Si / C ,' CVD-SiC

4. To develop a viable method of brazing PFC (consisting of either isotropic graphite or CFC) to copper base material.
   - (4-1) PFC / Mo / Cu Brazing

PHYSICAL PROPERTIES OF IG-430U AND CX-2002U

Grade:	IG-430U Isotropic Graphite	CX-2002U CFC (Felt Type) W/G	CX-2002U CFC (Felt Type) A/G
Density (Mg/m^3)	1.82	1.70	
Bend Strength (MPa)	54	54	--
Comp Strength (MPa)	83	61	64
Young's Mod (GPa)	11	--	
Thermal Cond (W/mK)	139	325	186
CTE (10^{-6}/°C)	4.4	1.8	5.8

TiC MIXED CFC

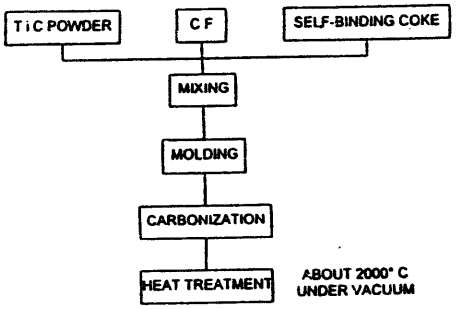

Fig. Manufacturing Process of TiC mixed CFC

Table: Physical Properties of TiC Mixed CFC

Ti Content (mass %)	0	10	21	29	47
Density (Mg/m^3)	1.29	1.46	1.65	1.91	2.48
Shore Hardness (-)	62/40	57/39	54/39	54/40	41/34
Specific Resistivity ($\mu\Omega \cdot m$)	28.4	19.1	15.4	10.4	3.0
Flexural Strength (MPa)	53	50	44	90	100
Compressive Strength (MPa)	86/106	90/100	84/98	94/90	78/74
C.T.E. ($10^{-6}/K$)	5.8/1.6	4.8/2.4	6.1/2.5	6.3/3.4	7.7/6.5
Thermal Conductivity ($W/m \cdot K$)				24/37	47/79

BORONIZED MATERIALS

(1) Manufacturing Process of B_4C mixed graphite

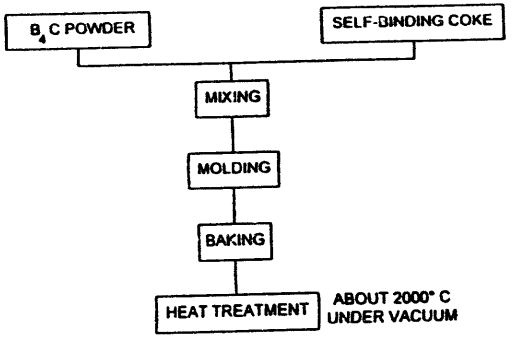

(2) Manufacturing Process of B_4C mixed CFC

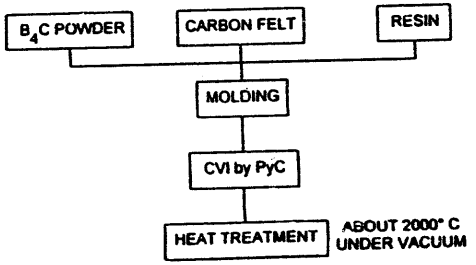

Table: Physical Properties of B_4C mixed Graphite and CFC

	GR-100	GR-101	GR-103	GR 110	GR-120	12% B-C/C
Boron Content (mass %)	0	1	3	11	22	12
Density (Mg/m^3)	1.80	1.79	1.85	1.82	1.78	1.75
Shore Hardness (-)	84	64	67	70	58	55
Specific Resistivity ($\mu\Omega \cdot m$)	19	10	9	15	25	10/12/26
Flexural Strength (MPa)	37	38	44	56	56	30
Compressive Strength (MPa)	100	79	104	137	159	101
CTE ($10^{-6}/K$)	5.7	5.5	5.3	4.9	4.6	3.6/3.5/5.0
Thermal Conductivity ($W/m \cdot K$)	54/26	48/29	33/26	35/28	33/23	76/72/33

SEM Micrograph of 12% B_4C Mixed CFC

Boron Mapping

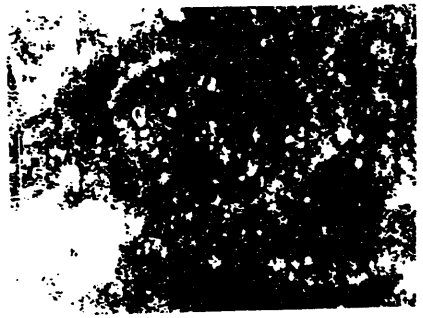

< 12% Boronized CFC >

(3) B_4C COATED MATERIALS

(3-1) Manufacturing Process of B_4C Coated Materials by Paste Method

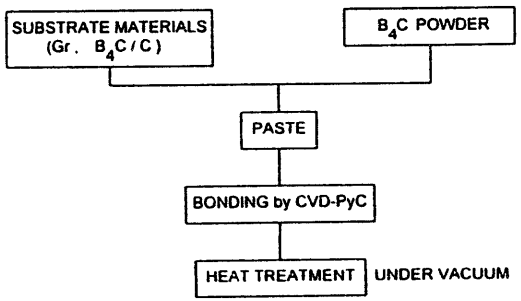

(a) Secondary Electron Image of the B_4C Coat on GB-120 <Paste Method>

(b) Backscattered Electron Image

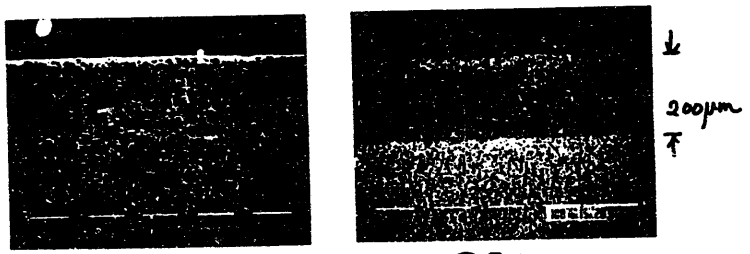

(a) SEI (b) BEI

B_4C コート材
GB-120 SEI. BEI

(3-2) Manufacturing Process of B_4C Coated Materials by CVD Method

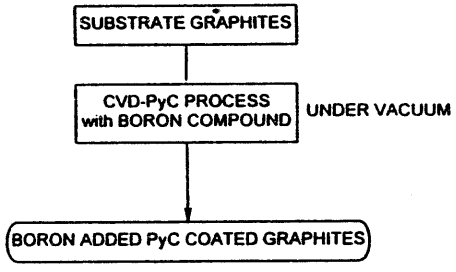

SILICONIZED MATERIALS

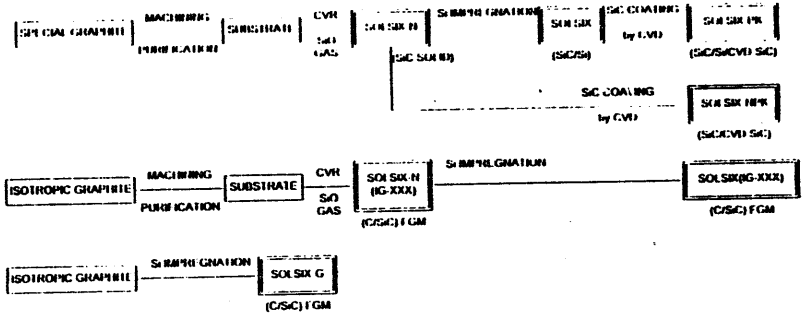

Fig Manufacturing Process of Siliconized Graphites

Table: Physical Properties of Siliconized Materials

	SOLSIX-PK	SOLSIX	SOLSIX-HPK	SOLSIX H	SOLSIX (IG 110)	SOLSIX H (IG 110)	SOLSIX G
Phase	SiC/Si/CVDSiC	SiC/Si	SiC/CVDSiC	Bulk SiC	C/SiC	C/SiC	C/SiC
Bulk Density (Mg/m^3)	3.0	2.9		2.1	2.1	2.0	2.6
C.T.E ($10^{-6}/K$)	4.7 (RT-1273K)	4.6 (RT-1273K)		4.4 (RT-1273K)	4.6 (623-723K)	4.6 (623-723K)	4.4 (RT-1273K)
Flexural Strength (MPa)	220	185		80	55	50	110
Compressive Strength (MPa)				300	135	110	630
Young's Modulus (GPa)	220	280		120	30	10	19
Thermal Conductivity (W/m • K)	110 (300K)	170 (300K)		50 (300K)	133 (300K)	110 (300K)	145 (300K)
Specific Heat (J/kg • K)	1270 (1000K)	1320 (1000K)		2030 (300K)	680 (300K)	680 (300K)	800 (300K)
Thermal Shock Resistance (K)	673-723	673-723	673-723	973-1073			1073-1113
Porosity	Pore Free	Pore Free	Pore Free (surface)	Porous	Pore Free	Porous	Pore Free

BRAZING STUDY*

OBJECTIVE: Develop a method of brazing PFC (IG-430U or CX-2002U) to copper base material. Evaluate integrity of braze joint. Evaluate application as diverters in the LHD.

TEST METHOD: Characterization of brazed surface and mechanical testing of brazed surface.

(1) PFC - Mo: 4-point Bending Test

(2) PFC - Mo - Cu: Thermal Shock Test

High-heat Load Test in ACT

RESULTS: "Dissolution and deposition of base metal" is a viable technique for joining PFC and copper based active cooling systems. Sample diverter plates for LHD show excellent braze joint stability at high temperature.

*Study done 1991-92. Results reported by [illegible] in US - Japan Workshop [illegible] and by S. [illegible] in High Heat Flux Engineering 1992

LASER MIRROR

背面冷却型反射鏡

(SiC Coated Graphite
- Cu Brazing)

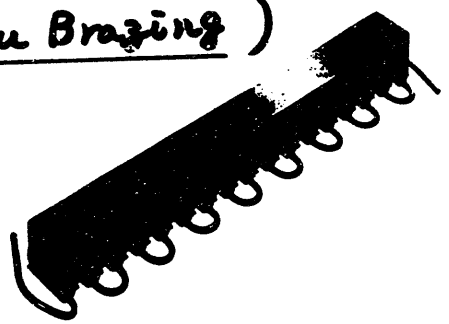

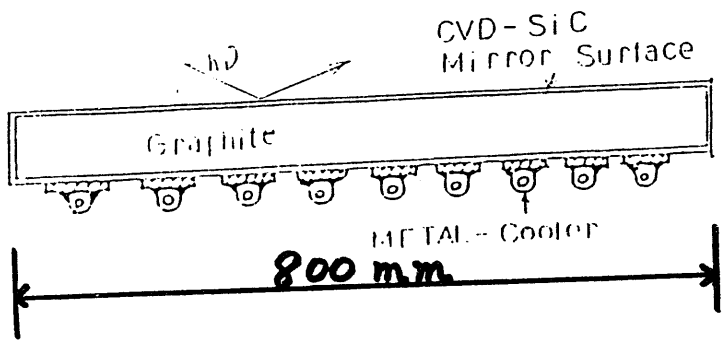

SUMMARY

The development work of PFC at Toyo Tanso Company has been ongoing for the past 10 years. Materials developed include:

(1) Isotropic Graphite: IG-430U
(2) Felt-type CFC: CX-2002U
(3) TiC mixed CFC
(4) Boronized Materials
  B_4C mixed graphite
  B_4C mixed CFC
  B_4C coated materials
(5) Siliconized Materials
(6) PFC / Cu Brazing Technology

CONCLUSION

The present generation, and future generations of large fusion devices require advanced graphite materials. Toyo Tanso is developing these materials to provide improved thermal performance, reduced contamination of the plasma, and active cooling of PFC. We are strongly committed to developing materials that meet the requirements of this demanding application.

Enhancement of H Trapping in Damaged B and Ti Doped Russian Graphites

W. R. Wampler and B. L. Doyle
SNL Albuquerque
and
V. N. Chernikov, A. E. Gorodetsky,
S. L. Kanashenko and A. P. Zakharov
IPC/RAS Moscow

US-Japan Workshop on PMI-HHF
UCSD, January 24-27, 1994

INTRODUCTION

- Retention of H isotopes in graphite can impact plasma fueling and tritium inventory.
- Lattice damage from neutron irradiation will increase tritium retention in graphite components in ITER.
- Our experiments measure D retention in graphites irradiated with C^+ ions to simulate neutron damage.
- Several types of graphite were examined to determine the influence of microstructure and composition on D retention.

Experimental Method

1. Graphite samples were irradiated at 77°C and 400°C with 200 keV C^+ ions to doses up to $9x10^{16}$ /cm^2, causing atomic displacements to ~ 7 dpa to a depth of 0.5 μm.
2. Samples were then exposed at 1200°C for 1 hour to D_2 gas at 5 millitorr and 1 torr.
3. The concentration of retained D was then measured to ~ 5 μm using D(^{3}He, p)^{4}He nuclear reaction analysis.

note: In ITER 1 MW yr/m^2 will produce ~ 1 DPA in graphite.

GRAPHITES EXAMINED:

Material	Microstructure	Grain size (μm)	Porosity	Source
AXF-5Q	Isotropic, graphitized	5	20% open	POCO, USA
PGI	Isotropic, turbostratic	1	10% closed	NIIGraphit, Moscow
USB-15 (15 wt.% B)	Isotropic, turbostratic	0.1	10% closed	NIIGraphit, Moscow
RG-Ti-91 (7.5 wt.% Ti)	Anisotropic, graphitized	10	low closed	NIIGraphit, Moscow
RG-Ti-91 +0.5 wt.% B	Anisotropic, graphitized	10	low closed	NIIGraphit, Moscow

MEAN DAMAGE (DPA)
0 1 2 3 4 5 6
2000
1500
1000
500
0
D RETENTION (appm)
POCO
PGI
RGT
USB
RGT+.5%B
DAMAGED BY 200 keV C+ IONS
AT 77°C
0 2 4 6 8 10
IRRADIATION DOSE (10^16 C+/cm^2)

1000
500
0
D RETENTION (appm)
POCO
PGI
RGT
USB
DAMAGED BY 200 keV C+ IONS
AT 400°C
0 2 4 6 8 10
IRRADIATION DOSE (10^16 C+/cm^2)

D Trapping depends on:

1. The trap concentration.
   Damage increases the number of traps.

2. The trap strength.
   Concentration of retained D did not increase when gas pressure was increased from 5 mtorr to 1 torr. This shows that traps are strong (E_b>4 eV) consistent with C-H bonds.

3. Microstructure.
   D access to traps is facilitated by open porosity and fast diffusion along graphite basal planes, eg. POCO, RGT, restricted by closed porosity and slow diffusion across graphite basal planes, eg. USB.

Conclusions

1. Damaged graphite (>0.2 dpa) traps much more D than undamaged graphite.
2. USB traps much less D than other graphites.
3. Adding 0.5 wt % B to RGT reduced D retention to ~50%.
4. Boron reduces D retention
5. Access of D to traps depends on the microstructure.
6. Increasing irradiation temperature to 400° C reduces D retention by a factor of ~2, except for USB.
7. Potential disadvantage of USB in ITER is the $^{10}B(n,^4He)^7Li$ reaction. Thermal neutron cross section is large (3840 b). Neutron flux from 1.5 MW yr / m^2 will consume the ^{10}B leaving ~ 3 at.% He and ^7Li and ~ 10 DPA from damage by reaction products.

Development of C/C with Controlled Fiber Orientation

Y. Gotoh
Hitachi Research Laboratory ,
Hitachi Ltd.

US-Japan Workshop Q181 on HHFC
and PSI for Next Devices,
Jan. 24-27, 1994, UCSD,
San Diego, CA, USA

Active Cooling C/C Divertor Armor

UD-, Felt-type C/C Armor:
- uniform fiber orientation through the tile,
- flat, saddle or monoblock,
- small in size

New C/C:
- controlled fiber orientations around the cooling channel,
- monoblock,
- larger in length

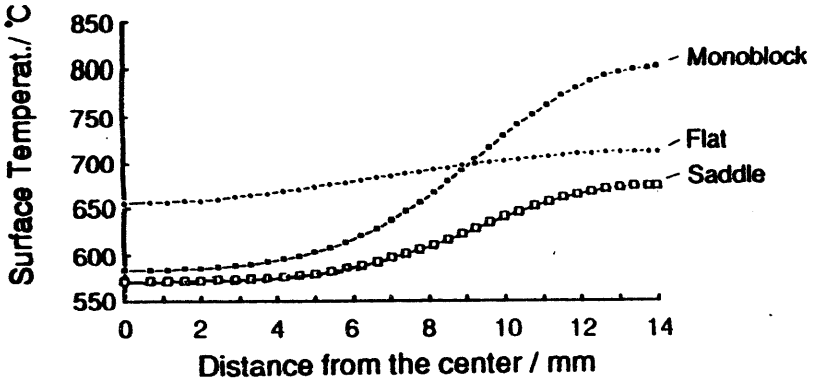

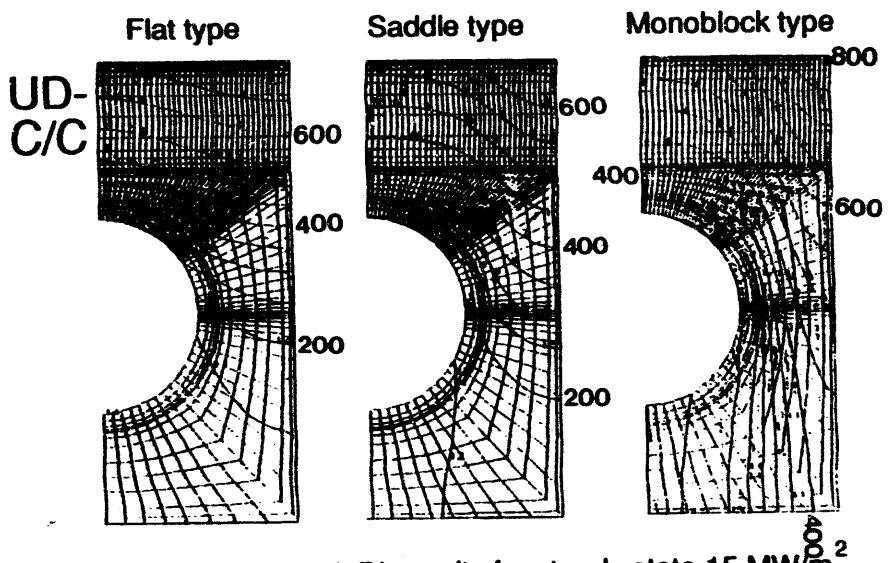

Thermal analysis (2D) results for steady state 15 MW/m^2 heat flux (coolant bulk temperature60℃, 70000W/m^{2}K)

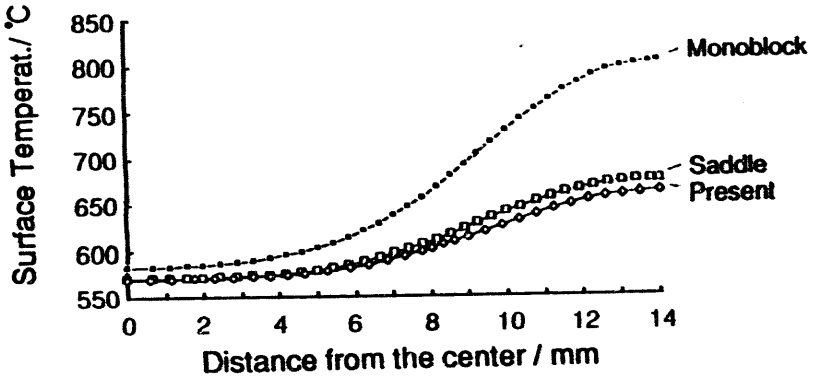

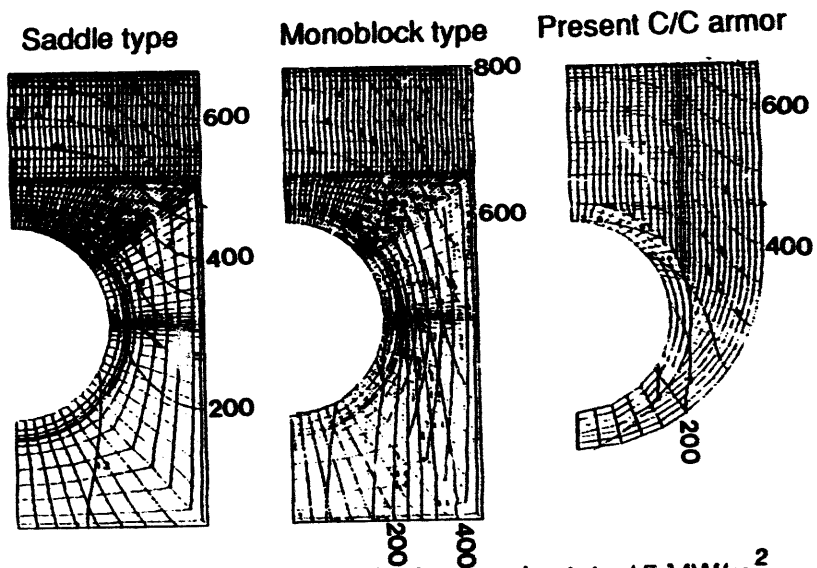

Thermal analysis (2D) results for steady state 15 MW/m^2 heat flux (coolant bulk temperature60℃, 70000W/m^{2}K)

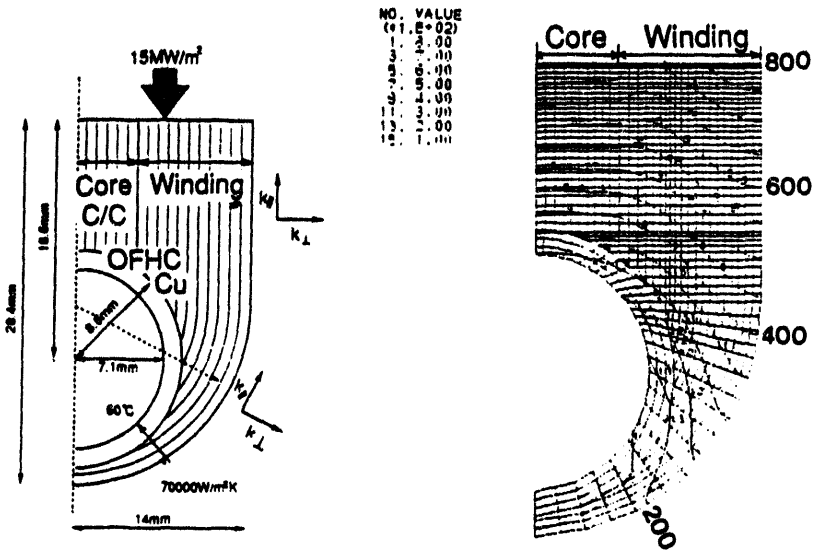

Model Result

2D-thermal analysis for steady state thermal load

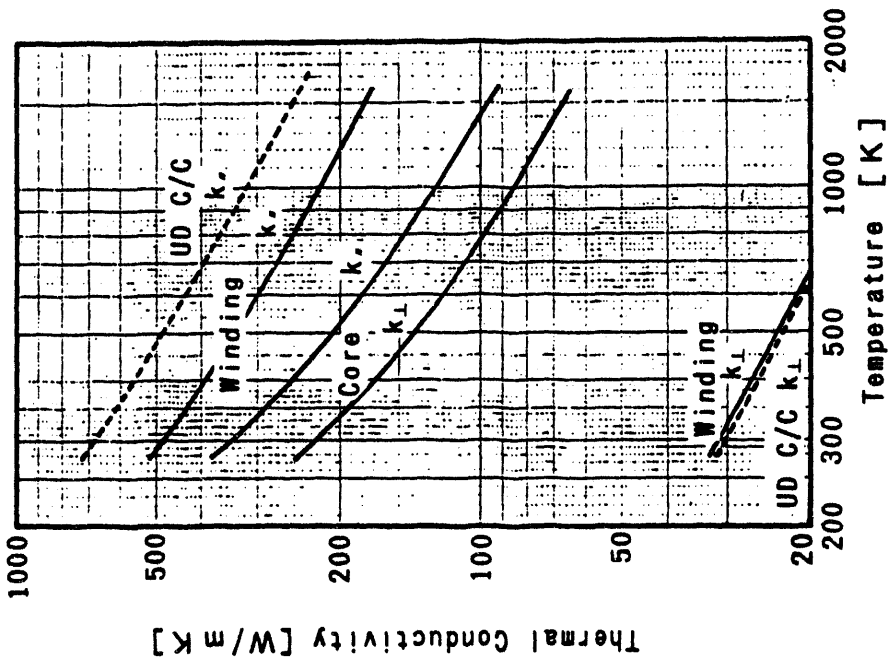

Thermal conductivity measurement results for the C/C with controlled fiber orientation

2D-thermal analysis

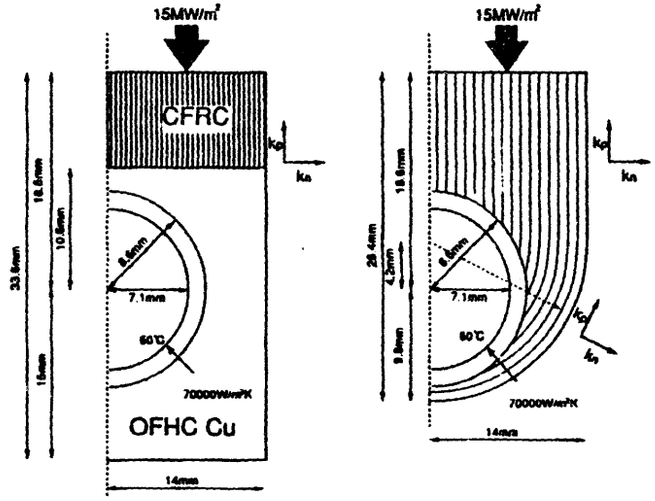

Model

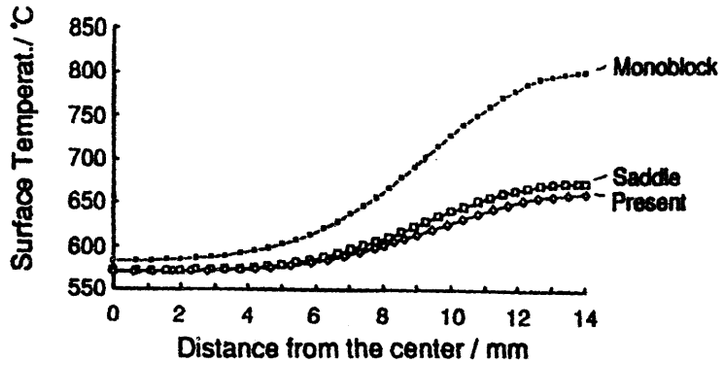

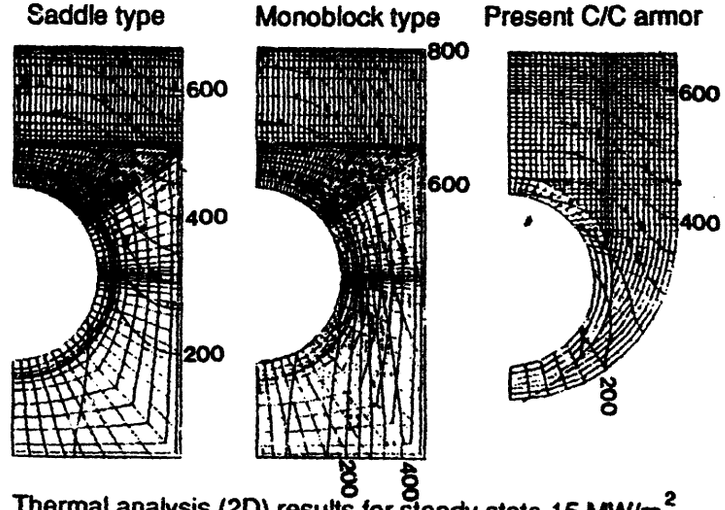

Thermal analysis (2D) results for steady state 15 MW/m^2 heat flux (coolant bulk temperature60℃, 70000W/m^{2}K)

2D-thermal analysis for steady state thermal load

Model

Result

Conclusion

1. New monoblock C/C armor with controlled fiber orientations around the cooling channel was proposed.

2. Thermal analysis showed that cooling performance of the present C/C is much better than that of monoblock UD-C/C.

3. Trial fabrication and thermal property measurements of the proposed C/C were made.

US-Japan Workshop Q181

25-January-94

Development of B_4C Coated Carbon Materials by Conversion Method

Y.Kikuchi,T.Suzuki,Y.Nakiri

Hitachi Chemical Co.,Ltd.

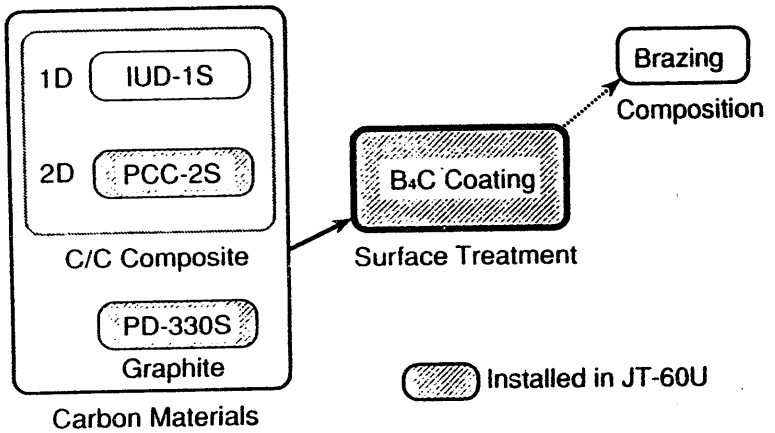

Fig.1 Development of Plasma Facing Materials in Hitachi Chemical

B_4C Conversion (Chemical Vapor Reaction)

$$2B_2O_3 + 7C \rightarrow B_4C + 6CO\uparrow$$

(Substrate)

Table. 1 Comparison of the B_4C coating method.

Method	C V D	Conversion
Structure	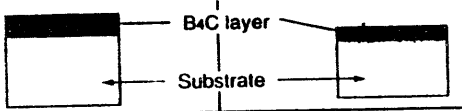	
Composition Change	Clear	Gradual

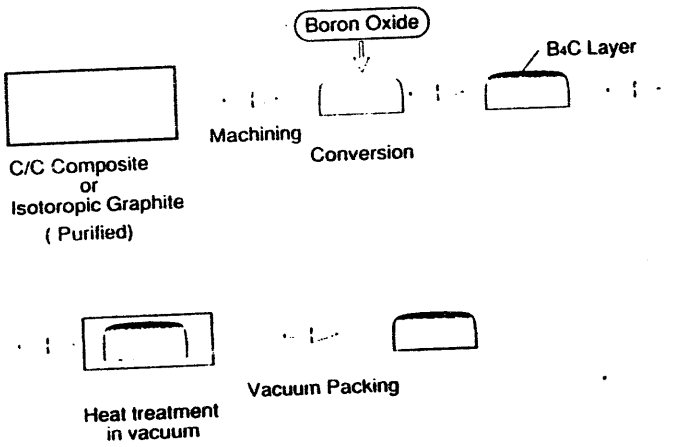

Fig. 2 Manufacturing process of B_4C converted carbon.

Table 2. Physical properties of B_4C layer and graphite substrates

Material / Properties	B_4C layer (Conversion)	C/C Composite PCC-2S		Graphite PD-330S
		//	⊥	
Density (g/cm^3)	1.5	1.83		1.82
Bending strength (MPa)	85	38.3	12.0	46
C.T.E ($10^{-6}/K$)	~5.2	1.0	5.8	4.8
Thermal Conduc. (W/mK)	10~20	280	150	150

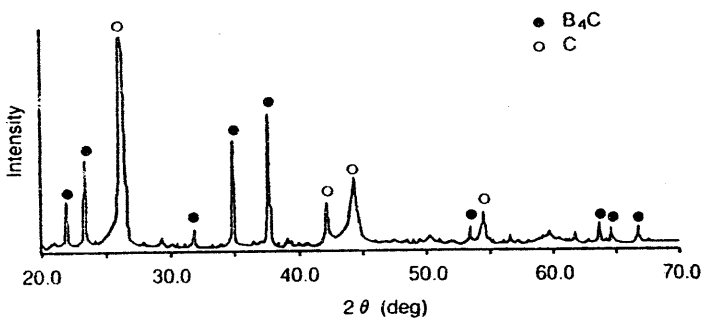

Fig. 3 The X-ray diffraction pattern of B_4C converted carbon.

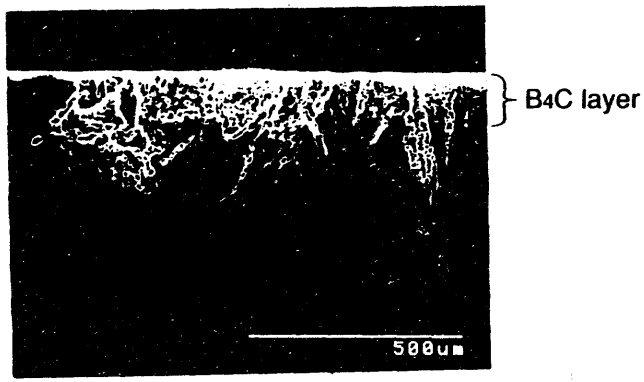

(a) B4C layer : 100 μm

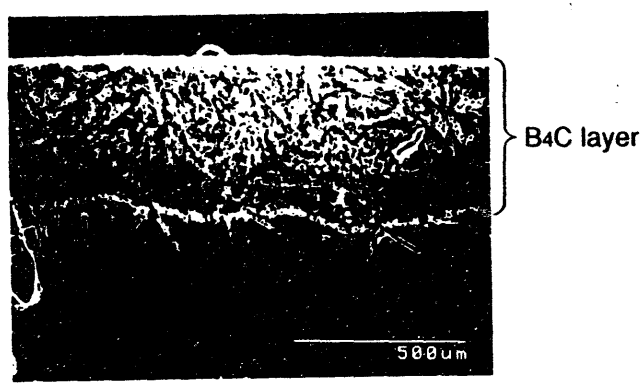

(b) B4C layer : 500 μm

Fig. 4 SEM photographs of the cross sectional view of B4C converted carbon.

Substrate: PCC-2S(C/C Composite)

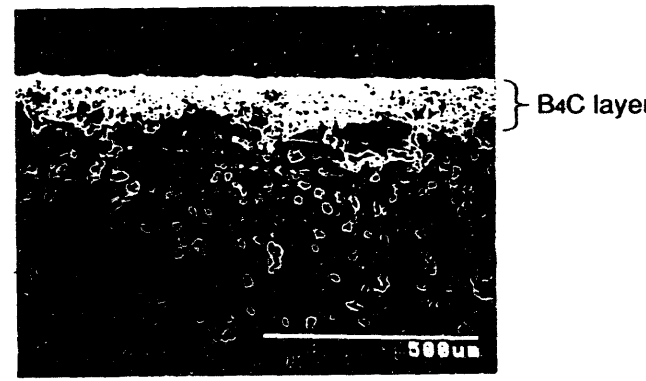

(a) B4C layer : 100 μm

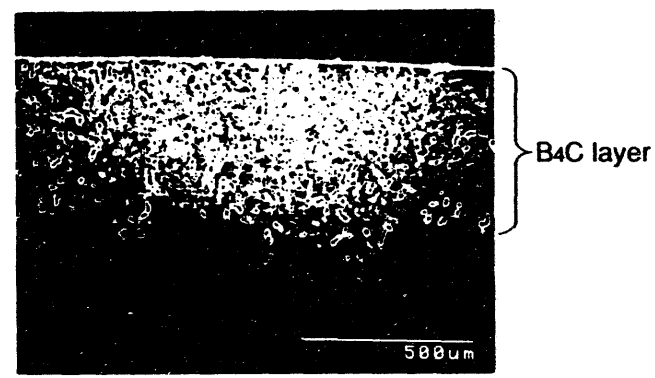

(b) B4C layer : 500 μm

Fig. 5 SEM photographs of the cross sectional view of B4C convertd carbon.

Substrate: PD-330S (Graphite)

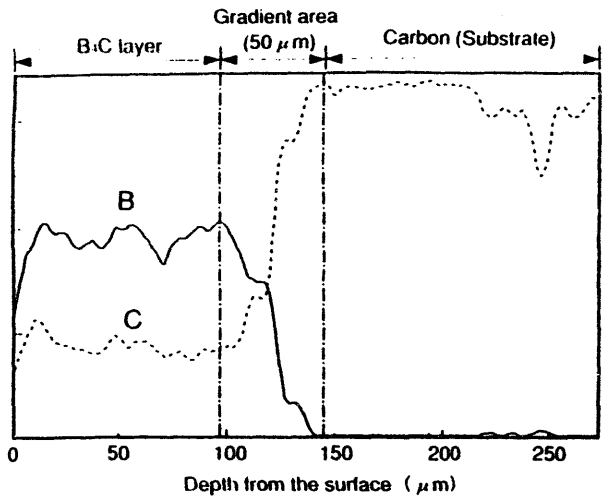

Fig. 6 Composition change in a cross-section of B_4C converted carbon.
(Auger Electron Spectroscopy)

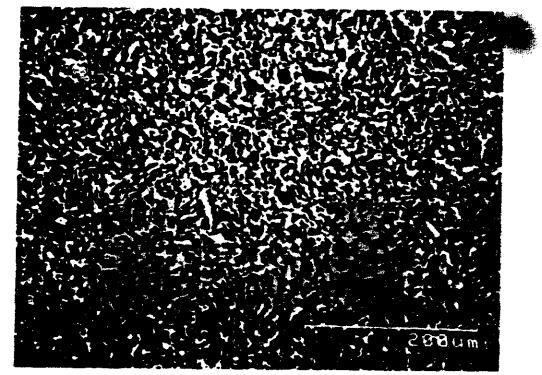

Fig. 7 SEM photograph of the surface of B_4C layer.
Substrate: PD-330S (Graphite)

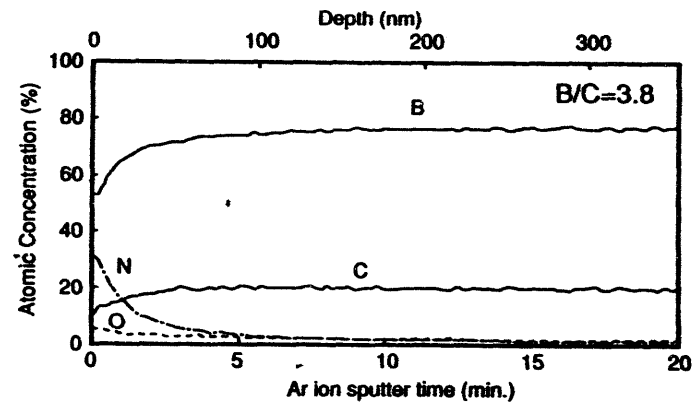

Fig. 8 AES depth profile of B_4C layer.
Substrate: PD-330S (Graphite)

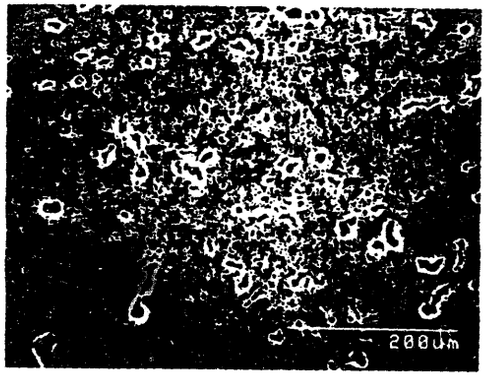

Fig. 9 SEM photograph of the polished surface of B_4C layer.
Substrate: PD-330S (Graphite)

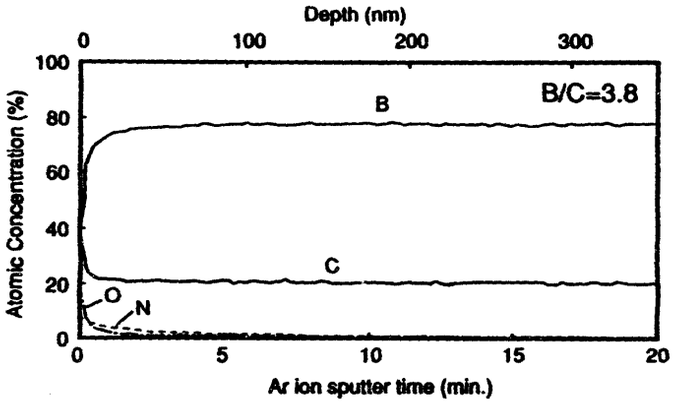

Fig. 10 AES depth profile of the polished surface of B_4C layer.
Substrate: PD-330S (Graphite)

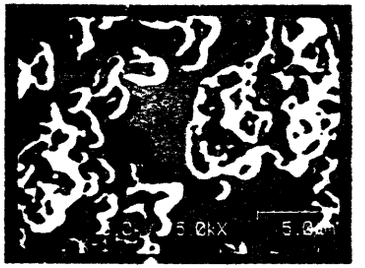

(1) SEM photograph

(2) SAM map of Nitrogen

(3) SAM map of Oxygen

Fig. SEM photograph and SAM maps of the polished surface of B_4C layer.
SAM: Scanning Auger Microscopy

Conclusions

We have developed the boron carbide coated carbon materials by using a conversion method (B4C converted carbon).

1. The surface layer material of the conversion method is presumed to be B4C by the X-ray diffraction pattern.

2. The thickness of B4C layer can be controlled from 100 to 700 μm.

3. The composition change is gradual near the boundary between the B4C layer and the carbon substrate.

4. Boron nitride is formed on the top surface of B4C layer several tens nm thick.

5. The converted layer is composed B4C + C with a B/C ratio of 3.8 .

The B4C converted carbon tiles with 300 μm thick B4C layer have been installed in JT-60U since Dec. 1993.

Preparation of Plasma Facing Materials Coatings at General Atomics

Paul W. Trester
Peter G. Valentine
W. Phil West

General Atomics
3550 General Atomics Court
San Diego, California 92121-1194, U.S.A.

U.S. - Japan Workshop Q181
High Heat Flux Components and
Plasma Surface Interactions for Next Devices
San Diego, California
24 - 27 January 1994

Materials and Processing R&D by General Atomics for Plasma Facing Components

Historical Summary:

Coating Designs	Substrates	Methods
• TiC	• Graphite	• CVD
• C + SiC; SiC	• Graphite	• CVD - Fluidized Bed
• B	• Graphite	• CVD (DIII-D in situ)

• Borides & Carbides
  - B_4C
  - B_4C + SiC
	• Graphite & C-C	• Reaction Sintering; Eutectic Melting

Advanced Substrates	Methods
• SiC-SiC	• CVI
• B_4C particles in C-C	• Pitch-fiber resin-matrix
• Fiber precoatings (e.g. of BN, C, SiC, or Si_3N_4) for tailored composites of C-C, MMC, or CMC	• CVD coating of continuous fiber (tows); sol-gel coating
• Fiber-reinforced Be-matrix composites	• new approach - exploratory

Outline

- Describe the coating method of reaction sintering a precursor layer of particles onto carbon substrates.
- Describe compositions and microstructures of B_4C and SiC mixtures investigated; a material design of interest for PFC radiative boundary experiments in TEXTOR.
- Summarize conclusions made from the materials R&D and from evaluation by electron beam and plasma gun tests and by TEXTOR plasma/NBI experiments.
- Discuss opportunities in coating materials and processing for carbon tile PFC's.

REACTION-SINTERED COATING PROCESS (TWO KEY STEPS)

1. Apply Particle Precursor Coating (With Organic Binder) Onto Graphite Substrate
   - B_4C Particles; Size ≈ 45 μm
   - B_4C-Coated SiC Particles; Uncoated Size ≤ 150 μm (CVD-FB Coating of B_4C Suppresses Dissociation of SiC and Promotes Reaction)

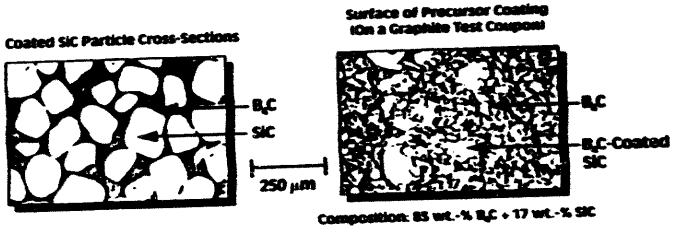

2. Form Adherent Multiphase B_4C-SiC Reaction-Sintered Coating
   - Rapid Thermal Cycle to 2270 C (Liquid Forms Through Eutectic Reaction)
   - Reaction-Sintering: Particles Sinter/React with Substrate and Pyrolyzed Binder

GENERAL ATOMICS

SCANNING ELECTRON MICROGRAPH OF $7B_4C + 2SiC$ MIXTURE REACTION-SINTERED COATING ON ATJ GRAPHITE

(Back-Scattered Electron Image, Cross-Section View)

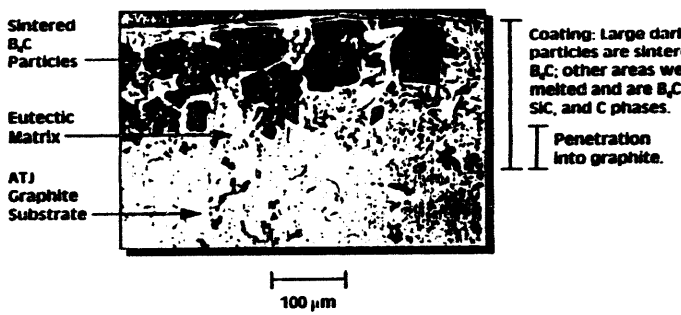

GENERAL ATOMICS

L-91529
9-16-93

Boron-Based Reaction-Sintered Coatings On Carbon Substrate Materials

Substrates

Graphite:
- Ringsdorfwerk EK 98
- Union Carbide ATJ
- Poco Graphite AXF 5Q
- NIIGrafit RGT-Ti-91

Carbon Composites:
- Le Carbon Lorraine AEROLOR A05
- Hercules 3D C-C

Coatings

(Particle Precursor Comp.)
- 100 % Boron Carbide (B4C)
- B4C with additions of Silicon Carbide (SiC)
  - 17, 31, and 55 wt.-% SiC

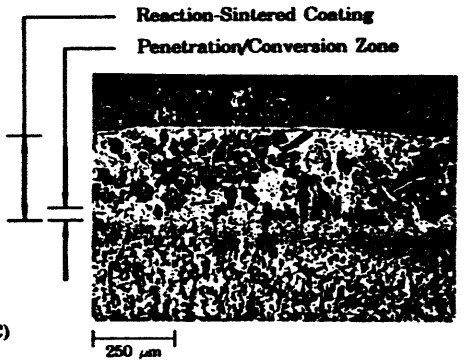

B4C + 31 wt.-% SiC Reaction-Sintered Coating on Russian RGT Graphite

Coating Microstructures Achieved With 100 % B_4C Precursor Composition

Coating formed after eutectic melting (B_4C + C reaction)

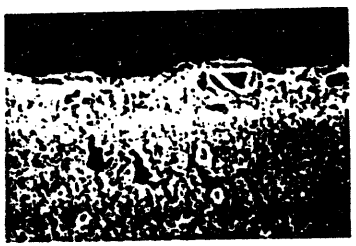

Coating is the result of B_4C penetration/conversion of the graphite substrate. Typical thin coating retained when dewetting occurs.

Substrate: Ringsdorfwerke EK 98 graphite
Images: Scanning electron microscope (SEM) secondary-electron images of cross-sectioned specimens.

Summary of Important Findings from R&D of Reaction-Sintered Coatings

- Boron-rich coatings on carbon substrates can be produced by methods of reaction sintering and eutectic melting of particle precursor layers (i.e., B_4C; mixtures of B_4C + SiC or SiC particles with a B_4C coating; or other boride/carbide mixtures).
- Control of thickness uniformity is achieved with B_4C + SiC mixtures.
- The B_4C-based coatings exhibit eutectic melting between 2200° and 2400°C under rapid heating in beams or plasma. Adherence of coating is maintained. The coating reduces the release of carbon at high temperature.
  - The coating method is attractive for:
    - Coating PFC's for near-future fusion devices,
    - Developing multiphase microstructure and multi-component composition coatings on graphite or carbon-carbon composite materials, and
    - In situ repair of eroded PFC surfaces (i.e., use heat sources such as laser beams, plasma/NBI, or induction heating) to provide new PFC design options.
- General Atomics is continuing R&D and evaluation of boron-rich coatings on PFC's.
  - Collaborations are on-going with:
    - KFA (Jülich, Germany)
    - Triniti Laboratory (Troitsk, Russia)
    - JAERI (Naka, Japan)

Session VII

Boundary Layer Plasmas

ITER Gas Target Divertor Modeling and Experimental Simulation

L. Schmitz, B. Merriman, A. Grossman, M. Day, L. Blush,
R. Doerner, R. Lehmer, F. Najmabadi, R. W. Conn
IPFR/UCLA

D. Stotler, PPPL

Presented by L. Schmitz

U.S./Japan IIIF/PMI Workshop
January 24-27, 1994
San Diego, CA

Outline

Introduction

1 1/2-D Modeling of ITER Divertor Scenarios

Recent PISCES-A Experimental Results and Modeling
(Momentum Balance, Pressure Balance, Flux Limit)

Summary / Future Work

Schematic of Highly Radiative (Gas Target) Divertor

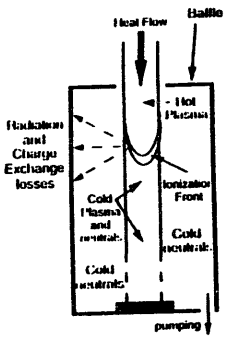

Detachment requires:

$\lambda_{in} << L_{div} B_\phi / B_\theta$

$\lambda_{ion} < d$

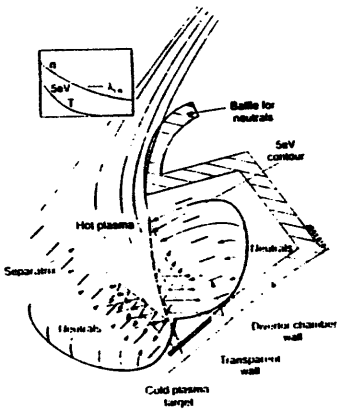

Conceptual Design of ITER Gas Target Divertor

Radiative/Gas Target Regimes for ITER

I. <u>High Density</u> Gas Target Divertor:

An Ionization Front is Produced by Interaction of the Plasma with a Neutral Gas Layer. The Plasma is Detached. The Divertor Heat Flux is Dissipated by Deuterium Line Radiation and/or Radial Transport (Volume Recombination or Gas Recirculation)

- Closed Divertor "Channel", High Target Neutral Pressure (≥ 1 Torr)

  Concerns: ***Radiation Trapping, Sidewall Sputtering, Stability of Ionization Front, Localized Radiation Layer***

II. Low Density Gas Target:

A Large Fraction (≤ 90%) of the Boundary Heat Flux is Dissipated by Impurity Radiation Inside or Outside the Separatrix.

- Moderately Open Divertor, Moderate Pressure (< 0.1Torr, D radiation and CX to Dissipate Momentum and Residual Energy)

  Concerns: ***Ion Heat Flux May not be Reduced Sufficiently, Required Impurity Concentration May be Too Large (Ignition Quenching), Radiative Instability***

ITER Gas Target Divertor Modeling Capabilities

1 1/2-D Coupled Plasma/Neutral Fluid Code (B. Merriman):

- Fully implicit code; solves plasma fluid equations with two species neutral diffusion model with high grid resolution (≤ 1600 pts)
- Sheath boundary conditions for momentum and heat flux
- Hydrogen atomic and molecular physics is included (H, H_2, H^+, H_2^+, H_3^+)
- Some perpendicular effects are included (recycling, distributed gas sources and pumping, perpendicular plasma transport)
- Benchmarked with PISCES-A data

2-D Plasma Solver (M. Day):

- Fully implicit code; accommodates wide range of physics models and multi-species, multi-group neutrals; robust, efficient numerics
- Flexible, non-orthogonal geometry
- Code is Benchmarked with ASDEX and PISCES-A data
- Higher order interpolation schemes are being implemented

2-D or 3-D DEGAS Simulations (A. Grossman):

- Used to calculate H and H_2 neutral distribution, wall loading, baffling and pumping requirements in realistic divertor geometry

ITER Gas Target Divertor Modeling

Present Status:

A fully implicit 1 1/2-D plasma/neutral model indicates possible high density gas target solutions ($P_{sep} \leq 200$ MW; 133 MW outboard, $n_{sep} \geq 3 \times 10^{19}$ m^{-3}, kT_e, $kT_{i,x} \leq 170$ eV)

Two scenarios have been explored:

A) Volume recombination scenario

B) Gas Injection/Recirculation Scenario (requires large radial plasma transport)

- ITER magnetics, closed slot divertor ($L_{pol} = 1.5$m, $a = 0.2$m)
- 2-D plasma profiles constructed by solving along $\underline{B}$ for various radii. Prescibed radial profiles at x-point

The DEGAS code is then used to calculate the 2-D neutral distribution and wall loading (A. Grossman)

ITER Model Equations

Atomic & Molecular Hydrogen Diffusion Equations

$$\frac{\partial}{\partial t} n_H + \frac{\partial}{\partial z}(-D_H \frac{\partial}{\partial z} n_H) = S_{n_H}$$

$$\frac{\partial}{\partial t} n_{H_2} + \frac{\partial}{\partial z}(-D_{H_2} \frac{\partial}{\partial z} n_{H_2}) = S_{n_{H_2}}$$

$$D_\alpha = \frac{kT_\alpha}{\mu_\alpha \nu_\alpha},$$

$$\alpha = H, H_2$$

Plasma Continuity Equation

$$\frac{\partial}{\partial t} n + \frac{\partial}{\partial z}(n v_{\rm pol}) = S_n$$

Plasma Parallel Momentum Equation

$$\frac{\partial}{\partial t}(M_i n v_\parallel) + \frac{\partial}{\partial z}(M_i n v_\parallel v_{\rm pol} + \frac{B_p}{B} P - (\frac{B_p}{B})^2 \eta \frac{\partial}{\partial z} v_\parallel) = S_{v_\parallel}$$

$$v_{\rm pol} = \frac{B_p}{B} v_\parallel$$

Electron & Ion Energy Equations

$$\frac{\partial}{\partial t}(\frac{3}{2} n k T_e) + \frac{\partial}{\partial z}(\frac{5}{2} n k T_e v_{\rm pol} + q_e) = S_{T_e}$$

$$\frac{\partial}{\partial t}(\frac{3}{2} n k T_i) + \frac{\partial}{\partial z}(\frac{5}{2} n k T_i v_{\rm pol} + q_i) = S_{T_i}$$

$$q_\alpha = \frac{q_{s,\alpha} q_{fl,\alpha}}{|q_{s,\alpha}| + q_{fl,\alpha}},$$

$$\alpha = e, i$$

Particle Balance in a Gas Target Divertor Relying on Volume Recombination

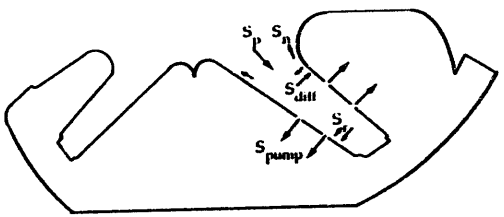

$$S_p = \underbrace{(S_{\rm diff} - S_r + S_{\rm recomb})}_{S_{\rm pump}} + \underbrace{S_n}_{\approx 0}$$

If Radial Transport Small: $\boxed{S_{\rm pump} \approx S_{\rm recomb} \approx S_p}$

ITER Gas Target Divertor with Volume Recombination (1½-D Model)

$T_{i,e\ sep}$ = 120 eV
n_{sep} = 3 x 10^{13}/cm^3
B field: ITER outer divertor magnetics
$D_\perp$ = D_{Bohm} + $D_{Classical}$
Pulling: none
Recombination
Recycling: $R_{sidewall,\ target}$ = 1.0

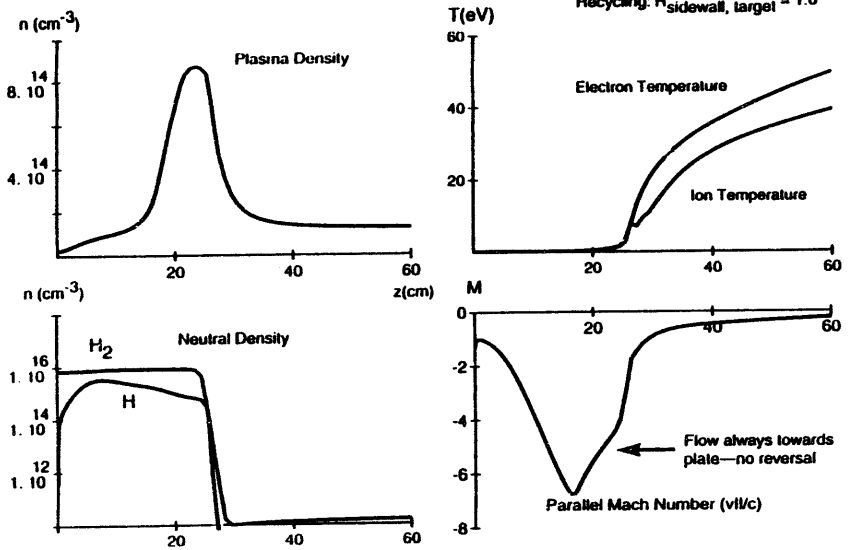

ITER Gas Target Divertor with Volume Recombination (1½-D Model)

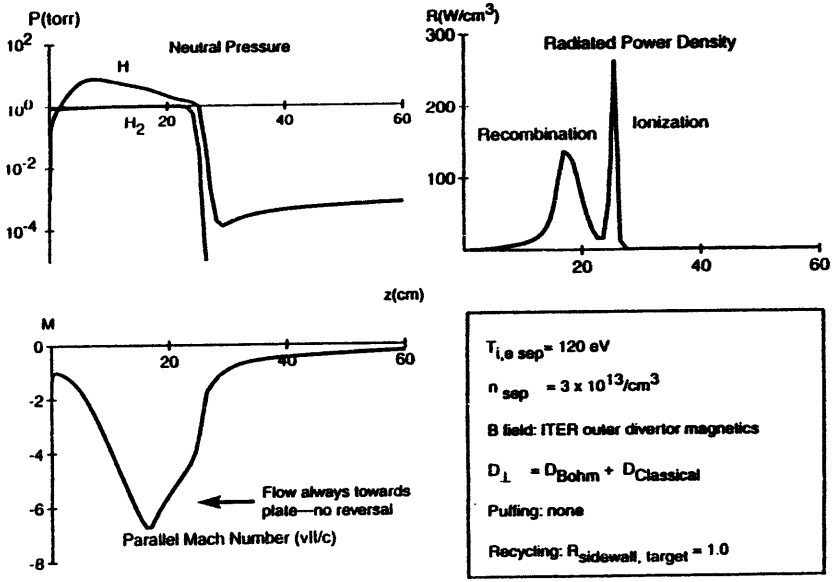

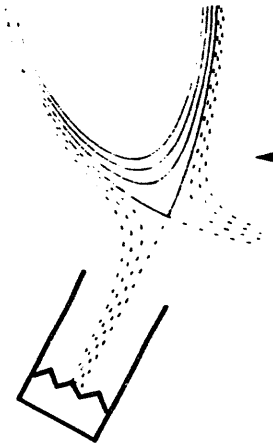

Poloidal View of
Gas Target Divertor

1 1/2 - D Model :

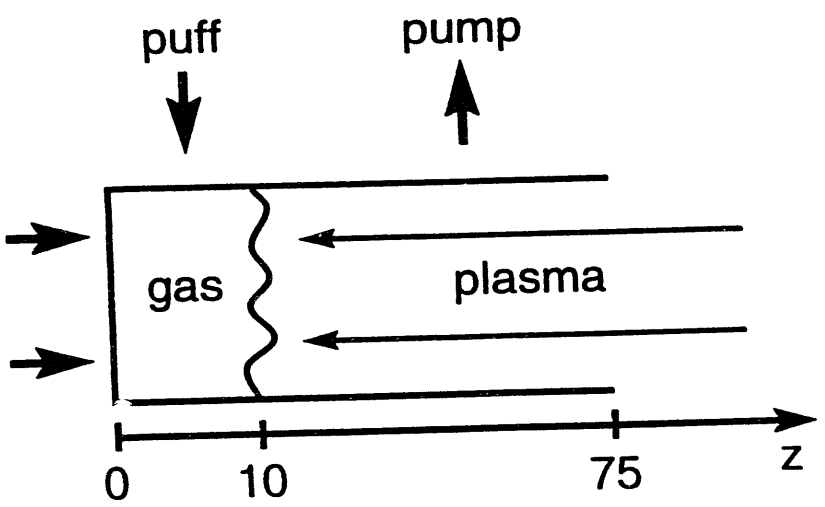

|| Braginskii Flow + ⊥ Diffusion

Particle Balance in a Gas Target Divertor

With Strong Gas Injection

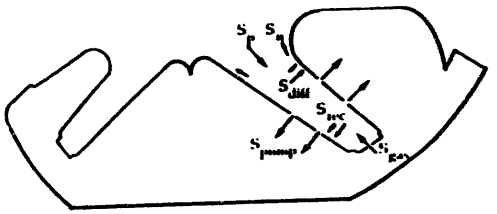

$$S_{gas} + S_p = \underbrace{(S_{diff} - S_{rec})}_{S_{pump}} + \underbrace{S_n}_{\sim 0}$$

$$\boxed{S_{diff} \geq S_{gas} + S_p} \Rightarrow \text{Large Radial Transport Required}$$

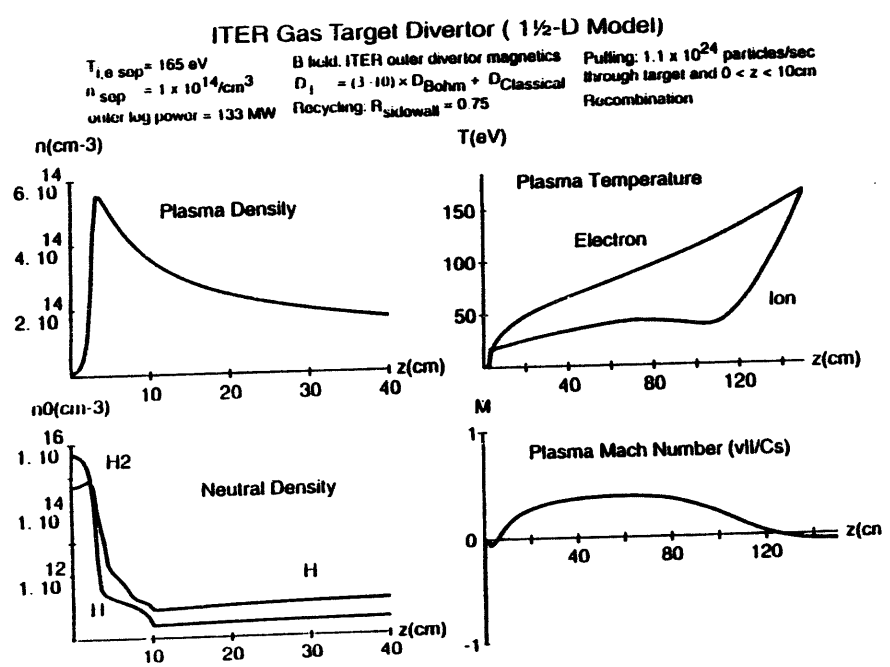
ITER Gas Target Divertor (1½-D Model)
T_i,e sep = 165 eV
n_sep = 1 x 10^14/cm^3
outer leg power = 133 MW
B field, ITER outer divertor magnetics
D_⊥ = (3 -10) x D_Bohm + D_Classical
Recycling: R_sidewall = 0.75
Pulling: 1.1 x 10^24 particles/sec through target and 0 < z < 10cm
Recombination
n(cm-3)
Plasma Density
z(cm)
T(eV)
Plasma Temperature
Electron
Ion
z(cm)
n0(cm-3)
H2
Neutral Density
H
H
z(cm)
M
Plasma Mach Number (vII/Cs)
z(cm

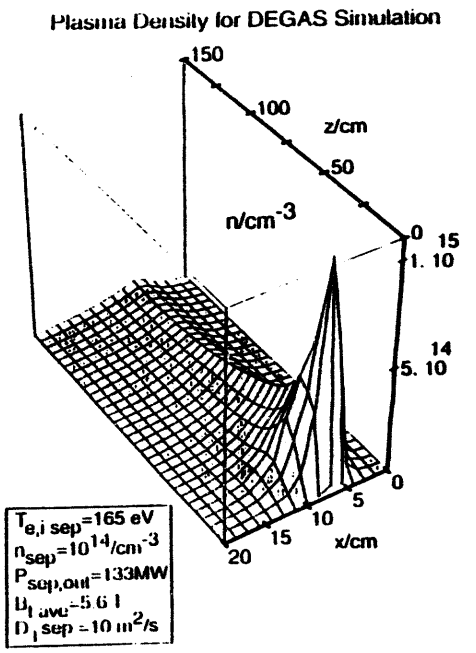
Plasma Density for DEGAS Simulation
z/cm
n/cm^-3
x/cm
T_e,i sep=165 eV
n_sep=10^14/cm^-3
P_sep,out=133MW
B_t ave=5.6 T
D_⊥ sep =10 m^2/s

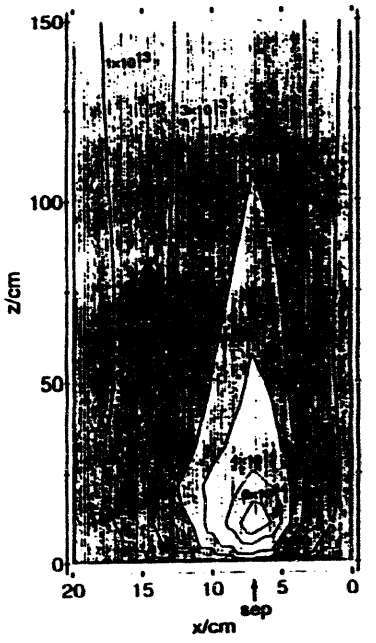
z/cm
sep
x/cm

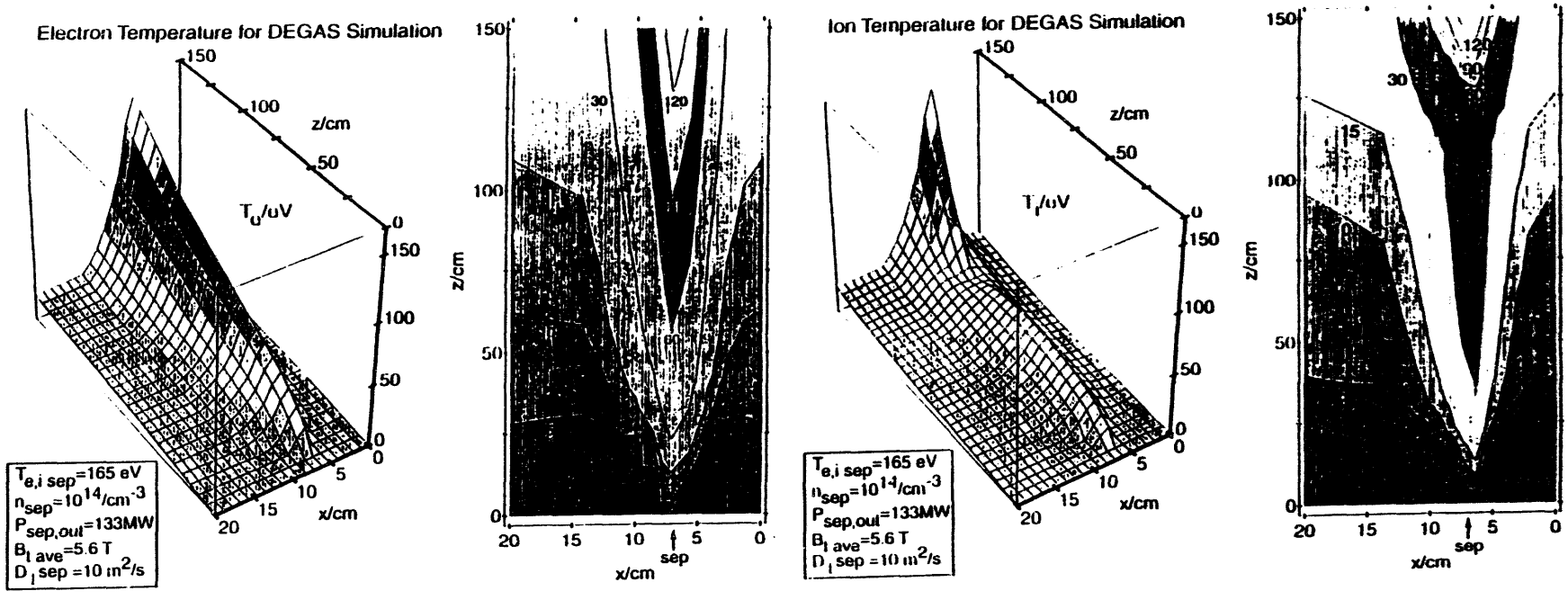
Electron Temperature for DEGAS Simulation
150
100
z/cm
50
0
T_e/eV
150
100
50
0
0
5
10
15
20
x/cm
$T_{e,i}$ sep=165 eV
$n_{sep}=10^{14}/cm^{-3}$
$P_{sep,out}$=133MW
B_t ave=5.6 T
$D_\perp$ sep =10 m^2/s
150
100
50
0
z/cm
30
120
60
20
15
10
5
0
sep
x/cm
Ion Temperature for DEGAS Simulation
150
100
z/cm
50
0
T_i/eV
150
100
50
0
0
5
10
15
20
x/cm
$T_{e,i}$ sep=165 eV
$n_{sep}=10^{14}/cm^{-3}$
$P_{sep,out}$=133MW
B_t ave=5.6 T
$D_\perp$ sep =10 m^2/s
150
100
50
0
z/cm
30
120
90
15
20
15
10
5
0
sep
x/cm

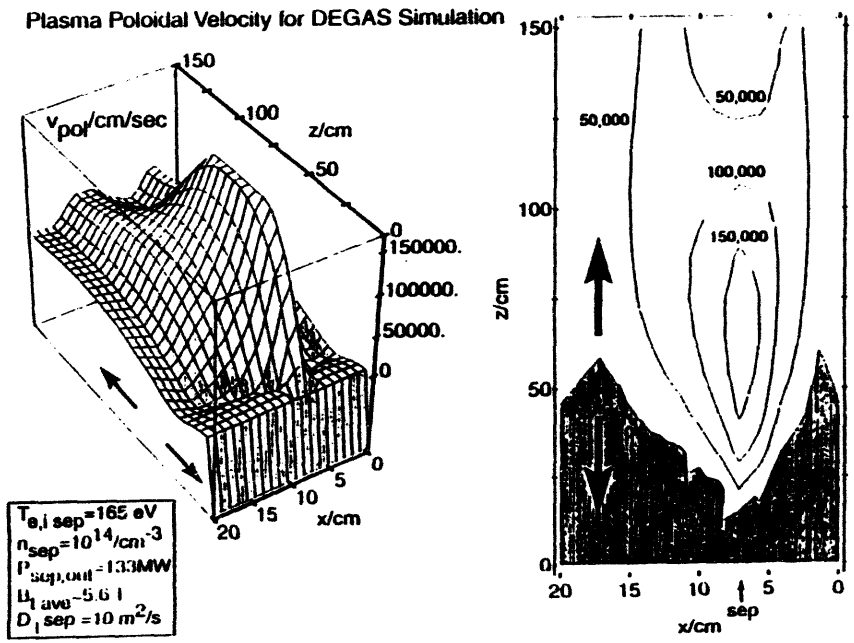

ITER Gas Target Divertor Modeling

IPFR/UCLA

Preliminary Results:

- "Detached" solutions ($kT_e \leq 3$ eV, $n_{target} \leq 10^{20}$ m^{-3}) have been found for $P_{sep} \leq 200$ MW).

  High separatrix density ($n_{sep} \leq 10^{20}$ m^{-3}) is required (Lower densities work for smaller P_{sep}).

  Line radiation tends to be strongly peaked and localized poloidally.

Active Gas Injection Scenario:

- Stable Solutions are found, but large particle diffusivity is required to control the particle inventory (avoid reversed flow): $D_{pump} > 10$ m^2/s
- Strong divertor pumping is necessary ($Q > 3 \times 10^4$ Torr l/s), possibly at some intermediate location upstream from the density peak.
- A substantial portion of the input power is dissipated by charged particle losses to the (slot) side walls.

Volume Recombination Scenario:

- Transient Solutions (stable on a 3 ms timescale) have been obtained with collapsed ion and electron temperatures (≤ 1 eV).

  The key factor is very high plasma density within the ionization front (≥ 5x 1021 m-3), leading to recombination rates comparable to the local ionization rate.

- Large radial particle diffusivity is not required.

- Stability depends critically on momentum damping. Correct treatment of the plasma momentum balance is essential. Momentum loss to neutrals (and, subsequently, the slot walls), may prevent plasma detachment and/or produce reversed plasma flow.

PISCES Gaseous Divertor Experiment

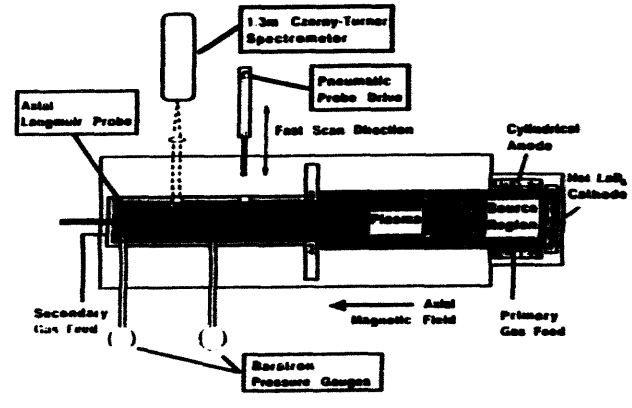

	$(Q_{\perp})^{peak}$ (MW/m^2)	B_{tot} (T)	kT_e^{sep} (eV)	kT_i^{sep} (eV)	λ_{cx}/R	λ_{ion}/R
PISCES-A	≥ 8	0.2	≤ 30	2.5	≥ 2	≥ 0.4
ITER	130-600	4.6	200	150-300	≥ 0.1	≥0.02

H^+ -- H_2 Gas Target: Plasma Pressure is Nearly Balanced by Neutral Pressure

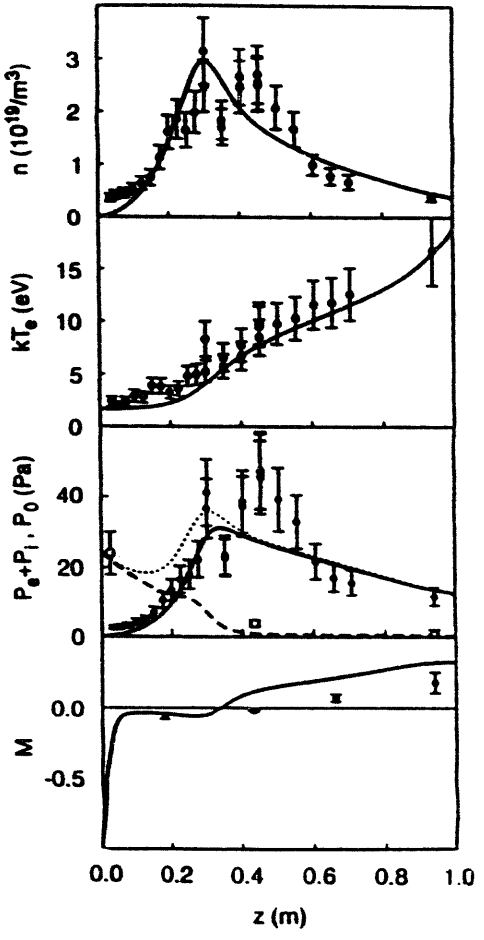

$q_{e\ source} \leq 7\ MW/m^2$

$q_{e\ target} \leq 0.22\ MW/m^2$

$Q_{rad} + Q_{ion} \sim 0.97\ Q_e$

H^+ -- H_2 Gas Target: Plasma Pressure is Nearly Balanced by Neutral Pressure

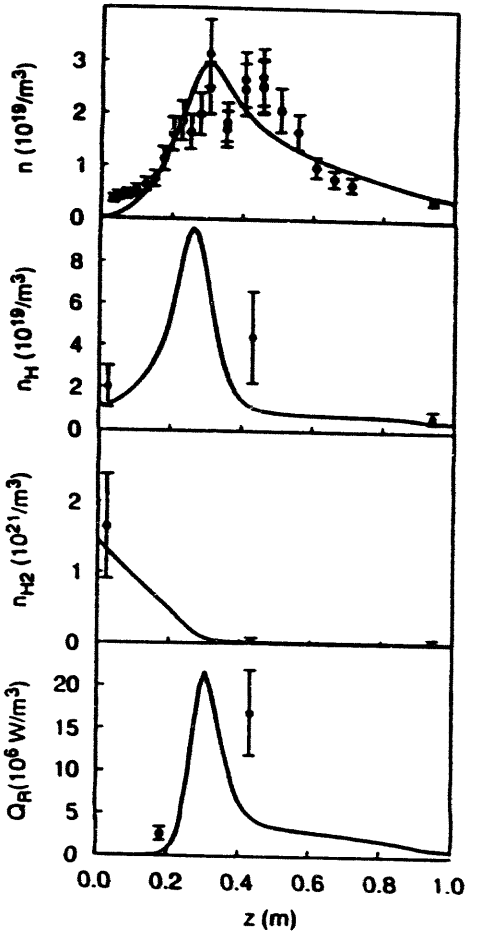

$q_{e\ source} \leq 7\ MW/m^2$

$q_{e\ target} \leq 0.22\ MW/m^2$

$Q_{rad} + Q_{ion} \sim 0.97\ Q_e$

Plasma Pressure can be Much Larger than Neutral Pressure in Argon Gas Target

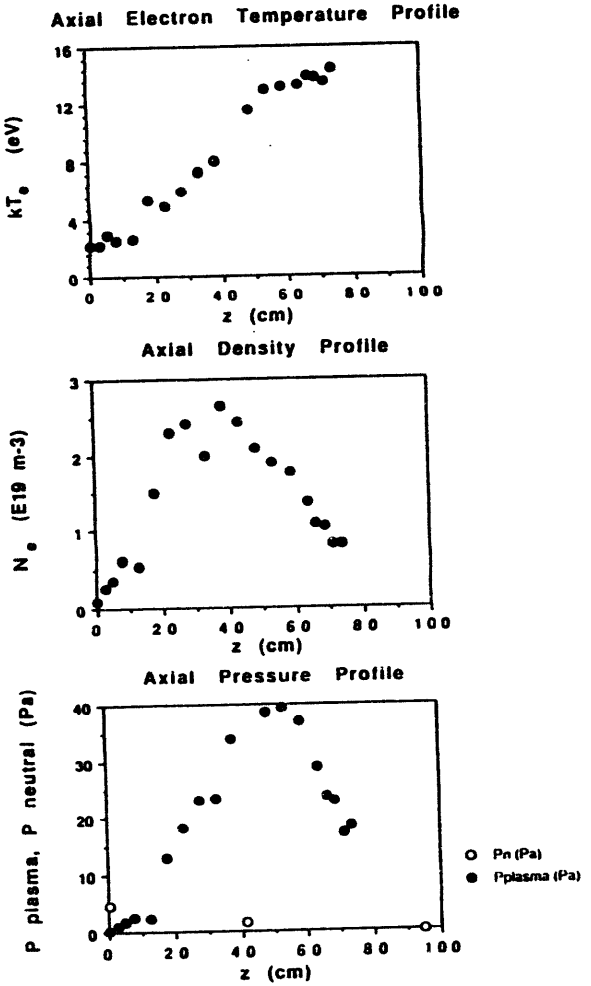

Plasma Momentum Balance

Balance equation:

$$\frac{\partial}{\partial z}\left(m_i n v_i^2 + n kT_i + n kT_e\right) = - m_i n v_i \left(\nu_{cx} + \nu_{in}\right)$$

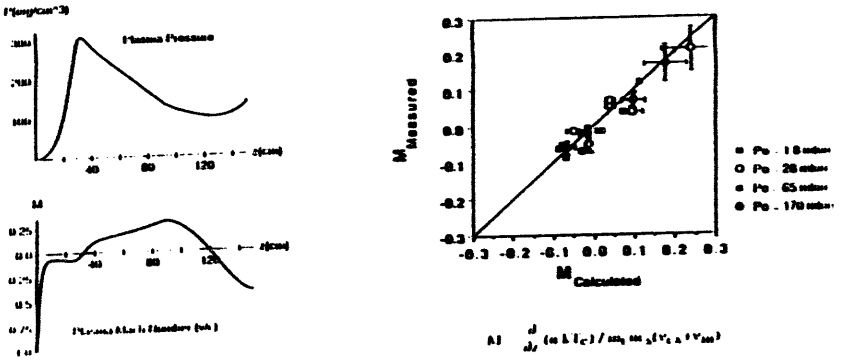

Plasma momentum is dissipated by ion-neutral collisions in PISCES!
The plasma flow speed is subsonic and severely damped.
A flow reversal is driven by the reversed pressure gradient.

The Parallel Electron Heat Flux is Classical with a Flux Limit $q/q_f = 0.5$

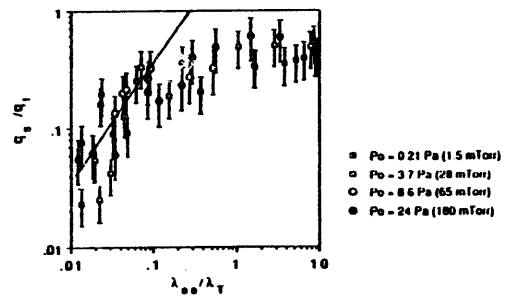

Free streaming limit: $q_f = (2/m_e)^{1/2}\, n(kT_e)^{3/2}$ $\qquad q_s/q_f \sim \lambda_{ee}/\lambda_T$

Spitzer heat flux: $q_s = 3.2\ (1/m_e\nu_{ee})n(kT_e)^{5/2}\,\partial kT_e/\partial z$

Gas Target Divertor Simulation in PISCES-A

L. Schmitz, L. Blush, R. Lehmer,
G. Tynan, B. Merriman, R. W. Conn
IPFR, UCLA

- Stable, detached ionization front demonstrated for $q_e \leq 7$ MW/m^2 (high density hydrogen plasma with typical divertor parameters $n_e < 2\times10^{13}$ cm^{-3}, $kT_e < 20$ eV)
- Up to 97% power dissipated on side walls (59% hydrogen line radiation, 38% CX and dissociated neutrals)
- Target electron temperature decreased to 2.5 eV
- Moderate neutral backflow due to plasma plugging ($p_{target}/p_s \leq 0.02$)
- Flow reversal due to strong gas puffing (momentum dissipation by neutrals)

Future Modeling/ Experimental Contributions

ITER Modeling:

- 2-D fluid modeling of ITER gas target scenarios (advanced numerics, 2-species diffusion or multi-group neutral model, impurities)
- realistic (non-orthogonal) geometry
- Study ionization front/plasma detachment with distributed puffing
- Helium transport (He_0, He^+, He^{2+})
- DEGAS runs for realistic ITER divertor geometry (non-orthogonal grid, He included)

Future Modeling/ Experimental Contributions

Experimental Work (PISCES-A and PISCES-Upgrade):

- Proof-of-principle tests of radiative divertor scenarios ($q_e \leq 35$ MW/m^2, $n_e \leq 20^{20}$ m^{-3}, $kT_e \leq 30$ eV)
- $kT_i \approx 10$-20 eV by ICRH to investigate ion cooling (charge exchange and ion-neutral collisions
- Dynamics of ionization front with distributed puffing (Momentum balance, 2-D flow pattern)
- Study radiative cooling by impurities (and radiative stability) (Injection of Ne, Ar, and Xe into high density hydrogen plasma)
- Investigate baffling schemes, pressure balance between hot and cold neutrals (divertor channel geometry) (Experiments as well as 2-D DEGAS simulations)

1.3m Czerny-Turner Spectrometer
Main Magnets
Anode
Antenna
Source Magnets
Cathode
Target Plate
Axial Langmuir Probe
Secondary Gas Valves
Neutralizer Tube
Trim Magnet
Baratron Gauge
Pump
B
RF, 1-2 MHz ≤ 5 kW
Pump
Primary Gas Feed
0.90 m
0.55 m

Modeling of Radiative and Gaseous Divertor Operation

Robert B. Campbell

Sandia National Laboratories

Dana A. Knoll

Paul R. McHugh

Idaho National Engineering Laboratory

Paper VII.2 at

U.S.-Japan Workshop Q181
High Heat Flux Components and Plasma Surface Interactions for Next Devices

San Diego, California
January 24-27, 1994

Sandia National Laboratories
Idaho National Engineering Laboratory

Talk Outline

- Definition of Problem
- Modeling Approach
- Description of Models
  - 1-D multifluid (SNL-NM)
  - 2-D multifluid (INEL)
- Modeling of Experiments
  - D III-D
  - C-Mod
- Modeling of ITER
  - Beryllium Transport
  - Radiative/Gaseous Divertor
- Future Directions

Sandia National Laboratories
Idaho National Engineering Laboratory

The Gas Target/Radiative Divertor is proposed to solve the high heat load problem in ITER

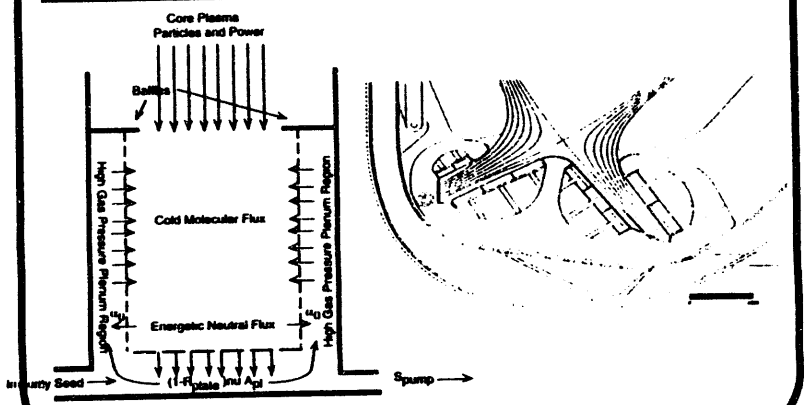

Sandia National Laboratories
Idaho National Engineering Laboratory

A two pronged approach is being taken to provide physics solutions to the ITER divertor problem.

Heat removal on plasma facing components is a major problem to be solved in ITER

Impurity control is crucial for long pulse operation.

We must understand divertor impurity entrainment under strongly collapsed, ultra-high recycling divertor conditions.

Parallel force balance of each separate impurity charge state is solved in 1-D, with full non-equilibrium radiation of an intrinsic impurity (e.g. beryllium or carbon) and an injected impurity (e.g. nitrogen or argon)

This 1-D impurity transport work is being implemented in 2-D, started from a reduced charge state impurity model now have multicharge state impurities, to include important cross field effects on both background and impurity fluids.

Example simulations of experimental devices and high power ITER computations follow to demonstrate this capability.

Sandia National Laboratories
Idaho National Engineering Laboratory

60.460/RBC/011994/61

Two-dimensional simulations are being performed at high power with the NEWEDGE code.

- Multifluid (ion, electron, neutral atom, choice of "average" impurity or multispecies) on a 2-D curvilinear, multiply connected geometry Non-orthogonal grids and tilted divertor plates treatable rigorously
- Hydrogenic atoms followed with convection-diffusion equation (inertia ignored in neutral momentum). Collisional-radiative corrections to rate coefficients. Volume recombination included.
- Momentum exchange between ions and neutrals through charge exchange is included (neutral pressure).
- "Non-equilibrium" ,"Average impurity", transport and radiation is performed using available atomic rate data.
- Neutral particle flows controlled by recycling and non-escape probabilities through slotted divertor walls.
- Local kinetic flux limiting of electron and ion heat fluxes.

Sandia National Laboratories
Idaho National Engineering Laboratory

We are also simulating experiments and ITER with a rapidly running 1-D code.

- Multi-charge state, multispecies self-consistent transport along B, with model terms for radial effects.
- Two hydrogenic neutral models have been considered:
  - Multiply-charge exchanged hydrogenic atoms and molecules followed in 1-D with diffusion theory.
  - Simple transport theory for first flight neutral hydrogen, full momentum balance for multiply charge exchanged group.
- Momentum exchange between ions and neutrals through charge exchange is included.
- Supersonic flow boundary conditions at the target are treated.
- Full non-equilibrium (i.e. "non-coronal") transport and radiation is performed using available atomic rate data.
- Neutral particle flows controlled by recycling and non-escape probabilities through slotted divertor walls.
- Local kinetic flux limiting of electron and ion heat fluxes.

Sandia National Laboratories
Idaho National Engineering Laboratory

Alcator C-Mod is being simulated in 1-D and 2-D

- Impurity (carbon) entrainment studies in 1-D. With and without D2 puffing. Low power ohmic heating shots.

  Before puffing, radiation zone is near the divertor plates

  After puffing, changes in divertor hydrogen flows cause (in the simulation) radiation zone move to the X-point.

  This compares well with the experimental observations.

- Puffing (D2 and Argon) studies are being performed in 2-D at high power (e.g. 4MW into SOL).

  Both D2 and Argon (quasi-avg. ion model) can reduce heat load by factors of 10 or more

  Extent of argon radiation zone is greater than the hydrogen zone. The cooling from the argon also extends the influence of the hydrogenic neutrals.

Sandia National Laboratories
Idaho National Engineering Laboratory

Alcator C-Mod Crossection

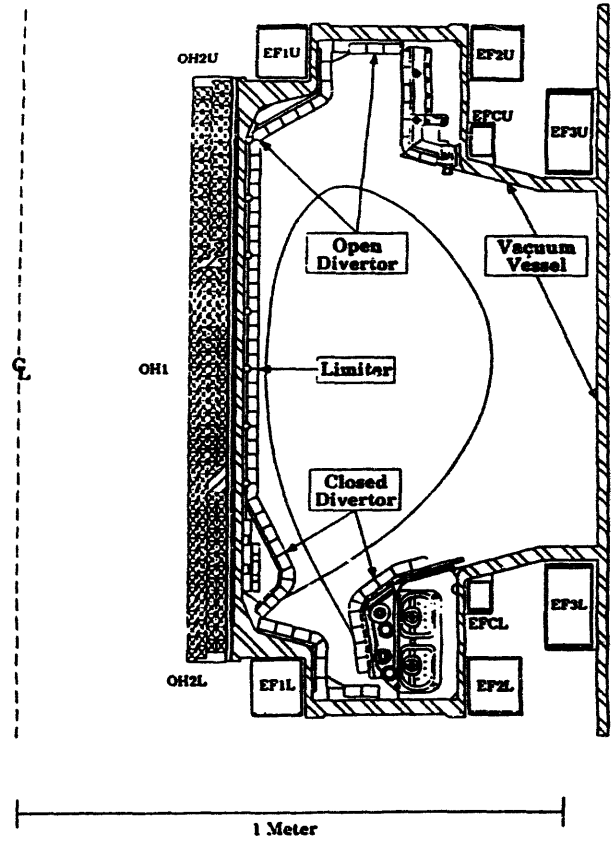

Before puffing, the Carbon Radiation is Localized to the Divertor Plate

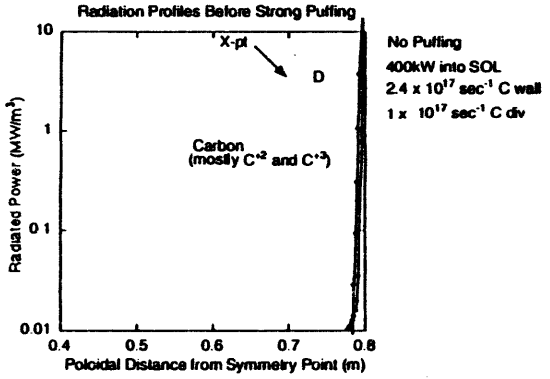

Sandia National Laboratories
Idaho National Engineering Laboratory

After Puffing, the Carbon Radiation Zone Moves Out to the X-point

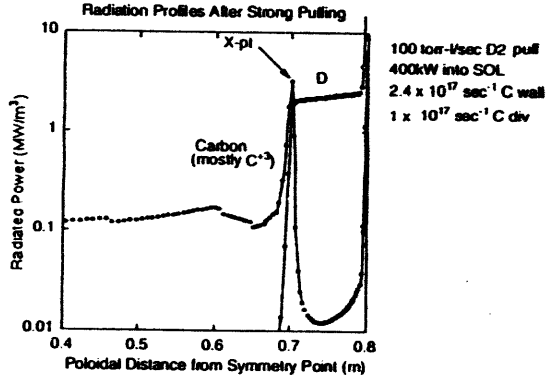

Sandia National Laboratories
Idaho National Engineering Laboratory

Alcator C-MOD Gaseous/Radiative Divertor, Deuterium and Argon Puffing

- Core B.C.'s n-1.7e20 (1/ m**3), Ti - Te - 100 eV
  Power crossing sep - 4.2 MW
  Q parallel approx 1 Gw/m**2
  1.5 Mw hydrogen Radiation before puffing

- After puffing 6.0e19 argon/sec (60/40)

  2.0 Mw neutral radiation
  1.6 Mw argon radiation
  3.6 Mw total 85 %

- After puffing 2.4e22 deuterium/sec (80/20)

  2.6 Mw neutral radiation 62 %
  Net particle flow is into core

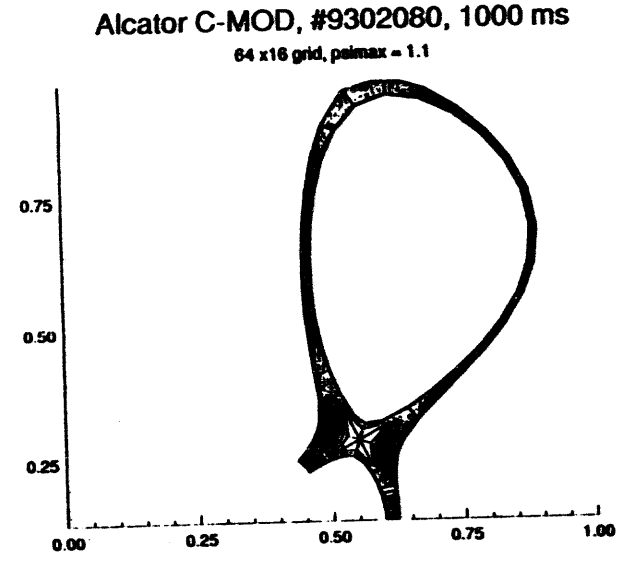

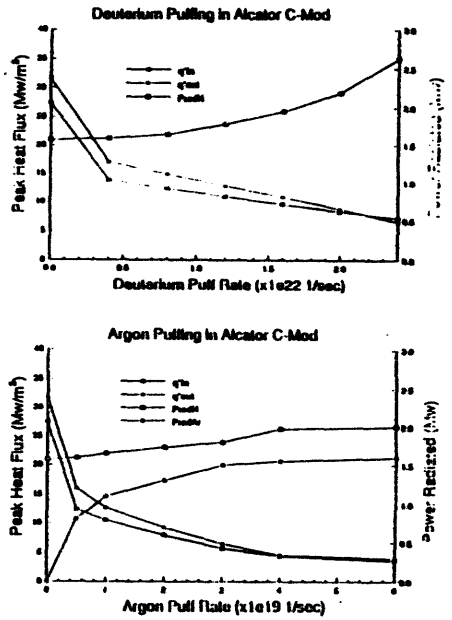

We are modeling D III-D in support of several projects

INEL

Radiative Divertor Upgrade

- Neutral impurity gas baffling (1-D)
- Strongly tilted slot walls to amplify recycling (2-D non-orthogonal)
- Performance of radiative divertor configurations (1-D and 2-D)

Ongoing experiments on existing machine

- Impact of neutral impurity confinement on core contamination
- Deuterium and Neon puffing experiments, role of intrinsic impurities.

Sandia National Laboratories
Idaho National Engineering Laboratory

One-D modeling examines the power handling capabilites of a slot/cold plasma/radiative divertor.

- Scrapeoff Layer Power 16MW (reflects upgraded D III-D power).
- Deuterium Molecular Puffing 300 t-l/sec puffed to outer divertor. Hydrogenic puffing alone at this strength does not cool divertor plasma adequately.
- What Argon puffing is required to extinguish the divertor plasma, and is it possible to maintain entrainment?
- Neutral albedo 0.95, hydrogen recycle 0.98, 50% in molecules, 15cm slot length. (ΔZ(wid,Ar,0)=0.25m along B, ~ 1 cm poloidally)
- The best steady state solution (28 t-l/sec Ar) we've found so far is shown below.

$N_{sep} = 2.5 \times 10^{19} m^{-3}$ $P_{ca} = 1.1$ MW

$Q_{peak} = 0.13$ MW/m^2 (outer) $N_{Ar,sep} = 6.5 \times 10^{17} m^{-3}$

$P_{rad} = 11$ MW (8MW Ar) $Z_{eff,sep} = 3.3$

$P_{brems} = 1.5$ MW

Sandia National Laboratories
Idaho National Engineering Laboratory

One-D calculations have been performed for D III-D with D2 and Argon puffing

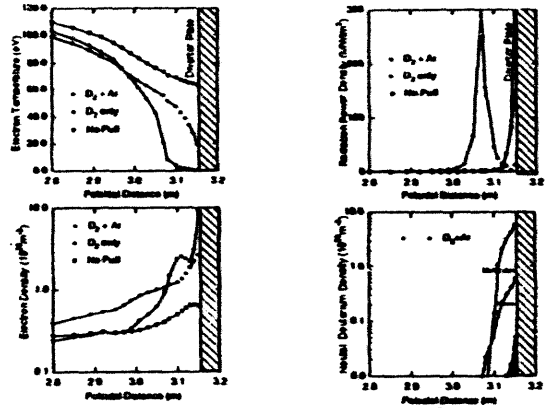

Sandia National Laboratories
Idaho National Engineering Laboratory

The fate of Neon neutrals have an important effect on maintaining core plasma purity.

INEL

Modeling of Neon Entrainment in D III-D, Shot 79349

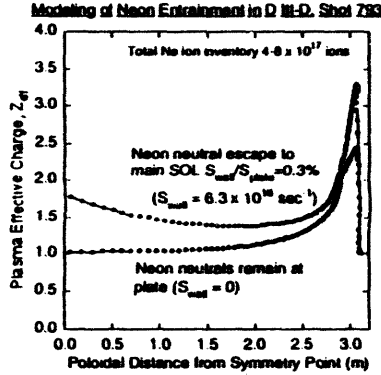

Sandia National Laboratories
Idaho National Engineering Laboratory

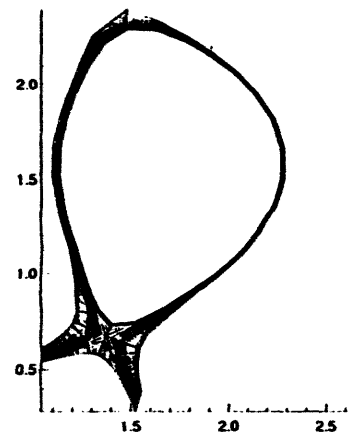

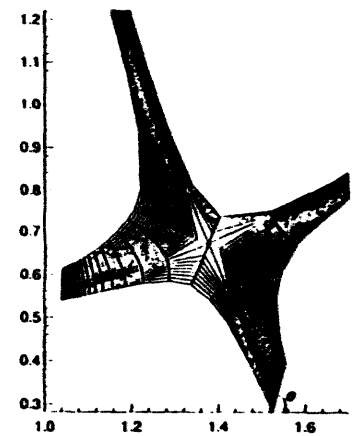

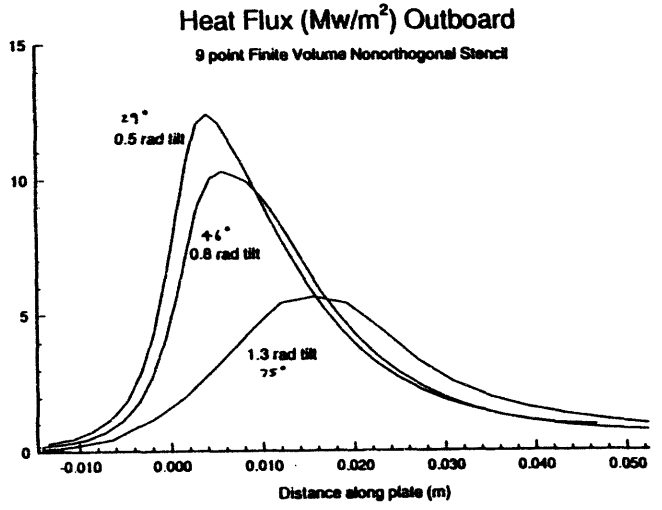
Heat Flux (Mw/m^2) Outboard
9 point Finite Volume Nonorthogonal Stencil
0.5 rad tilt
0.8 rad tilt
1.3 rad tilt
Distance along plate (m)

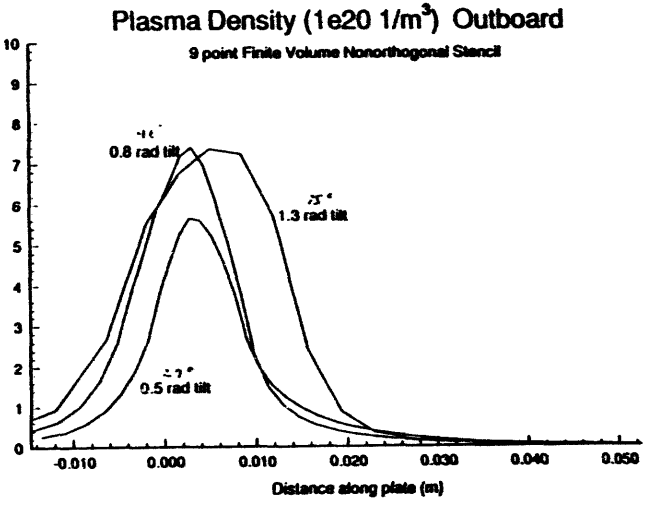
Plasma Density (1e20 1/m^3) Outboard
9 point Finite Volume Nonorthogonal Stencil
0.8 rad tilt
1.3 rad tilt
0.5 rad tilt
Distance along plate (m)

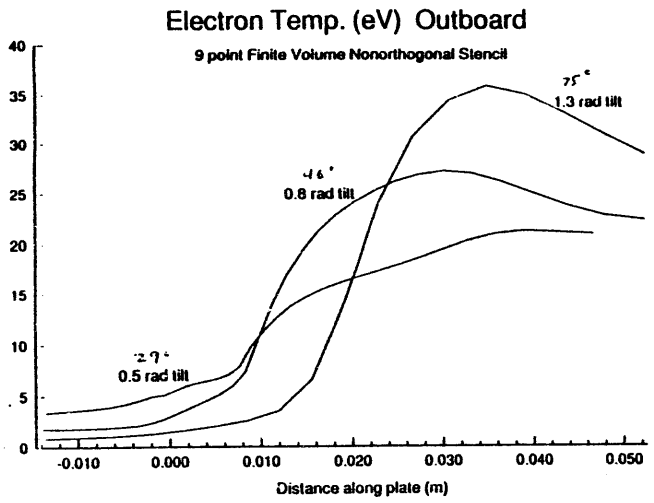

We have modeled ITER from various perspectives with the 1-D and 2-D work coordinated closely.

INEL

ITER Gaseous/Radiative Divertor Properties

- 1-D collapse at high power
- 2-D collapse difficult because of radial penetration of cooling gas.

Transport and entrainment of intrinsic and injected impurities

- Argon in radiative divertor
- Beryllium in high recycling divertor

Sandia National Laboratories
Idaho National Engineering Laboratory

One-dimensional simulations of ITER shed light the width of the radiation zone along the slot.

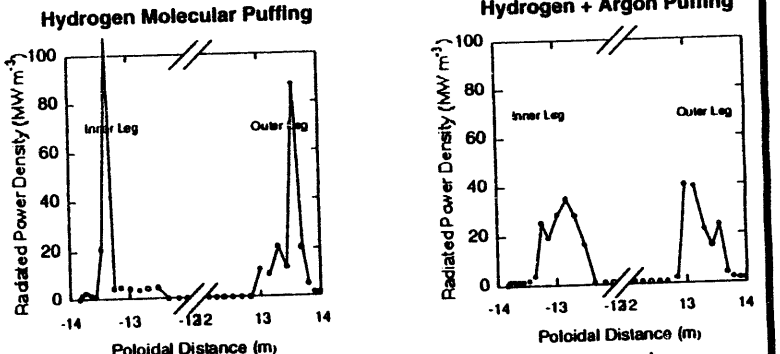

Calculations with intrinsic beryllium impurity instead of argon have been performed as well.

Sandia National Laboratories
Idaho National Engineering Laboratory

We have been successful in collapsing the divertor plasma in ITER @ 3250MW with Argon plus recycled DT, although neutral pressure is too high!

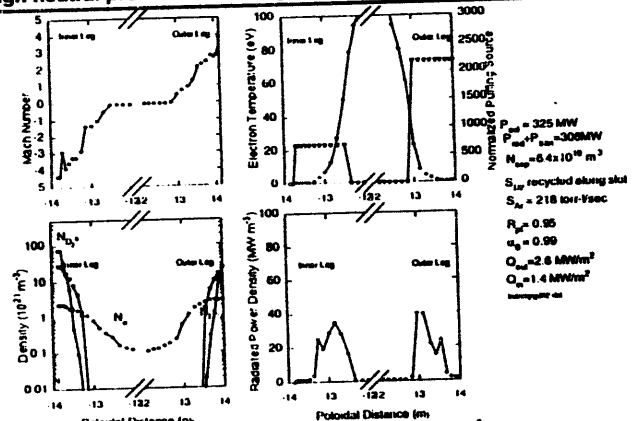

Sandia National Laboratories
Idaho National Engineering Laboratory

Impurities are well entrained if the hydrogen recycle fluxes in the divertor region are high enough.

INEL

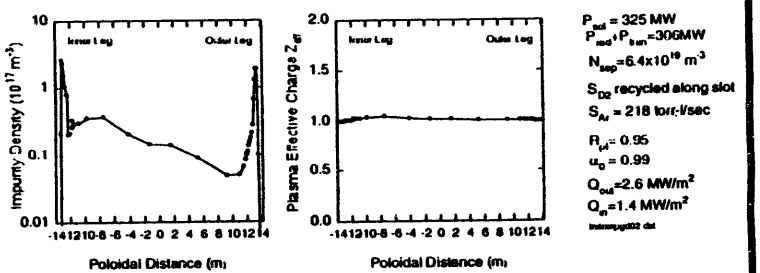

P_{sol} = 325 MW
P_{sol}+P_{beam}=306MW
N_{sep}=6.4x10^{19} m^{-3}
S_{D2} recycled along slot
S_{Ar} = 218 torr-l/sec
R_{pf}= 0.95
α_0 = 0.99
Q_{out}=2.6 MW/m^2
Q_{in}=1.4 MW/m^2

Sandia National Laboratories
Idaho National Engineering Laboratory

But at lower separatrix density, Argon can be poorly entrained

INEL

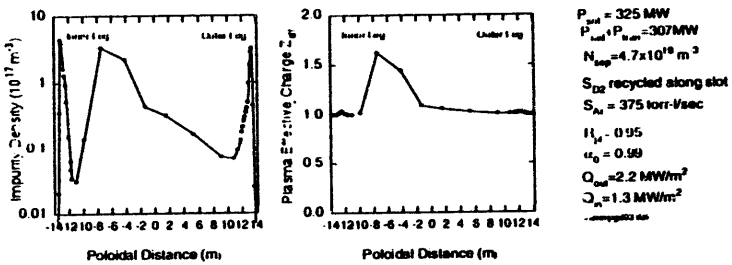

P_{sol} = 325 MW
P_{sol}+P_{beam}=307MW
N_{sep}=4.7x10^{19} m^{-3}
S_{D2} recycled along slot
S_{Ar} = 375 torr-l/sec
R_{pf} = 0.95
α_0 = 0.99
Q_{out}=2.2 MW/m^2
Q_{in}=1.3 MW/m^2

In addition, from the D III-D simulations, the baffling of the argon *neutrals* must be effective as well.

Sandia National Laboratories
Idaho National Engineering Laboratory

Beryllium transport in ITER is quite sensitive to background flows

INEL

For the Plasma Edge Theory meeting, we have performed both 1-D and 2-D transport studies of beryllium in the ITER divertor.

Flow reversal has an important effect on entrainment under high recycling conditions in 2-D.

Particle flows leaving the core plasma can be effective in isolating Be in the divertor region for parameters expected for ITER, but precise end wall conditions are important.

Wall sources of impurities (e.g. charge exchange sputtering of Be) can dominate the particle balance of Be in the SOL. Implies that "entrainment" of the divertor generated impurities may be moot.

Because of the sensitivity of the divertor impurity flows, all the relevant force terms should be in the models, including ExB and diamagnetic flows.

Virtually no models being used for cold plasma target studies have the proper terms.

Sandia National Laboratories
Idaho National Engineering Laboratory

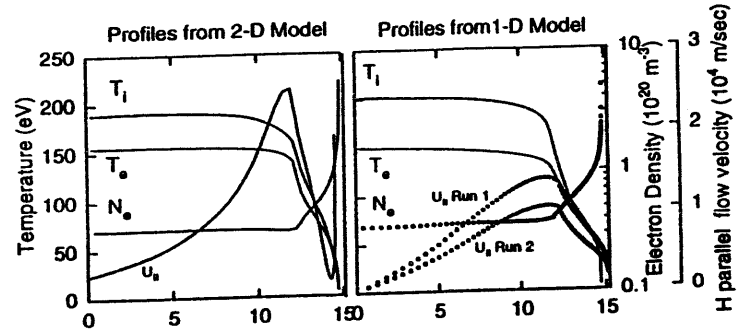

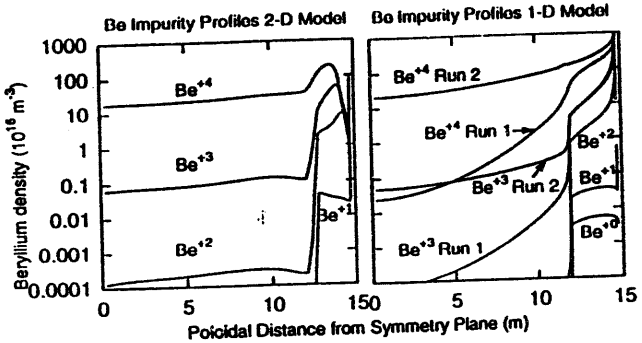

Figure 1-Comparison between 1-D and 2-D Profiles

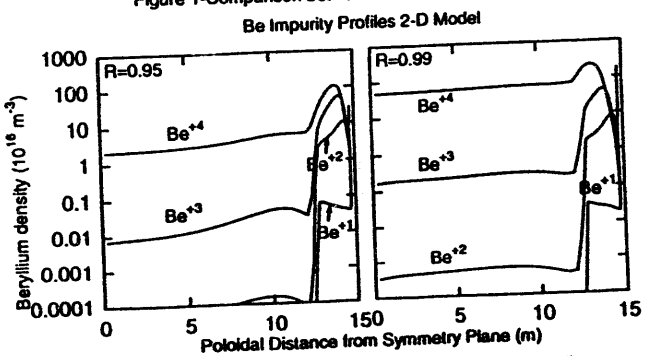

Figure 2- 2-D Be profiles as a function of plate recycling

Treat the 2-D transport of background flows in the edge plasma through the full Braginskii equations.

INEL

The usual fluid equations which are assumed to describe transport in the edge plasma of a tokamak are parallel or poloidal projections of the Braginskii equations

Ad-hoc "anomalous" diffusive radial terms of particles, momentum, and energy are added, replacing radial momentum balance.

Are these equations an accurate representation of transport in the scrape-off layer and divertor regions?

It may be useful to compare the solutions obtained from these semi-quantitative equations with the full two-fluid Braginskii equations.

Under the assumption of toroidal symmetry, we obtain 2-D balance relations for densities, temperatures, velocities, and electric potential in a suitable 3-D coordinate system.

Under this formulation, the fluid drifts appear in a natural and rigorous manner

Sandia National Laboratories
Idaho National Engineering Laboratory

Status of quasi-2D model

INEL

The contours of constant temperature resemble skewed parabolas

Cold recycled neutrals enter divertor region from walls in private region and outside region, their velocity is primarily radial.

The radial velocity of these cold neutrals when mapped to a system along the field is increased by an effective enhancement of $2/\Delta$, since they need to only travel a short distance radially to effectively fuel and cool the volume. (Watkins and Rebut)

This velocity enhancement (or equivalently lengthening of the mean free path) is important for cold neutral penetration, particularly for a machine like ITER, where the ionization mean free path in regions of interest is extremely short.

It is important to note that work has been reported using full Monte Carlo for neutrals (EIRENE) in ITER which still is plagued with the poor penetration characteristics of cold neutrals.

Work is in progress to distinguish between poloidal and radial directions in the coordinate transformation.

Sandia National Laboratories
Idaho National Engineering Laboratory

MODELING OF GAS TARGET SCENARIOS USING DEGAS

A.Grossman, L.Schmitz, B.Merriman, R.W.Conn

IPFR, UCLA

D.P.Stotler

PPPL

U.S./Japan HHF/PMI Workshop

San Diego, California January 24-27, 1994

Outline:

A. Introduction

B. Gas Target Models (Two Scenarios)

C. Particle and Energy Balance

D. 3D Model

E. Summary and Future Work

ITER Gas Target Divertor Modeling

- Input data for DEGAS obtained from $1\frac{1}{2}$D plasma/neutral model.
- 2-D plasma profiles constructed by solving along B for various radii.
- We have investigated a scenario with:

$$P_{sep} \leq 200MW$$

$$n_{sep} \geq 10^{20}m^{-3}$$

$$kT_e, kT_{i\ sep} = 170eV$$

- DEGAS code calculates 2-D atomic and molecular neutral distributions and wall loadings.

Two Possible Scenarios

I Gas Target Relying on **high radial plasma transport.**

(Large $D_\perp$).

II Gas Target Relying on **volume recombination.**

(Utilize new atomic data recently added to DEGAS to extend the range to lower temperatures and higher densities where recombination is important).

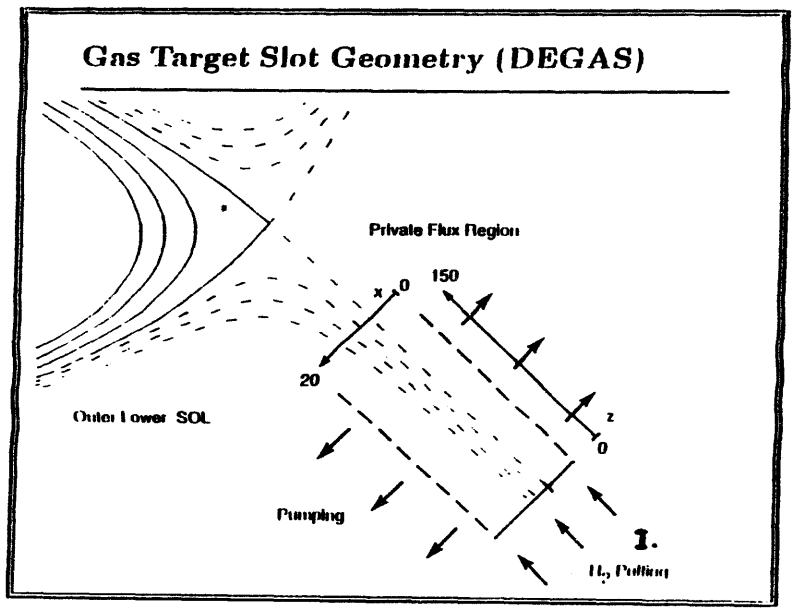
Gas Target Slot Geometry (DEGAS)
Private Flux Region
150
x
0
20
Outer Lower SOL
z
0
Pumping
1.

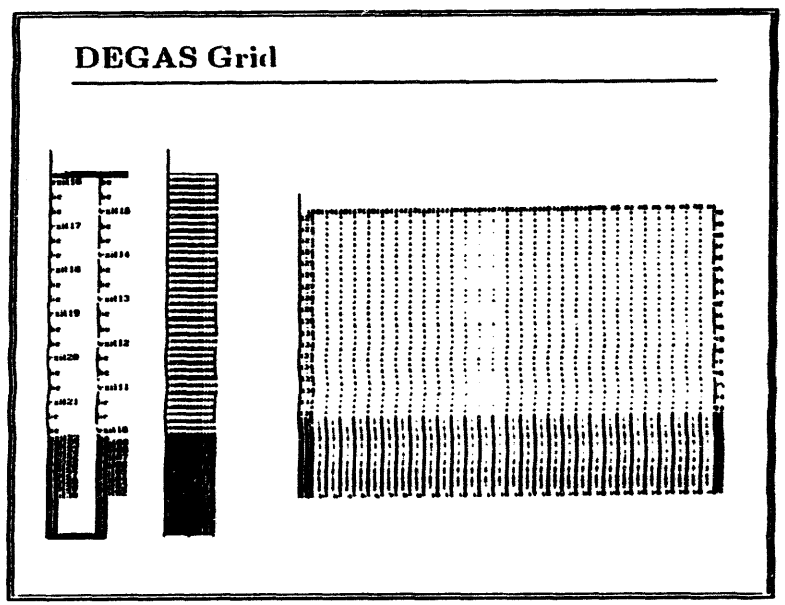
DEGAS Grid

Plasma Density (Scenario I)

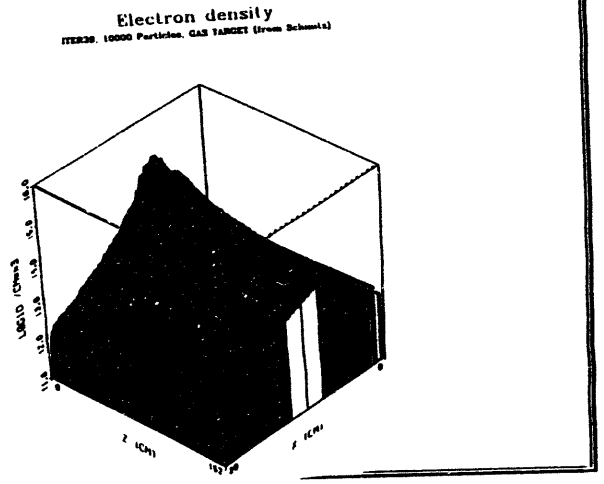

Electron Temperature (Scenario I)

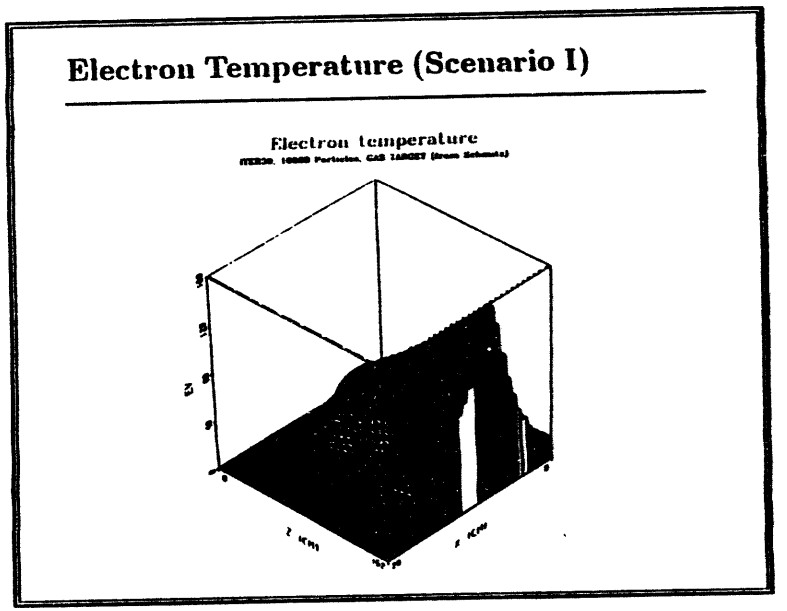

Neutral H Density Profile (Scenario I)

Pulling Needed
Need to Baffle
Strong Pumping Needed

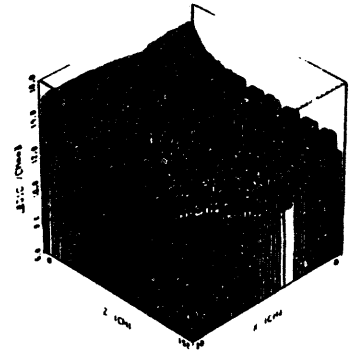

Neutral H Temperature (Scenario I)

- CX sputtering on the upper end of the slot is large.

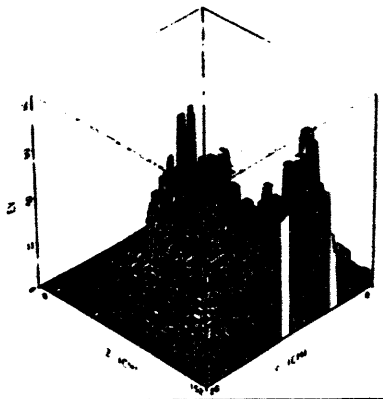

Neutral H Density Profile (Scenario II)

No Puffing Needed
No Need to Baffle
Moderate Pumping

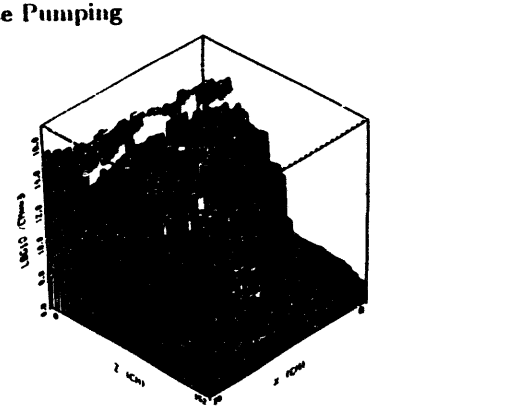

Neutral H Temperature (Scenario II)

- CX sputtering on the upper end of the slot is small.

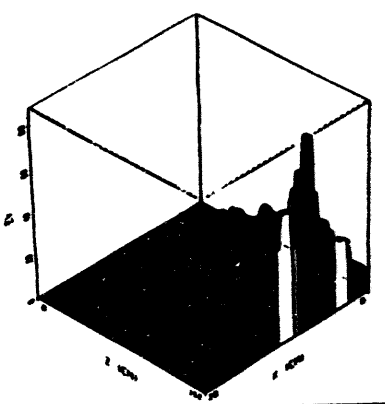

Neutral H_2 Density (Scenario I)

Density of neutral h2

Neutral H_2 Density (Scenario II)

Density of neutral d2

Line Emission Power (Scenario I)

Strongly Peaked.

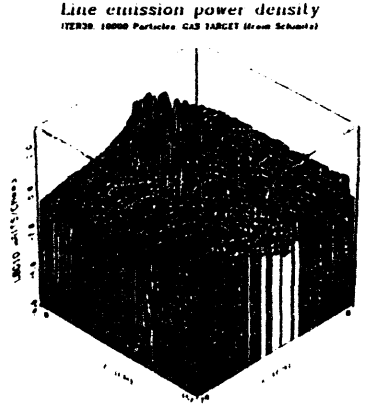

Line Emission Power (Scenario II)

Localized at Target.

Desirable to Increase Slot Width at Target.

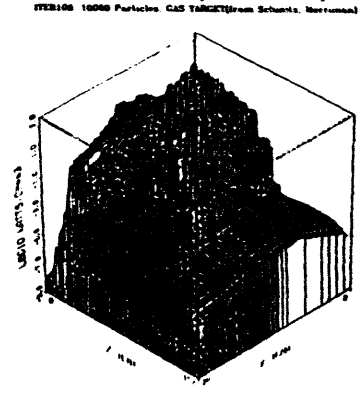

Power On Walls (Scenario I)

Neutral Wall Loading Not Excessive.

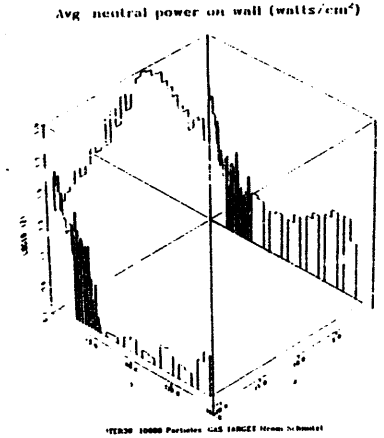

Power On Walls (Scenario II)

Neutral Wall Loading Not Excessive.

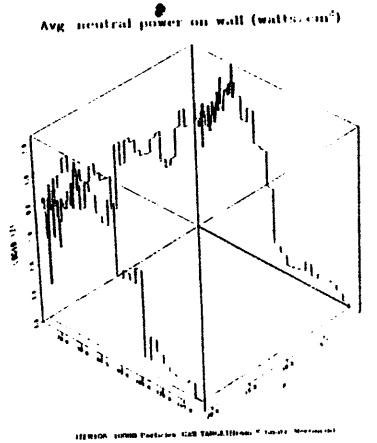

Particle and Power Balance (Scenario I)

NEUTRAL PARTICLE BALANCE (s^{-1})	
Total puffing rate	1.55×10^{25}
Target puffing rate	0.775×10^{25}
Ionization Rate	2.78×10^{25}
Pumping Rate	1.6×10^{25}
$D_\perp = 25\ D_{Bohm}$	

NEUTRAL POWER BALANCE (MW)	
Gain From D_2 Dissociation	16.6
Gain From Charge Exchange Collisions	29.3
Gain From Recycled Neutrals	10.1
Loss to Ion Population	-36.4
Loss to Wall	-21.8

ELECTRON POWER BALANCE (MW)	
Input	128
Ionization Power Loss	-61.6
Line Radiation	35.8
Dissociation Loss	30.5
Loss to Ions	?
Target Power Load	<1.0
Loss to Side Walls	<61

ION POWER BALANCE (MW)	
Input	8.0
Gain From Neutrals (CX, Ionization)	7.1
Gain From Electrons	?
Target Power Load	<1.0
Loss to Side Walls	>14.

Particle and Power Balance (Scenario II)

NEUTRAL PARTICLE BALANCE (s^{-1})	
Total puffing rate	0.0
Target puffing rate	0.0
Ionization Rate	2.99×10^{25}
Pumping Rate	1.81×10^{18}
$D_\perp = 0.5\ D_{Bohm}$	

NEUTRAL POWER BALANCE (MW)	
Gain From D_2 Dissociation	19.6
Gain From Charge Exchange Collisions	14.0
Gain From Recycled Neutrals	1.38
Loss to Ion Population	-24.4
Loss to Wall	-8.9

ELECTRON POWER BALANCE (MW)	
Input	
Ionization Power Loss	-11.1
Line Radiation	150.0
Dissociation Loss	34.9
Loss to Ions	?
Target Power Load	<0.1
Loss to Side Walls	<1.5

ION POWER BALANCE (MW)	
Input	
Gain From Neutrals (CX, Ionization)	10.4
Gain From Electrons	?
Target Power Load	<0.1
Loss to Side Walls	>1.5

I. Rely on High Radial Plasma Transport

- Large radial particle diffusivity (or convection) is required to control the particle inventory ($D_\perp > 10m^2/s$).
- Strong divertor pumping is necessary ($Q > 3 \times 10^4$ Torr/s), possibly at some intermediate location upstream from the density peak.
- Baffling will be required in the x-point region to reduce the neutral backflow to the core plasma by a factor of 100.
- Line radiation is strongly peaked, neutral wall loading is not excessive, but plasma loading close to the x-point may be a problem.

II. Rely on Volume Recombination

- Pumping Requirements are very moderate.
- X-Point Baffling may not be necessary if $D_\perp < 1m^2/s$ (sidewall recycling is small).
- Radiation is very localized poloidally. Increased slot width desirable near the target to spread out radiation wall load.
- Plasma and neutral wall loadings are not excessive.

Summary

- Both scenarios have been sucessfully modelled in 2-D for moderate power ITER cases.
- Volume recombination scenario combines many advantageous properties for ITER (moderate pumping requirements, low plasma sputtering from divertor channel side walls, tolerable heat loads).
- More realistic model geometry under development.

Development of More Realistic Geometry

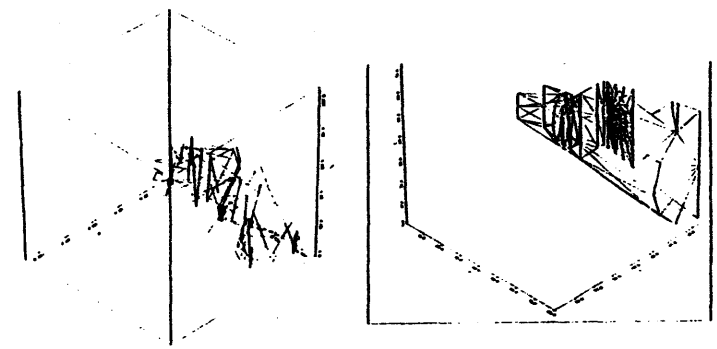

- Geometry part of DEGAS runs on a Workstation
- Interactively develop new geometries.

Possible Gas Target Configurations

Large Recirculating Neutral Flux
Plasma and CX Sputtering in Channel

Internal Recirculation?
Plasma and CX Sputtering in Channel

Possible Gas Target Configurations

Molecular "Blanket"
Plasma and CX Sputtering near X point

Possibly Larger CX Energy Loss
Extensive Baffling Required

Session VIII

Disruptions

US/J Workshop on HHF & PSI for
Next Fusion Devices,
San Diego, CA,
Jan. 24-27, 1994

JAERI

Overview of Disruption Simulations at JAERI

M. Akiba (JAERI)

Studies on Erosion by Simulated Plasma Disruption

JAERI

- Material erosion caused by simulated disruption heat loads has been studied at ~ 1000 °C.
- Materials tested are as follows;
  - Graphite and CFCs
  - B_4C-overlaid CFCs for JT-60
  - W, Mo
- Erosion has been evaluated by the erosion depth and/or weight loss.

Electron beam conditions for disruption and preheating

JAERI

- **Disruption Condition**
  - Electron Energy: 70 keV
  - Electron Current: 4 A
  - Peak Heat Flux: 1800 MW/m²
  - Duration: 1.5 ~ 2.0 ms
  - Bulk Temperature: RT ~ 1100 °C (at irradiation)
- **Preheating Condition**
  - Electron Energy: 25 keV
  - Electron Current: 0.7 A
  - Heat Flux: 0.8 MW/m²

Profile of heat flux of electron beam

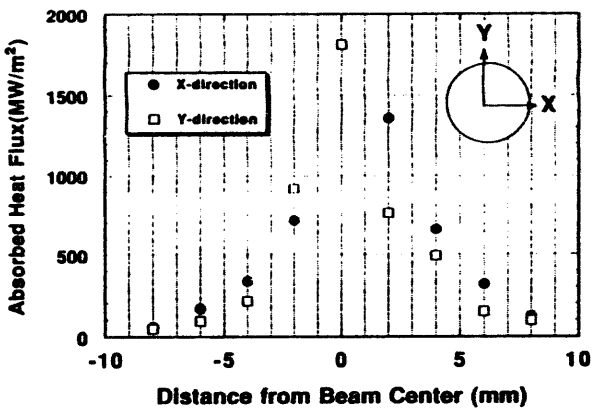

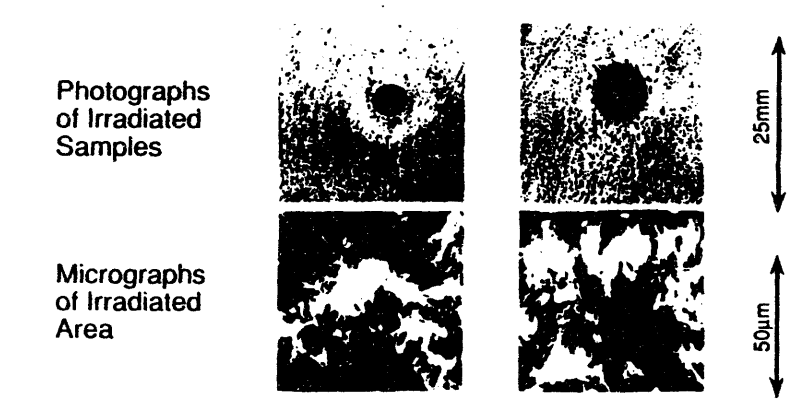

Typical mophologies of MFC-1 after loading

Erosion Loss of Carbon Based Materials at High Temperature

JAERI

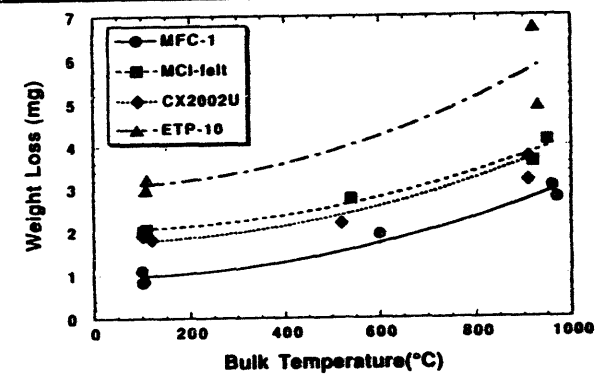

Next fusion devices, such as ITER, require material erosion database under disruption heat loads.

JAERI

- International collaboration becomes rather important in this field.

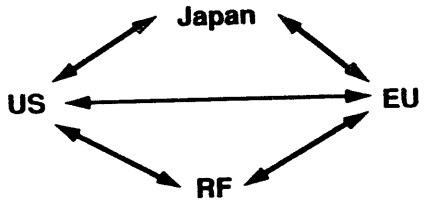

In particular, activities in the US/J collaboration is successful;

JAERI

- Effects of the incident electron energy have been investigated between UNM and JAERI.
- Erosion of high thermal conductivity CFCs have been studied in the plasma gun at UNM, and in the electron beam facility at JAERI.

Our approach was to apply transmission grating spectroscopy in the VUV (20-400 Å), to try to overcome the opacity of these large target plasmas.

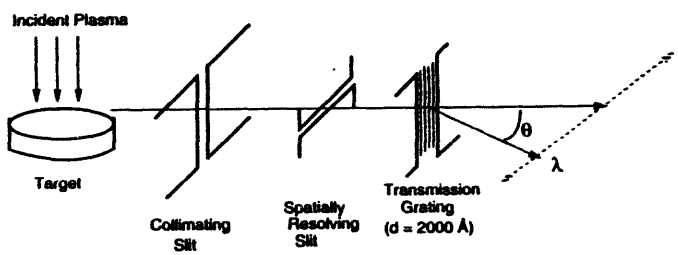

Target types included a variety of potential armor materials and substrates.

- POCO graphite
- ATJ graphite
- OFHC copper
- 1mm plasma sprayed tungsten on copper
- boron nitride

Paul D. Rockett and John A. Hunter
Sandia National Laboratories, Albuquerque, NM

Joseph T. Bradley III and John M. Gahl
Dept. of Electrical Engineering, Univ. of New Mexico, Albuquerque, NM

Anatoly Zhitlukhin, Kolja Arkhipov, Vitalja Bakhtin, and Dima Toporkov
Troitsk Institute for Innovation and Technology (TRINITI), Troitsk, Russia

Ivan Ovchinnikov
D. V. Efremov Institute of Electrophysical Apparatus, St. Petersburg, Russia

Recent Results from the US/RF Disruption Collaboration

-- Adding data to benchmark our disruption codes

Paul D. Rockett

Fusion Technology Dept.

Sandia National Laboratories

Presented to: **US/Japan Workshop**

26 January 1994

San Diego, CA

The goal of these experiments was to measure basic plasma parameters of target interactions in two plasma guns, and compare results to code simulations.

"Estimate $T_{e,i}$, $n_{e,i}$, and impurities vs. space and time"

on: *2MK-200* TRINITI, *Troitsk, RF*

- Incident T_i ~ 1 keV
- pure hydrogen plasma
- incident n_e ~ 10^{15} cm^{-3}
- Max energy density ~ 2 MJ/m^2
- pulselength ~ 20 µsec

and *VIKA* D. V. Efremov Lab., St. Petersburg, RF

- incident T_i ~ 100 eV
- hydrogen and fluorine plasma
- incident n_e ~ 10^{16} cm^{-3}
- Max energy density ~ 100 MJ/m^2
- pulselength ~ 100 µsec

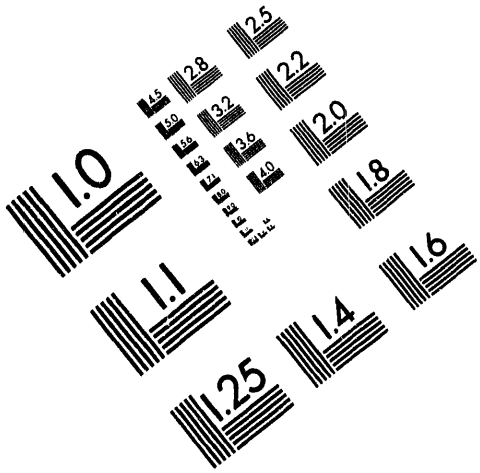

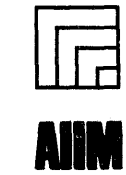

Association for Information and Image Management
1100 Wayne Avenue, Suite 1100
Silver Spring, Maryland 20910
301/587-8202

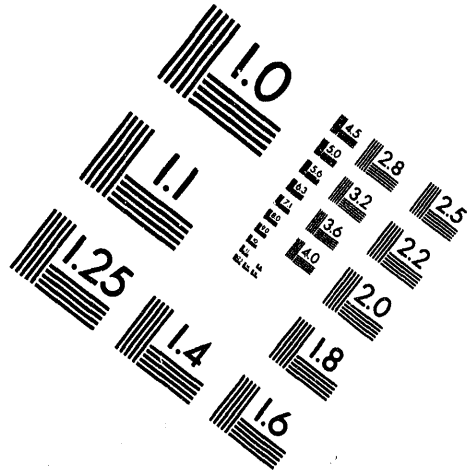

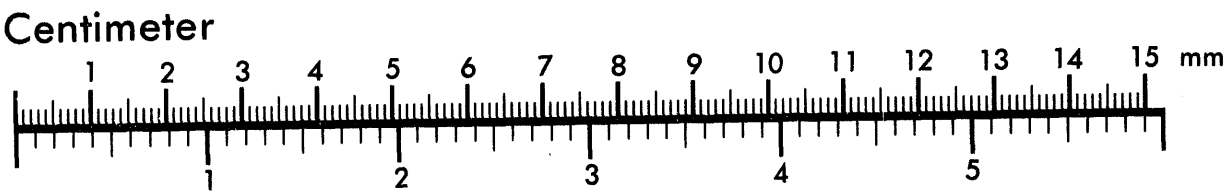

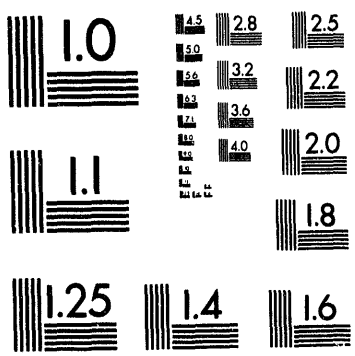

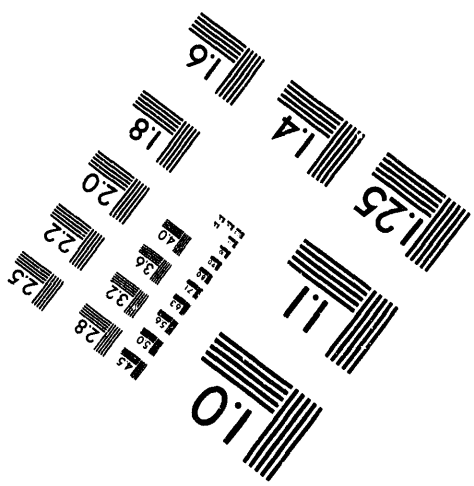

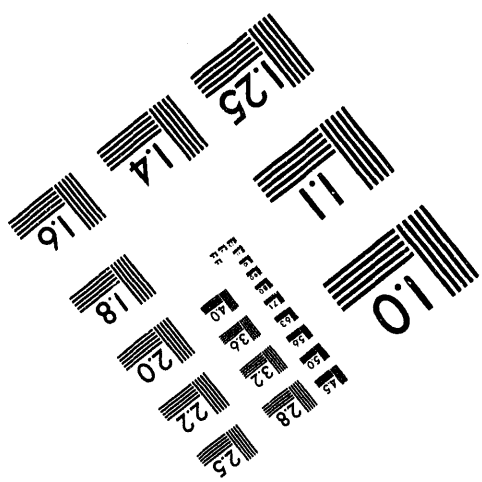

6 of 8

Recorded spectra revealed problems with sample handling and with plasma gun purity.

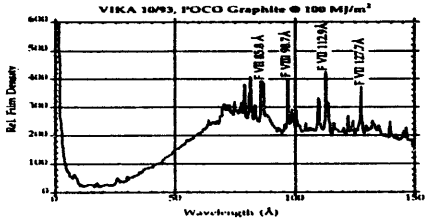

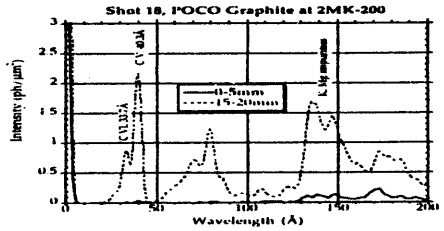

1-D spatial resolution indicated the height of hot regions above the target surface.

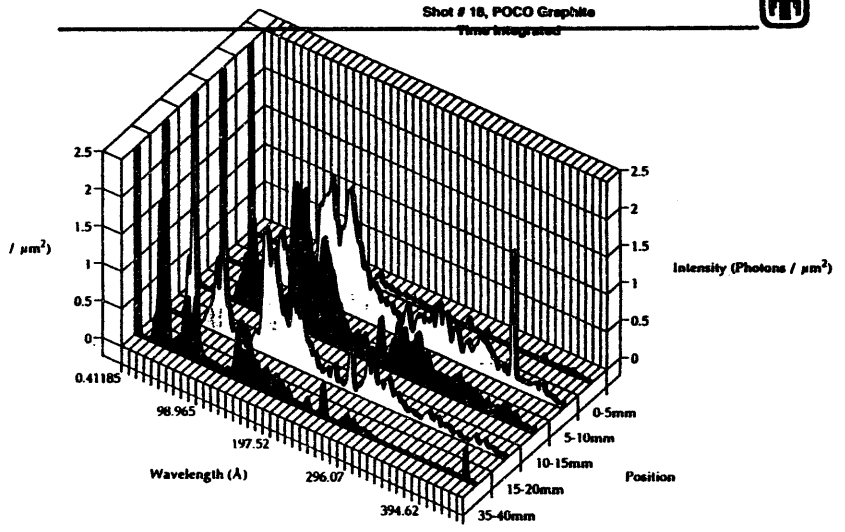

Both plasma gun facilities have received significant diagnostic attention over the last year. TRINITI completed interferometry, optical spectroscopy, and began Thomson scattering.

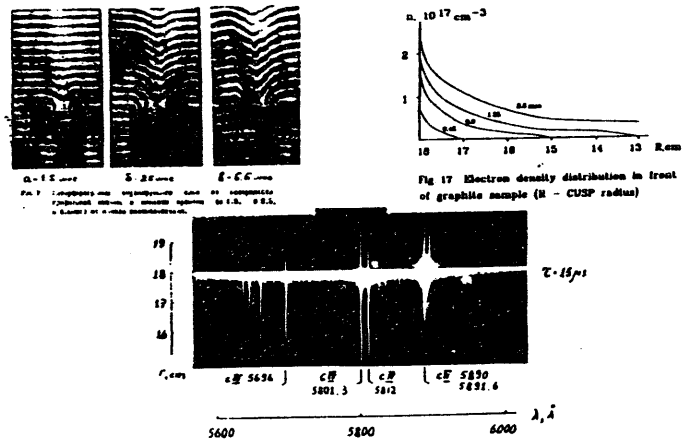

Fig 17 Electron density distribution in front of graphite sample (R - CUSP radius)

D. V. Efremov Labs have utilized interferometry, optical spectroscopy, and 1-D spatially resolved calorimetry to aid in characterizing their target plasma.

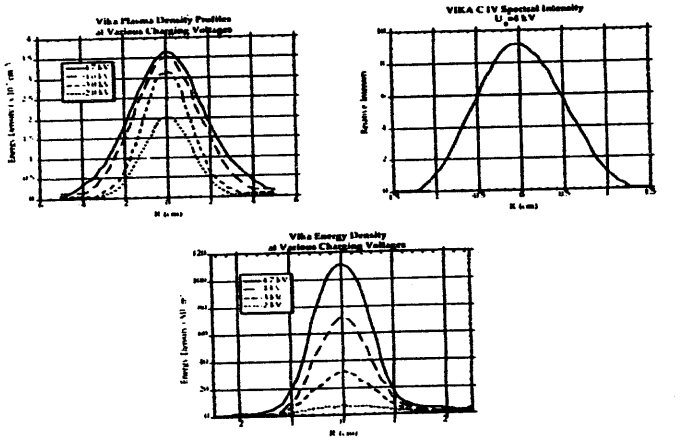

The dominant species observed in VIKA plasma spectra were impurities. No target spectral lines were apparent.

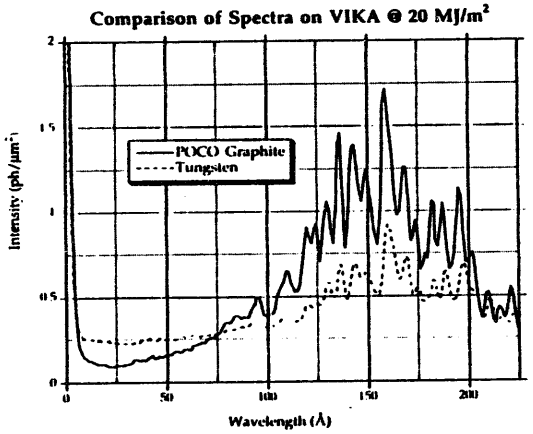

Incident flux in VIKA clearly influenced the plasma temperature, as observed in the level of impurity ionization.

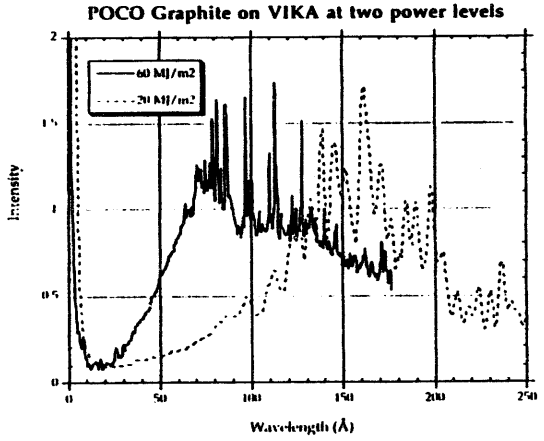

The boron nitride spectrum revealed significant qualitative features, but required greater spectral resolution to elicit plasma densities and temperatures.

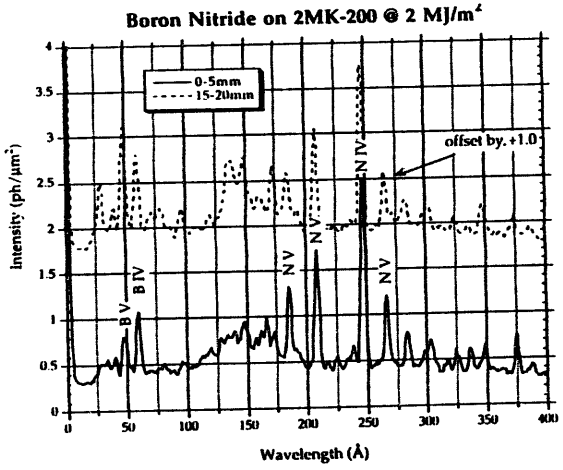

Null shots on VIKA showed the presence of Cu and/or Fe in the incident plasma. Null shots on 2MK-200 were plagued by material ablated from chamber wall surfaces.

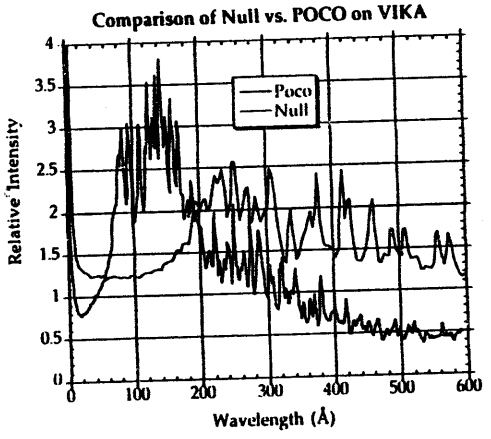

This initial acquisition of VUV spectra successfully identified relevant spectral regions for upcoming high resolution measurements, and isolated problems with impurities, both in the beam plasma and the target.

Phase I is well underway.

Phase II goals:

- Modify spectrograph to permit high resolution with large $\Delta\lambda$
- Utilize bake-out procedure for samples to eliminate hand-borne impurities
- Remove teflon insulators in VIKA, as is already in place in PLADIS
- Analyze spectra for temperature and density as a function of time and space; compare results to erosion rate code calculations

Status of Disruption Modeling and Simulations

Ahmed Hassanein

Argonne National Laboratory

Presented at

US-Japan Workshop Q181 on High Heat Flux Components and Plasma Surface Interactions for Next Devices

San Diego, California

January 24-27, 1994

Personnel Involved/Consulted

• A. Hassanein	ANL, USA
• D. Ehst	ANL, USA
• I. Konkashbaev	TRINITI, RF
• T. Scholz and H. Bolt	KfA, Germany
• V. Kozhevin	Efremov Inst., RF
• J. MacFarlane	UW, USA
• P. Rockett	SNL, USA
• J. Gahl	UNM, USA
• J. Linke	KfA, Germany

Objectives

- Understanding of basic physical *processes during both reactor disruption* and simulation experiments.
- *Accurate modeling of different disruption* simulation experiments (laser-electron beam-plasma gun).
- Define critical parameters and data needed to simulate reactor disruptions.
- Recommend, design, and evaluate disruption experiments relevant to reactor conditions (TEXTOR, DIII-D).
- Evaluate ITER first wall and divertor disruption lifetime.
- Analysis can be done for coating as well as for substrate structural materials.

Dynamics of Plasma-Vapor Interactions

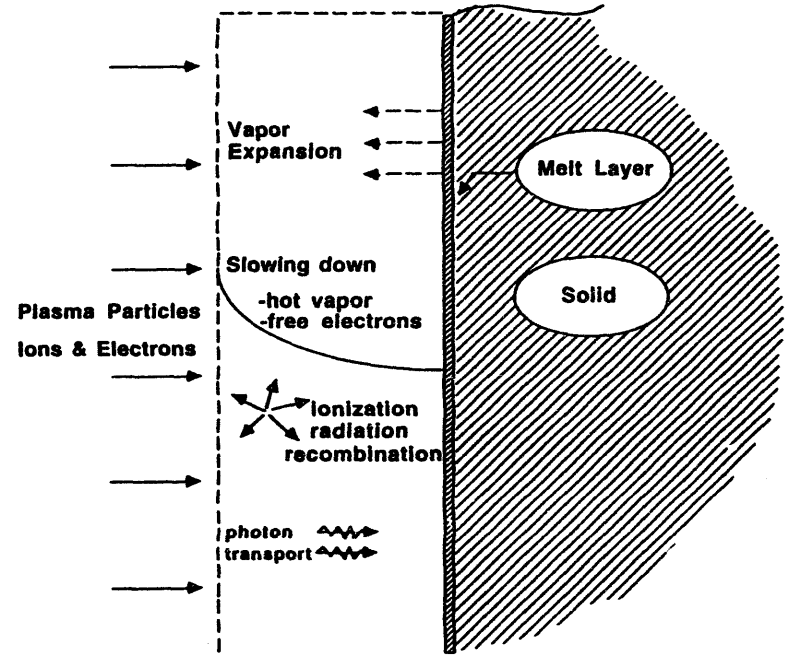

Radiation Transport Model

- Full hydrodynamic motion of vapor.
- Two-dimensional radiation transport capabilities.
- Non-local thermodynamic equilibrium model.
- Both continuum and line radiations are included.
- Up to 4000 photon energy groups.

A*Thermal-S Computer Code

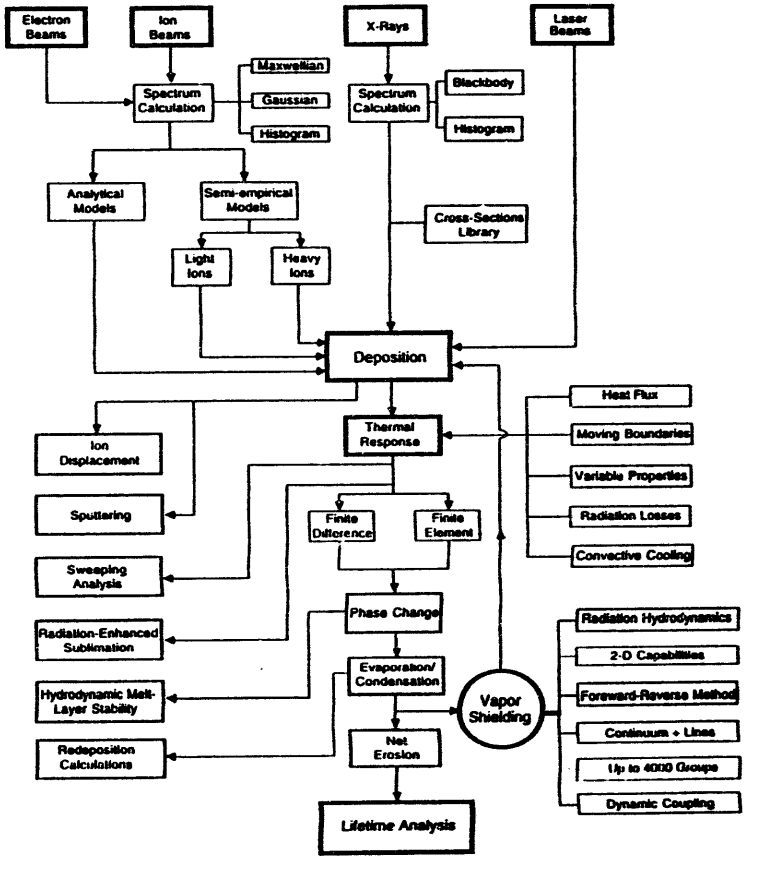

Recent Modeling Efforts

- Modeling the interaction of low-energy plasma particles (gun conditions) with ablated materials. All major atomic processes are included.
- Two-dimensional radiation transport model in the plasma-vapor interaction zones.
- Recent disruption simulation experiments on beryllium and graphite are carefully evaluated and compared.
- Key differences between simulation experiments and their relevancy to reactor conditions are discussed in detail.

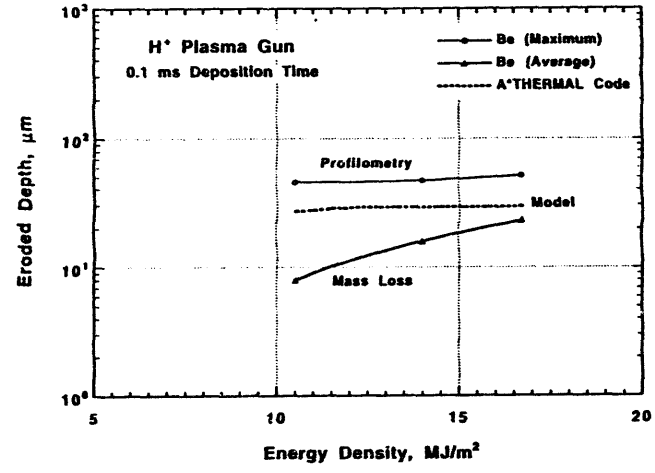

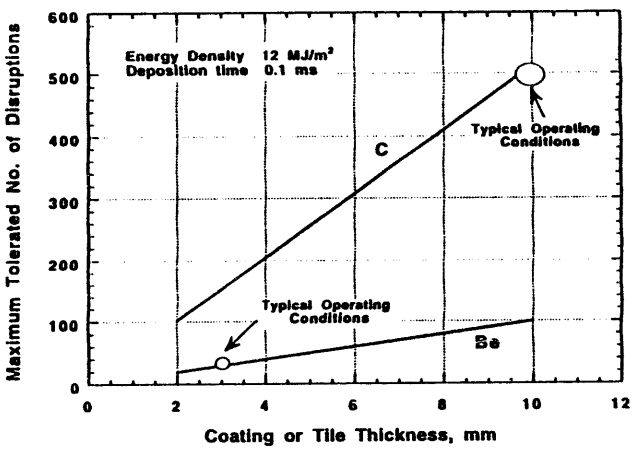

Reactor Disruption vs. Experiments

- Higher plasma-particle energies may result in more erosion and less shielding effect.
- Vapor shielding may be found less effective for electrons than for ions with the same particle energy.
- Longer disruption times ($\tau \approx 10$ ms) may result in less shielding effect by vapor and more erosion (particularly from melting).
- Magnetic field effects (oblique incidence).
  - vapor slide-off
  - edge effects
  - vapor expansion
- Higher reactor operating temperatures may increase net erosion rates.

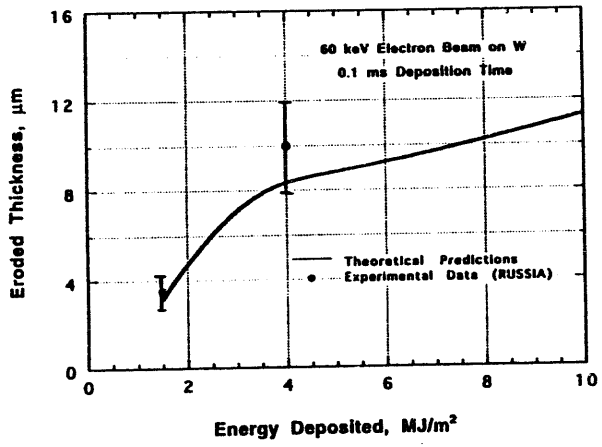

Evaluation of ITER Disruption Parameters

(ANL-TRINITI)

- Effect of multi-group radiation transport and hydrodynamics for light (C, Be) and heavy (W) materials. Implement better opacity data.
- Study the plasma-vapor interaction under the existence of a strong magnetic field.
- Study plasma-parameters of the scrape-off-layer during the thermal quench of a tokamak disruption.
- Results will be published at the PSI Meeting.

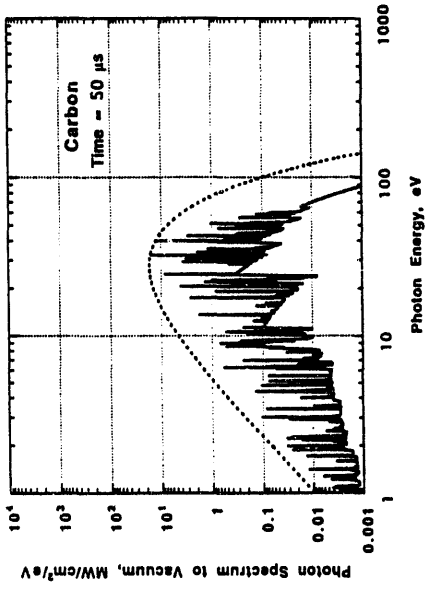
Carbon
Time = 50 μs
Photon Spectrum to Vacuum, MW/cm²/eV
Photon Energy, eV
10⁴
10³
10²
10¹
1
0.1
0.01
0.001
1
10
100
1000

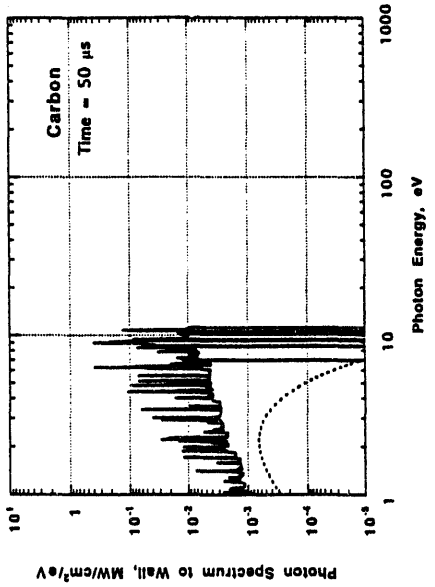
Carbon
Time = 50 μs
Photon Spectrum to Wall, MW/cm²/eV
Photon Energy, eV
10¹
1
10⁻¹
10⁻²
10⁻³
10⁻⁴
10⁻⁵
1
10
100
1000

Photon Spectrum to Vacuum, MW/cm²/eV
10⁻³
10⁻²
10⁻¹
10⁰
10¹
10²
1
10
100
1000
Photon Energy, eV
C
Be
Time = 50 μs

Vapor Temperature, eV
0
10
20
30
40
50
60
0
20
40
60
80
100
Distance, cm
C
Be
10 MJ/m²
0.1 ms Deposition Time
Time = 40 μs

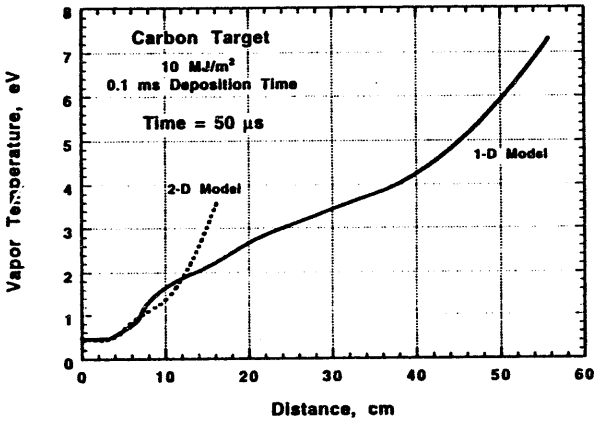

Reactor Simulation Experiment (TEXTOR)

[ANL-KfA]

- Using a fast probe, a material specimen will be inserted into TEXTOR plasma for short times (<100 ms).
- The surface heat flux is in the order of 1000 MW/m^2.
- Materials will be CFC, ceramics, and eventually higher Z materials.
- During the experiment, the tip of the probe will be viewed by a CCD camera to detect surface temperature and measure evolving radiation in the plasma near the probe.
- Post-experiment evaluation will include weight loss measurements, profilometry of damaged surface, SEM, etc.

Conclusions

- Comprehensive disruption model is developed and implemented in A*THERMAL-S computer code.
- Dynamic coupling between target thermal evolution, vapor hydrodynamics and the radiation transport.
- Simulation experiments as well as reactor disruption conditions can be evaluated.
- Good agreement with available experimental data.

Disruption Effects on the Substrate Structure

Normal Operating Parameters	First Wall	Divertor
• Neutron wall loading	2 MW/m^2	2 MW/m^2
• Surface heat flux	0.5 MW/m^2	5 MW/m^2
• Coolant temperature	300°C	300°C

Disruption Parameters	First Wall	Divertor
• Energy density in thermal quench	2 MJ/m^2	12 MJ/m^2
• Energy density in current quench	2 MJ/m^2	2 MJ/m^2
• Thermal quench time	0.1 ---------- 5.0 ms	
• Current quench time	5 ---------- 20 ms	

First Wall Design

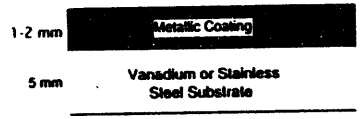

(Be or W Coating/Steel or Vanadium Structure)

Divertor Design

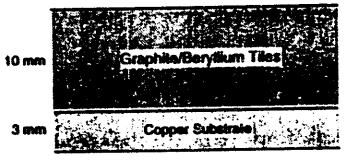

(Carbon or Beryllium Tiles/Copper Structure)

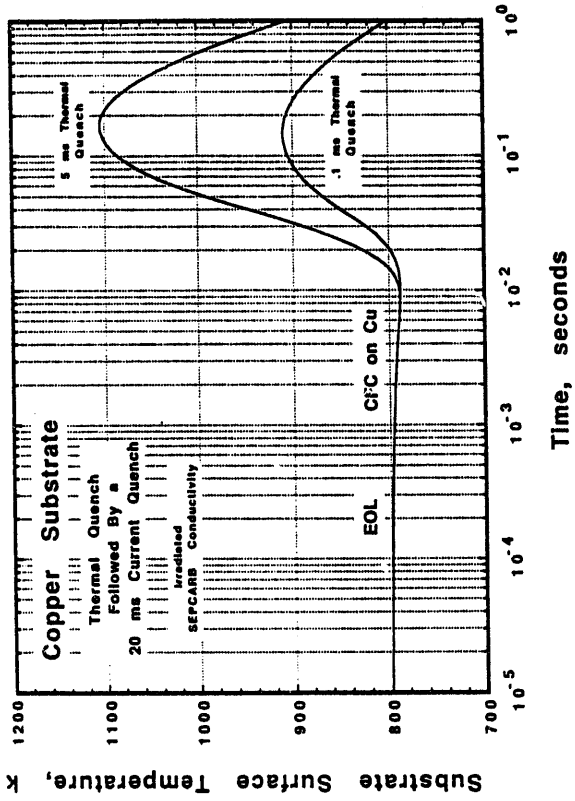
Copper Substrate
Thermal Quench
Followed By a
20 ms Current Quench
Irradiated
SEPCARB Conductivity
EOL
C-C on Cu
5 ms Thermal Quench
.1 ms Thermal Quench
Substrate Surface Temperature, K
Time, seconds

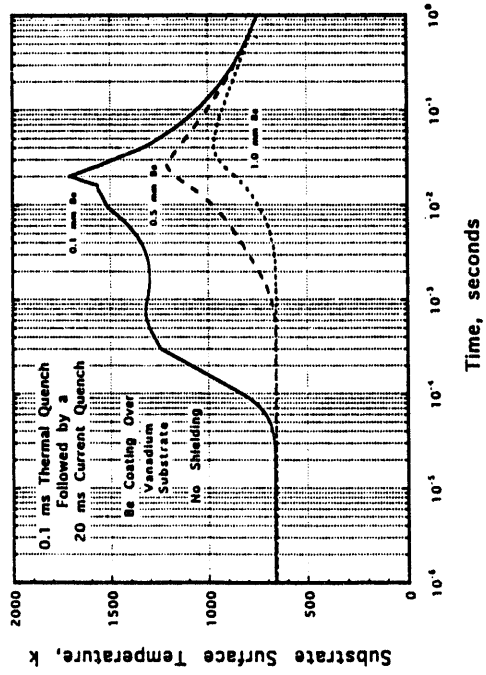
0.1 ms Thermal Quench
Followed by a
20 ms Current Quench
Be Coating Over
Vanadium
Substrate
No Shielding
0.1 mm Be
0.5 mm Be
1.0 mm Be
Substrate Surface Temperature, K
Time, seconds

Upgrade To MAGFIRE Code Modeling Of Disruptions And Comparison With Experimental Results*

John Gilligan, Eric Tucker, Mohamed Bourham
North Carolina State University
Department of Nuclear Engineering
Raleigh, NC 27695-7909
919/515-2301
919/515-5115 Fax
Email Gilligan@ncsu.edu

Presented at the
US-Japan Workshop on PMI-HHF
UCal-SD
January, 26, 1994

Support: Sandia-A
SDI/BMDO/Army

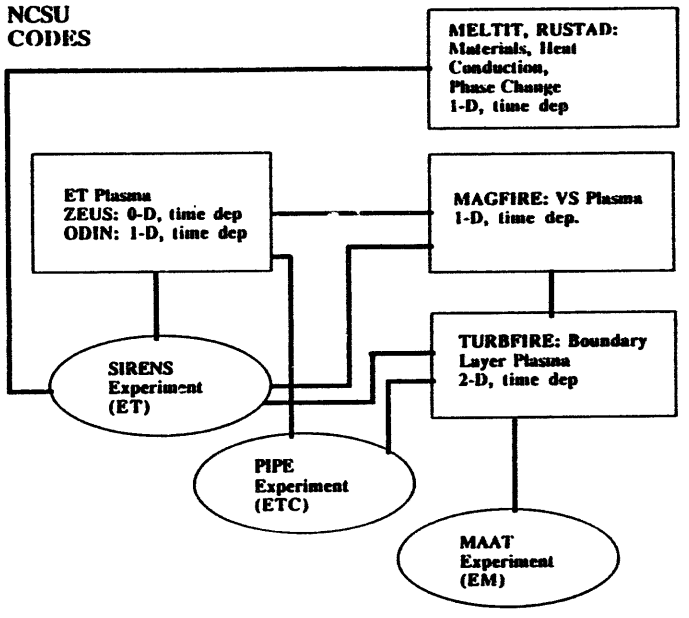

SIRENS OPERATIONAL CHARACTERISTICS

DISCHARGE VOLTAGE (10 kV max.)	1 - 8 kV
PEAK CURRENT (100 kA max.)	20 - 100 kA
NET INPUT ENERGY (15 kJ max.) (Upgraded to 150 kJ with PFN)	1 - 8 kJ
DISCHARGE PERIOD (Up to 1ms with PFN)	0.1 - 0.2 ms
RADIATED POWER (at max.)	2-120 GW/m^2
PEAK PRESSURE	> 1 kbar
PLASMA DENSITY	10^{25}-10^{26}m^{-3}
PEAK PLASMA TEMPERATURE	4 - 6 eV
AVERAGE PLASMA TEMPERATURE	1 - 3 eV
AVERAGE PLASMA VELOCITY	≈12 km/sec

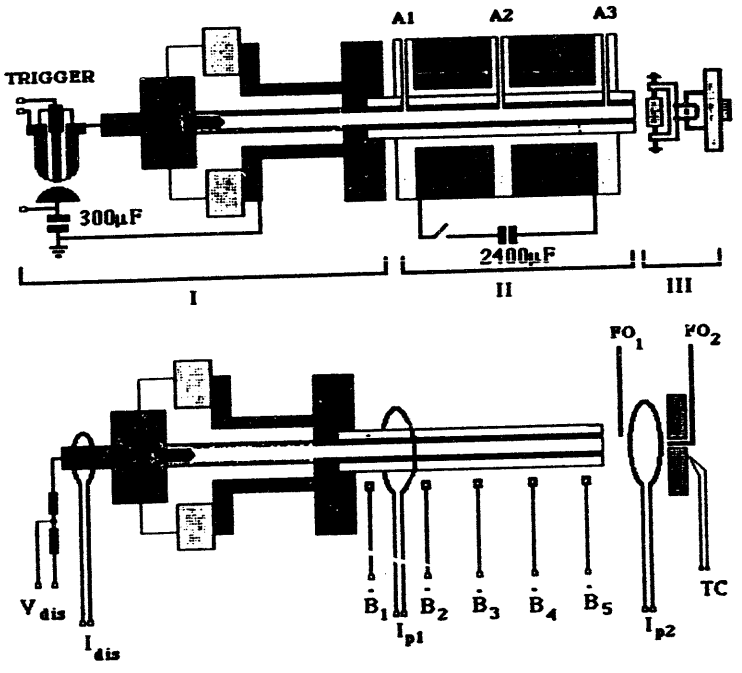

TOP: Schematic of SIRENS showing the source section (capillary), barrel section with magnet assembly (magnetic vapor shield studies).

BOTTOM: Diagnostics arrangement showing standard diagnostics (currents, voltage, B-dots), fiber optics for optical emission spectroscopy, and a thermocouple for heat flux measurements.

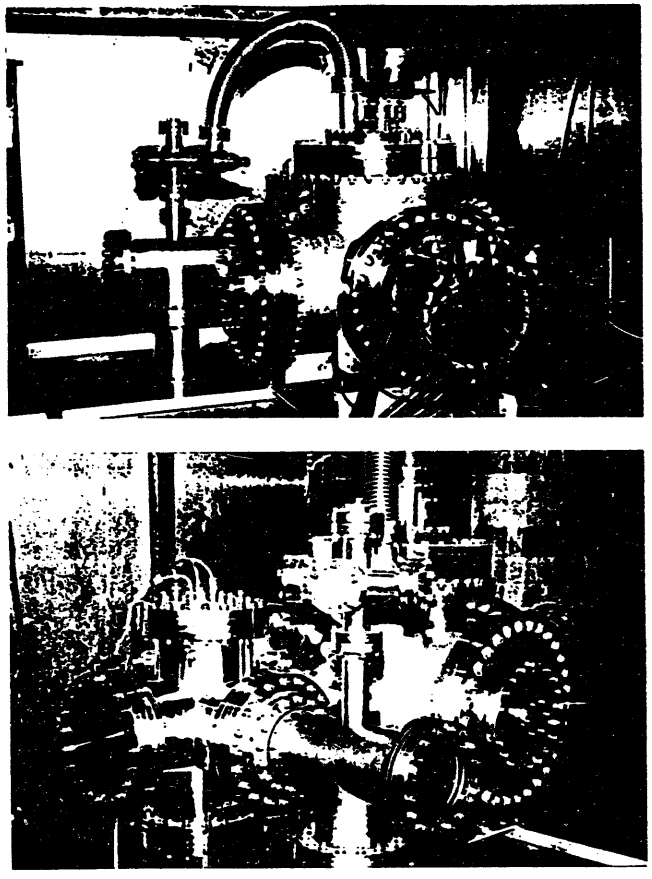

Photographs of SIRENS showing the source input section and magnet current feedthrough (top photo), and the target and expansion chamber with diagnostics feedthrough (bottom photo)

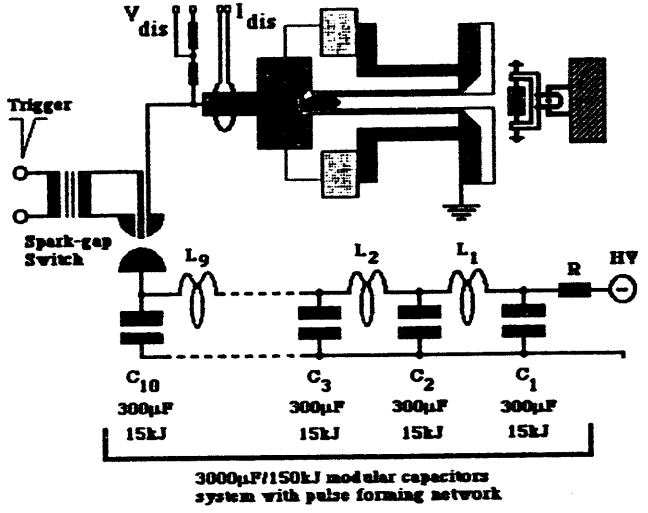

3000μF/150kJ modular capacitors system with pulse forming network

SCHEMATIC DRAWING OF THE MODIFIED SIRENS, OPERATING AT 150 KJ INPUT ENERGY

DIAGNOSTICS

PLASMA DIAGNOSTICS (UP TO 18 CHANNELS)

ROGOWSKI COILS -> DISCHARGE CURRENT, PLASMA CURRENT, MAGNET CURRENT)

B-DOT LOOPS -> B-DOT SIGNALS (WITHOUT BARREL, OR WITH SPECIAL BARREL)

COMPENSATED POTENTIAL DIVIDERS -> DISCHARGE POTENTIAL

MAGNETIC PROBES -> MAGNET B-FIELD

THERMOCOUPLES -> HEAT FLUX

CONDUCTIVITY PROBES -> PLASMA RESISTANCE

PRESSURE TRANSDUCERS -> TIME-RESOLVED ABSOLUTE PRESSURE

He-Ne LASER, PHOTO-TRANSISTORS, OPTO-INTERRUPTERS, BREAK WIRES -> VELOCITY

HEAT FLUX CALORIMETRY

OPTICAL MULTICHANNEL ANALYZER -> TIME-INTEGRATED VISIBLE SPECTRUM

MONOCHROMATORS -> TIME-RESOLVED SPECTRAL LINES

MATERIAL DIAGNOSTICS

MICROBALANCE -> WEIGHT LOSS

SEM -> SURFACE ANALYSIS

EDXA - > SURFACE ELEMENTAL ANALYSIS

AES -> SURFACE ELEMENTAL ANALYSIS

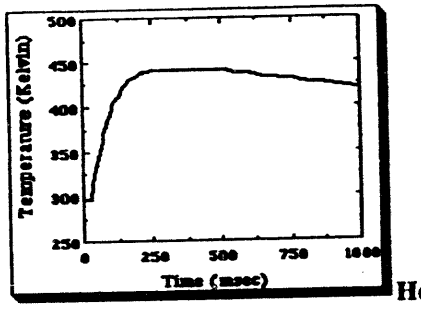

Heat Flux

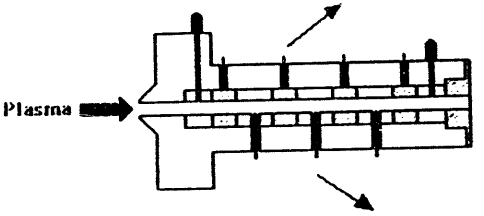

Conductivity

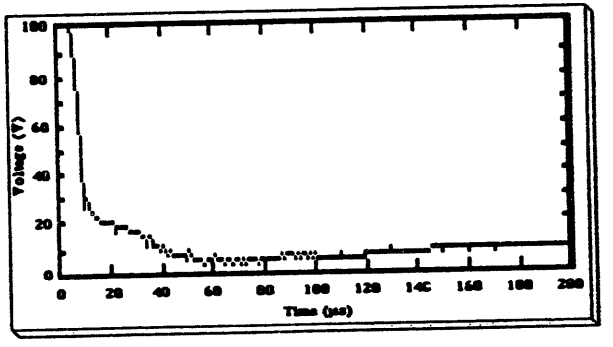

HEAT FLUX AND CONDUCTIVITY DIAGNOSTICS

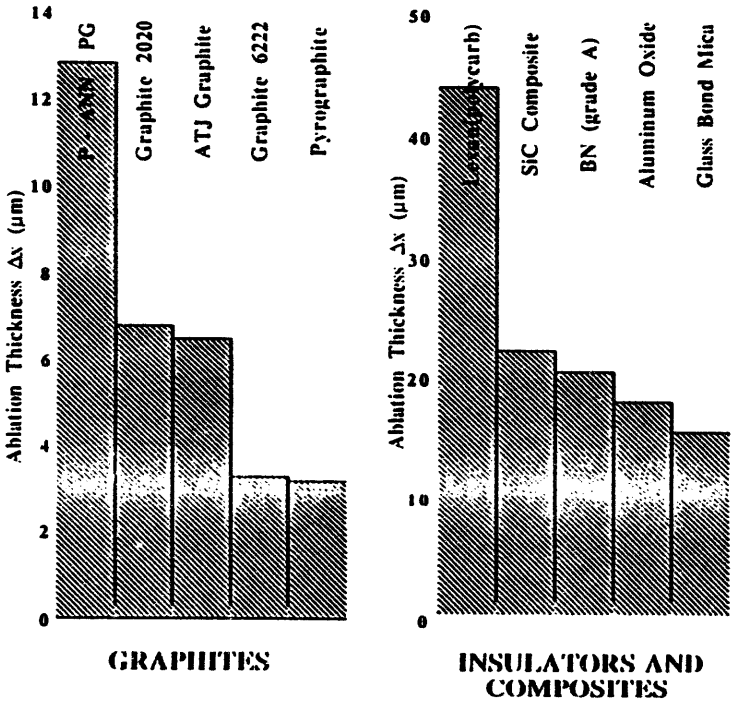

Ablation thickness of graphites, insulators and composites exposed to 33 GW/m² over 100 μs (5 kJ input energy to SIRENS source).

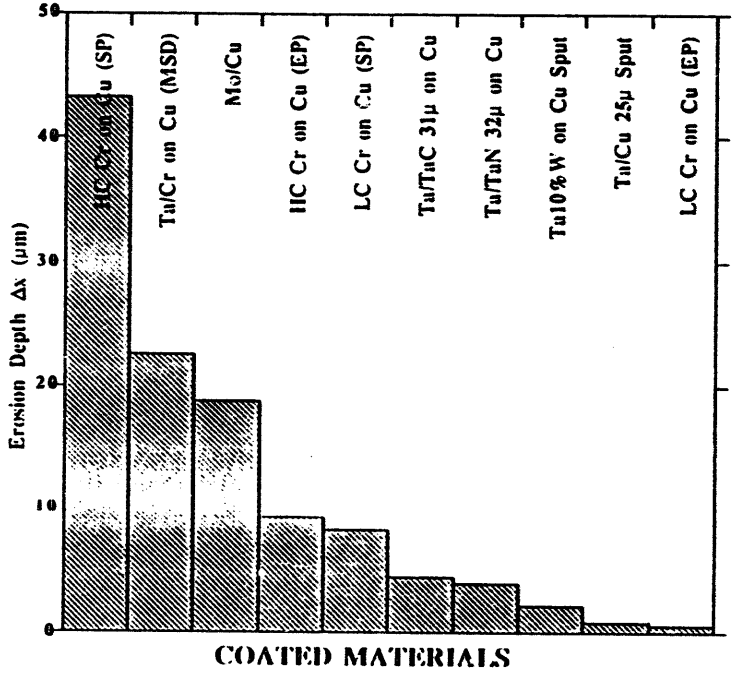

Erosion thickness of coated material surfaces exposed to 33 GW/m² over 100 μs (5 kJ input energy to SIRENS source).

SP, Sput	= Sputtering
EP	= Electroplated
MSD	= Molten Salt Deposition

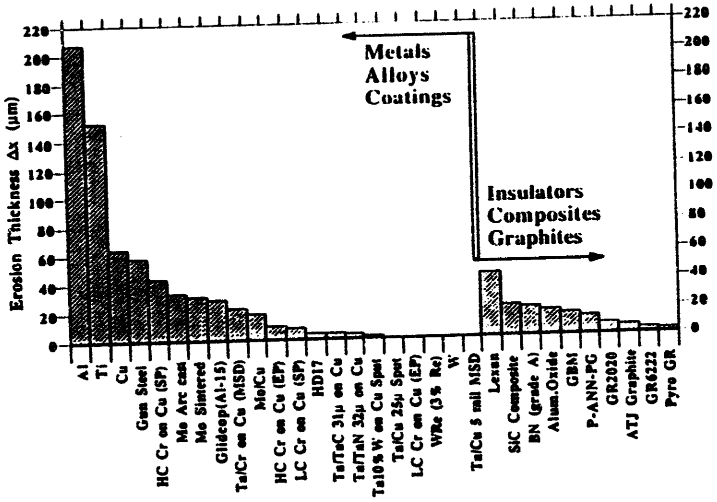

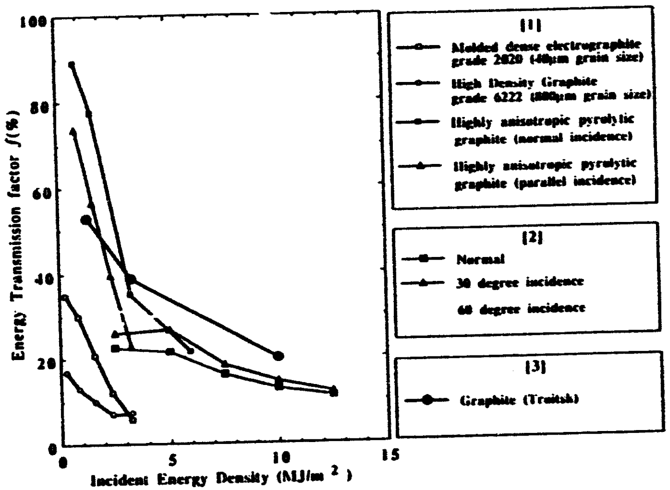

[1] M. Bourham, J. Gilligan and O. Hankins, SIRENS, NCSU, "see for example: Fusion technology, Vol. 21, 1852-1857 (1992)".
[2] J. Gahl and J. McDonald, "USSR/US Exchange Program of Cooperation for Magnetic Confinement Fusion", PMI/RHF Subtask Group Workshop on Tokamak Disruption Technology, July 30-31, 1991, Santa Fe, NM, page 291 "T. Kunoda et al., ITER Plasma Facing Components, ITER Documentation Series No. 30, IAEA, Vienna 1991"
[3] Anatoli Zhitlukhin, from his presentation at The Tokamak Disruption Workshop, Sandia National Lab., Albuquerque, NM, October 20-21, 1992.

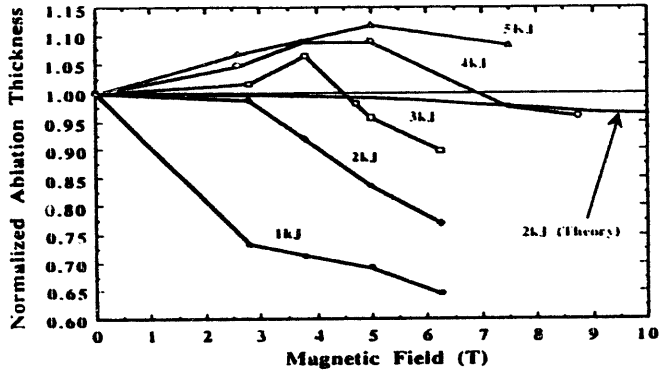

Effect of the applied magnetic field on the ablation of Lexan, at input energies between 1 and 5 kJ

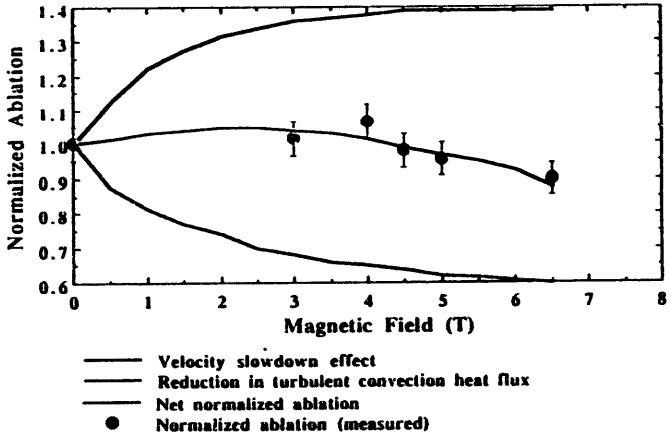

Magnetic Vapor Shield Analysis (Lexan Sample, 3 kJ)

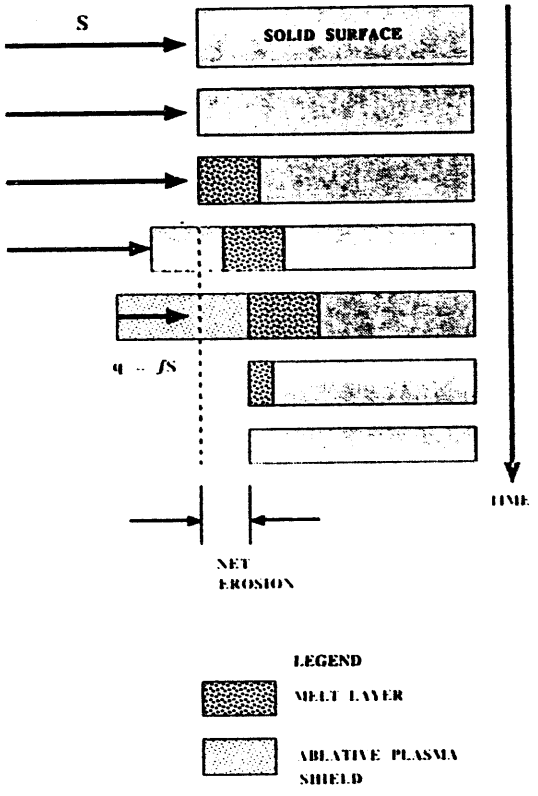

VAPOR SHIELD PROCESS

MODELS TO BE SOLVED

Simultaneous Solutions of :

- **Incident Radiation and Momentum Deposition**
- **Melting and Ablation of Wall Material**
- **MHD transport of the Shielding Vapor**
- **Radiation Transport in the Shielding Vapor**

Single part Fluid

Turbulence

Issues in Melt Layer/Vapor Shield

- Melt layer stability, ejection forces (EM, thermal, impulsive)

- Vapor shield

  Hydro motion

  Energy/momentum deposition in vapor/solid

  Radiation transport, equation-of-state, opacities, charge state

  Convective turbulence and instabilities in VS

  Magnetic field effects on convection, macro-motion

MAGFIRE Code Upgrades

Goal: Most complete description of vapor shield physics at a divertor plate surface during a disruption.

- Ion momentum transfer and electron angular scattering from higher energy disruption species.
- Charge separation fields in VS plasma.
- Mixing of disruption species with VS plasma.

IEEE Trans. Plasma
Magfire Code - Vapor Shield Physics

Equation of Motion

$$\frac{\partial u}{\partial t} = -V\frac{\partial}{\partial r}(P+q) + \frac{V}{c}\hat{r}\cdot\vec{J}_p \times (\vec{B}_{ind} + \vec{B}_{ext})$$

Energy Equations

Plasma

$$C_v\frac{\partial T_p}{\partial t} = \frac{\partial}{\partial m_0}(r\kappa_T\frac{\partial T_p}{\partial r}) - \frac{\partial P_p}{\partial T_p}\dot{V}T_p - q\dot{V} + A - J + \Psi$$

Radiation

$$V\frac{\partial E_h^g}{\partial t} = \frac{\partial}{\partial m_0}(r\kappa_h^g\frac{\partial E_h^g}{\partial r}) - \frac{4}{3}E_h^g\dot{V} - A^g + J^g \qquad g = 1,\ldots,G \quad G=20$$

Magnetic Diffusion Equation

$$\nabla\times\vec{B} = \frac{4\pi}{c}\vec{J}_p \quad ; \quad \nabla\times\vec{E} = -\frac{1}{c}\dot{\vec{B}}$$

$$\eta\vec{J}_p = \vec{E} + \frac{1}{c}\vec{u}\times(\vec{B}_{ind} + \vec{B}_{ext})$$

where

$$\Psi = \eta J_p^2 r\frac{dr}{dm_0}$$

$$A = \sum_{g=1}^{G} A^g = \sum_{g=1}^{G} c\sigma_p^g E_h^g$$

$$J = \sum_{g=1}^{G} J^g = \sum_{g=1}^{G} \frac{8\pi T_p^3}{c^2h^2}\sigma_p^g \int_{x_g}^{x_{g+1}} dx \frac{x^3}{e^x - 1} \quad ; \quad x = \frac{h\nu}{T_p}$$

$$\kappa_h^g = \frac{cV}{3\sigma_h^g}$$

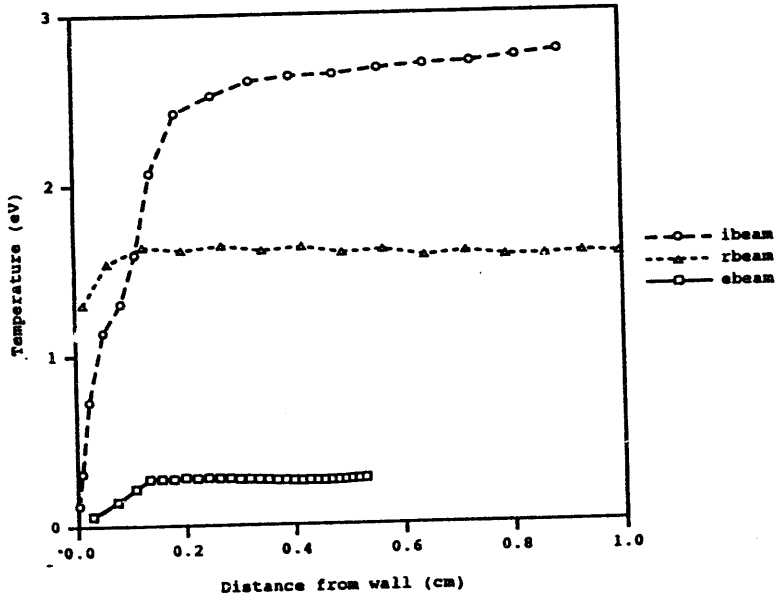

Fig.1 Incident heat flux = 10^{11}W/m^2 for 1 us.
Electron or ion incident energy/particle = 20keV.

Goals

1. Determine the transmission factor f for differing incident heat fluxes and species.

2. Determine the mechanisms by which energy is being transported to the wall.

3. Determine the vapor shield's thickness.

4. Determine if f reaches steady state for disruption relevant energies at ~100μs.

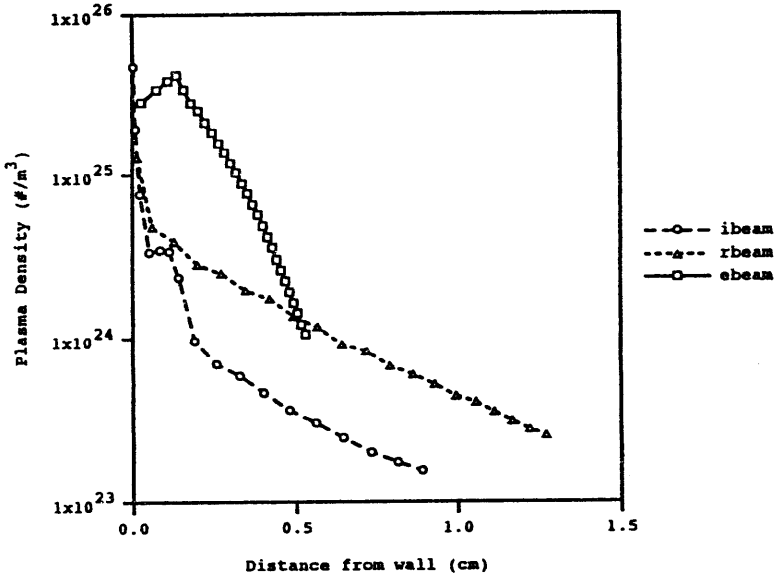

Fig.2 Incident heat flux = 10^{11}W/m^2 for 1 us.
Electron or ion incident energy/particle = 20keV.

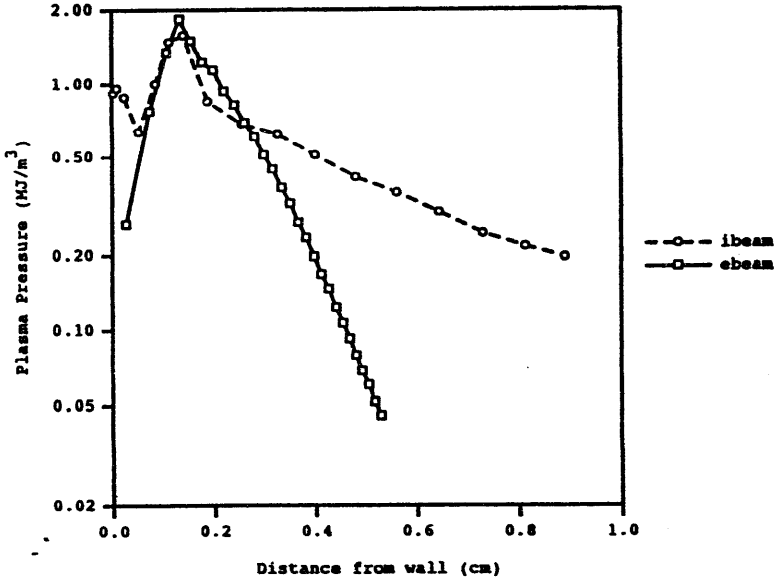

Fig.3 Incident heat flux = 10^{11}W/m^2 for 1 us.
Electron or ion incident energy/particle = 20keV.

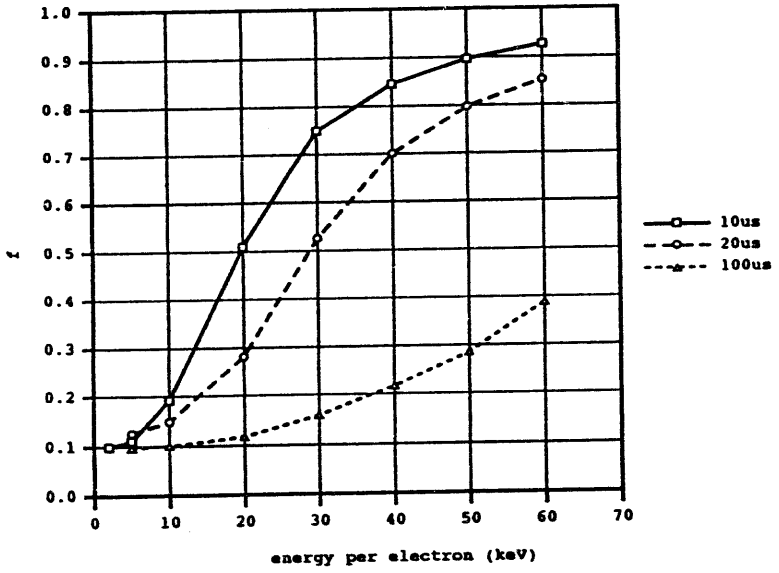

Fig.7 Total energy transmission fraction (f) for a 10^{11}W/m^2 electron beam.

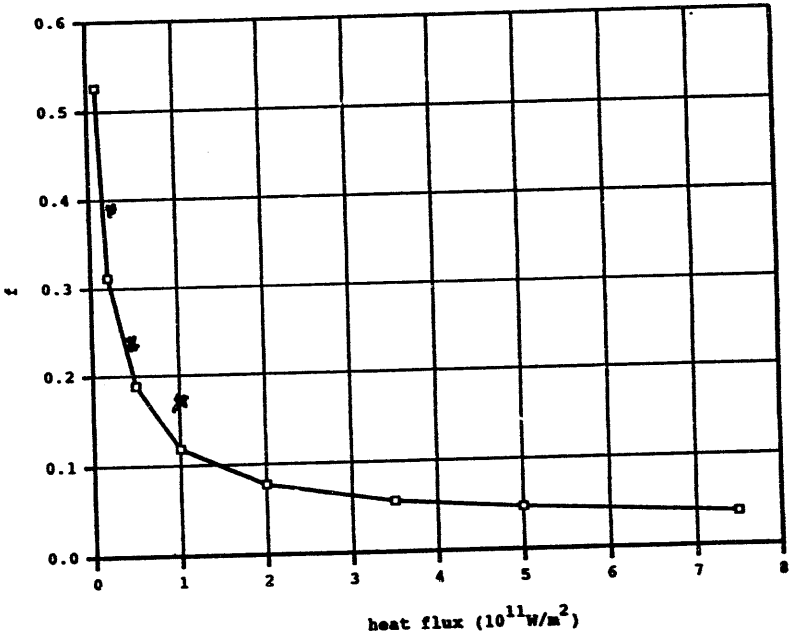

Fig.8 Total energy transmission fraction (f) vs. a 100us, 20keV incident electron heat flux.

* - Sirens exp. points on graphite

Future Work

1. Include beam electron (and maybe ion) 3D angle scattering.

2. Include beam momentum equation.

3. Include charge separation.

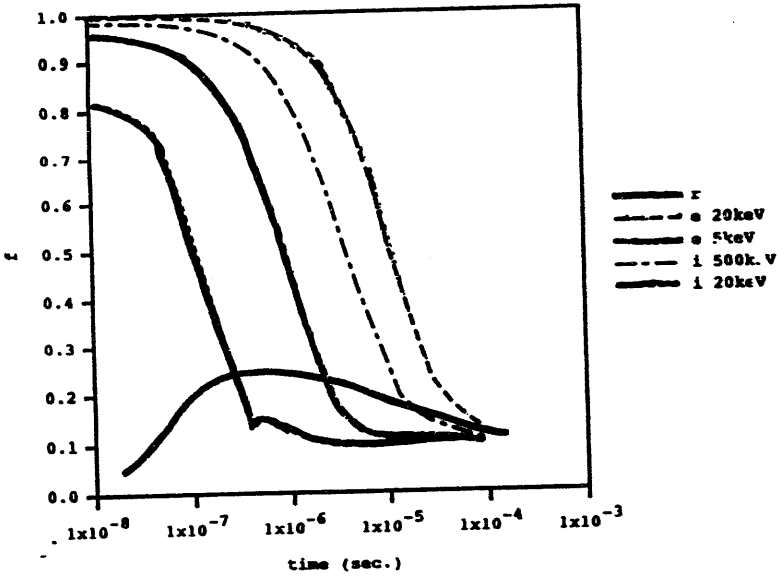

Fig.10 Total energy transport fraction for 10^{11} W/m^2, radiation (r), electron (e), ion (i) beams.

Needed

- Definitive disruption diagnostics on tokamaks
- Complete disruption model (entire plasma to divertor plate)
- Simulator testing

  long pulse, high energy fluence

  geometry, species, $\underline{B}$, energy effects, materials, etc.

Session IX

Conditioning and Tritium

US-J Workshop on PMI and HHF, San Diego, January 24 - 27, '94

Boronization in Japan

A. Sagara, N.Noda, N.Inoue, Y.Kubota, K.Akaishi and O.Motojima
NIFS, Japan
K.Iwamoto, I.Fujita, T.Hino and T.Yamashina
Hokkaido Univ., Japan
M.Yamage, H.Toyoda and H.Sugai
Nagoya Univ., Japan

1. Boronization Applied in Plasma Devices

- P-CVD : JT-60U, Heliotron-E, CHS
- STB : JIPP TII-U

2. Present State of R&D on Boronization for LHD

- Characterization of oxygen gettering : depth profiles
- Comparison between B_2H_6 and $B_{10}H_{14}$: oxygen gettering

JT-60U

Application of B/C materials (continued 6)
In situ boron coating (boronization)

* Summary of boronization sessions
  - uniform toroidal distribution after 3rd boronization due to an increase of gas inlets from one toroidal location to twelve
  - low carbon content
  - *10-14% hydrogen content*

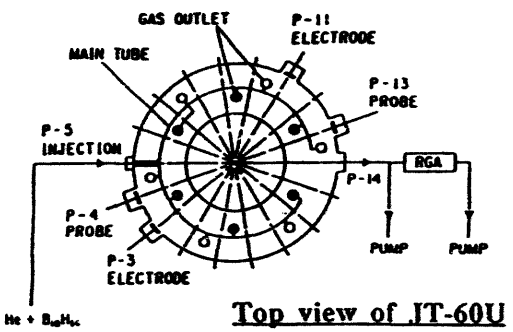

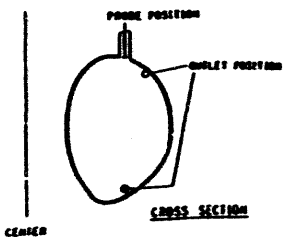

Top view of JT-60U

	1st	2nd	3rd	4th
Date	July 30 '92	Sep. 1 '92	Feb. 17 '93	July 2 '93
Amount of decaborane consumed (g)	10	15	50	100
Deposition time (h)	10	10	36	57
Wall temperature (deg C)	300	300	250	250
Number of gas inlets	1	1	12	12
Estimated boron film thickness (nm)	30	45	150	300
Measured thickness (nm)	--	2 - 80	100 - 400	--
Atomic composition (host)				
Boron content (%)	--	95	85 - 90	--
Carbon content (%)	--	< 5	10 - 15	--
Hydrogen content (H/Host) (%)	--	10	10 - 14	--

Application of B/C materials (continued 7)
In situ boron coating (boronization)

Effect of boronization on plasma performance

* Reduction of oxygen
  - 1/3 - 1/5 reduction in OH-discharge
  - - 1/2 reduction in NB-heated discharge
* Reduction of hydrogen recycling
  - 1/2 - 1/5 reduction in both OH- and NB-heated discharges
* Low n_e
  - wider density range operation available
* Operational improvements (vent recovery, disruption recovery(reduced number of He-TDC), reliable high Ip operation, etc.)

Particle Recycling in High-β_p Mode Discharges

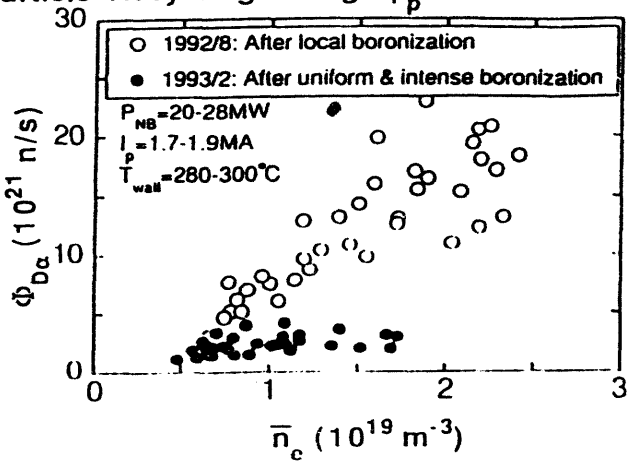

Heliotron-E

デカボラン導入経路

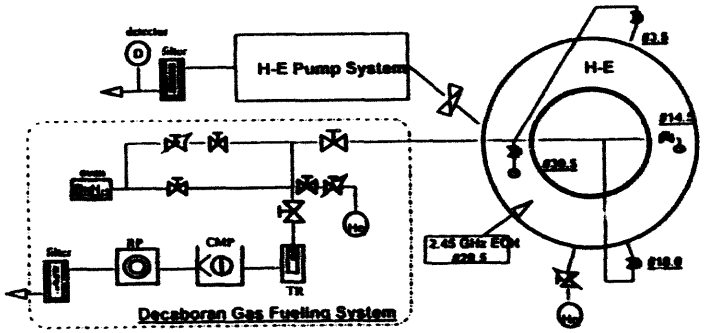

ヘリオトロンE装置における
ボロニゼーション

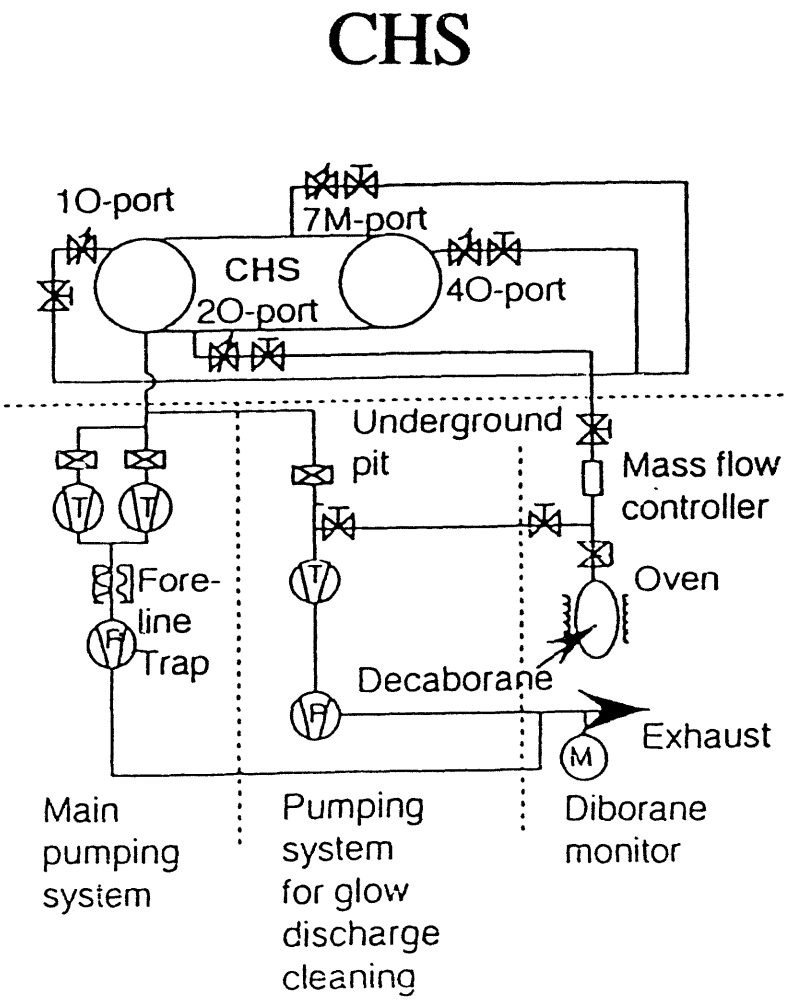

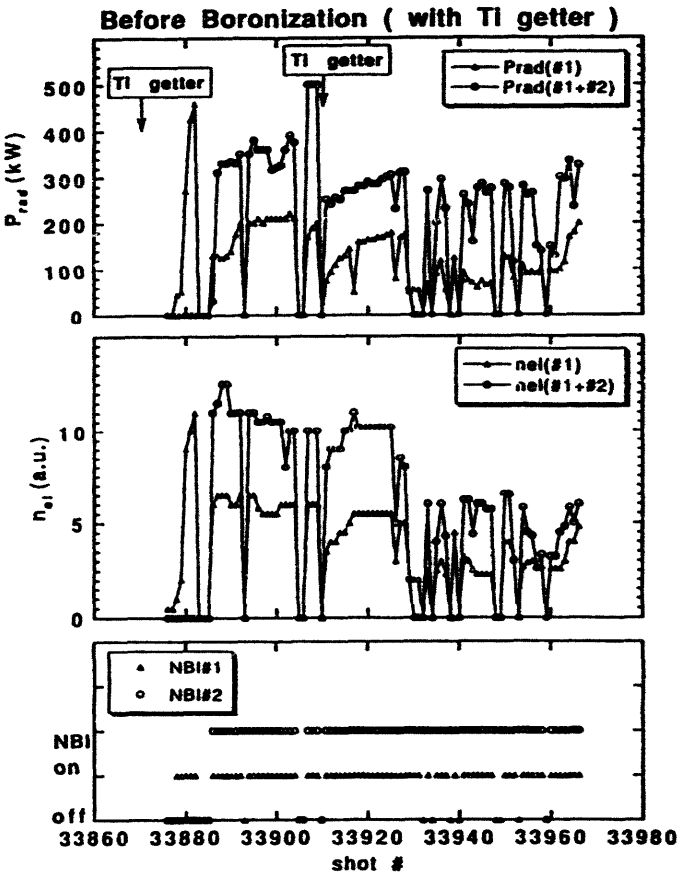

Fig.1 Diagram of boronization system in CHS

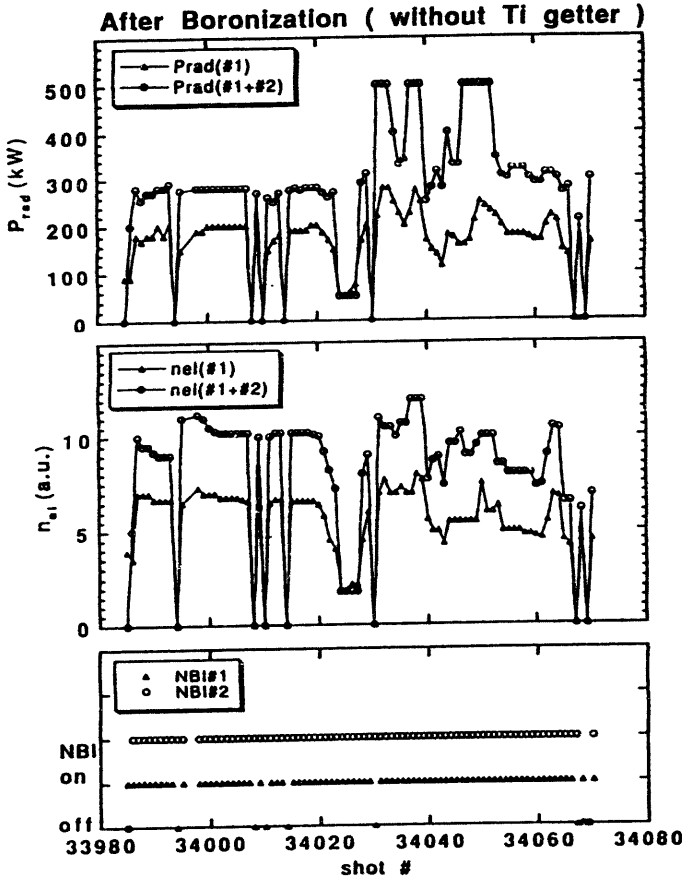
After Boronization (without Ti getter)
Prad(#1)
Prad(#1+#2)
P_{rad} (kW)
500
400
300
200
100
0
nel(#1)
nel(#1+#2)
n_{el} (a.u.)
10
5
0
NBI#1
NBI#2
NBI
on
off
33980
34000
34020
34040
34060
34080
shot #

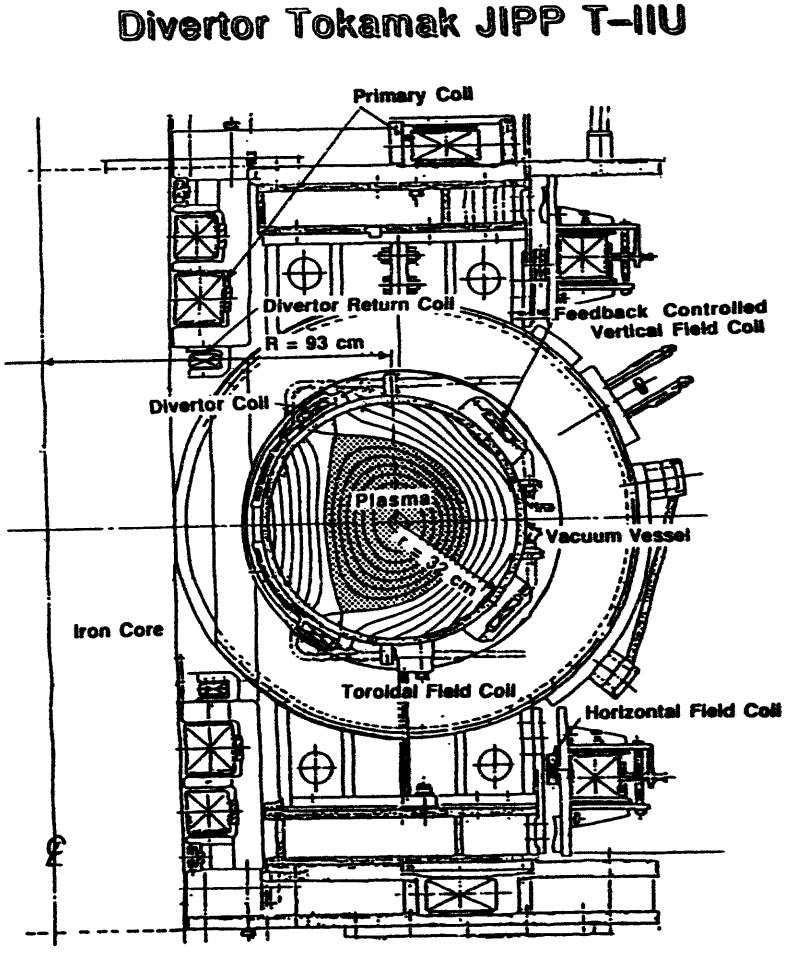
Divertor Tokamak JIPP T-IIU
Primary Coil
Divertor Return Coil
Feedback Controlled
Vertical Field Coil
R = 93 cm
Divertor Coil
Plasma
a = 32 cm
Vacuum Vessel
Iron Core
Toroidal Field Coil
Horizontal Field Coil

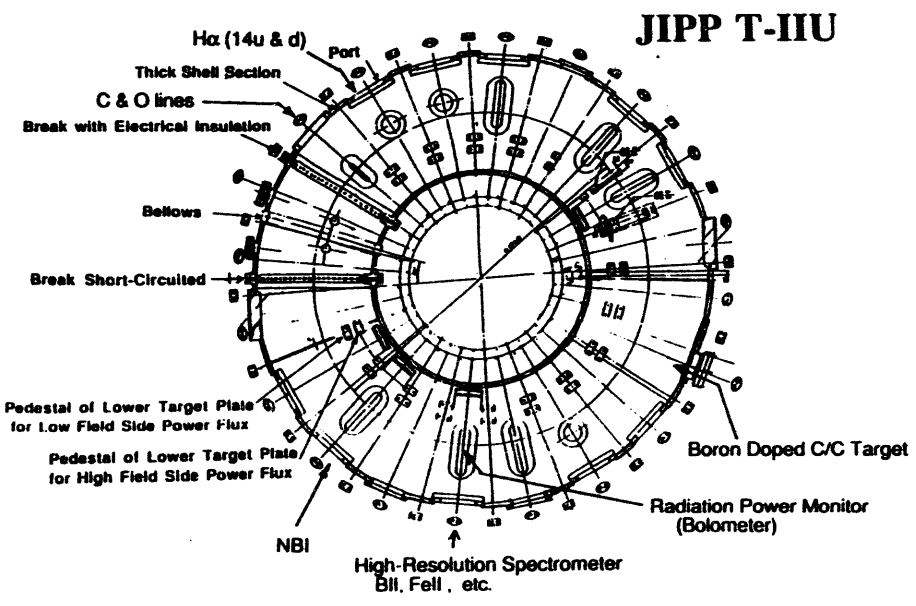
JIPP T-IIU
Hα (14u & d)
Port
Thick Shell Section
C & O lines
Break with Electrical Insulation
Bellows
Break Short-Circuited
Pedestal of Lower Target Plate for Low Field Side Power Flux
Pedestal of Lower Target Plate for High Field Side Power Flux
NBI
High-Resolution Spectrometer BII, FeII , etc.
Radiation Power Monitor (Bolometer)
Boron Doped C/C Target

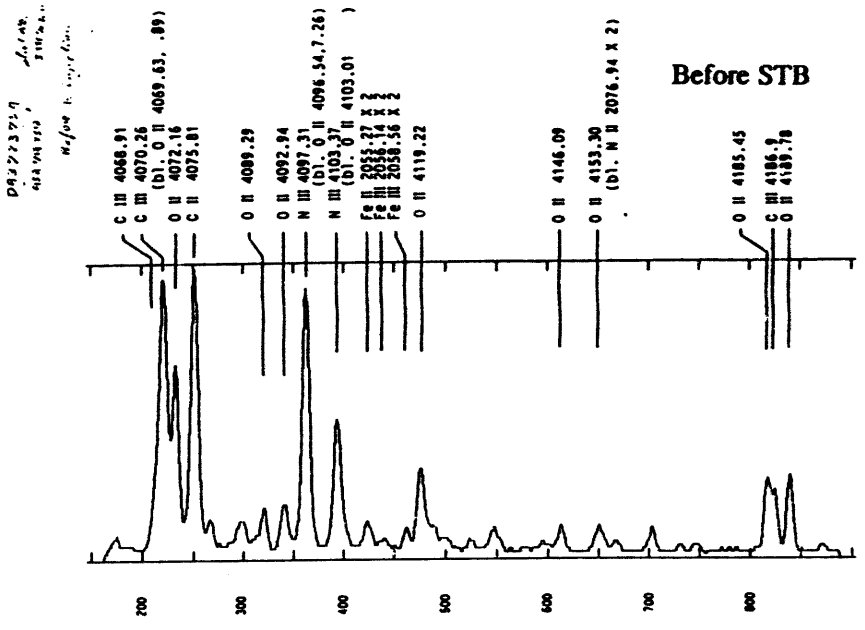
Before STB
C III 4068.91
C III 4070.26
(Dl. O II 4069.63, .89)
O II 4072.16
C II 4075.81
O II 4089.29
O II 4092.94
N III 4097.31
(Dl. O II 4096.54,7.26)
N III 4103.37
(Dl. O II 4103.01)
Fe III 2053.27 X 2
Fe III 2056.14 X 2
Fe III 2058.56 X 2
O II 4119.22
O II 4146.09
O II 4153.30
(Dl. N II 2076.94 X 2)
O II 4185.45
C III 4186.9
O II 4189.78
200
300
400
500
600
700
800

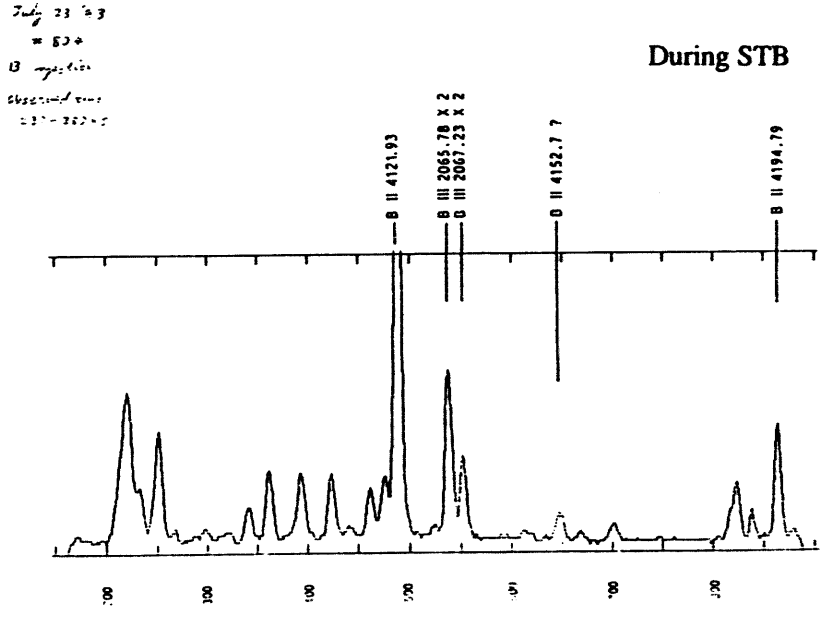
During STB
B II 4121.93
B III 2065.78 X 2
O III 2067.23 X 2
O II 4152.7 ?
B II 4194.79

Boronization in Fusion Oriented Plasma Machines in Japan

	JT-60U	Heliotron-E	CHS	JIPP T-IIU
Date	July 30 -, '92	July 6 -, '93	February 24 -, '93	July 23 -, '93
	JAERI	Kyoto Univ.	NIFS	NIFS
Method	DC-Glow	ECH (& DC-G)	DC-Glow	Solid Target Boronization
discharge	600 V x 8 A	-	~ 400V x 1A	-
RF	-	2.45GHz (0.045T)	-	-
discharge power	~ 5 kW	~ a few kW	~ 0.4 kW	ohmic ~ 250 kW (3T)
cathode material	carbon x 2		ss x 1	-
Gas				
discharge gas	$B_{10}H_{14}$ + He	$B_{10}H_{14}$ + He	$B_{10}H_{14}$ + He	CC + 20% B
mixing ratio	~ 1.5 %	~ a few % ?	~ a few %	-
total flow rate	380 sccm	~ 36 sccm	~ 1 sccm	-
nozzle number	6 x 2	3 (4)	4	-
pressure	~ 4×10^{-4} Torr	~ 8×10^{-5} Torr	~ 4.3×10^{-3} Torr	-
pumping speed	3,000 l/s	~ 6,000 l/s	~ 10 l/s	-
source distribution	6 x 2	3 (or 4)	4	2 (30φ)
Film and Condition				
total area	~ 200 m²	~ 30 m²	~ 12 m²	~ 12 m²
film growth rate	~ 5 nm/h	~ 30 nm/h ?	~ 9 nm/h	
consumed mass / time	100 g / 60 h	10 g / 11 h	12 g / 44 h	B ~ 7 g
film thickness	~ 250 nm	100 ~ 200 nm	(~ 400 nm)	
wall material	carbon	ss (Ti flashed)	Ti flashed ss	ss (+ C limiter)
wall temperature	250 °C	r.t.	r.t.	r.t.
Results				
Oxygen reduced	yes (--> 1/2 in NBI)	yes (--> 1/2 in NBI)	almost same in Ti	yes
Carbon reduced	divertor / carbon tile	yes (--> 1/2 in NBI)		yes
Metal reduced	carbon wall	no ? (after NBI)	yes	no ?
H recycling reduced	yes (--> 1/5 in NBI)	yes	no (He glow required)	yes (ohmic)
stored energy increased	yes	yes	yes (~10%)	-
lifetime		> 300 ECH shots	> 500 NBI shots	shot by shot
remarks	fast conditioning High βp + H mode	fast conditioning ECH up to cut-off	fast conditioning stable conditioning	fast conditioning impurity control
key person	M. Saidoh	T. Mizuuchi	H. Yamada	A. Sagara

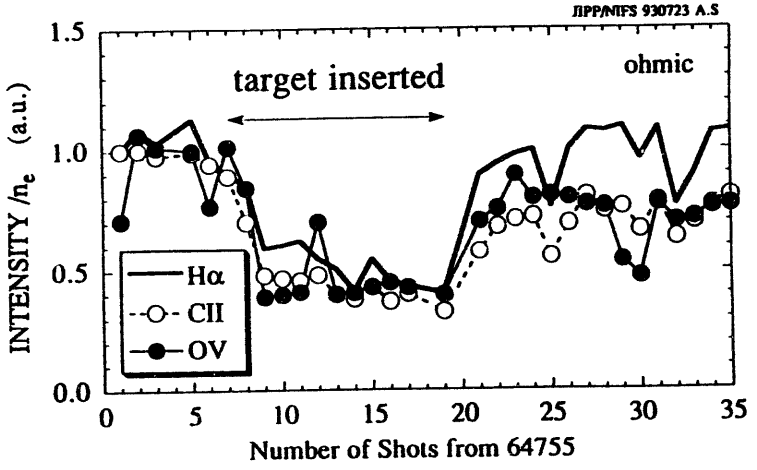

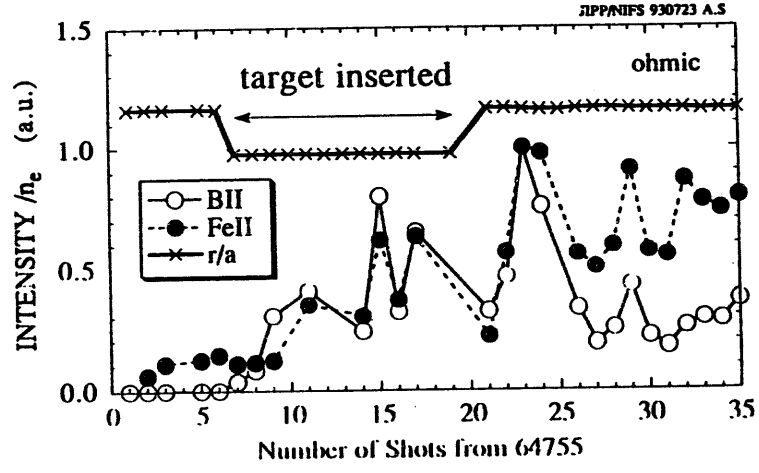

SUMMARY

(1) Boronization Applied in Plasma Devices

1. Decaborane has been commonly used with He.
2. Fast conditioning is commonly achieved in every morning and after exposure to air.
3. Boronization of once a few weeks gives stable wall-condition.
4. Oxygen impurity is effectively reduced.
5. Reduction of carbon and metal impurities depends on wall material and plasma operation.
6. Hydrogen recycling seems to depend on boronization condition and / or method.
7. STB has been confirmed to be clearly effective as quick conditioning to reduce both of impurity and H recycling, while its lifetime is limited within a few shots.

NIFS 940126 A.Sagara

Boronization

- He mixed B_2H_6(5vol.%)
- pressure of ~ 20 mTorr
- B_2H_6 flow rate ~ 2.4sccm
- glow of ~ 500V, 0.3A
- inner surface ~ 7,000 cm2
- growth rate ~ 180 nm/h
- at room temperature

Surface Modification Teststand

SUT in NIFS

(top view)

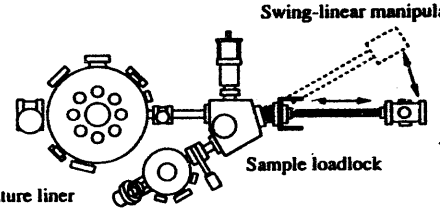

Main chamber
- UHV
- high temperature liner (< 600°C)
- surface modification
- optical analysys
- gas analysys
- quartz oscillator

Analysis chamber
- AES(in-situ)
- ion gun
- TDS

NIFS-94 0422 A. Sagara

表面元素組成 (AES)
Surface Composition

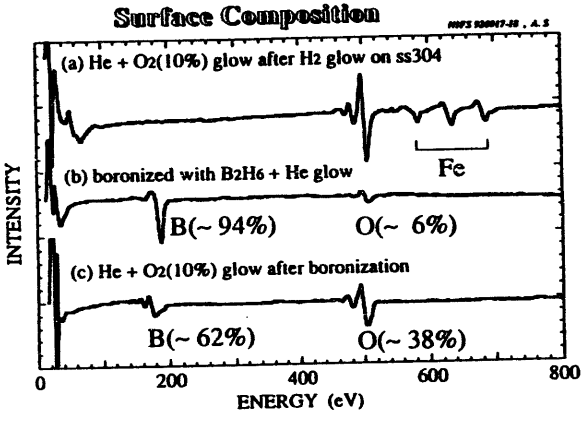

Oxygen penetrates into deeper layers over 50 nm .
However, the mechanism is not clear yet.

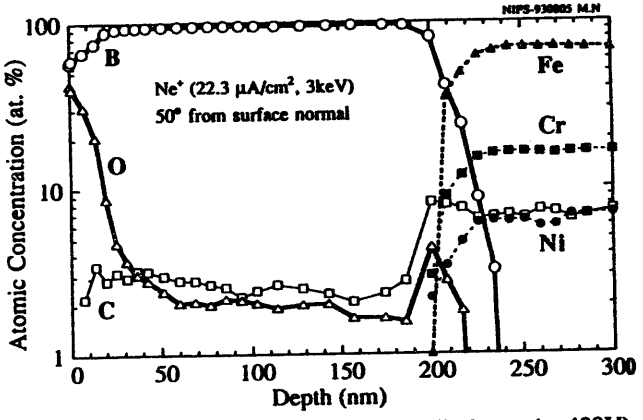

AES depth profiles taken after O_2 glow discharge (~ 400V).

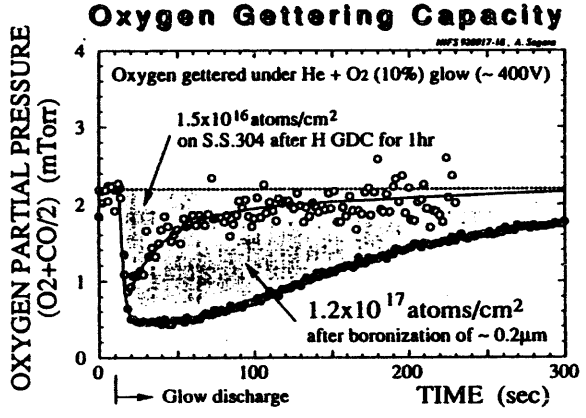

In good agreement with the capacity estimated from the AES depth profile.

B film of about 100nm thick is sufficient for oxygen gettering.

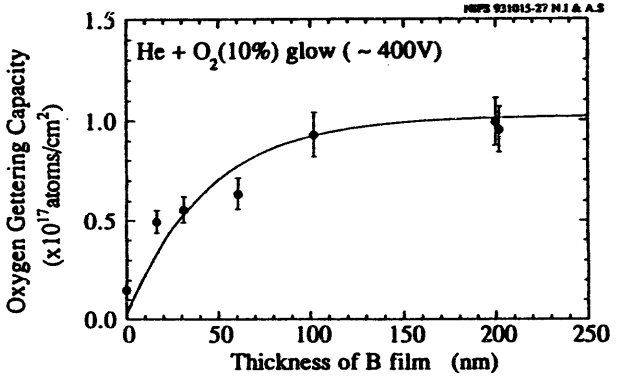

B film after O_2 glow keeps a quite passive state in the air.

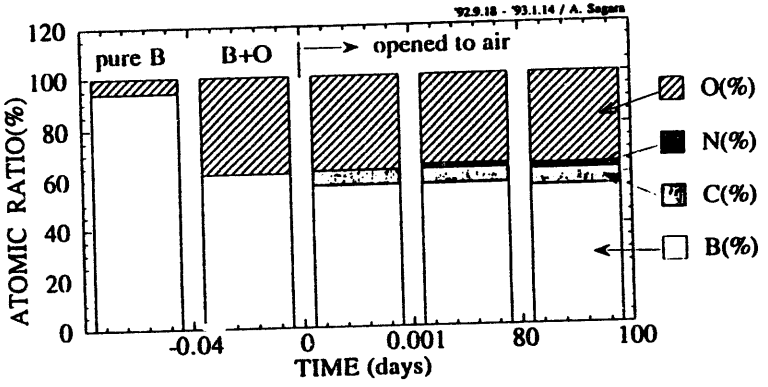

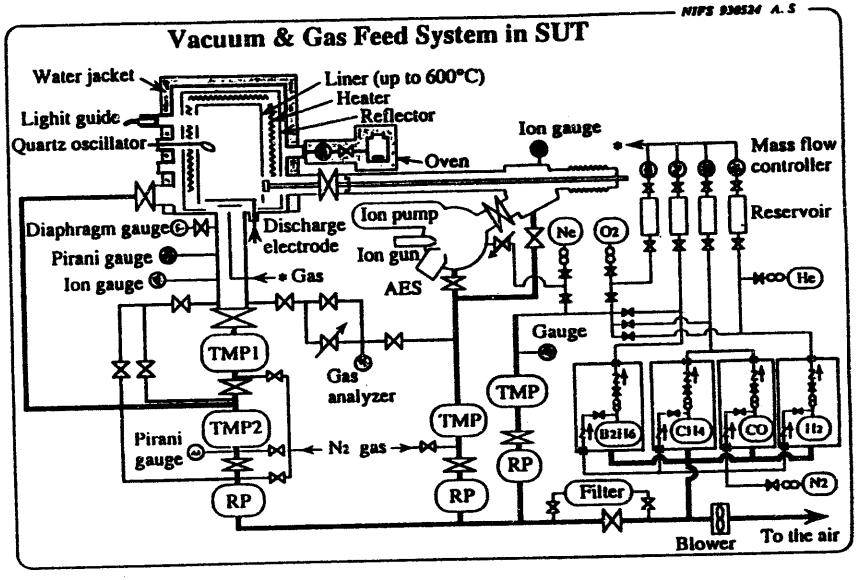

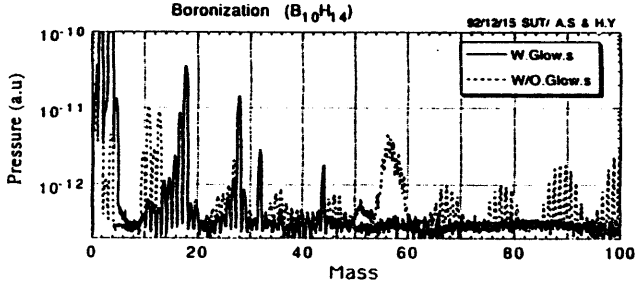

Decaborane is comparable with diborane as far as oxygen gettering capacity in B film is concerned.

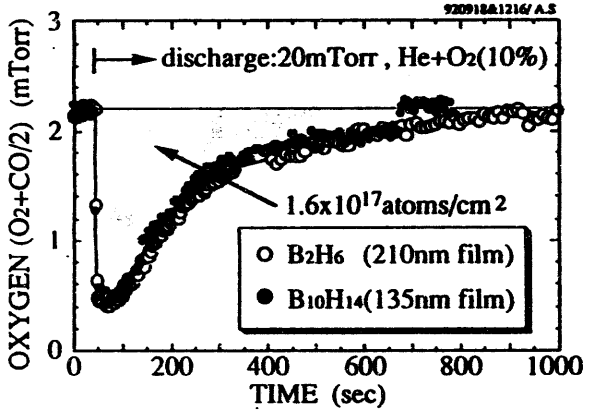

SUMMARY

(2) Present State of R&D on Boronization for LHD

1• Oxygen atoms penetrate into deeper layers over 50 nm,
and the B film of about 100nm thick is sufficient
for oxygen gettering.

This result coincides with the film thickness of about 200nm needed in plasma devices.

☞ *However, the penetration mechanism is not clear yet.*

2• B film after O_2 glow keeps a quite passive state in the air.

This result explains the fast conditioning observed in plasma devices.

NIFS 940126 A.Sagara

SUMMARY (cont.)

(2) Present State of R&D on Boronization for LHD

3• Decaborane is comparable with diborane as far as oxygen gettering capacity in B film is concerned.

4• Hydrogen in B film desorbs at lower temperature around 350°C than that around 500°C in carbon (TDS results presented by T.Hino)

This result explains the good discharges due to low H recycling performed in JT-60U, where the B film was prepared and operated at about 300°C.

☞ *R&D at room temperature is required for the V/V in LHD, because its temperature is limited below 100°C .*

NIFS 940126 A.Sagara

STUDIES ON TRITIUM RETENTION, PERMEATION AND RECOVERY OF PLASMA FACING MATERIALS AT JAERI

Kenji OKUNO

TRITIUM ENGINEERING LABORATORY
JAPAN ATOMIC ENERGY RESEARCH INSTITUTE

JAERI — TPL

OBJECTIVES

- From a tritium safety point of view, to estimate tritium amounts retained in plasma facing materials and permeated to first wall coolants
- To establish technology for tritium recovery from plasma facing materials

CONTENTS

1. TRITIUM RETENTION AND RECOVERY OF PFM

- ENERGY DEPENDENCE (< 1,000 eV)
- EXISTING CHEMICAL STATES OF TRITIUM
- RADIATION (neutron, γ-ray) DAMAGE EFFECTS
- TRITIUM RELEASE BEHAVIOR BY PHOTO IRRADIATION AND/OR HEATING

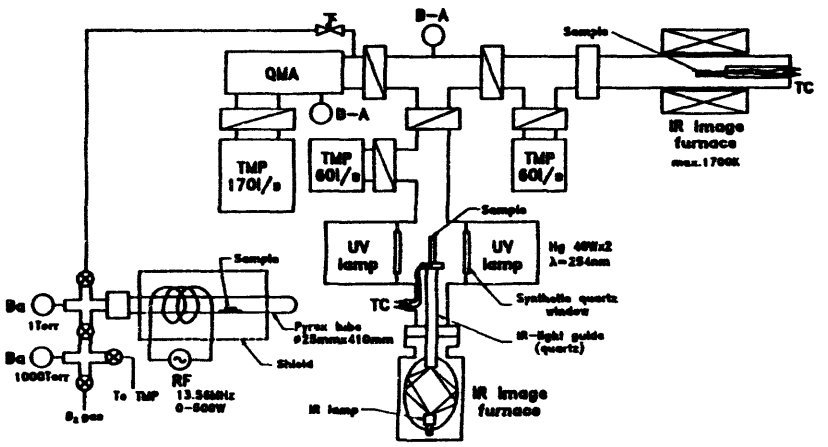

Schematic of apparatus for thermal/photo-desorption and retention research of hydrogen isotopes in plasma-exposed materials

Research of thermal/photo-desorption and retension of hydrogen isotopes in plasma-exposed materials

Specifications of apparatus

a) Plasma exposure system

-plasma chamber:	pyrex glass, 25mmOD x 410mm.
-plasma generation:	RF-discharge with external electrodes, 13.56MHz, 0 - 500W.
-gas pressure:	0.1 - 10Torr for D_2, (T_2).

b) Desorption system

-UV light irradiation:	40W low pressure Hg lamp, x2.
-IR light irradiation:	1kW IR lamp with focusing mirror and light guide, x2.
-thermal desorption:	max. 1700K with IR furnace.
-gas analysis:	quadrapole mass analyser.

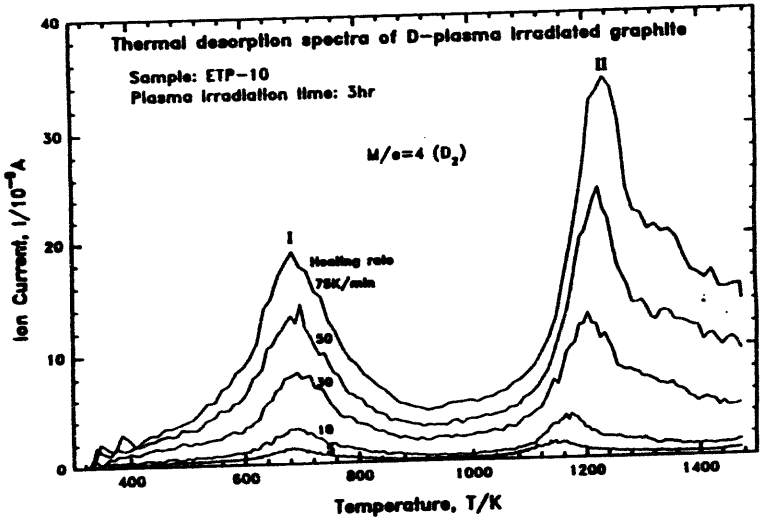
Thermal desorption spectra of D-plasma irradiated graphite
Sample: ETP-10
Plasma irradiation time: 3hr
M/e=4 (D_2)
I
II
Heating rate
75K/min
50
30
10
Ion Current, I/10^{-9}A
Temperature, T/K

M/e = 4

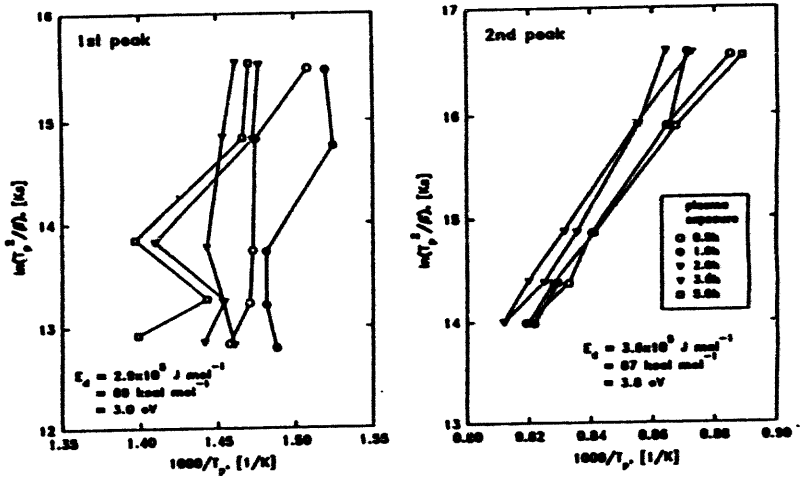
1st peak
2nd peak
E_d = 2.0x10^5 J mol^{-1}
= 48 kcal mol^{-1}
= 3.0 eV
E_d = 2.6x10^5 J mol^{-1}
= 67 kcal mol^{-1}
= 3.8 eV
1000/T_p, [1/K]

2. TRITIUM PERMEATION THROUGH PFM

- ION ENERGY (< 1,000 eV), ION FLUX, AND TEMPERATURE DEPENDENCES
- ISOTOPE EFFECTS
- RADIATION (neutron, γ-ray) DAMAGE EFFECTS
- DEVELOPMENT OF SIMULATION CODE FOR TRITIUM PERMEATION BEHAVIOR

JAERI TPL

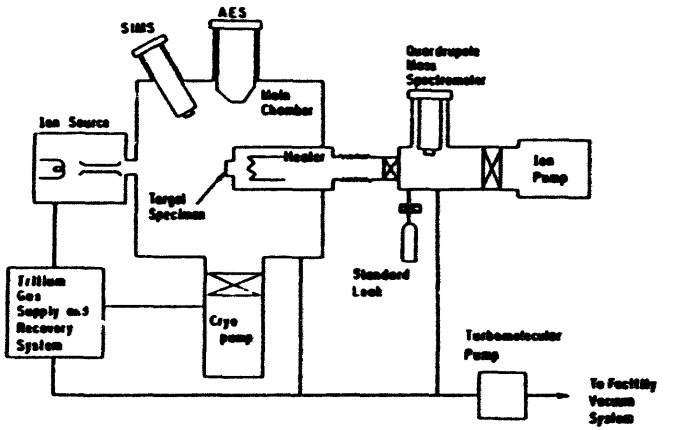

FIG. SCHEMATIC ILLUSTRATION OF THE APPARATUS FOR TRITIUM PERMEATION MEASUREMENT AT THE TRITIUM PROCESS LABORATORY OF JAERI

SPECIFICATION OF APPARATUS

- ION SPECIES : $D^+(T^+)$ >90%
- ION ENERGY : 100 - 2,000 eV
- ION FLUX : 1.5×10^{13} - 1.0×10^{15} $D^+(T^+)/cm^2s$
- TARGET TEMP. : ROOM TEMP. - 870 K
- PERMEATION MEASUREMENT
  1) QUADRUPOLE MASS SPECTROMETER
     (CALIBRATED BY AN ORIFICE CONDUCTANCE METHOD)
     m/e = 3 (HD) AND 4 (D_2)
  2) IONIZATION CHAMBER

- PRESSURE
  BASE PRESSURE
    MAIN CHAMBER : < 2.7×10^{-6} Pa
    DOWN STREAM : < 1.1×10^{-6} Pa
  UNDER IMPLANTATION
    MAIN CHAMBER : < 4.0×10^{-4} Pa
    DOWN STREAM : < 4.0×10^{-5} Pa
- TRITIUM : 1 g (MAXIMUM)
- TRITIUM STORAGE AND RECOVERY: ZrCo BED

JAERI ——— TPL

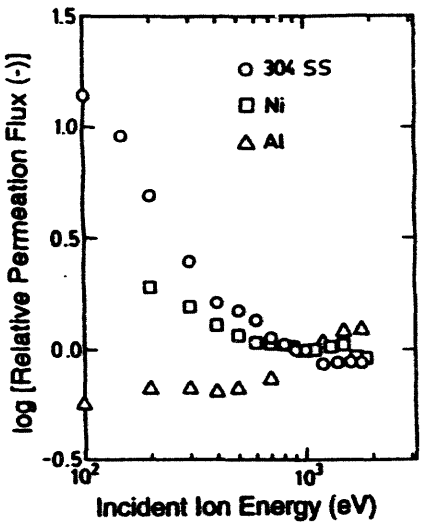

Incident Ion Energy Dependence of Deuterium Permeation Flux through Metals

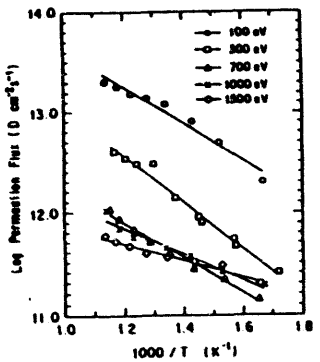

Fig. Temperature Dependency of Permeation Flux of D^+ Ions Through 304 SS

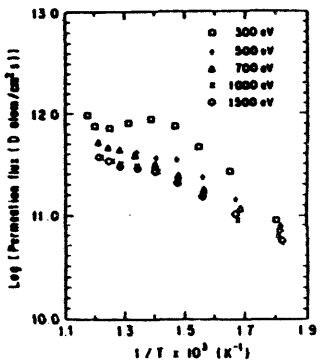

FIG. TEMPERATURE DEPENDENCE OF PERMEATION FLUX OF DEUTERIUM IMPLANTED INTO Ni

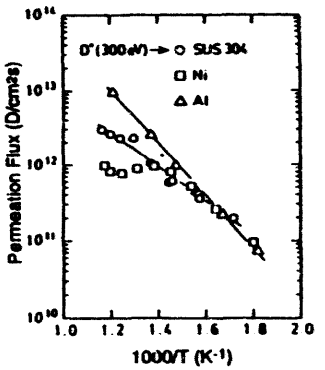

Temperature Dependence of Deuterium Permeation Flux through Metals

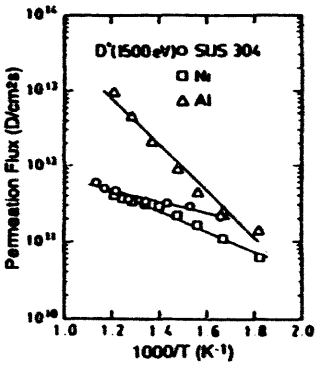

Temperature Dependence of Deuterium Permeation Flux through Metals

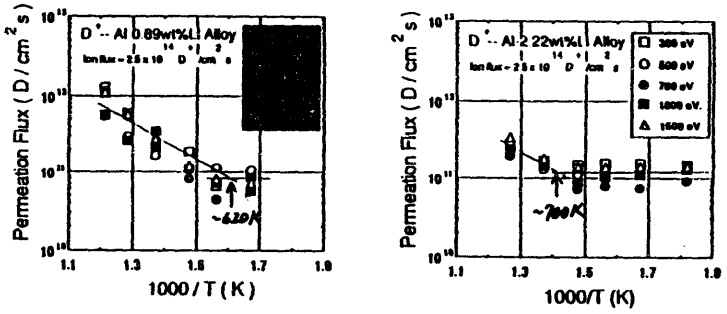

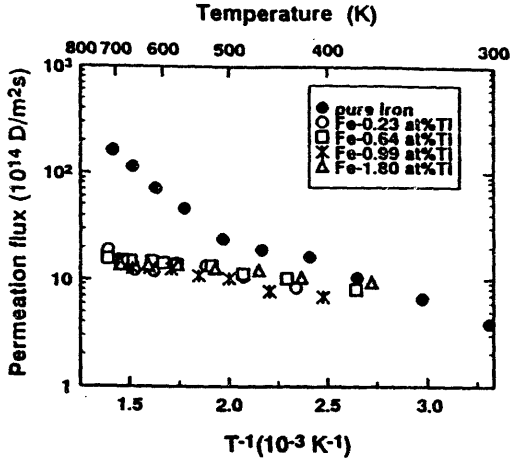

Fig. Temperature dependence of permeation flux for the incident ion energy of 300 eV.

R&D SCHEDULE FOR STUDIES ON TRITIUM RETENTION, AND RECOVERY OF PLASMA FACING MATERIALS

FISCAL YEAR	1992	1993	1994	1995	1996	1997	1998
Construction of experimental apparatus for photo/heating desorption and experiments using CI level tritium - Desorpion characteristics Heating temperature Wave langhth of photo - Existing chemical state - Measurement of tritium retention			Graphites, Be, Metals				
Design and construction of tritium recovery system for PMFs - Demonstration of tritium recovery using gram level tritium				Graphites, Be, Metals			

R&D SCHEDULE FOR TRITIUM PERMEATION STUDY

FISCAL YEAR	1999	1990	1991	1992	1993	1994	1995	1996	1997
-DEUTERIUM PERMEATION ENERGY DEPENDENCE TEMPERATURE DEPENDENCE		SUS	Ni,Fe,Al	Mo, Fe-Ti	W, Nb, V, Ti-Al Be				
-TRITIUM PERMEATION ENERGY DEPENDENCE TEMPERATURE DEPENDENCE						Mo,W, Ti	Al, V, Be	ETC.	
-TRITIUM RETENTION IN PFMs						GRAPHITE, Be		ETC.	
-SIMULATION CODE									

Report on the Tritium Plasma Experiment (TPE)

Tritium Inventory and Permeation in ITER

Outgassing and Conditioning

Rion Causey
and
Don Cowgill

US/Japan Workshop
San Diego, California
January 1994

The Tritium Plasma Experiment (TPE) is a Unique Facility Devoted to Tritium-Material Interaction Studies

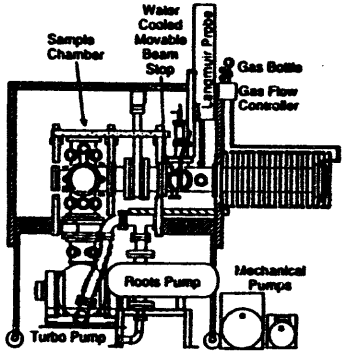

- TPE is presently being moved to the Tritium System Test Assembly (TSTA) at Los Alamos National Lab
- It should be ready for operation in June 1994
- It is capable of delivering a 100 eV tritium ion flux of 10^{19} T/cm^2-s to a 5 cm diameter sample

Sandia National Laboratories

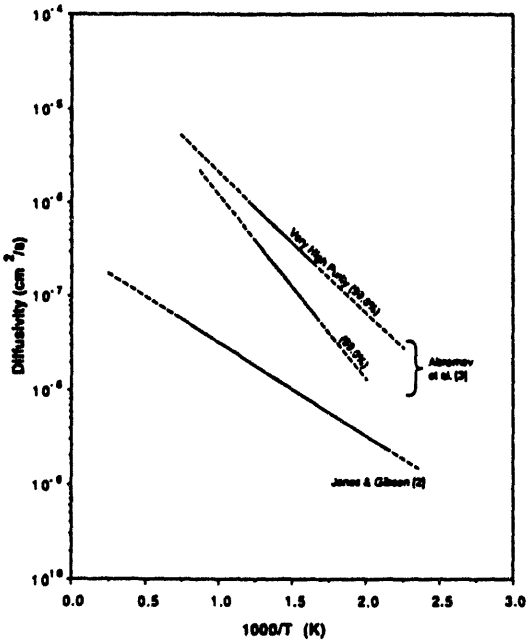

Hydrogen isotope diffusion in beryllium

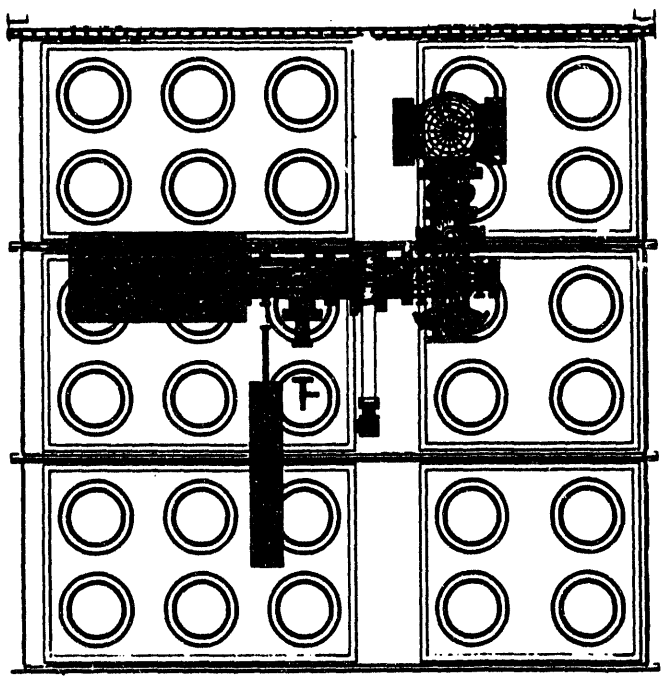

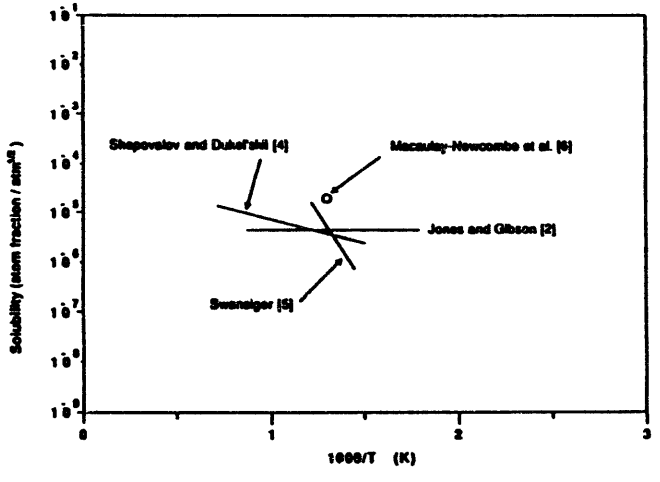

Hydrogen isotope solubility in beryllium

Recombination Rate Coefficient for Tritium on Beryllium

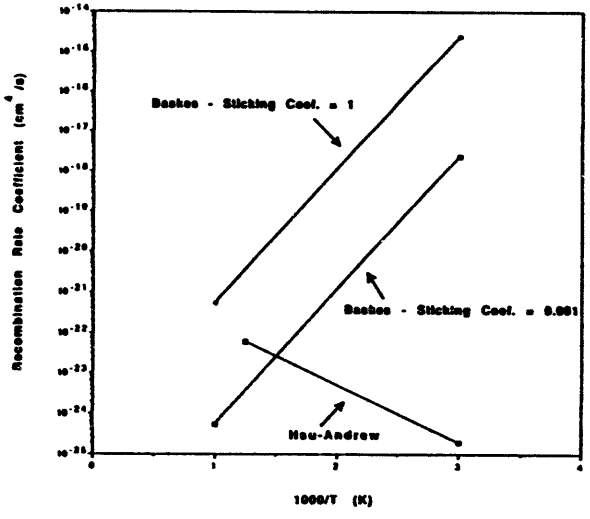

First Wall Calculations

- The first wall consists of 2 mm of beryllium on 5 mm of vanadium. This is backed by a compliant layer of lithium.
- The total surface area of the first wall is 1100 m^2.
- Between shots, the first wall is maintained at 500°C.
- At the beginning of each burn cycle, the front surface of the wall rapidly rises to 650°C. The back is held at 500°C.
- The D+T particle flux on the front surface is 10^{17} (D+T)/cm^2-s.
- The front boundary condition is recombination rate limited. The back boundary condition is zero concentration.

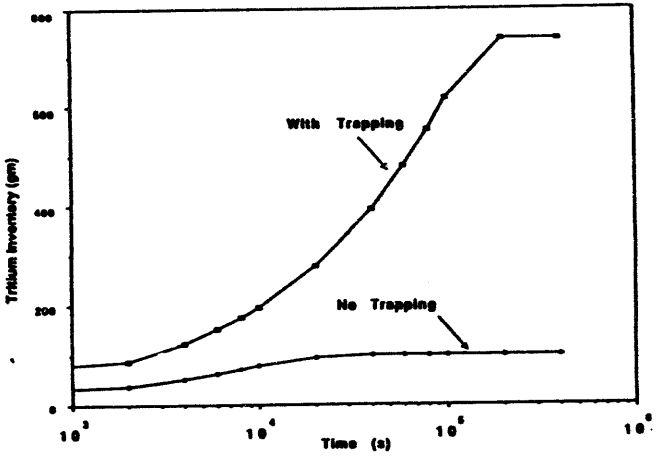

Tritium inventory in the ITER beryllium first wall using the best estimate of the surface recombination rate coefficient. Trapping case assumes trap density of 0.001 atomic fraction.

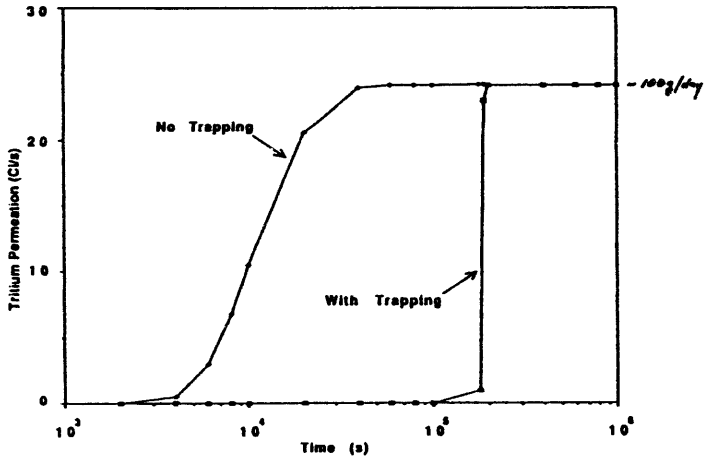

Tritium permeation through the ITER beryllium first wall using the best estimate of the surface recombination rate coefficient. Trapping case assumes trap density of 0.001 atomic fraction.

Limiter Calculations

- The ITER limiter consists of 20 mm thick slabs of beryllium between the first wall segments.
- The total area of the limiters is 500 m^2.
- Between shots, the limiters are maintained at a uniform 500°C.
- During the burn cycle, the limiter front surface rises to 800°C and the rear surface rises to 650°C.
- The D+T particle flux on the front surface is 10^{17} (D+T)/cm^2-s.
- The front surface boundary condition is recombination rate limited.

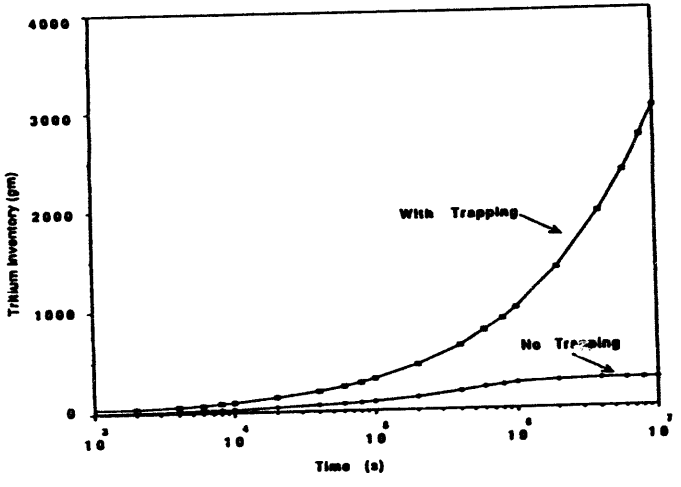

Tritium inventory into the 20mm thick beryllium limiters using the best estimate of the surface recombination rate coefficient. Trapping case assumes trap density of 0.001 atomic fraction

Divertor Calculations

- Our calculations for the divertor looked only at the tritium permeation through the 4 mm thick beryllium tubes into the compliant lithium layer.
- The total heated (plasma exposed) surface area was approximately 200 m^2.
- Between shots, the beryllium is held at 500°C.
- At the beginning of the burn cycle, the outer beryllium surface rapidly rises to 936°C. The inner surface is held at 500°C.
- The D+T particle flux on the heated sections of the divertor tubes averages about 10^{19} (D+T)/cm^2-s.
- The front surface is assumed to be recombination rate limited. The rear surface is assumed to have zero concentration.
- At this elevated temperature, the Baskes model for the recombination rate coefficient is assumed with a sticking coefficient of 1.0.

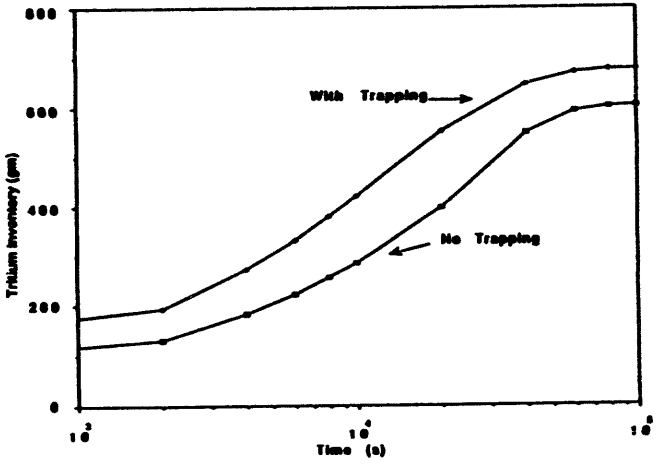

Tritium inventory in the beryllium section of the ITER divertor using the best estimate of the surface recombination rate coefficient. Trapping case assumes trap density of 0.001 atomic fraction.

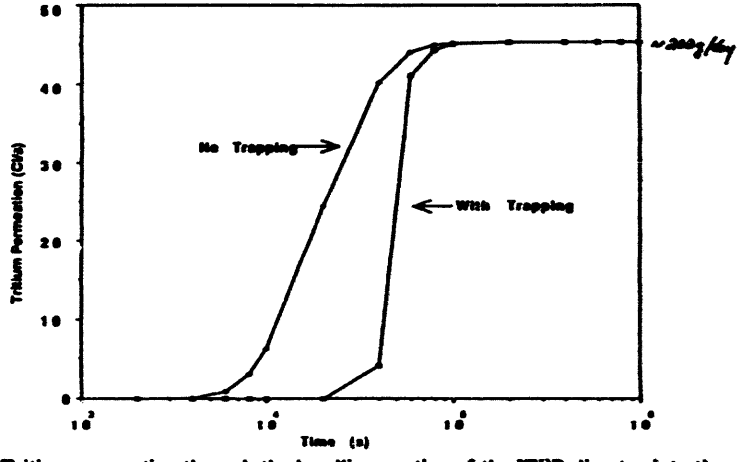

Tritium permeation through the beryllium section of the ITER divertor into the lithium using the best estimate of the surface recombination rate coefficient. Trapping case assumes a trap density of 0.001 atomic fraction.

Conclusions

- The calculations performed in this report show the tritium inventory and permeation in the ITER reactor to be very sensitive to both the surface recombination rate coefficient and the neutron induced trapping. Experimental data on both parameters is required to reduce the error bars on the calculated tritium inventories and permeation rates. Specifically, experiment using beryllium neutron irradiated at elevated temperatures is needed.

- At present, we can only say that the total tritium inventory in the beryllium components of the first wall, limiter, and divertor lies between 1 and 4.4 kilograms. The permeation rate of tritium into the lithium compliant layers of the first wall and divertor is calculated to be about 7 grams/1000 second shot (~300 grams/day with a 50% duty cycle).

Why Is Conditioning Needed?

- To reduce plasma contamination by minimizing impurity influx from walls and plasma-facing components.
  - Particularly O-bearing contaminants (water)
- To reduce H-recycling during plasma startup, to help provide reliable density control.
- To control in-vessel tritium inventory.

Porous Beryllium Materials Outgas Similar to Graphite

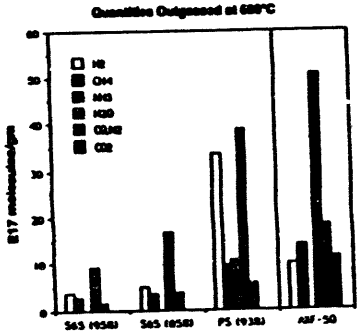

- Impurity gases:
  Primary = water & hydrogen
  Secondary = carbon & nitrogen compounds
- Plasma-spray Be outgases 4-times more water than S65 of comparible porosity
- Plasma-spray Be also outgases a small quantity the carrier gas, 0.3×10^{17} Ar/gm

Water Desorbs Very Slowly from Plasma-Sprayed Be, Even at 600°C

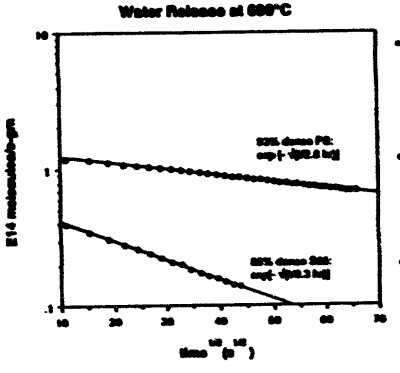

- Water release is diffusion controlled:
  Release varies as $\exp(-t^{1/2})$
  Using $2Dt \propto \ell^2$, gives
  t=280 hrs for ℓ=1cm thick
- Long, slow release indicates a very tortous diffusion path.
  Decreasing the porosity may further increase release time.
- This water is probably absorbed in the oxide (very hygroscopic) which is present on each powder particle.

Room Temperature Air Exposure Rapidly Reloads Be Materials with Impurities

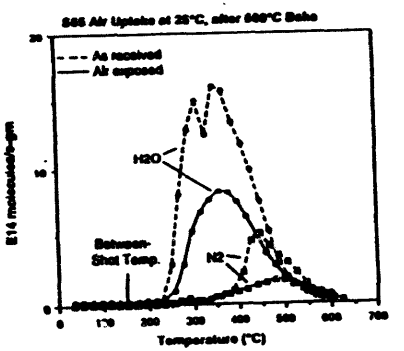

- Impurity absorption at 150°C is expected to be similar

Conclusions on Contaminant Behavior:

- O-bearing contaminants are not completely desorbed from either Be or Graphite by bakeout to 350°C.
- Some residual contaminants will be desorbed by plasma heating of PFC's. They will be rapidly desorbed by disruption events.
- These contaminants will be gettered by Be.
- BeO deposits at 150°C can act as sinks for weakly-bound gases, causing repeated recycling into the plasma.

Current Techniques Used to Condition Tokamaks:

- Prebaking of invessel materials
- Vacuum bakeout
- Operation at elevated temperatures
- Active contaminant gettering with B, Be, Li, Si, etc.
- Discharge conditioning: GDC (H, O, He)
  TDC, PDC, DDC (H, He)

US Tokamak Experience:

Graphite-Lined Machines

TFTR: Warm bakeout (150°C), RT operation
Boronization with diborane, Li pellets
He GDC overnight
He TDC, PDC every 5-30 shots

DIII-D: Hot bakeout (350°C), RT operation
Boronization with diborane
He GDC hot, overnight
He GDC for 5 min. every 2-3 shots

Be in Machines

ISX-B: 200°C operation
Be actively getters O and C impurities

GDC Removes Hydrogen and Weakly-Bound Contaminants by Ion-Induced Desorption

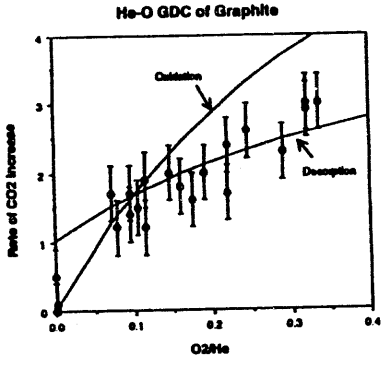

- He-O GDC is a 2-step process: Oxidation - Desorption
- GDC is very efficient: For 400eV He desorption of CO, CO_2 from graphite, the desorption yield ≈ 20C/He
- Shielded surfaces are not conditioned: He-O GDC erosion occurs normal to plasma sheath and textures the surface.

He GDC Is Used in All Tokamaks

- Most efficient method, particularly at high temperature
- He GDC: overnight and weekends between shots (DIII-D and JT-60U)
- Depletes the near-surface layer:
  300eV He range ≈3.6nm in Graphite
  ≈4.5nm in Be
- Penetrates into shadows better than Tokamak discharges
- He GDC won't work in a high toroidal magnetic field

Optimum Discharge Characteristics for Efficient Wall Conditioning

- Particle impact energies of few hundred eV, for large desorption yield.
- Random impact angle, for large yield, good depth, and no texturing.
- Low electron energies (< 10 eV), for minimal ionization or dissociation of desorbed impurity gases.
- Low background gas pressure ($<10^{-5}$ torr), for rapid evacuation and low gas throughput.

ICR Conditioning Can Produce Wall Impact Energies and Fluxes Similar to He GDC

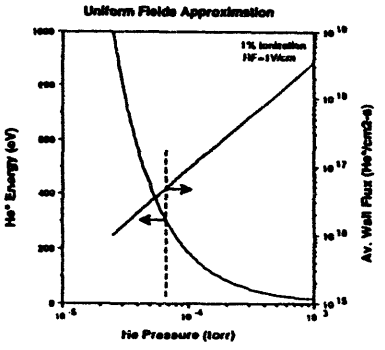

- Ion mean-free-path to charge exchange determines He^+ energy. At 400eV,
  $\sigma_{cx} \sim 10\,\sigma_{scatt} \sim 10\,\sigma_{ioniz}$
- Low gas pressure is required to produce energetic neutrals.
- Discharge is sustained at higher energies by an increase in the ionization cross-section.
- Typical He GDC parameters:
  300eV, 10^{13}-10^{14} He^+/cm^2 s

Computed Wall Flux Is Similar to GDC Flux

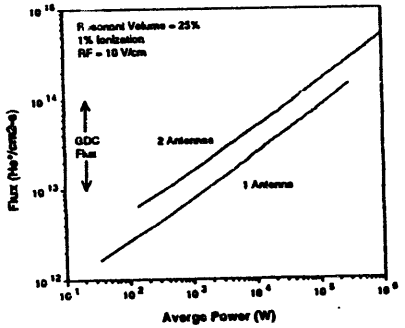

- Flux increases with
  - He° energy
  - degree of ionization
  - gas pressure
- ICR conditioning should be more efficient than GDC due to
  - lower pressure
  - random impact angle
  - better penetration into gaps between tiles

ECR Can Produce Large Neutral Wall Fluxes

- Sakamoto, et.al. compared the conditioning by low-P ECR with TDC (1% duty cycle) on JFT-2 (JAERI):

	ECR-DC (2 kW) $T_e = 60 \sim 100$°C	TDC (2 kW) $T_e = 80 \sim 180$°C	Background pressure
CH_4	3.3×10^{-6} Pa	6.6×10^{-6} Pa	2.7×10^{-7} Pa
H_2O	8.6×10^{-6} Pa	9.3×10^{-6} Pa	1.3×10^{-6} Pa
CO	3.4×10^{-6} Pa	3.1×10^{-6} Pa	4×10^{-7} Pa

Conclusion: Both methods have approximately equal cleaning effect.

- However, *He° energies are low.*

Major Findings:

- Graphite and porous Be have similar bakeout characteristics.
  Some impurities will remain after bakeout.

- Desorbed O-bearing contaminants are equally-well handled by Be or Boronization.
  Boronization is not needed with Beryllium.

- Between-shot discharge conditioning should be available to control:
  - impurities weakly bound on/in BeO deposits
  - startup H-recycling (including effects of BeO layers)
  - T-inventory in oxide-coated Be and C-T codeposits

- Low-pressure ICR conditioning has the best parameters for efficient discharge cleaning in high B-fields.

Real-Time Boronization in PBX-M Using Erosion of Solid Boronized Targets

H. W. Kugel[1], Y. Hirooka,[2] J. Timberlake[1], R. Bell[1], A. England[3], R. Isler,[3] S. Jones,[4] R. Kaita[1], S. Kaye[1], M. Khandagle,[2] R. Moore[5], M. Okabayashi[1], S. Paul[1], S.Sesnic[1], H. Takahashi[1], W. Tighe[1], S. Von Goeler[1], and A. Post-Zwicker[3]

1) PPPL, Princeton University, Princeton, NJ 08543
2) IPFR, University of California at Los Angeles, Los Angeles, CA 90024
3) Oak Ridge National Laboratory, Oak Ridge, TN 37831
4) Massachusetts Institute of Technology, Cambridge, MA 02139
5) Evans East, Inc. Plainsboro, NJ 08536

U.S.-Japan Workshop on
High Heat Flux Components
and
Plasma Surface Interactions for Next Devices
San Diego, CA
January 24-27, 1994

PBX-M's Advanced Physics Features

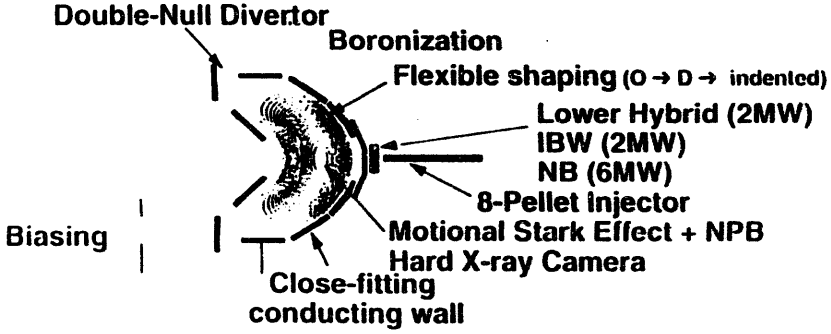

- **Typically PBX-M operations involve high duty cycles (~100-150 discharges per day) and the exploration of a wide range of experimental configurations.**

- **These conditions impose special requirements on possible boronization techniques.**

Real-Time Boronization in PBX-M Using Erosion of Solid Boronized Targets

Overview

- The initial boronization of PBX-M in 1992 used a Solid Target Boronization (STB) probe developed by Y. Hirooka, et al., IPFR, UCLA [1,2].

- This initial STB (Probe-1) used a mushroom shape and consisted of a 10.7% boronized 2-D Carbon-Carbon composite containing 3.6 gm of boron in a B_4C binder. Good PBX-M results and similar to those on TdeV [3] were obtained.

- These successful results encouraged the testing STB of probes with very high boron fractions and capacities for many boronizations to support the high PBX-M duty cycles and range of experimental configurations.

---

[1] Y. Hirooka and R.W. Conn, "A Review of Materials Erosion and Redeposition Research at UCLA for the Development of Plasma Facing Components in ITER", IPPL, University of California, Los Angeles, Report UCLA-PPG-81478, March 1983, and to be published in Atomic and Plasma Material Interaction Processes in Controlled Fusion, ed. R. Janev, IAEA (1993), Vienna.

[2] H.W. Kugel, Y. Hirooka, J. Timberlake, et al., "Initial Boronization of PBX-M Using Ablation of Solid Boronized Probes", Princeton University, Princeton Plasma Physics Laboratory, Report PPPL-2903, May 1993.

[3] Y. Hirooka, *et al.*, "Solid Target Boronization in the Tokamak de Varennes: A Technique for Real-Time Boronization", Nucl. Fus. 32(11), 2029 (1992).

Real-Time Boronization in PBX-M Using Erosion of Solid Boronized Targets

- Material (Probes-2,-3,-4)
  - ~86% boronized graphite-felt composite containing 40μ diameter boron particles
  - Typical dimensions ~ 6 cm x 2.5 cm x 2.5 cm containing ~ 30 g of boron
    - High boron content (≤ 86%)
    - High retention of heat (thermal conductivity < 2000 that of graphite)
    - High resistance to thermal shock (flexible)
    - High boron ablation yields per probe (1 to 8 g)

- Procedure
  - Insert target probe into edge plasma
  - Ablate boron using OH or NBI heated discharges
  - Optimize ablation and minimize spallation using
    - Plasma TV Camera
    - Probe floating potential
    - UV spectroscopy
  - 1-2 hrs per application (20-30 pulses [800 ms])
  - Available applications/probe varies with ablation rate
  - 3 graphite-felt probes tested
  - 29 applications
  - > 17 grams of boron deposited in PBX-M

STB probe (BP-1) developed by Y. Hirooka, et al., IPFR, UCLA for the initial PBX-M boronization in 1992. The probe is a mushroom shape consisting of a 10.7% boronized 2-D Carbon-Carbon composite similar to that used previously for STB on TdeV. Total ablation 0.37 g.

Boronized graphite-felt probe (BP-2) after exposure to PBX-M plasmas during real-time boronization. The ions were incident from the left. Total boron ablation 1 g.

93X3149

Boronized graphite-felt probe (BP-4) after exposure to PBX-M plasmas during real-time boronization. Shown is the side facing the incident ions. Total boron ablation 7.3 g.

93X3099

Boronized graphite-felt probe (BP-3) after exposure to PBX-M plasmas during real-time boronization. The ions were incident from the right. Total boron ablation 8.3 g.

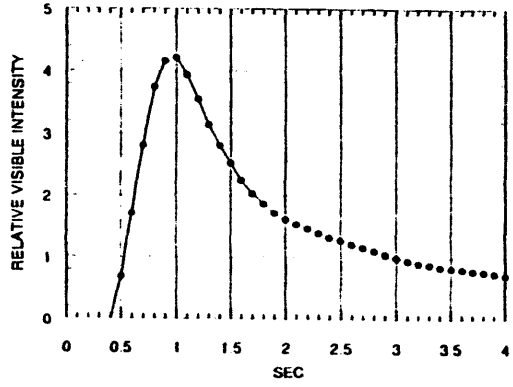

The visible light intensities emitted by boron probes during boronization discharges were monitored by a Plasma TV Camera. The waveforms exhibited a rise time characteristic of an approximately constant power density and an exponential-like decay.

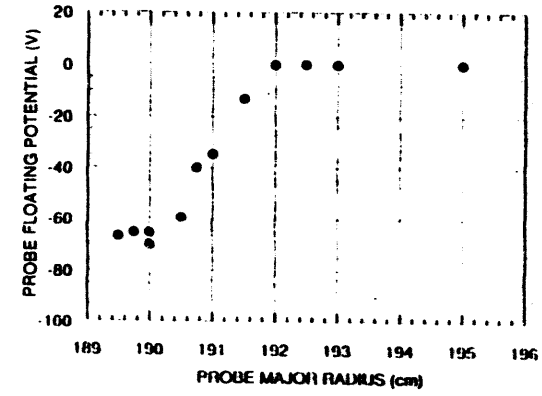

Floating potential of boron probe versus apparent radial position given by probe drive indicator. As a probe slowly erodes during many boronizations, the floating potential can be used to position the probe in the edge plasma

Real-Time Boronization in PBX-M Using Erosion of Solid Boronized Targets

- *EFFECTIVENESS*
  - DURING MODES OF OPERATION
    - ⇒ Continuous Real-Time Boronization Discharges
      - Boron is transported by the plasma around torus and into divertors
      - Little deposition on windows
      - Low-Z and high-Z impurities decrease significantly during application
      - Rapid improvement as plasma surfaces are covered during first 20-30 discharges with slower improvement thereafter
    - ⇒ Post Boronization Discharges
      - Low-Z and high-Z impurities decreased significantly after application
      - A short-term effect as boron is eroded
      - A long term effect as boron farther from the edge continues gettering
      - Up to 3-4 applications per week in PBX-M adequate; less depending on conditions
  - DURING DISRUPTIONS
    - After boronization, disruptions redistribute & reactivate boron

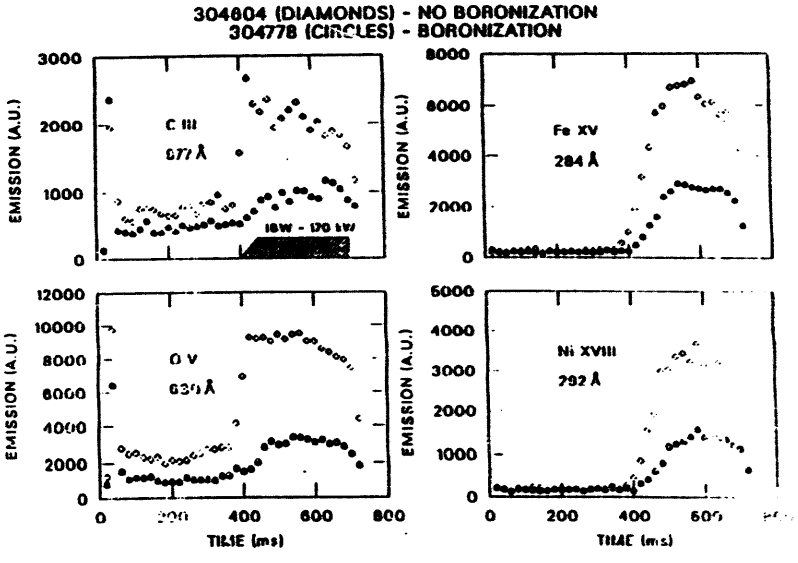

Boronization reduces impurities during ICW

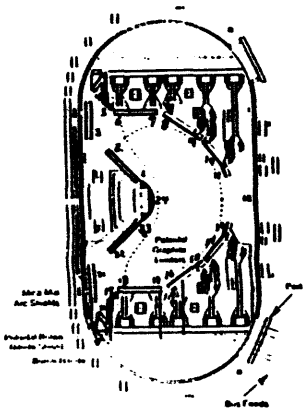

• Impurity deposition coupons for AUGER analysis were positioned poloidally at 24 locations at 4 toroidal locations.

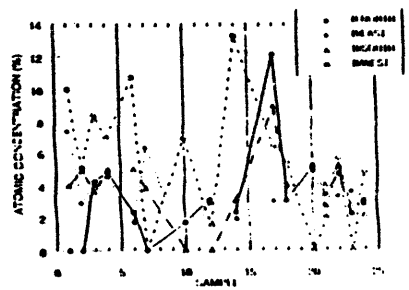

• Extensive boron distribution due to plasma transport and line of sight evaporation

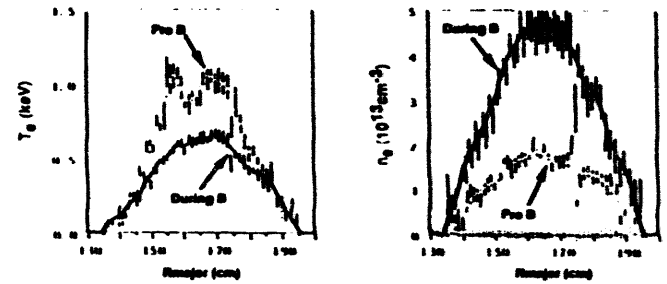

• During boronization (B) ohmic plasmas with steep, peaked density profiles are achieved.

• Less edge penetration and wider ablating surfaces may be useful for achieving target plasmas with steep, highly peaked density profiles.

Real-Time Boronization in PBX-M Using Erosion of Solid Boronized Targets

SUMMARY

- Evaporative, real-time, boronization is being performed routinely on PBX-M using boronized probes
  - 1-2 hrs per application
  - Up to several applications per week
  - 3 graphite-felt probes tested to date
  - 29 applications
  - >17 grams deposited in PBX-M to date

- Effectiveness
  - During Continuous Real-Time Boronization and Post Boronization Discharges
    - Low-Z and high-Z impurities are significantly lower
  - 3-4 applications per week seems adequate
  - Rapid recovery from recent air leak/N_2 vent
  - Reduced impurities during IBW
  - Disruptions redistribute & reactivate boron
  - Significantly accelerates conditioning to new regimes

- Possible method for achieving target plasmas with steep, highly peaked density profiles

ION BEAM MATERIALS RESEARCH LAB

Measurements of Fusion Synthesized T and T Fuel in JET, TFTR, DIII-D and TEXTOR

B.L. Doyle
Sandia National Laboratories
Albuquerque, NM

Credits:
W.R. Wampler, D.S. Walsh -- SNL/NM
R.A. Causey, R.J. Bastasz -- SNL/CA
F. Harmon, J. Knox ---------- ISU

Outline:

I. Motivation for measuring T
II. T measurement techniques
- Old
- New (T-monitor, NERD)
III. T measurement data in tokamaks
IV. Future research and development

WHY MEASURE TRITIUM ?

- **Provide data on the behavior of high energy ions in tokamak plasmas**
- **Tritium safety issues**
  - **Research (T permeation studies)**
  - **Operation (T accidents)**
  - **Decommissioning (Component decontamination)**

Tritium Detection Techniques

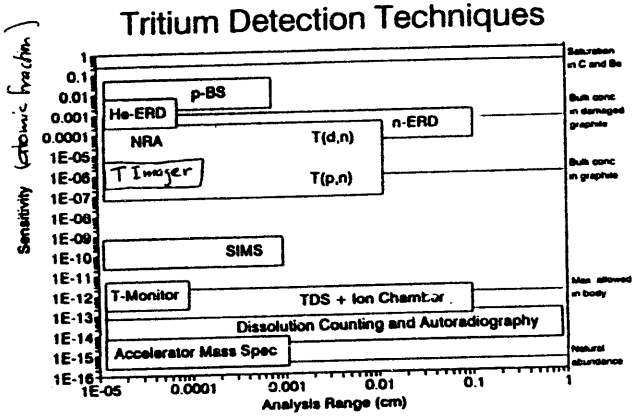

TRITIUM SURFACE CONTAMINATION MONITOR

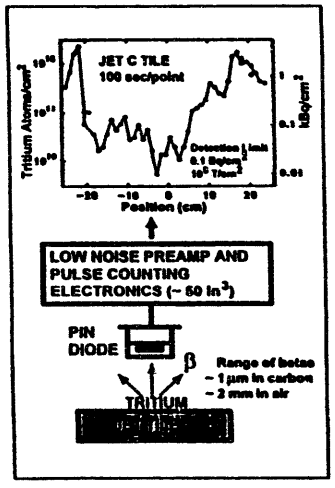

Counting betas using a PIN diode in air or vacuum provides quick real-time nondestructive measurement of tritium near surfaces.

Current applications:

- monitor build-up and clean-up of tritium inside TFTR during DT plasma experiments.
- map tritium on components from TFTR and JET.

Future potential applications for ITER:

- monitor in-vessel tritium.
- hand-held monitor for tritium on components after removal.

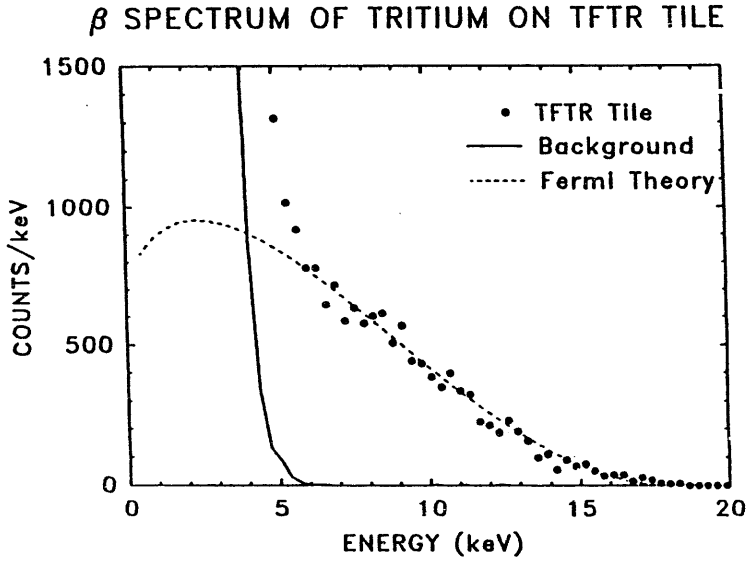

Bill Wampler (R) and Mark Adams use the new tritium monitor to measure tritium on a graphite tile that was used in the first tritium-fueled plasma experiments on the Joint European Torus Tokamak.

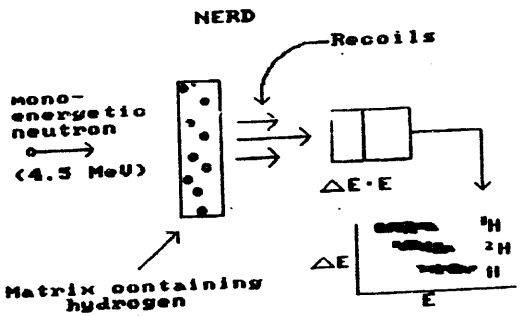

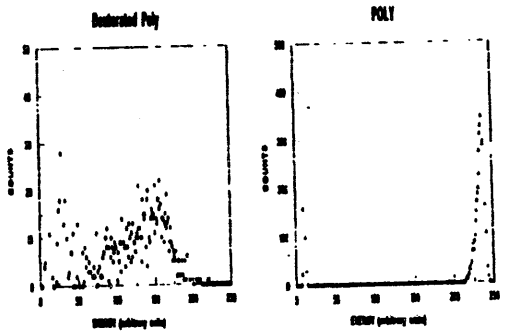

JET

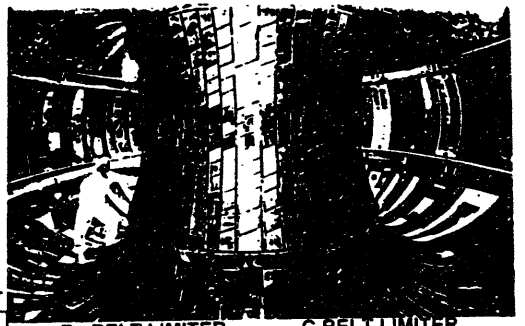

Be X-POINT

	#/cm²
T	~10¹¹
D	~10¹⁷

Be BELT LIMITER

TECHNIQUE	T/cm²
TDS	~10¹³
Dissolution	
T Monitor	~10¹¹

C BELT LIMITER

TECHNIQUE	T/cm²
TDS	
Dissolution	~10¹²
T Monitor	~10¹⁰

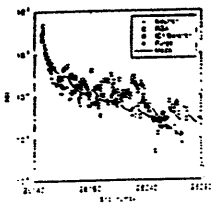

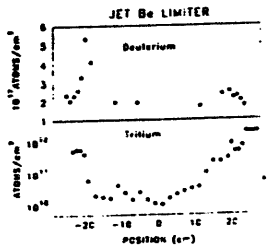

- T measurements prove that cleanup measures on JET (D_2 gas and isotope exchange) were highly effective in removing T from the torus.

TFTR

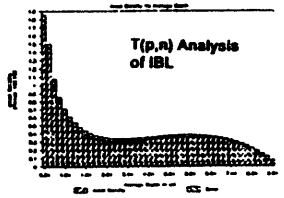

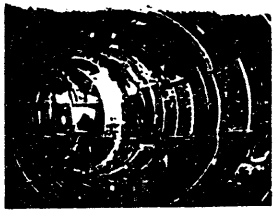

TFTR D(d,t) plasma
T implant profile in Si.

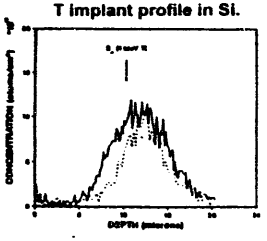

T Monitor
$8x10^{10}$ T/cm^2

D depth contours and
distribution on IBL tiles.

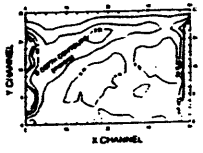

Technique	T/cm^2
ΣD(d,t)	~$2x10^{13}$
T(p,n)	$1.8x10^{13}$
SIMS	$5x10^{12}$
Dissolution	$1x10^{13}$
T Monitor	$1x10^{11}$

Measurements of T areal densities
on IBL tiles

- The difference between the T monitor and other measurements indicates deep implantation of HE T.

DIII-D and TEXTOR

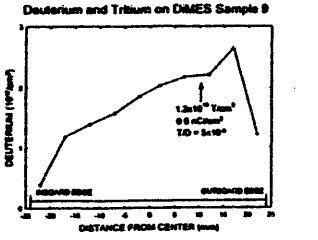

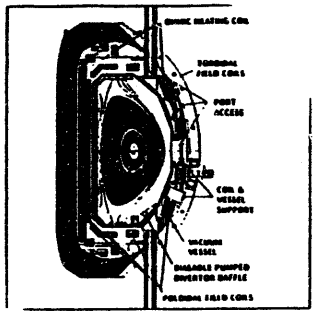

- T/D ≥ 10^{-7} ; TDS to determine true ratio
(deep T component)

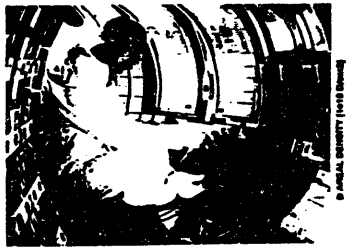

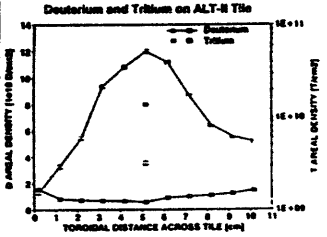

- T and D deposition patterns in TEXTOR differ
(co-dep. vs. implant)

Future Research and Development

1. Portable T-monitor
   - Working model
   - Screen components removed from US tokamaks
   - Transfer design to US, Japan, EC, RF Labs

2. TFTR in-situ monitor
   - Quantify effectiveness of T decontamination
   - Possible B-field interior scanning

3. Tritium Plasma Experiment (TPE)
   - On-line T measurements of coolant
   - Prototype T-monitoring systems for ITER

4. Advanced Tokamaks
   - TPX
     - d(d,t) measurements
     - T Safety
   - ITER
     - T62 Safety/Compatibility Task

Fig. 1 - Configuration of the beta probe on TFTR

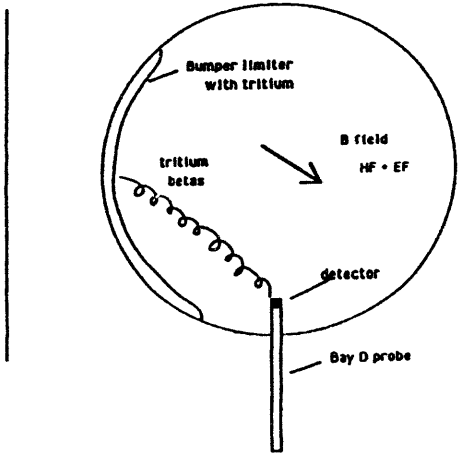

The betas emitted from the inner bumper limiter can be steered to the detector by the standard HF and VF fields (about 100 G)

The total beta flux emitted by the wall should be >10(7) /cm(2) sec. for a tritium inventory of 1 gram.

Miniaturized "remote-reporting" T-monitors could be placed throughout the ITER device to provide continuous, live-time measurements of T during operation.

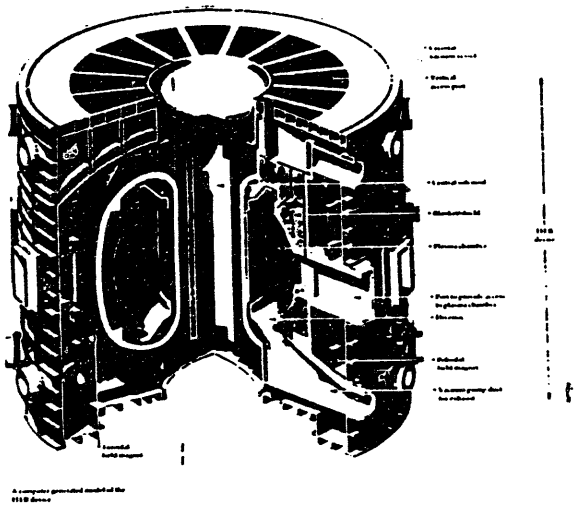

Sandia National Laboratories — Ion Beam Materials Research Lab

Main Points:

1. Convenient methods to measure the T content in solids for both research and tokamak labs are becoming very important as we enter the era of DT-burning devices.
2. The Sandia solid state T-monitor is such a method when the region of interest is in the first micron of the sample.
3. We will be glad to share the design of the T-monitor with our Japanese colleagues.

Session X

Erosion/Redeposition

Recent progress in the ITER-R&D related erosion and redeposition studies at UCLA

US-Japan Workshop on PMI/HHF
1/24-1/27/1994, UCSD

Yoshi Hirooka

PISCES Plasma-Surface Interactions Reserach Laboratory
Institute of Plasma and Fusion Research
University of California, Los Angeles

IPFR-UCLA

Table of Contents

IPFR-UCLA

Impurity transport exps.

A schematic diagram of the impurity transport experiment

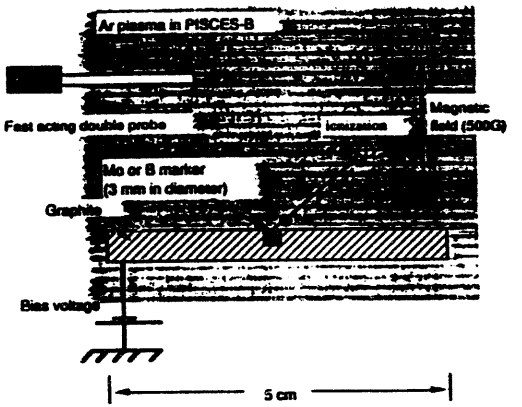

Concentration profile of Mo on the graphite surface

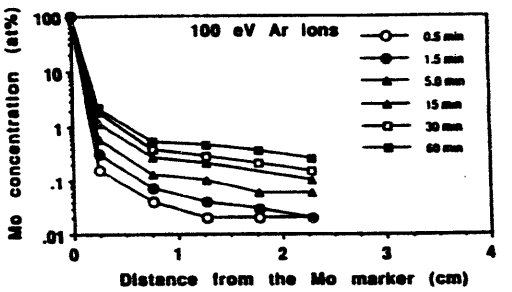

Trajectory of a sputtered particle simulated using the WBC Monte Carlo code

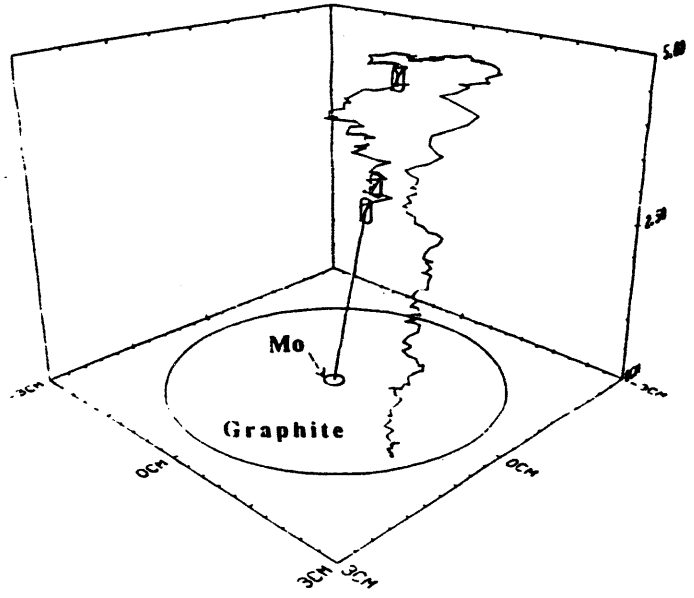

○ denotes an ionization event

Comparison of Mo redeposition data at 0.5 minute exposure with the result of WBC simulation

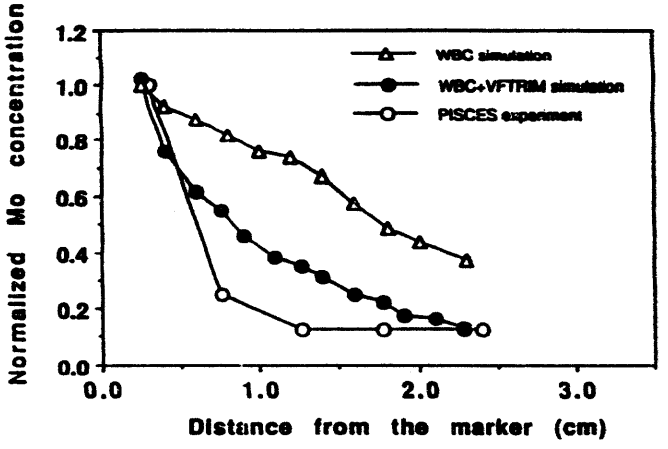

Beryllium facilities for PISCES

IPFR-UCLA

Beryllium handling facility for PISCES experiments

1. Major features
   - *Ultra-clean room for PISCES-B Mod (<0.01mg-Be/m^3)
   - *High-rate ventilation (3000 CFM) with HEPA-filtered exhaust
   - *Negative internal pressure
   - *Double-door limited access
   - *Computer-controlled interlock safety system
   - *Operation in full-face, air-supplied resparator

2. Milestones
   - *SOP reviewed (UCLA-EH&S, SNL, LANL) by: Aug. 92
   - *Facility conceptual design finished by: Sep. 92
   - *Detailed design of Be facilities finished by: Mar. 92
   - *School construction approval by: Jun. 93
   - *Complete facility construction by: Nov. 93
   - *On-site safety review by: Nov. 93
   - *First erosion experiments by: Jan. 93

IPFR-UCLA

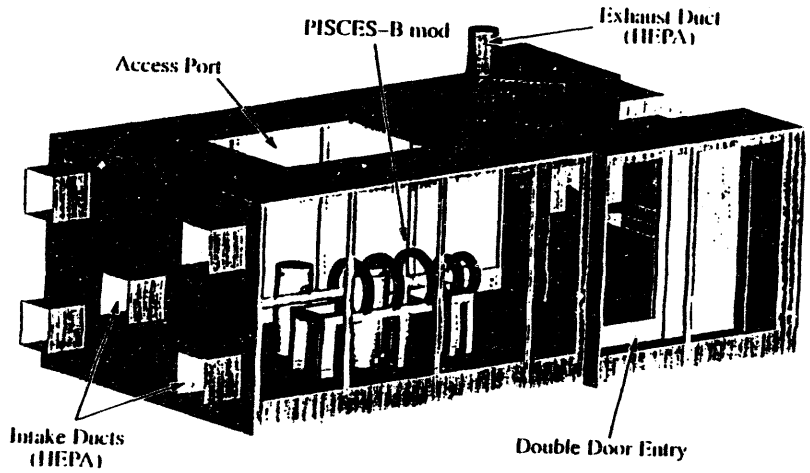

Fig. 10 The beryllium handling facility for PISCES–B mod.

1994 experimental plans

Erosion and redeposition studies in PISCES-B mod

***Start Be operation in the safety facility**

***Be erosion/redep. exps. under ITER-relevant conds.**

Characterization of redep. Be
Hydrogen retention in Be
Evaluation of new mateials (Be+C:C)

***Continue impurity transport exps. + modeling (w/ANL)**

IPFR-UCLA

AIIM

Association for Information and Image Management

1100 Wayne Avenue, Suite 1100
Silver Spring, Maryland 20910

301/587-8202

Centimeter

Inches

MANUFACTURED TO AIIM STANDARDS
BY APPLIED IMAGE, INC.

7 of 8

DIMES PROGRAM 1993 ACTIVITIES AND 1994 PLAN

by the DIMES TEAM
and presented by C.P.C. WONG

Presented at the
U.S./Japan HHF/PMI Workshop
San Diego, California

JANUARY 24–27, 1994

GENERAL ATOMICS

DIMES COLLABORATORS

• Samples preparation and characterization, plasma diagnostics, planning	SNL
• Modeling	ANL
• Disruption Studies	UNM, NCSU
• Erosion/Redeposition	UCLA

INTERNATIONAL

- TRINITI, Troitsk, Russia
- JAERI, Japan
- KFA, Jülich, Germany
- SWIP, Chengdu, PRC

GENERAL ATOMICS

OUTLINE

- Introduction
- 1993 activities
- Improved instrumentation
- In-situ measurement, reflectometry
- CY94 plan
- Long term plan

GENERAL ATOMICS

DiMES
DIVERTOR MATERIALS EXPOSURE SYSTEM

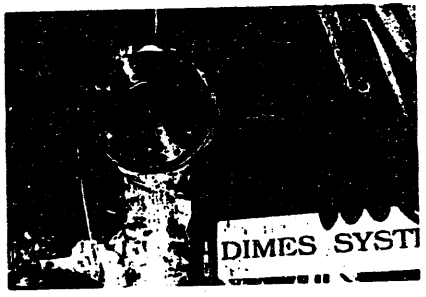

GENERAL ATOMICS

DIII-D DIVERTOR FLOOR AND DIMES SAMPLE

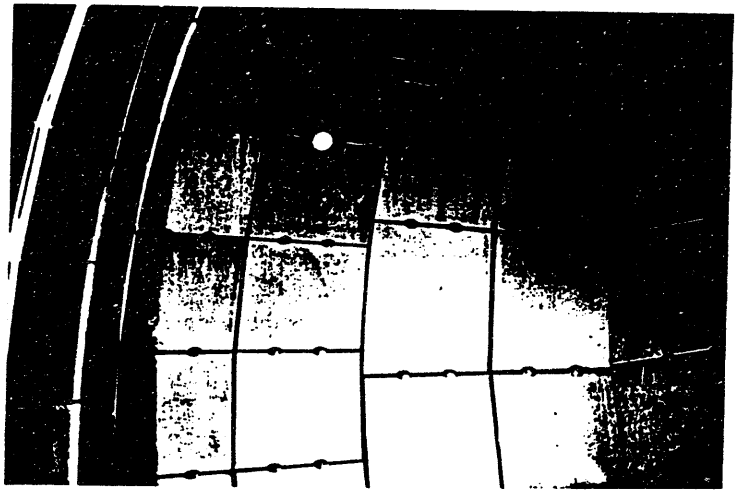

GENERAL ATOMICS

DIII-D DIVERTOR MATERIAL EVALUATION SYSTEM (DIMES)

- DIMES allows exposure of various materials to the DIII-D divertor plasma.
- Capabilities:
  - Strike point sweeping across sample.
  - 4.8 cm sample diameter.
  - Exposure for one or more shots.
  - Can be changeout.
  - Active instrumentation.
- In-situ, on-line measure technique being developed.

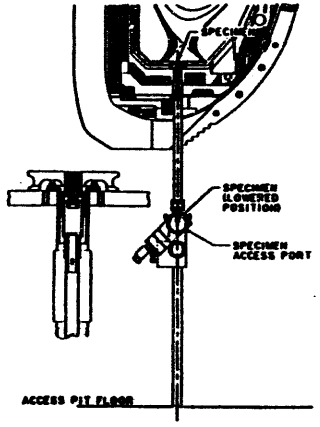

GENERAL ATOMICS

1993 DIMES SAMPLES EXPOSURE

DATE	SAMPLE #	MATERIALS	COMMENTS
March 2	15	ATJ graphite	Exposed to 2 pre-shots
March 3, 16–18	22, 21	ATJ graphite with Si chip insert	Bakeout and conditioning
March 29 & 30	16	ATJ graphite	Piggyback on 13 and 23 shots
July 14	35	ATJ graphite	Piggy on 16 shots
July 19	27	ATJ graphite with Si chip insert	He glow discharge cleaning
July 22	9	ATJ graphite with ^{29}Si chip implant	15 plasma shots with last second strike point on DIMES
August 23, September 11	30, 24	ATJ graphite with Si chip insert	Borosteel in DIII-D
September 13	TRINTI sample	MPGSB$_4$C	Exposed to 16 shots
October 1–29	SNL probe	Sheath physics	Testing of 3 different Langmuir probes
October 21	8	ATJ graphite W-coating with ^{29}Si implant	Dedicated experiment, sample exposed to 6 plasma shots

GENERAL ATOMICS

DIMES 1993 MATERIALS STUDIES ACTIVITIES SUMMARY

	No. of Experiments
Dedicated Experiments:	
ATJ graphite, ^{29}Si implant, 1 cm dia. W coating (sample #8)	1
Piggy-Back Experiments:	
ATJ graphite, ^{29}Si implant (sample #9)	1
ATJ graphite	3
MPGSB$_4$C	1
Surface Characterization Experiments:	
ATJ graphite	5
Sheath Physics Experiments:	
Langmuir probe	1
Disruption:	
MPGSB$_4$C coated sample	1

GENERAL ATOMICS

DiMES IMPROVED INSTRUMENTATION FEEDTHRU

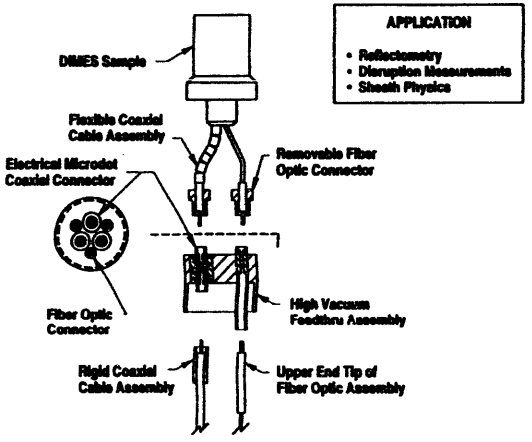

GENERAL ATOMICS

MATERIAL EVALUATION EXPERIMENTS IN DIII-D DIVERTOR

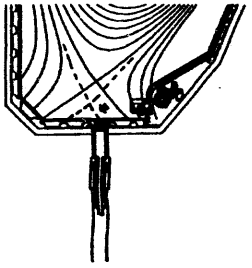

DIMES Sample Insertion

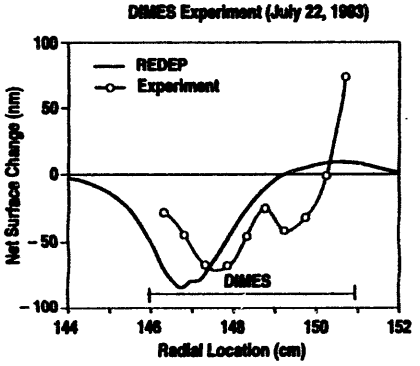

Comparison of Net Erosion with REDEP Model

GENERAL ATOMICS

IN-SITU REFLECTOMETRY

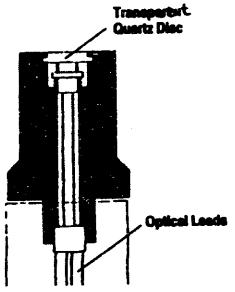

Sample Design

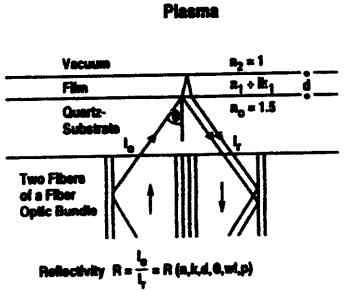

Optical Schematic

GENERAL ATOMICS

DRAFT DIMES EXPERIMENTAL PLAN CY94

	No. of Experiments
Dedicated Experiments:	
(Based on 2 of 43 DIII-D running days, DIMES can do 4 half-day experiments.)	
1. Erosion and redeposition experiments (including Be when possible)	2
2. International collaboration sample	1
3. Disruption	1
Piggy-Back Experiments:	
4. International collaboration samples	4
5. Surface characterization experiments	6
6. In-situ reflectometry	2
Others:	
7. Sheath physics experiments	2
8. Ion implantation experiments	2

NOTE: ITER CREDIT IS NECESSARY FOR THE PROGRAM

DIMES LONG TERM PLAN

- FY95 DIII-D projected to run for 21 weeks
  - This can become the most productive year for DIMES
- We have started to investigate the modification of DIMES for the Radiative Divertor configuration

SUMMARY

- DIMES system operated since early 1993
- Dedicated erosion/redeposition experiment performed
- DIMES team in place: sample changer, plasma diagnostics, modeling, samples preparation and characterization
- Other activities performed in 1993
- Conceptual design of improved instrumentation completed
- Design of reflectometry experiment underway
- Planning initiated for the 1994 campaign
- With 105 DIII-D running days planned, FY95 can be most productive for DIMES
- ITER credit is essential for 1994 and 1995

X-17

CHARACTERIZATION OF DIVERTOR PLASMA DURING DIMES8 SAMPLE EXPOSURE

Presented by

N.H. BROOKS

with contributions from

J. CUTHBERTSON,* D. BUCHENAUER,* C. LASNIER,†
W.P. WEST, and C.P.C. WONG

* Sandia National Laboratory.
† Lawrence Livermore National Laboratory.

Erosion/Redeposition studies with DIMES is a joint program of GA with the Argonne and Sandia National Laboratories.

JANUARY 24, 1994

GENERAL ATOMICS

Compound Tungsten/Graphite Erosion/Redeposition Sample

ATJ Graphite with implanted Si 29 layer and 100 nm Tungsten deposited in 1 cm diameter spot in center.

Net erosion/deposition of carbon outside W spot determined from change of depth of Si marker.

Erosion of tungsten from change in thickness of W film.

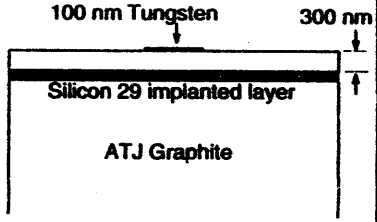

GENERAL ATOMICS

MECHANICS OF SAMPLE EXPOSURE

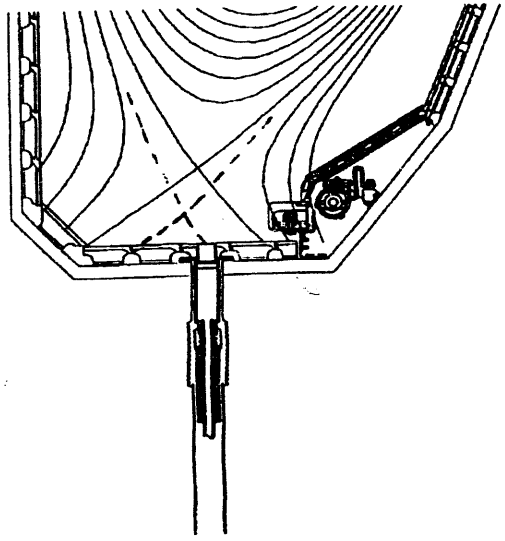

- Shelter sample in private flux region below X-point during set up of confinement regime
- Sweep outer strike point onto sample; hold fixed during each period of ELM-free H-mode

GENERAL ATOMICS

IR IMAGE DURING ELM-FREE H-MODE

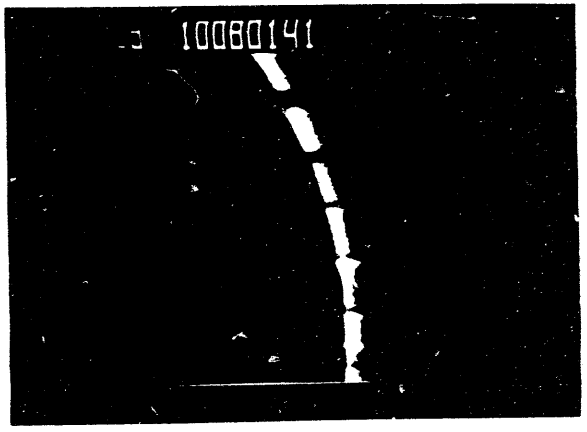

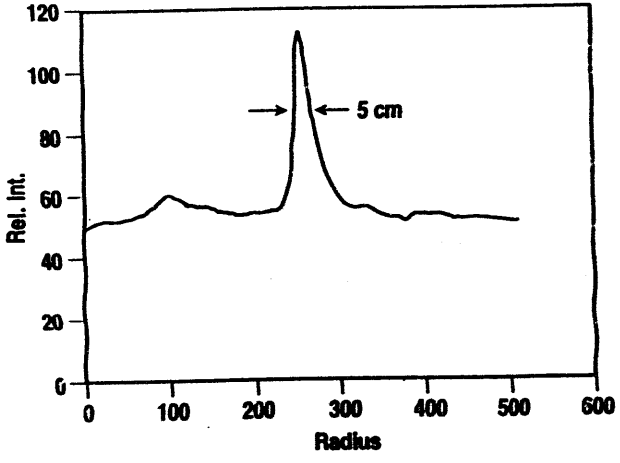

GENERAL ATOMICS

IMAGE OF C II LIGHT FROM CCD CAMERA

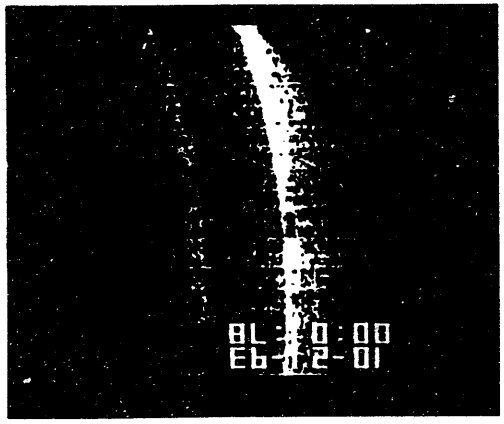

- Bright, narrow ring is visible when strike point initially moved to DIMES radius
- C II image provides visual confirmation that strike point is well-centered on DIMES sample

GENERAL ATOMICS

TOKAMAK DISCHARGE FOR DIMES8 EXPOSURE

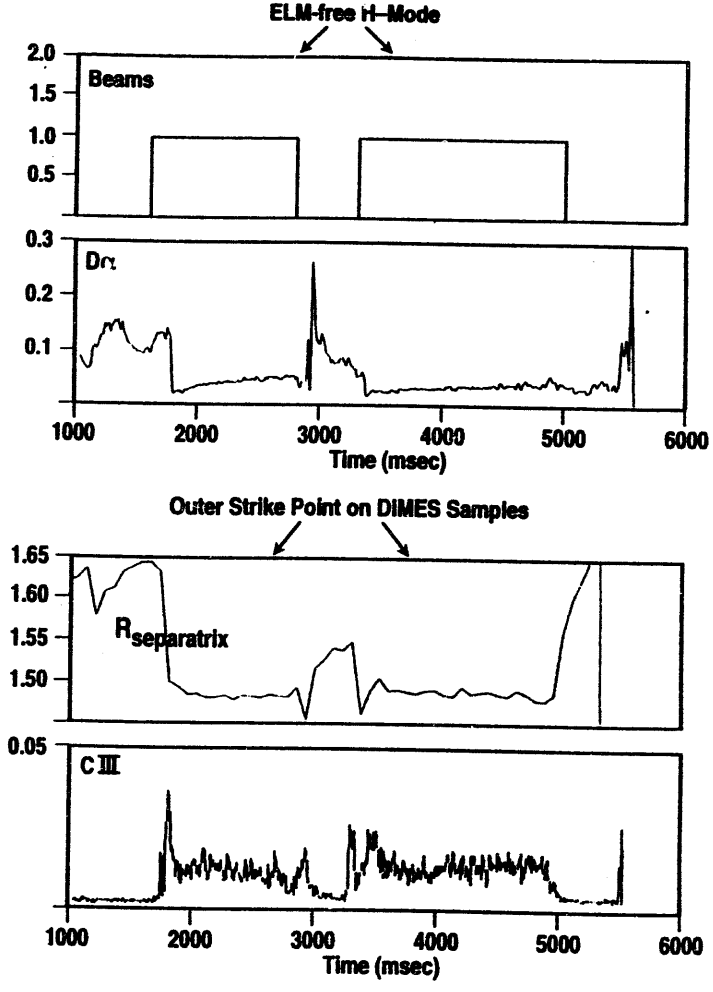

GENERAL ATOMICS

DIII-D DIAGNOSTICS FOR CHARACTERIZING DIVERTOR PLASMA

n_e, T_e, V_{FL}	—	Langmuir Probe Array
q_{DIV}	—	IR TV
$R_{separatrix}$	—	Global MHD fit to magnetic probes
C II, C III	—	Visible spectroscopy
C II image	—	CCD camera with spectral line filter

GENERAL ATOMICS

HEAT FLUX TO DIMES SAMPLE

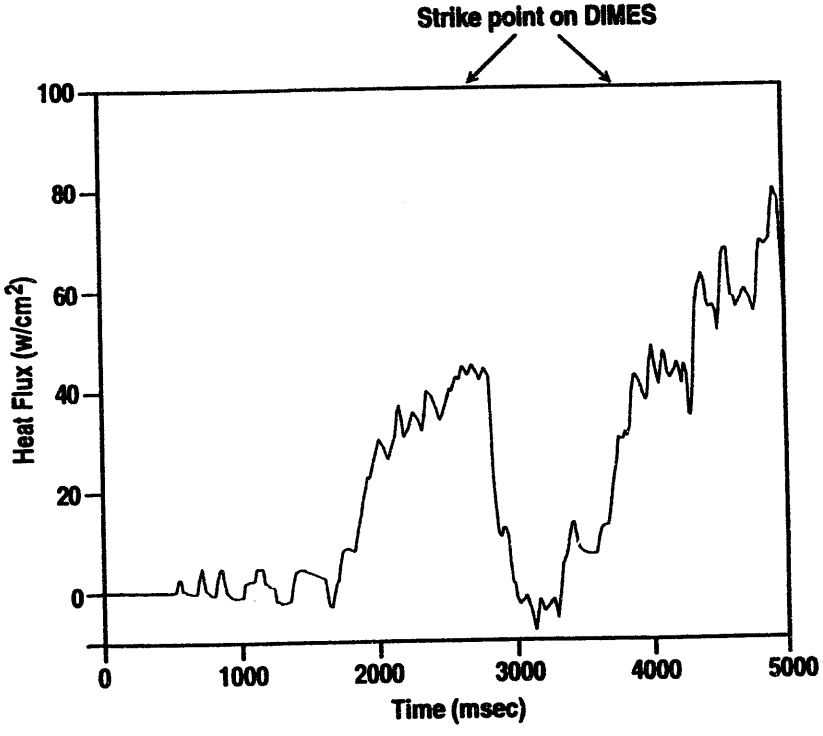

GENERAL ATOMICS

SPATIAL COVERAGE OF DIVERTOR DIAGNOSTICS

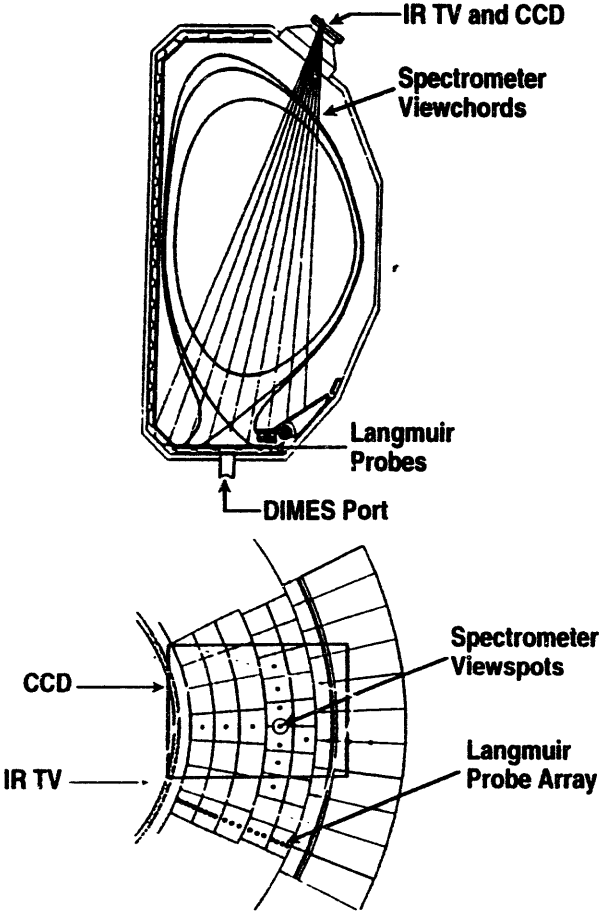

GENERAL ATOMICS

SUMMARY

- DIMES sample exposed to ELM-free H-mode in six, near-identical DIII-D discharges
- Key divertor parameters measured for input to REDEP modeling code of erosion and redeposition
- Collaborative program among GA, Sandia, and Argonne bench tests modeling code against real tokamak data

Measurements of Erosion and Deposition of Carbon and Tungsten by the DIIID Divertor Plasma

W. R. Wampler, R. Bastasz,
W. Cuthbertson, D. A. Buchenauer
Sandia National Laboratories
and
N. Brooks, R Junge and C. P. C. Wong,
General Atomics

US-Japan Workshop on PMI-HHF
UCSD, January 24-27, 1994

Two DiMES Samples have been exposed and analysed.

- ATJ graphite 5 cm diameter.
- Both were implanted with 200 keV ^{29}Si to provide a marker ~300 nm beneath the surface for C erosion measurements. Peak Si concentration is ~ 0.004 Si/C.
- A tungsten film ~ 100 nm thick by 1 cm diameter was deposited on one of the samples.

Exposures:

- Sample 9 was exposed on July 22, 1993. The outer strike point plasma was centered on the sample for 1 second during each of 15 shots.
- Sample 8, with the tungsten spot, was exposed October 21, 1993 for 13.5 seconds during 6 shots.
- H mode D plasmas

Analysis:

- Samples were analysed by Rutherford Backscattering Spectroscopy (RBS) using 2 MeV ^{4}He ions before and after exposure in DIIID.
- The change in depth of the Si marker gives the net erosion or deposition of carbon.
- On sample 8 the change in thickness of the W film gives the net erosion of W. Also the thickness of W deposited on C and C deposited on W were determined.

DIMES 8
TUNGSTEN FILM
COUNTS
CHANNEL
25000
20000
15000
10000
5000
0
0
100
200
300
400
500

DIMES 8
TUNGSTEN FILM
COUNTS
CHANNEL
30000
25000
20000
15000
10000
5000
0
440
450
460
470
480
490
500

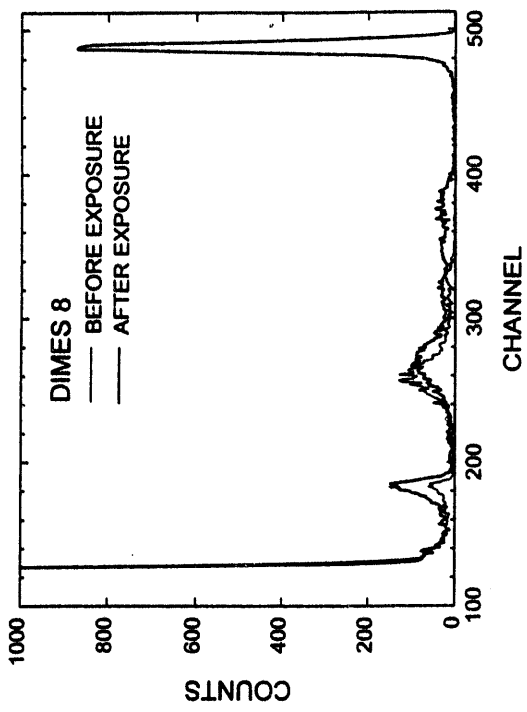
DIMES 8
BEFORE EXPOSURE
AFTER EXPOSURE
COUNTS
CHANNEL
0
200
400
600
800
1000
100
200
300
400
500

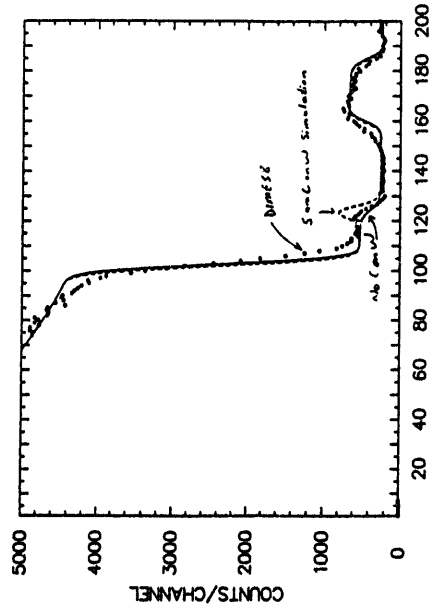
COUNTS/CHANNEL
CHANNEL
0
1000
2000
3000
4000
5000
20
40
60
80
100
120
140
160
180
200

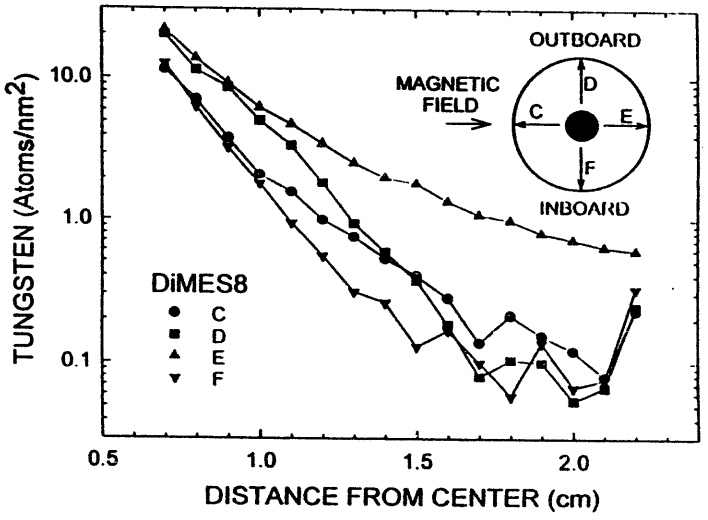
TUNGSTEN (Atoms/nm^2)
10.0
1.0
0.1
0.5
1.0
1.5
2.0
DISTANCE FROM CENTER (cm)
DiMES8
C
D
E
F
MAGNETIC FIELD
OUTBOARD
INBOARD
C
D
E
F

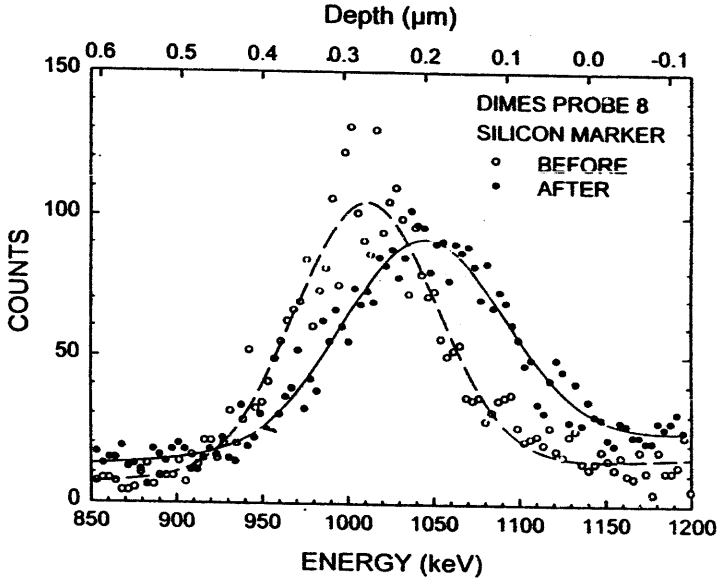
Depth (μm)
0.6
0.5
0.4
0.3
0.2
0.1
0.0
-0.1
COUNTS
150
100
50
0
850
900
950
1000
1050
1100
1150
1200
ENERGY (keV)
DIMES PROBE 8
SILICON MARKER
BEFORE
AFTER

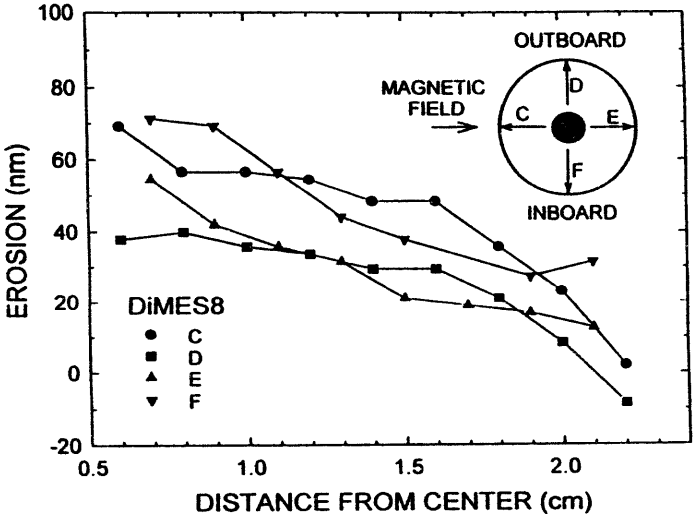
EROSION (nm)
DISTANCE FROM CENTER (cm)
DiMES8
C
D
E
F
MAGNETIC FIELD
OUTBOARD
INBOARD
100
80
60
40
20
0
-20
0.5
1.0
1.5
2.0

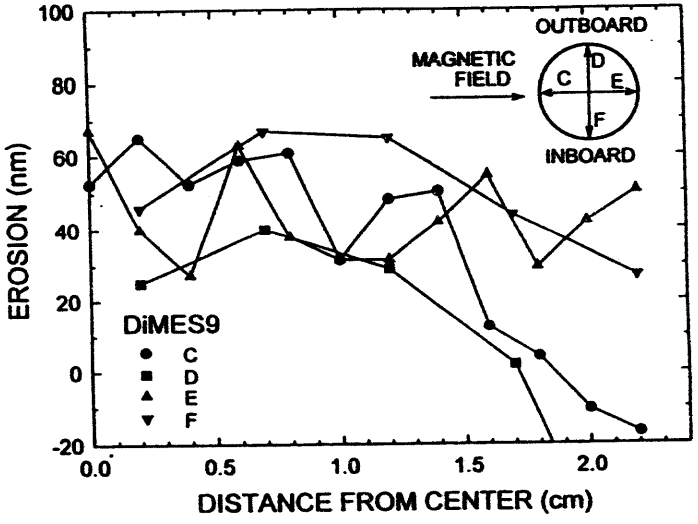
EROSION (nm)
DISTANCE FROM CENTER (cm)
DiMES9
C
D
E
F
MAGNETIC FIELD
OUTBOARD
INBOARD
100
80
60
40
20
0
-20
0.0
0.5
1.0
1.5
2.0

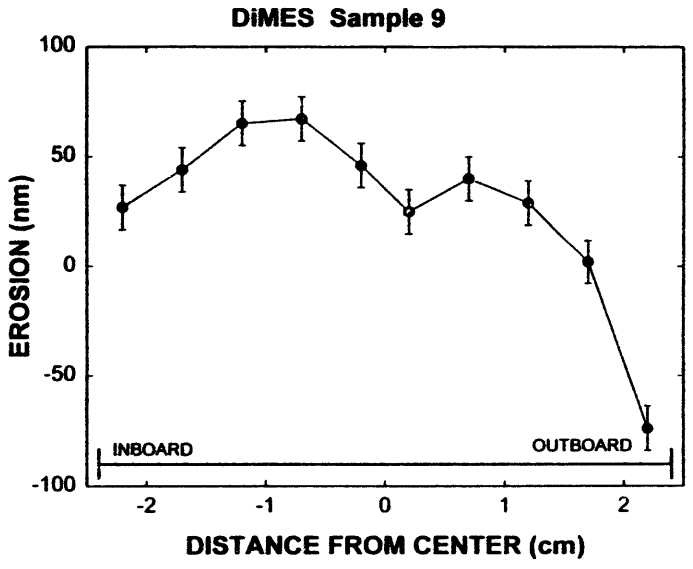
DiMES Sample 9
EROSION (nm)
100
50
0
-50
-100
INBOARD
OUTBOARD
-2
-1
0
1
2
DISTANCE FROM CENTER (cm)

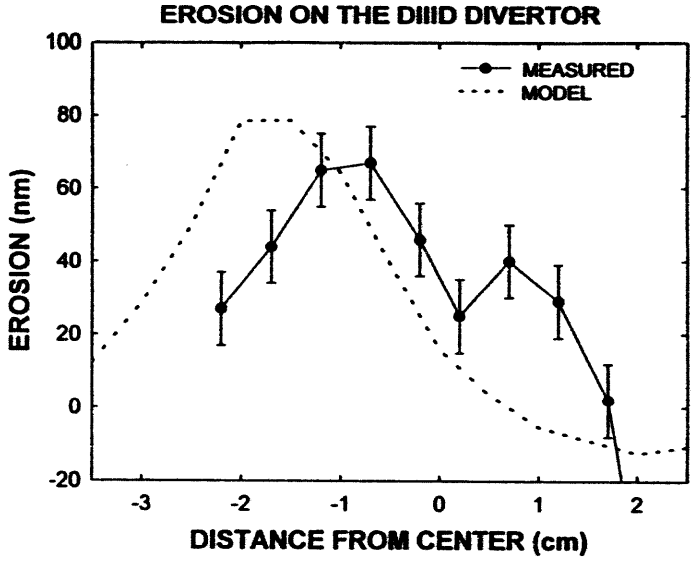
EROSION ON THE DIIID DIVERTOR
MEASURED
MODEL
EROSION (nm)
100
80
60
40
20
0
-20
-3
-2
-1
0
1
2
DISTANCE FROM CENTER (cm)

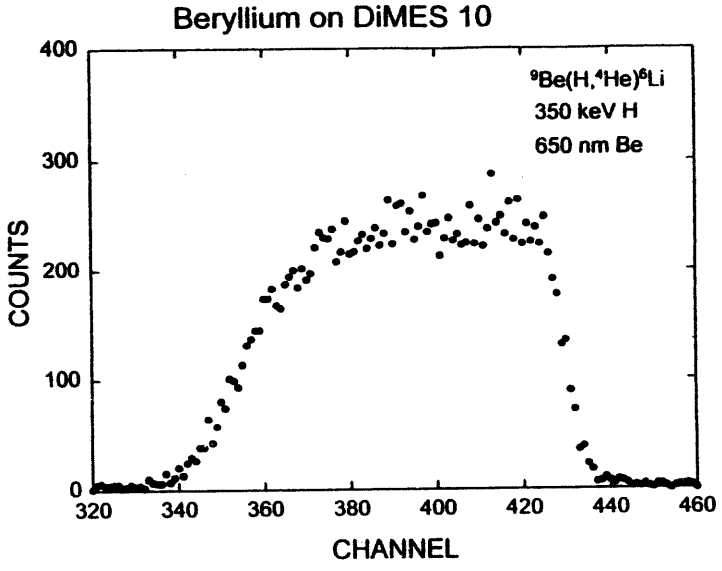

Conclusions:

1. Peak carbon erosion was ~ 60 nm or ~ 4 nm/sec. (12 cm/yr) Agrees with REDEP model.
2. Erosion of tungsten was < 5 nm.
3. Deposition of carbon on tungsten was < 5 nm.
4. Deposition of tungsten on carbon was ~ 1 monolayer near the edge of the spot and decreased exponentially with distance from the spot with an e-folding length of ~ 1.7 mm. There is more tungsten downfield from the spot than in other directions.

Erosion/Redeposition Analysis for ITER, DIII-D, and PISCES, and Tokamak Sheath Modeling

J. N. Brooks and T.Q. Hua

Argonne National Laboratory
9700 South Cass Avenue
Argonne, IL 60439 USA

US-Japan Workshop Q181 on High Heat Flux Components and Plasma Surface Interactions for Next Devices

January 24-27, 1994

San Diego, California

Introduction	J. Brooks
ITER Erosion Analysis	J. Brooks
PISCES Erosion Analysis	J. Brooks
DIII-D Erosion Analysis	T. Hua
Sheath Analysis	T. Hua

Erosion/Redeposition and Related Analysis

- Personnel (ANL) J. Brooks, A. Hassanein, T. Hua; (U of I) D. Ruzic et al.
- Goal: Use, Develop, and Validate Models and Codes to Predict:
  1) Erosion-limited surface component lifetime
  2) Impurity transport
  3) Tritium co-deposition
  4) Heat deposition
- Previous Studies:
  - TEXTOR limiters (C, TiC)
  - TFTR bumper limiter (C)
  - INTOR divertor
  - ITER/CDA divertor
  - DIII-Divertor

<u>Current Work</u>

- DIII-D: REDEP, WBC Erosion/Redeposition Code Analysis of:
  - Carbon divertor tiles
  - Carbon, tungsten, beryllium DIMES probes (with GA, SNL)

- ITER: REDEP, WBC, BPHI Code Analysis of:
  - Dissipative divertor plate and sidewall erosion
  - Sputtered impurity transport

  (with UCLA, PPPL)

- PISCES: WBC/VFTRIM Code Analysis of:
  - Normal incidence impurity transport experiments (Mo, B)
  - Oblique incidence impurity transport experiments

  (with UCLA)

- Divertor Sheath: BPHI Kinetic Code Analysis of:
  - ITER oblique incidence sheath parameters
  - In-sheath impurity, hydrogen atom, and hydrogen molecule ionization, transport, charge exchange, and elastic collisions.
  - Heat transmission factor
  - Redeposited ion parameters

Impurity Transport Codes for Erosion/Redeposition

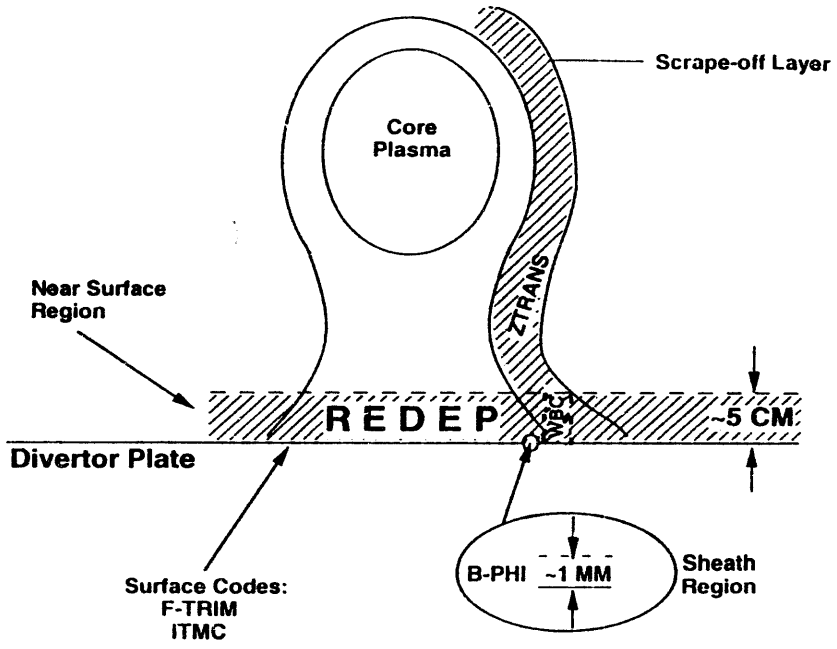

Code	Type
REDEP	Kinetic, Gyro Averaged, Finite Difference
WBC	Kinetic, Sub-Gyro, Monte Carlo
B-PHI,	Kinetic, Finite Difference
ZTRANS	Quasi Fluid, Monte Carlo
F-TRIM, ITMC	Binary Collision, Monte Carlo

ITER Erosion/Redeposition Analysis

- **Previous Work:**
  - REDEP and WBC code analysis of ITER high recycling divertor; $q_o \approx 10$ MW/m^2, $T_{e_o} \approx 10$ - 100 eV. Results show:
  - High peak net erosion rates for beryllium and carbon coated divertor plate (~ 30 cm/burn-yr).
  - High tritium co-deposition rates for carbon ($\gtrsim$ 10 ci/s).
  - Low and very low erosion rates for niobium (~2 cm/burn-yr), and tungsten (~1 mm/burn-yr).
  - Little or no core contamination by divertor plate sputtering.
- **Present Work:**
  - REDEP and WBC code analysis of ITER dissipative divertor; $q \lesssim 5$ MW/m^2, plasma may be extinguished at divertor plate, sidewalls used for baffling.
  - UCLA (Schmitz et al.), and PPPL (Petravic) plasma solutions with DEGAS neutral calculations (Ruzic et al.) used as inputs to REDEP.
  - Models are currently highly uncertain, plasma results are speculative, ongoing work is focusing on sidewall boundary conditions, stability of solutions, sputtering coefficients, etc.
  - Preliminary REDEP results show very high peak net erosion for Be (~ 4000 Å/s) due to both charge exchange D-T neutrals and D-T ions.

REDEP Analysis--ITER Gas Target Divertor*

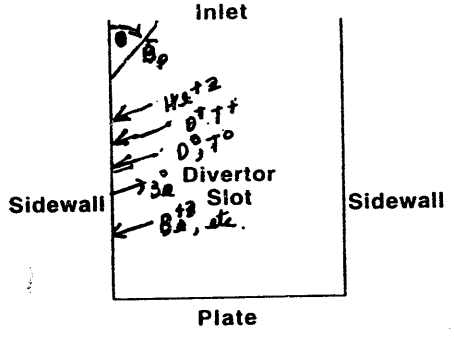

Parameter	Reference Value
1) Region analyzed	Sidewalls - assumed identical - assumed continuous
2) D-T plasma parameters	a) per UCLA solution (Schmitz et al.) b) per PPPL solution (Petravic/Ruzic)
3) He^{+2} flux	10% of D-T ion flux
4) Be sputt. coefficients	WBC/FTRIM/DSPUT calculations for oblique incidence, D, T, He, Be → Be
5) Poloidal field-to-sidewall angle, θ	3°
6) Plasma sheath at sidewall	eϕ/kTe = 3

* J.N. Brooks, in "US Design Support Study for the ITER Divertor," MDC report, to be issued.

PLASMA PARAMETERS FOR REDEP CALCULATION

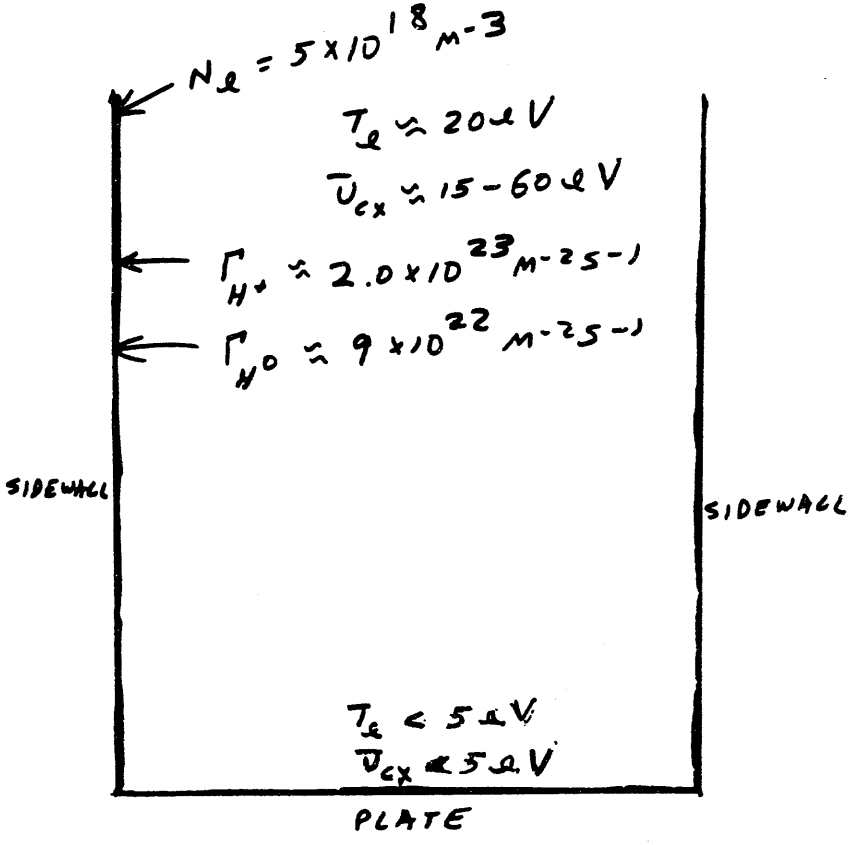

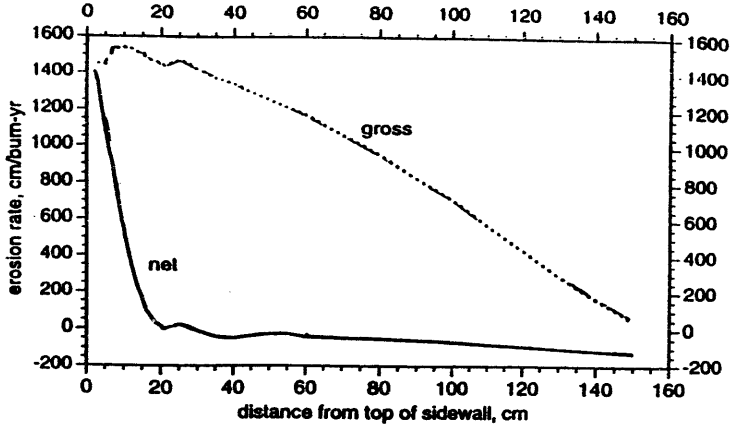

Fig. 4.4-1. ITER/REDEP Analysis: Erosion of beryllium coated gaseous divertor sidewall; for UCLA plasma solution.

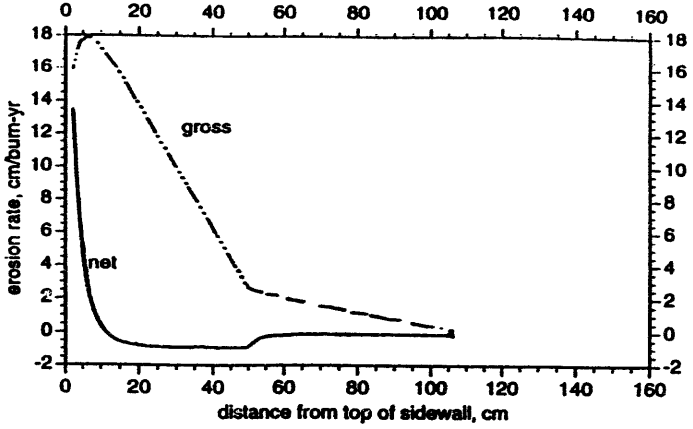

Fig. 4.4-2. ITER/REDEP Analysis: Erosion of molybdenum coated gaseous divertor sidewall; for UCLA plasma solution.

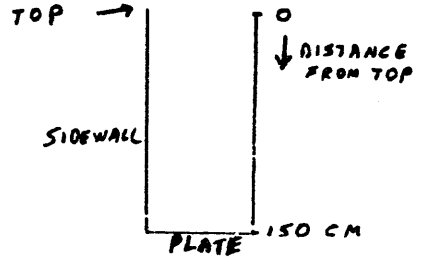

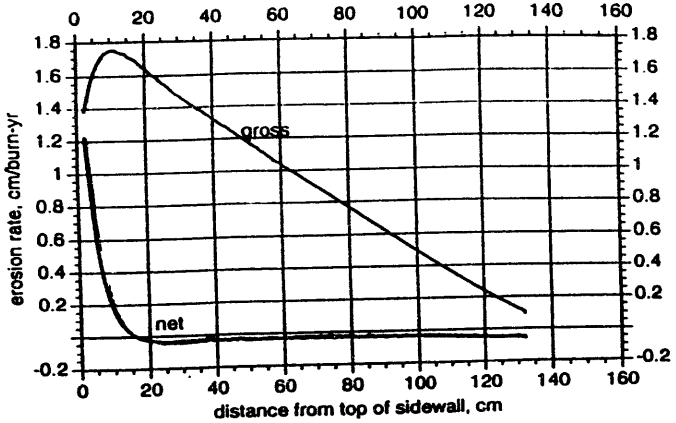

Fig. 4.4-3. ITER/REDEP Analysis: Erosion of tungsten coated gaseous divertor sidewall; for UCLA plasma solution.

PISCES Erosion/Redeposition Analysis

- **Previous Work: WBC/VFTRIM/ITMC Code Analysis of Normal Incidence Impurity Transport Experiments (M. Khandagle et al., J. Nuc. Mat. to be published).**
  - **Mo, B impurity markers sputtered by 100-150 eV Ar+ ions, redeposited on 2.5 cm dia. carbon disc, normal (90°) incidence magnetic field.**
  - **Good agreement observed between measured and computed redeposited impurity concentrations.**
- **Current Work: WBC/VFTRIM/ITMC Analysis of Oblique Incidence Impurity Transport Experiments.**
  - **Mo etc. marker sputtering at 45°, and 10° B-field incidence.**
  - **MoI, MoII lines will be computed (WBC) and compared with spectroscopic measurements.**
- **Future Work: Be Target Experiment Simulation**

PISCES OBLIQUE INCIDENCE
IMPURITY TRANSPORT EXPERIMENT;
WBC/VFTRIM/ITMC SIMULATION

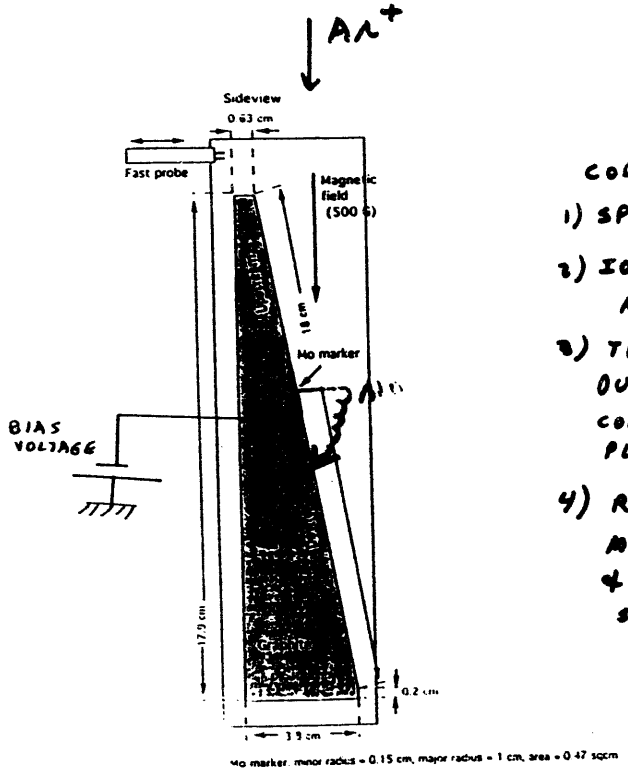

CODES COMPUTE:

1) SPUTTERING OF Mo^0
2) IONIZATION OF Mo^0, Mo^{+1} etc.
3) TRANSPORT OF Mo DUE TO $\bar{F} = q(\bar{v} \times \bar{B} + \bar{E})$ COLLISIONS WITH Ar PLASMA
4) REDEPOSITION OF Mo^{+k} ON SURFACE & EFFECTS ON SURFACE CONCENTRATION

PISCES, 100 eV $Ar \rightarrow Mo^*$
WBC SIMULATION.
(NORMAL INCIDENCE)

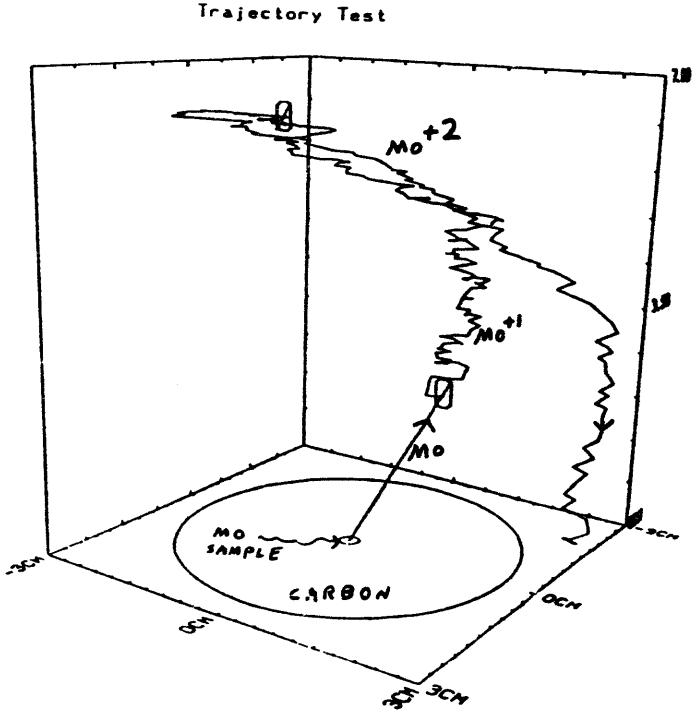

WBC/VF-TRIM CODE: $T_i = 0.2$ eV, $T_e = 20$ eV, $N_{e_0} = 2 \times 10^{18}$ m^{-3}
$B = .05$ T, $D = D_{BOHM}$, $\Delta\phi = 6$ V at $r = 3$c

PISCES OBLIQUE INCIDENCE NO TRANSPORT EXPAT.
COMPARISON BETWEEN MEASURED DATA + WBC CODE SIMULATION.

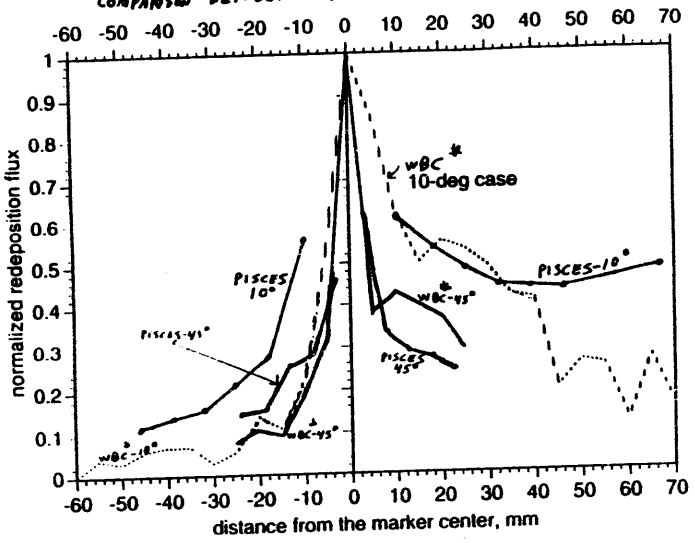

* PRELIMINARY PLASMA MODEL

Conclusions

- **Preliminary REDEP code analysis for ITER dissipative divertor shows very high (~10 m/burn-yr) sidewall Be erosion rates. This is due to high particle fluxes and low redeposition fractions. Much more detailed analysis is needed, and is being worked on.**

- **WBC code analysis is being performed for PISCES oblique incidence impurity transport experiments. Results should help to validate models/codes for erosion redeposition calculations.**

Erosion/Redeposition Analysis of DIII-D DIMES Experiments (with GA, SNL)

- **Analysis are being done for the following:**

DIMES Sample No.	Material	No. of Plasma Discharges	Date
9	C	15 (during last second of discharge)	July 22, 1993
8	C with 1 cm W at center	6	October 4, 1993
10	C with 1 cm Be at center		Future

- **Codes used for the analysis: REDEP and WBC with selected input data from ITMC, VFTRIM, and BPHI code results.**

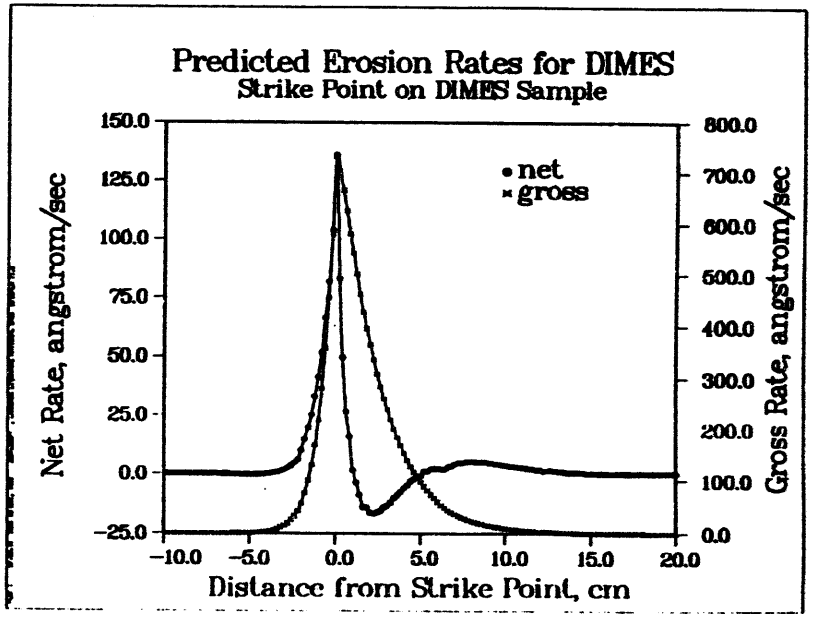

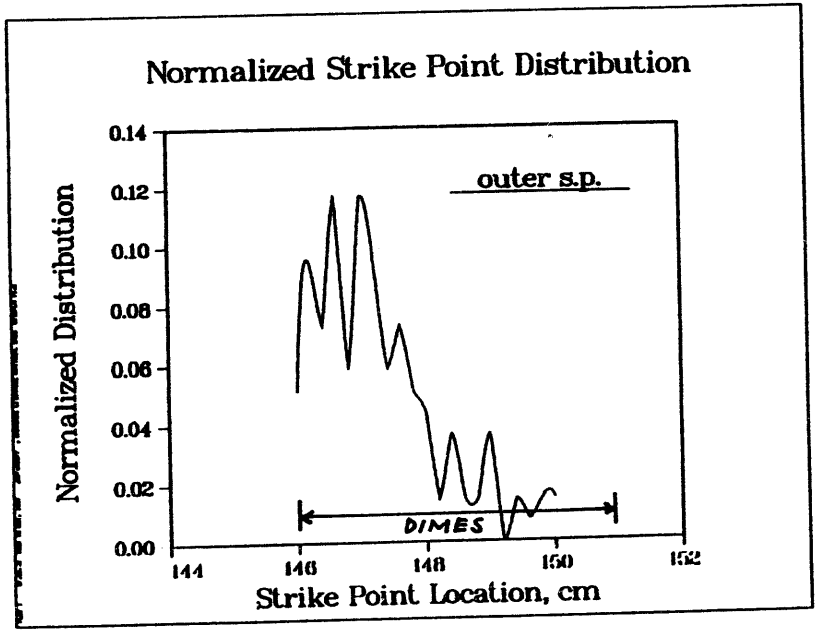
Normalized Strike Point Distribution
Normalized Distribution
0.14
0.12
0.10
0.08
0.06
0.04
0.02
0.00
outer s.p.
DIMES
144
146
148
150
152
Strike Point Location, cm

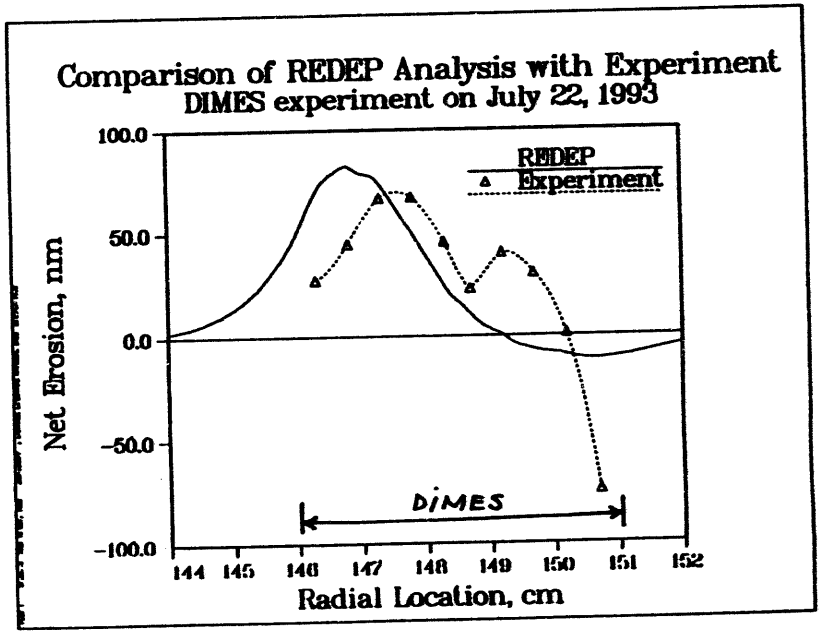
Comparison of REDEP Analysis with Experiment
DIMES experiment on July 22, 1993
Net Erosion, nm
100.0
50.0
0.0
-50.0
-100.0
REDEP
Experiment
DIMES
144
145
146
147
148
149
150
151
152
Radial Location, cm

The BPHI Code

- BPHI is a kinetic/Monte Carlo code, developed at ANL, for the analysis of the tokamak sheath region with oblique magnetic field.
- In-sheath ionization and transport of surface emitted particles, charge exchange, elastic collisions, and physical sputtering are modeled.
- The code computes the sheath potential, electric field, heat transmission factor, surface impact parameters of DT and redeposited ions (charge state, incident angle, and energy).
- Effects on the sheath parameters due to surface reflection of DT, surface material evaporation and physical sputtering have been analyzed.
- The code is fast running on the cray. Typical cpu ~ 1 minute.

Hydrogen Desorption

- $H_2 + e \rightarrow H_2^+ + 2e$
- $H_2^+ + e \rightarrow H + H^+ + e$
- $H_2 + e \rightarrow H + H + e$
- $H + e \rightarrow H^+ + 2e$

} insignificant

- Hydrogen reflection coefficients for DT on C, W, Nb, Be were computed by the VFTRIM code for a wide range of T_e and incidence angle.

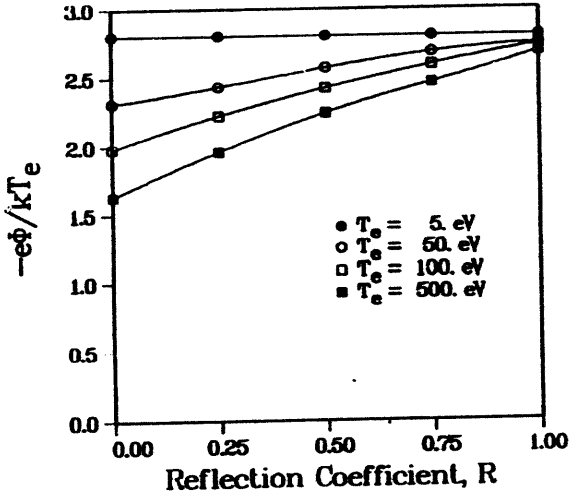

$n_i = 1 \times 10^{20}\ m^{-3}$

$\theta_B = 87^\circ$

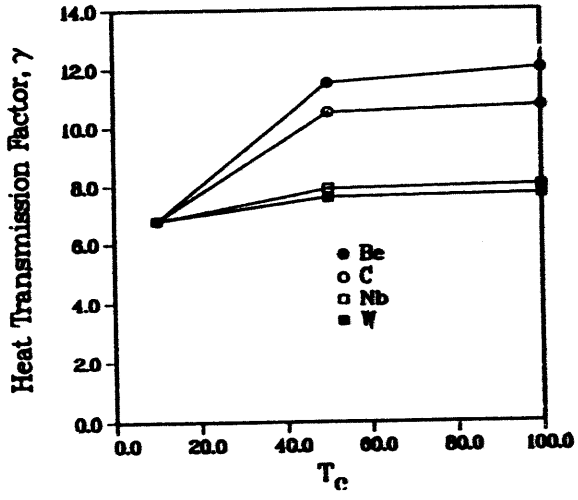

$n = 1 \times 10^{20}\ m^{-3}$,

$\theta_B = 87^\circ$

Thermal Evaporation of Be

- **Motivation: an overheated hot spot may thermally emit Be atoms. These may be ionized in the sheath. The resulting ions and electrons can alter the sheath profile and <u>increase</u> heat transmission. This may result in <u>positive</u> <u>feedback</u> causing more overheating.**

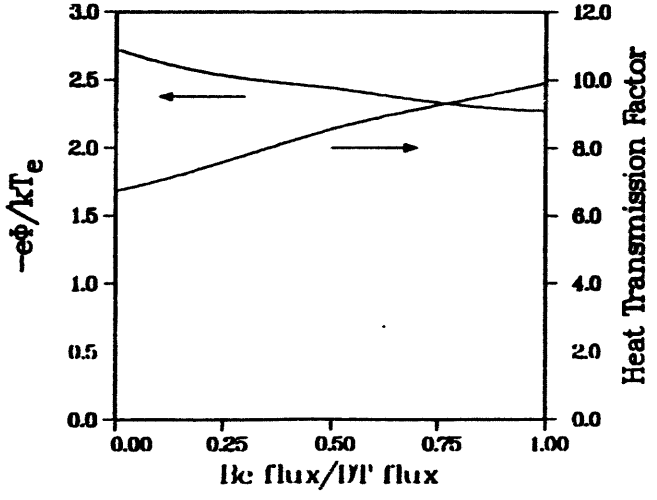

$n = 1 \times 10^{20}\ m^{-3}$, $\theta_B = 57°$

$T_e = 50\ eV$

Conclusions and Future Work

I. <u>DIMES</u>

- **Preliminary erosion analysis for carbon DIMES sample shows good agreement with experiment.**
- **Analysis is continuing for the C/W and C/Be DIMES samples.**
- **Experimentally measured plasma parameters and computed strike point distributions are critically needed to complete the modeling.**

II. <u>Sheath</u>

- **Kinetic analysis is being performed for ITER sheath region.**
- **Hydrogen desorption and Be evaporation tend to decrease the sheath potential but increase the heat transmission factor.**
- **In-sheath elastic collisions (results not shown here) are unimportant for the plasma regime studied.**
- **Improved plasma-surface interaction models and additional processes will be incorporated in BHPI.**

Session XI

Workshop Summary and Conclusion Viewgraphs

Session II

PFC Issues for Future Machines

Summary Viewgraphs

compiled by

O. Motojima and K. Wilson

Session II: PFC Issues for Future Machines

Co-Chair:
O. Motojima
K. Wilson

II.1	O. Motojima	Present Status of LHD
II.2	S. Tanaka	Design of ITER PFCs
II.3	R. Matera	R&D for ITER PFCs
II.4	D. Hill	PFCs for TPX

The Missions of Future Machines Are Quite Varied

LHD Currentless steady helical plasma production that is complimentary to the tokamak approach. Physics extrapolatable to fusion conditions with contribution to fusion technology.

TPX Testing of the compatibility of steady-state power and particle control techniques with advanced tokamak operation (non-induction current drive with high beta and high confinement).

ITER The demonstration of the scientific and technological feasibility of fusion through controlled ignition and extended burn of D-T plasmas, with steady-state as the ultimate goal.

The Future Machines Share Some Common Challenges

LHD, TPX, and ITER must make tremendous advances in plasma facing component technology:

Steady-State Heat Removal The steady state heat flux of order 10 MW/m^2 requires active heat removal.

Pumping Particle and impurity control require active pumping.

Erosion Lifetime Sputtering may limit the lifetime of the PFC elements.

Conditioning Conditioning techniques must be developed that are compatible with the steady state magnetic field.

All of These Devices Use a Divertor for Steady State Heat Removal

LHD Helical or Local Island Divertor
- 5-10 MW/m^2 heat flux
- CFC brazed to copper
- Water cooling (helium)

TPX Radiative Divertor
- 15 MW/m^2
- CFC brazed to copper
- Water cooling

ITER Radiative Divertor
- 5 MW/m^2
- Beryllium brazed to copper alloy
- Water cooling (helium and liquid metal)
- Sacrificial components for disruption (compliant layer)
- Neutron and tritium issues

Pumping Systems Concepts

LHD - Carbon Sheet Pumping
- Metal Membrane Pumping

TPX - External Cryopumps
- Turbo Pumps

ITER - Cryopumps inside the cryostat

Common Issues for Divertor Technology

Low Z Materials Development

- Ductile Beryllium
- Fiber Reinforced Beryllium
- Carbon Fiber Composites
- Innovative Approaches

Joining

- Brazing
- Thixotropic Compliant Layer

Conditioning

- Boronization
- High Magnetic Field Techniques

Lifetime and Performance Testing

- High Heat Flux Testing
- Sputter Erosion Lifetime
- Disruptions (tokamaks)

Remote Handling

- TPX and ITER

Session III

Recent PMI Results from Several Tokamaks

Summary Viewgraphs

compiled by

N. Yoshida and D. K. Owens

Session III.

Recent PMI Results from Several Tokamaks

Chairmen: N. Yoshida and D. K .Owens

This session contained many interesting reports of progress on device performance, plasma materials interaction and plans for future work. The groups reporting were TRIAM-1M, C-MOD, TEXTOR, JT-60 U, DIII-D, and TFTR.

Contributions to PMI from this session fall into three categories:

- Wall Conditioning and Low Z Materials (DIII-D, TFTR, JT-60 U)
- High Z Limiter and Divertor Tiles (TRIAM-1M, C-MOD, TEXTOR, JT-60)
- Radiative Divertors, Divertor Pumping (C-MOD, DIII-D)

1. Wall Conditioning and Low Z Materials

DIII-D reports dramatic improvement in N-τ-T, doubling the value every two years. Wall and conditioning techniques are credited with this improvement. Wall coverage has gone from 9% to 100% graphite and carbonization, boronization, and He glow discharge cleaning are employed.

Similar performance improvements in the high-βp mode were reported by JT-60 U. CFC divertor tiles were B_4C converted on the surface and installed at the outer divertor strike point. These tiles survived 30 MW of NBI for 2 seconds without significant damage. By optimizing tile shape and B_4C thickness to reduce erosion, they have obtained record values of N-τ-T.

The attainment of fusion powers in excess of 6MW on TFTR was possible only with a low Z carbon limiter, the reduction in hydrogen isotope recycling by discharge cleaning and the reduction in carbon influx by coating the limiter with lithium, also low Z.

The effect of Li coatings on deuterium retention were investigated on the Tokamak de Varennes, with the result that D retention is increased slightly, from 40% (without Li) to 50% (with Li).

The initial retention measurements for T on the graphite TFTR limiter are at least 9% (values of 50-80% are expected).

2. High Z Limiters and Divertor Tiles

Analysis of the PM-Mo moveable limiter on TRIAM-1M and TiC/Mo limiter and divertor tiles on JT-60 show melting and cracking. The estimated heat flux to the edge of the JT-60 divertor tiles was in the range 140-200 MW/m^2. The melting appears to initiate cracking at the grain boundaries. The high heat load also initiates grain growth and recrystallization above 1200C, resulting in reduced intergranular strength. Alloying of the TiC and Mo was observed on JT-60. Intergranular fracture was the failure mechanism.

On TRIAM-1M, the Mo cracking has been understood on the basis of 3d finite element stress analyses. The cure to the problem is to raise the recrystallization temperature. Possible improvements are summarized in the following table:

Alloy	Recrystallization Temperature
Pure Mo	1200C
Mo + Ti, Ce, Th - TZM	1300 - 1400C
Mo + rare earth metals - TEM	1200 - 1800C
Mo + TiC	1800 - 2000C

C-MOD has a Mo first wall. During normal operation (no auxiliary heating), the dominant impurities are C, O, and H. The carbon flux is typically two to three times the oxygen flux and comes mostly from the walls. Mo is not observed. However, with Ar puffing, Mo is observed. This is attributed to the increased sputtering of Mo by Ar.

Extensive work was done on TEXTOR with high Z limiters since tungsten is the primary candidate for the divertor plates in the ITER/CDA (technical phase). It was suggested that the question should not be whether high Z materials are acceptable, but under what conditions high Z materials can be allowed for use as plasma facing materials.

With the Mo moveable limiter on TEXTOR, no strong dependence of Z_{eff}, density or radiated power on limiter position was seen. (Note that the limiter was sharing power with the ALT II limiter. The power fraction going to the limiter was less than 7%).

Effects on plasma stability were observed in high density ohmic discharges which had unstable, hollow T_e profiles. Peaked tungsten radiation profiles were sometimes seen in auxiliary heated plasmas, though conditions were found which did not have such behavior.

An interesting observation is that central Mo radiation did not increase in spite of melting of the Mo limiter.

3. Radiative Divertors, Divertor Pumping

Normal operation of the C-MOD divertor is "radiative", with the radiated power fraction in the divertor region on the order of 40%. With gas puffing, detached divertor operation is achieved with greatly reduced conducted power flow to the target plates. The radiating region moves from a volume near the target plates to the X-point.

Radiative divertor operation was also accomplished in DIII-D with a factor of 2 reduction in conducted power flow to the target plates with heavy gas puffing.

The divertor cryopump is in operation in DIII-D with 30 kl/s pumping speed for D_2 and 10 kl/s pumping speed for He using the argon frost technique. For He pumping, $\tau^*_{He}/\tau_E \approx 11\text{-}14$, comparable to the values required for ITER (7-15).

The pumped divertor has also permitted density control independent of plasma current in H-modes. Confinement is found to be weakly dependent on density.

Session IV

High Heat Flux Technology

Summary Viewgraphs

compiled by

M. Ulrickson and M. Akiba

Session Summary IV: High Heat Flux Components

by M. Ulrickson, M. Akiba

Development of high heat flux components have extensively been performed in both US and Japan. These efforts have been oriented to develop high heat flux components for not only operating fusion devices, but also next fusion devices, in particular, for ITER. The US/Japan collaboration in this field has successfully been carried out as before!
This session can be summarized as follows;

JAPAN Contribution

1. The divertor plates for LHD have successfully been developed at NIFS, which could endure a heat load of 10 MW/m^2, 30 s for 5000 thermal cycles.
2. The divertor plates for JT-60U have been developed at JAERI, which successfully demonstrated to satisfy the design values.
3. The 1 m-long divertor plates with a sliding support structure have been developed at JAERI, which successfully demonstrated the sliding performance, and suppress deformation less than 0.5 mm.
4. The divertor plates with 1-D CFC armors brazed onto W-Cu alloy heat sinks endured a heat load of 15 MW/m^2, 30 s for over 1000 thermal cycles in a flat plate type. The W30Cu alloy can be a promising candidate for the ITER divertor plate.
5. Development of functionally gradient materials has intensively been performed at Mitsubishi Heavy Industries, which will be a promising technique to reduce stresses at a bonding interface of the ITER divertor plate.
6. Residual stresses of bonded structures have intensively been measured and compared with numerical analyses at Toshiba Corp., whose efforts are necessary to design the ITER divertor plate in a bonded structure.

U.S Contribution

7. The results of testing of carbon brazed to copper are very encouraging for TPX and ITER. The samples have survived large numbers of cycles at heat fluxes above 10 MW/m^2.
8. Activation of silver used in most of the carbon-copper braze joints is a potential problem for ITER. Development of non-silver containing brazes should be pursued.
9. Helium cooled divertor heat removal modules have been tested at ITER relevant heat fluxes. The results indicate helium should be further developed as a back-up to the baseline water cooling planned for ITER.
10. The plasma sprayed Be materials being produced are very promising for use in ITER. Further optimization to improve the thermal conductivity is required. This technique has potential for being used for in-situ repair of ITER PFC's.
11. Functionally graded layers are being developed to reduce braze stresses.
12. Liquid metal coolants for the divertor were discusses. Insulating layer development is the major R&D issue. Healing of cracked insulating layers is the most critical topic.

Session V

Plasma Facing Component Design and Applications

Summary Viewgraphs

compiled by

A. Komori and J. Davis

Session V.

PFC Design and Application
Chairmen: A. Komori and J. Davis

* The LID for LHD should be very useful for developing actively cooled divertor components as well as benefiting LHD.

* The results of the Tore Supra pumped limiter development have shown that perfect brazing as PFM to cooling tubes is not required. This increases the likelihood actively cooled components can be developed for future devices.

* The US ITER divertor design study has shown that there are several clear optimizations that can be made in divertor design once the materials are chosen.

Principle of LID

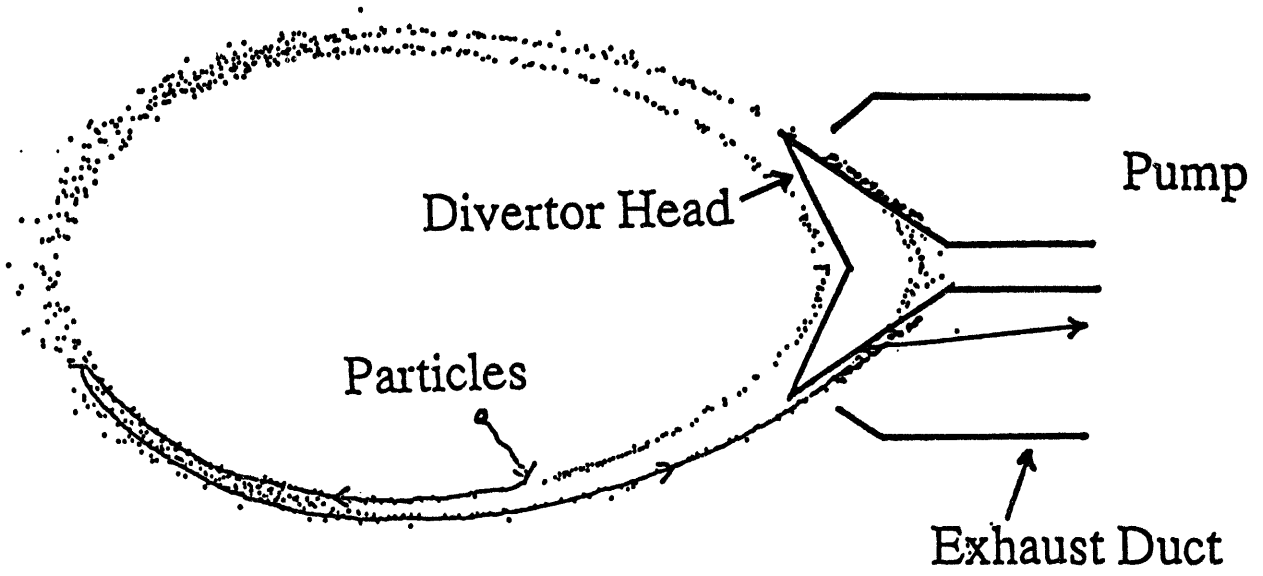

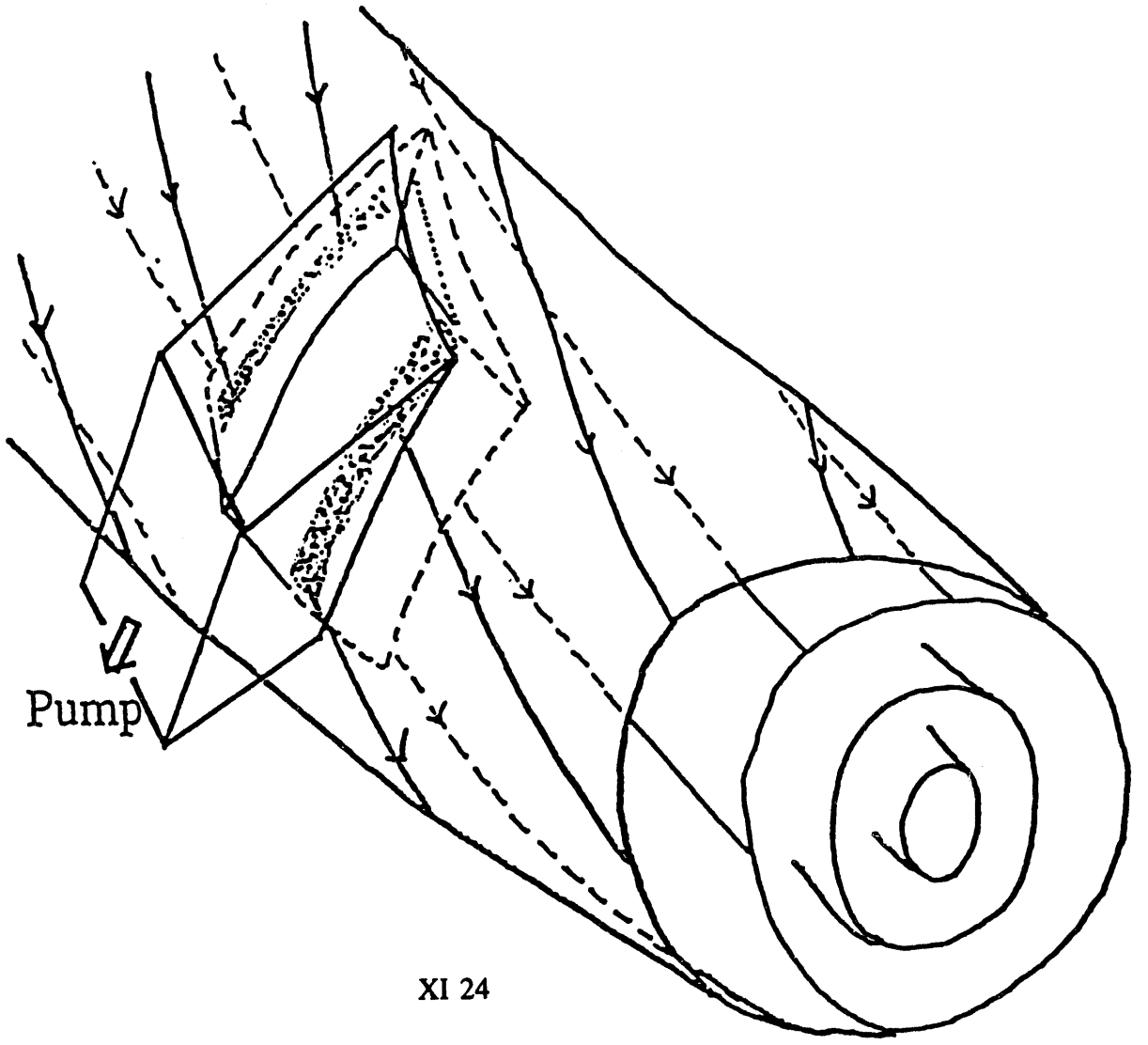

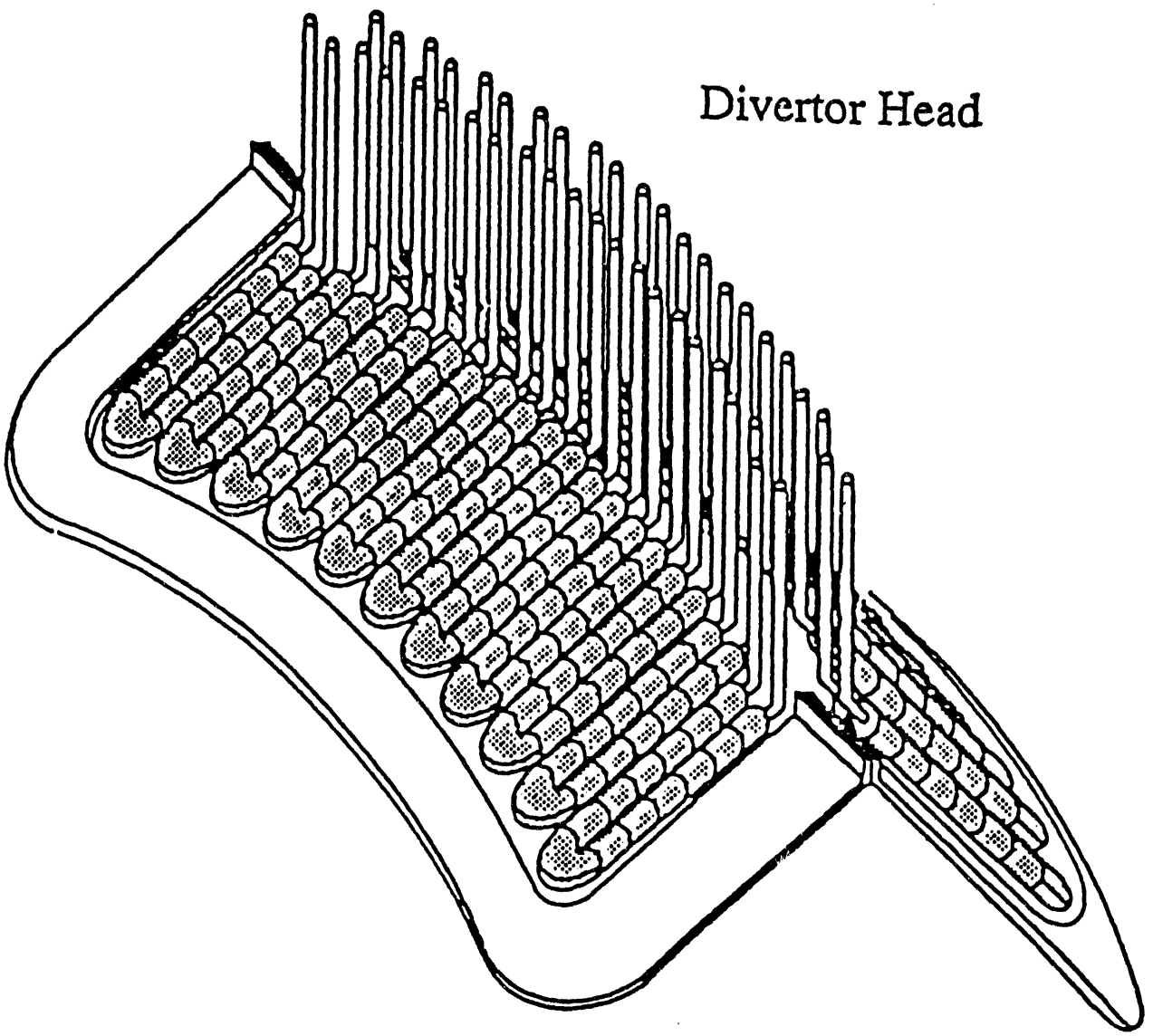
Divertor Head

Initial Operation May 13th - 14th (Thurs.- Fri.)

Shots 11002-11084

- Phase III Outboard Pump Limiter (OPL) operated successfully.

> Tests at progressively higher powers, longer shots
>
> example: shot 11044
>
> ~0.8 MW absorbed for 8 seconds
>
> $n_e = 3 \times 10^{19}\ m^{-3}$, $T_e = 42$ eV, $I_p = 1.5$ MA

- TCs (32) and flowmeters (10) provided excellent data.
- Limiter surface was surveyed with endoscope (large lens) - minor hot spots where expected. (Grafoil inserted between tiles was a problem.)
- "Cold wall" operation (T<100°C) did not appear to be a problem.
- Limited data on pumping (ducts open versus closed) were obtained.

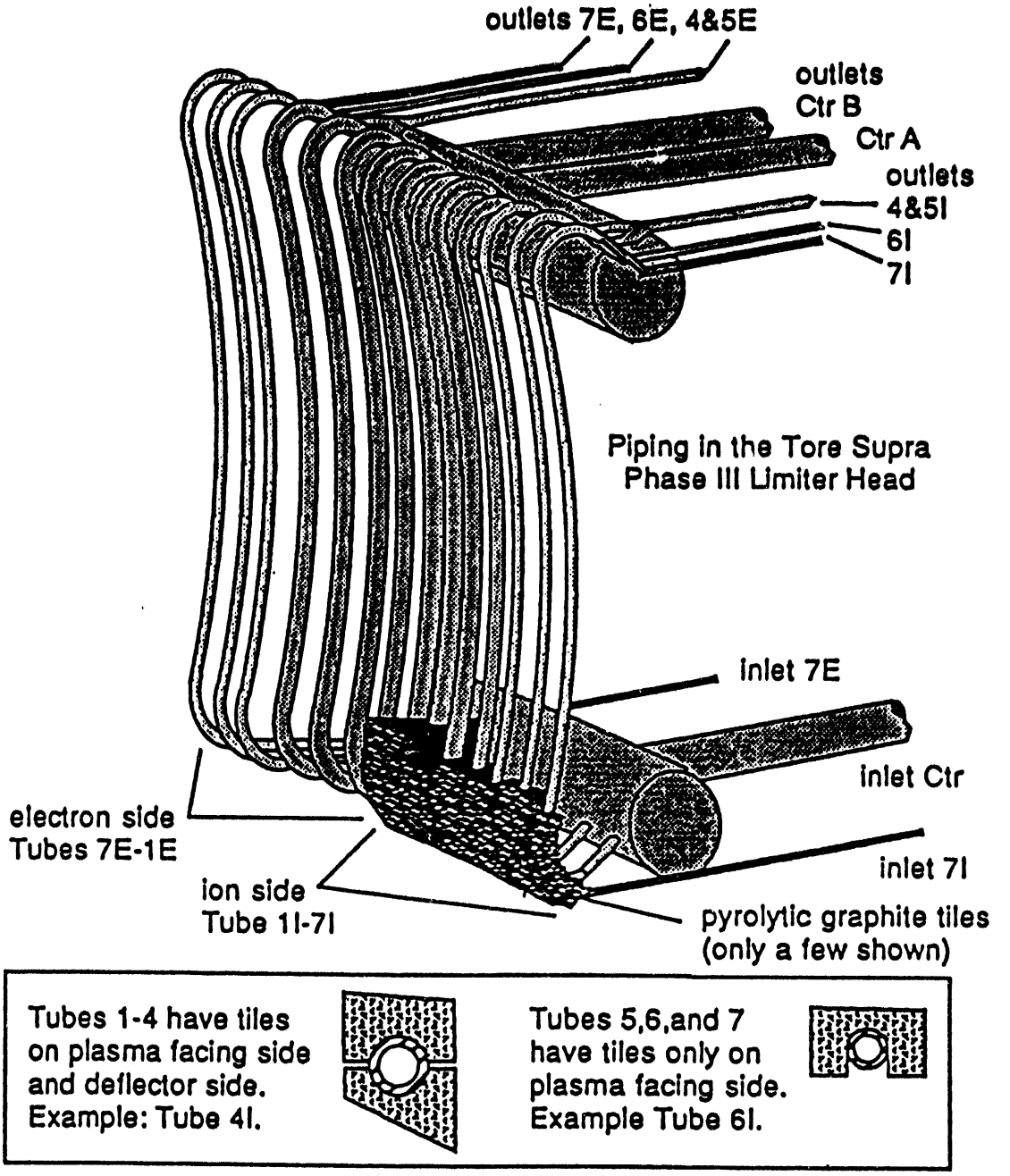

Figure 1. Piping in the Phase III Outboard Pump Limiter -- From left to right the tubes are numbered from 7I (leading edge tube) to 1I on the ion side and 1E to 7E (leading edge tube) on the electron side. The leading edge tubes, 7I and 7E, and Tubes 6I and 6E each have (separate) flowmeters. Tubes 4I and 5I are joined to a single manifold which has a flowmeter; the same is true for 4E and 5E. The center tubes flow into a single header which has two outlet pipes (Center A and Center B). Tubes 1-6 one each side plus the shelves (the heat sink and armor just outboard of the throat) are fed from a single header supplied by one large inlet pipe. The leading edge tubes (7I and 7E) are fed by a separate inlet line that splits into two lines before the diagnostic flange. (See also Figure A1 in Appendix A.)

Be Is a Viable Armor Material at Lower Heat Fluxes

- Coolant Temperature = 150°C
- Convective Heat Transfer Coefficient = 50 kW/m^2-K
- 10 mm Thick Armor
- 2 mm Thick Copper Structure

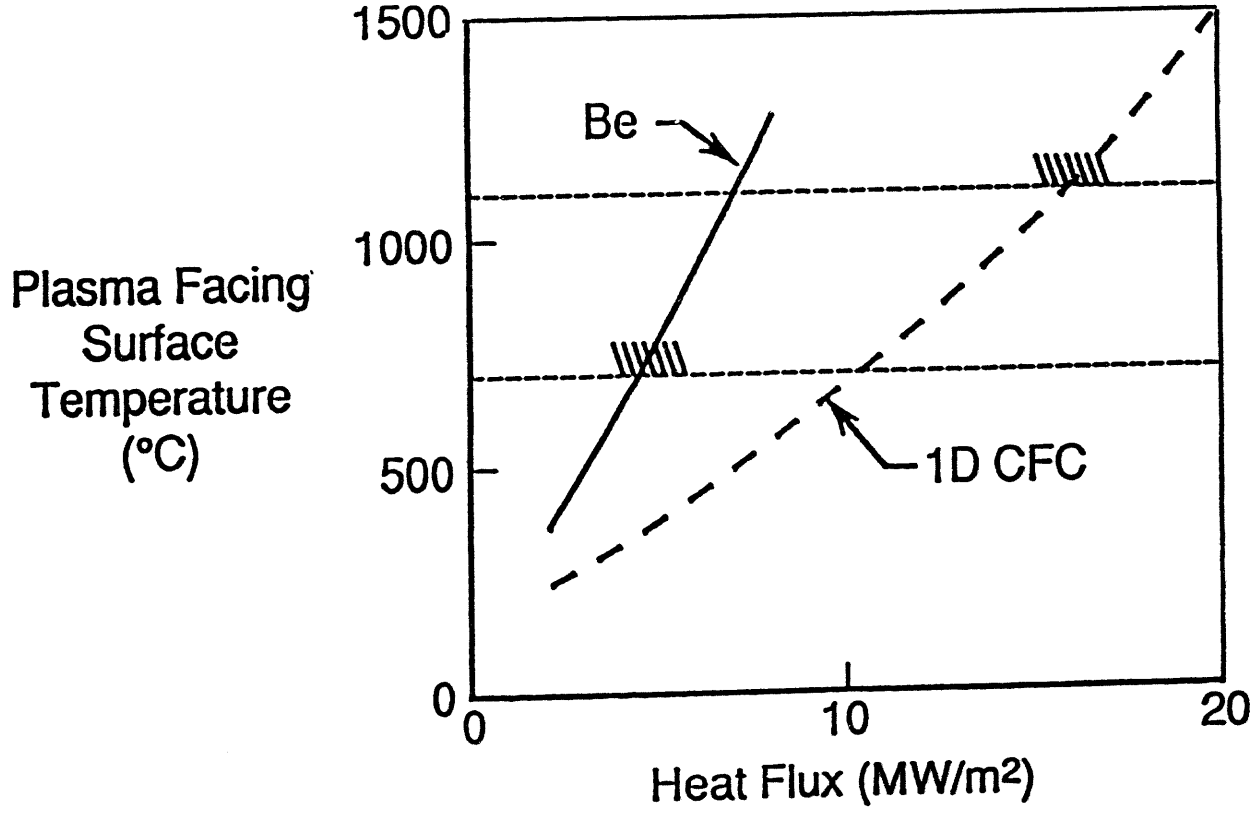

Thermal Performance Limits for Divertor Depend on Tube Material Selection

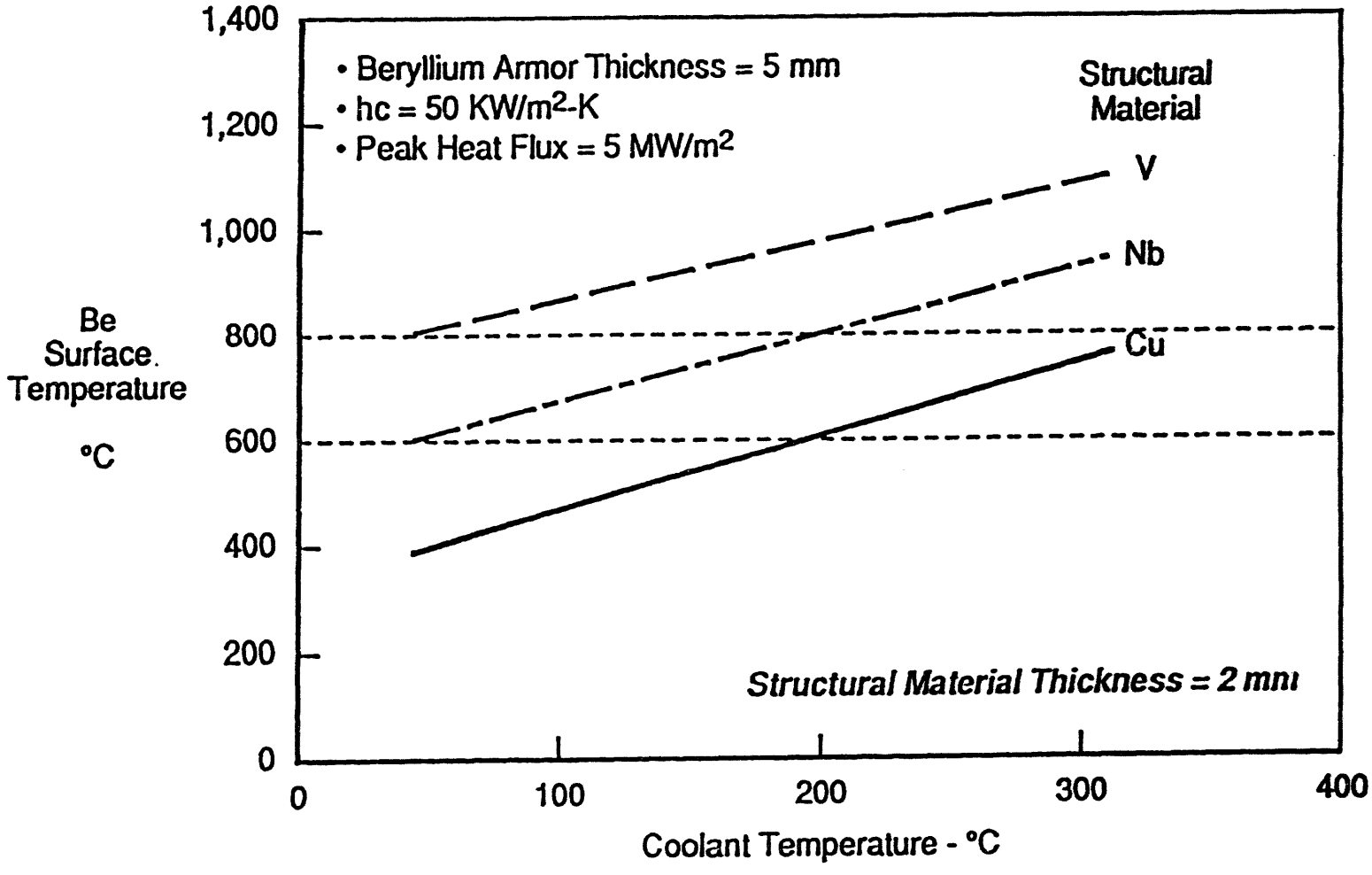

Session VI

Plasma Facing Component Materials and Irradiation Damage

Summary Viewgraphs

compiled by

T. Muroga and L. Snead

Enhancement of H Trapping in Damaged B and Ti Doped Russian Graphites

W. R. Wampler and B. L. Doyle
SNL Albuquerque
and
V. N. Chernikov, A. E. Gorodetsky,
S. L. Kanashenko and A. P. Zakharov
IPC/RAS Moscow

US-Japan Workshop on PMI-HHF
UCSD, January 24-27, 1994

W. R. Wampler

- Studied D retention in several Russian-made graphites.

- Samples were irradiated with e-beam at 77°C and 400°C.
  - Saturation observed at 77°C
    * Possibly due to amorphization
    * Neutron damage should be different
  - The higher the graphitization (higher TC), the greater the D retention
  - Boron addition significantly affects (reduces) D retention

- ... ion due to amorphization!

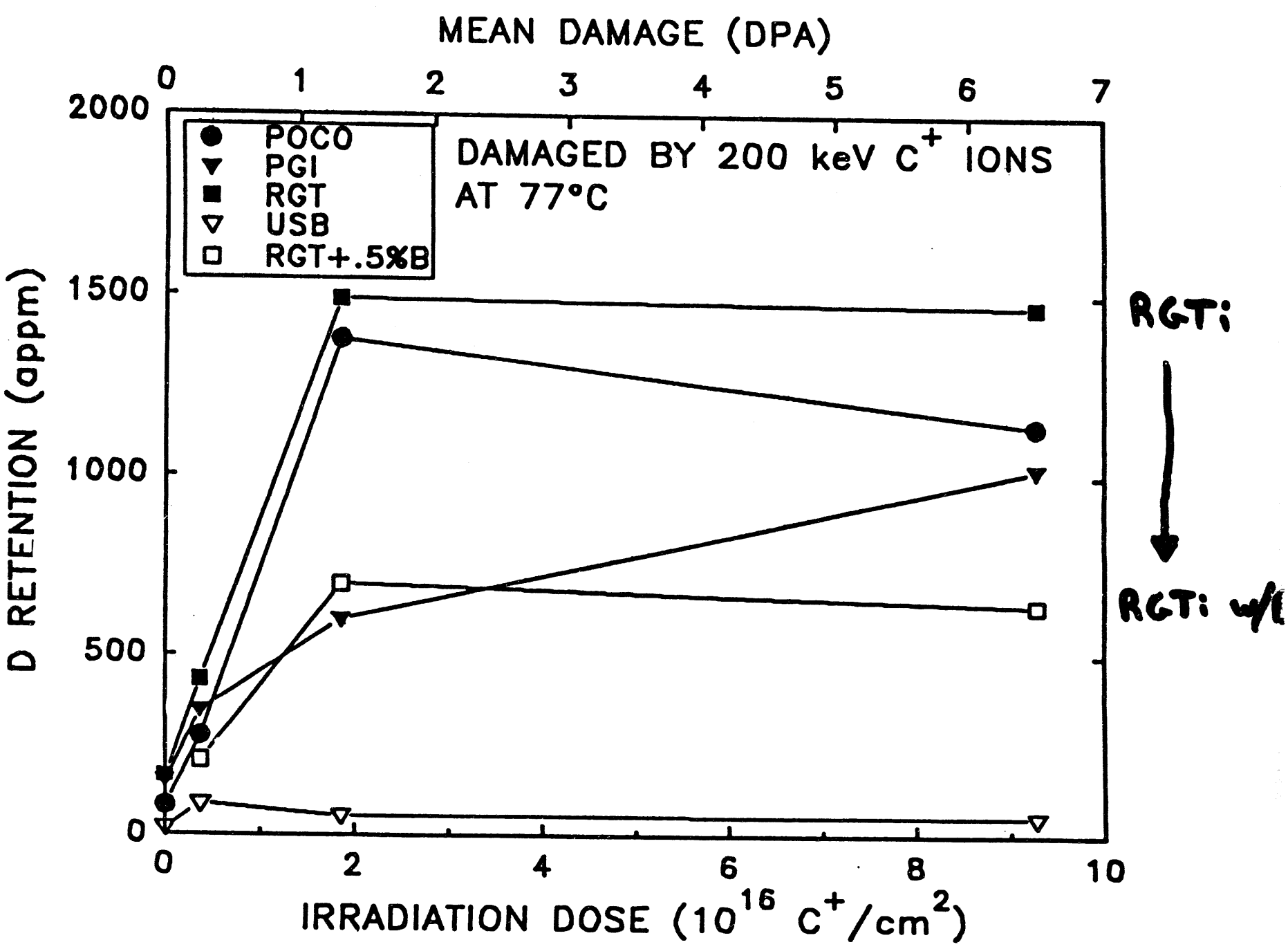

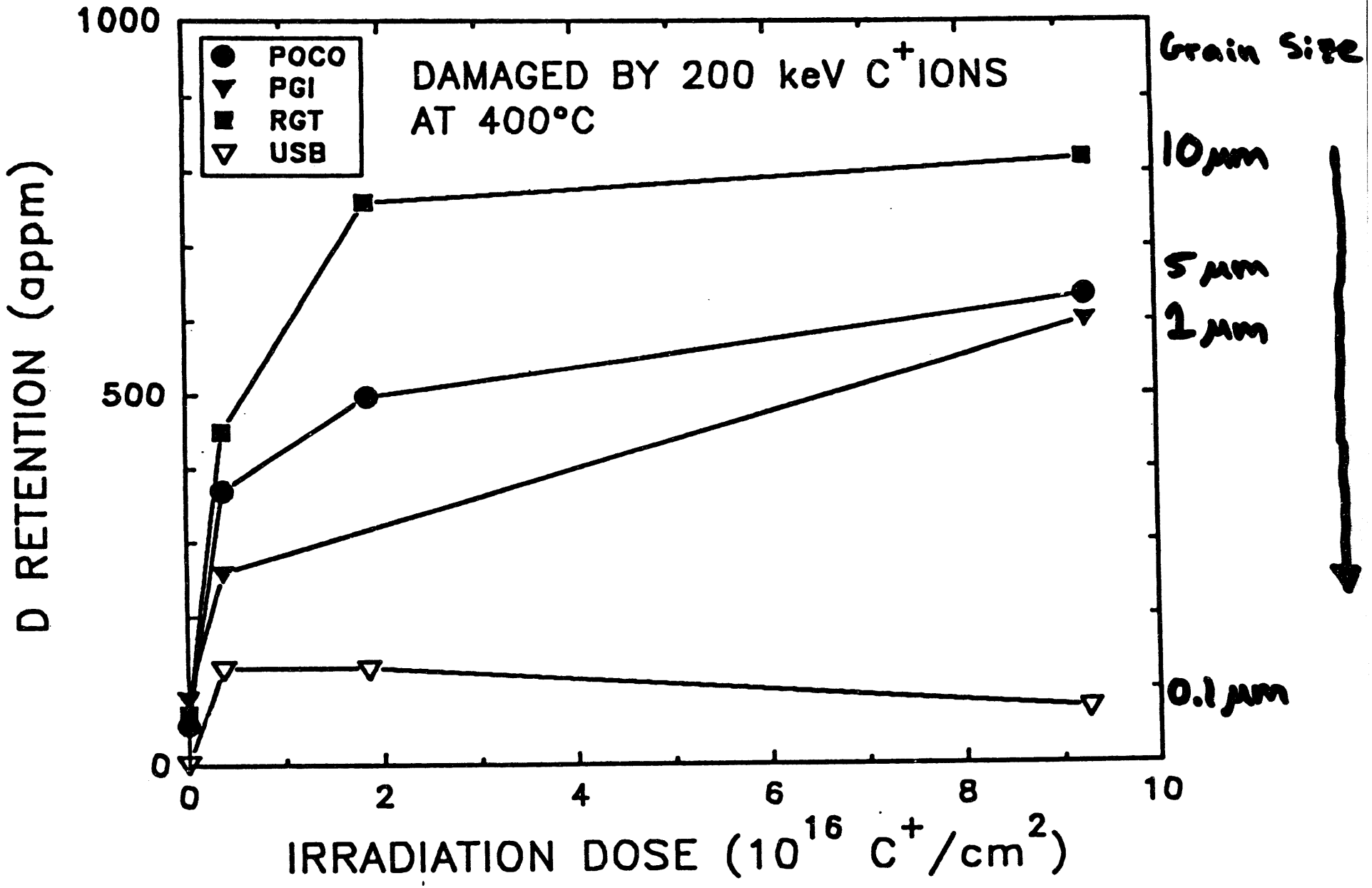
POCO
PGI
RGT
USB
DAMAGED BY 200 keV C+ IONS
AT 400°C
Grain Size
10 μm
5 μm
2 μm
0.1 μm
D RETENTION (appm)
1000
500
0
0
2
4
6
8
10
IRRADIATION DOSE (10^16 C+/cm^2)

ITER Relevance

- Will B be in bulk materials?

- B surface treatment may be adequate to limit uptake of tritium.

Preparation of Plasma Facing Materials Coatings at General Atomics

Paul W. Trester
Peter G. Valentine
W. Phil West

General Atomics
3550 General Atomics Court
San Diego, California 92121-1194, U.S.A.

U.S. - Japan Workshop Q181
High Heat Flux Components and Plasma Surface Interactions for Next Devices
San Diego, California
24 - 27 January 1994

SCANNING ELECTRON MICROGRAPH OF $7B_4C + 2SiC$ MIXTURE REACTION-SINTERED COATING ON ATJ GRAPHITE

(Back-Scattered Electron Image, Cross-Section View)

GENERAL ATOMICS

L-015(3)
9-16-93

Trester et al.

- Oxide getter coating with excellent adherence has been demonstrated.

- Thermal shock resistant.

ITER Relevance

- It is possible to paint slurry onto surface and use laser sintering.

- Possible for spot repair or surface coverage.

ORNL Irradiation Effects Program

L. L. Snead and T. D. Burchell

Metals and Ceramics Division
Oak Ridge National Laboratory

Thermal Conductivity Degradation of Selected Graphite Materials

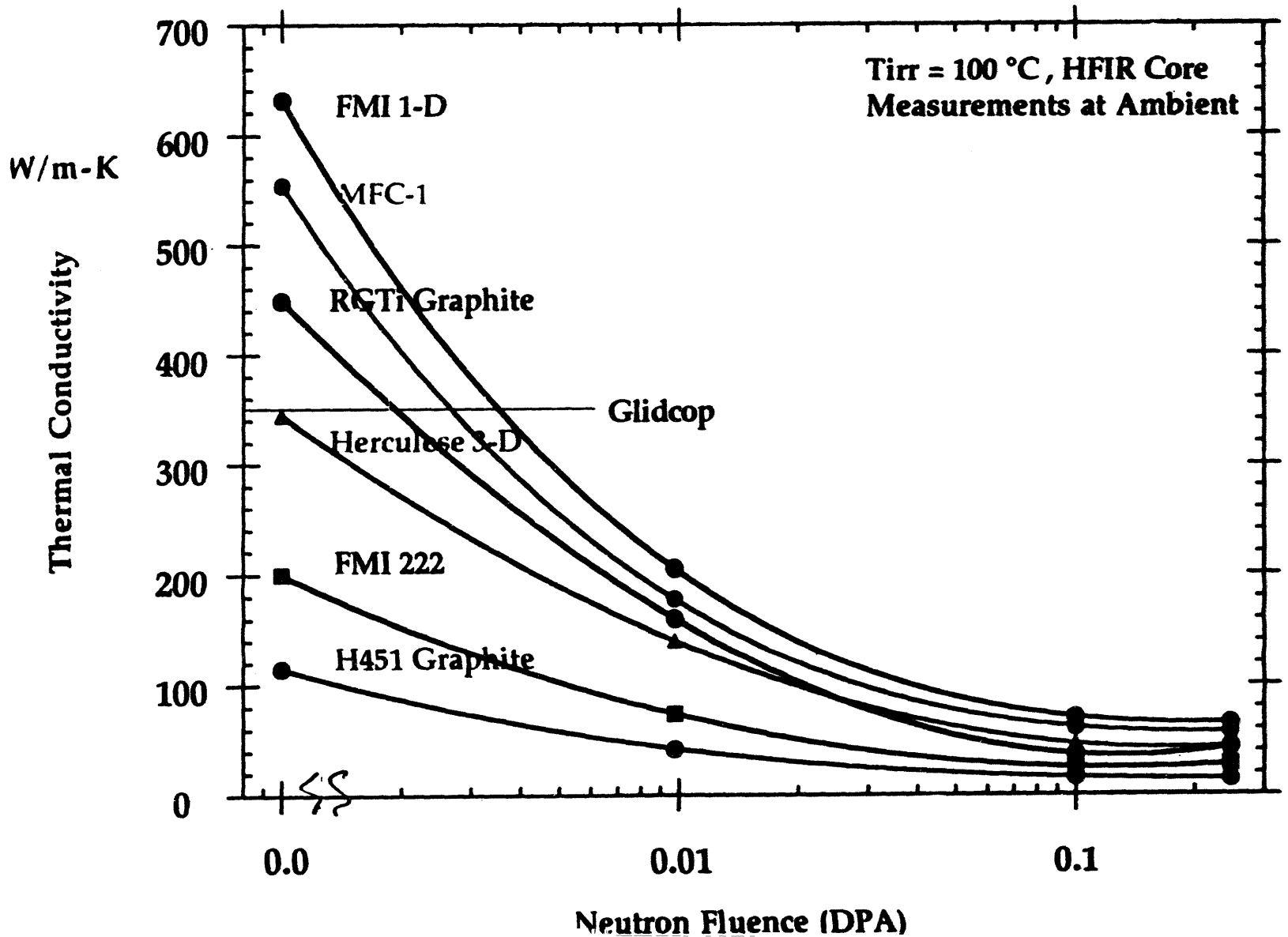

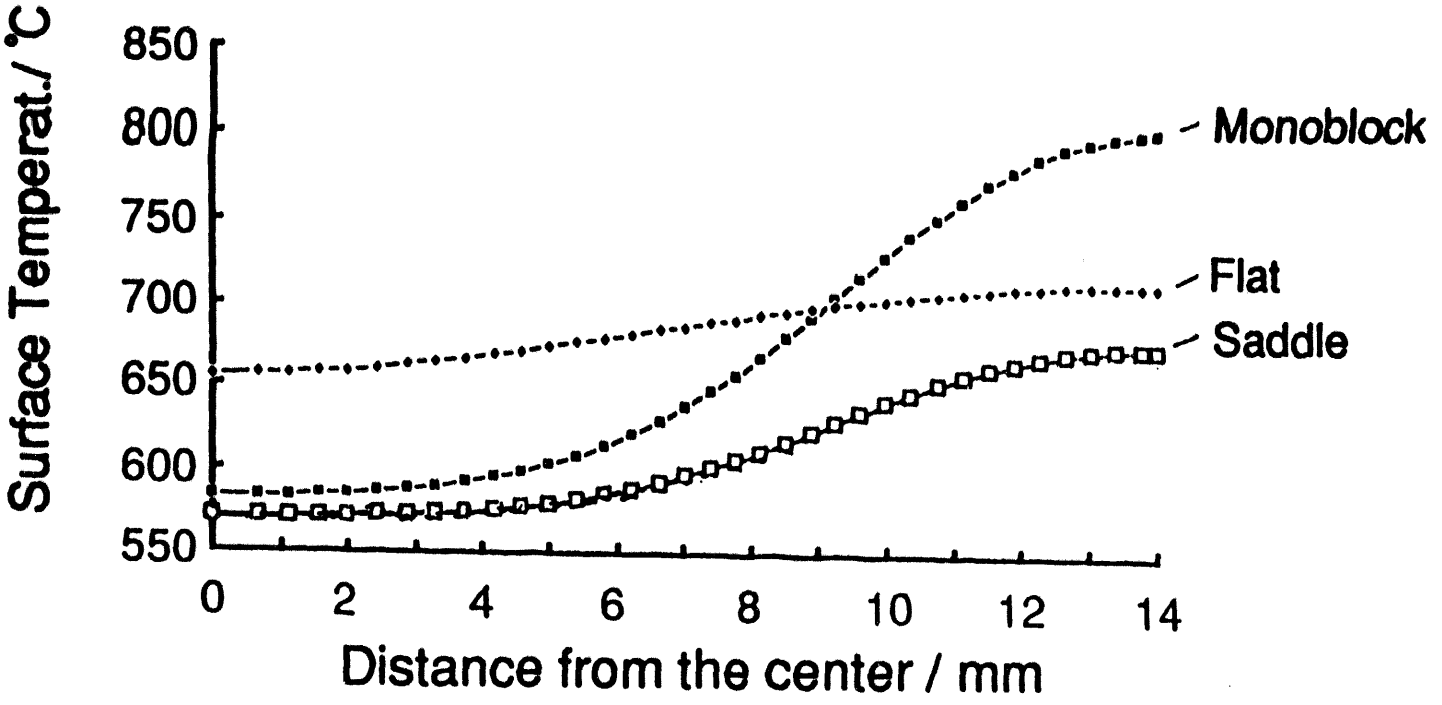

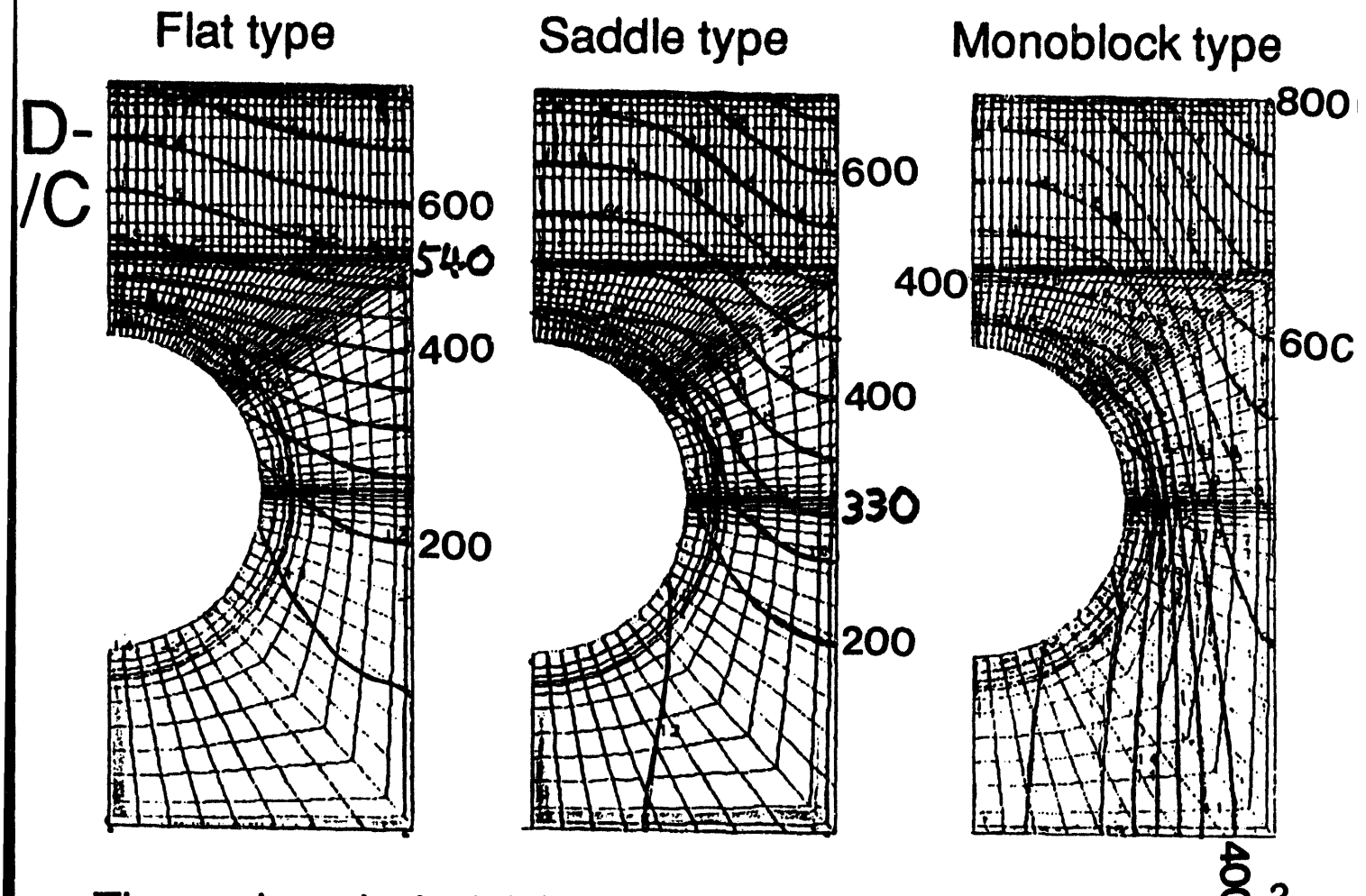

Thermal analysis (2D) results for steady state 15 MW/m^2 heat flux (coolant bulk temperature60℃, 70000W/m^{2}K)

Percent of Original T.C.

Effect of Annealing on Room Temperature Thermal Conductivity

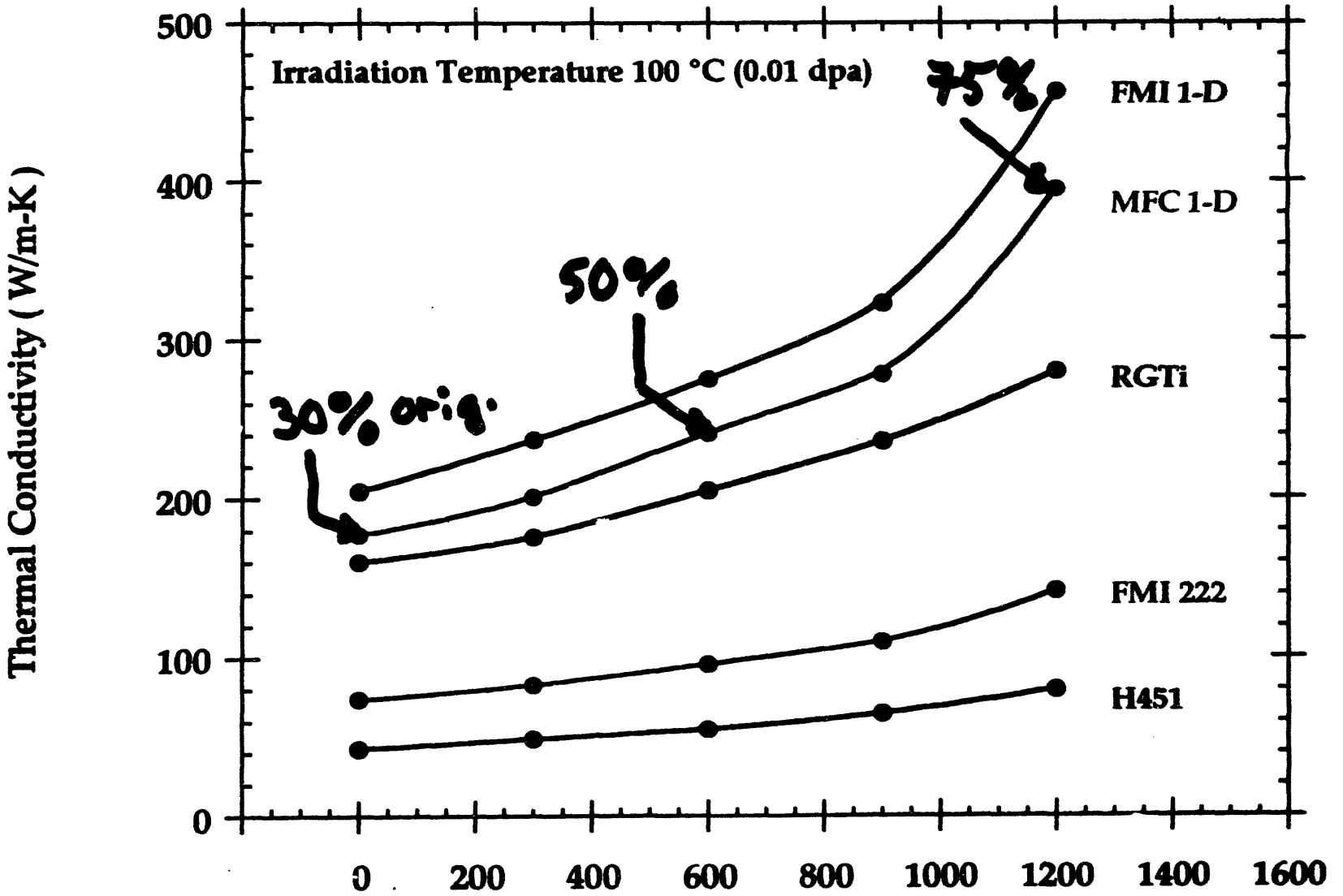

Snead et al.

- Use of C/C at elevated temperature significantly enhances performance.

  MFC 1, Flat Plate (Gotoh)

	Surface
ΔT (0 dpa) = 200°C	(700 max)
ΔT (0.01) = 400°C	(900 max)
ΔT (>1) ~ 500-700	(~1200°C)

- RGTi shows no advantage in irradiation performance.

- An algorithm has been developed to yield thermal conductivity as a function of T and OPA.

Session VII

Boundary Layer Plasmas

Summary Viewgraphs

compiled by

N. Noda and L. Schmitz

Boundary Layer Plasmas

Control of plasma boundary is one of the critical issues in next devices.

- Heat flux and particle flux to target plates and side walls of a divertor are determined by the boundary control.

- Design of divertor pumping scheme is also strongly dependent on the boundary control.

- The boundary control is not well established in the existing plasma experimental devices.

- A lot of efforts are ongoing to have a reasonable and reliable modeling of the boundary plasmas.

Radiative/Gas Target Regimes for ITER

I. High Density Gas Target Divertor:

An Ionization Front is Produced by Interaction of the Plasma with a Neutral Gas Layer. The Plasma is Detached. The Divertor Heat Flux is Dissipated by Deuterium Line Radiation and/or Radial Transport (Volume Recombination or Gas Recirculation)

- Closed Divertor "Channel", High Target Neutral Pressure ($\geq$ 1 Torr)

  Concerns: ***Radiation Trapping, Sidewall Sputtering, Stability of Ionization Front, Localized Radiation Layer***

II. Low Density Gas Target:

A Large Fraction ($\leq$ 90%) of the Boundary Heat Flux is Dissipated by Impurity Radiation Inside or Outside the Separatrix.

- Moderately Open Divertor, Moderate Pressure (< 0.1Torr, D radiation and CX to Dissipate Momentum and Residual Energy)

  Concerns: ***Ion Heat Flux May not be Reduced Sufficiently, Required Impurity Concentration May be Too Large (Ignition Quenching), Radiative Instability***

ITER Gas Target Divertor Modeling

Present Status:

A fully implicit 1 1/2-D plasma/neutral model indicates possible high density gas target solutions ($P_{sep} \leq 200$ MW; 133 MW outboard, $n_{sep} \geq 3 \times 10^{19}$ m^{-3}, kT_e, $kT_{i\,x} \leq 170$ eV), $n_2 = 0$!

Two scenarios have been explored:

A) Volume recombination scenario

B) Gas Injection/Recirculation Scenario (requires large radial plasma transport)

- ITER magnetics, closed slot divertor ($L_{pol} = 1.5$m, $a = 0.2$m)
- 2-D plasma profiles constructed by solving along $\underline{B}$ for various radii. Prescibed radial profiles at x-point

The DEGAS code is then used to calculate the 2-D neutral distribution and wall loading (A. Grossman)

ITER Gas Target Divertor Modeling

IPFR/UCLA

Preliminary Results:

- "Detached" solutions ($kT_e \leq 3$ eV, $n_{target} \leq 0.1\ n_{midplane}$ have been found for $P_{sep} \leq 200$ MW (133 MW to the outboard divertor).

  High separatrix density ($n_{sep} \leq 10^{20}$ m^{-3}) is required.

Active Gas Injection Scenario:

- Large radial particle diffusivity (or convection) is required to avoid reversed plasma flow ($D_{perp} > 10$ m^2/s).

  Charged particle flux to side walls ($\Gamma_i > 10^{19}$ /s cm^2) required to carry a substantial fraction (30-60%) of the total input power

- Strong divertor pumping is necessary ($Q > 5 \times 10^4$ Torr l/s), possibly at some intermediate location upstream from the density peak.

  Baffling will be required in the x-point region to reduce the neutral backflow to the main chamber by at least two orders of magnitude.

- Line radiation is strongly peaked, neutral wall loading is small but plasma wall loading close to the x-point may be a problem.

Volume Recombination Scenario:

- Transient Solutions (stable on a 3 ms timescale) have been obtained with collapsed ion and electron temperatures ($\leq$ 1 eV).

  The key factor is very high plasma density within the ionization front ($\geq$ 5x 10^{21} m^{-3}), leading to recombination rates comparable to the local ionization rate.

- Large radial particle diffusivity is not required.

- Correct treatment of the plasma momentum balance is essential. Momentum loss to neutrals (and, subsequently, the slot walls), may prevent plasma detachment and/or produce reversed plasma flow.

- The long-term stability in the presence of plasma influx and divertor pumping needs to be investigated.

Gas Target Divertor Simulation in PISCES-A

L. Schmitz, L. Blush, R. Lehmer,
G. Tynan, B. Merriman, R. W. Conn
IPFR, UCLA

- Stable, detached ionization front demonstrated for $q_e \leq 7. MW/m^2$ in a high density hydrogen plasma with typical divertor plasma parameters ($n_e \leq 2x10^{13}$ cm^{-3}, $kT_e \leq 20$ eV)
- Radiative Loss of up to 97% demonstrated (~60% line radiation, ~37% radial loss w/surface recombination on side walls)
- Target electron temperature decreased to 2.5 eV
- Moderate neutral backflow due to plasma plugging ($p_{o\ target}/p_{o\ source} \leq 0.02$)
- Strong momentum damping by ion-neutral collisions (leads to reversed plasma flow)
- Classical parallel electron heat transport
- Pressure Balance in H_2, but not in Ar!

Discussion:

Backflow of neutrals may be a problem ($p_o \geq 1$ Torr)
Extensive baffling required.

Existing tokamaks have $p_o/pc_{ore} \leq 1000$ (DITE, DIII-D)

Impuri. / radiation may ease requirements; but:
Entrainment is not experimentally established (Ignition quenching)

"Radiative mantle"(core impurity radiation) may be an option,
but may be insufficient at high input power.

We need to couple modeling of SOL impurity transport with
core radial impurity transport (find the right "species mix", etc.

He removal needs to be investigated for radiative divertor options, along with impurity behavior.

PFC requirements in the presence of injected (or intrinsic) impurities should be evaluated

Realistic models for SOL physics (drift flows, thermal forces, radial E-Field, etc., needs to be coupled with divertor (atomic physics) simulation

One-D modeling examines the power handling capabilites of a slot/cold plasma/radiative divertor.

INEL

- Scrapeoff Layer Power 16MW (reflects upgraded D III-D power).
- Deuterium Molecular Puffing 300 t-l/sec puffed to outer divertor. Hydrogenic puffing alone at this strength does not cool divertor plasma adequately.
- What Argon puffing is required to extinguish the divertor plasma, and is it possible to maintain entrainment?
- Neutral albedo 0.95, hydrogen recycle 0.98, 50% in molecules, 15cm slot length. (ΔZ(wid,Ar,0)=0.25m along B, ~ 1 cm poloidally)
- The best steady state solution (28 t-l/sec Ar) we've found so far is shown below.

$N_{sep} = 2.5 \times 10^{19} m^{-3}$

$Q_{peak} = 0.13$ MW/m (outer)

$P_{rad} = 11$ MW (8MW Ar)

$P_{trans} = 1.5$ MW

$P_{cx} = 1.1$ MW

$N_{Ar,sep} = 6.5 \times 10^{17} m^{-3}$

$Z_{eff,mid} = 3.3$

Alcator C-Mod is being simulated in 1-D and 2-D

- Impurity (carbon) entrainment studies in 1-D. With and without D2 puffing. Low power ohmic heating shots.

  Before puffing, radiation zone is near the divertor plates

  After puffing, changes in divertor hydrogen flows cause (in the simulation) radiation zone move to the X-point.

  This compares well with the experimental observations.

- Puffing (D2 and Argon) studies are being performed in 2-D at high power (e.g. 4MW into SOL).

  Both D2 and Argon (quasi-avg. ion model) can reduce heat load by factors of 10 or more

  Extent of argon radiation zone is greater than the hydrogen zone. The cooling from the argon also extends the influence of the hydrogenic neutrals.

Sandia National Laboratories
Idaho National Engineering Laboratory

AIIM

Association for Information and Image Management
1100 Wayne Avenue, Suite 1100
Silver Spring, Maryland 20910
301/587-8202

8 of 8

Session VIII

Disruptions

Summary Viewgraphs

compiled by

P. Rockett, A. Hassanein and N. Yoshida

Disruptions

I. P. Rockett

- Presented spectroscopic analysis of two RF plasma guns:

  - 2MK-200 TRINITI
  - VIKA Efremov

- Detailed spectral analysis in VUV showed that VIKA has impurities (Teflon).

- Need better high-resolution plasma characterization for accurate modeling.

- Presented new data from J. Gahl that showed higher erosion at lower energy density and longer disruption time.

- In Phase II study will modify spectrograph to permit higher resolution to analyze T_e (x,t), n_e (x,t).

II. A. Hassanein

- Developed comprehensive 2-D multi-group, continuum + lines, hydrodynamic radiation transport model → A * THERMAL-S

- Capabilities to model

  - Various simulation experiments (gun, E-beam, ion, etc.)

  - In-reactor conditions

- Good agreement with erosion measurements as well as fine details of plasma vapor characteristics.

- Simulate and help design TEXTOR disruption experiments with KFA.

III. J. Gilligan

- Showed results from SIRENS, electrothermal gun.

- Compared erosion measurements for different graphites and metals.

- Their data of erosion is much higher than other simulation experiments.

- Has 1-D MAGFIRE code to model disruption experiments.

What We Need to Do/ Recommendations

- Do disruption experiments that are reactor relevant:
  - DIII-D
  - TEXTOR

- Further study the effect of higher surface temperatures on the total erosion rate.

- Disruption modeling of reactor conditions:
  - ions + e's
  - magnetic field
  - melt layer hydrodynamics
  - longer disruption time ~ 10 ms
  - higher energy deposited ~ 200 MJ/m^2

- Develop collaboration between the U.S. and Japan in disruption modeling.

Session IX

Conditioning and Tritium

Summary Viewgraphs

compiled by

A. Sagara and R. Causey

Conditioning and Tritium

Boronization in Japan, A. Sagara (NIFS)

Boronization has been applied in plasma devices, JT-60U, Heliotron-E, CHS and JIPP T-IIU. Results are summarized as follows: (1) Decaborane has been commonly used with He. (2) Fast conditioning is commonly achieved every morning and after exposure to air. (3) Boronization once every few weeks gives stable wall condition. (4) Oxygen impurity is effectively reduced. (5) Reduction of carbon and metal impurities depends on wall material and plasma operation. (6) H recycling seems to depend on boronization condition and/or method. (7) STB has been confirmed to be clearly effective as quick conditioning to reduce both impurity and H recycling, while its lifetime is limited within a few shots.

Present state of R&D on boronization for LHD is summarized as follows: (1) Oxygen penetrates into deeper layers over 50 nm, and B film of about 100 nm thick is sufficient for oxygen getter. This result coincides with the thickness needed in plasma devices, but the penetration mechanism is not clear yet. (2) B film after O_2 glow keeps a quite passive state in the air. This result explains the fast conditioning observed in plasma devices. (3) Decaborane is comparable with diborane as far as oxygen getting capacity is concerned. (4) H in B film desorbs at lower temperature than that in carbon. This result explains the good discharges due to low H recycling in JT-60U, but R&D at room temperature is still required for the V/V in LHD, because its temperature is limited below 100°C.

Studies on Tritium Retention, Permeation and Recovery of Plasma Facing Materials at JAERI, M. Akiba (JAERI) on behalf of K. Okuno

The Tritium Processing Laboratory (TPL) were discussed. It is capable of handling 40 grams of tritium. The tritium permeation and inventory in plasma facing materials was discussed. The experimental facilities used in these experiments were shown. Permeation studies performed so far have used only deuterium. The R&D schedule for studies on tritium retention and recovery of plasma facing materials was shown. Tritium permeation experiments are scheduled to begin this year.

Report on the Tritium Plasma Experiment (TPE) Tritium Inventory and Permeation in ITER Outgassing and Conditioning, R. Causey and D. Cowgill (SNL/CA)

This talk covered three different areas: (1) Tritium Plasma Experiment (TPE), (2) tritium inventory prediction for ITER, and (3) conditioning. The TPE has been moved to the Tritium System Test Assembly (TSTA) at Los Alamos National Laboratory. It should be ready for operation in June of this year. Dr. Causey suggested TPE is available for collaborative research by ITER researchers from Japan, the European Community, and Russia.

Tritium inventory predictions for ITER were given to be as high as several kilograms. The upper limit is determined by the amount of trapping. Permeation into the coolant could be as high as 300 grams per day.

ICR was given as the recommended way to condition plasma machines with permanent high magnetic fields.

Real-Time Boronization in PBX-M Using Erosion of Solid Boronized Targets, H. Kugel (PPPL)

Evaporative, real-time boronization is being performed routinely on PBX-M using boronized probes. The most recent STB probes consist of 86% boronized graphite-felt composite containing loose 40 μm diameter boron particles. Three graphite-felt probes have been tested to date, resulting in more than 17 g deposited in PBX-M to date (1-2 hours per application, up to several applications per week, 29 applications total).

Effectiveness is summarized as follows: (1) During continuous real-time boronization and post boronized discharges, low Z and high Z impurities are significantly lower. (2) During disruptive conditions on new regimes, 3-4 applications per week seem adequate. (3) Rapid recovery from an air leak followed by N_2 vent. (4) Reduced impurities during IBW core confinement mode. (5) Disruptions redistribute and reactivate boron. (6) Significantly accelerate conditioning to new regimes.

STB may provide a possible method for achieving target plasmas with steep, highly peaked density profiles.

Measurements of Fusion Synthesized T and T Fuel in JET, TFTR, DIII-D and TEXTOR, B. Doyle (SNL/NM)

Motivation for measuring T was discussed: to provide data on the behavior of high energy ions in tokamak plasmas and T safety issues.

T measurement techniques were characterized with respect to sensitivity and analysis range. A new T-monitor by counting β's using a PIN diode in air or vacuum was introduced, which provides quick, real-time, nondestructive measurement of tritium near surface. Another new technique, neutron elastic recoil detection (NERD) method, was introduced for H isotope depth profiling.

Tritium measurement data on materials in tokamaks, JET, TFTR, DIII-D and TEXTOR, were shown and discussed from points of view of T cleanup, behavior of high energy T, and deposition patterns of T and D.

Future research and development were discussed concerning portable or in-situ T-monitor and their applications for advanced tokamaks, TPX and ITER.

Session X

Erosion/Redeposition

Summary Viewgraphs

compiled by

Y. Hirooka and T. Hino

Erosion/Redeposition

PRESENTATIONS

PISCES Experiment (1)
DiMES Experiments (3)
Modeling (1)

- Experiments and modeling well coordinated
- Emphasis shifting to Be materials for ITER

PISCES Experiments

- Impurity transport (Figure 1)
  (more transport to downstream)
- Be erosion experiments ready to go (Figure 2)

DiMES Experiments

- Instrumented probe available (Figure 3)
- In-situ elipsometry under way
  (real-time erosion measured during discharges)
- Four half days of experiment time available
- Good agreement with REDEP and experimental data on net carbon erosion (Figure 3)
- W-probe—very small erosion
- Downstream erosion observed (Figure 4)

Erosion and Redeposition Modeling

- Observed close agreement with DIII-D, PISCES experiments
- More work planned for 1994
- ITER gas target conditions
  - REDEP predictions (Figure 5 and Figure 6)
  - with dissipative divertor
    - Be—short life [3 hours (?)]
    - Mo, W—long life [x 100 (?)]
  - Need experimental data on Be sputtering
- Sheath modeling
  - Possible positive feedback
  - Effect due to:
    - H desorption
    - Be evaporation

Issues (directions)

- More experiments and modeling comparison for ITER R&D
- In general, coordination is good
- More tokamak machine time for PMI work (in DIII-D) (this means more funding from D&T)
- Lab tours:
  - DIII-D/DiMES on January 27, 1994—C. Wong
  - PISCES on January 28, 1994—Y. Hirooka

After Hirooka

Fig. 1

45 degree experiment, 100 eV Ar^+ bombarbment
Mo concentration profile on the graphite target

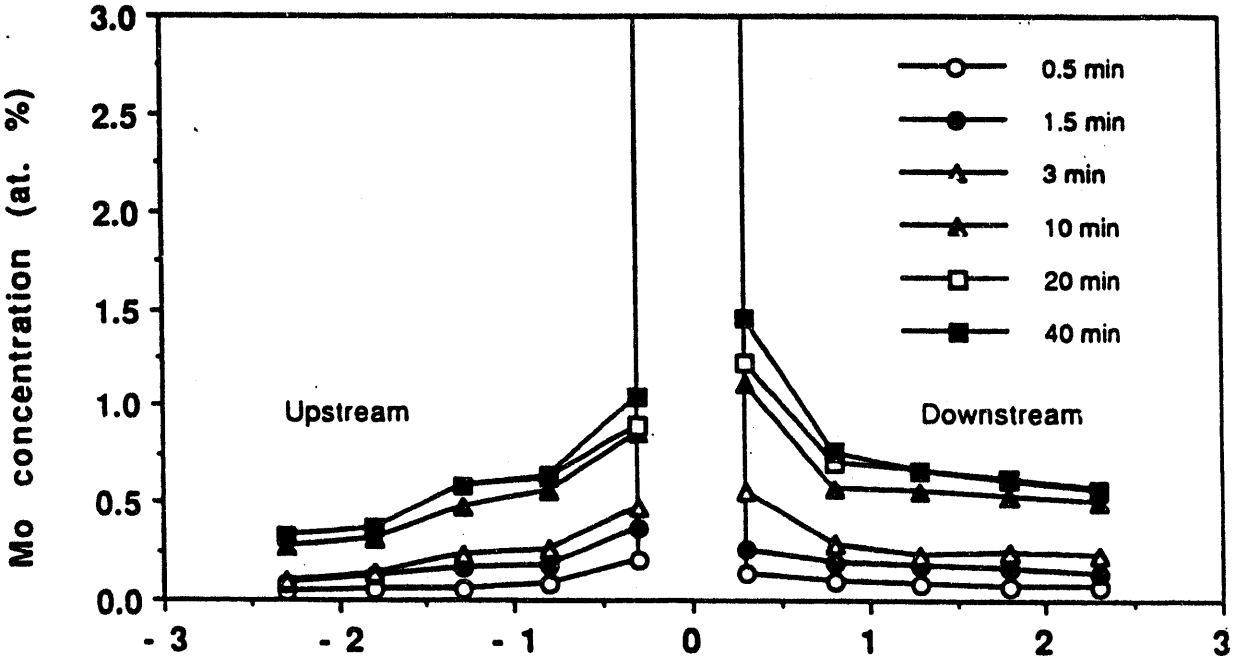

Radial distance on sample surface (cm)

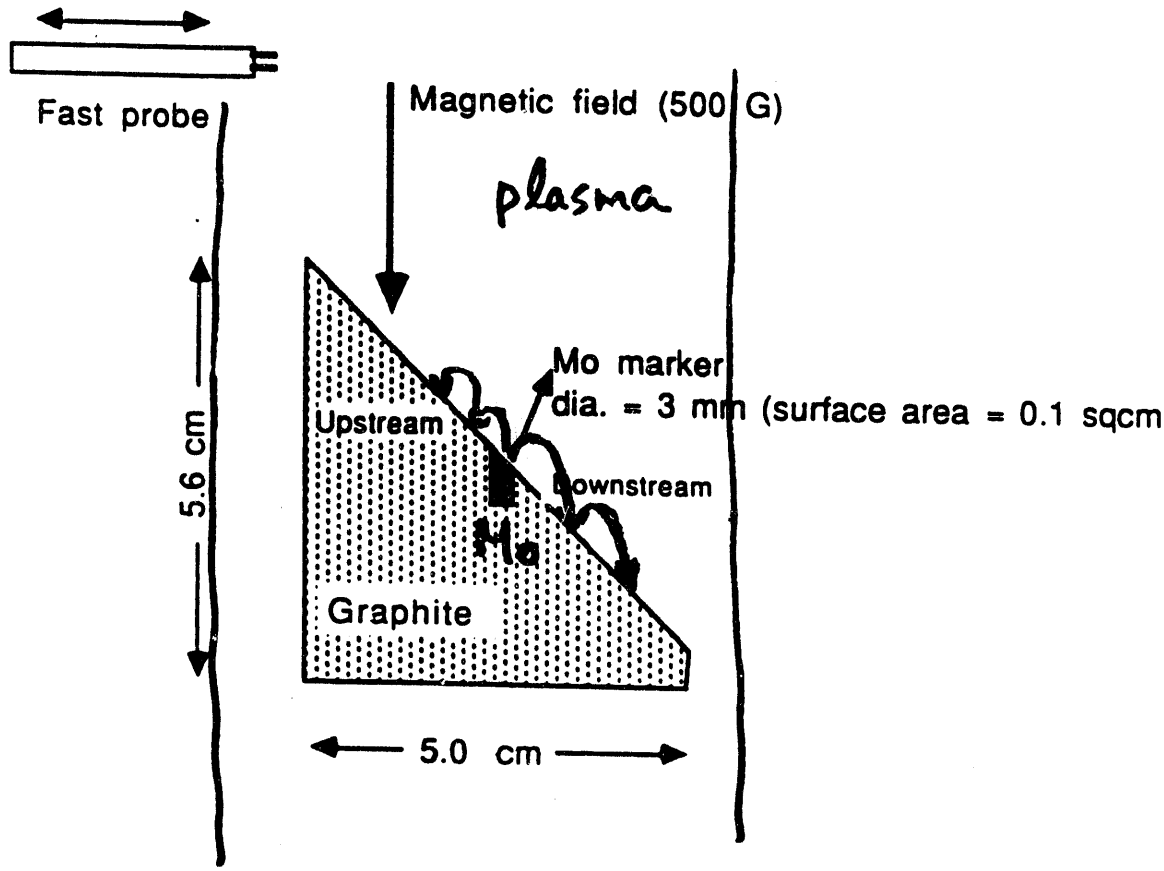

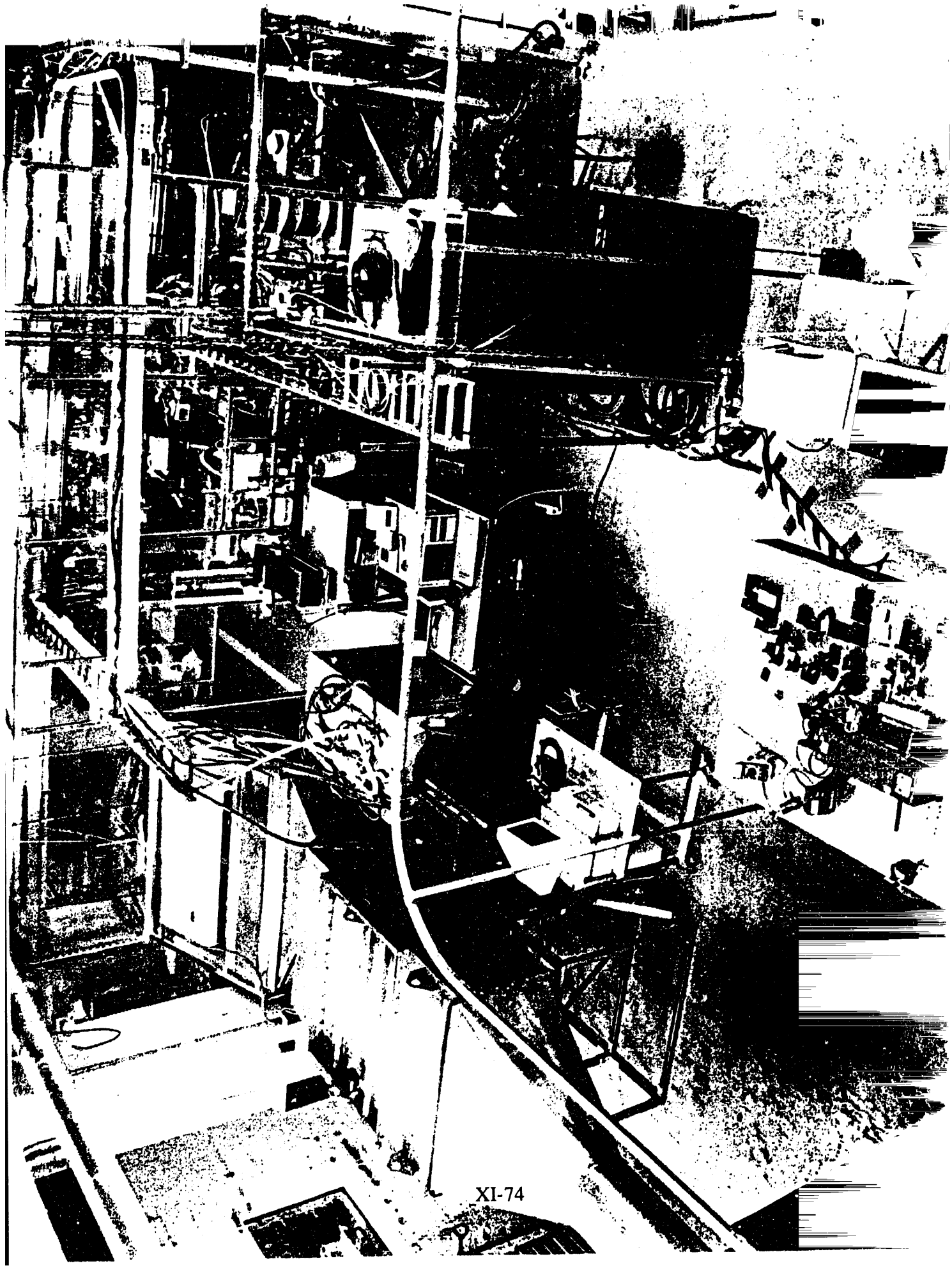

Hitter Wong

GENERAL ATOMICS

Fig. 3

DiMES IMPROVED INSTRUMENTATION FEEDTHRU

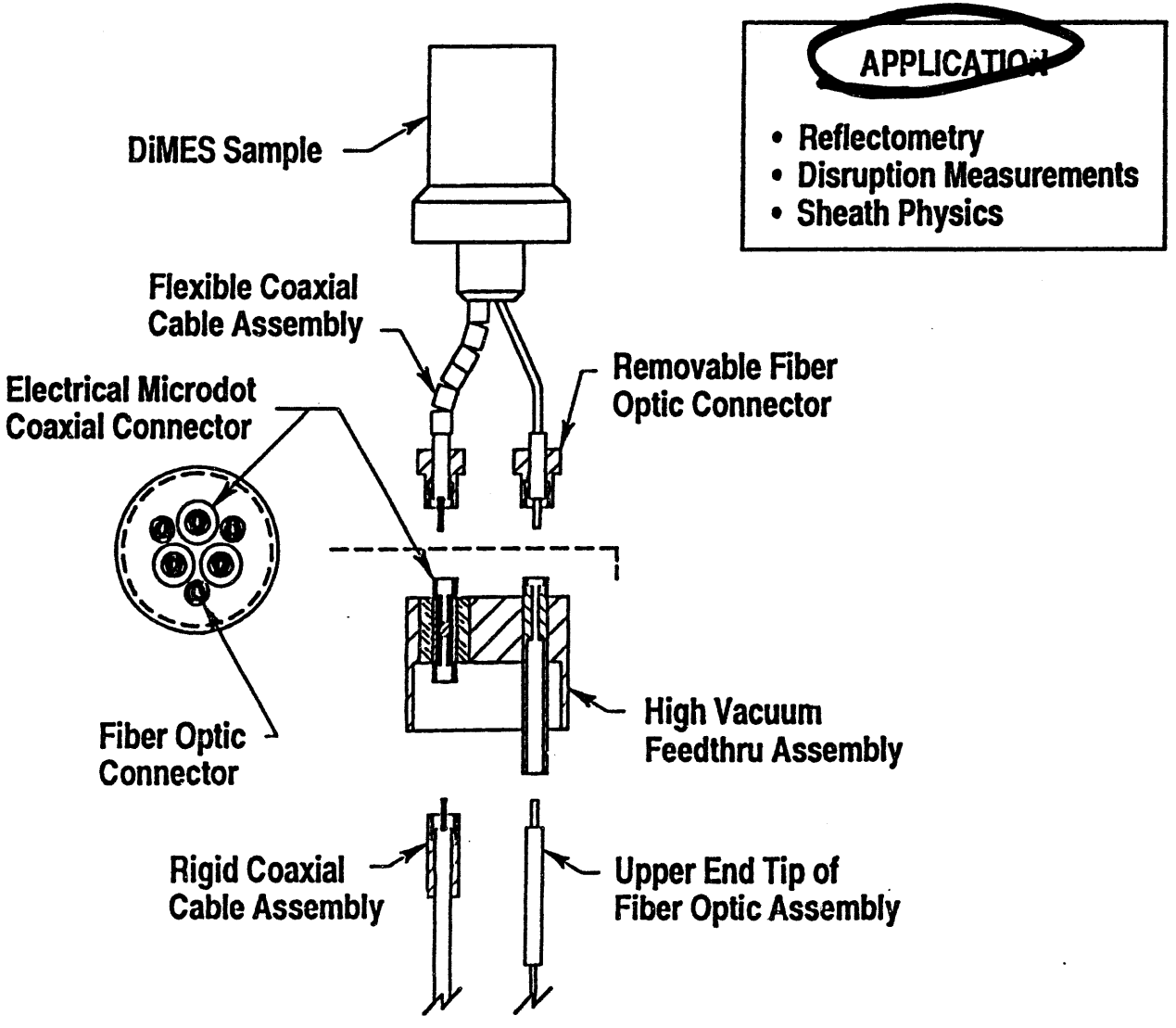

After Wong

Fig. 3

GENERAL ATOMICS

MATERIAL EVALUATION EXPERIMENTS IN DIII–D DIVERTOR

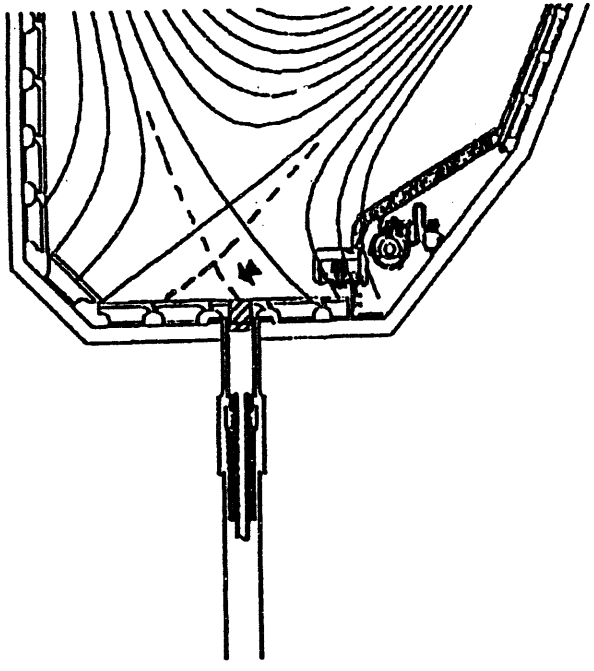

DIMES Sample Insertion

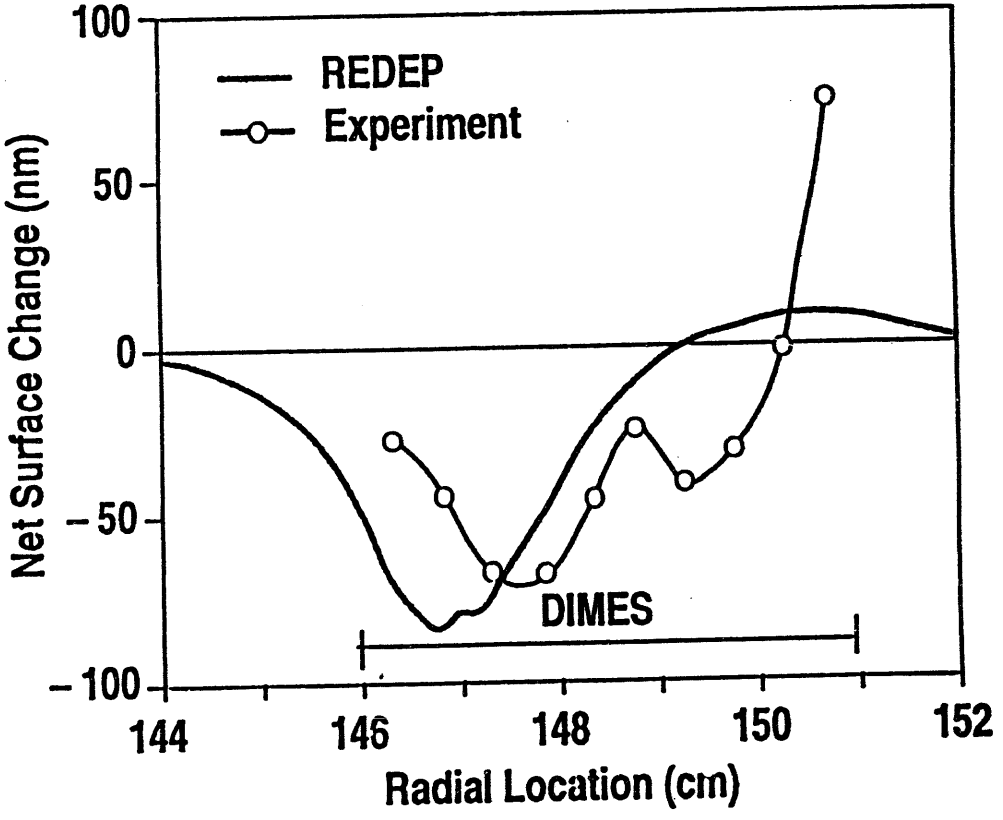

Comparison of Net Erosion with REDEP Model

PW 1/94

After Wampler

Fig. 4

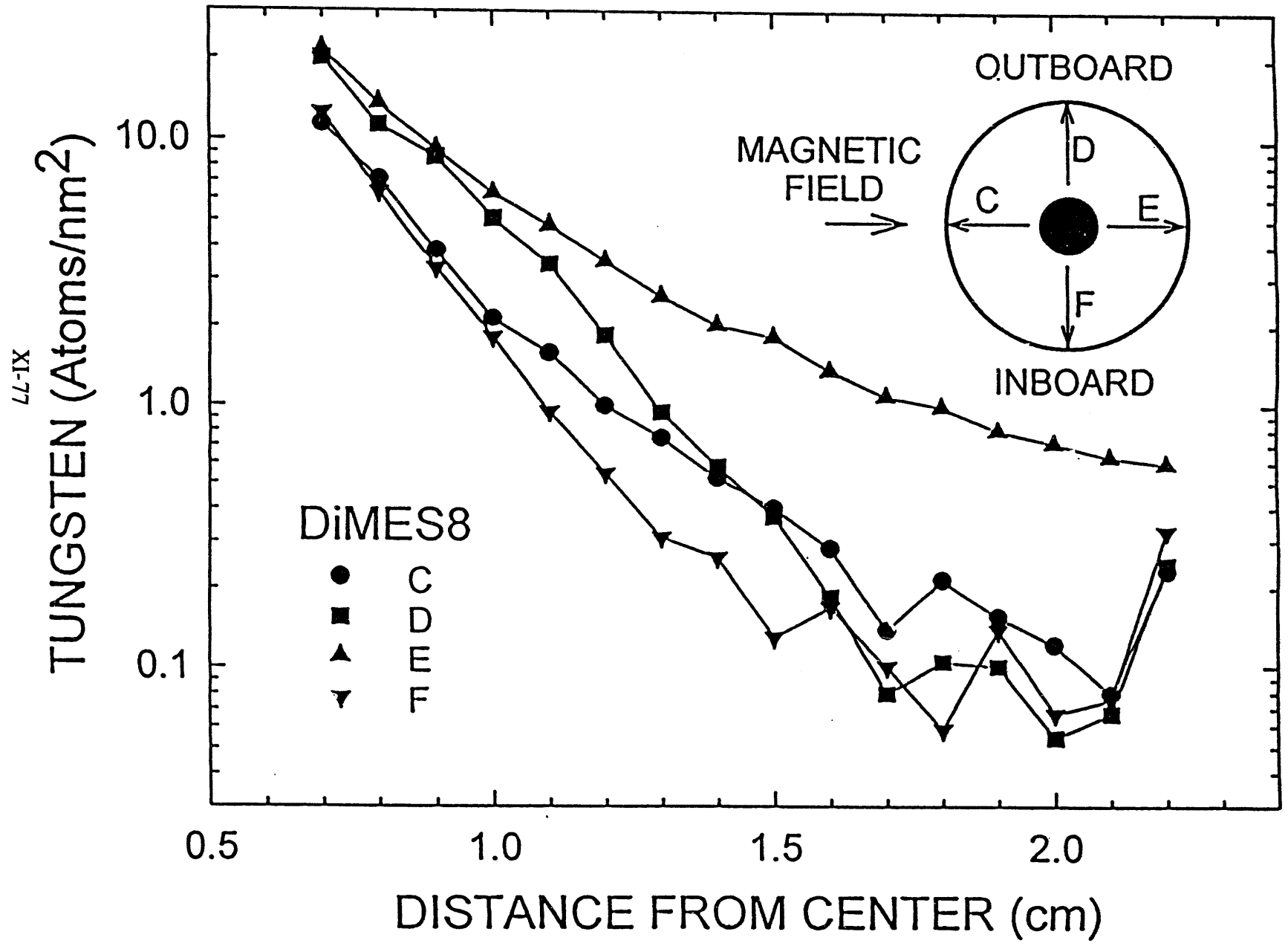

After Brooks

Fig. 5

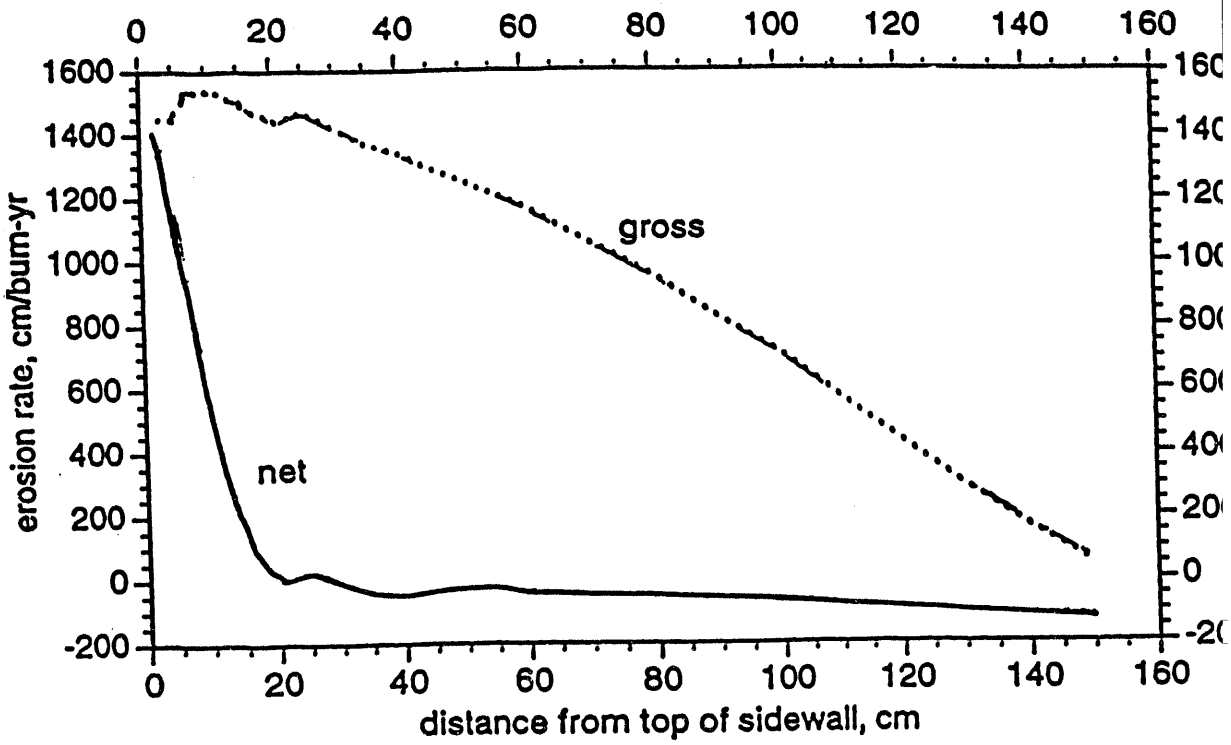

Fig. 4.4-1. ITER/REDEP Analysis: Erosion of beryllium coated gaseous divertor sidewall; for UCLA plasma solution.

Dissipative divertor conditions

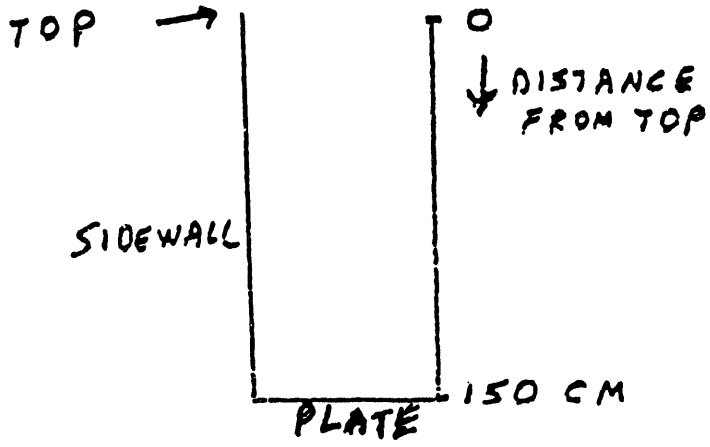

-for Breeder

Fig. 6

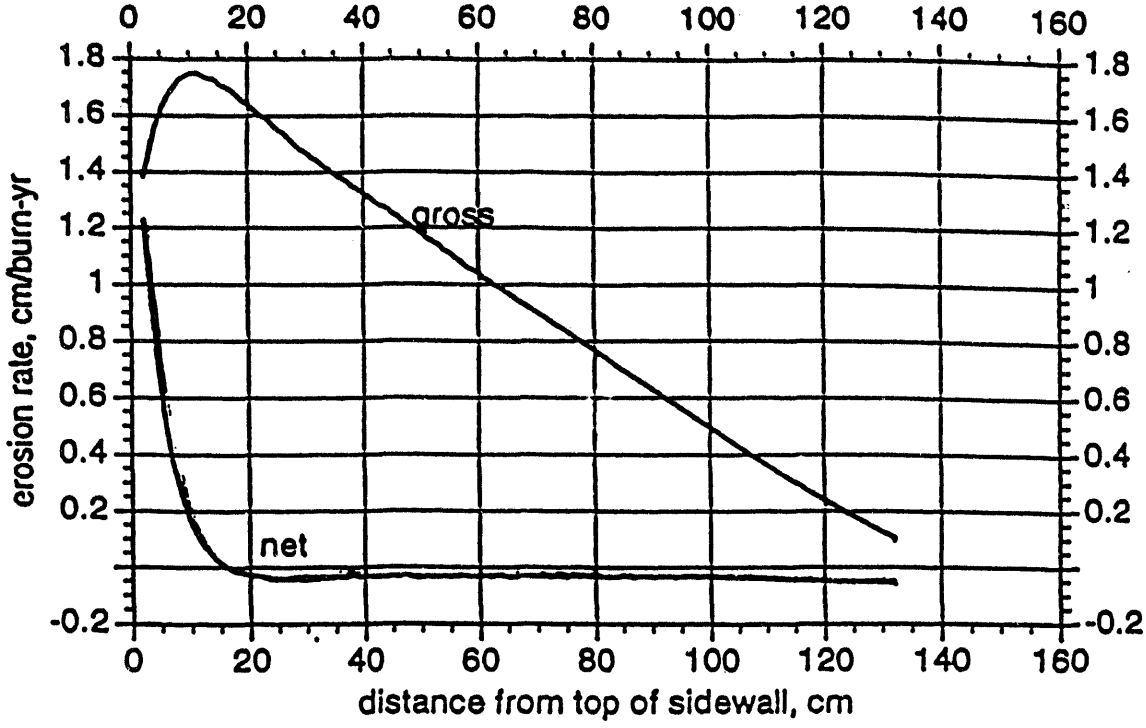

Fig. 4.4-3. ITER/REDEP Analysis: Erosion of tungsten coated gaseous divertor sidewall; for UCLA plasma solution.

Appendix A

Workshop Agenda

U.S.-Japan Workshop Q-181
High Heat Flux Components and Plasma-Surface Interactions for Next Devices

University of California at San Diego
San Diego, California
January 24-27, 1994

AGENDA

Monday
24-January-94

Arrival: Coffee and Danish 7:45 - 8:30 a.m.

Session I: Welcome/Organization and Overviews
Chairman: R. T. McGrath (SNL/NM)

I.1	M. Cohen (DOE)	Welcome, Workshop Objective	8:30 a.m.	(15)
I.2	T. Yamashina (Hokkaido University)	Opening Remarks	8:45 a.m.	(15)
I.3	R. Conn (UCLA)	Opening Remarks	9:00 a.m.	(15)
I.4	T. Hino (Hokkaido University)	Overview of HHFC and PMI Studies in Japan	9:15 a.m.	(30)
I.5	M. Ulrickson (SNL/NM)	Overview of HHFC and PMI Studies in the U.S.	9:45 a.m.	(30)
	Break		10:15 a.m.	(15)

Session II: PFC Issues for Future Machines
Chairmen: O. Motojima (NIFS) and K. Wilson (SNL/CA)

II.1	O. Motojima (NIFS)	Present Status of the Large Helical Device (LHD)	10:30 a.m.	(30)
II.2	S. Tanaka (JCT)	Design of ITER Plasma Facing Components	11:00 a.m.	(20)
II.3	R. Matera (JCT)	R&D for ITER Plasma Facing Components	11:20 a.m.	(20)
II.4	D. Hill (LLNL)	Power Handling in the TPX Tokamak—Tokamak Physics Experiment	11:40 a.m.	(30)
	Lunch		12:10 p.m.	(75)

Session III: Recent PMI Results from Several Tokamaks
Chairmen: N. Yoshida (Kyushu University) and D. K. Owens (PPPL)

III.1	D. K. Owens (PPPL)	Results from the Initial D-T Experiments on TFTR	1:25 p.m.	(30)
III.2	N. Yoshida (Kyushu University)	PFC and PSI Studies on TRIAM-1M	1:55 p.m.	(30)
III.3	B. LaBombard (MIT)	Initial Results from Alcator C-Mod	2:25 p.m.	(30)
	Break		2:55 p.m.	(15)
III.4	N. Noda (NIFS)	High Z Limiter Experiments in TEXTOR	3:10 p.m.	(30)
III.5	T. Ando (JAERI)	PFCs and PSI in JT-60U	3:40 p.m.	(30)
III.6	M. Caorlin (PPPL)	DT-Relevant PMI Studies on TFTR	4:10 p.m.	(30)
III.7	P. West (GA)	Divertor Plasma and Plasma Facing Wall Research on DIII-D	4:40 p.m.	(30)
	Open Discussion on Day-One Presentations: **Discussion Leaders: O. Motojima (NIFS) and P. West (GA)**		5:10 p.m.	(35)
	Depart for Reception		5:45 p.m.	
	Reception at Faculty Club, UCSD (return transportation to hotel provided)		6:00-8:30 p.m.	

Session IV: High Heat Flux Technology
Chairmen: M. Akiba (JAERI) and M. Ulrickson (SNL/NM)

IV.1	M. Akiba (JAERI)	Development of High Heat Flux Components at JAERI	8:30 a.m.	(30)
IV.2	N. Noda (NIFS)	HHFC Development at NIFS	9:00 a.m.	(30)
IV.3	C. Baxi (GA)	Design, Fabrication and Testing of Helium Cooled Divertor Module	9:30 a.m.	(15)
IV.4	S. Suzuki (JAERI)	Heating Tests on JT-60 Actively Cooled Divertor Mock-ups	9:45 a.m.	(15)
IV.5	K. Sato (JAERI)	Thermal Cycling Experiment on 1D CFC/W-Cu Divertor Mock-up	10:00 a.m.	(15)
	Break		10:15 a.m.	(15)
IV.6	D. Youchison (SNL/NM)	Recent EBTS Results and Planned HHF Tests on Beryllium Armored Mock-ups	10:30 a.m.	(15)
IV.7	R. Castro (LANL)	Plasma-Spraying of Beryllium for Fusion Applications	10:45 a.m.	(15)
IV.8	F. Kudough (Mitsubishi Atomic Power Industries, Inc.)	High Heat Flux Load Experiments on Functionally Graded Materials	11:00 a.m.	(10)
IV.9	T. Hua (ANL)	Liquid Metal Coolants for Blanket and Divertor	11:10 a.m.	(10)
IV.10	K. Kitamura (Toshiba Corp.)	Residual Stress Measurements in Tungsten-Copper Duplex Structures after Cyclic Thermal Testing	11:20 a.m.	(10)

Session V: Plasma Facing Component Design and Applications
Chairmen: A. Komori (NIFS) and J. Davis (MDA)

V.1	A. Komori (NIFS)	Local Island Divertor Concept for LHD	11:30 a.m.	(30)
	Lunch		12:00 noon	(90)
V.2	R. Nygren (SNL/NM)	Tore Supra Phase III Outboard Pump Limiter (OPL)	1:30 p.m.	(30)
V.3	J. Davis/D. Driemeyer (MDA)	U.S. Design Studies for ITER PFCs	2:00 p.m.	(30)

Session VI **Plasma Facing Component Materials and Irradiation Damage**
Chairmen: T. Muroga (Kyushu University) and T. Burchell (ORNL)

VI.1	T. Muroga (Kyushu University)	Radiation Damage of Plasma-Facing Materials	2:30 p.m.	(30)
VI.2	L. Snead (ORNL)	ORNL Irradiation Effects Program	3:00 p.m.	(30)
VI.3	S. Miki (Toyo Tanso USA, Inc.)	Development of PFC Materials at Toyo Tanso	3:30 p.m.	(15)
VI.4	W. Wampler (SNL/NM)	Enhancement of Hydrogen Isotope Trapping in Damaged B and Ti Doped Russian Graphites	3:45 p.m.	(15)
	Break		4:00 p.m.	(15)
VI.5	Y. Gotoh (Hitachi Research Lab)	Development of C/C with Controlled Fiber Orientation	4:15 p.m.	(15)
VI.6	Y. Kikuchi (Hitachi Chemical Co.)	Development of B_4C Coated Carbon Materials by Conversion Method	4:30 p.m.	(15)
VI.7	P. Trester (GA)	Preparation of Plasma Facing Materials Coatings at General Atomics	4:45 p.m.	(15)
	Discussion: Sessions IV, V, and VI **Discussion Leaders: M. Akiba (JAERI) and M. Ulrickson (SNL/NM)**		5:00 p.m.	(30)
	Adjourn		5:30 p.m.	
	U.S.-Japan Joint Projects Meeting (limited attendance)		5:30 p.m.	(90)

Session VII: Boundary Layer Plasmas
Chairmen: N. Noda (NIFS) and L. Schmitz (UCLA)

VII.1	L. Schmitz (UCLA)	ITER Gas Target Divertor Modeling and Experimental Simulation	8:30 a.m.	(30)
VII.2	R. Campbell/D. Knoll (SNL/NM) (INEL)	Modeling of Radiative and Gaseous Divertor Operation	9:00 a.m.	(30)
VII.4	A. Grossman (UCLA)	Modeling of Gas Target Scenarios Using Degas	9:30 a.m.	(30)
	Break		10:00 a.m.	(15)

Session VIII: Disruptions
Chairmen: N. Yoshida (Kyushu University) and P. Rockett (SNL/NM)

VIII.1	M. Akiba (JAERI)	Overview of Disruption Simulations at JAERI	10:15 a.m.	(15)
VIII.2	P. Rockett (SNL/NM)	Recent Results from the US/RF Disruption Collaboration	10:30 a.m.	(15)
VIII.3	A. Hassanein (ANL)	Status of Disruption Modeling and Simulations	10:45 a.m.	(15)
VIII.4	J. Gilligan (NCSU)	Upgrade to MAGFIRE Code Modeling of Disruptions and Comparison with Experimental Results	11:00 a.m.	(15)
	Discussion: Sessions VII and VIII **Discussion Leaders: N. Yoshida (Kyushu University) and L. Schmitz (UCLA)**		11:15 a.m.	(45)
	Lunch		12:00 noon	(60)

Session IX: Conditioning and Tritium
Chairmen: R. Causey (SNL/CA) and A. Sagara (NIFS)

IX.1	A. Sagara (NIFS)	Boronization in Japan	1:00 p.m.	(30)
IX.2	K. Okuno (JAERI)	Studies on Tritium Retention, Permeation and Recovery of Plasma Facing Materials at JAERI	1:30 p.m.	(30)
IX.3	R. Causey/D. Cowgill (SNL/CA)	Report on the Tritium Plasma Experiment (TPE) Tritium Inventory and Permeation in ITER Outgassing and Conditioning	2:00 p.m.	(30)
	Break		2:30 p.m.	(15)
IX.4	H. Kugel (PPPL)	Real-Time Boronization in PBX-M Using Erosion of Solid Boronized Targets	2:45 p.m.	(15)
IX.5	B. Doyle (SNL/NM)	Measurements of Fusion Synthesized T and T Fuel in JET, TFTR, DIII-D and TEXTOR	3:00 p.m.	(15)

Session X: Erosion/Redeposition
Chairmen: T. Hino (Hokkaido University) and Y. Hirooka (UCLA)

X.1	Y. Hirooka (UCLA)	Recent Progress in the ITER-R&D Related Erosion and Redeposition Studies at UCLA	3:15 p.m.	(30)
X.2	C. P. C. Wong (GA)	DiMES Program 1993 Activities and 1994 Plan	3:45 p.m.	(15)
X.3	N. Brooks (GA)	Characterization of Divertor Plasma During DiMES8 Sample Exposure	4:00 p.m.	(15)
X.4	W. Wampler (SNL/NM)	Measurements of Erosion and Deposition of Carbon and Tungsten by the DIII-D Divertor Plasma	4:15 p.m.	(15)
X.5	J. Brooks/T. Hua (ANL)	Erosion/Redeposition Analysis for ITER, DIII-D, and PISCES and Tokamak Sheath Modeling	4:30 p.m.	(30)

Wednesday
26-January-94

Discussion: Sessions IX and X **Discussion Leaders: N. Noda (NIFS) and Y. Hirooka (UCLA)**	5:00 p.m.	(45)
Adjourn	5:45 p.m.	
Conference Banquet: Bus departs Embassy Suites Hotel	6:15 p.m.	
Hornblower Yacht Dinner Cruise (the *Zumbrota*, private yacht))		
Board: B Street Pier, 1066 N. Harbor Dr., San Diego	6:45 p.m.	
Cruise:	7:00 p.m.	
Return:	9:45 p.m.	
Disembark:	10:00 p.m.	

Thursday
27-January-94

Session XI: Workshop Summary and Conclusions

Working Group Sessions	8:30 a.m.	2.5 hr
Meeting Summary and Conclusions	11:00 a.m.	2.0 hr
Workshop Adjourns	1:00 p.m.	

Appendix B

List of Participants and Addresses

Masato Akiba
Japan Atomic Energy Research Institute (JAERI)
Naka-machi, Naka-gun, Ibaraki-ken
311-01 Japan
Phone: 81-292-70-7552
FAX: 81-292-70-7558
E-mail: akiba@vax011

R. Bolvin
Institute of Plasma & Fusion Research
University of California, Los Angeles
44-139 Engineering IV
Los Angeles, CA 90024-1597
FAX: (310) 206-4832

Susumu Amemiya
Nagoya University
Department of Nuclear Engineering
Furo-cho, Chikusa-ku, Nagoya
464 Japan

J. Brooks
Argonne National Laboratory
9700 South Cass Avenue
Argonne, IL 60439
Phone: (708) 252-4830
FAX: (708) 252-5287
E-mail: u1646@f.nersc.gov

Paul Anderson
General Atomics
P.O. Box 85608
San Diego, CA 92186
FAX: (619) 455-4156

N. Brooks
General Atomics
P.O. Box 85608
San Diego, CA 92186
Phone: (619) 455-3979
FAX: (619) 455-4156
E-mail: brooks@gav.gat.com

Toshiro Ando
Japan Atomic Energy Research Institute
(JAERI)
Naka-machi, Naka-gun, Ibaraki-ken
311-01 Japan
Phone: 81-292-70-7432
FAX: 81-292-70-7449

D. Buchenauer
Sandia National Laboratories, Org. 8347
PO Box 969
MS9162
Livermore, CA 94551-0969
Phone: (510) 294-3570
FAX: (510) 294-3231
E-mail: buchenaue@vaxm.gat.com

C. Baxi
General Atomics
P.O. Box 85608
San Diego, CA 92186
FAX: (619) 455-4156

T. Burchell
Oak Ridge National Laboratory
Bldg. 4508, MS6088
PO Box 2008
Oak Ridge, TN 37831
FAX: (615) 574-7659

R. Campbell
Sandia National Laboratories, Org. 6531
PO Box 5800
MS1129
Albuquerque, NM 87185-1129
Phone: (505) 845-3147
FAX: (505) 845-3130
E-mail: campbel@pmtf.sandia.gov

R. Conn
Office of the Dean
School of Engineering
University of California, San Diego
La Jolla, CA 92093-0403
Phone: (619) 534-6237
FAX: (619) 534-4771

M. Caorlin
Princeton Plasma Physics Laboratory
PO Box 451
Princeton, NJ 08543
Phone: (609) 243-3627
FAX: (609) 243-2874
E-mail: mcaorlin@pppl.gov

J. Cuthbertson (SNL/CA)
General Atomics
P.O. Box 85608
San Diego, CA 92186
Phone: (619) 455-2832
FAX: (619) 455-4156
E-mail: cuthbertson@vaxm.gat.com

R. Castro
Los Alamos National Laboratory
PO Box1663
Los Alamos, NM 87545
Phone: (505) 667-5191
FAX: (505) 667-5268
E-mail: rcastro@lanl.gov

J. Davis
McDonnell Douglas Aerospace
Mail Code 306-4204
PO Box 516
St. Louis, MO 63166
Phone: (314) 233-6200
FAX: (314) 234-4506
E-mail: davis@lllsrv.mdc.com

R. Causey
Sandia National Laboratories, Org. 8347
PO Box 969
MS9162
Livermore, CA 94551-0969
Phone: (510) 294-3326
FAX: (510) 294-1489
E-mail: causey@california.sandia.gov

B. Doyle
Sandia National Laboratories, Org. 1111
PO Box 5800
MS1056
Albuquerque, NM 87185-1056
Phone: (505) 844-7568
FAX: (505) 844-7775
E-mail: bldoyle@sandia.gov

M. Cohen
Office of Fusion Energy
Office of Energy Research
ER-533, Germantown
U.S. Department of Energy
Washington, DC 20585
Phone: (301) 903-4253
FAX: (301) 903-8681

John Gilligan
Department of Nuclear Engineering, Rm. 1110C
North Carolina State University
Box 7909
Raleigh, NC 27695-7909
Phone: (919) 515-2301
FAX: (919) 515-5115
E-mail: gilligan@ncsu.edu

Yoshitaka Gotoh
Hitachi Laboratory, Hitachi Ltd.
Saiwaicho 3-1-1, Hitachi
317 Japan
Phone: 81-294-23-5773
FAX: 81-294-23-6955

Yoshi Hirooka
Institute of Plasma & Fusion Research
University of California, Los Angeles
44-139 Engineering IV
Los Angeles, CA 90024-1597
Phone: (310) 825-6996
FAX: (310) 206-4832

A. A. Haasz
Institute of Aerospace Studies
University of Toronto
4925 Dufferin Street
Downsview, Ontario, M3H 5T6
Canada
Phone: (416) 667-7734
FAX: (416) 667-7799

T. Hua
Argonne National Laboratory
9700 South Cass Avenue
Argonne, IL 60439
Phone: (708) 252-7753
FAX: (708) 252-5287
E-mail: u30277@f.nersc.gov

A. Hassanein
Argonne National Laboratory
9700 South Cass Avenue
Argonne, IL 60439
Phone: (708) 252-5889
FAX: (708) 252-5287
E-mail: u1647@f.nersc.gov

G. Jackson
General Atomics
P.O. Box 85608
San Diego, CA 92186
FAX: (619) 455-4156

D. Hill (LLNL)
General Atomics
P.O. Box 85608
San Diego, CA 92186
FAX: (619) 455-4156
E-mail: hilld@gam.gat.com

Scott Keller
Institute of Plasma & Fusion Research
University of California, Los Angeles
44-139 Engineering IV
Los Angeles, CA 90024-1597
Phone: (310) 206-2468
FAX: (310) 206-1531
E-mail: keller@fusion.ucla.edu

Tomoaki Hino
Hokkaido University
Department of Nuclear Engineering
Kita-13, Nishi-8, Kita-ku, Sapporo
060 Japan
Phone: 81-11-716-2111, ext. 6660
FAX: 81-11-709-6413

Yoshihiro Kikuchi
Yamazaki Works (Sakuragawa)
Hitachi Chemical Co., Ltd.
3-3-1, Ayukawa-cho, Hitachi, Ibaraki-ken
316 Japan
Phone: 81-294-33-1111
FAX: 81-294-36-5342

Kazunori Kitamura
Heavy Apparatus Engineering Laboratory
Toshiba Corporation
2-4, Suehiro-cho, Tsurumi-ku, Yokohama
230 Japan
Phone: 81-45-509-6698
FAX: 81-45-509-6646

G. Longhurst
Idaho National Engineering Laboratory
PO Box 1625
Idaho Falls, ID 83415
Phone: (208) 526-9950
FAX: (208) 526-0528

Akio Komori
National Institute for Fusion Science
Furocho, Chikusa-ku, Nagoya
464 Japan
Phone: 81-52-781-5111
FAX: 81-52-782-8493
E-mail: komori@robin.nifs.ac.jp

Toshikazu Maeda
Mitsubishi Kasei America Inc., California Office
2180 Sand Hill Road, Suite 440
Menlo Park, CA 94025
Phone: (415) 854-5690
FAX: (415) 854-9797

Fumio Kudough
Mitsubishi Fusion Center
2-3, Marunouchi 2 Chome, Chiyoda-ku, Tokyo
100 Japan
Phone: 81-3-3218-2047
FAX: 81-3-3211-3123

R. Matera
ITER Garching Joint Work Site
Max Planck Institut für Plasmaphysik
Boltzmannstrasse 2
D-85748 Garching bei München
Germany
FAX: 011-49-89-3299-4313

H. Kugel
Princeton Plasma Physics Laboratory
PO Box 451
Princeton, NJ 08543
Phone: (609) 243-3146
FAX: (609) 243-2418
E-mail: hkugel@pppl.gov

Chris Mays
Institute of Plasma & Fusion Research
University of California, Los Angeles
44-139 Engineering IV
Los Angeles, CA 90024-1597
Phone: (310) 206-6440
FAX: (310) 206-1531
E-mail: cmays@fusion.ucla.edu

B. LaBombard
Massachusetts Institute of Technology
175 Albany Street
Cambridge, MA 02139
FAX: (617) 253-8000

Bob McGrath
Sandia National Laboratories, Org. 6503
P.O. Box 5800
MS0740
Albuquerque, NM 87185-0740
Phone: (505) 844-1522
FAX: (505) 844-6055
E-mail: rtmcgrath@pmtf.sandia.gov

Sokan Miki
Toyo Tanso USA
2575 NW Graham Circle
PO Box 280
Troutdale, OR 97060
Phone: (503) 661-7700
FAX: (503) 669-9107

R. Nygren
Sandia National Laboratories, Org. 6531
PO Box 5800
MS1129
Albuquerque, NM 87185-1129
Phone: (505) 845-3135
FAX: (505) 845-3130
E-mail: nygren@pmtf.sandia.gov

Osamu Motojima
National Institute for Fusion Science
Furocho, Chikusa-ku, Nagoya
464 Japan
Phone: 81-52-782-8395
FAX: 81-52-782-8493

D. K. Owens
Princeton Plasma Physics Laboratory
PO Box 451
Princeton, NJ 08543
Phone: (609) 243-3181
FAX: (609) 243-2874
E-mail: kowens@pppl.gov

R. Moyer
General Atomics
P.O. Box 85608
San Diego, CA 92186
Phone: (619) 455-2275
FAX: (619) 455-4156

P. Rockett
Sandia National Laboratories, Org. 6531
PO Box 5800
MS1129
Albuquerque, NM 87185-1129
Phone: (505) 845-7466
FAX: (505) 845-3130
E-mail: rockett@pmtf.sandia.gov

Takeo Muroga
Research Institute of Applied Mechanics
Kyushu University
Kasuga-koen 6-1, Kasugashi, Fukuoka-ken
816 Japan
Phone: 81-92-573-9611
FAX: 81-92-582-4201

Akio Sagara
National Institute for Fusion Science
Furocho, Chikusa-ku, Nagoya
464 Japan
Phone: 81-52-781-5111
FAX: 81-52-782-8493

Nobuaki Noda
National Institute for Fusion Science
Furocho, Chikusa-ku, Nagoya
464 Japan
Phone: 81-52-781-5111
FAX: 81-52-782-8493
E-mail: noda@nifs.ac.jp

Kazuyoshi Sato
Japan Atomic Energy Research Institute (JAERI)
Naka-machi, Naka-gun, Ibaraki-ken
311-01 Japan
Phone: 81-292-70-7552
FAX: 81-292-70-7558

L. Schmitz
Institute of Plasma & Fusion Research
University of California, Los Angeles
44-139 Engineering IV
Los Angeles, CA 90024-1597
Phone: (310) 825-6919
FAX: (310) 206-4832
E-mail: schmitz@fusion.ucla.edu

S. Tanaka
ITER Garching Joint Work Site
Max Planck Institut für Plasmaphysik
Boltzmannstrasse 2
D-85748 Garching bei München
Germany
FAX: 49-89-3299-4110
E-mail: tanakas@sat.ipp-garching.mpg.de

L. Sevier
General Atomics
P.O. Box 85608
San Diego, CA 92186
Phone: (619) 455-4769
FAX: (619) 455-4156
E-mail: sevier@gav.gat.com

D. Taylor
Los Alamos National Laboratory
PO Box 1663
Los Alamos, NM 87545
FAX: (505) 665-1687
E-mail: dtaylor@lanl.gov

J. Smith
General Atomics
P.O. Box 85608
San Diego, CA 92186
Phone: (619) 455-3836
FAX: (619) 455-4156
E-mail: smithj@gav.gat.com

P. Trester
General Atomics
PO. Box 85608
San Diego, CA 92186
Phone: (619) 455-2914
FAX: (619) 455-4268

L. Snead
Oak Ridge National Laboratory
PO Box 2009
Oak Ridge, TN 37831-8070
Phone: (619) 574-9942
FAX: (615) 574-7659

M. Ulrickson
Sandia National Laboratories, Org. 6531
P.O. Box 5800
MS1129
Albuquerque, NM 87185-1129
Phone: (505) 845-3020
FAX: (505) 845-3130
E-mail: maulric@pmtf.sandia.gov

Satoshi Suzuki
Japan Atomic Energy Research Institute (JAERI)
Naka-machi, Naka-gun, Ibaraki-ken
311-01 Japan
Phone: 81-292-70-7552
FAX: 81-292-70-7558
E-mail: suzuki@vax001.naka.jaeri.go.jp

M. Wade
Oak Ridge National Laboratory
PO Box 2009
Oak Ridge, TN 37831-8070

B. Wampler
Sandia National Laboratories, Org. 1111
PO Box 5800
MS1056
Albuquerque, NM 87185-1056
Phone: (505) 844-4114
FAX: (505) 844-7775

J. Won
Institute of Plasma & Fusion Research
University of California, Los Angeles
44-139 Engineering IV
Los Angeles, CA 90024-1597
Phone: (310) 206-7759
FAX: (310) 206-4832
E-mail: won@fusion.ucla.edu

J. Watkins (SNL)
General Atomics
P.O. Box 85608
San Diego, CA 92186
Phone: (619) 455-3670
FAX: (619) 455-4156
E-mail: watkins@vaxm.gat.com

C. Wong
General Atomics
P.O. Box 85608
San Diego, CA 92186
Phone: (619) 455-2266
FAX: (619) 455-2266
E-mail: wongc@gav.gat.com

P. West
General Atomics
P.O. Box 85608
San Diego, CA 92186
Phone: (619) 455-2863
FAX: (619) 455-4156
E-mail: west@gav.gat.com

Toshiro Yamashina
Hokkaido University
Department of Nuclear Engineering
Kita-13, Nishi-8, Kita-ku, Sapporo
060 Japan
Phone: 81-11-716-2111, ext. 6659
FAX: 81-11-747-9366

Scott Willms
Los Alamos National Laboratory
PO Box 1663
Los Alamos, NM 87545
Phone: (505) 667-5802

Naoaki Yoshida
Research Institute of Applied Mechanics
Kyushu University
Kasuga-koen 6-1, Kasugashi, Fukuoka-ken
816 Japan
Phone: 81-92-573-9611
FAX: 81-92-582-4201

K. Wilson
Sandia National Laboratories, Org. 8304
PO Box 969
MS9163
Livermore, CA 94551-0969
Phone: (510) 294-2497
FAX: (510) 294-3231
E-mail: klwilso@california.sandia.gov

D. Youchison
Sandia National Laboratories, Org. 6531
PO Box 5800
MS1129
Albuquerque, NM 87185-1129
Phone: (505) 845-3138
FAX: (505) 845-3130
E-mail: dlyouch@pmtf.sandia.gov

EXTERNAL DISTRIBUTION:

Masato Akiba (5)
Japan Atomic Energy Research Institute
Naka-machi, Naka-gun
Ibaraki-ken 311-01
JAPAN

Yoshi Hirooka (2)
Institute of Plasma & Fusion Research
University of California, Los Angeles
44-139 Engineering IV
Los Angeles, CA 90024-1597

M. Cohen
Office of Fusion Energy
Office of Energy Research
ER-533, Germantown
U.S. Department of Energy
Washington, DC 20585

Osamu Motojima
National Institute for Fusion Science
Furocho, Chikusa-ku
Nagoya 464
JAPAN

R. Conn
Office of the Dean
School of Engineering
University of California, San Diego
La Jolla, CA 92093-0403

Nobuaki Noda (3)
National Institute for Fusion Science
Furocho, Chikusa-ku
Nagoya 464
JAPAN

J. Davis
McDonnell Douglas Aerospace
Mail Code 306-4204
PO Box 516
St. Louis, MO 63166

Akio Sagara
National Institute for Fusion Science
Furocho, Chikusa-ku
Nagoya 464
JAPAN

Tomoaki Hino (10)
Hokkaido University
Department of Nuclear Engineering
Kita-13, Nishi-8, Kita-ku
Sapporo 060
JAPAN

L. Sevier
General Atomics
P.O. Box 85608
San Diego, CA 92186

L. Snead
Oak Ridge National Laboratory
PO Box 2009
Oak Ridge, TN 37831-8070

C. Wong
General Atomics
P.O. Box 85608
San Diego, CA 92186

P. Trester
General Atomics
PO. Box 85608
San Diego, CA 92186

Toshiro Yamashina
Hokkaido University
Department of Nuclear Engineering
Kita-13, Nishi-8, Kita-ku
Sapporo 060
JAPAN

P. West
General Atomics
P.O. Box 85608
San Diego, CA 92186

Naoaki Yoshida (3)
Research Institute of Applied Mechanics
Kyushu University
Kasuga-koen 6-1, Kasugashi
Fukuoka-ken 816
JAPAN

INTERNAL DISTRIBUTION:

1	MS1056	B. L. Doyle, 1111
5	MS0740	R. T. McGrath, 6503
1	MS1129	M. A. Ulrickson, 6531
1	MS1129	R. E. Nygren, 6531
1	MS1129	D. L. Youchison, 6531
1	MS9163	K. L. Wilson, 8304
1	MS9162	R. Causey, 8347
1	MS9018	Central Technical Files, 8523-2
5	MS0899	Technical Library, 7141
1	MS0619	Technical Publications, 7151
10	MS1119	Document Processing for DOE/OSTI, 7613-2

*U.S. GOVERNMENT PRINTING OFFICE 1994-0-573-026/80029

DATE
FILMED
8/24/94

END